

**1972**  
international  
clay  
conference

**PREPRINTS**  
VOLUME I

*E. Galois*

# 1972 INTERNATIONAL CLAY CONFERENCE

Madrid, June 25 - 30, 1972

## P R E P R I N T S

### VOLUME I

Editor

*J. M. Serratosa*

Assistant

*A. Sánchez*

Editorial Staff

*A. Hidalgo*

*J. A. Raussell-Colom*

*A. Mifsud*

*V. Fornes*

Secretary

*M. T. Miranda*

S.E.A.

Sociedad Española de Arcillas

A.I.P.E.A.

Association Internationale  
pour l'Etude des Argiles

D. L. M. 16294 - 1972

«Realigraf», Rodón, 12. MADRID-20

In conformity with the policy of previous meetings, the A. I. P. E. A. Council agreed that the 1972 Clay Conference should be conducted mainly as a discussion meeting, devoting a minimum time to presentation of papers. At the same time, the Council paid serious consideration to the difficulties inherent in producing a volume of Proceedings of high quality before the Conference, due to the rigid time schedule. Consequently, it was decided to postpone the appearance of the Proceedings after the Conference, and to publish the contributions selected in Preprint form.

This publication consist of two volumes, the first corresponding to section I and II, and the second to the remaining sections. It contains papers selected for presentation at the scientific sessions, together with the Introductory Lectures by the section chairmen. The selected papers are automatically regarded as submitted for publication in the Conference Proceedings. Additional contributions, which may be presented during discussion periods at the discretion of the chairmen, have also been included.

The Organizers wish to express their deepest gratitude to Prof. Lisa Heller and to the section chairmen for their selection of papers. In response to the Second Circular, some 167 abstracts were received. Time available for the scientific sessions permits the discussion of only about 70 of these papers. Because of that limitation, the Organizing Committee, regrets that many excellent contributions have been turned away. It is hoped that authors whose papers have not been included in the programme will nevertheless be able to attend the Conference and contribute with their comments to the discussions.

The assistance of Mrs. A. Muro, Mrs. C. Vizcaíno, Mr. M. Fernández, Mr. J. A. Martín Rubí and Mr. C. Serna in checking the original manuscripts and the proofs is grateful acknowledged.

The Organizing Committee



# CONTENTS

## SECTION I. CRYSTALCHEMISTRY OF CLAY MINERALS

(structures included)

	<u>Page.</u>
Chairman's Introduction.	
Recent advances in the crystal structures and crystal chemistry of layer silicates, <i>S. W. Bailey</i> ... ..	3
Some structural and crystallochemical features of layer silicates, <i>V. A. Drits</i> ... ..	15
× The defect structure of dehydrated clay mineral crystals, <i>F. Freund</i> ...	29
The hydrous magnesium-nickel silicate minerals (so-called garnierites), <i>G. W. Brindley</i> and <i>Pham Thi Hang</i> ... ..	41
A quantitative study of one-layer polytypism in the kaolin minerals, <i>R. W. Wolfe</i> and <i>R. F. Giese Jr.</i> ... ..	51
The nature of the cohesion energy in kaolin minerals, <i>M. Cruz</i> , <i>H. Jacobs</i> and <i>J. J. Fripiat</i> ... ..	59
Electron spin resonance studies of kaolins, <i>B. R. Angel</i> and <i>P. L. Hall</i> ...	71
× Infrared study of chromium-bearing halloysites, <i>Z. Maksimovic</i> and <i>J. L. White</i> ... ..	87
× Mixed-layer kaolinite-smectite from lower Silesia, Poland. Final report, <i>A. Wiewióra</i> ... ..	101
Correlation between the hydroxyl stretching bands and the chemical composition of trioctahedral micas, <i>J. M. Rousseaux</i> , <i>C. Gómez</i> , <i>Y. Nathan</i> and <i>P. G. Rouxhet</i> ... ..	117
Le spectre infrarouge des biotites: vibrations d'elongation basse fréquence des OH du reseau, <i>J. Chaussidon</i> ... ..	129
Deprotonation of nontronite resulting from chemical reduction of structural ferric iron, <i>C. B. Roth</i> and <i>R. J. Tullock</i> ... ..	143
Analyse structurale de la sepiolite à partir des données de la diffraction électronique, <i>M. Rautureau</i> , <i>C. Tchoubar</i> and <i>J. Mering</i> ... ..	153
Triangular diagrams in use of a survey of crystal chemistry of chlorites, <i>K. Oinuma</i> , <i>S. Shimoda</i> and <i>T. Sudo</i> ... ..	161

	<i>Page.</i>
Reaction at low temperatures between kaolin and lithium carbonate, <i>A. García Verduch</i> and <i>J. S. Moya Corral</i> ... ..	173
Formation of $\beta$ -spodumene by solid state reaction between pyrophyllite and lithium carbonate, <i>S. Udagawa</i> and <i>H. Ikawa</i> ... ..	185

Additional Contribution,

Infrared study of attapulgite and HCl treated attapulgite, <i>E. Mendelovici</i> .	193
--	-----

SECTION II. GENESIS AND SYNTHESIS OF CLAY MINERALS

Chairman's Introduction.	
Data and tendencies of recent years in the field «Genesis and synthesis of clays and clay minerals», <i>G. Millot</i> ... ..	205
Contribution a la connaissance de la synthese des kaolins, <i>B. Siffert</i> and <i>R. Wey</i> ... ..	213
A contribution to the synthesis of kaolinite, <i>A. La Iglesia Fernández</i> and <i>J. L. Martín Vivaldi</i> ... ..	227
Importance of the silica subtraction process during the hydrothermal kaolinitization of amorphous silico-aluminas, <i>L. Rodrique, G. Poncelet</i> and <i>A. Herbillon</i> ... ..	241
Geochemical evolution of clay minerals in weathered products and soils of mediterranean climates, <i>H. Paquet</i> and <i>G. Millot</i> ... ..	255
Distribution and genesis of imogolite in volcanic ash soils of northern Kanto, Japan, <i>S. Aomine</i> and <i>Ch. Mizota</i> ... ..	263
Clay mineralogy of soils on ultrabasic rocks from Sabah, Borneo, <i>H. Eswaran</i> and <i>C. Sys</i> ... ..	271
Origin and specific structural features of clay minerals from the lateritic bauxites in the european part of the U. S. S. R., <i>A. P. Nikitina</i> and <i>B. B. Zvyagin</i> (abstract) ... ..	283
Phase equilibria for dioctahedral expandable phases in sediments and sedimentary rocks, <i>B. Velde</i> ... ..	285
Clay mineralogy of bottom sediments in the Adriatic Sea, <i>F. Veniale, F. Soggetti, B. Pigorini, A. Dal Negro</i> and <i>A. Adami</i> ... ..	301
Distribution of clay minerals in the spanish triassic sedimentary basins, <i>M. Caballero</i> and <i>J. L. Martín Vivaldi</i> ... ..	313
Clay mineral provinces in european malm, <i>W. M. Bausch</i> (abstract) ... ..	325
Crystallochemical heterogeneity of glauconite as depending on the conditions of its formation and post-sedimentary change, <i>V. D. Shutov, M. Ya. Katz, V. A. Drits</i> and <i>A. L. Sokolova</i> ... ..	327

	Genetic types and paragenetic associations of minerals of the corrensite group, <i>A. G. Kossovskaya</i> (abstract) ... ..	341
	Genesis and thermodynamic stability of dioctahedral and trioctahedral mixed-layer minerals in sedimentary rocks, <i>S. G. Sarkisyan</i> and <i>D. D. Kotelnikov</i> ... ..	343
X	Genesis of chlorite, vermiculite, serpentine, talc and secondary oxides in ultrabasic rocks, <i>J. Rimsaite</i> ... ..	353
	Some aspects of structural transformations of clay minerals under hydrothermal conditions, <i>V. Frank-Kamenetskij</i> , <i>N. Kotov</i> , <i>E. Goilo</i> and <i>G. Klotchkova</i> ... ..	365
	Kinetics of alteration of k-feldspar to kaolinite and its application to the genesis of kaolin deposits, <i>Y. Tsuzuki</i> , <i>S. Mizutani</i> , <i>H. Shimizu</i> and <i>H. Hayashi</i> ... ..	377
	Kinetics and mechanism of dissolution of Fifthian illite in two complexing organic acids, <i>W. H. Huang</i> and <i>W. D. Keller</i> ... ..	385
✓	New data on iron oxides in the weathering zone, <i>F. V. Chukrov</i> , <i>B. B. Zvyagin</i> , <i>L. P. Ermilova</i> and <i>A. I. Gorshkov</i> ... ..	397
	The transformation of lepidocrocite to goethite, <i>U. Schwertmann</i> and <i>R. M. Taylor</i> ... ..	405

## Additional Contributions

	Geochemistry of trace elements during the genesis of coloured bentonites, <i>J. Linares</i> , <i>F. Huertas</i> , <i>M. Lachica</i> and <i>E. Reyes</i> ... ..	415
	Remarques sur la transformation de quelques minéraux en milieu alcalin, <i>S. Caillère</i> , <i>H. Besson</i> and <i>S. Herin</i> ... ..	429
	Wall rock alteration in the Neogene hydrothermal areas in the Gutin Mountains (Rumania), <i>O. Anton</i> ... ..	435
	Author index ... ..	441

can be seen in the  
 ... ..



S E C T I O N I

CRYSTALCHEMISTRY OF CLAY MINERALS  
(Structures included)



## CHAIRMAN'S INTRODUCTION

### RECENT ADVANCES IN THE CRYSTAL STRUCTURES AND CRYSTAL CHEMISTRY OF LAYER SILICATES

S. W. Bailey

ABSTRACT. - Discontinuities in the cell dimensions of synthetic lithian muscovites and lepidolites can be used to map out the region of immiscibility in the ternary system muscovite-polyolithionite-triolithionite. The structure of the end member 1M polyolithionite shows a nearly hexagonal tetrahedral ring, partial ordering of octahedral Al and Li, and an hexagonal antiprism of CN 12 around K. A 2M<sub>2</sub> lepidolite on the margin of the miscibility gap shows a slightly distorted hexagonal ring and an hexagonal prism around K. The amount of tetrahedral rotation and the difference between inner and outer K--O distances can be predicted from chemical composition alone. Octahedral ordering of the xanthophyllite type (two large and one small octahedra) has been predicted for zinnwaldite micas. Four observed structural types of trioctahedral chlorite can be used to interpret diagenetic versus detrital origins in sediments and soils. Di, trioctahedral cookeite has a nearly constant tetrahedral composition, perhaps due to its structural type, and octahedral totals ranging from 4.90 to 5.35 ions per formula unit. Four distinct structural types have been reported for palygorskite.

## INTRODUCTION

I appreciate the opportunity to deliver this Introductory Lecture for the AIPEA 1972 International Clay Conference. Due to time limitations my survey necessarily will be restricted to a few topics of special interest and will not pretend to be comprehensive. I will

attempt to summarize some of the recent advances in our knowledge of the crystal structures and crystal chemistry of selected layer silicates. Where appropriate, I will mention problems that are still unsolved or could benefit from additional research. Most of the advances mentioned will be from the literature of the three years since the last AIPEA Conference, with references to earlier work where necessary for background information. Although most of the research on crystal structures of layer silicates necessarily must be conducted on macroscopic crystals, the information derived should be equally applicable to clay-size particles of the same and related species.

### LEPIDOLITE MICAS

It is now well known that natural micas in the Li-Al system do not exhibit a continuous solid solution series that would bridge the gap between dioctahedral muscovite and trioctahedral lepidolite (Levinson, 1953; plus others). Instead, lithian muscovites with total octahedral occupancies from 2.0 to approximately 2.4 atoms per formula unit crystallize with the  $2M_1$  layer stacking sequence characteristic of muscovite, and more Li-rich lepidolites with approximately 2.6 to 3.0 octahedral atoms adopt one or another of the different stacking sequences designated 1M,  $2M_2$ , or 3T. Intermediate compositions in the approximate octahedral range of 2.4 to 2.6 atoms are two-phase mixtures of dioctahedral lithian muscovite and trioctahedral lepidolite.

Foster (1960) showed that lepidolites should be subdivided into polyolithionite and trilithionite end members. Polyolithionite  $K(AlLi_2)Si_4O_{10}F_2$  is derived from muscovite  $KAl_2(Si_3Al)O_{10}(OH)_2$  by a 2:1 replacement of octahedral Al by Li with concomitant decrease in tetrahedral Al to maintain charge balance and by replacement of OH by F. Trilithionite  $K(Al_{1.5}Li_{1.5})(Si_3Al)O_{10}(OH,F)_2$  is derived from muscovite by a 3:1 replacement of octahedral Al by Li. Natural lithian muscovites and lepidolites show replacement ratios between 2:1 and 3:1, and should be plotted in a triangular diagram with muscovite (Ms), polyolithionite (P1), and trilithionite (T1) at the corners.

Munoz (1968) has synthesized Li-Al micas along the three edges of this ternary system Ms-P1-T1. Starting materials of oxide-fluorite mixes or gels were crystallized both in the dry state and with excess  $H_2O$  present at pressures ranging from 2 kbars to 5 kbars and at temperatures ranging from 250° to 800°C.

(1) Micas along the Ms-P1 join were found to crystallize only with the 1M structure from  $P1_{100}$  to  $P1_{40}Ms_{60}$ , with the  $2M_1$  structure only for  $Ms_{100}$  and  $Ms_{90}P1_{10}$ , and as mixtures of  $2M_1 + 1M$  for intermediate compositions. The 1M structure is not necessarily

the stable form over all its composition range, however, under the conditions of synthesis. The structural break between the dioctahedral and trioctahedral end members is confirmed by a discontinuity in the (005) basal spacing for intermediate compositions.

(2) Along the join P1-T1 the 1M structure formed exclusively from P<sub>100</sub> to P<sub>31</sub>T<sub>69</sub>, with mixtures of 1M + 2M<sub>1</sub> for more T1-rich compositions. Polylithionite itself was found to crystallize only in the fluorine form and not to accept hydroxyl in its structure.

Trilithionite, however, accepts variable amounts of F and OH. Although all compositions along this join are trioctahedral, both the octahedral and tetrahedral compositions change continuously. Sharp discontinuities are observed in both the *a* and *c* cell dimensions around P<sub>30</sub>T<sub>70</sub>, which also marks the break between one-layer and two-layer structures. Moreover, between P<sub>40</sub>T<sub>60</sub> and P<sub>25</sub>T<sub>75</sub> reproducible cell dimensions cannot be obtained from identical starting materials under duplicate conditions.

(3) Along the Ms-T1 join the 2M<sub>1</sub> structure formed exclusively between Ms<sub>100</sub> and Ms<sub>70</sub>T<sub>30</sub>, with a mixture of 2M<sub>1</sub> + 1M for more T1-rich compositions. But the 2M<sub>1</sub> structure was considered to be the stable form across the entire join. There is a hint of a discontinuity in the (005) basal spacing between Ms<sub>70</sub>T<sub>30</sub> and Ms<sub>60</sub>T<sub>40</sub>, but the powder data are inconclusive. Such a break might be anticipated between dioctahedral and trioctahedral end members even if the 2M<sub>1</sub> structure is adopted throughout. Because of this indeterminacy the results of the ternary system can be plotted in two ways (Fig. 1).

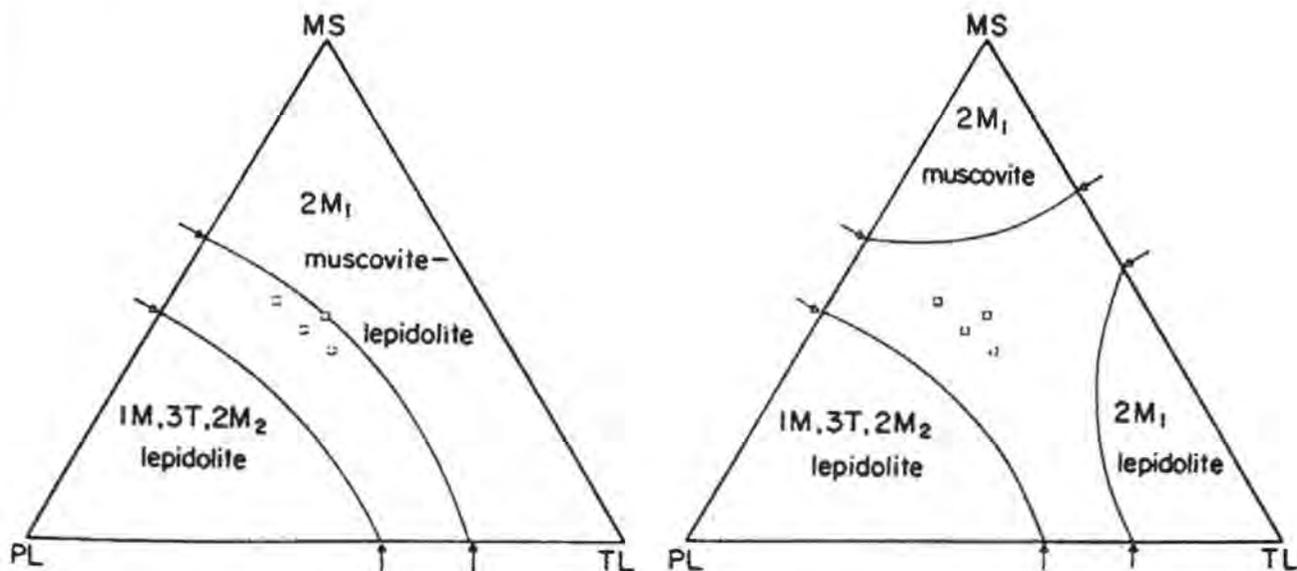


Figure 1. Two different interpretations of immiscibility region in ternary system muscovite-polyolithionite-trilithionite. Data points represent natural two-phase Li-micas. From Munoz (1968).

The foregoing interesting study by Munoz could be extended very fruitfully in the following ways.

a) Further study of the possible break along the Ms-T1 join by single crystal X-ray methods.

b) Crystal structure analysis of a natural trioctahedral trili-  
thionite  $2M_1$  structure to determine differences from the muscovite  
 $2M_1$  structure.

c) Examination of many more natural lepidolites of known bulk composition to outline better the structural immiscibility regions of Fig. 1.

d) Determination of the compositions and cell parameters of the individual phases present in the immiscibility regions.

The crystal structure of the trioctahedral 1M polyolithionite end member synthesized by Munoz has been determined by Takeda and Burnham (1969). Some of the interesting features found are:

a) Partial ordering of octahedral Al and Li so that the large octahedron, which would correspond to the vacant site in muscovite, contains more Li than the other two sites.

b) A nearly hexagonal tetrahedral ring with a rotation angle  $\alpha$  of only  $3^\circ$ . This lesser distortion relative to muscovite had been predicted by Levinson (1953) on the basis of the weakened intensities of the  $06\ell$  reflections with  $\ell$  odd in lithian muscovites and by Radoslovich (1959) on the basis of the assumption that interlayer stacking vectors of  $\pm 60^\circ$ , needed for the  $2M_2$  lepidolite structure, should be possible only for layers not distorted in ditrigonal fashion.

c) The effective oxygen coordination around the interlayer K approaches 12, in the form of an hexagonal antiprism. The difference ( $\Delta$ ) between the inner and outer K--O distances is only 0.132 Å because of the small value of  $\alpha$ . Because there is no tetrahedral substitution, the positive charge on K is balanced by negative charges on the apical oxygens and fluorine coordinating the octahedral cations. The K antiprism is noticeably flattened as a result of this attraction as well as by the absence of OH with its repulsing proton.

Takeda, Haga, and Sadanaga (1971) have analyzed the structure of a natural  $2M_2$  lepidolite having 2.6 octahedral cations and thus lying on the border of the miscibility gap. Because the  $2M_2$  stacking sequence involves  $\pm 60^\circ$  interlayer vectors, the K coordination polyhedron is a slightly distorted hexagonal prism rather than an antiprism. The inner and outer K--O distances differ by 0.24 Å due to a slightly larger tetrahedral rotation angle ( $5.3^\circ$ ) than was found for polyolithionite. This larger  $\alpha$  value undoubtedly is due to the substitution of 0.61 atoms of Al for Si. The hexagonal prism polyhedron around K normally would be unstable due to close mutual approach of negatively charged basal oxygens from adjacent layers. This configuration becomes increasingly more stable toward the end member polyolithionite due to lessening of charge on the basal oxygens (lesser tetrahedral substitution) and concomitant replacement of OH by F. The authors note that with increasing trioctahedral character

the H proton in OH turns toward the interlayer K. The resulting increasing repulsion between H and K, which results in instability of the OH form of polyolithionite, is avoided by replacement of OH by F which will attract rather than repel the K. In  $2M_1$  muscovite, on the other hand, the H proton in OH is oriented differently so that it can interact with the basal oxygens. Replacement of OH by F here would be unfavorable. It is likely that this is the reason F does not replace OH completely in the  $2M_1$  form of trilithionite.

The preceding 3-dimensional structural analysis supersedes an earlier 1-dimensional analysis of  $1M$  and  $2M_2$  lepidolites by Franzini and Sartori (1969). The latter study reported an  $\alpha$  value of  $11^\circ$  and a trigonal antiprism (octahedron) around K, but was based on only 12 00 $\ell$  reflections.

McCauley and Newnham (1971) have made the most quantitative and convincing study to date of the causes of distortions in the mica structure. They show a linear relation between tetrahedral rotation angle  $\alpha$  and the difference  $\Delta$  between inner and outer K--O distances. By means of statistical analysis  $\alpha$  is shown to depend primarily on misfit between the ideal lateral dimensions of unconstrained tetrahedral and octahedral sheets, expressed as the ratio  $b_t/b_o$ . The interlayer cation contributes on the average only about 10% to the amount of rotation. By use of the graphs, or equivalent equations,  $\alpha$  and  $\Delta$  can be predicted from chemical composition alone. The results of Takeda and Burnham (1969) on  $1M$  polyolithionite were not used in this analysis, but fit the curves exceedingly well.

The crystal structure of a  $3T$  lepidolite is presently under refinement by B.E. Brown (pers. comm., 1971). This will be of special interest as the  $3T$  muscovite structure is the only mica to date in which appreciable Si, Al ordering has been documented (Güven and Burnham, 1967). Güven (1971) attributes this ordering to the differences in the symmetry of individual layers in the  $3T$  as opposed to the  $2M_1$  structure. In  $2M_1$  muscovite adjacent tetrahedral sheets within the layer are related by a center of symmetry. If the tetrahedral ordering pattern also obeys the center of symmetry there will be two oxygens with unbalanced electrostatic charges along the octahedral shared edges. In  $3T$  muscovite, where the tetrahedral sheets within each layer are related by a 2-fold axis, the unbalanced oxygens do not lie on the same shared edge. This factor, if valid, presumably becomes less important in trioctahedral species due to less shortening of shared edges.

## ZINNWALDITE MICAS

Rieder (1968, 1970, 1971) and Rieder and others (1970, 1971) have studied the crystal chemistry and crystallography of natural and synthetic Li-Fe micas. Rieder and others (1970) point out that

the Ms-P1-T1 triangle used by Munoz (1968) may not involve three true compositional parameters, but only two parameters such as octahedral occupancy and octahedral  $R^{3+}$ . If so, it is permissible to project the triangle onto the Ms-P1 join to form one edge of a triangle with Ms, P1, and a hypothetical Fe-mica at the corners. A diagram of this type was used to show that natural zinnwaldites from Czechoslovakia and Germany plot near the siderophyllite  $KFe_2^{2+}(Al, Fe^{3+})(Si_2Al_2)O_{10}(OH, F)_2$ -polyolithionite join. In these samples there is always close to one small and two large octahedral cations, neglecting vacancies. Li tends to replace  $R^{2+}$  on a 1:1 basis along the join, and there is about a 1:1 ratio of Li to F. Several different polytypic varieties were recognized, but no relation of the polytypes to compositional or temperature-pressure parameters was noted.

Based on the favorable ratio of big and small octahedral cations and the observation of smaller  $d(00\ell)$  values for these specimens than for annite, trilithionite, and synthetic zinnwaldites, Rieder (1968) proposed that natural zinnwaldites show an octahedral ordering pattern of the type found in xanthophyllite (one small and two large octahedra) by Takeuchi and Sadanaga (1966). Although this appears to be a reasonable assumption, it must be remembered that it is based on indirect evidence and needs experimental verification by crystal structure analysis. The only pertinent structure known in sufficient detail for testing purposes is the previously described synthetic 1M polyolithionite by Takeda and Burnham (1969), and this does not support the assumption. Partial ordering was found, but it was of the muscovite type with one large and two small octahedra. The two large atoms of Li present are distributed with 0.9 Li in the large octahedron (plus 0.1 Al), and the remaining 1.1 Li distributed equally (with 0.9 Al) between the two smaller octahedra. Perhaps consideration must be given to structural features or to cation charge, not just to cation numbers and sizes, in determining the ordering tendency and pattern. For example, two ions of  $Li^{1+}$  may distribute differently than two ions of  $Mg^{2+}$  or  $Fe^{2+}$ . Clearly, more structural analyses are needed to resolve this question.

## CHLORITES

Hayes (1970) has made the most detailed study to date of the environmental significance of chlorites in sedimentary rocks. Four different structural arrangements of the 2:1 layer and the interlayer hydroxide sheet, designated Ia, Ib ( $\beta = 97^\circ$ ), Ib ( $\beta = 90^\circ$ ), and IIb by Bailey and Brown (1962), were recognized by X-ray powder patterns in his study. Textural and morphological evidence from thin

section petrography and scanning electron microscopy led to the conclusion that type I chlorite structures are formed almost exclusively by diagenetic processes, rarely by halmyrolysis. They form from a variety of parent materials at temperatures and pressures only moderately above earth-surface conditions. A diagenetic crystallization and stability sequence with increasing temperature was proposed from type I chlorite with disordered layer stacking  $Ib_d$  to  $Ib(\beta = 97^\circ)$  to  $Ib(\beta = 90^\circ)$ . Weathering or hydrothermal alteration may lead to the  $Ia$  structure. Thermal energy approaching that of low-grade metamorphism is usually necessary to cause  $Ib(\beta = 90^\circ)$  chlorites to convert to the more stable  $IIb$  structure characteristic of igneous and metamorphic rocks. Hence the  $IIb$  chlorite in unmetamorphosed sediments or soils is most likely of detrital origin. Chemical composition has little or no influence upon relative structural stabilities. Temperature is much more important. Hayes recommends greater use of chlorite structural types in geothermometry, recognition of diagenetic facies or gradients, and detection of hydrothermal and incipient metamorphic effects.

Černý (1970) has studied the crystal chemistry of cookeite on the basis of the 14 best chemical analyses in the literature. Cookeite is a di, trioctahedral chlorite of ideal composition  $(LiAl_4)(Si_3Al)O_{10}(OH, F)_8$  normally based on the  $Ia$  structural type. Černý finds a nearly constant tetrahedral composition of  $Si_3Al$  throughout, but with occasional substitution of minor Be or B for Al. He suggests this constant 3:1 ratio may result from the particular ordering pattern that is possible only in the  $Ia$  structure. Ordering and local charge balance can be achieved here because a trivalent element in the hydroxide interlayer sheet, which is the source of overall positive charge for that sheet, can be positioned vertically midway between superimposed ordered Al tetrahedra, which are the sources of the overall negative charges on the layers immediately above and below. Ordering patterns of this sort have been identified in a  $Ia$  Cr-chlorite by Brown and Bailey (1963) and in  $Ia$  vermiculite by Shirozu and Bailey (1966). A detailed structure of cookeite is now in progress.

Total octahedral occupancy in cookeite was found to be close to 5 per formula unit, as required for a di, trioctahedral chlorite, but varying from 4.90 to 5.35. The main substitutions found are  $3(Li, alk)^{1+}/Al^{3+}$  and  $3R^{2+}/2Al^{3+}$ . Fluorine substitutes frequently for OH, but no quantitative relationship could be established from the data. Small amounts of Na, Ca, K are reported in some analyses of supposedly pure cookeites. Černý suggests these are accommodated in the hexagonal rings between the 2:1 layer and the interlayer. Linear relationships between  $(R^{1+} + 2R^{2+})$  and  $(Al + Fe^{3+})^{VI}$  or  $(\sum R^{VI} + R^{2+})$  could be achieved only by including these alkalis with the octahedral  $R^{1+}$  and  $R^{2+}$  cations. Černý postulates these linear trends extrapolate beyond cookeite to Li-low and Li-free di, dioctahedral chlorites. The di, dioctahedral end member of ideal

composition  $\text{Al}_{4.33}(\text{Si}_3\text{Al})\text{O}_{10}(\text{OH})_8$  has been designated donbassite by the AIPEA Nomenclature Committee, whereas the di, trioctahedral chlorite without Li has been designated sudoite (Pedro, 1970).

### PALYGORSKITE AND SEPIOLITE

Because of their fibrous nature precise 3-dimensional crystal structures of palygorskite and sepiolite have not been determined. In gross outline it is agreed that the structures consist of talc-like ribbons parallel to the fiber axis, in which the tetrahedral sheet is continuous throughout but inverts apical directions in adjacent ribbons.  $\text{H}_2\text{O}$ , OH, and exchangeable cations lie in channels parallel to the fiber axis between the backs of inverted tetrahedra (Caillère and Hénin, 1961a, b).

Until recently the accepted 2-dimensional model of palygorskite has been that of Bradley (1940), in which the width of the ribbons is due to the lateral linkage of two pyroxene-like single tetrahedral chains into a double chain. This leaves room for 5 octahedral cation sites per formula unit, not necessarily all occupied. Drits and Aleksandrova (1966) showed that normally 4 out of 5 sites are occupied in a dioctahedral pattern. The accepted model for sepiolite has been that of Brauner and Preisinger (1956), in which a ribbon width of 3 linked pyroxene tetrahedral chains and a total of 8 octahedral cation sites are postulated. By analogy with pyroxenes the direction of the tetrahedral chains, which parallel the fiber axis, was chosen as the Z axis. The AIPEA Nomenclature Committee recognizes these minerals as phyllosilicate species because of the continuous nature of the tetrahedral sheet (Pedro, 1970), however, so the suggestion of Zvyagin, Mishchenko, and Shitov (1963) that the fiber axis (of periodicity 5.2-5.3 Å) should be called X is more appropriate.

Christ and others (1969) now have shown that X-ray powder patterns of palygorskite can be indexed on the basis of three different structures, perhaps of different composition. One is based on an orthorhombic-shaped unit cell and exhibits diffraction aspect  $p^{**}n$ . The other two have primitive monoclinic-shaped cells and show systematic absences interpreted as due to n-glide planes parallel to (001). The latter structures differ in that the unique monoclinic axis is the Y axis for one and the X axis for the other (retaining the earlier convention of Z for the fiber axis). Thus, the monoclinic angle of  $95^\circ 46'$  is  $\beta$  for the former, but the angle of  $92^\circ 14'$  is  $\alpha$  for the latter. The authors point out that Bradley's 2-dimensional model, stated of probable space group  $C2/m$  with monoclinic angle undetermined, is compatible with all three observed unit cells viewed in projection on (001). So also is an orthorhombic structure of space group  $Pbmn$  reported by Preisinger (1963) without supporting details.

The monoclinic space group P2/c and  $\beta$  angle of 95°50' found by Zvyagin and others (1963) by electron diffraction for one specimen of palygorskite is reported not to be consistent with any of the three preceding X-ray patterns. Gard and Follett (1968), however, accept P2/c as correct for the specimen investigated. They also report that this space group requires an alternation of ribbons of three pyroxene chain width with those of one chain width. Dioctahedral occupancy of 4 out of 5 octahedral sites is still possible. A hypothetical orthorhombic structure of space group Pnmc can also be constructed with this same structural motif by alternating the direction of mutual stagger of tetrahedral ribbons parallel to the fiber axis. The possible existence of ribbons of different widths supports the intergrowths of palygorskite and sepiolite postulated by Martin Vivaldi and Linares Gonzalez (1962) and of possibly more complex structural variants. Drits and Sokolova (1971) have confirmed the Bradley monoclinic model, with  $\beta = 107^\circ$ , by comparison of observed and calculated F values for a palygorskite from Kazakh, but consider other structures possible for other specimens. Nathan and others (1970) found three vein palygorskites, presumably of hydrothermal origin, from Israel to be monoclinic whereas a fourth specimen of probable sedimentary origin is orthorhombic. They propose an order-disorder mechanism to explain the symmetry differences.

Additional research is needed on palygorskite specimens of known composition to document the several proposed structures of different symmetry. Principles of polytypism found useful in other layer silicates should be of value in relating the structures to one another. Single crystal electron diffraction methods appear to offer the most promise in testing possible 3-dimensional models. Although only an orthorhombic model has been recognized to date in sepiolite, there is no a priori reason to rule out the same sort of structural variants as found for palygorskite.

#### REFERENCES

- BAILEY, S. W. and BROWN, B. E. (1962): Chlorite polytypism: I. Regular and semirandom one-layer structures. *Am. Mineralogist* 47, 819-850.
- BRADLEY, W. F. (1940): The structural scheme of attapulgite. *Am. Mineralogist* 25, 405-410.
- BRAUNER, K. and PREISINGER, A. (1956): Struktur und Entstehung des Sepioliths. *Mineral. Petrogr. Mitt.* 6, 120-140.
- BROWN, B. E. and BAILEY, S. W. (1963): Chlorite polytypism: II. Crystal structure of a one-layer Cr-chlorite. *Am. Mineralogist* 48, 42-61.

- CAILLÈRE, S. and HÉNIN, S. (1961a): Sepiolite. Chap. VIII in "The X-ray Identification and Crystal Structures of Clay Minerals" (Ed.: G. BROWN). Mineral. Soc. (London), 325-342.
- CAILLÈRE, S. and HÉNIN, S. (1961b): Palygorskite. Chap. IX in "The X-ray Identification and Crystal Structures of Clay Minerals" (Ed.; G. BROWN). Mineral. Soc. (London), 343-353.
- ČERNÝ, Petr (1970): Compositional variations in cookeite. *Can. Mineral.* 10, 636-647.
- CHRIST, C. L., HATHAWAY, J. C., HOSTETLER, P.B. and SHEPARD, Anna O. (1969): Palygorskite: New X-ray data. *Am. Mineralogist* 54, 198-205.
- DRITS, V. A. and ALEKSANDROVA, V.A. (1966): (The crystallochemical nature of palygorskite). *Zap. Vses. Min. Obshch.* 95, 551-560.
- DRITS, V. A. and SOKOLOVA, G. V. (1971): (Structure of palygorskite). *Soviet Physics--Crystallography* 16, 183-185 (Engl. transl.).
- FOSTER, Margaret D. (1960): Interpretation of the composition of lithium micas. *U. S. Geol. Surv. Prof. Paper* 354-E, 147.p.
- FRANZINI, Marco and SARTORI, Franco (1969): Crystal data on 1M and 2M<sub>2</sub> lepidolites. *Contr. Mineral. Petrology* 23, 257-270.
- GARD, J. A. and FOLLETT, E. A. C. (1968): A structural scheme for palygorskite. *Clay Minerals* 7, 367-370.
- GÜVEN, Necip (1971): Structural factors controlling stacking sequences in dioctahedral micas. *Clays and Clay Minerals* 19, 159-165.
- GÜVEN, Necip and BURNHAM, Charles W. (1967): The crystal structure of 3T muscovite. *Z. Krist.* 125, 163-183.
- HAYES, John B. (1970): Polytypism of chlorite in sedimentary rocks. *Clays and Clay Minerals* 18, 285-306.
- LEVINSON, Alfred A. (1953): Studies in the mica group; Relationship between polymorphism and composition in the muscovite-lepidolite series. *Am. Mineralogist* 38, 88-107.
- MARTIN VIVALDI, Juan L. and LINARES GONZALEZ, Jose (1962): A random intergrowth of sepiolite and attapulgite. *Clays and Clay Minerals* 9, 592-602.
- McCAULEY, James W. and NEWNHAM, R. E. (1971): Origin and prediction of ditrigonal distortions in micas. *Am. Mineralogist* 56, 1626-1638.
- MUNOZ, J. L. (1968): Physical properties of synthetic lepidolites. *Am. Mineralogist* 53, 1490-1512.
- NATHAN, Y., BENTOR, Y. K. and WURTZBURGER, U. (1970): Vein palygorskites in Israel and Sinai: their origin and symmetry. *Israel J. Chem.* 8, 477-485.
- PEDRO, G. (1970): Report of the AIPEA Nomenclature Committee. *AIPEA Newsletter* No. 4, 3-4.
- PRESINGER, Anton (1963): Sepiolite and related compounds: Its stability and application. *Clays and Clay Minerals* 10, 365-371.
- RADOSLOVICH, E. E. (1959): Structural control of polymorphism in micas. *Nature* 183, 253.

RIEDER, Milan (1968): Zinnwaldite: Octahedral ordering in lithium-iron micas. *Science* 160, 1338-1340.

RIEDER, Milan (1970): Lithium-iron micas from the Krušné hory Mountains (Erzgebirge): Twins, epitactic overgrowths and polytypes. *Z. Krist.* 132, 161-184.

RIEDER, Milan (1971): Stability and physical properties of synthetic lithium-iron micas. *Am. Mineralogist* 56, 256-280.

RIEDER, Milan, HUKA, Miroslav, KUČEROVÁ, Dagmar, MINAŘÍK, Luděk, OBERMAJER, Jiří and POVONDRA, Pavel (1970): Chemical composition and physical properties of lithium-iron micas from the Krušné hory Mts. (Erzgebirge). Part A: Chemical composition *Contr. Mineral. Petrology* 27, 131-158.

RIEDER, M. PÍCHOVÁ, A., FASSOVÁ, M., FEDIUKOVÁ, E. and ČERNÝ, P. (1971): Chemical composition and physical properties of lithium-iron micas from the Krušné hory (Erzgebirge), Czechoslovakia and Germany. Part B: Cell parameters and optical data. *Mineral. Mag.* 38, 190-196.

SHIROZU, Haruo and BAILEY, S. W. (1966): Crystal structure of a two-layer Mg-vermiculite. *Am. Mineralogist* 51, 1124-1143.

TAKEDA, Hiroshi and BURNHAM, Charles W. (1969): Fluor-polyolithionite: A lithium mica with nearly hexagonal  $(\text{Si}_2\text{O}_5)^{2-}$  ring. *Mineral. J.* 6, 102-109.

TAKEDA, Hiroshi, HAGA, N. and SADANAGA, R. (1971): Structural investigation of polymorphic transition between  $2\text{M}_2$ ,  $1\text{M}$ -lepidolite and  $2\text{M}_1$  muscovite. *Mineral. J.* 6, 203-215.

TAKEUCHI, Y. and SADANAGA, R. (1966): Structural studies of brittle micas. (1) The structure of xanthophyllite refined. *Mineral. J.* 4, 424-437.

ZVYAGIN, B. B., MISHCHENKO, K. S. and SHITOV, V. A. (1963): Electron diffraction data on the structures of sepiolite and palygorskite. *Soviet Physics--Crystallography* 8, 148-153 (Engl. transl.).



## SOME STRUCTURAL AND CRYSTALLOCHEMICAL FEATURES OF LAYER SILICATES

V.A. Drits

Geological Institute, USSR Academy of Sciences, Moscow, USSR

ABSTRACT. - A bonding model is suggested for tetrahedra of layer silicates, assuming that the cation is in the "centre of gravity" of a tetrahedron of an irregular shape, if the order of each bond  $n = 1.5$ . The lengths of the individual bonds in that case may be different. The displacement of the cation from the "centre of gravity" in the direction of the anion linked with it by a bond having  $n > 1.5$ , is proportional to

$$\frac{n - 1,5}{1,5}$$

Experimental data are in accordance with the calculations.

### INTRODUCTION

In 1961, Cruickshank discussed in detail the role of  $\pi$ -bonding in silicates. He showed that in the  $\text{TO}_4^{n-}$  ion only two d-orbitals of the central atom can form strong d-p  $\pi$ -bonds with the P-orbitals of oxygen. Cruickshank's theory enabled to predict the lengths of T-O bonds and thus paved the way for studies which analyzed the variations of the lengths of bonds and angle between these in silicate tetrahedra in terms of  $\pi$ -bonding. It turned out meanwhile that to explain the observed data one needed certain additional assumptions and in particular had to take account of the electronegativity of the nontetrahedral cations (McDonald, Cruickshank, 1967).

On the other hand, some authors held that the variations of the inter-atomic distances in the silicate groups are to be explained on the basis of local balance of charges, justifying the existence of the ionic model bonding in such silicates as pyroxenes, amphiboles, etc. (Clark et al., 1969). Bauer (1971) proceeded from the Pauling's electrostatic valence rule to show that for  $\text{SiO}_4$ -tetrahedra a simple relation exists between the bond length and bond strength received by the given anion from its surrounding cations.

This paper proposes a bonding model for layer silicate tetrahedra which is somewhat different from those mentioned above and discusses on this basis the observed variations of the lengths of tetrahedral bonds and angles between them for this mineral group.

### GENERAL ASPECTS

A typical feature of tetrahedra in layer silicate structures is that their three cation-anion bonds are directed towards oxygen atoms that are common for the two tetrahedra ("bridge" bonds), while one bond is directed towards the oxygen atom which is at the same time the apex of the octahedron ("nonbridge" bond). For simplicity's sake we shall consider an idealized model of tetrahedron, in which three "bridge" bonds are equivalent between themselves but different from the fourth, "non-bridge", bond. Let us determine for that case the set of hybrid orbitals  $sp^3$ , formed by the tetrahedral cation (Coulson, 1961).

We denote by  $\Psi_1$ ;  $\Psi_2$ ;  $\Psi_3$  and  $\Psi_4$ , the wave functions of the hybrid orbitals, taking into account that  $\Psi_3$  and  $\Psi_4$  are equivalent to  $\Psi_2$ . Then

$$\Psi_1 = N_1 (s + \alpha P_1); \quad \Psi_2 = N_2 (s + \beta P_2) \quad (1)$$

where  $N_1$  and  $N_2$  are the normalization factors

$\alpha$  and  $\beta$  - mixture coefficients whose squares define the relative weight of s- and p-atomic orbitals.

Since the functions  $\Psi_i$  must be orthogonal,

$$1 + \alpha \beta \cos \varepsilon = 0 \quad 1 + \beta^2 \cos \varepsilon_1 = 0 \quad (2)$$

where  $\varepsilon$  and  $\varepsilon_1$  are the angles between the non-equivalent and equivalent hybrids.

By the condition

$$\cos \varepsilon_1 = 1 - \frac{3}{2} \sin^2 \varepsilon \quad (3)$$

Solving equations system (2), taking into account (3), we find that

$$\alpha^2 = \frac{1 - 3 \cos^2 \xi'}{2 \cos^2 \xi'}; \beta^2 = \frac{2}{1 - 3 \cos^2 \xi'}, \text{ where } \xi' = 180^\circ - \xi \quad (4)$$

Since the hybrid orbital is "asymmetric" and the "gravity centre" of its electron cloud is at some distance from the nucleus (Coulson, 1961), let us analyze the relation of the distances  $\bar{X}_1$  and  $\bar{X}_2$  between the "gravity centres" and the nucleus of each hybrid orbital:

$$\bar{X}_1 = 2 N_1^2 \alpha \int X_{sp} d\tau; \bar{X}_2 = 2 N_2^2 \beta \int X_{sp} d\tau \quad (5)$$

Since the orbitals belong to one atom, taking into account equations (4), we have

$$\frac{\bar{X}_1}{\bar{X}_2} = \frac{\alpha (1 + \beta^2)}{\beta (1 + \alpha^2)} = 3 \cos \xi' \quad (5')$$

Hence, for this type of hybridization, the "gravity centres" of the charges of hybrid orbitals are positioned in such a manner that the common "gravity centre" of the charges of all the four orbitals coincides with the origin of coordinates, that is with the atomic nucleus.

The wave function of the molecular orbital describing the relationship between the heteropolar atoms A and B and in LCAO approximation can be written as

$$\Psi = N(\Psi_A + \lambda \Psi_B); N^{-2} = 1 + \lambda^2 + 2\lambda S_{AB}; S_{AB} = \int \Psi_A \Psi_B d\tau \quad (6)$$

where  $\lambda$  is the degree of polarity,  $\Psi_A$  and  $\Psi_B$  are the hybrid orbitals of the atoms A and B, and  $S_{AB}$  is the overlap integral.

Suppose that, in the MO, the wave functions  $\Psi_A$  and  $\Psi_B$  are identical as regards the content of the s- and p-character, i.e.

$$\Psi_A = N_1(s_A + \alpha p_A); \Psi_B = N_1(s_B + \alpha p_B) \quad (7)$$

This arbitrary assumption leads to interesting consequences, which we shall analyze considering Si atoms as the cations (atoms A) and oxygen atoms as the anions (atoms B).

Table I gives the wave functions of the hybrids orbitals as dependent on the value of the angle  $\xi$  (see equations (1) and (4)).

Si cations were assumed to be located in the "gravity centre" of the tetrahedron. For each given average distance  $r_{av}$  (Si - O), the individual interatomic cation-anion distances were found to depend on the angle  $\xi$ . For these initial data the values of the over-

lap integrals were calculated using the table data of Milliken et al. (1949). Table I shows that for a given average distance  $r_{av}$  (Si-O) independent of the angle  $\epsilon$  and the individual values  $r_i$  (Si-O) the overlap integrals are practically equal and have the same value as in the geometrically regular tetrahedron having all bonds equivalent. The value of the overlap integral can be regarded as measure of the strength of the bond. Therefore, under the above conditions, all four Si-O bonds are equivalent as regards the strength of the bond independent of the relationship of s- and p-character in each particular bond.

Table I

Values of overlap integrals  $S$  and  $\frac{\bar{X}_{Si-O}}{R}$ , calculated for bonds Si-O at different  $r_{av}$ (Si-O) and  $\epsilon$

	$\epsilon = 109^{\circ}28'$	$\epsilon = 110^{\circ}$		$\epsilon = 110^{\circ}28'$		$\epsilon = 109^{\circ}28'$	$\epsilon = 110^{\circ}$		$\epsilon = 110^{\circ}28'$	
		$i = 1$	$i = 2$	$i = 1$	$i = 2$		$i = 1$	$i = 2$	$i = 1$	$i = 2$
$r_i(\text{\AA})$	1.62	1.65	1.61	1.68	1.60	1.76	1.793	1.749	1.826	1.738
$S_i$	0.503	0.502	0.503	0.501	0.503	0.467	0.465	0.468	0.464	0.470
$\frac{\bar{X}_i}{R_i}$	-0.103	-0.102	-0.104	-0.100	-0.106	-0.083	-0.081	-0.083	-0.079	-0.083
$r_{av}(\text{\AA})$	1.62					1.76				
	$\epsilon = 109^{\circ}28'$	$\epsilon = 110^{\circ}$		$\epsilon = 110^{\circ}28'$		$\epsilon = 109^{\circ}28'$	$\psi = 0.5 s + 0.866 p$			
		$i = 1$	$i = 2$	$i = 1$	$i = 2$		$\epsilon = 110^{\circ}$	$\psi_1 = 0.515 s + 0.857 p$		
$r_i(\text{\AA})$	1.83	1.866	1.818	1.900	1.807	$\epsilon = 110^{\circ}28'$		$\psi_2 = 0.495 s + 0.869 p$		
$S_i$	0.448	0.446	0.449	0.440	0.450		$\psi_1 = 0.528 s + 0.849 p$			
$\frac{\bar{X}_i}{R_i}$	-0.073	-0.072	-0.073	-0.071	-0.074	$\psi_2 = 0.490 s + 0.872 p$				
$r_{av}(\text{\AA})$	1.83									

The basic feature of the heteropolar MO is the parameter  $\lambda$ , which characterizes the orbital polarity, and hence, essentially determines the dipole moment. Let us calculate the average value  $\bar{X}$  of the "gravity centre" of the charge cloud on the molecular orbital. If  $X$  and  $\bar{X}$  is measured from the middle point of the line connecting atoms A and B in the direction of atom B, then, according to Coulson and Rogers (1961), the expression of the average value of the coordinate of the "gravity" centre of the charge cloud is:

$$\bar{X} = \frac{\bar{X}_A + \lambda^2 \bar{X}_B + 2\lambda \bar{X}_{AB}}{1 + \lambda^2 + 2\lambda S_{AB}} \quad (8)$$

where

$$\bar{X}_A = \int X \Psi_A^2 d\tau; \quad \bar{X}_B = \int X \Psi_B^2 d\tau; \quad \bar{X}_{AB} = \int X \Psi_A \Psi_B d\tau$$

According to equations (5) and (7), it is evident that for the "non-bridge" bond

$$\begin{aligned} \bar{X}_{1A} &= -\frac{R_1}{2} + 2N_1^2 \alpha \bar{X}(S_A^P A); & \bar{X}_{1B} &= \frac{R_1}{2} - 2N_1^2 \alpha \bar{X}(S_B^P B) \\ \bar{X}_{1AB} &= N_1^2 \bar{X}(S_A S_B) + N_1^2 \alpha [\bar{X}(S_B^P A) + \bar{X}(S_A^P B)] + N_1^2 \alpha^2 \bar{X}(P_A P_B) \end{aligned} \quad (9)$$

The expressions of  $\bar{X}_{2A}$ ;  $\bar{X}_{2B}$ ;  $\bar{X}_{2AB}$  for three equivalent bonds are analogous to expressions (9), if  $R_1$  is substituted by  $R_2$ ,  $\alpha$  by  $\beta$ , and  $N_1$  by  $N_2$  ( $R_1$ , and  $R_2$  are the lengths of the "non-bridge" and "bridge" Si-O bonds).

Let us proceed again from the assumption that the general properties of a tetrahedron with one specific bond are the same as those of a tetrahedron with all equivalent bonds, which must be manifested, in particular, in the total dipole moment being zero. Let us show that this requirement is practically equivalent to that of the cations being in the "gravity centre" of the tetrahedron. We denote the coordinate of the "gravity centre" of the charge of the electron cloud of the first ("non-bridge") bond by  $\bar{X}_1$  and of the second bond by  $\bar{X}_2$ .

In that case it must be true that  $\bar{X}_1 = 3 \bar{X}_2 \cos \epsilon'$  or

$$\begin{aligned} & \frac{-\frac{1}{2} R_1 + 2N_1^2 \alpha \bar{X}(S_A^P A) + \frac{\lambda^2}{2} R_1 - 2N_1^2 \alpha \lambda^2 \bar{X}(S_B^P B) + \bar{X}_{1AB}}{1 + \lambda^2 + 2\lambda S(\Psi_{1A} \Psi_{1B})} = \\ & = \frac{-\frac{3}{2} R_2 \cos \epsilon' + 6N_2^2 \beta \cos \epsilon' \bar{X}(S_A^P A) + \frac{3}{2} \lambda^2 R_2 \cos \epsilon' - 6N_2^2 \beta \lambda^2 \cos \epsilon' \bar{X}(S_B^P B) + 3 \bar{X}_{2AB} \cos \epsilon'}{1 + \lambda^2 + 2\lambda S(\Psi_{2A} \Psi_{2B})} \end{aligned} \quad (10)$$

Taking into account the above results that  $S(\Psi_{1A} \Psi_{1B}) = S(\Psi_{2A} \Psi_{2B})$  and also equation (5'), we obtain:

$$\frac{\bar{X}_{1AB}}{R_1} = \frac{\bar{X}_{2AB}}{R_2} \quad (11)$$

Hence, the dipole moment is zero, if condition (11) is fulfilled.

Basing on the data of Coulson and Rogers (1961) and of Katani et al. (1938), the values of

$$\frac{\bar{X}_{Si-O}}{R}$$

were calculated for various average and individual Si-O lengths. Table I shows that the values of

$$\frac{\sum \text{Si-O}}{R}$$

for non-equivalent bonds are very close to one another. It is noteworthy that the data obtained are valid for any value of  $\lambda$  i.e. are practically independent of the share of the ionic character of the bond.

Thus, the assumption that the hybrid orbitals constituting a given molecular orbital are characterized by the same s- and p-character leads to the conclusion of the cation being located practically in the "gravity centre" of the tetrahedron whose three equivalent bonds differ from the fourth one.

So far only  $\sigma$ -bonds have been considered to each of which the anion and the cation supply a single electron each. The presence of  $\pi$ -bonds between the d-orbitals of the cation and P-orbitals of the anion (Pauling, 1952; Cruickshank, 1961) leads to a shortening of the bonds and an increase of the number of electrons participating in the bonding. It is assumed that if the  $\pi$ -bonding potential is equal for each bond, the presence of  $\pi$ -bonding does not change the angles between the bonds and leads to such shortening of the bonds that the cation still remains in the "gravity" centre of the tetrahedron.

To examine a bond independent of the relationship of  $\sigma$ - and  $\pi$ -bonding, it is convenient to characterize it by the bond order  $n$ , which determines the average number of the electron pairs accessible to this bond. It is assumed that if the cation is in the tetrahedron "gravity" centre, the order of each bond will be the same, even though the bond lengths may differ. Under these conditions one can apply the following technique to analyze layer silicate structures: placing the cations into the "gravity centres" of their tetrahedra, let us assume that the order of all the bonds is the same. The displacement of the cation from the "gravity centre" will be obviously in the direction of the anion the bonding with which is characterized by a greater (as compared with the average) bond order. The shortening of the bond will be determined by the difference of the actual and average bond orders.

In order to find the mathematical relation between the shortening of the bond and the difference of bond orders, we shall use the well known Pauling's formula (1960).

$$r = r_1 - \frac{r_1 - r_2}{1 + \frac{K_1}{K_2} \frac{2 - n}{n - 1.5}} \quad \text{where}$$

$n$  is the order of the bond of length  $r$  being considered,  $K_1$ ,  $K_2$  and

$r_1$ ,  $r_2$  are respectively, the force constants and the lengths of the single and double bonds.

Gillespie and Robinson (1963) and Robinson (1963) found that for  $\text{ClO}_4$ ,  $\text{SO}_4$ ,  $\text{PO}_4$  and  $\text{SiO}_4$  tetrahedra it holds that:

$$r_{\text{Cl-O}} = 1.70 - \frac{0.33}{1 + 0.44 \left( \frac{2-n}{n-1} \right)}; \quad r_{\text{S-O}} = 1.70 - \frac{0.30}{1 + 0.46 \left( \frac{2-n}{n-1} \right)}$$

$$r_{\text{P-O}} = 1.76 - \frac{0.32}{1 + 0.45 \left( \frac{2-n}{n-1} \right)}; \quad r_{\text{Si-O}} = 1.83 - \frac{0.32}{1 + 0.60 \left( \frac{2-n}{n-1} \right)}$$

(12)

On an analogy with expressions (12) one can write the following approximate expression for the inter-atomic distance Al-O in  $\text{AlO}_4$ -tetrahedra:

$$r = r_1 + \frac{0.32}{1 + 0.60 \left( \frac{2-n}{n-1} \right)} \quad (13)$$

In the conditions of Si-for-Al-substitution and fulfilment of the additivity rule in tetrahedra with the average  $\text{Si}_x \text{Al}_{1-x}$  composition the average cation-anion distance is

$$r = r(\text{Si-O})x + r(\text{Al-O})(1-x) = r'_1 - \frac{0.32}{1 + 0.6 \left( \frac{2-n}{n-1} \right)} \quad (14)$$

where

$$r'_1 = r_1(\text{Si-O})x + r_1(\text{Al-O})(1-x)$$

In other words, if expression (13) holds, the shortening of the bond length with the increasing bond order does not depend on the single bond and on Si-for-Al substitution.

It should be noted that expressions (12), (13) and (14) apply to a geometrically regular tetrahedron with equal cation-anion distances. We have supposed earlier that for a given bond order bond lengths may differ. For the case of layer silicate tetrahedra we shall distinguish between "bridge" and "non-bridge" bonds, which, at a given  $n$ , are equal to

$$r_{nbr} = \frac{4 \cos \xi'}{1 + \cos \xi'} \left[ r_1 - \frac{r_1 - r_2}{1 + 0.60 \left( \frac{2-n}{n-1} \right)} \right] \quad (15)$$

$$r_{br} = \frac{4}{3(1 + \cos \xi')} \left[ r_1 - \frac{r_1 - r_2}{1 + 0.60 \left( \frac{2-n}{n-1} \right)} \right]$$

if the cation is in the tetrahedron "gravity centre" at  $n = 1$  and  $n = 2$ . Let us find the difference of the values of  $r_{nbr}$  for different  $n$ .

$$\Delta r_{nbr} = r_{nbr}(n_1) - r_{nbr}(n_2) = \frac{4 \cos \xi'}{1 + \cos \xi'} \left[ \frac{15 (r_1 - r_2) (n_2 - n_1)}{(2n_1 - 1)(2n_2 + 1)} \right]$$

In conformity with the results of Robinson (1963), we shall assume that for bonding cations Si and Al (as well as Cl, S, and P) with the oxygen atoms in the groups  $\text{SiO}_4$  and  $\text{AlO}_4$  12 valent electrons are necessary. In that case, when all the bonds have an equal number of common electrons,  $n = 1.5$ . When the cation is in the "gravity centre", all the bonds have  $n = 1.5$ . The displacement of the cation from the "gravity centre" at an increasing order  $n$  is equal to

$$\Delta r_{nbr} = r_{nbr}(1.5) - r_{nbr}(n) = \frac{4 \cos \xi'}{1 + \cos \xi'} \left[ \frac{3.75(n - 1.5)(r_1 - r_2)}{2n + 1} \right] \quad (16)$$

and with decreasing  $n < 1.5$

$$\Delta r_{br} = r_{br}(n) - r_{br}(1.5) = \frac{4}{3(1 + \cos \xi')} \left[ \frac{3.75(1.5 - n)(r_1 - r_2)}{2n + 1} \right]$$

Figure 1 shows the dependence between

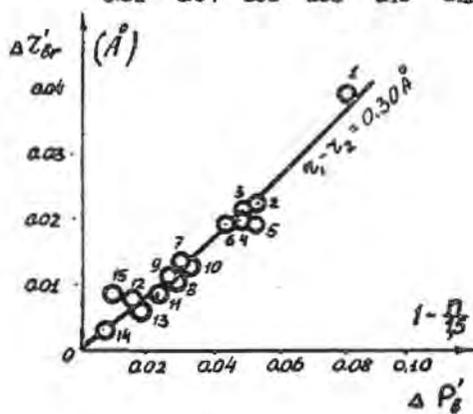
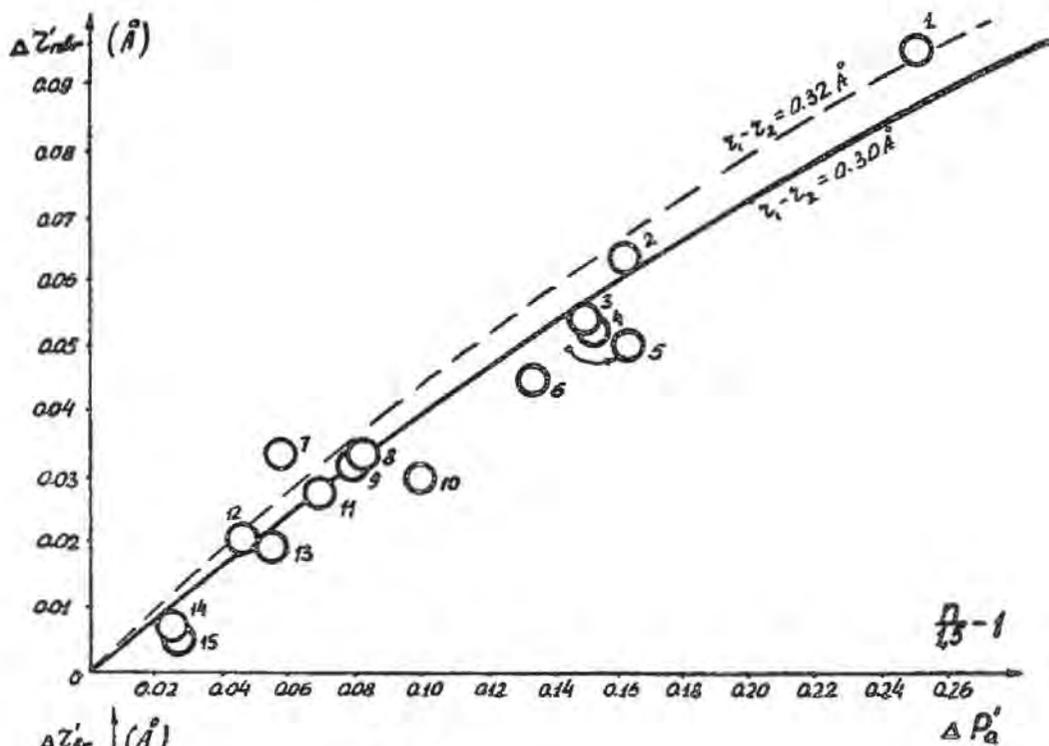
$$\Delta r'_{nbr} = \frac{1 + \cos \xi'}{4 \cos \xi'} \Delta r_{nbr}$$

and the value of

$$\frac{n - 1.5}{1.5}$$

at  $r_1 - r_2 = 0.32$  and  $0.30 \text{ \AA}$  ( $n > 1.5$ ) and between

$$\Delta r'_{br} = \frac{3(1 + \cos \xi')}{4} \Delta r_{br}$$



1. Polylitionite (Takeda et al. 1967)
2.  $2M_2$  muscovite (Takeda et al. 1971)
3. Nacrite (Blount et al. 1969)
4. Dickite (Newham, 1961)
5. Margarite (Takeuchi, 1965)
6.  $2M_1$  phengite (Güven, 1967)
7. Mg-vermiculite (Shirozu, Bailey, 1966)
8. Cr-chlorite (Brown, Bailey, 1963)
9.  $2M_1$  muscovite (Güven, 1967)
10. 3T muscovite (Güven, Burnham, 1967)
11. Dioctahedral chlorite (Alexandrova et al. 1972)
12. Ditrioctahedral chlorite (Alexandrova et al. 1972)
13. Fe-chlorite (Shirozu, Bailey, 1965)
14. Fe-biotite (Tepikin et al. 1969)
15. Lanthophyllite (Takeuchi, 1965)

Figure 1

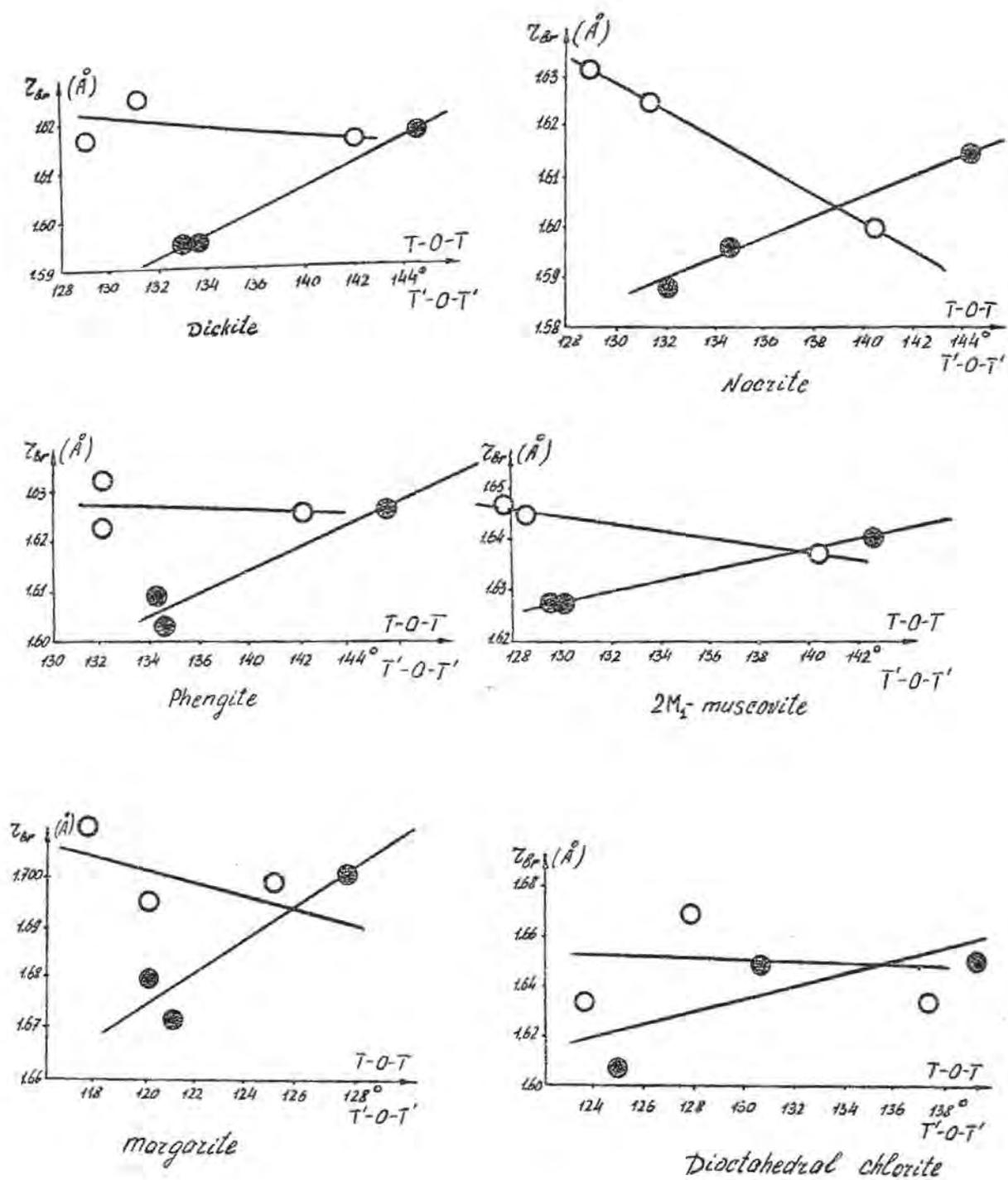


Fig. 2

and the value of

$$\frac{1.5 - n}{1.5}$$

at  $r_1 - r_2 = 0.30 \text{ \AA}$  ( $n < 1.5$ ).

## EXPERIMENTAL

The experimental material was comprised of the results of refinements of layer silicate structures conducted by various authors and data on the chemical composition of the minerals. The following calculations were previously carried out.

1. For the tetrahedra of all analyzed structures the coordinates of their "gravity centres" were found, equal to the arithmetic means of the coordinates of oxygen atoms forming the apices of the tetrahedra. For each tetrahedron the distances from the "gravity centre"  $T'$  to each of its apices  $r(T'-O)$  and the angles  $O-T'-O$  and  $T'-O-T'$  were computed. For the structures having two tetrahedra not connected by symmetry per unit cell the corresponding interatomic distances and angles were averaged.

2. For each tetrahedral anion the sum of bond strengths received by that anion from the surrounding cations was counted according to Pauling's (1960) rule of electrostatic valence. The following notations were used:  $P_a$  = the sum of bond strengths received by the apical "non-bridge" oxygen and  $P_b$  = the sum of bond strengths received by the "bridge" oxygen. The resulting values of  $P_a$  and  $P_b$  were averaged to find the mean bond strength per anion of the given tetrahedron

$$P_{av} = \frac{3P_b + P_a}{4}$$

The data obtained showed that, on the whole, for all layer silicates  $P_a < P_{av}$  and  $r_{nbr}(T-O) < r_{nbr}(T'-O)$ . The greater was  $\Delta P_a = P_{av} - P_a$ , the greater was  $\Delta r_{nbr} = r_{nbr}(T'-O) - r_{nbr}(T-O)$ . Conversely,  $P_b > P_{av}$  and  $r_{br}(T-O) > r_{br}(T'-O)$ , the greater  $\Delta P_b = P_b - P_{av}$ , the greater  $\Delta r_{br} = r_{br}(T-O) - r_{br}(T'-O)$ . Characteristically, the angles  $O_{nbr} - T' - O_{br}$  are significantly similar for the tetrahedra of all layer silicates  $110^\circ$  on the average, usually differing from the "ideal" tetrahedral angle  $109^\circ 28'$  by  $+40'$  at most. These results were to be expected from the viewpoint of the above discussion, since it has been assumed that all the bonds  $r(T'-O)$  have equal  $n$ . On the other hand, the angles  $O_{nbr}-T'-O_{br}$  vary in a

very broad range (from 109°40' to 113°50'), and  $O_{br}-T-O_{br} < O_{br}-T-O_{nbr}$ . The greater  $\Delta P_a$  and  $\Delta r_{nbr}$ , the greater the difference of the angles  $O_{nbr}-T-O_{br}$  and  $O_{br}-T-O_{br}$ . In qualitative terms this can be explained by the fact that the greater the order of the bond  $r_{nbr}(T-O)$ , the stronger the repulsion existing between the "bridge" and "non-bridge" bonds and the greater the angle  $O_{nbr}-T-O_{br}$ . Since the average bond order is constant, an increase of  $n$  on the  $r_{nbr}$  bond leads to a decrease of the repulsion between the "bridge" bonds and of the angle  $O_{br}-T-O_{br}$ . Finally, the variations of the individual  $r_{nbr}(T-O)$ ;  $r_{nbr}(T'-O)$ ;  $r_{br}(T-O)$  and  $r_{br}(T'-O)$  are observed in a very broad range, which does not contradict to our propositions but disagrees both with Bauer's data and Cruickshank's theory. According to Cruickshank's theory,  $r_{nbr}$  must be shorter than  $r_{br}$ . In layer silicate tetrahedra various relationships between  $r_{nbr}$  and  $r_{br}$  are observed in absence of a correlation with the electronegativity of nontetrahedral cations. For instance, in Fe-biotite  $r_{nbr} > r_{br}$ . The values of the individual  $r$  (Si-O) for  $SiO_4$  tetrahedron, as calculated by Bauer's formula disagree with those experimentally observed (polytitionite).

Such examples are numerous enough. Certainly, one could say that the theories of the above authors "do not work" because, except for polytitionite, dickite and nacrite, all other structures contain in tetrahedra not only Si but also Al cations. However, this seems unlikely, for the general regularities of the change of bond lengths must be the same for  $SiO_4$  and  $AlO_4$  -tetrahedra, which on the whole follows both from the notions of the theory of  $\pi$ -bonding and, all the more so, from the ionic model of bonding.

Let us consider a tetrahedron which has  $Si_xAl_{1-x}$  average composition. When the cation is in the "gravity centre", it is assumed that  $n = 1.5$  and the bond strength from the tetrahedral cation to the anion is equal to  $(0.25x + 0.75)$  v.u. The value  $\Delta P_a = P_{av} - P_a$  characterizes the degree of "undersaturation" of  $O_{nbr}$  by the negative charge, which is supplied to the tetrahedral cation by  $O_{nbr}$  in the form of "donor" electrons. The order of the "non-bridge" bond in that case is increased to  $n > 1.5$ . Hence,

$$\frac{n - 1.5}{1.5} = \frac{\Delta P_a}{0.25x + 0.75} = \Delta P'_a$$

Similarly, at  $n < 1.5$

$$\frac{1.5 - n}{1.5} = \frac{\Delta P_b}{0.25x + 0.75} = \Delta P'_b$$

It should be noted that for a majority of layer silicates (except for margarite)  $\Delta P_a \approx \Delta P'_a$ ;  $\Delta P_b \approx \Delta P'_b$ . Let us now consider the pattern of change of  $\Delta r'_{nbr}$  and  $\Delta r'_{br}$  depending on  $\Delta P'_a$  and  $\Delta P'_b$

$$\Delta r_{nbr}' = \frac{\Delta r_{nbr} (1 + \cos \xi')}{4 \cos \xi'} \quad \text{and} \quad \Delta r_{br}' = \frac{\Delta r_{br} 3 (1 + \cos \xi')}{4}$$

The relevant data for all structures known to the author are represented on Fig. 1a, b. It can be easily seen that all the points on the diagrams are very close to the curves described by equations (16), which is a sufficiently convincing corroboration of the bonding model discussed above. The study of the bond length  $r_{br}$  (T-O) as depending on T-O<sub>br</sub>-T for layer silicates shows that for all mineral tetrahedra the length  $r_{br}$  (T-O) either does not depend on the angle T-O<sub>br</sub>-T, or decreases with the increase of that angle. Fig. 2 shows the curves reflecting the variation of  $r_{br}$  (T-O) from the value of T-O<sub>br</sub>-T for dioctahedral minerals. The diagrams also represent the bond lengths  $r_{br}$  (T'-O) and the corresponding T'-O<sub>br</sub>-T'. For the tetrahedra of all minerals,  $r_{br}$  (T'-O) decreases with decreasing T'-O<sub>br</sub>-T'. With an increase of the order of a "non-bridge", the "redistribution" of n on the "bridge" bonds is such that the bond order decreases most of all on the bonds with the smallest T-O-T. In other words, the smaller the angle T-O-T the easier it is, ceteris paribus, for the order of the "bridge" bonds to decrease.

#### REFERENCES

- ALEXANDROVA, V.A. and DRITS, V.A. (1972): Structural features of one-packet dioctahedral chlorite. *Kristallografiya*, 17, 3. [In Russian].
- ALEXANDROVA, V.A., DRITS, V.A., and SOKOLOVA, G.V. (1972): Crystalline structure of ditrioctahedral chlorite. *Kristallografiya* (in press). [In Russian].
- BAUER, W.H., (1971): The prediction of bond length variations in silicon-oxygen bonds. *Am. Mineral.* 56, 9-10, 1573-1599.
- BLOUNT, A.M., THREADGOLD I.M., and BAILEY, S.W., (1969): Refinement of the crystal structure of nacrite, *Clays and Clay Minerals*, 17, 185-194.
- BROWN B. and BAILEY S.W., (1963): Chlorite polytypism: II Crystal structure of a one-layer Cr-chlorite. *Am. Mineral.* 48, 42-61.
- CLARK, J.R., APPLEMAN, D.E., PAPIKE, J.J. (1969): Crystal-chemical characterization of clino-pyroxenes based on light new structures refinements. *Mineral. Soc. of Amer. Spec. Pap.*, 2, 31-50.
- COULSON, C.A. (1961): Valence. "Oxford University Press".
- COULSON, C.A., ROGERS, M.T. (1961): Homopolar dipole. *J. Phys.* 35, 593-598.
- CRUICKSHANK, D.W. (1961): The role of 3d-orbitals in  $\pi$ -bonds between (a) silicon, phosphorus, sulfur or chlorine and (b) oxygen or nitrogen. *J. Chem. Soc.*, 5486-5504.

- GILLESPIE, R.J. and ROBINSON, E.A. (1963): The sulphur-oxygen bond in sulphuryl and thionyl compounds: correlation of stretching frequencies and force constants with bond lengths, bond angles and bond order. *Canad. J. Chem.* 41, 2074-2085.
- GUVEN, N. (1967): The crystal structure of  $2M_1$ -phengite and  $2M_1$ -muscovite, *Carnegie Inst. Year Book*, 487-490.
- GUVEN, N. and BURNHAM, C.W. (1967): The crystal structure of  $3T$  muscovite, *Z. Kristallogr.* 125, 163-183.
- KATANI, M., AMEMIYA, A., SIMOSE, T. (1938): Tables of integrals useful for the calculations of molecular energies. *Proceed. Phys-Math. Soc. Jap.* 20, Extra number one.
- MILLIKEN, R.S., RIEKE, C.A., ORLOFF, D., ORLOFF, H. (1949): Formulas and numerical tables for Overlap integrals; *J. Chem. Phys.* 17, 1248-1260.
- NEUNHAM, R.E. (1961): A refinement of the dickite structure and some remarks on polymorphism in kaolin minerals. *Min. Mag.* 32 683-704.
- PAULING, L. (1952): Interatomic distances and bond character in the oxygen acids and related substances. *J. Phys. Chem.*, 56, 361-365.
- PAULING, L. (1960): The nature of the chemical bond. 3rd edition Cornell. Univ. Press, Ithaca New-York.
- ROBINSON, E.A. (1963): Characteristic vibrational frequencies of oxygen compounds of silicon, phosphorus, and chlorine: correlation of stretching frequencies and force constants with bond lengths and bond order. *Canad. J. Chem.* 41, 3021-3033.
- SHIROZU, H. and BAILEY, S.W. (1965): Chlorite polytypism: III. Crystal-structure of an orthohexagonal iron chlorite. *Am. Mineral.*, 50, 868-885.
- SHIROZU H. and BAILEY S.W. (1966): Crystal structure of a two-layer Mg-vermiculite, *Am. Mineral.* 51, 1124-1143.
- TAKEDA, H. (1969): The crystal structure of a polytitionite. *Miner J.*
- TAKEDA, H., HAGA, N. and SADANAGA, R. (1971): Structural investigation of polymorphic transition between  $2M_2$ - $1M$ -lepidolite and  $2M_1$  muscovite. *Miner. J.* 6, 4, 203-215.
- TAKEUCHI, Y. (1965): Structures of brittle micas. *Clays and Clay Minerals*, Proc. 13th Conf. Pergamon Press, 1-25.
- TEPIKIN, V.E., DRITS, V.A. and ALEXANDROVA, V.A. (1969): Crystal structure of iron biotite and construction of structural models for trioctahedral micas. *Proceed. Inter. Clay Conf.* 1, 43-51.

# "THE DEFECT STRUCTURE OF DEHYDRATED CLAY MINERAL CRYSTALS"

F. Freund

Mineralogisch-Petrographisches Institut der Universität zu  
Köln

ABSTRACT.- The exothermal transformations observed in DTA-curves of numerous clay minerals are due to the energy release associated with the lattice collapse of high defect structures. Anion-sized vacancies, introduced by the loss of structural OH-groups from kaolinite, are responsible for unusually low density values of metakaolinite. The unsaturated coordination of Al causes marked shifts of the Al  $K\alpha$ - and Al  $K\beta$ -bands which differ from those of known tetrahedrally coordinated Al-compounds.

## INTRODUCTION

The endothermal effects in the DTA-curves of clay minerals are related to dehydration processes, by which  $H_2O$  is removed either from inner and outer surfaces, where it had been held in a relatively weakly bound state, or from within the clay minerals structure, where it was held mostly in form of  $OH^-$ -groups. The exothermal effects are generally attributed to recrystallisation reactions, by which intermediate forms recrystallize into anhydrous silicate phases.

In Fig. 1 a compilation of typical DTA- curves of a variety of  $OH^-$  containing layer silicates is shown. The endothermal reaction "A" in the range below  $200^\circ C$  can be attributed to the removal of adsorbed water. It will not be treated in this paper. The large endothermal reaction "B", clearly separated from all other thermal reactions in the case of kaolinite between  $400-600^\circ C$ , is attributed to the removal of "structural water", e.g. of  $OH^-$ -groups from within the clay mineral structure. This removal of  $OH^-$ -groups, or -

more precisely - of  $H_2O$  molecules, which have been formed by proton exchange reactions between the  $OH^-$ -groups inside the lattice, leads then to highly disordered structures which undergo recrystallisation during the exothermal reaction "D". The nature of this recrystallisation reaction is still not fully understood and subject to controversial discussions. Also the nature of the reaction type "C" in Fig. 1 is uncertain.

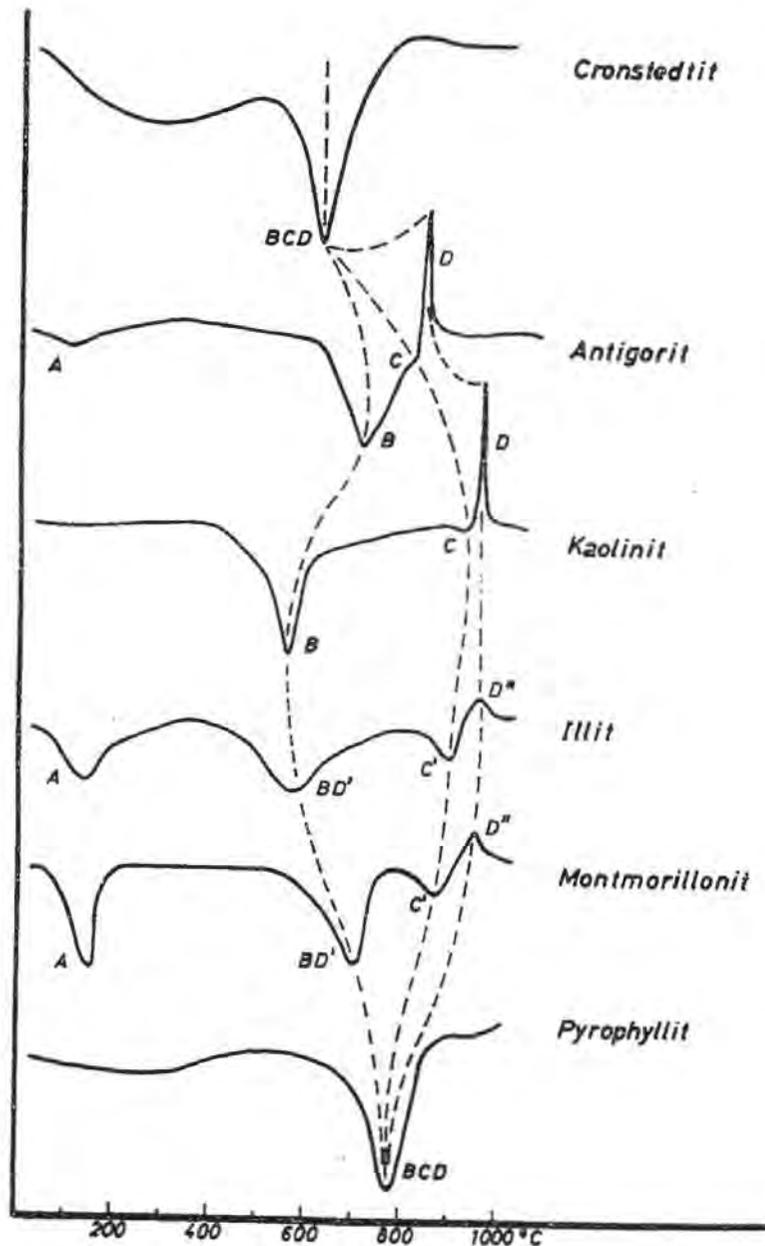


Figure 1. Typical differential thermal analysis curves of various layer silicates

By the connecting lines in Fig. 1 the interdependence of these different thermal reactions is tentatively indicated for the different types of layer silicates. The arguments which lead to this assignment will become more clear from the subsequent discussion of the kaolinite - metakaolinite - spinel reaction series, which is at once the best investigated of all and the most suitable for model considerations.

## DENSITY AND DEFECT STRUCTURE

Metakaolinite is the dehydrated form of kaolinite,  $Al_2 [(OH)_4/Si_2O_5]$ . The structure of metakaolinite has been discussed since many years. In powder diffraction diagrams metakaolinite appears to be an x-ray amorphous phase, but already Buessem, Tscheischwili and Weyl (1939) reported a residual crystallinity. Brindley and Nakahira (1959) studied the kaolinite-metakaolinite-mullite reaction series in the great detail and showed, that in single crystal aggregates the crystallinity of the original structure is retained in two dimensions, but lost in the third.

The plane, in which crystallinity is retained, is the basal plane, as shown by the persistence of (hk0) reflection. The  $a_0$  and  $b_0$  parameters of metakaolinite differ only slightly from those of kaolinite. Recent x-ray investigation by Range et al. (1970) confirm and supplement these earlier results.

No value for  $c_0$  the layer spacing of metakaolinite could be obtained from x-ray data, since all (hk1) and (001) reflections disappear early in the course of dehydration. Density values (Fig. 2) were therefore used to calculate the average layer spacing in metakaolinite. Unfortunately, however, a misleading value has thus found its way persistingly into the literature. Instead of own density values Brindley and Nakahira (1959) used data taken from an earlier paper by Rieke and Mauve (1942). Among a choice of density values, strongly dependent upon the previous heat treatment, they selected the value reached at 800°C. A  $d(001)$  distance was deduced on the assumption that this particular density value - obtained on fine-grained kaolin with 1.7 to 2.7 weight % alkaline impurities - corresponds to the density of single crystal material of relatively high purity, heated to approximately the same temperature for approximately the same length of time. This, however, is not the case for any intermediate form of dehydrated clay minerals, which are never in thermodynamic equilibrium and sensitive to thermal prehistory.

In untreated kaolinite the  $c_0$ -parameter has a value of 7.13 Å corresponding to a layer spacing of 7.08 Å. Its density is given as 2.55 g/cm<sup>3</sup>. Rieke and Mauve (1942) employed the pycnometer method on pressed powder samples heated accumulatively 12 hours

each at the temperatures indicated in Fig. 2, curve 1. Brindley and Nakahira (1959) singled out the 800°C-value and deduced from it the 6.3 Å value for the layer a spacing in metakaolinite. Meyer (1940) had heated kaolin samples of similar impurity content 3 hours each and obtained pycnometer density values which were lower over the whole temperature range (Fig. 2, curve 2).

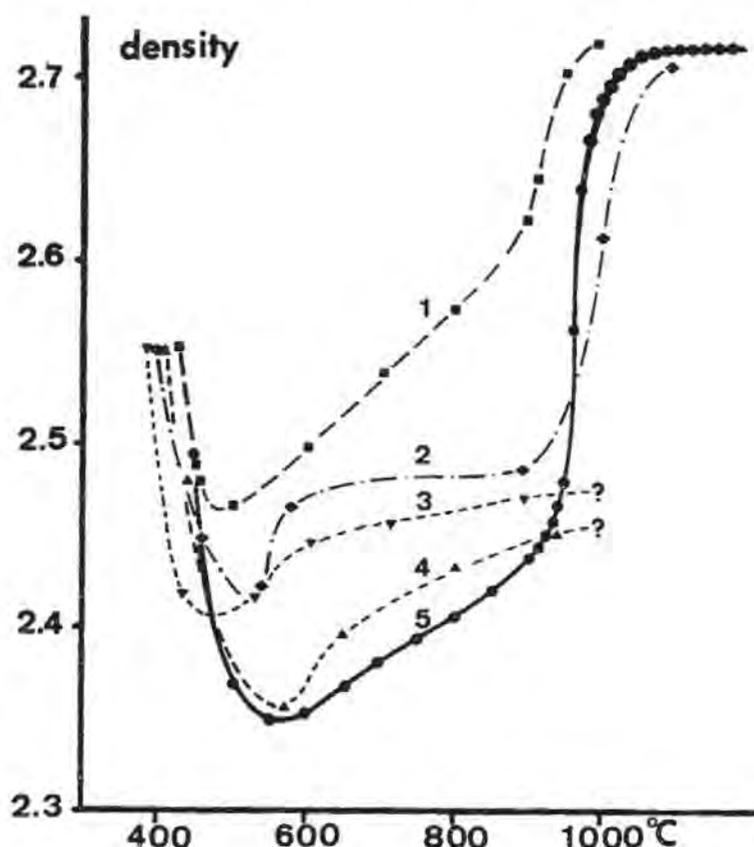


Figure 2. Density data for kaolinite-metakaolinite-spinel  
 Curve 1: RIEKE and MAUVE  
 Curve 2: MEYER  
 Curves 3 and 4: RANGE et al.  
 Curve 5: FREUND

Freund (1967) obtained density data from the shrinkage behaviour of pressed powder samples of a coarse-grained, high purity kaolinite from Hirschau, Germany. Cylinders of 7 mm diameter and 10 mm height were loaded with 7 kg/cm<sup>2</sup> unidirectional pressure and heated at a rate of 7°/min. The shrinkage in direction of the pressure and perpendicular to it was registered photographically in a Leitz heating microscope. From these shrinkage values the density changes were calculated by fitting the curve on the room temperature density value of kaolinite and taking into account the weight

loss of the sample as determined by thermogravimetric methods. The results are shown in curve 5 in Fig. 2 (It should be noted that the values here correspond to densities at the indicated temperatures, not after cooling the sample again to room temperature).

Curves 3 and 4 in Fig. 2 represent density data by Range et al. (1970) using large single crystal aggregates of kaolinite from the Columbian deposit described by Paetsch et al. (1963). In this case cleaved central sections of the kaolinite crystals were heated for 6 and 48 hours to the temperatures indicated in curve 3 and 4 respectively. The density was then measured after cooling to room temperature by suspending the dehydrated samples in chloroform/bromoform mixtures of adjusted density. The agreement is surprisingly good between these values and those deduced from shrinkage values by Freund (1967).

This compilation of density data in Fig. 2 indicates that the 6.3 Å value originally selected by Brindley and Nakahira (1959) for the layer spacing in metakaolinite will need comment and revision.

Taking the  $a_0$ - and  $b_0$ -parameters of metakaolinite as determined by x-ray diffraction and any of the new density values from the "plateau" shown by curve 3, 4 or 5 in Fig. 2, the  $d(001)$ -value turns out to range between 6.75 and 6.85 Å with a tendency to the higher  $d(001)$ -value for shorter heating times at the high temperatures. This is also the range of the electron diffraction values which were obtained by Radczewski and Schädel (1962) using ultra thin sections of kaolinite single crystals cut normal to the layer plane. Larger values than 6.85 Å were not observed, which is in agreement with the earlier statement (Freund, 1967) that 6.85 Å is the upper limit for the layer spacing in metakaolinite. After the sample had been exposed to a high flux of electrons in the electron microscope values smaller than 6.75 Å were observed. The lowest value was 5.56 Å. The 6.3 Å-value was not statistically favored.

Theoretically an anhydrous metakaolinite structure, in which the anion packing comes to the same space filling coefficient as in the original kaolinite, should have a layer spacing of 5.54 Å. This is close to the lowest value mentioned above, observed by electron diffraction. The experimental 5.56 Å layer spacing value is therefore to be assigned to the completely collapsed metakaolinite structure.

This sheds light on the actual defect structure of metakaolinite, which is characterized by a large mean  $d(001)$ -value. It should be kept in mind, that the kaolinite structure is - with the exception of one anion position in the pseudo-hexagonal ring at the base of the  $\text{Si}_2\text{O}_5$ -layer - an essentially close anion packing. The metakaolinite structure is not, as the density values show. In kaolinite 4 out of 9 anions are  $\text{OH}^-$ -groups. Half of these, 2 out of a total of 9, will be removed as  $\text{H}_2\text{O}$  molecules, leaving vacancies in a 2-dimensional array parallel to the basal plane. The concentration of these anion-sized vacancies is ranging close to 20% for the fully dehydra-

ted not yet collapsed metakaolinite structure. This is far more than thermodynamic equilibrium. The metakaolinite structure is therefore necessary unstable. This statement can be generalized for all intermediate forms of dehydrated clay minerals, as far as they give rise to strong exothermal reactions. The reaction "D" in Fig. 1 is caused by the energy release, when the high defect structures collapse to a close anion packing. The entropy decreases markedly, though it is often still high in the reaction product thermodynamically unstable Al-Si-spinel in the kaolinite case with its inherent disorder in the cation distribution. The relative stability of the metakaolinite between 600 to nearly 1000°C is due to the fact that, in the absence of fluxes, the activation energy needed to rupture Si-O-bonds is quite high. May be the small endothermal reaction "C" in Fig. 1 is connected with the on-set of the Si-O-bond rupture.

Range et al. (1970) showed, that by heating kaolinite single crystals to 800°C for many weeks they loose their residual crystallinity and become completely x-ray amorphous. Unfortunately, no density values were reported but most likely the density ranges high. At the same time the exothermal reaction near 1000°C will have vanished.

Brandley and Nakahira (1959) showed, that a completely collapsed metakaolinite structure has a cubic over-all symmetry. In an almost dense packing of  $O^{2-}$  -ions, Si occupies tetrahedral voids. Al occupies both tetrahedral and octahedral voids. This phase has therefore be termed an Al-Si-spinel. Its topotactic relationship to the parent structure is such that the (001) plane of kaolinite becomes the (111) plane of the spinel phase, and the b-axis of kaolinite becomes the (110) -direction of the spinel phase. This orientational relationship persists - with a varying degree of perfection - up to the mullite formation at higher temperatures (Johns, 1953; Comer, 1960).

## UNSATURATED COORDINATION OF AL

We now come to the question of the coordination of Al in metakaolinite, which is intimately connected to the defect structure. We have to consider the coordination number, but also the geometry of the ligand configuration.

Brindley and Nakahira (1959) assumed tetrahedral coordination of Al in metakaolinite e.g. four  $O_2$ -ligand arranged in a more or less tetrahedral array. Brindley and McKinstry (1961) and De Kimpe et al. (1964) observed a slight shift of the Al  $K\alpha_{1,2}$ -band of metakaolinite with respect to kaolinite. When kaolinite was further heated beyond the temperature of the exothermal transformation to form the spinel-type phase and subsequently mullite, the shift reserved to nearly the original value. Comparison with the  $K\alpha_{1,2}$ -bands of

Al-silicates of known structure (White and Gibbs, 1969; Wardle and Brindley, 1971) provided support of the assumingly tetrahedral coordination of Al in metakaolinite.

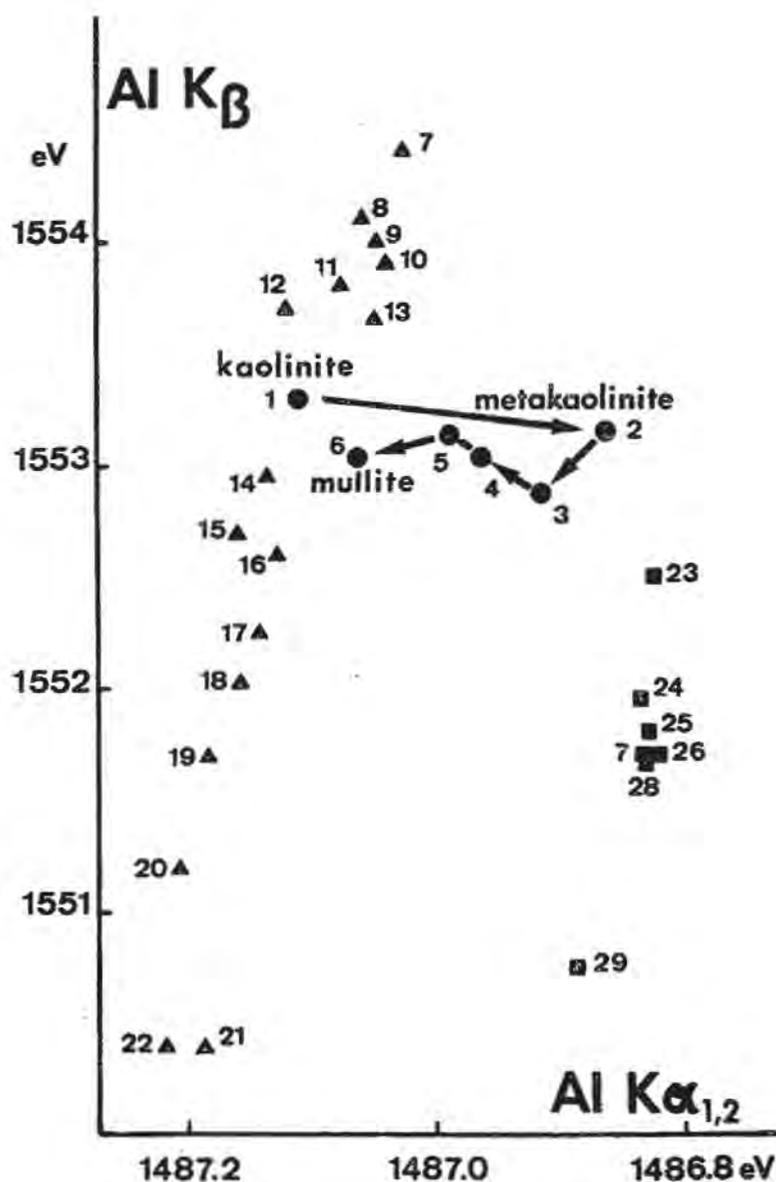


Figure 3. K $\alpha$  and K $\beta$  x-ray line shift for various Al-compounds (Läuger, 1.968, 1.971). Läuger's data are complemented with points 1-6, corresponding to kaolinite heated at 30 $^{\circ}$ , 580 $^{\circ}$ , 970 $^{\circ}$ , 1050 $^{\circ}$ , 1200 $^{\circ}$  5 min., 1200 $^{\circ}$ C 6 hrs.

However, Läuger (1968, 1971), measuring the Al K $\alpha_{1,2}$ - and Al K $\beta$ - bands of a large number of Al-compounds, showed that the shift of the Al K $\alpha_{1,2}$ -band is intercorrelated with the shift of the Al K $\beta$ -band. In Fig. 3 Läuger's data are presented in a K $\beta$  vs. K $\alpha_{1,2}$  plot. All oxy-compounds with Al in octahedral coordination

(no. 7-16) lie together in the upper left corner of the plot. The octahedrally coordinated halides (no. 21-22) form separate sets in the lower left. All tetrahedrally coordinated Al-silicates, (no. 23-28) and  $\text{AlPO}_4$  are at the lower right hand side of the diagram. The upper right hand side of the diagram is void of known stable compounds.

Lauger (1968, 1971) did not include the kaolinite-mullite reaction series in his measurements. We have therefore redetermined the Al  $K_{\alpha 1,2}$ - and Al  $K_{\beta}$ -bands of this series. These points are included in Fig. 3 (no. 1-6).

While kaolinite clearly lies in the range of octahedrally coordinated, Al, the point representing metakaolinite (no. 2) has moved

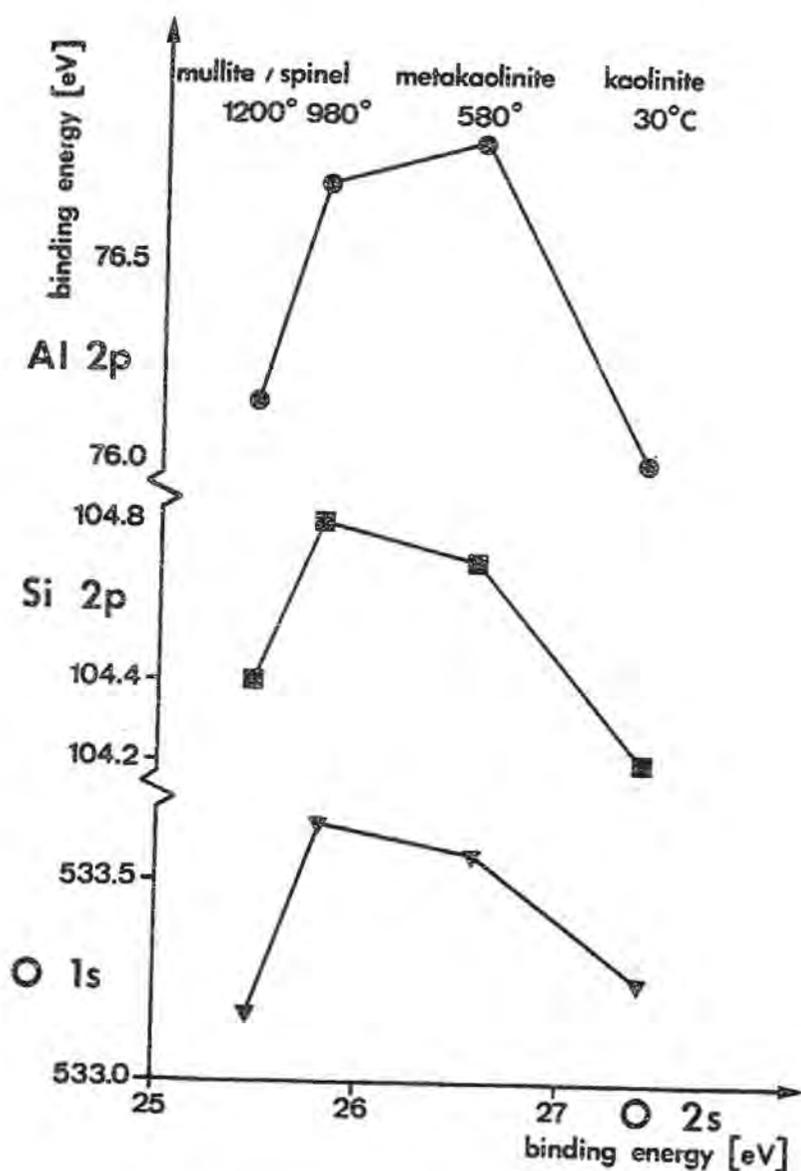


Figure 4. Core level binding energies Al 2p, Si 2p and O 1s vs. O 2s for the kaolinite thermal reaction sequence.

to the right hand side, where no stable compounds with tetrahedral coordination are found. When metakaolinite is transformed into the spinel-type phase, the representative point (no. 3 in Fig. 3) moves downward as if it were to join the group of known compounds with Al in tetrahedral coordination. Further heating and gradual formation of mullite causes the points (no. 4-6) to return to the group of octahedrally coordinated Al-compounds.

Recently, Iwai et al. (1971) have reported results on an electron density distribution determination on partially dehydrated dickite by x-ray diffraction techniques. In metadickite the  $\text{AlO}_4$ -polyhedra, have only a remote resemblance to normal  $\text{AlO}_4$ -tetrahedra. They are strongly elongated in the (001)-plane of the original dickite structure and compressed normal to it. These polyhedra are intermediate between tetrahedra and truncated octahedra, where two of the six ligands are moved.

This now leads us to a dynamic view of the dehydration reaction. If the original kaolinite structure is capable of withstanding, with minor displacements of the atomic positions in the 2-dimensional  $\text{SiO}_4$  network, the loss of half of the  $\text{OH}^-$ -groups as  $\text{H}_2\text{O}$  molecules, the original  $[\text{Al}(\text{OH})_4\text{O}_2]$  coordination will necessarily turn into a  $[\text{AlO}_4\Box_2]$  coordination. The symbol  $\Box$  stands for a missing ligand, e. g. an uncharged vacancy comparable in size with an  $\text{O}^{2-}$ - or  $\text{OH}^-$ -ion. The dehydroxylation reaction is statistical. Adjacent pairs of  $\text{OH}^-$ -groups will have a preference for reacting to form  $\text{H}_2\text{O}$  molecules. This given a higher probability of reaction to those  $\text{OH}^-$ -groups which are in a closed layer parallel to (001). Iwai et al. (1971) state that these  $\text{OH}^-$ -groups in dickite are driven off first and followed by those  $\text{OH}^-$ -groups which are located more inside the octahedral layer.

Also the unusual fact, deduced by Iwai et al. (1971), that the  $\text{AlO}_4$  polyhedra share edges, does not appear strange in the light of a dehydroxylation reaction occurring in an essentially rigid lattice frame. In the original kaolinite structure, the  $[\text{Al}(\text{OH})_4\text{O}_2]$  octahedra share edges. The two  $\text{O}^{2-}$ -ions connect the octahedral layer to the supporting  $\text{Si}_2\text{O}_5$ -sheet. After the dehydration the  $[\text{AlO}_4\Box_2]$  polyhedra still must share edges in 2 dimensions, unless the 2-dimensional structure of the whole sheet is disrupted. This, however, is not the case except along mosaic grain boundaries, where the stress has overridden the strength of the Si-O bonds.

From crystallographic data on the mean Al-O distance in tetrahedrally coordinated Al (Smith, 1954) one can estimate that - assuming similar Al-O distance in the  $\text{AlO}_4\Box_2$  polyhedra in metakaolinite - the  $\text{AlO}_4$ -layer will not match any more with the  $\text{Si}_2\text{O}_5$  tetrahedral layer. After about 10  $\text{SiO}_4$ -repeat units the two layers will presumably be out of phase (Freund, 1967). Therefore, mosaic grain boundaries are to be expected every 50 Å. This is the value also deduced from x-ray line broadening by Brindley and Nakahira (1959). Furthermore, the structural units which cohere might

have a tendency to bend either bidirectional to form a cup-like shape, or unidirectional like the crystals of halloysite, the tubular polymorph of kaolinite with additional interlayer water molecules.

This then would explain the reported loss of a well-defined  $c_0$ -parameter already in the early stages of the kaolinite dehydration. Also the reluctance of the metakaolinite structure to collapse up to 1000°C may thus find its ready explanation because each such spherically or cylindrically deformed layer section need to be in contact only at a few points with neighboring sections. This stabilizes the defect structure up to the temperature which is sufficiently high to thermally provide the activation energy for an over-all rupture of Si-O bonds.

The unsaturated coordination of Al in metakaolinite affects the core and valence shell electron binding energies of Al, Si and O - as determined by photo electron spectroscopy (ESCA) - in a very characteristic way. It was shown for Mg-silicates having 4-fold, 6-fold and 8-fold coordination (Freund and Hamich, 1970a, 1970b) that a plot of the mean Mg-O distance vs. the Mg 1s, 2s and 2p-binding energies gives an approximately linear relationship. The larger the Mg-O distance the higher the Mg core level binding energies. If the values for carefully dehydrated chrysotile and serpentine - "meta-forms" with unsaturated  $[MgO_4]_{2-}$ -coordination were included, the apparent Mg-O distance turned out to be exceedingly large and clearly different from regular tetrahedral  $[MgO_4]$ -coordination in the stable Mg-silicate phase åkermanite. In metakaolinite the results are more complicated, probably due to the lower symmetry of the ligand field inherent to Al. Yet, including O 1s and O 2s, a very similar behaviour as for its Mg-equivalent was formal showing a steady decrease in O 2s binding energy in the sequence kaolinite-metakaolinite -Al-Si-spinel-mullite while the Al 2p-, Si 2p-, and O 1s-binding energies first increase and then decrease as shown in Fig. 4.

Preliminary results on illites and montmorillonites (Freund unpublished) indicate that, prior to the high temperature endothermal/exothermal reaction, C'/D' in Fig. 1, similar unsaturated ligand sites around some cations are to be expected which arise from the loss of structural water from the more or less rigid clay mineral structure.

This justifies the tentative assignment of the thermal reactions given in Fig. 1 with the possible exception, that in the case of talc the occurrence of the exothermal lattice collapse "D" is not fully concurrent with the main dehydration reaction but - at least partially - retarded up to almost 1100°C. In the case of cronstedtite, however, the high Fe-content efficiently prevents the formation of any metaform, due to the "fluxing" effect of the transition metal oxide component.

## REFERENCES

- BRINDLEY, G.W. and MCKINSTRY, H.A.: (1961): The kaolinite-mullite reaction series IV. *J. Amer. Ceram. Soc.* 44, 506-507.
- BRINDLEY, G.W. and NAKAHIRA, M. (1959): The kaolinite-mullite reaction series I-III. *J. Amer. Ceram. Soc.* 42, 311-324.
- COMER, J.J. (1960): Electron microscope studies of mullite development in fired kaolinites. *J. Amer. Ceram. Soc.* 43, 378-384.
- DE KIMPE, C., GASTUCHE, M.C. and BRINDLEY, G.W. (1969): Ionic coordination in alumino-silicic gels in relation to clay mineral formation. *Amer. Miner.* 49, 1370-1381.
- FREUND, F. (1967): Kaolinite, metakaolinite a model structure for high defect concentrations. *Ber. Dtsch. Keram. Ges.* 44, 5-17.
- FREUND, F. and HAMICH, M. (1971):  $K_{\alpha}$  and  $K_{\beta}$  spectra of magnesium in different coordination in oxides and silicates. *Z. anorg. allg. Chem.* 385, 209-229.
- FREUND, F. and HAMICH, M. (1971): Photoelectron and x-ray fluorescence spectroscopy on Mg-minerals. *Fortschr. Miner.* 48, 243-258.
- IWAI, S., TADAI, H. and SHIMAMUNE, T. (1971): Studies of the structural changes of dickite during dehydration. *Acta Cryst. B* 27, 248-250.
- JOHNS, W.D. (1953): High temperature phase changes in kaolinites. *Mineral Mag.* 30, 186, -198.
- LÄUGER, K. (1968): Ph. D. thesis München 1968.
- LÄUGER, K. (1971): On the influence of bonding and crystal structure on the K -spectrum of Al. I. *Phys. Chem. Solids* 32, 609-622.
- MEYER, F.W. (1940). Constitution of kaolin when treated at high temperatures. *Sprechsaal* 75, 5-14.
- PAETSCH, D., FELTKAMP, K. and SCHIMMEL, G. (1963): A new occurrence of kaolinite. *Ber. Dtsch. Keram. Ges.* 40, 386-392.
- RADCZEWSKI, O.E. and SCHÄDEL, J. (1962): Ultra-thin sections of kaolinite. *Ber. Dtsch. Keram. Ges.* 39, 48-51.
- × RANGE, K.J., RUSSOW, J., DEHLINGER, G. and WEISS, A. (1970): New investigation about the thermal decomposition of kaolinite I. *Ber. Dtsch. Keram. Ges.* 47, 545-549.
- RIECKE, R. and MAUVE, L. (1942): About the mineral components of kaolin. *Ber. Dtsch. Keram. Ges.* 23, 119-151.
- SMITH, J.V. (1954): Review of the Al-O and Si-O distances. *Acta Cryst.* 479-481.
- TSCHEISCHWILI, L., BÜSSEM, W. and WEYL, W. (1939): About metakaolin. *Ber. Dtsch. Keram. Ges.* 20, 249-276.
- WARDLE, R. and BRINDLEY, G.W. (1971): The dependence of the wavelength of Al K radiation from alumino-silicates on the Al-O-distance. *Amer. Miner.* 56, 2123-2128.
- WHITE, E.W. and GIBBS, G.U. (1967): Structural and chemical effects on the Si  $K_{\beta}$  x-ray line for silicates. *Amer. Miner.* 52, 985-993.



# THE HYDROUS MAGNESIUM-NICKEL SILICATE MINERALS (so-called garnierites)

G. W. Brindley and Pham Thi Hang

Department of Geosciences, and Materials Research Laboratory  
The Pennsylvania State University, University Park,  
PA 16802 U.S.A.

**ABSTRACT.** - Some forty hydrous Mg, Ni silicates from localities throughout the world have been studied. The most commonly occurring types have basal spacings of about 7.2-7.5 and 10.0-10.5 Å. Frequently both types are intimately associated and not easily separable. The spacings are largely independent of humidity, low-temperature heat-treatment, and ethylene glycol saturation. Both types give two-dimensional x-ray diffraction bands, generally similar in form and position.

Electron micrographs show a variety of morphological forms including tube- and rod-like particles, platy and ill-defined fluffy particles. At 10<sup>6</sup>x magnification, regions of clearly defined 7 Å and 10 Å spacings can be seen and also less clearly defined regions, which may be highly disordered or even amorphous.

Chemical analyses of samples showing dominantly 7 Å and 10 Å basal spacings give formulae intermediate between those of serpentine- and talc-like minerals. The 10 Å-type minerals are considerably more hydrous than corresponds to a mixture of serpentine and talc forms. The results indicate a talc monohydrate composition combined with hydrated brucitic material or hydrated serpentine-like material.

## INTRODUCTION

A detailed study of magnesium-nickel hydrous silicates, so-called garnierites, has been made by x-ray powder diffraction analysis, electron-optical observations, chemical analysis, thermo-gravimetric analysis, and high temperature transformations. The term

"garnierite" will be used in the general sense defined by Pecora et al. (1949) and Faust (1966), and will include the nickel-poor samples termed kerolites by Russian investigators (see Vitovskaya and Berkhin, 1968, 1970, and with Yashina, 1969). Considerable evidence has accumulated tending to show that many garnierites are intimate mixtures of two components resembling serpentine and talc (or stevensite). In some samples, the two components are clearly indicated by x-ray reflections corresponding to basal spacings of about 7 Å and 10 Å respectively. In other samples, the components are less obvious. The present study was undertaken with the intention of obtaining garnierites essentially of one type which could be examined in detail by a variety of techniques.

About forty samples of garnierites were available for the investigation and from these a selection was made on the basis of x-ray powder diffraction analysis after careful hand-picking of uniformly green particles under a binocular microscope. Samples were selected which showed dominantly 7 Å or 10 Å basal reflections and little or no crystalline impurities. Small percentages of quartz which could not be eliminated were measured directly by an x-ray method.

Space limitations permit only a brief outline of the results obtained and attention will therefore be focussed on the chemical analysis of selected samples.

## RESULTS AND DISCUSSION

### X-RAY DIFFRACTION DATA:

Almost all samples, but especially the 10 Å-types, showed strong two-dimensional diffraction bands indicating considerable layer stacking disorder. None of the samples exhibited marked swelling characteristics when immersed in water or in ethylene glycol, and the usual simple procedures for studying interstratified systems when one component is expandable were of no assistance. Also only small changes in the basal spacings were observed on heating at 110°C for several days.

7 Å-type garnierites: The diffraction patterns are variable in detail but all show resemblances to patterns of lizardite and/or chrysotile. One sample appeared to be a good two-layer orthochrysotile, but most samples could be described only as resembling the serpentine group minerals. There was little indication of basal plane orientation so the samples clearly did not have a good basal plane development.

10 Å-type garnierites: The diffraction patterns were more nearly identical than those of the 7 Å-type minerals. They also closely resembled a pattern of a so-called  $\beta$ -kerolite supplied by Dr. Z. Maksimovic, and appeared almost free of 7 Å-type material. The (001) peak profiles showed some asymmetry spreading towards smaller values of  $2\theta$ . Heating at 110°C for 3 days gave stronger

and more nearly symmetrical profiles and a basal spacing ranging from 10.0-10.3 for nine different samples. The patterns obtained are essentially identical with those reported by Maksimovic (1966), and indicate a non-expanding 10 Å-type mineral with considerable layer stacking disorder. His description of these minerals as representing a series from a magnesian end-member ( $\beta$ -kerolite) to a nickelian end-member (pimelite) is questioned only as regards the nomenclature. The name pimelite has been applied (Spangenberg, 1938; Faust, 1966) to an expanding mineral, possibly a member of the smectite group, and this does not apply to the 10 Å-type garnierites studied here and by Maksimovic.

### ELECTRON-OPTICAL DATA

Electron micrographs recorded at  $5 \cdot 10^4$  -  $10^5 \times$  magnifications show that the 7 Å-type garnierites have a variety of morphological forms, including tube- and rod-shaped particles and also platy forms and poorly defined, fluffy particles which are probably aggregates.

Among the 10 Å-type minerals, less morphological variety is found. They consist mainly of fine platy particles, with ill-defined outlines and often appear as fluffy aggregates. Very few elongated forms are observed.

In a collaborative study with Dr. Natsu Uyeda, of Kyoto University, these 7 Å- and 10 Å-type garnierites have been studied at  $10^6 \times$  magnifications. The individual lattice planes with 7 Å and 10 Å spacings are seen directly. The 7 Å spacings are usually clearer and more regularly defined than the 10 Å spacings. Many examples have been found where as many as ten-twenty 7 Å layers have been observed in a measurable sequence. The 10 Å spacings are revealed by no more than three or four parallel layers. Fig. 1 shows part of a sample which is predominantly of 10 Å-type, but there is clear evidence of small areas with regular 7 Å spacings and a regularity of 4.5 Å, possibly corresponding to  $b/2$ , along some of the layers. In general these micrographs suggest the presence of highly distorted or even amorphous material.

### CHEMICAL ANALYSIS, AND STRUCTURAL FORMULAE

Chemical analyses have been made on four 7 Å-type garnierites and seven 10 Å-type garnierites including the magnesian mineral  $\beta$ -kerolite, by atomic absorption spectrometry on materials dried at 110°C. The content of  $H_2O^+$  has been taken as the weight loss on samples between 110°C and 950°C. Quartz impurities have been measured directly by an x-ray intensity method and subtracted from the total  $SiO_2$ . The analyses are given in Tables I and II where the total weight percentages including  $H_2O^+$  are seen to add to values mainly between 98.5 and 100.5%.

Table I. Chemical Analyses and Structural Formulae of Some 7 Å-Type Garnierites

	(1) # MN6 Morro do Niquel, Brazil	(2) # 3996 Morro de Cerisco Brazil	(3) # HMC5 Riddle, Oregon	(4) # New Cal New Caledonia
Quartz	1.5	1.3	1.2	-
SiO <sub>2</sub> (d)	43.5	43.7	43.2	35.0
Al <sub>2</sub> O <sub>3</sub>	0.25	0.51	0.24	0.47
Fe <sub>2</sub> O <sub>3</sub>	2.20	6.10	2.74	0.10
MgO	35.1	30.4	22.7	2.70
NiO	4.40	5.50	18.6	49.3
CaO	0.20	0.05	0.12	< 0.05
Na <sub>2</sub> O	0.04	0.13	-	0.14
K <sub>2</sub> O	0.03	0.05	-	0.08
H <sub>2</sub> O <sup>+</sup> (a)	12.8	12.7	11.9	11.4
Total	100.0	100.4	100.7	99.2
	A B	A B	A B	A B
Si	2.00 2.09	2.00 2.11	2.00 2.18	2.00 2.14
Al	0.01 0.01	0.03 0.03	0.01 0.01	0.03 0.03
Fe <sup>3+</sup>	0.08 0.08	0.21 0.22	0.09 0.10	0.00 0.00
Mg	2.41 2.51	2.07 2.19	1.57 1.71	0.23 0.25
Ni	0.16 0.17	0.20 0.21	0.70 0.76	2.27 2.43
∑ Oct. (b)	2.70 2.81	2.63 2.77	2.42 2.62	2.54 2.70
H <sub>2</sub> O <sup>+</sup>	1.96 2.05	1.94 2.05	1.85 2.01	2.17 2.31
x (c)	0.110	0.141	0.240	0.180

(a) H<sub>2</sub>O<sup>+</sup> = weight loss from 110° - 950°C.

(b) ∑ Oct. = ∑(R<sup>2+</sup> + 3/2 R<sup>3+</sup>)

(c) x = Proportion of 10 Å-type layers, calculated from [Si/∑ Oct.].

(d) Total silica - quartz.

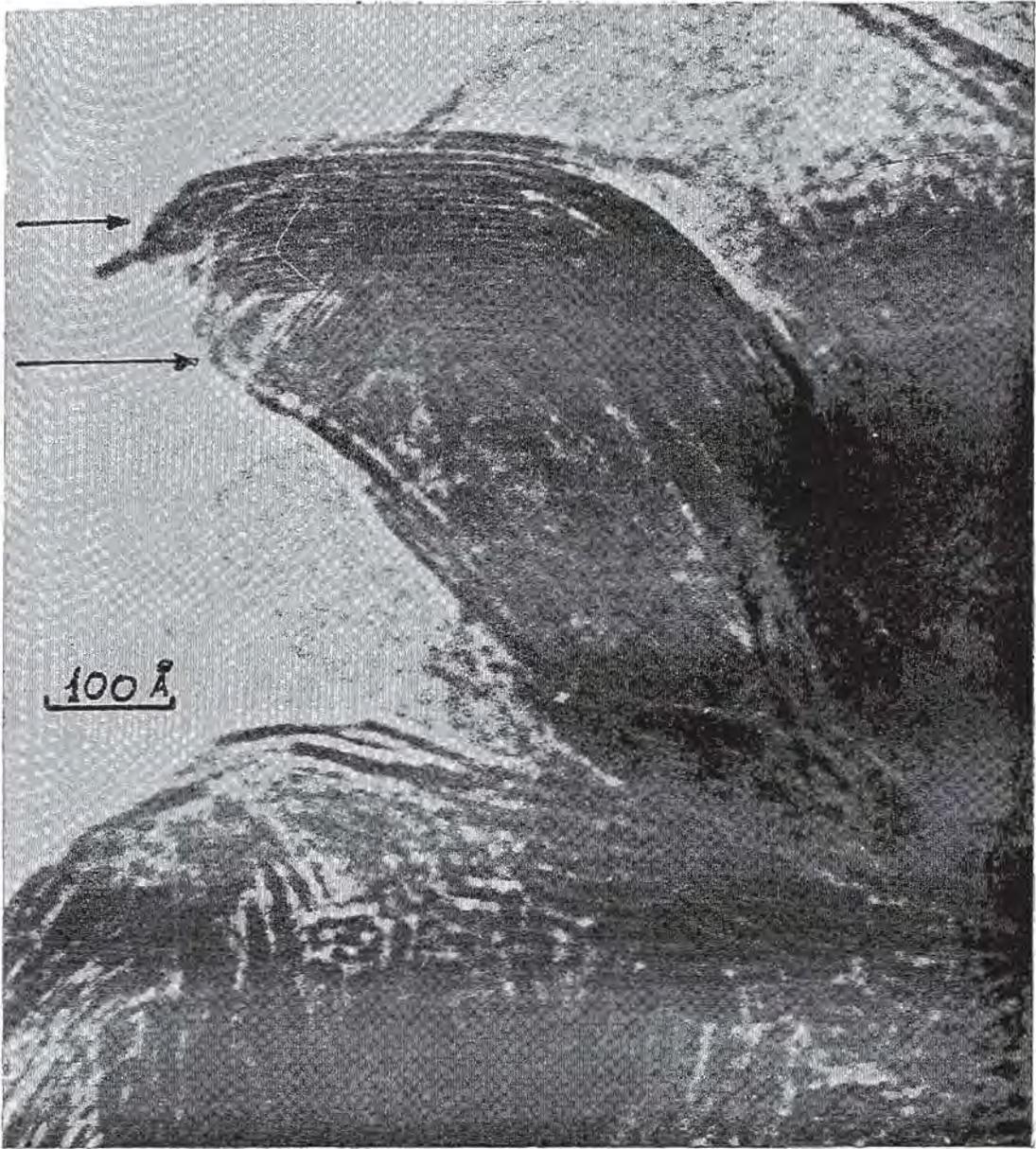


Figure 1. Electron micrograph of garnierite sample from unknown source, probably New Caledonia. Original magnification  $1,5 \times 10^6 \times$ . Scale mark = 100 Å. Sample is mainly 10 Å garnierite, but arrows point to 7 Å spacings. (Courtesy of Dr. N. Uyeda)



Table II. Chemical Analyses and Structural Formulae of Some 10 A-Type Garnierites

	(1) $\beta$ -kero- lite Goles Mt. Yugoslavia	(2) # NC Durham, N. Caroli- na	(3) # MN4A Morro do Niquel, Brazil	(4) # RO3B Riddle, Oregon	(5) # RO24 Riddle, Oregon	(6) RO3A Riddle, Oregon	(7) GUS, Unknown Source
Quartz (d)	-	2.0	4.1	-	2.2	-	-
SiO <sub>2</sub>	58.35	58.0	52.9	52.0	47.8	52.3	46.0
Al <sub>2</sub> O <sub>3</sub>	0.03	0.05	0.12	-	0.14	-	0.20
Fe <sub>2</sub> O <sub>3</sub>	0.11	0.20	0.25	-	0.15	-	0.35
MgO	31.6	25.9	18.3	18.5	18.6	16.3	9.40
NiO	0.26	5.51	16.8	18.2	19.6	20.8	31.5
CaO	0.32	0.05	0.05	-	0.05	-	0.05
Na <sub>2</sub> O	0.24	0.04	0.01	0.02	0.01	-	0.14
K <sub>2</sub> O	0.04	0.13	0.05	0.04	0.03	0.08	0.03
H <sub>2</sub> O <sup>+</sup>	9.8	8.4	7.4	10.0	12.7	8.6	10.3
Total	100.7	100.3	100.0	98.8	101.3	98.1	98.0
	A B	A B	A B	A B	A B	A B	A B
Si	4.00 3.91	4.00 4.01	4.00 3.96	4.00 3.91	4.00 3.77	4.00 3.95	4.00 3.83
Al	- -	- -	0.01 0.01	- -	0.01 0.01	- -	0.02 0.02
Fe <sup>3+</sup>	- -	0.01 0.01	0.01 0.01	- -	0.01 0.01	- -	0.02 0.02
Mg	3.23 3.16	2.66 2.66	2.06 2.04	2.12 2.08	2.32 2.19	1.86 1.84	1.22 1.17
Ni	0.01 0.01	0.31 0.31	1.02 1.01	1.13 1.10	1.32 1.24	1.28 1.26	2.20 2.11
Oct. (b)	3.24 3.17	2.98 2.98	3.11 3.08	3.25 3.18	3.67 3.46	3.14 3.10	3.48 3.34
H <sub>2</sub> O <sup>+</sup>	2.24 2.18	1.93 1.93	1.87 1.85	2.56 2.51	3.55 3.35	2.20 2.17	2.99 2.86
x (c)	0.148	-0.015	0.070	0.154	0.364	0.088	0.274

(a) H<sub>2</sub>O = weight loss from 110° - 950°C(b)  $\sum \text{Oct.} = \sum (\text{R}^{2+} + 3/2 \text{R}^{3+})$ (c) x = Proportion of 7 Å-type layers calculated from  $(\text{Si}/\sum \text{Oct.})$ .

(d) Total silica - quartz

Derivations of structural formulae are subject to many uncertainties. Essentially atom ratios can be derived and the problem is to choose a valid basis for normalizing the composition to obtain a unit cell formula. In the present case, two methods are used; method A supposes that the tetrahedral cation positions are fully occupied by Si, with 2 Si per formula unit in the serpentine-like minerals ( $Mg_3 Si_2 O_5 (OH)_4$ ) and 4 Si in the talc-like minerals ( $Mg_3 Si_4 O_{10} (OH)_2$ ). Method B assumes a (tetrahedral + octahedral) cation valence of +14 and +22 in the corresponding formulations. The results are given in columns A and B of Tables I and II. Both methods lead to the conclusion that the total octahedral cations, chiefly  $Mg^{2+}$  and  $Ni^{2+}$ , are distinctly less than the ideal value 3.0 for serpentines, and distinctly more than the ideal value, also 3.0, for talc. The results suggest that talc-like layers are associated with the 7 Å-garnierites, and serpentine-like layers with the 10 Å-garnierites. Similar conclusions have been reached by other investigators.

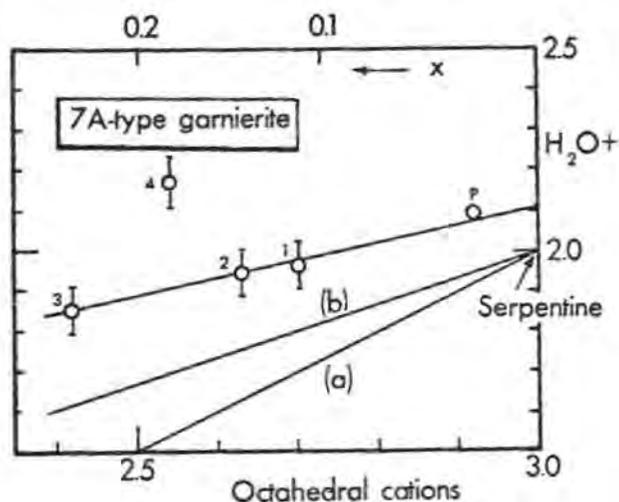


Figure 2. 7 Å-type garnierites.  $H_2O+$  versus  $\Sigma$  octahedral cations for  $Si = 2.00$ . Experimental points correspond to data of Table I. Vertical lines attached to data points correspond to  $\pm 3\%$  uncertainty.

Line (a). Mixture of  $(1-x)$  serpentine layers,  $x$  talc layers.

Line (b). Mixture of  $(1-x)$  serpentine layers,  $x$  talc monohydrate layers.

#### Tetrahedral/Octahedral Cation Ratios and Mixtures of Layers

The calculations are made most easily as follows: In 7 Å-garnierites let  $(1-x)$  be the proportion of serpentine-like layers, and  $x$  the proportion of talc-like layers. In 10 Å-garnierites, let the converse arrangement hold. If the basic formulae are written in the oxide forms,  $3MgO \cdot 2SiO_2 \cdot 2H_2O$  for serpentine and  $3MgO \cdot 4SiO_2 \cdot H_2O$  for talc, where Mg also includes Ni and other octahedral cations,

then the resulting mixed formulae are:

7 Å-type garnierites:  $3\text{MgO} \cdot (2+2x)\text{SiO}_2 \cdot (2-x)\text{H}_2\text{O}$ ,  $x$  = proportion of talc layers

10 Å-type garnierites:  $3\text{MgO} \cdot (4-2x)\text{SiO}_2 \cdot (1+x)\text{H}_2\text{O}$ ,  $x$  = proportion of serpentine layers

Then for 7 Å-type garnierites,  $x = 1.5 [\text{SiO}_2/\text{MgO}] - 1$

and for 10 Å-type garnierites,  $x = 2 - 1.5 [\text{SiO}_2/\text{MgO}]$

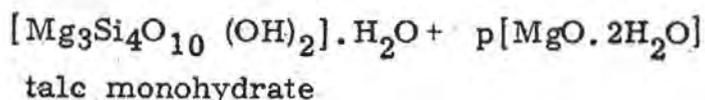
where  $[\text{SiO}_2/\text{MgO}]$  is the mole ratio of the oxides, or simply the tetrahedral/octahedral cation ratio. The values of  $x$  calculated from these equations are given in Tables I and II. The smaller values of  $x$  may well represent interstratified layers, particularly in the 10 Å-type garnierites, and/or phase mixtures, but the higher values of  $x$  are less easily "explained" in this way and may arise in part from the amorphous-looking regions seen at  $10^6\times$  magnification.

#### THE WATER CONTENT, $\text{H}_2\text{O}^+$ , OF GARNIERITES

The  $\text{H}_2\text{O}^+$  contents of garnierites are difficult to obtain reliably. In defense of the  $\text{H}_2\text{O}^+$  values given in Tables I and II, it should be noted that the total analyses with  $\text{H}_2\text{O}^+$  included come close to 100%. The values given, however, are subject to an uncertainty of the order of 2-3%. In Fig. 2 and 3, the  $\text{H}_2\text{O}^+$  values given under A are plotted against total octahedral cations,  $\Sigma (R^{2+} + 3/2 R^{3+})$ , relative to Si = 2.00 for 7 Å-type garnierites and to Si = 4.00 for 10 Å-type garnierites. These figures also show a scale of  $x$  values derived from the  $[\text{SiO}_2/\text{MgO}]$  mole ratios as described earlier.

10 Å-type garnierites: Fig. 3 shows that the  $\text{H}_2\text{O}^+$  values of five of the seven samples listed in Table II plot close to the line marked (c) which passes through  $\text{H}_2\text{O}^+ = 2$  when octahedral cations = 3.0 and Si = 4.0. The composition of this point is  $3\text{MgO} \cdot 4\text{SiO}_2 \cdot 2\text{H}_2\text{O}$ , or  $[\text{Mg}_3\text{Si}_4\text{O}_{10}(\text{OH})_2] \cdot \text{H}_2\text{O}$  which can be called "talc monohydrate". The composition point for normal talc also is shown. Line (a) in Fig. 3 corresponds to a mixture of normal talc and normal serpentine layers. Evidently the garnierites are considerably more hydrated. Line (b) corresponds to a mixture of talc monohydrate and normal serpentine, and this also falls below most of the experimental values.

Line (c) can be fitted by compositions derived as follows: The slope of this line corresponds to an increment of 2 units of  $\text{H}_2\text{O}^+$  per unit increment of octahedral cations and therefore corresponds to compositions



where  $p$  = octahedral cations in excess of 3.0, when referred to  $Si = 4.0$ . The additional term can be written in various ways, but its relation to brucite is shown by writing  $(p/2)[(Mg_2O)(OH)_4 \cdot 2H_2O]$ ; in other words, the additional material appears as a hydrated form of brucite. Other interpretations are possible, involving combinations of talc monohydrate and hydrated forms of serpentine, such as  $Mg_3Si_2O_5(OH)_4 \cdot 2H_2O$ , giving the same net composition, but they cannot be discussed at length here.

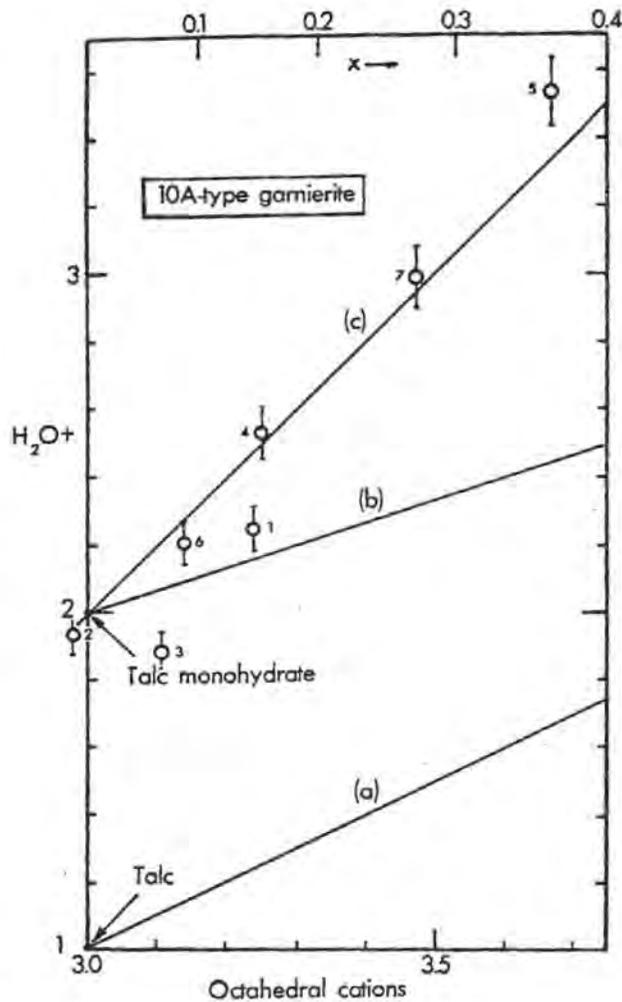


Figure 3. 10 Å-type garnierites,  $H_2O +$  versus  $\Sigma$  octahedral cations for  $Si = 4.00$ . Experimental points correspond to data of Table II. Vertical lines attached to data points correspond to  $\pm 3\%$  uncertainty.

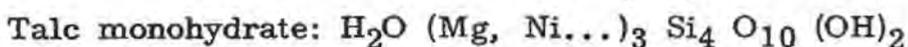
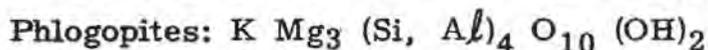
- Line (a). Mixture of  $(1-x)$  talc layers,  $x$  serpentine layers.
- Line (b). Mixture of  $(1-x)$  talc monohydrate layers,  $x$  serpentine layers.
- Line (c). Mixture of  $(1-x)$  talc monohydrate layers,  $x$  serpentine dihydrate layers; or alternative model with talc monohydrate layers and hydrated brucite layers.

7 Å-type garnierites: Fig. 2 shows the  $H_2O^+$  values plotted against octahedral cations with respect to  $Si = 2.0$  for the four samples listed in Table I, together with an additional point P, corresponding to the analysis of pecoraite by Faust et al. (1969). The composition of serpentine is indicated in Fig. 2 and the experimental line extrapolates to 2.1  $H_2O$  in place of the ideal 2  $H_2O$ . Line (a) corresponds to mixtures of normal talc and normal serpentine, line (b) to mixture of talc monohydrate and normal serpentine. Line (b) is approximately parallel to the experimental line.

It appears that the 7 Å-type garnierites can be described as consisting mainly of a serpentine-type mineral with slightly more water than the ideal composition and possibly included in the tubular forms, together with a hydrated talc component approximating to the monohydrate found in the 10 Å-type garnierites.

### TALC MONOHYDRATE

It is of interest to speculate on the nature of this component in garnierites. A comparison can be made with phlogopites:



This comparison suggests a reason for the talc monohydrate composition, namely the incorporation of  $H_2O$  molecules, like the  $K^+$  ions of micas, in the holes of the quasi-hexagonal oxygen networks. One recalls that  $H_2O$  and  $K^+$  have similar packing radii, about 1.35 Å. The suggested arrangement is compatible with the observed basal spacing, about 10 Å, and not 9.4 Å as in normal talc. The additional water is gradually released between 110° and 500°C. The basal spacing does not readily diminish with heat treatment and 9.7 Å is about the smallest spacing observed in the heated 10 Å-type garnierites. Usually thermal transformation begins before a collapse to 9.4 Å occurs.

### CONCLUSIONS

Samples selected by x-ray diffraction data as consisting dominantly of 7 Å and 10 Å-type garnierites, are found by electron microscopy to consist of a variety of morphological types. At  $10^5 \times$  magnification, the individual layers can be seen and 7 Å and 10 Å spacings are measured where a regular succession of layers occurs, but also regions are found in which the layers are not clearly revealed as either 7, or 10 Å-types. In agreement with other investigations, the chemical analyses are shown not to conform with normal serpentine and normal talc compositions, and from the ratio of tetrahedral/octahedral cations, the proportion  $x$  of admixed layers

is derived, but no independent proof of the reality of these mixtures is obtained. The water content,  $H_2O^+$ , is particularly interesting and especially the very strong indication of a talc monohydrate, which is compared with a mineral such as phlogopite, with  $H_2O$  possibly occupying interlayer positions analogous to  $K^+$  ions.

Many other aspects of this study, including electron-optical study, thermogravimetric data, and high temperature phase transformations will be discussed in detail elsewhere.

#### ACKNOWLEDGMENTS

Thanks are extended to the U. S. Administration for International Development (U.S.A.I.D.) for a scholarship to Pham Thi Hang, and to the Georgia Kaolin Company for a grant supporting the research program. We are also greatly indebted to many donors of mineral samples whom we thank collectively here. We thank also Dr. Natsu Uyeda of Kyoto University for high resolution, high magnification electron micrographs of some of our samples; a joint publication of this work will be given later.

#### REFERENCES

- FAUST, G. T. (1966): The hydrous nickel-magnesium silicates - the garnierite group. *Amer. Mineral.* 51, 279-298.
- FAUST, G. T., J. J. FAHEY, BRIAN MASON and E. J. DWORNIK (1969): Pecoraite,  $Ni_6 Si_4 O_{10} (OH)_8$ , the nickel analog of clinochrysotile, formed in the Wolf Creek meteorite. *Science* 165, 59-60.
- GINZBURG, I. I. and I. A. RUKAVISHNIKOVA (1951): Minerals from the ancient crust of weathering of the Urals. *Izdat. Akad. Nauk SSSR*, 714 pp. [CA 11267, 1954].
- MAKSIMOVIC, Z. (1966):  $\beta$ -kerolite-pimelite series from Goleš Mountain, Yugoslavia. *Proc. Internat. Clay Conf., Jerusalem.* 1, 97-105.
- PECORA, W. T., S. W. HOBBS and K. J. MURATA (1949): Variations in garnierite from the nickel deposit near Riddle, Oregon. *Econ. Geol.* 44, 13-23.
- SPANGENBERG, K. (1938): Die Wasserhaltigen Nickelsilikate. *Cent. Mineral. Abt. A*, 360-364.
- VITOVSKAYA, I. V. and S. I. BERKHIN (1968): The problem of the nature of kerolite Kora *Vyvetrivaniya* 10, 134-159.
- VITOVSKAYA, I. V. and S. I. BERKHIN (1970): Nature of garnierite. *Kora Vyvetrivaniya* 11, 26-39.
- VITOVSKAYA, I. V., S. I. BERKHIN, and R. S. YASHINA (1969): The serpentine component of nickel silicates. *Doklady Akad. Nauk SSSR* 189, 1092-1094. *English Trans. Earth Science Section.* 189, 160-162.

## A QUANTITATIVE STUDY OF ONE-LAYER POLYTYPISM IN THE KAOLIN MINERALS

R. W. Wolfe and R. F. Giese, Jr.

State University of New York at Buffalo  
P.O. Box U, Station B, Buffalo 14207, New York, U.S.A.

ABSTRACT. - In the past, clay mineral polytypes have been derived on the basis of geometric relations and the relative stabilities of these polytypes have been assessed by very qualitative arguments. We have developed a very general technique for quantitatively treating the relative stabilities of polytypes. As an example, we have studied the one-layer polytypes based on a kaolin-type clay layer. Generation of these polytypes involves the translation of one layer with respect to another in two dimensions with interlayer distances held constant. The translations used here are in increments of  $a/6$  and  $b/12$  where  $a$  and  $b$  are the unit cell edges of the kaolinite structure. Initially, the structure of the single layer was taken to be that of kaolinite (including hydrogen positions). For each of the possible translations, the electrostatic energy was calculated. These energies represent samples of a continuous potential energy surface when plotted against the two translation increments and the minima in this surface are the stable structures. On the basis of geometric relations (oxygen atoms in one layer adjacent to hydroxyl groups in the next layer) there are six different one-layer polytypes. The potential energy surface for all possible translations has only three minima, two of which represent the mineral kaolinite (right- and left-handed). The surface was recomputed using the structural data for dickite and shows no substantial difference.

### INTRODUCTION

Relative stabilities have been assigned to polytypes based on their frequency of occurrence in nature and the degree to which they form large, well-ordered crystals. Bailey (1966) has noted that,

for the muscovites and chlorites, some polytypes occur nearly to the exclusion of others in environments having sufficient thermal energy or pressure and that metastable polytypes which crystallize early may persist indefinitely. By petrographic methods, Hayes (1970) has applied the occurrence of various chlorite polytypes to the determination of whether these minerals are detrital or authigenic. He also proposed that the presence of certain polytypes may serve as a geothermometer. In order that the polytypes of phyllosilicates may be useful as indicators of geological environments, it is necessary to determine which of the geometrically possible polytypes are stable, which are metastable, and which of the metastable polytypes are resistant to conversion to the stable form. However, predictions of polytype stabilities based on geometric considerations have been only very qualitative.

## BACKGROUND

It has been noted by Hendricks (1938) that, for the kaolin minerals, layers are stacked such that oxygen atoms in one layer are adjacent to hydroxyl groups in the next layer and long hydrogen bonds may be formed. The six possible stacking translations which lead to the formation of the bonds were determined by Brindley (1951). By considering that the layers could be rotated with respect to one another by multiples of  $\pi/3$ , Newnham (1961) derived thirty additional configurations. There are, then, six theoretically possible one-layer and 138 two-layer polytypes based on a kaolin-type layer. Of these 144 structures, only four or five are found in nature: the two enantiomorphs of kaolinite, dickite, nacrite, and possibly the "monoclinic kaolinite" from Yugoslavia reported by Krstanović and Radošević (1961).

In explaining the stabilities of the kaolin minerals, Newnham (1961) eliminated, as being energetically unfavorable those polytypes: (1) with the greatest amount of cation-cation superposition in adjacent layers, (2) those which, because of layer distortions, had less favorable oxygen-hydroxyl pairings, and (3) those for which the surface corrugations of adjacent layers fit poorly. He found that, of all possible two-layer structures, only those of dickite and nacrite met none of these criteria for instability. The kaolinite structure does not possess a favorable fit of corrugations but is nevertheless seen as the most stable one-layer polytype by the above criteria. Bailey (1963) has proposed that the "monoclinic kaolinite" of Krstanović and Radošević (1961) may have a structure similar to kaolinite but with the octahedral site A vacant rather than sites B or C (Fig. 1). Alternatively, he proposed a structure in which the

vacant site is randomly distributed among the three. In Newnham's (1961) analysis, the proposed ordered structure is considered unstable, having more cation-cation superposition than the kaolinite structure though possessing favorable oxygen-hydroxyl pairings and fit of corrugations.

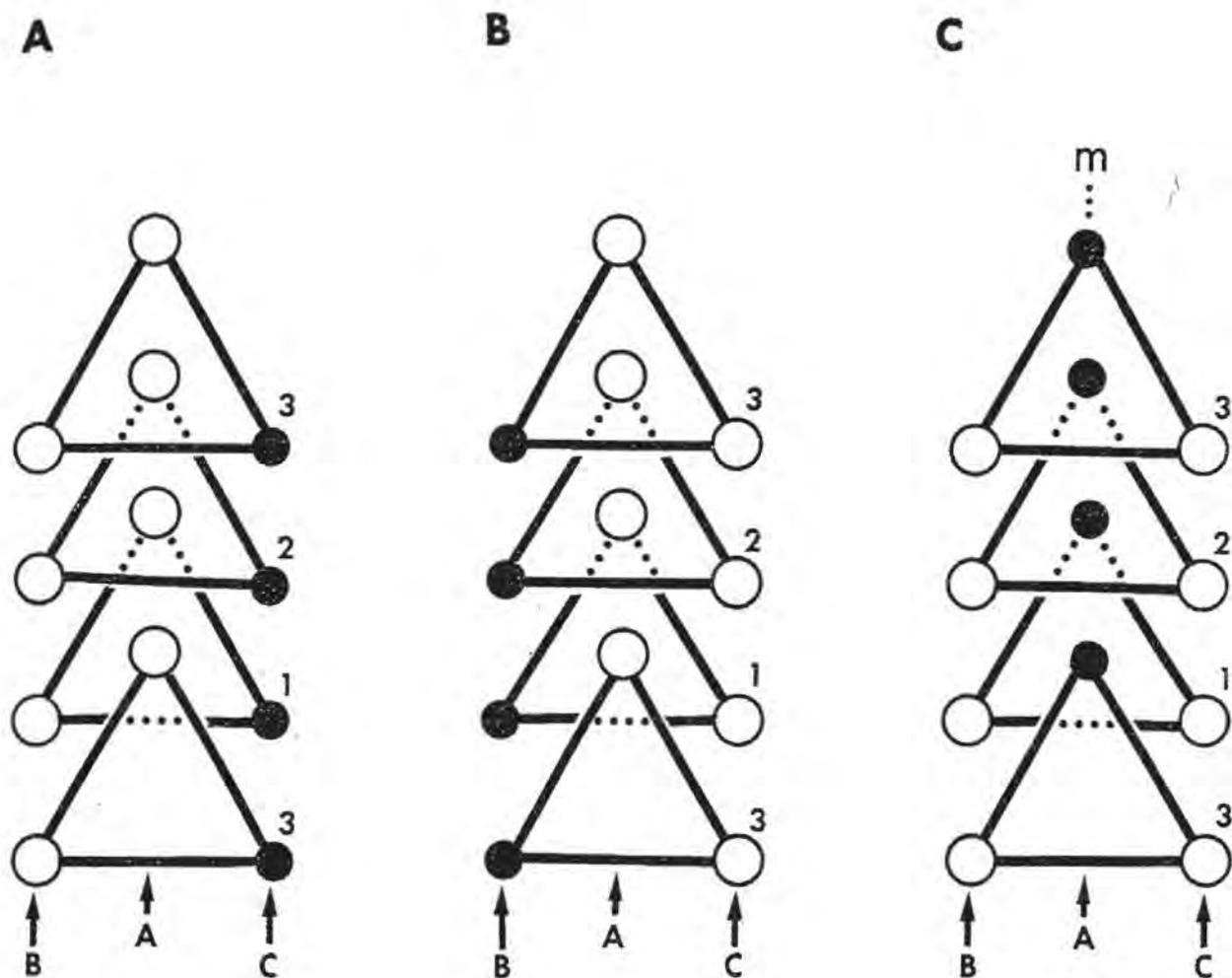
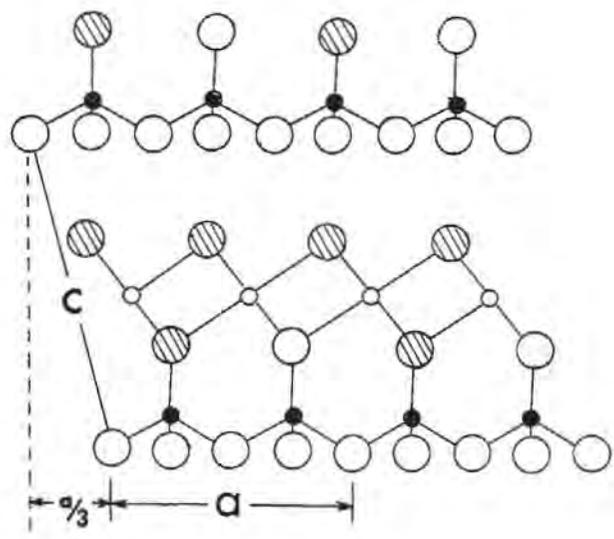


Figure 1. - Projections onto (001) of the octahedral sites of three layers (1, 2, 3) based on a kaolin-type layer, showing the distribution of cations (open circles) and vacancies (closed circles).

- A. Kaolinite
- B. Kaolinite enantiomorph
- C. "Monoclinic kaolinite"

**A**



- ⊘ OH
- O
- Si
- Al

**B**

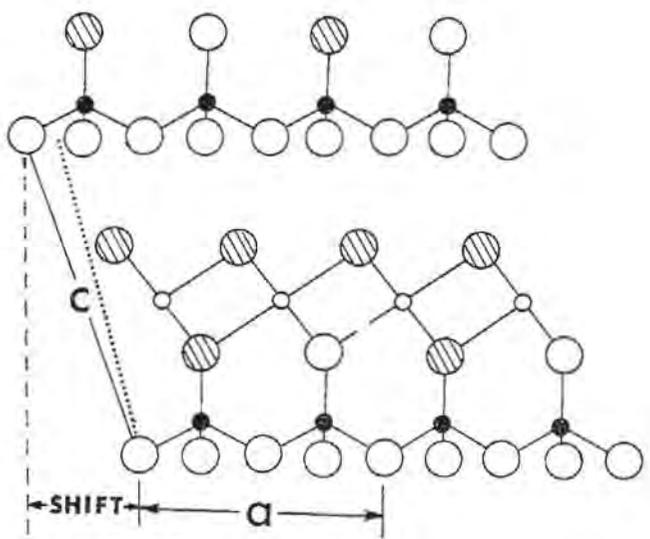


Figure 2. - Projections onto (010) of idealized polytypes.  
 A. "Kaolinite", showing shift of  $-a/3$   
 B. A "new" structure with c-axis of kaolinite shown dotted for comparison.

Radoslovich (1963) extended Newnham's work by considering the directed nature of O-H...O bonds even though the orientations of the hydroxyls were not known. Despite torsion of these bonds in all stacking configurations, the stress is seen to be least in the two enantiomorphs of kaolinite and greatest in the proposed structure of "monoclinic kaolinite". This criterion of minimal angular strain of O-H...O bonds leads also to a prediction of greater stability of dickite than nacrite.

Relative stabilities for the trioctahedral 1:1 polytypes have been predicted by Bailey (1969) using much the same criteria as Newnham (1961), but weighting the relative importance of each of the various factors based on the ionic charges involved and the distances over which the interatomic forces operated.

On the basis of electrostatic energy calculations using a simple ionic model, Giese and Datta (1972) have proposed hydroxyl orientations for the minerals kaolinite, dickite, and nacrite based on the observation that hydroxyls orient themselves in the structure so that the electrostatic energy is minimized. More recently, Giese (1972) has used this approach to study the role of hydrogen atoms in the interlayer bonding in these minerals. By extending the method of Giese (1972), we have developed a very general technique for quantitatively treating the relative stabilities of polytypes. This treatment is based on the assumption that, for a stable structure, not only atoms but larger portions of the structure, such as clay layers, occupy positions relative to one another such that the electrostatic energy of the structure is minimized.

## METHOD

All possible one-layer kaolin polytypes can be generated by appropriately shifting the adjacent clay layers in two dimensions. Each shift will correspond to a different unit cell with invariant a and b dimensions and the angle between. If one begins with all layers superimposed, that is, with  $\alpha$  and  $\beta = 90^\circ$ , the c-axis length will be the separation distance of the kaolin layers. To correctly compare different shifts, this interlayer distance must be kept constant even though the real c-axis must change as the layers are shifted. Furthermore, the relative positions of the atoms within each kaolin layer must remain constant, that is, the interatomic distances and angles must not vary.

To generate each new cell and the fractional coordinates of the atoms in it, we started with the kaolinite structure determination by Zvyagin (1967) with the hydrogen positions of Giese and Datta (1972). The procedure we have followed is to first compute "new" unit cells corresponding to shifts between layers. The shift increments were multiples of  $a/6$  and  $b/12$  all possible shifts with the-

se grid intervals were examined in the asymmetric part of the structure. The atomic positions in the kaolinite structure were then converted to orthogonal coordinates which in turn were converted to fractional coordinates in a new cell corresponding to one of the shifts to be examined. This process produces the effect of shifting rigid silicate layers relative to each other (Fig. 2). For each of the new shifted structures, the electrostatic energy was computed using a program written by Baur (1965).

## RESULTS

The result of all the calculations can be represented as a potential energy surface as a function of the two shift directions and is shown in Fig. 3 which is a stereographic view of the surface. The absolute values of the potential energy surface are not given because they are very sensitive to the structure one starts with. It is sufficient to note that the depths of the three depressions are not greatly different and average approximately -15 kcal/mole relative to the saddle points.

If our assumptions are correct, the stable structures will be those whose potential energy lies at or near the bottoms of closed depressions on the potential energy surface. The positions marked A and B, both in closed depressions, correspond to the structures of a right- and left-handed kaolinite (A is Zvyagin's structure). There is only one other such depression, C, and this corresponds to the "monoclinic" kaolinite of Bailey (1963) shown in Fig. 1-c. This stacking, to use Newnham's approach, has a favorable pucker and a favorable rotation for hydroxyl-oxygen approach but an unfavorable Si-Al superposition. Kaolinite has an unfavorable pucker, favorable rotation, and unfavorable Si-Al superpositions for half the cations. Apparently, the pucker is of about the same weight in determining stability as is half the Si-Al superposition. The letters D, E, and F correspond to the remaining three stackings for one-layer structures and appear at or very near saddle points.

It is quite possible that the hydroxyl orientations on the clay layer surfaces is influenced by the next layer (Giese and Datta, 1972). Hence, the potential energy surface might be influenced by the choice of hydroxyl orientations. The kaolinite structure used has two of the three unique surface hydroxyls nearly normal to the layer and the third almost horizontal. All our calculations were redone using the structure of the dickite layer based on Newnham (1961) with the three surface hydroxyls nearly normal to the clay layer (Giese and Datta, 1972). The resulting potential energy surface was not substantially different from that shown in Fig. 3. We therefore conclude that changes in hydroxyl orientation are minor features and do not radically influence the stacking stability.

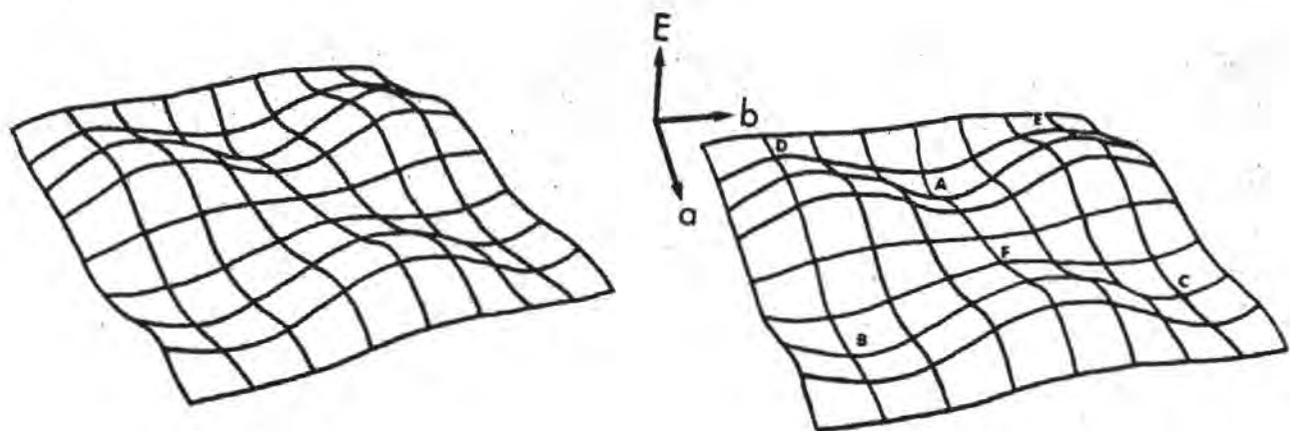


Figure 3. Stereographic view of the potential energy surface for one-layer polytypes based on a kaolin-type layer. The letters A, B, and C lie in closed depressions; D, E, and F are on saddle points.

#### REFERENCES

- BAILEY, S.W. (1963): Polymorphism of the kaolin minerals. *Am. Mineral.* 48, 1196-1208.
- BAILEY, S.W. (1966): The status of clay mineral structures. 14th National Conf. on Clays and Clay Minerals, 1-23.
- BAILEY, S.W. (1969): Polytypism of trioctahedral 1:1 layer silicates. *Clays and Clay Minerals* 17, 355-371.
- BAUR, W. (1965): On hydrogen bonds in crystalline hydrates. *Acta Crystallogr.* 19, 909-916.
- BRINDLEY, G.W. (1951): *X-ray Identification and Structure of the Clay Minerals*, Mineralogical Society, London.
- GIESE, R.F., Jr. (1972): Interlayer bonding in kaolinite, dickite and nacrite. In preparation.
- GIESE, R.F., Jr. and DATTA, P. (1972): Hydroxyl orientations in kaolinite, dickite and nacrite. In preparation.
- HAYES, J.B. (1970): Polytypism of chlorite in sedimentary rocks. *Clays and Clay Minerals* 18, 285-306.
- HENDRICKS, S.B. (1938): The crystal structure of nacrite  $\text{Al}_2\text{O}_3 \cdot 2\text{SiO}_2 \cdot 2\text{H}_2\text{O}$  and the polymorphism of the kaolin minerals. *Zeit. Krist.* 100, 509-518.
- KRSTANOVIĆ, I. and RADOŠEVIĆ, S. (1961): Monoclinic kaolinite from Kocevje mine, Yugoslavia. *Am. Mineral.* 46, 1198.

- NEWNHAM, R.E. (1961): A refinement of the dickite structure and some remarks on polymorphism in kaolin minerals. *Min. Mag.*, 32, 683-704.
- RADOSLOVICH, E. W. (1963): The cell dimensions and symmetry of layer-lattice silicates. IV. Interatomic forces. *Am. Mineral.* 48, 76-99.
- ZVYAGIN, B.B. (1967): *Electron-diffraction Analysis of Clay Mineral Structures*, Plenum Press, New York.

# THE NATURE OF THE COHESION ENERGY IN KAOLIN MINERALS

M. Cruz, H. Jacobs and J. J. Fripiat

Department of Geology, The University of Illinois at Urbana  
(Illinois) and Laboratoire de Physico-chimie minérale,  
Université de Louvain, (Belgium)

**ABSTRACT.** - It is still a general belief that in kaolinite the most important contribution to the cohesion inside the microcrystals is due to hydrogen bonds between the OH of the upper octahedral layer and the adjacent oxygen atoms of the tetrahedral layer.

A recent assignment of the 4 components of the complex OH stretching bands by Jacobs, Rouxhet and Fripiat has shown that the three high frequency components are due to a coupling phenomenon between almost identical OH, whilst, as known already, the low frequency OH band is assigned to the inner layer OH. When the coupling is prevented, the frequency of the single high frequency component is about  $3680 \text{ cm}^{-1}$ , suggesting a hydrogen bond energy lower than 1 kcal.

The Van der Waals forces being more energetic, the cohesion energy between the layers is mostly dispersive. The intercalation process of kaolinite, very often performed by proton acceptor organic molecules, is then explained by a diffusion process, the driving force of which is due to rather strong hydrogen bonds formed between the intercalating agent and the upper OH of the octahedral layer. The release of the original H-bond in the unattacked crystal is a secondary effect which is not at the origin of the intercalation process.

## INTRODUCTION

In 1939, S. B. Hendricks stated that the chief factor determining the relationship between adjacent kaolinite layers must be the interaction of the hydroxyl groups in the bottom of one layer with

the oxygen ions in the top of another, a linkage of "hydroxyls bonds", in agreement with ideas discussed by Bernal. Since that time, this concept has been generally accepted (Grim, 1953 and G. W. Brindley, 1961).

Four OH stretching bands are observed in kaolinite namely at 3696, 3672, 3654 and 3620  $\text{cm}^{-1}$ . The latter is assigned to OH in the medium plane the octahedral layers (inner hydroxyls, R. Ledoux, 1964). Various assignments of the three others bands have been proposed (R. Ledoux 1964, V. C. Farmer, 1964 and R. Pampuch and K. Wilkos, 1965) but all the authors agree that they correspond to OH in the upper octahedral layer.

According to recent data of Jacobs et al. (1972), these frequency components originate in a coupling of three OH oscillators, as shown schematically in Fig. 1. The angles fitting the best the intensity ratios are  $a = 17^\circ$  and  $b = 14^\circ$ . In a still more recent work the orientation of the hydroxyl groups in kaolinite has been determined by Giese (1972) by an iterative process, based on the minimization of the electrostatic energy with the surrounding lattice. It was found that two, out of three OH, are tilted by  $13^\circ$  to the  $c^x$  axis whilst the third, tilted by  $76^\circ$  is close to the kaolin layer. In dickite the three OH are tilted by  $20^\circ$  in average to  $c^x$  whilst in nacrite, one OH is tilted by  $52^\circ$  and the two others by an average angle of  $14^\circ$ .

Obviously according to the usual views some of these OH should be responsible for the hydrogen bond energy linking the layers to each others. It is well known that the stretching frequency of a free OH is observed around 3750  $\text{cm}^{-1}$  and that any tendency for hydrogen bonding results in a shift towards lower frequency. According to calculations carried out by Lippincott and Schroeder (1965) and by others, the energies corresponding to the shifts of the stretching bands of the OH in the interlamellar space should be lower than 1 kcal. This raises a question about the reality of the hydrogen bonding effect invoked to explain the cohesion between the layers and therefore the origin of cohesion.

## THE COHESION ENERGY OF KAOLINITE LAYERS

The cohesion energy is contributed by three main factors:

1. the electrostatic energy
2. the van der Waals energy
3. the energy of hydrogen bonds.

### 1. The van der Waals energy

Consider the dispersion-repulsion energy between a pair of atoms 1 and 2 separated by distance  $l$  and let  $l_e$  be the equilibrium

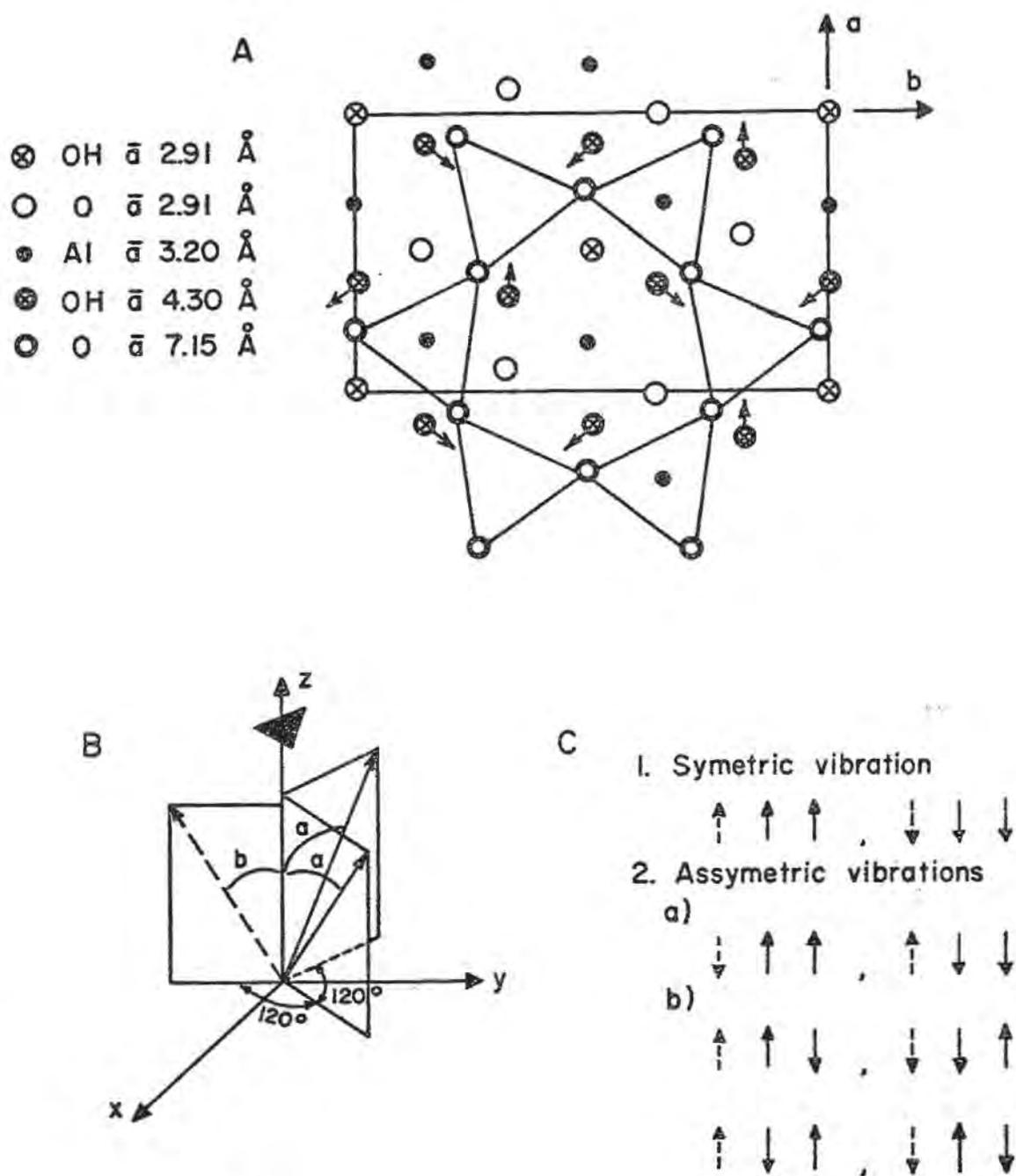


Figure 1. A. Structure of kaolinite. Arrows indicate the OH directions in the upper octahedral layer, according to Veith and Radoslovich.  
 B. Simplified model showing the direction of the OH oscillators obtained from IR spectroscopy.  
 C. Schematic model showing the origin of the 3 high frequency OH stretching bands.

distance, i.e. that for which  $(\delta E / \delta l)_{l_e} = 0$

$$E = - A \phi \quad (1)$$

where

$$\phi(l) = \frac{1}{16} - \frac{1}{2} \frac{l_e^6}{l^{12}}$$

$$A = 6 m C^2 \alpha_1 \alpha_2 / (\alpha_1 / X_1 + \alpha_2 / X_2)$$

A is the Kirkwood-Muller constant. m and C are the electron mass and the speed of the light,  $\alpha$  and X, the polarisability and magnetic susceptibility of atoms (1) and (2) respectively. Consider that atoms (1) and (2) form two continuous planes parallel to each other. The average value of  $\phi(l)$ , i.e.  $\langle \phi(l) \rangle$ , for one of these atoms (1) or (2) with respect to all the others of the opposite plane may be obtained by integrating  $\phi(l)$  on a circular surface element:

$$\langle \phi(l) \rangle = \int_{r=0}^{\infty} \phi(l) \quad 2\pi r \quad dr$$

where

$$l = l_e \{1 + (r^2/l_e^2)\}^{1/2}$$

The energy is then given by  $n\langle \phi(l) \rangle$  where n is the number of atoms per surface unit i.e.  $n = 6/45.9 \text{ \AA}^2$

$$E = - \frac{nr}{2l_e^4} (1 - 1/5) A$$

Assume that  $l_e$  is the distance between the two planes. In first approximation it will be supposed that the two planes are made of the same kind of atoms and that  $\alpha_1 = \alpha_2$  and  $X_1 = X_2$  are those used for oxygen in similar calculations performed on zeolite (Barrer and Coughlan, 1968), i.e.

$$\alpha = 1.65 \cdot 10^{-24} \text{ cm}^3; X = 20.9 \cdot 10^{-30} \text{ cgs}$$

Per g. atom,

$$A = 1.7 \cdot 10^{-45} \text{ kcal cm}^{-6}$$

$$E = 3.75 \text{ kcal per unit cell.}$$

## 2. Hydrogen bond energy

If we consider  $3680 \text{ cm}^{-1}$  as the degenerate stretching frequency of the OH in the interlamellar space (Jacobs et al. 1972) and  $3750 \text{ cm}^{-1}$  as the frequency of the free OH, the shift towards low frequency due to hydrogen bonding should be  $90 \text{ cm}^{-1}$ . This corresponds to an OH...O hydrogen bond energy of  $\sim 1 \text{ kcal}$ .

Taking into account the result obtained by Giese, i.e. that in kaolinite 4 OH out of 6 are hydrogen bonded per unit cell, the hydrogen bond energy is of the order of the van der Waals energy and the sum of these two terms is of the order of 8 kcal.

## 3. The electrostatic energy contribution

Consider the interlamellar space as a condenser bearing a surface density of charge  $\sigma$  on each plane. Inside the condenser the electrical field and the electrostatic energy per unit volume are respectively:

$$H = 4\pi\sigma$$

$$\rho = \frac{H^2}{8\pi}$$

The surface density of charge may be evaluated as follows. It is known that the kaolinite lattice is not polar. Assume that in the interlamellar space, the total dipole moment  $\mu_t$  of the OH protruding outwards the layer is balanced locally by a dipole moment arising from a formal positive charge on the OH layer and from a negative charge on the opposite oxygen layer, the separation of these charges being, in average,  $l_0 = 2.95 \text{ \AA}$ . Per unit cell there are 6 OH and 6 O: if each of them bears a fractional formal charge  $x$ , then

$$\mu_t = 6 \times 4.8 \times 2.95 \text{ D.u.} \quad (1 \text{ D.u.} = 10^{-18} \text{ cgs})$$

If, in agreement with Giese (1971), out of 6 OH, 4 are tilted by  $13^\circ$  and 2 by  $76^\circ$  to the  $c^x$  axis and if the dipole moment of an isolated OH is 1.5 Debye unit (D.u.), then

$$\mu_t = 6.575 \text{ D.u.}$$

$$x = 0.0775$$

If the structural scheme proposed by Jacobs et al. is correct, namely that the 6 OH are tilted by an average angle of  $16^\circ$  to the  $c^x$  axis:

$$\mu_t = 8.65 \text{ D.u.}$$

$$x = 0.102$$

The density of charge per surface unit is  $0.627 \times 10^6$  esu  $\text{cm}^{-2}$  and the field amounts to

$$7.87 \times 10^6 \text{ esu cm}^{-2} \text{ whilst } \rho = 2.47 \times 10^{12} \text{ esu cm}^{-3}$$

The energy per unit cell is given by:

$$E = 4.8 \times 10^3 \text{ kcal}$$

Within the limits of the two hypotheses on the orientation of the OH:

$$28.8 < E < 48.8 \text{ kcal per unit cell.}$$

The sum of the electrostatic, of the van der Waals and of the hydrogen bond contributions is thus

$$37 < E < 56 \text{ kcal per unit cell}$$

It may thus be concluded that the hydrogen bond energy contribution is of the order of the van de Waals contribution and that the hydrogen bond energy represents roughly 10% of the total cohesion energy.

Using the direction of the OH dipole moment proposed by Giese (1971) for Dickite and Nacrite the values shown in Table I are obtained for the electrostatic contributions.

Table I

Electrostatic contribution to the cohesion energy

	x fractional formal charge	H esu/cm <sup>2</sup> $\times 10^{-6}$	E (electrostatic) kcal per unit cell
Dickite	0.0993	0.781	47.4
Nacrite	0.0902	0.710	39.1
Kaolinite	0.0775	0.610	28.8

## DISCUSSION

In a paper presented in 1971 at the Geological Society of America, Giese (Giese, 1972), as a continuation of his previous work,

has calculated the derivative of the electrostatic potential energy with respect to a small change in the interlayer separation. This electrostatic force between the layer should be equal to  $F = He$  where  $H$  is the electrostatic field calculated according to our technique and  $e$  is the elementary charge. As shown in Fig. 2, a close similarity exists between our results and those obtained by Giese and founded on a complete evaluation of the lattice energy

$$F(\text{Giese}) = 0.46 \cdot 10^{-4} \text{ cgs} + 1.1 F(\text{this work})$$

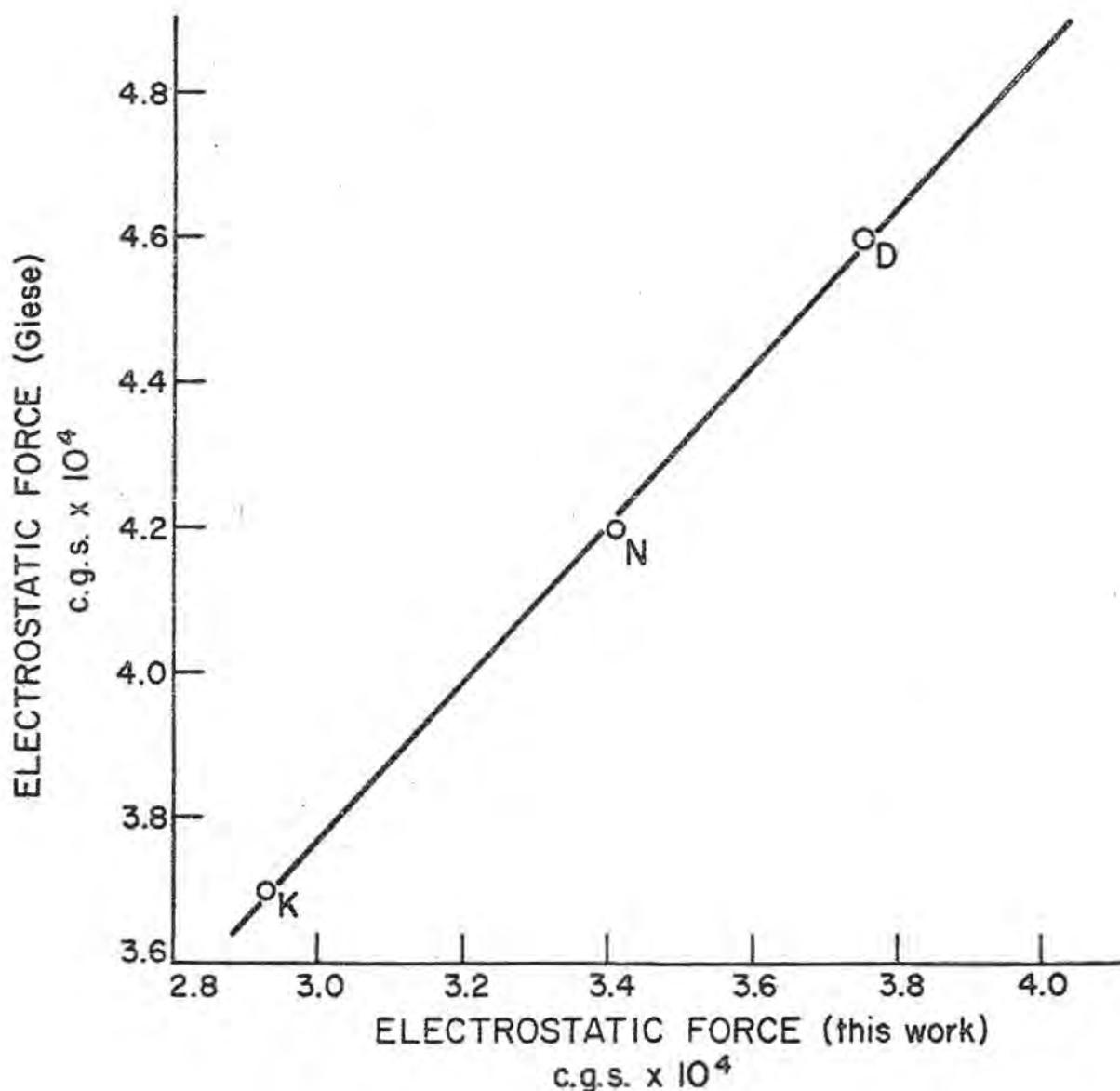


Figure 2. Relationship between the electrostatic force between the layers obtained by Giese (1972), and that obtained in this work.

The positive intercept could be accounted for by the fact that we have considered only the contribution of the lattice planes forming both sides of the interlamellar space. However, it represents no more than 13% of the lowest electrostatic force (in Kaolinite) and therefore we are founded to believe that the calculation that we propose here for the electrostatic energy contribution is essentially correct.

Consequently, the electrostatic contribution appears essentially as due to an attractive effect between the positive and negative charges of the oxygen and hydroxyl oxygen of the interlamellar planes. This difference is required to balance the OH dipole moments. Should the OH be replaced by a negative monovalent anion and this electrostatic contribution would disappear. Again this is in agreement with Giese (1972) findings since his calculations show that a slight repulsive effect arises when OH<sup>-</sup> is replaced by F<sup>-</sup>.

An important question, directly relevant to the present problem rises up. Since the OH are mostly responsible of the main electrostatic contribution to the cohesion energy, it might be considered that the cohesion is mainly due to hydrogen bonds. If hydrogen bonding is considered as essentially electrostatic in nature, then the answer is obviously positive whilst if it is considered essentially as an exchange of protons between two oxygen atoms, the answer is no. In the case where an exchange mechanism is prevailing, the vibrational levels of the OH oscillator are perturbed (Rouxhet and Fripiat, 1971) and to account for the cohesion, the position of the OH stretching bands should be modified to an extent which is not compatible with the frequencies observed in kaolin minerals. The case of a magnesian trioctahedral 1:1 layer lattice silicate such as antigorite is very illustrative of this view point. The main OH stretching band is observed at 3700 cm<sup>-1</sup> approximately, i.e. still closer the "free OH" frequency than in kaolinite. Yet, assuming that, in antigorite, the 6 OH are perpendicular to the layer, the electrostatic contribution calculated according to our method reaches its maximum value of 53.7 kcal.

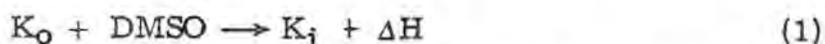
It seems thus more meaningful to consider that in 1:1 layer lattice minerals the proton plays a role more similar to that of cation in the interlamellar space of micas rather than an exchange particle coordinating the layers.

In this sense, cohesion in these minerals is not due to hydrogen bonding.

A critical examination of the intercalation process of kaolinite seems interesting in view of this statement since it has been usually considered that the intercalation agents were mainly active by breaking the "hydrogen bonds" between the layers.

THE ENERGY BALANCE IN KAOLINITE  
INTERCALATION PROCESSES

Consider the intercalation process



where  $K_0$  is the kaolinite lattice in the initial state,  $K_i$  the intercalated lattice:  $\Delta H$  must be of the order of magnitude of  $E$  in order for the intercalation reaction to proceed at a measurable rate.

According to Jacobs and Sterckx (1970) and in good agreement with Weiss et al. (1966), in the expanded kaolinite lattice there are 1.5 DMSO molecule per unit cell. Each DMSO molecule reacts with 2 OH forming with them hydrogen bonds appreciably stronger than

Table II

Position of the perturbed hydroxyl stretching frequencies in kaolinite complexes.

Complexes	OH Frequency (cm <sup>-1</sup> )	Ref.
Formamide	3590	M. Cruz, A. Laycock and J. L. White (1969)
Urea	3585-3560 (shoulder)	M. Cruz, A. Laycock and J. L. White (1970)
Methyl urea	3595 3540 3515	idem
Dimethyl urea	3565 3515	idem
Methyl formamide	3550	M. Cruz, A. Laycock and J. L. White (1969)
Dimethylsulfoxide	3546 3507	H. Jacobs and M. Sterckx (1970)
Dimethylformamide	3415	M. Cruz, A. Laycock and J. L. White (1969)

the initial hydrogen bonds in kaolinite. The average frequency shift is  $225 \text{ cm}^{-1} = 3750-3525 \text{ cm}^{-1}$  for these OH. This corresponds to an energy of the order of 5 kcal per bond and thus a contribution to  $\Delta H$  of  $3 \times 5 \text{ kcal (K}_i) - 4 \times 1 \text{ kcal (K}_o) = 11 \text{ kcal}$ .

As shown in Table II, it is a matter of fact that intercalation agents shift the high frequency stretching bands of kaolinite within a range of 150 to  $350 \text{ cm}^{-1}$ .

However this contribution is obviously not high enough to account for the intercalation. The formation of stronger hydrogen bonds between the intercalating molecules and the internal surface OH may provide the chemical driving force but the energy balance is still not favorable.

The dielectric constant ( $\epsilon$ ) of liquid DMSO is 48.9 at  $20^\circ\text{C}$ . As soon as a few molecules have gone inside the layers on the edges of the crystal the electrostatic attractive force is strongly decreased by the high increase of the dielectric constant and this is most probably the important energetic factor.

This hypothesis is in line with the observation by Olejnik et al. (1968) who have shown that the rate of intercalation is increased by adding some water ( $\epsilon \approx 80$ ) to the intercalating agent. It is interesting to note also that according to the same work, the intercalation rate is higher in dickite (API 15) than in kaolinite (API 9) although these two samples have similar surface areas. This is in good agreement with a higher contribution of electrostatic energy to cohesion (Table I).

Finally since lattice defects should influence much more the electrostatic contribution than the hydrogen bond contribution (in the sense defined above) or the van der Waals contribution, it is understandable that particle size is an important factor, as outlined by Wiewiora and Brindley (1969). It may thus be concluded that the characteristics reported so far for the intercalation process favor the idea developed here, namely that cohesion in kaolinite minerals is not due to hydrogen bonding.

#### ACKNOWLEDGEMENTS

We wish to thank deeply Professor Giese of the State University of New York at Buffalo for unpublished data which were essential for the discussion and Professor J. White of Purdue University for stimulating discussion on intercalation.

## REFERENCES

- BARRER, R.M. and GOUGHLAN, B. (1968): Influence of crystal structures upon zeolitic carbon dioxide. I. Isotherms and selectivity. *Molecular Sieves*, 233, Soc. Chem. Ind., London.
- BRINDLEY, G.W. (1961): The X-ray identification and crystal structure of clay minerals. The Mineralogical Society, London 2d edition, p. 60.
- CRUZ, M., LAYCOCK, A., and WHITE, J.L. (1969): Perturbation of OH groups in intercalated kaolinite donor-acceptor complexes. I. Formamide, methyl formamide and dimethyl formamide kaolinite complexes. *Proc. Inter. Clay Conference, Tokyo*, 1, p. 785-789.
- CRUZ, M., LAYCOCK, A., and WHITE, J.L. (1970): Les complexes de la kaolinite avec l'uree et ses derives methyles. *Reunion Hispano-Belga de Minerale de la Arcilla, Madrid*, p. 148.
- FARMER, V.C. (1964): I. R. Absorption of OH groups in kaolinite. *Science*, 145, p. 1189-1190.
- GIESE, R.F., JR., and DATTA, P. (1971): Hydroxyl orientation in kaolinite, dickite and nacrite. (to be published).
- GIESE, R.F., JR. (1972): Interlayer bonding in kaolinite, dickite and nacrite. (to be published).
- GRIM, R.E. (1953): *Clay mineralogy*. McGraw-Hill, p. 48
- HENDRICKS, S.B. (1939): The crystal structure of nacrite and the polymorphism of the kaolin minerals. *Zeitsch. fur Kristallographie*, 100, p. 509-518.
- JACOBS, H., and STERCKX, M. (1970): Contribution a l'etude de l'intercalation du dimethyl sulfoxide dans le reseau de la kaolinite. *Reunion Hispano-Belga de Minerale de la Arcilla, C.S.I.C., Madrid*, p. 154.
- LEDoux, R. and WHITE, J.L. (1964): I. R. Study of the OH groups in expanded kaolinite, *Science*, 143, p. 244-246.
- LIPPINCOTT, E.R. and SCHROEDER, R. (1965): One dimensional model of the hydrogen bond. *The Journal of Chem. Phys.*, 23, p. 1099-1106 (1965).
- OLEJNIK, S., AYLMORE, S., POSNER, A.M. and QUIRK, J.P. (1968): Infrared spectra of kaolin mineral-dimethyl sulfoxide complexes. *J. Phys. Chem.*, 72, 241.
- PAMPUCH, R., and WILKOS, K. (1963): Assignment of I. R. absorption bands in the hydroxyl region of kaolin group minerals and kaolinitic clays. 7th. Conference on the Silicate Industry, Budapest, , p. 179-182.
- ROUXHET, P.G. and FRIPIAT, J.J. (1971): Effet de la temperature sur l'intensite apparente des bandes de vibration de valence OH de solides inorganiques. *Bull. Classe des Sciences. Acad. Royal de Belgique* 57, 101-123.
- WEISS, A., THIELEPOPE, W. and ORTH, H. (1966): Neue Kaolinit - Einlagerungs-verbindungen. *Proc. Int. Clay Conf.*, Jerusalem,

1, 277-293 (1966).

WIEWIORA, A.W. and BRINDLEY, G.W. (1969): Potassium acetate intercalation in kaolinite and its removal; effect of material characteristics. Proc. Int. Clay Conf., Tokyo, 1, p. 723-739.

# ELECTRON SPIN RESONANCE STUDIES OF KAOLINS

B.R. Angel and P.L. Hall

Department of Physical Sciences  
Plymouth Polytechnic, Plymouth, Devon, England

**ABSTRACT.** - Previous studies of electron spin resonance in clay minerals have been extended. The most intense features of the spectra of three clays, centred at  $g$ -values of 2.0 and 4.2, are not significantly affected by the presence of exchangeable cations, organic matter or mineralogical impurities, except for variations in the lineshape and intensity of the  $g = 4.2$  feature caused by the presence of micaceous impurities, which could be reproduced by mixing kaolinite with powdered muscovite in varying proportions.

By studying the changes in the E.S.R. spectra of the samples caused by preferential orientation, X-irradiation, or thermal treatment, it is concluded that the observed features may be attributed to  $\text{Fe}^{3+}$  ions occupying three distinct sites in the kaolinite structure, together with small contributions from trapped hole centres.

Marked changes in the spectra occur for samples heated at or above the dehydroxylation temperature, and are discussed in terms of the kaolinite-metakaolin phase transformation.

## INTRODUCTION

Relatively few reports of electron spin resonance (ESR) in clay minerals have been published. Boesman and Schoemaker (1961) reported two resonances common to a number of kaolins; a 3-line resonance centred at  $g = 4.2$ , attributed to  $\text{Fe}^{3+}$  replacing  $\text{Si}^{4+}$  in distorted tetrahedral sites, and an asymmetric 2-line resonance at  $g = 2.0$  attributed to  $\text{Fe}^{3+}$  replacing  $\text{Al}^{3+}$  in axially distorted octahedral sites. In contrast, Freidlander et. al. (1963) suggested that resonances at  $g = 2.0$  in samples of kaolinite, illite and montmorillonite were due to free radicals possibly related to humic acids

present in residual organic matter. However, Wauchope and Haque (1971) showed that the resonances at  $g = 2.0$  in kaolinite and montmorillonite were unaffected by chloroform extraction or oxidising agents, and therefore suggested that they were due to paramagnetic defects located within the clay mineral structures. Hall, Angel and Braven (1972) investigated the ESR spectra of a closely related South Devon ball clay and lignite and solvent extracts from both materials, and showed that resonances due to stable organic free radicals occurred in each fraction but could not account for the asymmetric  $g = 2.0$  resonance in the ball clay.

A detailed ESR study of an illitic mica (Matyash et al., 1969) has indicated the presence of a resonance at  $g = 4.37$  characteristic of isolated  $Fe^{3+}$  ions occupying sites of orthorhombic symmetry, together with a broad resonance at  $g = 2.03$  characteristic of strong exchange interactions between clusters of paramagnetic centres. Similar resonances have been observed in muscovite and phlogopite (Kemp, 1971) and in a synthetic fluorophlogopite (Novozhilov et al., 1970).

None of the previous studies have considered the possible effect of mineralogical impurities, point defects, exchangeable cations or the possibility of preferred orientation upon the ESR phenomena. In the present work, an attempt has been made to clarify the interpretation of the ESR spectra of natural and calcined kaolins taking these factors into account.

## EXPERIMENTAL

The samples investigated in this work consisted of two kaolins and one ball clay. The kaolins, supplied by English Clays, Lovering, Pochin & Co. Ltd., St. Austell, England, consisted of a St. Austell clay of particle size distribution 94% <  $2 \mu$  e. s. d., and a Georgia clay which was predominantly <  $5 \mu$  e. s. d.

The ball clay, supplied by Watts, Blake, Bearne & Co. Ltd., Newton Abbot, Devon, England, is a sample typical of the South Devon ball clays and has been described elsewhere (Hall, Angel and Braven, 1972). The analyses of the chemical and mineralogical composition of these samples are given in Table I.

The ESR spectra reported here were all recorded at X-band. Spectra of the three clay samples covering the magnetic field range 0 - 6 kG are illustrated in Fig. 1, which shows the two principal resonances at  $g = 2.0$  (A) and  $g = 4.2$  (B).

The spectra of the three clays differ mainly in the relative intensities of resonances A and B, and in the lineshape associated with resonance B, the central line at  $g = 4.2$  being more intense in the Georgia kaolinite and the South Devon ball clay. The Georgia kaolinite exhibits a number of additional weak resonance lines centred at about  $g = 2.0$  (C), due to a vanadium impurity. An investigation by the au-

TABLE 1. Chemical and mineralogical analyses of samples. (Total iron concentration calculated as  $\text{Fe}_2\text{O}_3$ ).

	<u>St. Austell Kaolinite</u>	<u>Georgia kaolinite</u>	<u>S. Devon ball clay</u>
$\text{SiO}_2$	46.6	-	48.5
$\text{Al}_2\text{O}_3$	38.3	38.6	31.9
$\text{Fe}_2\text{O}_3$	0.49	0.46	1.08
$\text{TiO}_2$	0.05	1.75	0.90
$\text{MgO}$	0.20	-	0.28
$\text{CaO}$	0.20	-	0.15
$\text{K}_2\text{O}$	0.68	-	1.68
$\text{Na}_2\text{O}$	0.07	-	0.20
Ign	13.4	-	15.6
<hr/>			
Kaolinite	94%	98%	67.5%
Mica/Illite	5 - 6%	1%	19%
Quartz	-	-	7.5%
Anatase	-	1%	-
Rutile	-	Tr.	-
Carbonaceous matter	Tr.	-	6%

thors of similar resonances in a number of clay minerals is to be reported shortly, and the lines are not considered further here.

Washing the clays with dilute acids or preparation of their hydrogen-exchanged forms produced no changes in the spectra. In addition, the only effect of removing part of the micaceous impurities from the St. Austell kaolinite by magnetic extraction was to produce a very slight reduction in the intensity of the central peak of resonance B.

Removal of the organic matter from the ball clay by successive benzene-methanol extraction and hydrogen peroxide treatment had only a marginal effect on resonances A and B (Hall, Angel and Braven, 1972). Similar treatments applied to the two kaolinites had no effect on the ESR spectra.

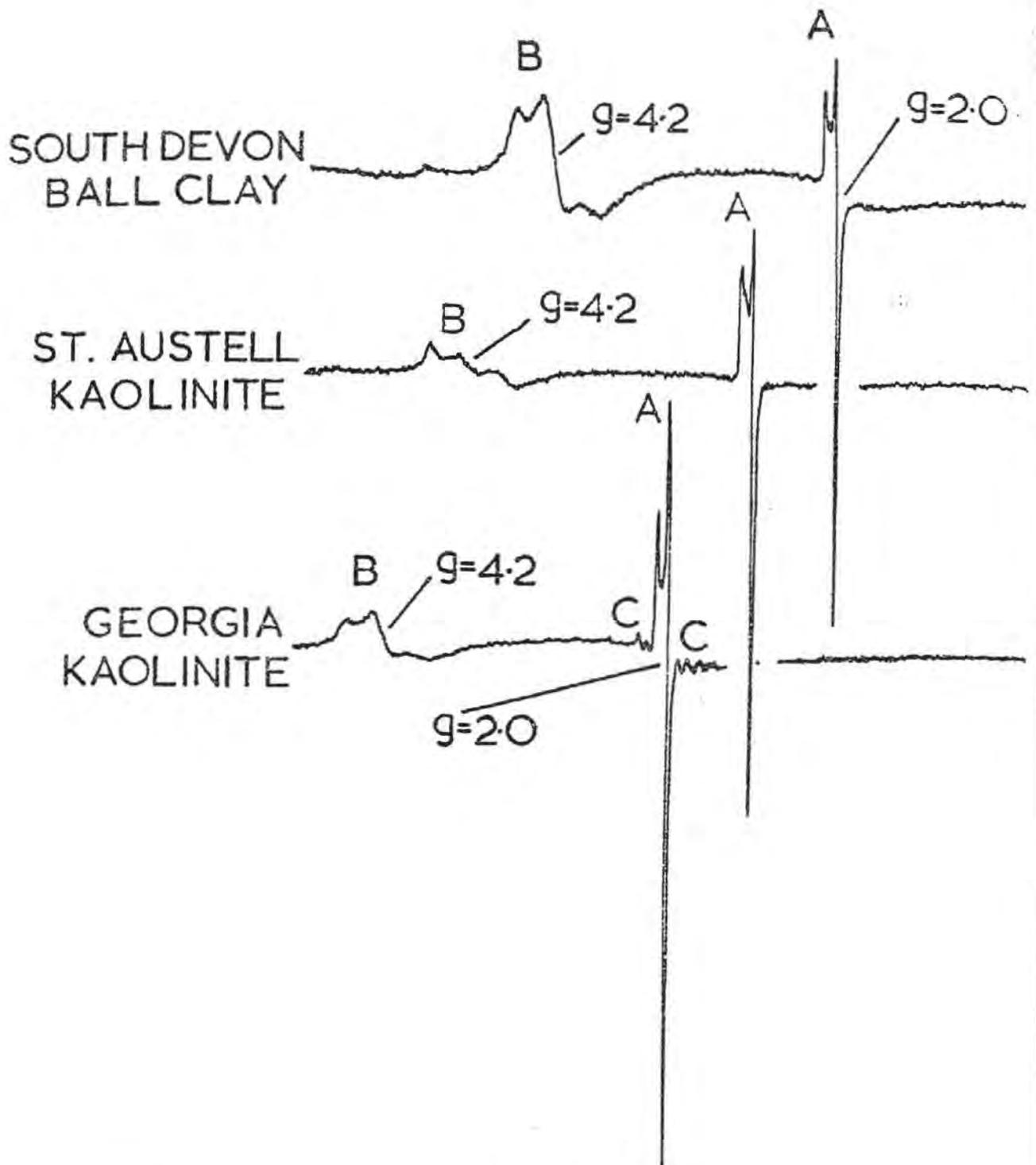


Figure 1. ESR spectra over the range 0 - 6 kG recorded at room temperature

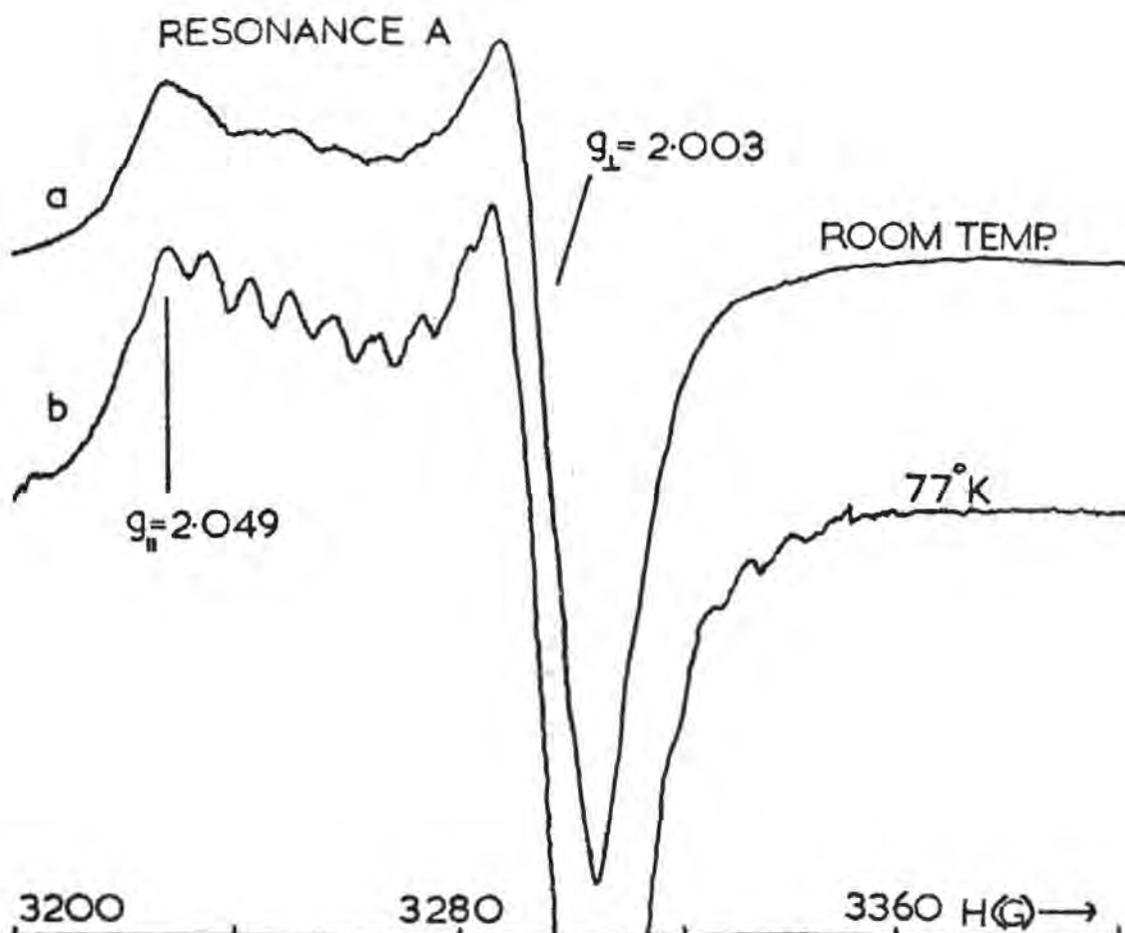


Figure 2. ESR spectra of the  $g = 2.0$  region of St. Austell kaolinite (a) at room temperature; (b) at 77°K.

The resonances A and B were studied in more detail and are now considered in turn. Fig. 2 (a) illustrates resonance A of St. Austell kaolinite at room temperature on an expanded scale. The observed lineshape is characteristic of a paramagnetic centre in an axially symmetric environment in a powder sample (Searl et. al., 1961). From the spectrum we obtain the principal values of the  $g$ -tensor as  $g_{\parallel} = 2.049 \pm 0.001$ ;  $g_{\perp} = 2.003 \pm 0.001$ .

The measured concentration of unpaired spins calculated by a numerical double integration technique (Hall, 1972) is approximately  $3.2 \times 10^{18}$  spins/gram. The only chemically detectable paramagnetic impurity which could account for a resonance with this intensity is iron. The presence of point defects could provide an alternative explanation.

Figs. 2 (a) and 2 (b) show that at least six weak lines are observed between the main peaks of resonance A and are considerably enhanced when the sample is cooled to 77°K. This effect was common to all three samples. Preheating the clays for 24 hours at 200°C or for 2 hours at 300°C removed the subsidiary lines without causing any

measurable changes in the main peaks. In contrast, irradiation of untreated and heated clays with 40 kV X-rays reproduced and considerably enhanced the subsidiary lines without causing any change to the main peaks. It was considered probable, therefore, that a point defect characterized by a resonance with a positive  $g$ -shift, such as a vacancy or trapped hole centre, contributed to the  $g = 2.0$  resonance at room temperature and below, and was annealed in the heated samples. A discussion of the possible nature of such a centre is given later.

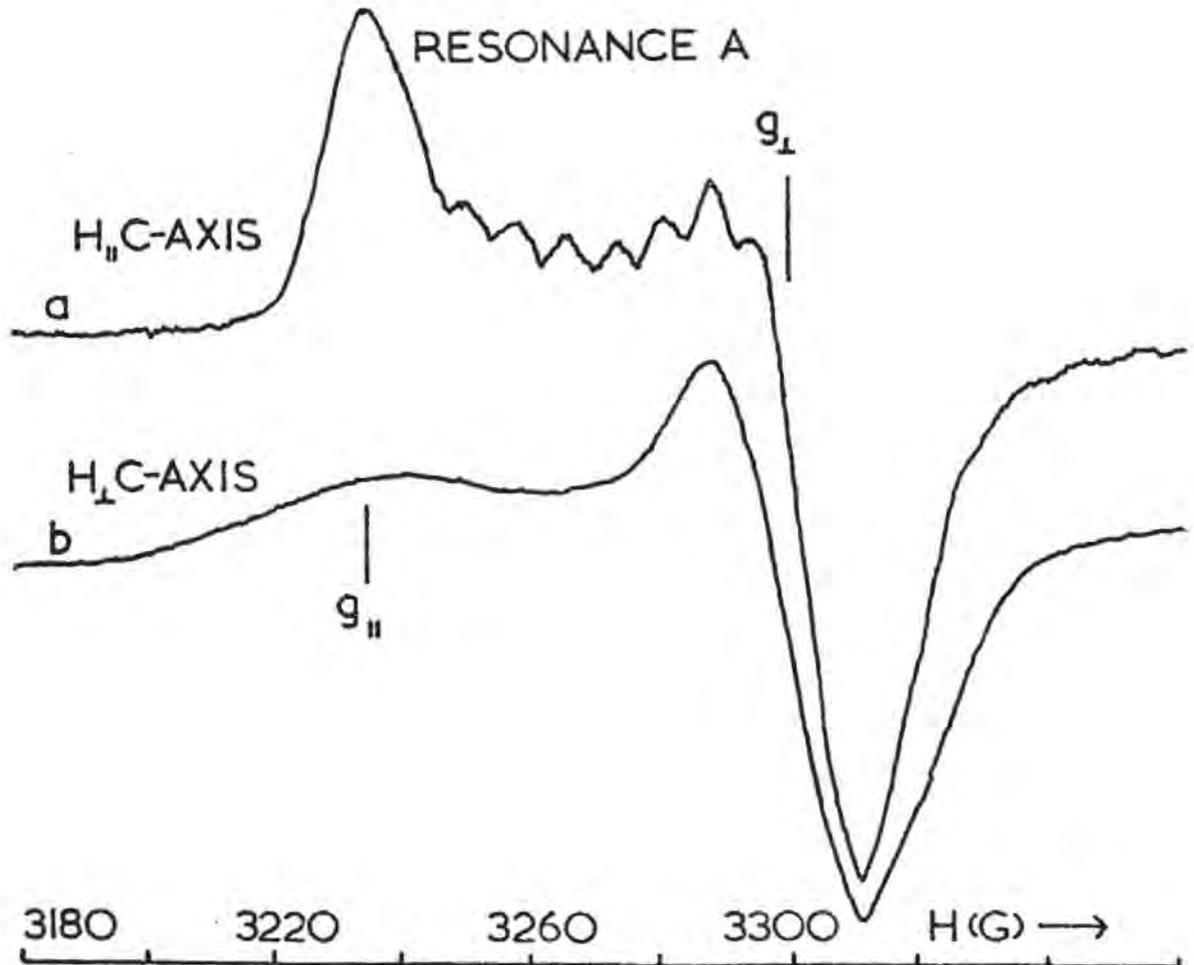


Figure 3. ESR spectra of St. Austell kaolinite pressed disc ( $g = 2.0$  region) with applied magnetic field (a) perpendicular and (b) parallel to disc plane.

A complete investigation of the nature of the main asymmetric resonance A was not possible since no single crystals of kaolinite large enough for studies of the effect of crystal orientation on the ESR spectra were available. Nevertheless valuable information was obtained by

investigating the effects of partial alignment of a bulk sample. Samples of St. Austell kaolinite were pressed into discs using a hydraulic press. A fairly high degree of preferential orientation was obtained, with the basal planes of the particles predominantly in or near to the disc plane. The ESR spectra of the discs were then recorded at room temperature with the discs orientated either perpendicular or parallel to the applied magnetic field, corresponding to the magnetic field being aligned either approximately parallel or perpendicular to the kaolinite c-axis. The spectra are illustrated in Figs. 3(a) and 3(b), respectively.

The results clearly indicate an enhancement of each of the component lines in turn, the line at the lower field value (corresponding to  $g_{\parallel}$ ) being enhanced when the magnetic field is approximately perpendicular to the disc plane (Fig. 3(a)) and the line at the higher field value (corresponding to  $g_{\perp}$ ) being enhanced when the field is parallel to the plane of the disc (Fig. 3(b)). These results indicate that the axis of symmetry of the centre lies close to the kaolinite c-axis. In addition, it is notable that the intensity and resolution of the lines which can be attributed to a hole centre are enhanced when the magnetic field is perpendicular to the disc plane.

Results similar to those just described were obtained using a sample in which preferred orientation was obtained by sedimentation from Colombia, South America.

For the resonances in the region of  $g = 4.2$ , previous studies (Hall, Angel and Braven, 1972) have shown that  $Fe^{3+}$ -organic complexes make only a small contribution to the ESR spectrum of the ball clay. Furthermore, the two kaolins contained little or no organic matter. It was therefore considered unlikely that such species could ac-

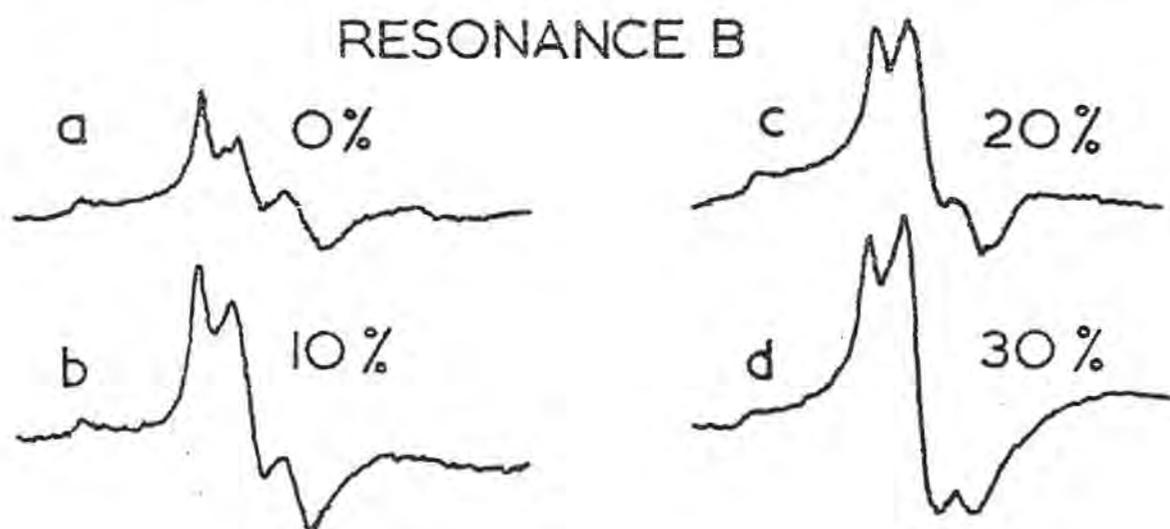


Figure 4. Resonance B in kaolinite-muscovite mixtures: (a) 0% muscovite, (b) 10%, (c) 20%, (d) 30%.

count for the marked variations in lineshape and intensity of the resonances in the three clays reported here. However, the occurrence of resonances in the  $g = 4.2$  region in micas have been reported (Matyash et. al., 1969), and the effect of micaceous impurities was therefore taken into consideration.

In this work, the effect of such impurities on resonance B was studied by recording the ESR spectra of mixtures of St. Austell kaolinite with powdered muscovite. Differences in the lineshape of resonance B similar to those occurring between the natural clays were easily demonstrated. In Fig. 4 (a) - (d) the spectra of mixtures containing 0, 10, 20 and 30 % muscovite respectively are illustrated.

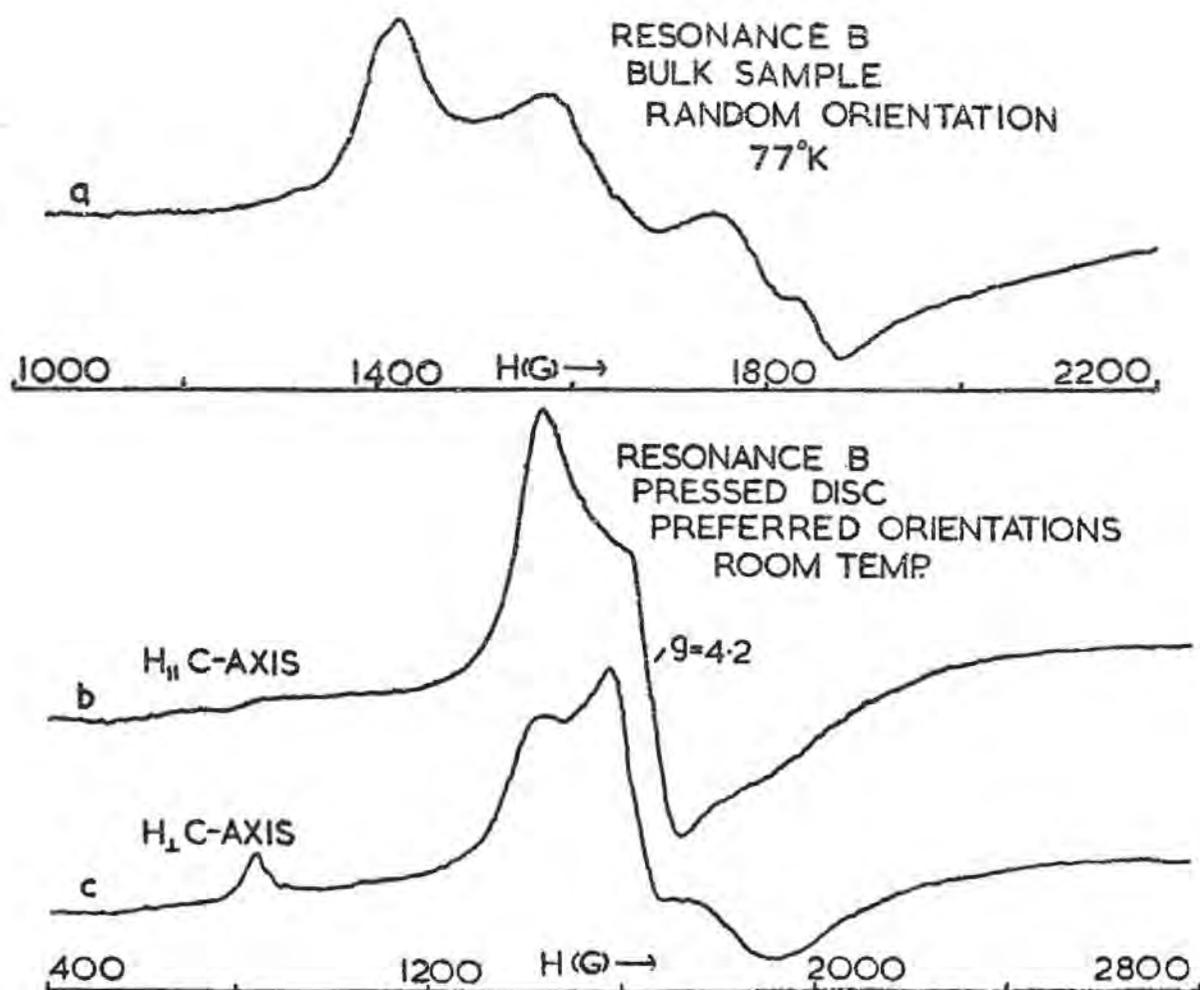


Figure 5. ESR spectra of St. Austell kaolinite, low-field region. (a) Bulk sample at 77°K; (b) Pressed disc, H perpendicular to disc plane; (c) Pressed disc, H parallel to disc plane.

These results provide one explanation for the differences in lineshape between the ball clay (containing ~19 % mica) and the St. Austell kaolinite (containing ~5 % mica), but is not consistent for the Georgia kaolinite, whose mica content is extremely low, and yet has a lineshape similar to that of the ball clay, though of lower intensity. Another effect was therefore sought in order to fully explain the observed variations in lineshape for all three samples.

By recording the low-field region of the spectrum of St. Austell kaolinite at 77°K it was possible to resolve a fourth line (Fig. 5 (a)). The  $g$ -values of the four lines were estimated as being approximately 4.9, 4.2, 3.7 and 3.5. In addition, it was found that for the pressed discs, regardless of the orientation with respect to the magnetic field, the intensity, shape and position of the line at  $g = 4.2$  remained constant, while significant changes occurred in the remainder of the spectrum (Figs. 5 (b) - 5 (c)).

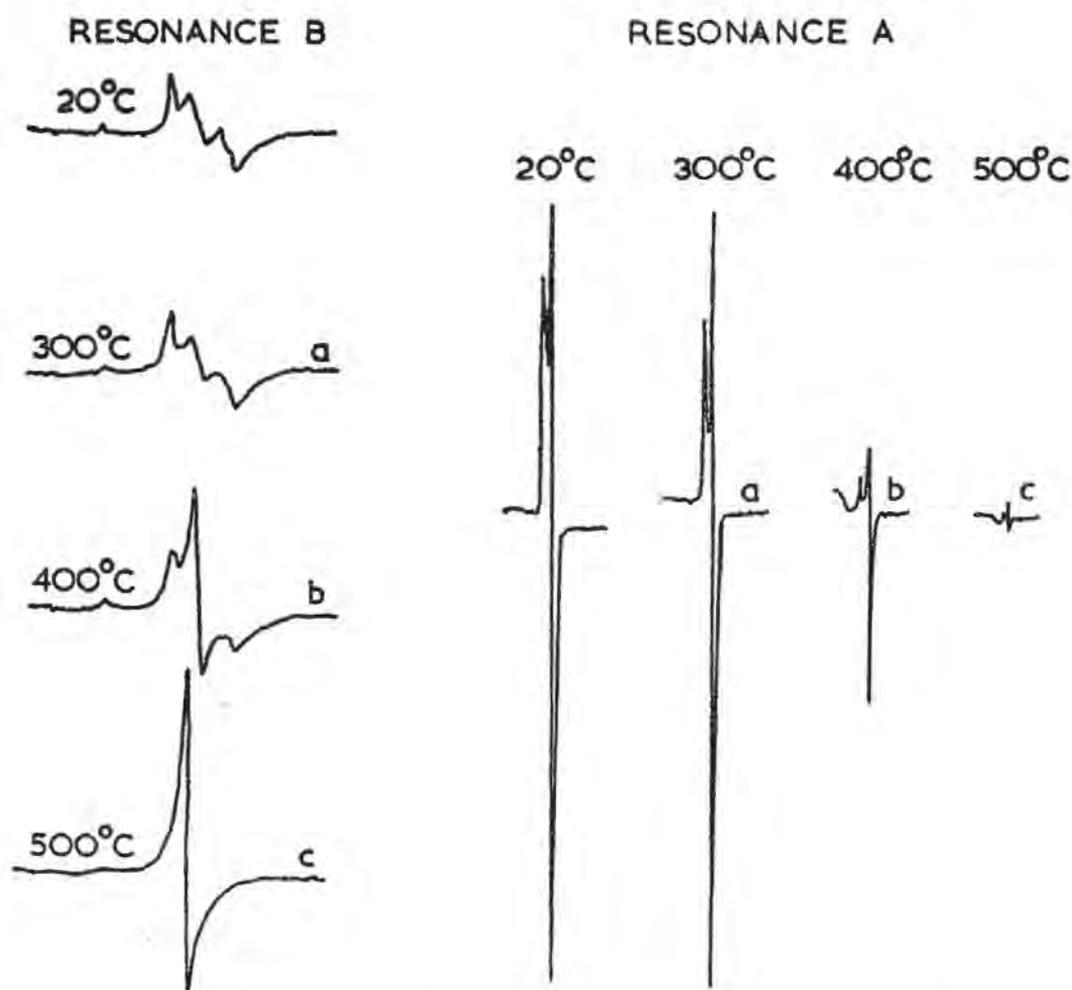


Figure 6. ESR spectra of heated St. Austell kaolinite (a) 24 hrs. at 300°C; (b) 24 hrs. at 400°C; (c) 24 hrs. at 500°C.

These results suggest that resonance B is probably a composite feature due to two overlapping resonances arising from two distinct centres:

Centre I: a system giving a single isotropic line at  $g = 4.2$ .

Centre II: a system giving three lines having principal  $g$ -values

$$g_z = 4.9; g_x = 3.7; g_y = 3.5$$

Theoretical considerations which favour this assignment are included in the discussion.

Further supporting evidence for the existence of centres I and II was obtained by studying the effect of thermal treatment on the ESR spectra.

Samples of St. Austell kaolinite were heated in air for 24 hours at various temperatures up to 1000°C. Marked changes in the spectra occurred for samples heated at or above the dehydroxylation temperature. Fig. 6 illustrates the spectra of St. Austell kaolinite in the regions of  $g = 4.2$  and  $g = 2.0$  after heating at various temperatures.

It can be seen that the spectrum characteristic of the unheated clay persists up to pre-heating temperatures of 300°C, except for the annealing out of the weak lines attributed to trapped hole centres, as described previously. In the sample heated at 400°C (Fig. 6(b)) the spectra show two main changes:

- (i) The main  $g = 2.0$  resonance (A) is markedly reduced in intensity;
- (ii) The isotropic line at  $g = 4.2$  (Resonance B) has increased in intensity in comparison with the other lines in the low-field region.

Heating at temperatures of 500°C and above causes an elimination of the  $g = 2.0$  resonance, together with a collapse of the low-field resonance to a single line of width about 50 gauss at  $g = 4.2$  (Fig. 6(c)). These transitions in the ESR spectra coincide with both the collapse of the kaolinite X-ray diffraction pattern to the broad, diffuse band characteristic of metakaolin and to the related changes in the hydroxyl bands in the infrared spectrum.

## DISCUSSION OF RESULTS

### Resonances at $g = 2.0$

Apart from the small contribution made by point defects to the main asymmetric resonance (A) at  $g = 2.0$ , and contributions from organic free radicals, which may be significant in organic-rich clays (Hall, Angel and Braven, 1972), the main features of the resonance were unaffected by a variety of physical and chemical treatments which

would be expected to produce and anneal point defects and to remove organic matter and surface-adsorbed or dispersed mineralogical impurities. It is therefore concluded that none of these are likely to be responsible for the resonance.

The only chemically detectable paramagnetic ion in the clays which can satisfactorily account for the occurrence of the resonance with the observed spin concentration is  $\text{Fe}^{3+}$ .

The substitution of  $\text{Fe}^{3+}$  for  $\text{Al}^{3+}$  in kaolinite is fairly well established (Grim, 1968), and in particular Malden and Meads (1967) have demonstrated by Mössbauer spectroscopy the occurrence of  $\text{Fe}^{3+}$  in the octahedral sites of a St. Austell kaolinite similar to that used in the present work.

The disappearance of the resonance following the kaolinite-metakaolin phase transformation may be attributed to a change in the local symmetry of the octahedrally coordinated ferric ions since at the same time the single-line resonance at  $g=4.2$  exhibits a corresponding increase in intensity. It is suggested that this is consistent with an increase in the number of ferric ions occupying distorted tetrahedral configurations after the change in  $\text{Al}^{3+}$  coordination from 6 to 4 (Brindley and Nakahira, 1959).

As further experimental evidence for the assignment of resonance A to octahedrally coordinated  $\text{Fe}^{3+}$  ions, we mention that treatment of two of the clays with acid fluoride solutions, known to attack principally the octahedral layer (Semmens, 1965), resulted in significant changes in the  $g = 2.0$  resonance, details of which are to be published shortly.

The axial symmetry associated with the  $g = 2.0$  resonance in kaolinites may be related to the well-known distortions from ideal octahedral symmetry via a flattening of shared octahedral edges (Radoslovich, 1963). The results obtained from the preferentially orientated bulk samples are in accordance with this conclusion.

Weak broad resonances which have been observed in the  $g = 2.0$  region in natural and calcined clays have not been considered here, but are probably attributable to exchange interactions between clusters of  $\text{Fe}^{3+}$  ions. We have observed intense broad resonances in samples of muscovite, phlogopite and biotite in which the concentration of substitutional iron is greater than in the clays and therefore more likely to produce this effect.

The subsidiary lines between the main peaks of resonance A are most probably due to a hole centre interacting with an  $^{27}\text{Al}$  nucleus, whose spin  $I = 5/2$  would account for the predominant 6-line hyperfine structure. The hyperfine splitting parameter of  $7.7 \pm 0.2$  gauss and  $g$ -value  $2.03 \pm 0.01$  are not far removed from values previously reported by Griffiths et. al. (1955) for a defect centre in irradiated natural quartz crystals, and by Lee and Bray (1962) for a similar centre in irradiated aluminosilicate glasses which consisted of a trapped hole centre located on an Al-O bond following aluminium substitution for silicon. It is suggested that a small degree of  $\text{Al}^{3+}$

substitution in the tetrahedral sheet of kaolinite could account for the observed features. Considerable enhancement of the centres by X-irradiation has been demonstrated. It is considered possible that the weak lines in the natural clays may arise from natural background radiation.

The enhancement of the hole-centre spectrum caused by irradiation or cooling to low temperatures reveals the presence of additional lines, indicating that the system is fairly complex and probably involves multiple nuclear hyperfine interactions. Further ESR studies of defect centres induced by X-irradiation of aluminosilicate minerals are currently in progress in this laboratory.

### Resonances at low fields

Resonances at low field values corresponding to  $g$ -values of about 4.2 have been observed for  $\text{Fe}^{3+}$  replacing  $\text{Si}^{4+}$  in silicate glasses, and subsequently in a larger number of materials containing  $\text{Fe}^{3+}$  impurity centres (Castner et. al. 1960; Kedzie et. al. 1965, Matyash et. al. 1969). The theory appropriate to resonances of this type has been outlined by Griffith (1964), Holuj (1966) and Blumberg (1967) among others.

For powder samples, the spectra may be described by a Spin Hamiltonian of the form.

$$\mathcal{H} = g\beta H \cdot S + D[S_z^2 - \frac{1}{3}S(S+1)] + E[S_x^2 - S_y^2]$$

where the effective spin,  $S$ , for the  $\text{Fe}^{3+}$  ion is  $5/2$ , and  $D$  and  $E$  are energy terms related to the axial and rhombic components of the local crystal field at the  $\text{Fe}^{3+}$  sites. If  $D$  and  $E$  are much greater than the Zeeman term,  $g\beta H$ , it can be shown that resonances at  $g$ -values greatly removed from the free spin value can occur. In particular, if  $E/D = 1/3$ , representing completely orthorhombic symmetry, an isotropic resonance at  $g = 4.28$  is predicted, together with resonances described by extremely anisotropic  $g$ -tensors, from which weak lines at lower magnetic fields, corresponding to  $g$ -values up to about  $g = 9$ , may be expected.

If the value of the ratio  $E/D$  is less than  $1/3$ , representing a symmetry of partially orthorhombic character, it can be shown that instead of an isotropic resonance at  $g = 4.28$ , an anisotropic resonance having three principal  $g$ -values is expected. The position of the principal  $g$ -values depends both on the ratio  $E/D$  and the relative magnitude of  $D$ (or  $E$ ) and  $g\beta H$ . The averaging out of such an anisotropic resonance in a powder sample gives rise to a characteristic lineshape (Kneubuhl, 1960) similar to that observed in kaolinite. On this basis, and using the perturbation calculation of Castner et. al., (1960), Boesman and Schoemaker (1961) interpreted the resonance in terms of  $\text{Fe}^{3+}$  replacing  $\text{Si}^{4+}$  in distorted sites of approximately orthorhombic symmetry, and measured the principal  $g$ -values from their spectrum as 5.00, 4.16, and 3.52.

The difficulty of making accurate g-value measurements from powder spectra makes any detailed assignment slightly tentative, but a closer examination of the argument of Boesman and Schoemaker reveals that their use of perturbation theory is untenable, and that the more rigorous exact computational solutions of the Spin Hamiltonian given by Dowsing and Gibson (1969) show that in no case would three equally spaced g-values of 5.00, 4.16, and 3.52 be expected. However, for certain symmetries, two of the three principal g-values may be fairly close together, and might not give rise to well-resolved lines in a powder spectrum.

We therefore suggest that the resonance B in kaolinite is a superimposition of resonances arising from two centres:

Centre I :  $\text{Fe}^{3+}$  ions occupying sites of orthorhombic symmetry, with  $E/D = 1/3$ , giving rise to an isotropic line at  $g = 4.2$ .  
Centre II :  $\text{Fe}^{3+}$  ions occupying sites of partially orthorhombic character, having  $E/D < 1/3$  and principal g-values (referred to a proper axis system, as described by Blumberg (1967)),  $g_z = 4.9$ ,  $g_x = 3.7$ ,  $g_y = 3.5$ .

The weak line at about  $g = 8.8$  in all three clays probably arises from an extremely anisotropic g-tensor which may be related to either of the two centres.

A precise fitting of the parameters of the Spin Hamiltonian to the principal g-values of Centre II is currently in progress using an exact computational method (Dowsing, 1972) in conjunction with ESR spectra obtained at Q-band. However, we have found close agreement between calculated and observed g-values by a perturbation treatment if it is assumed that  $E/D = 0.22$  and that  $D \gg g\beta H$ . (At X-band, the Zeeman energy corresponds to about  $0.3 \text{ cm}^{-1}$ ). This calculation gives  $g_x = 3.89$ ,  $g_y = 3.53$ ,  $g_z = 4.94$  which compares favourably with measured values  $g_x = 3.7$ ,  $g_y = 3.5$ , and  $g_z = 4.9$ .

It is suggested that centres I and II may both be explained in terms of  $\text{Fe}^{3+}$  ions substituting for  $\text{Si}^{4+}$  in distorted tetrahedral sites, one possible explanation for the difference in symmetry between the centres being differences in the mechanism of charge compensation. Variations in the relative population of the two centres would then account in part for the observed lineshape differences in different samples. [It is noteworthy that evidence for tetrahedrally coordinated  $\text{Fe}^{3+}$  ions in a number of layer silicates has been obtained from Mössbauer spectroscopy (Taylor et. al., 1968)].

The effect of heat treatment on the ESR spectra of kaolinites may then be explained in the following manner;  $\text{Fe}^{3+}$  ions replacing  $\text{Al}^{3+}$  and giving rise to resonance A at  $g = 2.0$  experience a change in environment on dehydroxylation, and occupy sites having the symmetry of Centre I in the disordered metakaolin structure (Fig. 6 (b) and (c)). At the same time, a conversion of Centre II to Centre I occurs, the latter representing the stable environment for  $\text{Fe}^{3+}$

ions in the metakaolin structure. It is notable that the lineshape observed in metakaolin closely resembles that observed for  $\text{Fe}^{3+}$  ions in tetrahedral silicon sites in glasses (Castner et. al., 1960).

In summary, the principal features of the ESR spectra of kaolinites may be attributed to a number of centres.

- (1)  $\text{Fe}^{3+}$  ions occupying axially distorted octahedral sites;
- (2)  $\text{Fe}^{3+}$  occupying a site of orthorhombic symmetry (Centre I);
- (3)  $\text{Fe}^{3+}$  occupying a site of partially orthorhombic symmetry (Centre II);
- (4) At least one type of point defect, probably a trapped hole centre interacting with an aluminium nucleus, which may be reversibly induced and destroyed by irradiation and thermal annealing.

In addition, small contributions to the  $g = 2.0$  resonance from organic free radicals or weak broad resonances due to strongly interacting clusters of paramagnetic centres may be observed.

Further ESR studies of natural and irradiated aluminosilicate minerals are currently in progress. Clearly, the technique of ESR spectroscopy can provide detailed information regarding the nature of the paramagnetic impurities and defect centres in clay minerals and their higher temperature phases which it is hoped may contribute to the knowledge of the structure of disordered and X-ray amorphous phases.

#### ACKNOWLEDGEMENTS

Our thanks are due to the Board of Governors of Plymouth Polytechnic for the provision of research facilities and for the award to one of us (P.L.H.) of a Research Assistantship; to Watts, Blake, Bearne & Co. Ltd. and English Clays, Lovering, Pochin & Co. Ltd. for supplying samples and analytical data; to Professor G.W. Brindley for supplying an orientated kaolinite stack from Colombia, S. America; and to Dr. R.D. Dowsing for assistance with computer programming.

#### REFERENCES

- BLUMBERG, W.E. (1967); In: Magnetic Resonance in Biological Systems, Ehrenberg, A. and Vänngård, T., editors, Pergamon, New York.
- BRINDLEY, G.W. and NAKAHIRA, M. (1959): The kaolinite-mullite reaction series. *J. Amer. Ceram. Soc.*, 42, 311 - 324.

- BOESMAN, E. and SCHOEMAKER, D. (1961): Resonance paramagnetique de l'ion  $Fe^{3+}$  dans la kaolinite. *Compt. Rend. Acad.Sci.*, 252, 1931 - 1933.
- CASTNER, T., NEWELL, G.S., HOLTON, W.C. and SLICHTER, C.P. (1960): Note on the paramagnetic resonance of iron in glass. *J. Chem. Phys.*, 32, 668 - 673.
- DOWSING, R.D. (1972); Private communication.
- DOWSING, R.D. and GIBSON, J.F. (1969): Electron spin resonance of high-spin  $d^5$  systems, *J. Chem. Phys.*, 50, 294 - 303.
- FRIEDLANDER, H.Z., FRINK, C.R. and SALDICK, J. (1963): Electron spin resonance spectra in various clay minerals. *Nature*, 199, 61 - 62.
- GRIM, R.E. (1968): *Clay Mineralogy*, 2nd ed., McGraw-Hill, New York.
- GRIFFITH, J.S. (1964): Theory of the isotropic g-value of 4.27 found for some high-spin ferric ions, *Mol. Phys.*, 8, 213 - 216.
- GRIFFITHS, J.H.E., OWEN, J. and WARD, I.M. (1955): In: Report of Conference on Defects in Crystalline Solids, p.81. Physical Society, London.
- HALL, P.L. (1972); Errors in the determination of ESR spin concentrations by numerical double integration, *J. Phys. D.*, 5.
- HALL, P.L., ANGEL, B.R. and BRAVEN, J. (1972): Electron spin resonance and related studies of lignite and ball clay from South Devon. To be published.
- HOLUJ, F. (1966): The Spin Hamiltonian and intensities of the ESR spectra originating from large zero-field effects on  $6S$  states. *Can. J. Phys.*, 44, 503 - 508.
- KEDZIE, R.W., LYONS, D.H. and KESTIGAN, M. (1965): Paramagnetic resonance of the  $Fe^{3+}$  ion in  $CaWO_4$ . *Phys. Rev.*, 138, A918 - A924.
- KEMP, R.C. (1971): Orthorhombic iron centres in muscovite and phlogopite micas. *J. Phys. C.*, 4, L11 - L13.
- KNEUBÜHL, F.K. (1960): Lineshapes of electron paramagnetic resonance signals produced by powders, glasses and viscous liquids. *J. Chem. Phys.*, 33, 1074 - 1078.
- LEE, S. and BRAY, P.J. (1962): Electron spin resonance studies of irradiated aluminosilicate glasses. *Phys. Chem. Glasses*, 3, 37 - 41.
- MALDEN, P.J. and MEADS, R.E. (1967): Substitution by iron in kaolinite. *Nature*, 215, 844 - 846.
- MATYASH, I.V., POL'SHIN, E.V. and KALINICHENKO, A.M. (1969): Investigation of the effect of thermal treatment on hydromica by radiospectroscopy. *Geokhimiya*, 7, 840 - 845.
- NOVOZHILOV, A.I., SAMILOVICH, M.I., ANIKIN, I.M. and SERGEEV-BOBR, A.A. (1970): Paramagnetic V, Fe, Mn impurities in crystals of fluorophlogopite, a synthetic mica. *Izvest. Akad. Nauk SSSR, Neorg.Mater*, 6(1), 108 - 112.
- RADOSLOVICH, E.W. (1963): Cell dimensions and symmetry of la-

yer lattice silicates. IV. Interatomic forces. *Am. Mineralogist*, 48, 76 - 79.

SEARL, J.W., SMITH, R.C. and WYARD, S.J. (1961): Electron spin resonance absorption for polycrystalline substances. *Proc. Phys Soc.*, 78, 1174 - 1176.

SEMMENS, B. (1965): Disruption of the aluminosilicate lattice by acid fluoride solutions. Ph.D. Thesis, London University.

TAYLOR, G.L., RUOTSALA, A.P. and KEELING, R.O. Jr. (1968): Analysis of iron in layer silicates by Mössbauer spectroscopy. *Clays and Clay Minerals*, 16, 381 - 391.

WAUCHOPE, R.D. and HAQUE, R. (1971): ESR in clay minerals. *Nature Phys. Sci.*, 233, 141 - 142.

## INFRARED STUDY OF CHROMIUM-BEARING HALLOYSITES

Zoran Maksimović

Faculty of Mining and Geology  
University of Belgrade  
Belgrade, Yugoslavia

and

Joe L. White

Department of Agronomy  
Purdue University  
Lafayette, Indiana USA

**ABSTRACT.** - Chromium-bearing halloysites occur in Yugoslavia (a) as products of hydrothermal alteration of ultramafic rocks, (b) in contact-karst nickel deposits, and (c) as a result of weathering of chromium-bearing illites.

Most frequently Cr-halloysites constitute a part of the argillic zone outward from epithermal and mesothermal sulfide veins in ultramafic rocks. In this case the most common pattern of argillic zoning is: Cr-smectites  $\longrightarrow$  Cr-halloysites  $\longrightarrow$  a silicic zone with sulfides and Cr-illites.

Six samples of halloysites from three localities in Serbia having chromium contents varying from 1.34 to 8.02% Cr have been studied by infrared, x-ray diffraction, chemical, and optical techniques.

In the structure of halloysite chromium replaces aluminum in octahedral positions. Structural formulas of Cr-halloysites, derived from chemical analyses, indicate that from 0.14 to 0.92 chromium ion per 18 (O, OH) is present in octahedral sites.

In addition to the OH stretching frequencies at 3692 and 3624  $\text{cm}^{-1}$  normally observed in halloysites, our infrared spectra show the presence of hydroxyl stretching frequencies at 3588 and 3550  $\text{cm}^{-1}$  in Cr-halloysites. The behavior of the bands at 790 and 750  $\text{cm}^{-1}$  reflects the presence of Cr in octahedral sites and provides a basis for more definitive assignment of these frequencies. The intensity of a band at 1080  $\text{cm}^{-1}$ , normally assigned to Si-O-Si vibrations, is inversely related to the chromium content.

## INTRODUCTION

Cr-bearing halloysites occur in Yugoslavia (a) as products of hydrothermal alteration of ultramafic rocks, (b) in contact-karst nickel deposits, and (c) as a result of weathering of Cr-bearing illites.

Due to the lack of aluminum, the clayey alteration products of ultramafic rocks often contain variable amounts of  $\text{Cr}^{3+}$  replacing  $\text{Al}^{3+}$  in octahedral positions (Maksimović, 1959; Maksimović and Crnković, 1968). Enrichment of chromium is encountered particularly in clays of hydrothermal origin. Some illites and smectites may contain up to 14.59% and 13.74%  $\text{Cr}_2\text{O}_3$ , respectively.

Most frequently Cr-halloysites constitute a part of the argillic zone outward of epithermal and mesothermal sulfide veins in ultramafic rocks. In this case, the most common pattern of argillic zoning is: a silicic rock with sulfides and Cr-illites  $\longrightarrow$  Cr-halloysites  $\longrightarrow$  Cr-smectites  $\longrightarrow$  partly altered rock. Halloysites of hydrothermal origin may be very rich in chromium, containing up to about 12% of  $\text{Cr}_2\text{O}_3$ .

A few samples of Cr-halloysites were found in contact-karst nickel deposits in Ural and in Serbia, where they also form mixtures with various hydrous nickel minerals (Godlevskii and Ivanova, 1935; Alexeieva and Godlevskii, 1937; Gritsaienko and Grum-Grzhimailo, 1949; Maksimović, 1957; Maksimović and Crnković, 1968). In these deposits halloysites contain up to 2.65%  $\text{Cr}_2\text{O}_3$ , indicating that the weathering did not promote the concentration of chromium as did hydrothermal processes.

A suite of samples of bluish halloysites from three localities in Serbia with different chromium content have been studied and characterized by infrared, x-ray diffraction, optical, DTA, and chemical techniques. The data obtained are presented and the changes of properties with increasing  $\text{Cr}^{3+} \longrightarrow \text{Al}^{3+}$  substitution are discussed.

## EXPERIMENTAL

### Materials

Cr-halloysites occur in nests and veins which may attain a thickness of a few meters. This bluish clayey material from the locality of Rudnjak in Serbia was originally described by Breithaupt (1838) as a new mineral "miloschite". Later, this mineral was redefined as Cr-bearing halloysite (Maksimović, 1953; Stangačilović, 1953).

Samples of Cr-halloysites have a clay-like to earthy appearance without any recognizable traces of primary rock structure. Very rarely, however, some structural rock features have been preser-

ved--in a blue, earthy groundmass of transformed olivine the crystals of orthopyroxenes, also completely transformed into bluish Cr-halloysite, can be recognized. In this case, the hydrothermal alteration of harzburgite took place without appreciable change in volume.

The following samples of Cr-halloysites were chosen for investigation:

1. Pale blue halloysite, contact-karst nickel deposit, village of Ba, with Cr = 1.34%,  $n_{Na} = 1.558 \pm 0.002$ .

2. Pale blue halloysite of hydrothermal origin, locality of Rudnjak Cr = 2.02%,  $n = 1.562$ .

3. Sky blue halloysite, locality of Rudnjak, Cr = 2.64%,  $n = 1.570$ .

4. Blue halloysite, locality of Rudnjak, Cr = 3.95%,  $n = 1.573$ .

5. Dark blue halloysite, locality of Rudnjak, Cr = 5.40%,  $n = 1.580$ .

6. Dark blue halloysite of hydrothermal origin, village of Takovo, Cr = 8.02%,  $n = 1.587$ .

### Optical Methods

Cr-halloysites are various shades of blue, the intensity of the color increasing with the chromium content. There is also a direct relation between mean index of refraction and the chromium content the  $n_{Na}$  varying from 1.558 (1.34% Cr) to 1.587 (8.02% Cr) (Fig. 1).

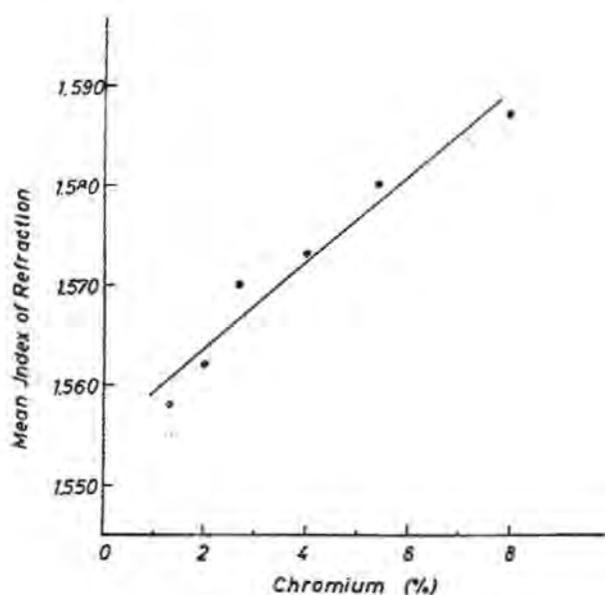


Figure 1. Relation of mean index of refraction and chromium content for halloysites. The indices were determined after drying at 105°C.

It should be noted that the blue color and the chromium content often vary in one sample. For this reason, the mean index of refraction of a sample analyzed for chromium was obtained by measuring a great number of grains.

Under the microscope Cr-halloysite appears as pale blue to sky blue, very fine aggregates. Rare chromite grains were observed in some cases as well as a very small amount of fine grained magnetite. The yellow-brown coatings were found sporadically due to the presence of iron hydroxides. The content of iron hydroxides estimated by use of the microscope is quite closely related to the content of  $\text{Fe}_2\text{O}_3$  of the sample. This suggests that all  $\text{Fe}_2\text{O}_3$  is present as an impurity. In sample No. 6 about 3 to 5% of free silica in the form of amorphous, spongy particles was observed. X-ray powder data did not detect the presence of quartz.

Electron micrographs of halloysites were taken with a Philips EM 300 electron microscope with direct magnification of 20,500X. The micrographs showed the halloysites to have the familiar morphology of elongate tubular particles of extremely small size, regardless of the chromium content.

#### X-ray Diffraction Measurements

The x-ray diffraction patterns were obtained with a Philips PW 1051 x-ray diffractometer using Ni-filtered  $\text{CuK}\alpha$  radiation. Instrument settings were: voltage - 40 kV; current - 20 mA; divergence slit =  $1^\circ$ ; scatter slit =  $1^\circ$ ; receiving slit = 0.1 mm; scale factor = 16; multiplier = 1; time constant = 4 seconds; scanning speed =  $1^\circ$ , or  $1/2^\circ$ , or  $1/4^\circ$  per minute; chart speed = 0.6 cm per minute.

#### Differential Thermal Analyses

The differential thermal analyses were made using a Stanton Instruments Model Standata 6-25 DTA apparatus. Samples weighing 0.1 g. were heated at a rate of  $10^\circ$  per minute.

#### Chemical Composition

Elemental analyses of the halloysites were made using conventional procedures for silicate analysis.

#### Cation Exchange Determination

The halloysites were saturated with ammonium by treating with ammonium acetate, the excess removed by washing and the total cation exchange capacity determined by measurement of the adsorbed ammonium using the Kjeldahl distillation method.  $\text{Mg}^{2+}$ ,  $\text{Ca}^{2+}$ ,  $\text{Na}^+$ ,

$K^+$ , and  $Ni^{2+}$  were determined in the ammonium acetate extract. The small quantity of material available for the cation exchange analysis (0.30 to 0.85 g) and the possible errors in determinations impose some caution in the interpretation of the results.

### Infrared Measurements

Infrared spectra were recorded with a Perkin-Elmer Model 180 Infrared Spectrophotometer operated in the absorbance mode. Samples were prepared as KBr pellets and as capillary films of nujol between two Irtran-2 windows.

## RESULTS AND DISCUSSION

### X-ray Diffraction Measurements

X-ray diffractometer traces for six randomly oriented low to high Cr-halloysites are shown in Fig. 2. X-ray powder diffraction data are listed in Table I.

As seen from Table I and Fig. 2, the powder data indicate the presence of hydrated, partially-hydrated, and dehydrated halloysites. Sample No. 2 represents a dehydrated halloysite while all other samples are partially dehydrated forms with spacings corresponding both to hydrated (10.0 - 9.6 Å) and dehydrated halloysite (about 7.4 Å). After drying these samples at 105°C., the 001 reflection of the hydrated form disappeared the intensity of a spacing at about 7.4 Å. increased, as the hydrated form passed into the dehydrated one.

The x-ray diffractometer traces in Fig. 2 indicate an increase of disorder in going from low to high Cr-halloysite. This is in agreement with the results of the DTA measurements.

X-ray diffraction data did not reveal the presence of impurities in these halloysite samples. However, it is possible that the third order reflection of hydrated halloysite at about 3.3 to 3.4 Å. may coincide with the 3.34 Å. reflection of quartz. Sample No. 3 may possibly contain a small amount of quartz.

As would be predicted on the basis of ionic radii, the substitution of  $Cr^{3+}$  for  $Al^{3+}$  in octahedral sites causes an increase in the b-dimension, as measured by the (060) spacing. There is an increase from 1.482 Å. up to 1.486 Å. as the content increases (Table I, Fig. 1). This shift in (060) spacing has been established by recording the (060) peak at high sensitivity.

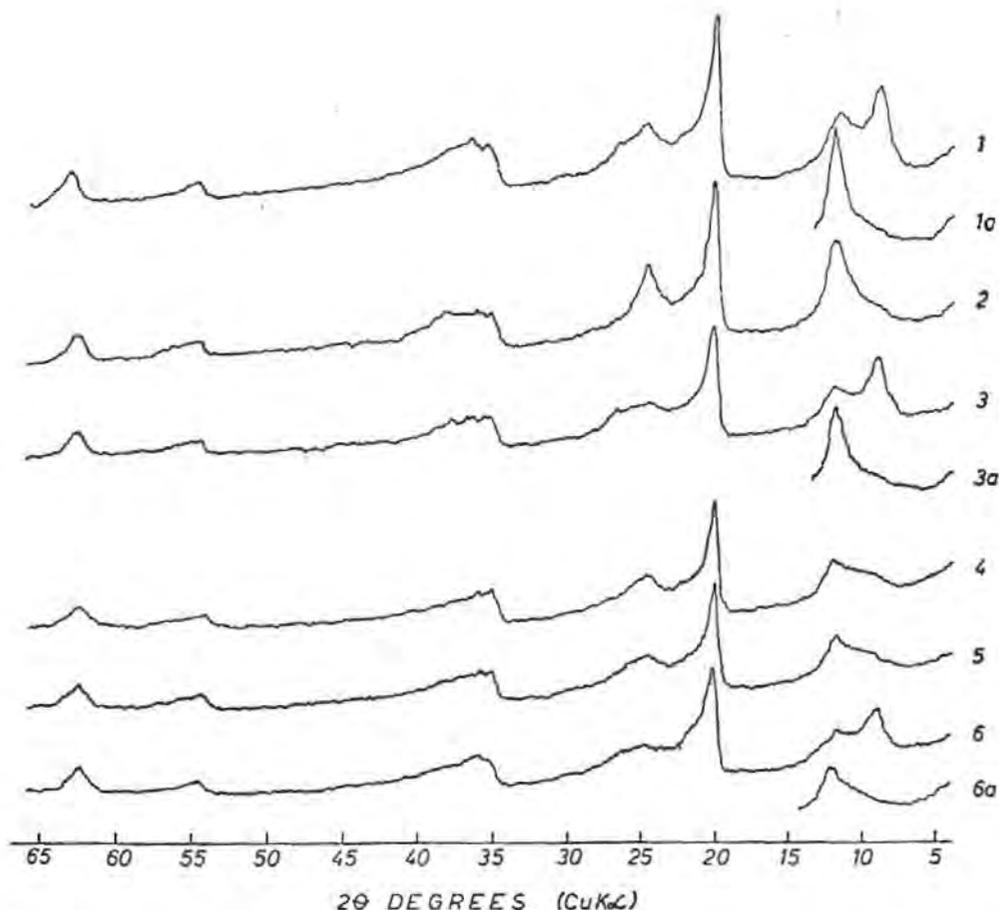


Figure 2. X-ray diffraction patterns of Cr-bearing halloysites. 1a, 3a, and 6a represent the samples 1, 3 and 6 after drying at 105°C.

Table I. X-ray powder diffraction data for Cr-bearing halloysites.

1		2		3		4		5		6	
d(A)	I										
9.0	48			9.9	66	9.6	27	9.6	23	10.0	61
7.47	30	7.47	56	7.50	35	7.43	40	7.48	50	7.48	38
4.440	100	4.417	100	4.420	100	4.412	100	4.440	100	4.417	100
3.604	30	3.612	41	3.610	30	3.610	30	3.612	30	3.604	33
3.333	18			3.338	25			3.412	25	3.340	22
2.561	23	2.567	19	2.554	20	2.553	25	2.563	23	2.550	25
2.468	26	2.485	20	2.462	20	2.479	25	2.496	24	2.508	30
2.370	22	2.351	20	2.383	18						
1.683	10	1.681	9	1.688	11	1.683	10	1.682	13	1.685	11
1.482	22	1.483	20	1.484	20	1.485	20	1.486	18	1.486	22

## Differential Thermal Analysis

The DTA curves (Fig. 3) correspond to typical hydrated, partially dehydrated and dehydrated halloysites described previously. Differences between low and high Cr-halloysites are demonstrated on DTA curves by the magnitude of the exothermic peak; from low to high chromium samples the intensity of this peak becomes gradually smaller. The change of the magnitude of this peak might be explained (a) by the decrease of aluminum content due to  $\text{Cr}^{3+} \longrightarrow \text{Al}^{3+}$  diadochy and the reduced heat of reaction, and (b) by the increased degree of disorder in the stacking of structural layers affected by this substitution. The influence of particle size is not responsible in this case because there is no significant difference in particle size between the halloysite samples. A slight decrease of the exothermic peak temperature with increase of chromium may be observed, also suggesting a more disordered lattice of high Cr-halloysite.

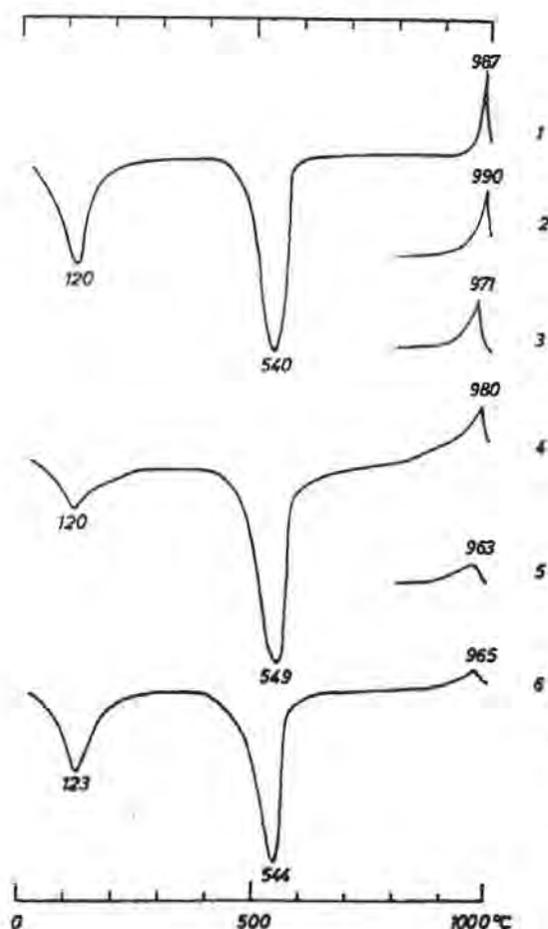


Figure 3. Differential thermal analyses of Cr-bearing halloysites.

Table II. Chemical analyses of Cr-bearing halloysites.

Element	1	2	3	4	5	6
SiO <sub>2</sub>	40.04	44.25	41.34	43.45	42.52	40.55
Al <sub>2</sub> O <sub>3</sub>	32.08	35.53	31.50	30.53	28.87	24.56
Cr <sub>2</sub> O <sub>3</sub>	1.96	3.02	3.86	5.78	7.90	11.72
Fe <sub>2</sub> O <sub>3</sub>	0.30	0.32	0.35	1.28	1.30	0.94
NiO	0.20	0.08	0.28	0.16	0.15	0.19
MgO	0.64	0.42	Tr	0.66	0.58	0.54
CaO	0.91	0.30		0.56	0.72	0.46
Na <sub>2</sub> O	0.27	0.10	0.31	0.10	0.14	0.20
K <sub>2</sub> O	0.32	0.03	0.27	0.10	0.08	0.10
H <sub>2</sub> O <sup>+</sup>	12.98	13.32	13.32	12.75	12.73	12.20
H <sub>2</sub> O <sup>-</sup>	10.08	2.70	2.70	4.65	4.52	8.22
Total	99.78	100.07	100.44	100.02	99.51	99.68

Number of ions on the basis of 18 (O, OH)

Si	3.89	3.96	3.95	4.08	4.00	4.01
Al	3.67	3.76	3.55	3.35	3.20	2.86
Cr	0.15	0.21	0.29	0.42	0.58	0.92
Fe <sup>3+</sup>	0.02	0.01	0.03	0.09	0.10	0.07
Ni	0.02	0.01	0.02	0.01	0.01	0.01
Mg	0.09	0.05	-	0.09	0.08	0.08
Ca	0.09	0.03	-	0.06	0.07	0.05
Na	0.05	0.02	0.06	0.02	0.02	0.04
K	0.04	0.00	0.03	0.01	0.01	0.01
OH	8.40	7.96	8.46	7.90	8.00	8.05

1. Village Ba (Maksimović, 1957). Anal. Z. Maksimović.
2. Rudnjak. Anal. D. Nikolić.
3. Rudnjak. (Maksimović, 1959). Anal. J. Stupar.
4. Rudnjak. Anal. D. Nikolić.
5. Rudnjak. Anal. D. Nikolić.
6. Takovo. (Maksimović, 1957). Anal. J. Stupar.

### Chemical Composition

The chemical composition of the kaolin minerals is subject to only slight variation. Analyses in Table II show, however, that these specimens of Cr-halloysites are exceptions to this general rule. The substitution of Cr<sup>3+</sup> for Al<sup>3+</sup> is very marked and approaches a limit of approximately 1.0 atom per unit cell. The range of this isomorphous substitution is facilitated by the similarity in ionic size

( $\text{Cr}_{\text{VI}}^{3+} = 0.70 \text{ \AA}$ ,  $\text{Al}_{\text{VI}}^{3+} = 0.61 \text{ \AA}$ , Whittaker and Muntus, 1970). Because  $\text{Cr}^{3+}$  is slightly larger than  $\text{Al}^{3+}$  this substitution causes an increase in the b-dimension; this may also increase disorder of the lattice. Both x-ray and DTA results suggest there is increased disorder with increasing Cr-content.

Considering that  $\text{Mg}^{2+}$  and  $\text{Ni}^{2+}$  are partially to completely exchangeable, and that iron is present as an impurity, the number of ions in octahedral sites is obviously less than calculated in Table II. The apparent excess of  $\text{Si}^{4+}$  in tetrahedral positions in samples No. 3 to No. 6 might be explained by the presence of quartz or amorphous silica. Free silica is not present in large amounts in these samples. Moreover, the excess of  $\text{Si}^{4+}$  in tetrahedral sites does not regularly increase going from low to high Cr-halloysites. Therefore, we conclude that the increase of  $\text{Cr}^{3+}$ -- $\text{Al}^{3+}$  substitution is the main cause for the increase in disorder.

### Cation Exchange Determinations

The cation exchange capacities for the halloysites in this study are shown in Table III, along with the exchangeable cations. The values range from 21 to 35 milliequivalents per 100 g. The degree of hydration appears to influence the cation exchange capacity values markedly; this factor may be responsible for the values determined in this study being somewhat lower than the 40-50 milliequivalents per 100 g. value given by Grim (1968, p. 189).

Table III. Cation exchange capacity and exchangeable cations in Cr-halloysites (milliequivalents per 100 g).

Samples	1	2	3*	4	6
Total cation exchange capacity	35	21	21.3	22	34
Exchangeable cations					
$\text{Mg}^{2+}$	15	19	3.2	6	15
$\text{Ca}^{2+}$	16	9	-	18	16
$\text{Na}^+$	8	3	9.6	4	6
$\text{K}^+$	6.6	0.5	5.5	0.9	2
$\text{Ni}^{2+}$	0.2	0.1	6.8	0.4	0.8

\* Z. Maksimović (1959).

## Infrared Measurements

The compositional variations in the kaolin minerals are much more limited than those in smectites and micas. As a result of the rather limited variation in composition, the infrared spectra of the kaolin minerals have rather similar characteristics with the absorption bands occurring in more or less constant positions. The elegant work of Stubičan and Roy (1961a, 1961b) provided assignments for most of the bands of kaolinite. The synthesis of minerals of varying composition was the basis for this empirical approach.

The suite of Cr-halloysites collected and characterized by Maksimović (1957) appeared to offer a unique opportunity to examine the effect of isomorphous substitution on the infrared vibrations of this group of kaolin minerals.

Figure 4 shows the OH stretching region for the Cr-halloysites. The normal OH stretching frequencies at  $3692\text{ cm}^{-1}$  and  $3624\text{ cm}^{-1}$  are the dominant ones for samples No. 1 through 4 (1.34 to 3.95% Cr). There is also a distinct shoulder at about  $3588\text{ cm}^{-1}$  for samples No. 3 and 4. In samples No. 5 and 6 (5.40 and 8.02% Cr, respectively) the  $3692\text{ cm}^{-1}$  band is somewhat lower than the  $3624\text{ cm}^{-1}$  band and new bands appear at  $3588$  and  $3550\text{ cm}^{-1}$ . The predicted effect of the substitution of chromium (at. wgt. 52) for aluminum (at. wgt. 26.98) would be a shift of OH stretching frequencies to lower values.

In sample No. 6 (Table II) chromium substitutes for almost one-fourth of the aluminum. The OH stretching intensity for the  $3692\text{ cm}^{-1}$  band for the low-chromium samples (No. 1 - 4) is only slightly less than that of the  $3624\text{ cm}^{-1}$  band. In samples 5 and 6 the  $3692\text{ cm}^{-1}$  band is about one-fourth less intense than the  $3624\text{ cm}^{-1}$ . Assuming that the hydroxyls giving rise to the  $3692\text{ cm}^{-1}$  band are perturbed by the chromium ions to produce the  $3588\text{ cm}^{-1}$ , this would represent a shift of about  $104\text{ cm}^{-1}$ . Similarly, perturbation of the hydroxyls responsible for the  $3624\text{ cm}^{-1}$  band to produce the  $3550\text{ cm}^{-1}$  band represents a shift of  $74\text{ cm}^{-1}$ .

This shift of  $74\text{ cm}^{-1}$  is very close to the effect of substituting iron (at. wgt. 55.85) for aluminum in the smectite structure, as seen by comparison of the OH stretching band at  $3620\text{ cm}^{-1}$  in montmorillonite with that of nontronite at  $3550\text{ cm}^{-1}$ . The hydroxyl assigned to the  $3620\text{ cm}^{-1}$  band in kaolinite has an environment very similar to that in dioctahedral smectites.

Turning next to the region between  $1200$  and  $800\text{ cm}^{-1}$  (Fig. 5), the low Cr-halloysites (samples 1-4) show bands at  $1120$ ,  $1080$ ,  $1040$ , and  $910\text{ cm}^{-1}$ . The three former bands have been assigned to antisymmetric stretching modes of Si-O-Si bonds by Pampuch and Blaszcak (1964); the  $910\text{ cm}^{-1}$  band has been assigned to an Al-O-H bending mode (Stubičan and Roy, 1961a, 1961b). The most striking feature of this spectral region is the gradual diminution in the in-

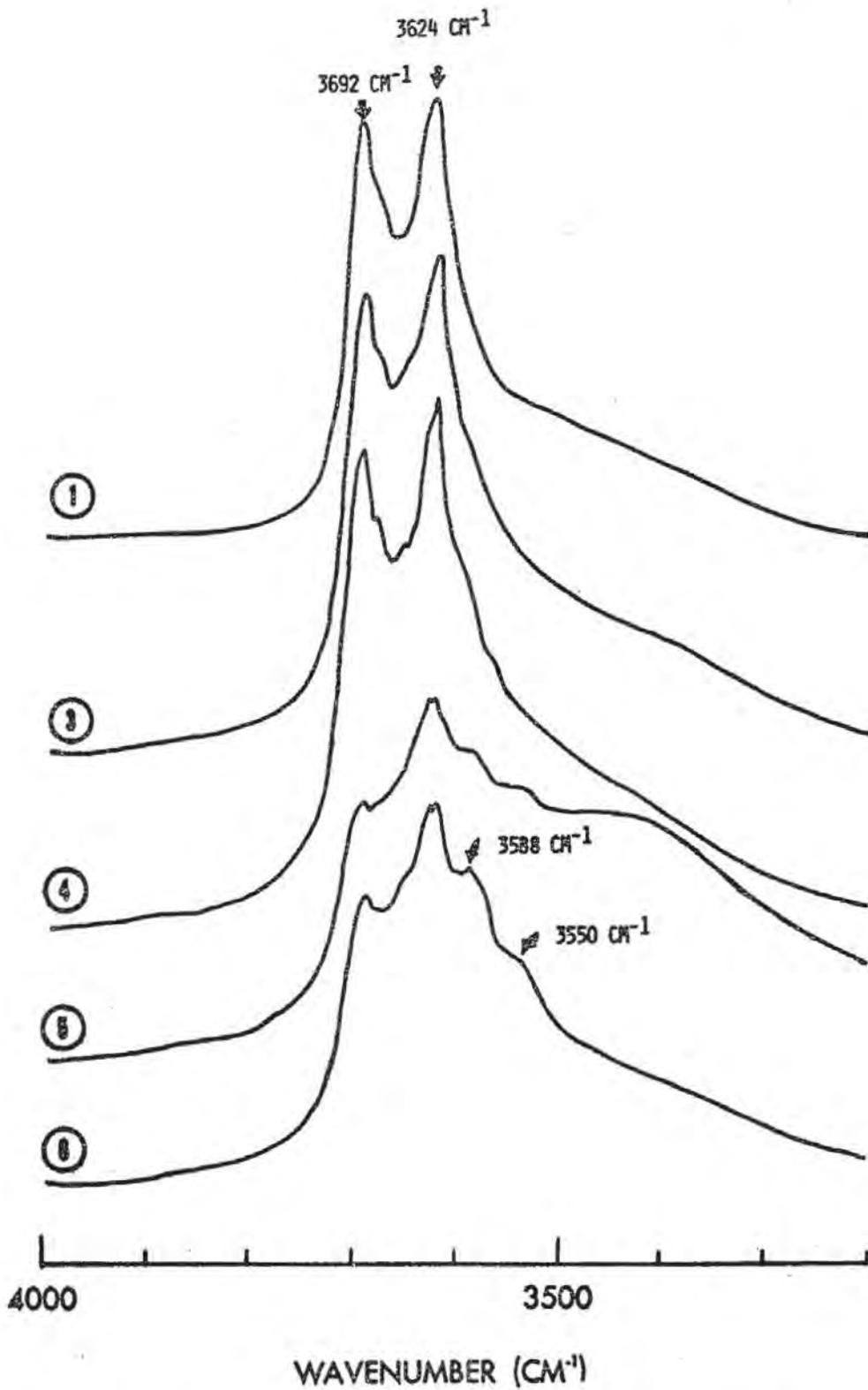


Figure 4. Infrared absorbance spectra in OH-stretching region of Cr-bearing halloysites.

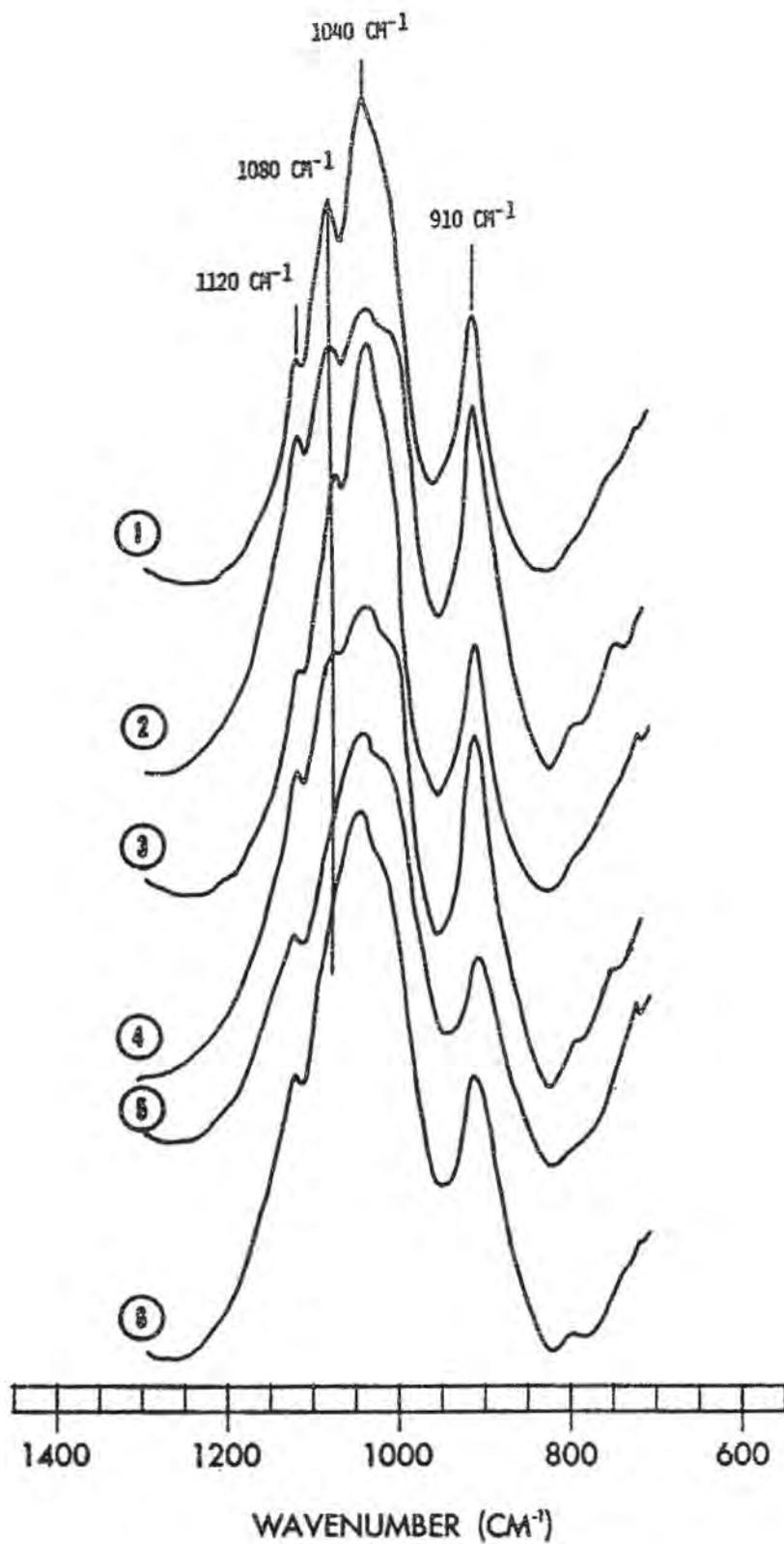


Figure 5. Infrared absorbance spectra in 1200 to 800  $\text{cm}^{-1}$  region of Cr-bearing halloysites.

tensity of the  $1080\text{ cm}^{-1}$  band with increasing chromium content. This suggests that the octahedral chromium ions perturb the Si-O-Si stretching frequency. The shift from  $1040$  to  $960\text{ cm}^{-1}$  for Si-O-Si stretching bands in comparing a dioctahedral with a trioctahedral 1:1 layer lattice silicate (Pampuch and Ptak, 1969, p. 23) also suggests strongly a considerable interaction between the octahedral cations and the silicate tetrahedra vibrations.

Stubican and Roy (1961a, 1961b) suggested that the  $792$  and  $750\text{ cm}^{-1}$  bands were both Al-O-Si vibrations. Pampuch and Blaszczyk (1964) questioned this assignment on the basis of calculations of frequencies and group-theoretical considerations; these workers assigned these vibrations to symmetrical Si-O-Si stretching modes. Careful examination of the intensities of the  $795\text{ cm}^{-1}$  and  $752\text{ cm}^{-1}$  as related to chromium content of the halloysite showed little change in the  $795\text{ cm}^{-1}$  band but a decreasing intensity of the  $752\text{ cm}^{-1}$  band with increasing chromium content. The intensity ratio  $795\text{ cm}^{-1}/750\text{ cm}^{-1}$  as a function of chromium content is shown in Fig. 6. There appears to be a definite trend for this ratio to increase with increasing chromium content. The relative constancy of the  $795\text{ cm}^{-1}$  band suggests that this is an Si-O-Si vibration, while the decrease in intensity of the  $752\text{ cm}^{-1}$  with increasing chromium content indicates that this may be an Al-O-Si vibration.

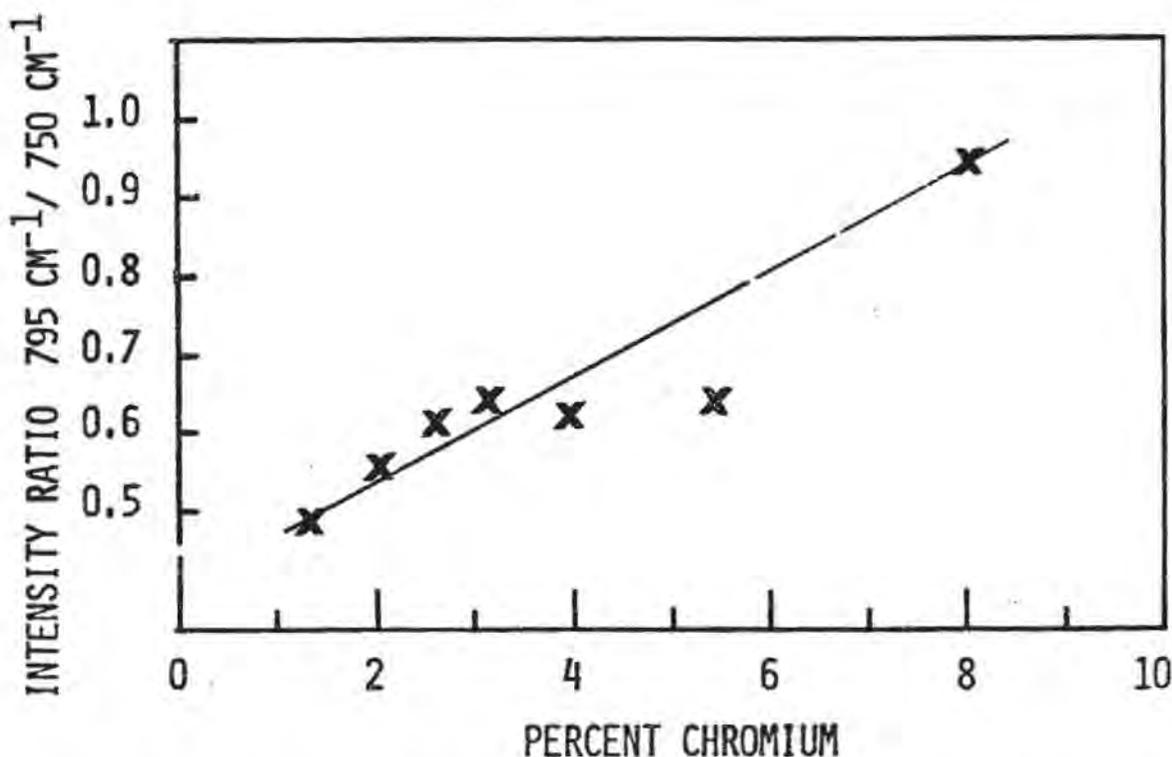


Figure 6. Relation between intensity ratio  $795\text{ cm}^{-1}/750\text{ cm}^{-1}$  absorption bands and chromium content of Cr-bearing halloysites.

Thus, examination of these halloysites with variable chromium content by infrared techniques has shown that the OH stretching vibrations, Si-O-Si, and Al-O-Si vibrations are affected by the chromium content and confirms the substitution of chromium for aluminum in octahedral sites.

#### REFERENCES

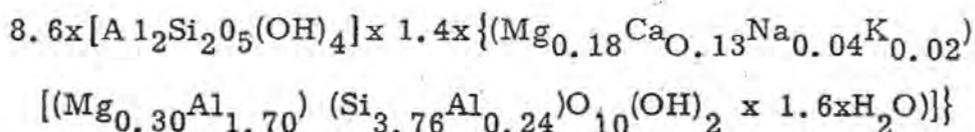
- ALEXEIEVA, E. F., and GODLEVSKII, M. N. (1937): Rentgenometricheskoie izuchenie gidrosilikatov nikelya. Zapiski vses. min. obshchestva, 66, 51-106.
- GODLEVSKII, M. N. and IVANOVA, V. P. (1935): Galluazit iz Aidyrlinskogo mestorozhdeniya nikelovykh rud. Zapiski vses. min. obshchestva 64, 108-117.
- GRIM, R. E. (1968): Clay Mineralogy. p. 189. McGraw-Hill Book Co., N. Y.
- GRITSAIENKO, G. S., and GRUM-GRZHIMAILO, S. V. (1949): O khromovon galluazite iz Aidyrlinskogo mestorozhdeniya na juzhnom Urale. Zapiski vses. min. obshchestva 78, 61-63.
- MAKSIMOVIC, Z. (1953): Milosin-hromni halojzit. Glasnik srp. Akad. nauka 6, 67-68.
- MAKSIMOVIC, Z. (1957): The mineralogy and geochemistry of weathering and hydrothermal alteration of ultramafic rocks in Serbia. Doctor's thesis, Faculty of Mining and Geology, Belgrade (in Serbian) Bull. Sci. Acad. Yugoslave 4, p. 49 (1958) (abstract in English).
- MAKSIMOVIC, Z. (1959): The use of spectrochemical analysis for estimation of exchangeable cations in clay minerals. Bull. Acad. serbe Sci. 25, 163-165.
- MAKSIMOVIC, Z., and CRNKOVIC, B. (1968): Halloysite and kaolinite formed through the alteration of ultramafic rocks. XXIII Intern. Geol. Congress, 14, 95-105, Prague.
- PAMPUCH, R., and BLASZCZAK, K. (1964): Infrared vibrational spectra of kaolin group minerals. Prace Komisji Nauk Tech. O/PAN w Krakowie, Ceramika 3, 5-30.
- PAMPUCH, R., and PTAK, W. (1969): Infrared spectra and structure of 1:1 layer lattice silicates. Part I. The vibrations of the tetrahedral layer. Prace Mineralogiczne 15, 1-50. O/PAN w Krakowie.
- STANGACILOVIC, D. (1953): Milosin sa Rudnjaka-hromni halojzit. Zapisnici srp. geol. drustva, Belgrade, 41-42.
- STUBICAN, V., and ROY, R., (1961a): Isomorphous substitution and infrared spectra of the layer lattice silicates. Amer. Mineral, 46, 32-51.
- STUBICAN, V., and ROY, R., (1961b): New approach to assignment of absorption bands of layer lattice silicates. Z. Kristallogr. 115, 200-214.
- WHITTAKER, E. J. W., and MUNTUS, R. (1970): Ionic radii for use in geochemistry. Geochim. Cosmochim. Acta 34, 945-956.

MIXED-LAYER KAOLINITE-SMECTITE FROM LOWER SILESIA,  
POLAND: FINAL REPORT

A. Wiewiora

Institute of Geological Sciences, Polish Academy of Sciences, War -  
saw, Poland

ABSTRACT. - Kaolinite-like clay, ocuring in veins in the quartz-schists, was found in the quarry situated between Jeglowa and Krzywina near Strzelin. Under careful examination of optically homogeneous material by several methods have been identified non-expanding 1:1 (kaolinite) and expanding 2:1 (smectite) layers. By means of visual method of interpretation of X-ray diffraction patterns risen by the mixed-layer system and subsequently by the Fourier transform method 86 per cent of kaolinite and 14 per cent of smectite has been computed to be irregularly interlayered within the one phase. These data were helpful for calculation of the chemical formulae from chemical composition of the kaolinite smectite:



Electron diffraction measurement of basal spacings of single crystals revealed regular 3:1, 4:1 and 4:2 interstratification of kaolinite and smectite layers within the individual domains.

INTRODUCTION

Occurrence of interstratified clay minerals composed of 1:1 and 2:1 layers is a kind of curiosity and happens very seldom. Hitherto such clays are known from: Japan (Sudo and Hayashi) 1956;

Shimoyama et al., 1969), Florida (Altschuler et al., 1963), Yucatan Peninsula, Mexico (Schultz et al., 1971) and Poland (Wiewióra, 1971).

Numerous studies of irregularly interstratified different clay minerals not only kaolinite-smectite, were based upon the X-ray examination of polycrystalline aggregates. According to the present author structure, which could be derived from the summary diffraction effects in such usual procedure, should be called "statistical" or "summary" structure. Exemplifying the investigation of kaolinite-smectite from Poland, there has been shown, that statistical structure was not consistent with a real structure of individual crystals.

## OCCURRENCE

Kaolinite-like clay found in the quarry situated between Jegłowa and Krzywina fills veins in the quartz-schists, which are ranked among the metamorphic shield rocks associated with the granite intrusion of Strzelin in Lower Silesia, western Poland, Quartz-schists and sericite-schists modified in a different degree by secondary processes are thought to be of Devonian age by analogy to similar Devonian rocks of Eastern Sudety Mountains.

According to Oberc (1966) the granite of Strzelin has been shaped by longlasting processes. They might be bound with Bretonian up to Asturian orogeneses. The latter generated pegmatite and hydrothermal processes like: leaching of feldspar, kaolinization of sericite and crystallization of rock crystal in association with the kaolinite-like clay. Detailed studies of products of transformation of sericite (in situ) and clay material in veins revealed beyond doubt that kaolinization of sericite produced greyish-white striped, but normal kaolinite, while hydrothermal processes created snow white, optically homogeneous kaolinite-smectite.

## IDENTIFICATION OF COMPONENTIAL LAYERS

### Morphology

Optical homogeneity of the clay from Jegłowa has been fully confirmed under the electron microscope. Apart macro-crystals of quartz, mica and anatase no other minerals were traced. Lack of the halloysite tubes has been also proved.

Individual crystals of the kaolinite-smectite have appearance of rather irregular grains shaped in stocks of very thin laminae (Photo 1-4). Some top laminae partially saved their hexagonal symmetry (Photo 3). A surface of most laminae is highly corrugated.

An average diameter of a clay particle reaches 2 microns; particles  $< 0.2\mu$  are rather missing. Granulometric analysis completed by elutriation method proved that the clay material is coarse crystalline, as there are 98 per cent particles  $< 20\mu$ , 87 per cent  $< 5\mu$ , 32 per cent  $< 1\mu$  (Szpila et al. 1972).

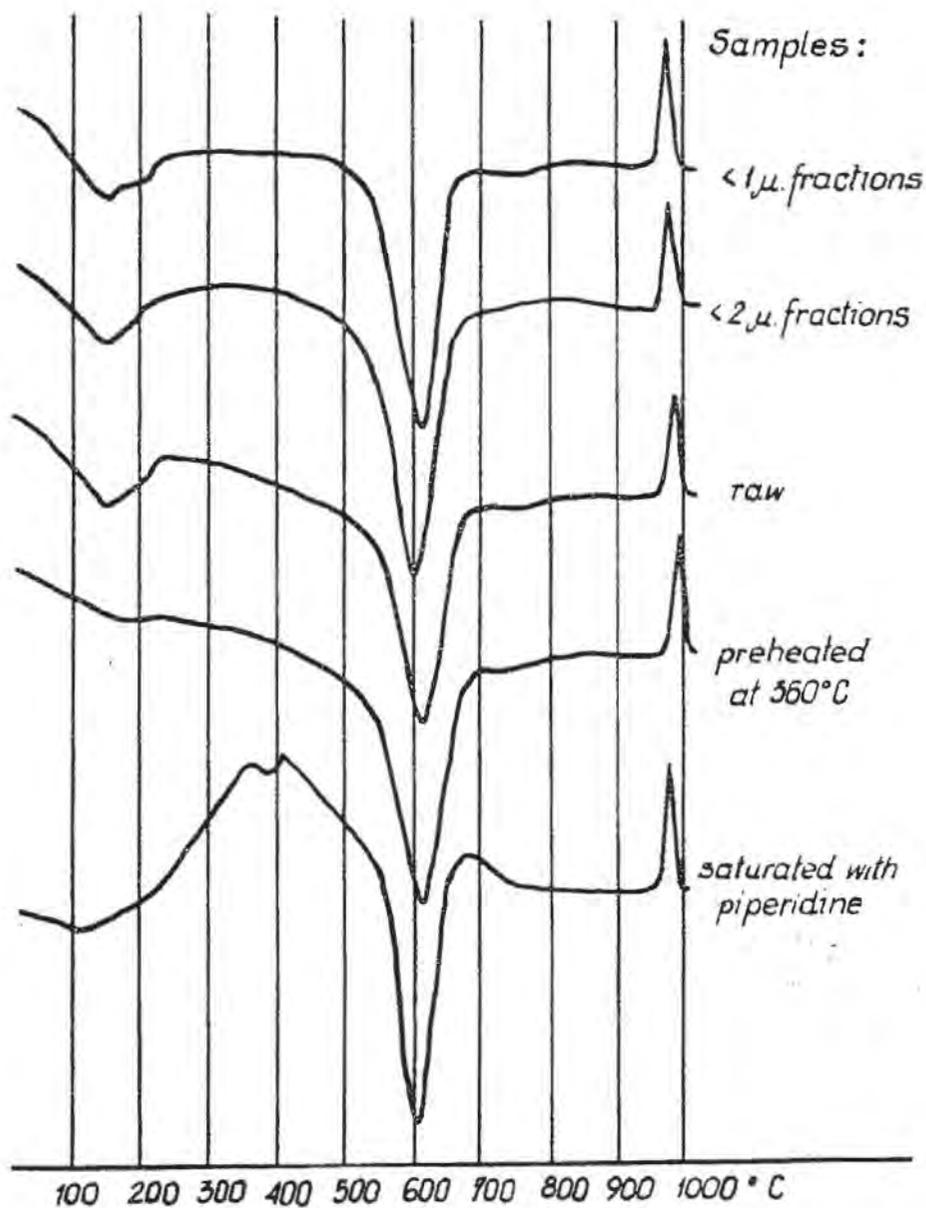


Figure 1. - DTA curves.

#### Differential Thermal Analysis

DTA curves (Fig. 1) show typical kaolinite effects at  $600^{\circ}\text{C}$  and  $980^{\circ}\text{C}$  (curves 1, 2, 3) besides weaker double effect at  $150^{\circ}$  -  $200^{\circ}\text{C}$  and hardly visible bending at  $740^{\circ}\text{C}$ . An additional information

on non kaolinite endothermic peaks may be provided by analyses of samples: preheated to 380°C and piperidine saturated (curves 4 and 5 respectively). There are reactions typical for the smectite layers.

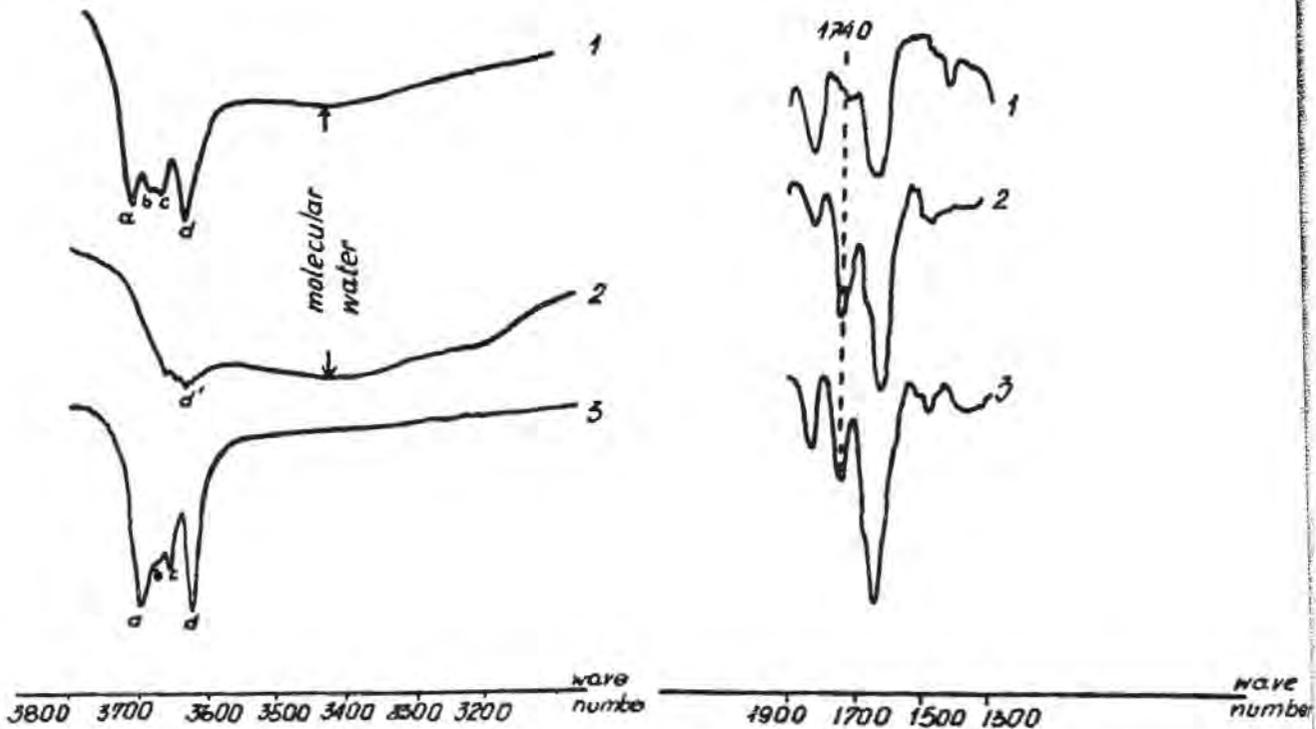


Figure 2. Infrared absorption spectra;

1. Kaolinite-smectite
  2. Ca-montmorillonite
  3. Kaolinite 0.5-2  $\mu$  fractions
- a-3692  $\text{cm}^{-1}$ , b-3662  $\text{cm}^{-1}$ ,  
c-3648  $\text{cm}^{-1}$ , d-3621  $\text{cm}^{-1}$ ,  
d'-3635  $\text{cm}^{-1}$

Figure 3. Infrared absorption spectra;

1. raw sample
2. sample saturated with trietazine
3. < 1  $\mu$  fractions saturated with trietazine

#### Infrared Absorption Data

Infrared absorption spectra in the range of 3200 - 3800 wave number (Fig. 2) show a general resemblance of the clay from Jeglowa to kaolinite. Nevertheless, there is a clearly visible enhancement of the 3620  $\text{cm}^{-1}$  absorption band (which is due to the internal  $\text{OH}^-$  groups in kaolinite; it coincides with the 3635  $\text{cm}^{-1}$  band due to the  $\text{OH}^-$  groups in a smectite layer), as well as appearance of the 3410  $\text{cm}^{-1}$  bending due to interlayer molecular water. Similar effects but better expressed were described by Oinuma and Hayashi (1965) for the interstratified system from Japan.

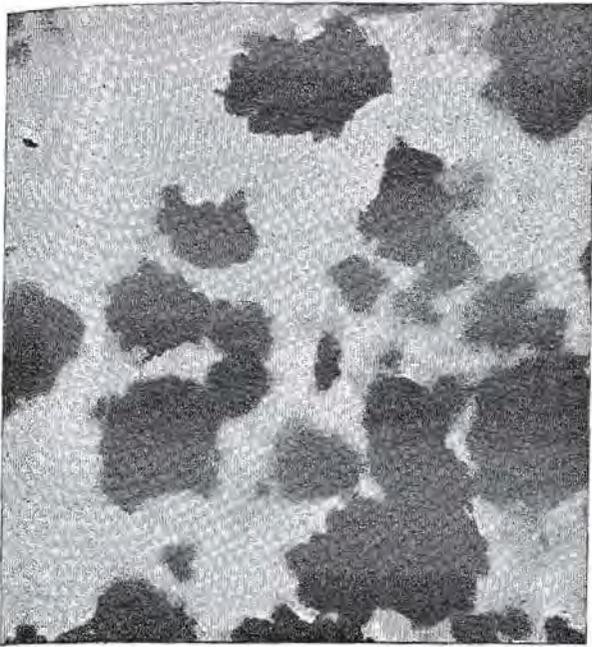


Photo 1. Electron micrograph, dispersion; 4000 x.



Photo 2. Electron micrograph, dispersion replica; 10.800 x.



Photo 3. Electron micrograph, dispersion replica; 16.800 x.



Photo 4. Electron micrograph, dispersion replica; 21.400 x.



A raw sample and  $<1\mu$  size fractions were saturated with trietazine (Cruz and White, 1968; Russel et al., 1968; Brown and White, 1969). The products of the hydrolytic reaction were analysed by infrared spectra (Fig. 3). At both diagrams strong absorption band at the 1740 wave number appeared, which was absent in spectra of the untreated sample. This gives evidence for the presence of highly charged surface in the mineral system.

### X-Ray Diffraction Analysis

DTA and I.R. were helpful in identification procedure of the layers existing in the clay, but they were not universal enough to distinguish the phases they form. This problem may be solved by means of X-ray diffraction analysis. An optical homogeneity of the clay may indicate that both types of layer compose the only one mineral phase.

For the study of interstratification were prepared oriented aggregates. They were characterised by an excellent orientation due to the platy shape of the clay particles (see electron micrographs). The presence of swelling layers has been revealed by saturation of the specimen with the ethylene glycol (Fig. 4). A shift of an angular position of 001 toward smaller, and 002 peaks toward higher angles and changes in their relative intensities and shape were clearly visible. They might be assigned only to the interstratified mineral system.

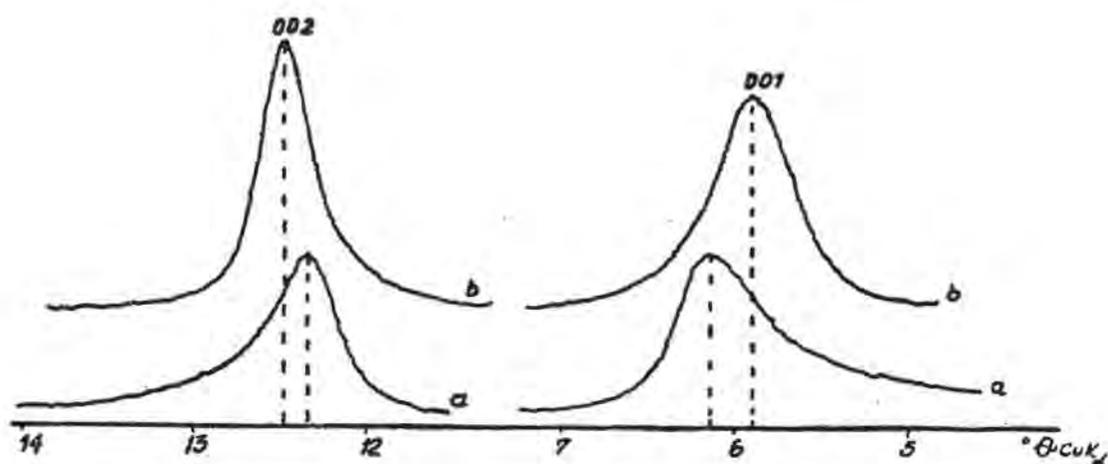


Figure 4. Basal reflections; a-raw sample; b-saturated with ethylene glycol.

Visual treatment (Mering, 1949) of the diffraction curves resulted by differently modified samples, by saturation and heating, used to show that the observed peaks were the summary diffraction, pro-

ved that kaolinite-nonexpanding and smectite-expanding layers were interlayered within the structure (Wiewióra, 1971). An additional evidence has been provided by the study of products of thermal transformation of the clay. In  $< 1 \mu$  size fractions heated to  $380^{\circ}\text{C}$  decrease of intensity of basal reflections of kaolinite and appearance of smectite reflections were observed (b in Fig. 5). After heating for 3 hours in  $500^{\circ}\text{C}$  kaolinite layers fully dehydroxylated. The only observed diffraction (c in Fig. 5) belonged to smectite or rather to a system of smectite and X-ray amorphous zones intermixed within a structure. Similar shift of diffraction peaks has been theoretically derived by Ross (1968) for thin crystals of mica and montmorillonite.

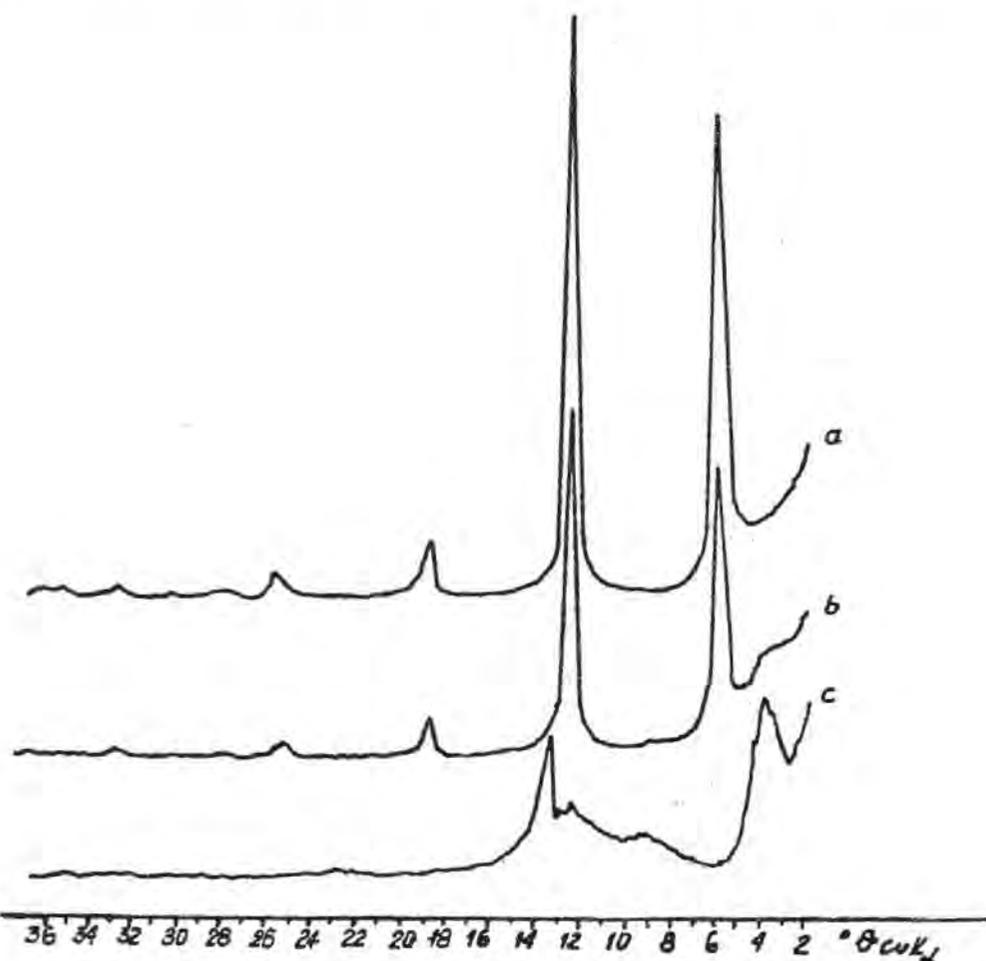


Figure 5. X-ray diffractograms of oriented aggregates of  $< 1 \mu$  particle size fractions; a-raw, b-heated to  $380^{\circ}\text{C}$ , c-heated to  $500^{\circ}\text{C}$ .

Further heating to  $700^{\circ}\text{C}$  produced a decrease of the described peaks and to  $900^{\circ}\text{C}$  gave complete dehydroxylation of the investigated sample (Fig. 6).

In the raw sample heated to  $500^{\circ}\text{C}$  smectite and mica layers were not changed. In  $900^{\circ}\text{C}$  only mica did not dehydroxylate (c in

Fig. 7). Heating to 1200°C produced well crystallized mullite with some admixture of crystobalite-typical products of thermas transformation of both: kaolinite and smectite.

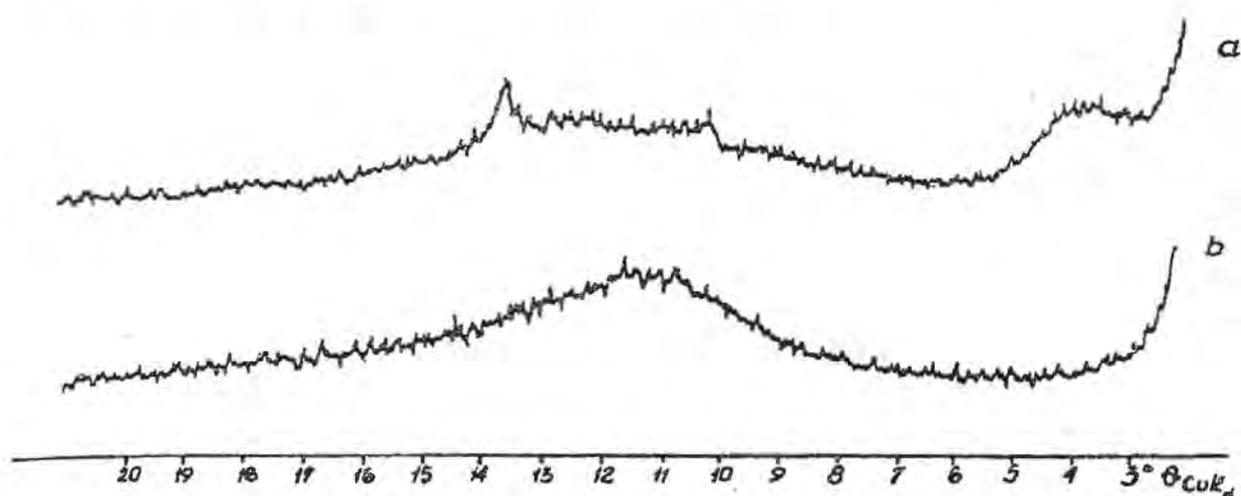


Figure 6. X-ray diffractograms of oriented aggregates of  $< 1 \mu$  particle size fractions heated to: a-700°C, b-900°C.

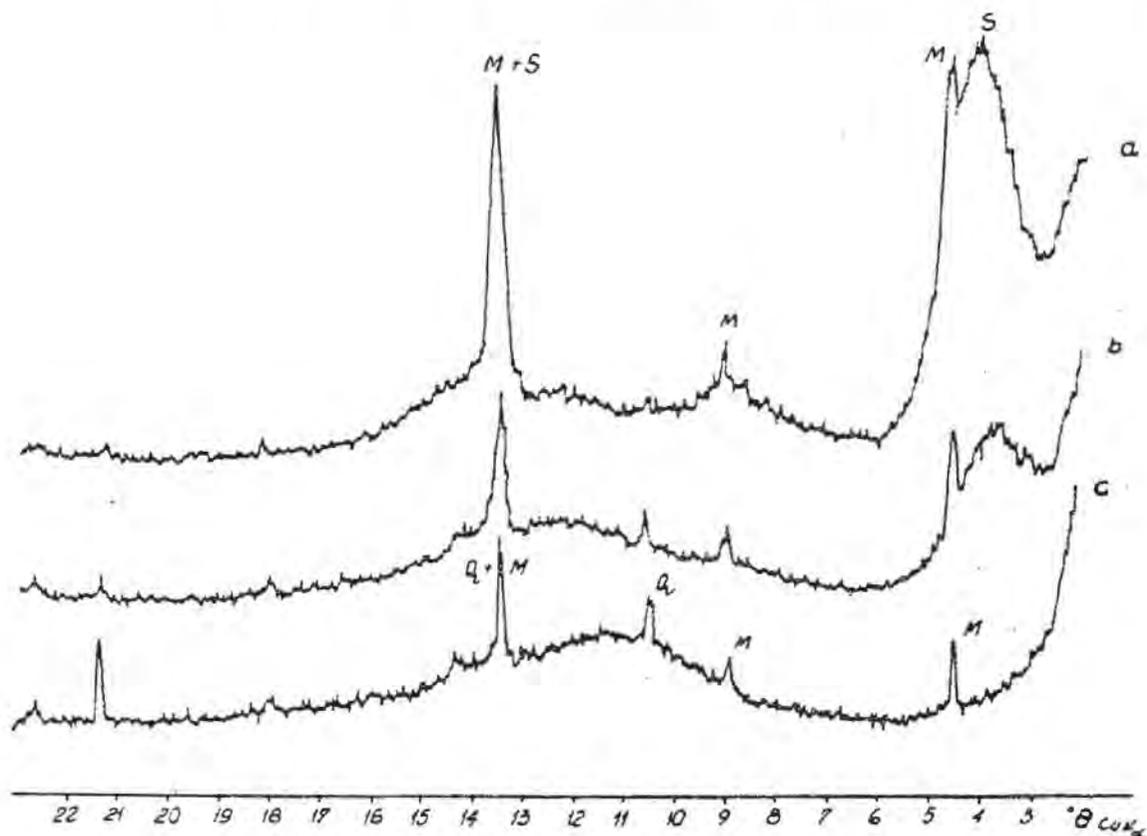


Figure 7. X-ray diffractograms of oriented aggregates of raw samples heated to: a-500°C, b-700°C, c-900°C; M-mica, S-smectite, Q-quartz.



the three mentioned samples. The applied Fourier transform method gave as an average of three:  $P_K = 0.86$ ,  $P_S = 0.14$ ,  $P_{KK} = 0.86$ ,  $P_{KS} = 0.14$ ,  $P_{SS} = 0.14$ ,  $P_{SK} = 0.86$  and subsequently  $P_K \cdot P_{KK} \cdot P_{KS} + P_K \cdot P_{KS} \cdot P_{SK} + P_S \cdot P_{SK} \cdot P_{KK} = 0.3$ . These coefficients indicate irregularly interstratified structure, zonal with tendency for regular interstratification, due to partial segregation of layers.

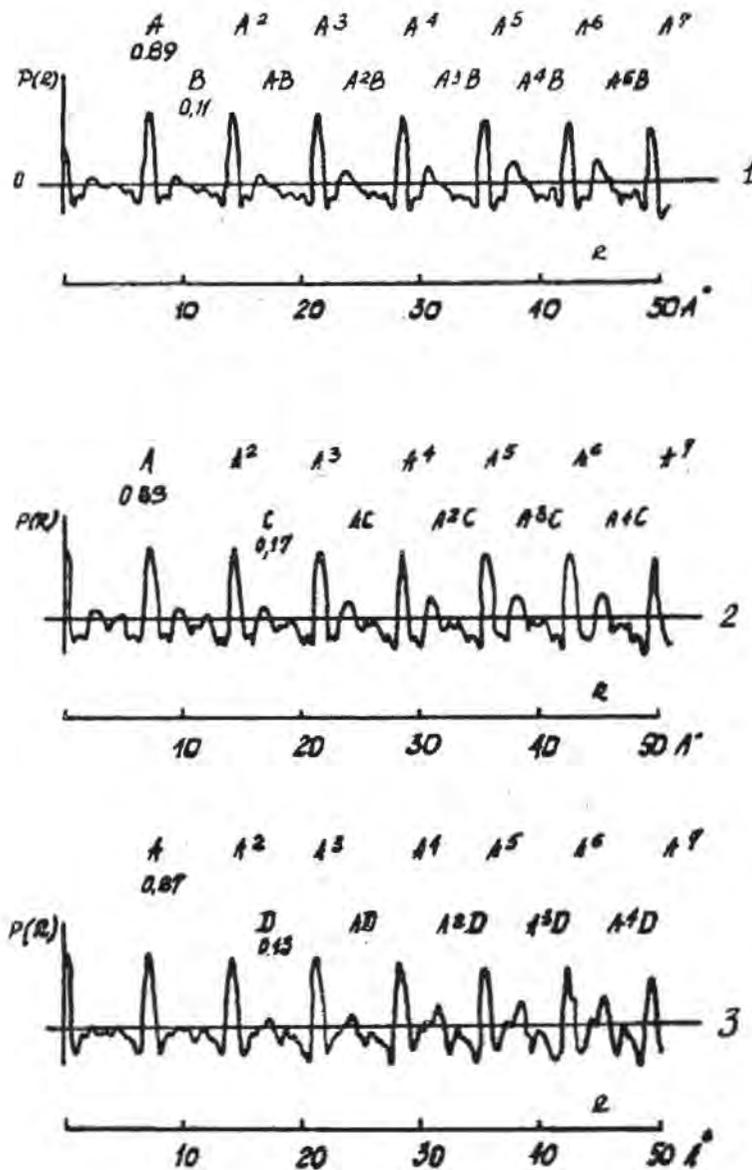


Figure 8. Fourier transforms of  $< 2 \mu$  particle size fractions: 1-heated to  $360^\circ\text{C}$ ; 2-saturated with ethylene glycol; 3-saturated with glycerol;  $A-d_K = 7.15 \text{ \AA}$ ;  $B-d_s = 9.6 \text{ \AA}$ ;  $C-d_s = 16.8 \text{ \AA}$ ;  $D-d_s = 17.6 \text{ \AA}$ .

## DERIVATION OF CHEMICAL FORMULA

< 1  $\mu$  size fractions were free of quartz, anatase and mica, could be then used for derivation of chemical formula. Calculation was performed on following assumptions:

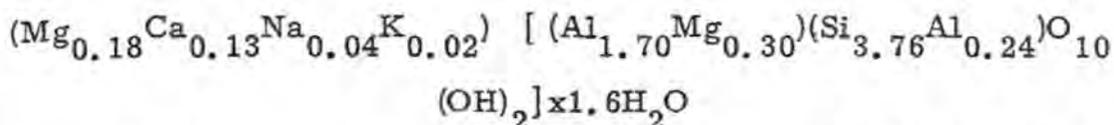
- (1) Kaolinite layers have an ideal composition -  $Al_2Si_2O_5(OH)_4$ .
- (2) Smectite layers have the general formulae -  $M_{x+y} [ /Al_{2-y}Mg_y / Si_{4-x}Al_x / O_5 / OH /_2 ]$ , where M means Mg, Ca, Na, K. An additional assumption is necessary that  $x = y$ .
- (3) According to the Fourier transform data 86 per cent of kaolinite and 14 per cent of smectite are interlayered in the investigated sample.
- (4) Iron exists in the form of hydrated oxides and is not taken into account.

Table 1

Chemical analysis < 1  $\mu$  size fractions

Compound	weight per cent
SiO <sub>2</sub>	47,02
TiO <sub>2</sub>	0,02
Al <sub>2</sub> O <sub>3</sub>	35,28
Fe <sub>2</sub> O <sub>3</sub>	0,58
FeO	0,03
MnO	trace
MgO	0,96
CaO	0,41
Na <sub>2</sub> O	0,08
K <sub>2</sub> O	0,05
H <sub>2</sub> O <sup>+</sup>	13,04
H <sub>2</sub> O <sup>-</sup>	2,53

Chemical analysis is presented in the Table 1. These data were used for calculation of the chemical formulae of the smectite layer:



A layer charge per formula unit equals then to 0.54, which is in the range characteristic for smectite (Brindley, 1966; Bailey et al., 1971).

Measurements of CEC, completed by aid of X-ray determination of Sr, when exchanged for the interlayer cations, gave 27 meq./100g.

According to the written formula 0.24 per four silica has been substituted by Al in the tetrahedral sheet. This has been well consistent with the Green-Kelly test, which revealed partial collapsing in the course of common treatment by Li-saturation, heating, and ethylene glycol saturation.

### BASAL SPACING BY ELECTRON DIFFRACTION

X-ray studies concerned polycrystalline material. Summary diffraction cannot be used for the control of the interlayering in the individual crystal. The control may be provided by monocrystal methods. For quick check on clay particles only electron diffraction may be seriously taken into account, but one must realize, that we need 001 reflections, instead of usually obtained hk reflections. Gorshkhov (1970) has shown, that this is practically possible. He also photographed basal reflections of 9 crystals of kaolinite-smectite for the present writer. At none of 9 photographs basal reflections of natural kaolinite were found. All examined crystals appeared to be mixed-layer kaolinite-smectite. Basing upon the  $d(001)$  spacing three kinds of interstratification were traced. For each of them  $d(001)$  were as follow:

$$(1) d_{(001)} = 3d_K + d_S = 31.3 \text{ \AA} \quad \text{where } d_K = 7.15 \text{ \AA}$$

$$(2) d_{(001)} = 4d_K + d_S = 38.8 \text{ \AA} \quad d_S = 9.8 \text{ \AA}$$

$$(3) d_{(001)} = 4d_K + 2d_S = 48.2 \text{ \AA}$$

Each of these combinations of spacings is the only possible one. Schematic representation of the structure of three kinds of crystals have been drawn in Fig. 9.

Judging from many orders of diffraction the interstratification in the investigated crystals is a very regular one.

One may be confused however, that kaolinite to smectite layers ratio is lower, than calculated from X-ray diffraction. This may be easily explained. Basal reflections were obtained from the curved edges of thin laminae. The rule is: the more of smectite layers,

the better curving; the thinner laminae, the better for diffraction. Then crystals containing more smectite layers than commonly occurring, thicker crystals were purposely chosen for the experiment.

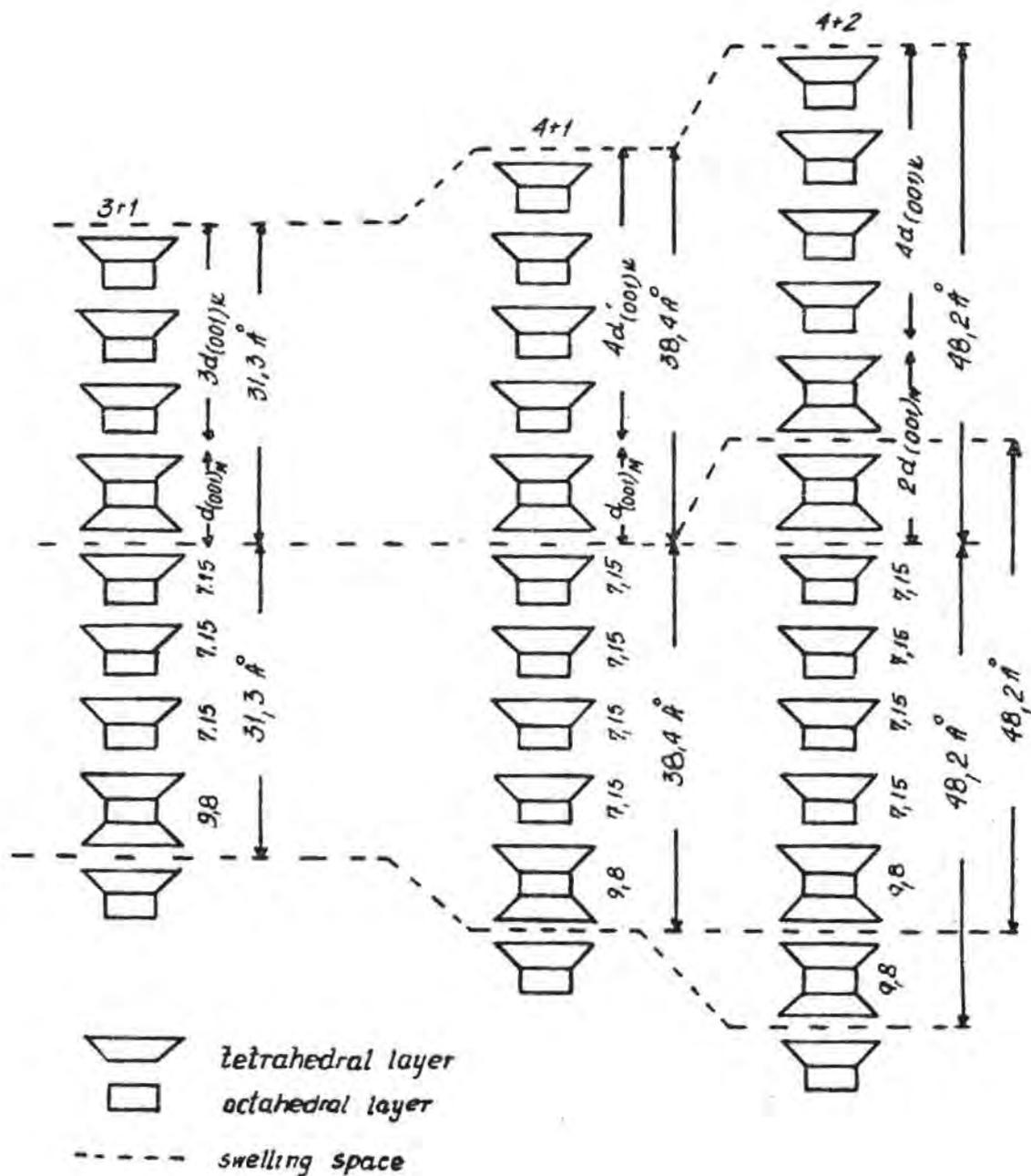


Figure 9. Diagrammatic representation of structure of regularly interstratified domains.

## ORIGIN

Presented data have shown than kaolinite and smectite layers - different in the sense of structure, chemical composition and bonds - are arranged in the definite mineral species, neglecting the rule of homogeneity of crystalline material. Moreover, kaolinite and smectite needs different physico-chemical environment for crystallization. Why then kaolinite-smectite could be formed in Jeglowa?. This question could be answered due to clear geologic relation of rocks exposed in quarry in Jeglowa. Against expectation and elementary logic, the one of two neighbouring clays, which substituted sericite was normal kaolinite, but mixed-layer clay was found in veins. Traces of the latter clay included in the rock crystal at the boundary of higher ( $\geq 300^{\circ}\text{C}$  according to Kozowski and Karwowski, 1971) and lower ( $220^{\circ}\text{C}$ ) temperatures generations were identified by infrared analysis (Fig. 10).

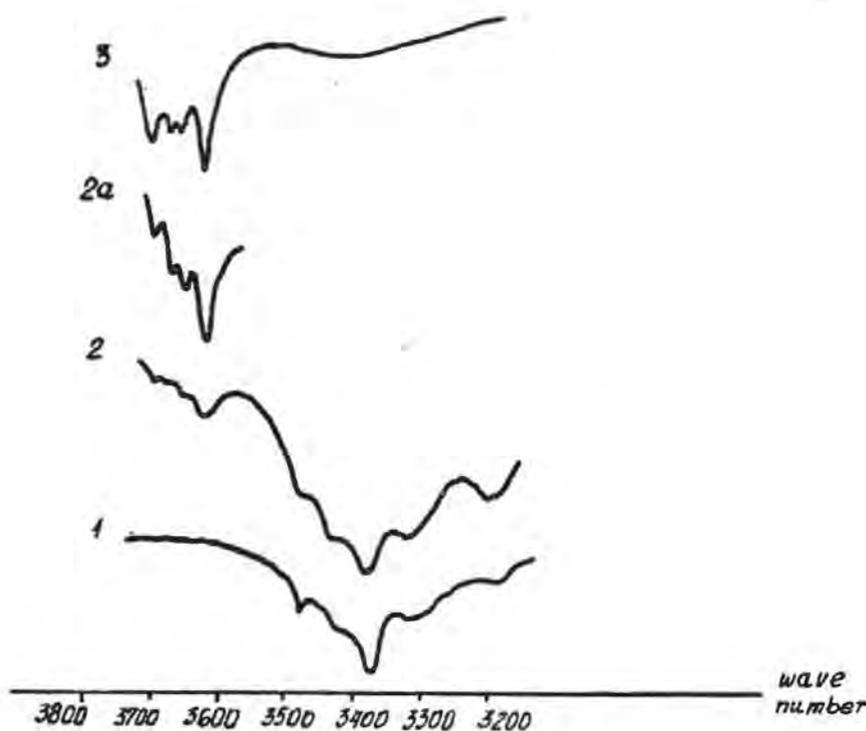


Figure 10. Infrared absorption spectra;

1. quartz of a low temperature generation without clay inclusions;
2. quartz of a high temperature generation with clay inclusion;
- 2a. the same like 2; more sensitive recording;
3. raw kaolinite-smectite.

Discussion of hydrothermal origin of kaolinite-smectite from Poland may be based on the well known rule, that chemical composition of geologic solutions determines the order of crystallization of minerals, and vice-versa, the type of newly created solid phase influences chemical composition of geologic solution. Paragenesis of kaolinite-smectite and quartz plus minor anatase and mica indicates the system  $\text{Al}_2\text{O}_3 - \text{SiO}_2 - \text{H}_2\text{O}$  plus some lesser amount of  $\text{MgO}$  and  $\text{TiO}_2$ . Quartz, which crystallizes and dissolves very slowly, could not influence the composition of the solution. Kaolinite and smectite were quickly crystallizing, thermodynamically metastable intermediate phases between quartz and diaspore. Simultaneous formation of kaolinite layers could then be possible if chemical composition of geologic solution and physical factors of temperature and pressure oscillated around a border point of formation of each type of layer. This could happen rarely, which determined that kaolinite-smectite has been quite unique in the world.

## CONCLUSIONS

Many characteristic features of the studied clay could be established, because various analytical methods were applied. All data appeared consistent. However some explanation should be given to the summary X-ray and single electron diffraction. The individual domains constructed in a regular way gave integral series of reflections of the type  $n \cdot d^x(001)$ . Domains might be created from different number of kaolinite and smectite type of layers. In consequence basal spacing in various domains could be one of many possible:  $d(001) = x d_K + y d_S$  (where  $x, y =$  small integers). This is a clue why summary X-ray diffraction indicated irregularly interstratified, zonal structure. The discovered arrangement seems to have broader significance, as disordered interstratification is much less probable than ordered from many points of view, most of all bonds. The described case calls for careful searches of regularly interstratified domains in clays giving non integral X-ray series of diffraction maxima (see also Reynolds and Hower, 1970).

## ACKNOWLEDGEMENTS

Words of deepest gratitude are due to Dr. K. Szpila and Mr A. Pelc from Poland, to Drs. G.W. Brindley and J.L. White from U.S.A., to Dr B.B. Zvyagin and Mr A.I. Gorshkhov from U.S.S.R. for their generous assistance in producing several results, which were extremely valuable for this study and which helped the author to believe in what he has traced.

## REFERENCES

- ALTSCHULER, Z.S., DWORNIK, E.J., and KRAMER, H. (1963): Transformation of montmorillonite to kaolinite during weathering. *Science*, 141, 148-152.
- AMIL, A.R., GARCIA, A.R., MACEWAN, D.M.C., (1967): *Curvas de difraccion de rayos x para el analisis de estructuras interstratificadas*. Volturna Press.
- BAILEY, S.W., BRINDLEY, G.W., JOHNS, W.D., MARTIN, R.T., ROSS M. (1971): Summary of national and international recommendations on clay mineral nomenclature, 1969-70 MCS Nomenclature Committee. *Clays and Clay Minerals*, 19, 129-132.
- BRINDLEY, G.W., (1966): Discussion and recommendations concerning the nomenclature of clay minerals and related phyllosilicates. *Proc. 14th Nat' l. Conf. Clays and Clays Minerals* 27-34.
- BROWN, C.B., WHITE, J.L. (1969): Reactions of s-triazines with soil clays. *Soil. Science Soc. of America, Proc.* 33, 863-867.
- CRUZ, M., WHITE, J.L. (1968): Montmorillonite - S - triazine interactions. *Israel Journ. of Chem.*, 6, 315-323.
- GORSHKOV, A.I. (1970): *Primenenie mikrodifrak sii elektronov dla polucheniya bazalnykh reflektsov ot plaslintsatykh sloistykh silikatov*. *Izv. AN SSSR*.
- KOZOWSKI, A., KARWOWSKI, L. (1972): Hydrothermal origin of quartz from Jeglowa, Lower Silesia, *Bull. d. Acad. Polon. Sci. ser. geol. et geogr.* (in press).
- MACEWAN, D.M.C., AMIL, R.A., BROWN, G. (1961): Interstratified clay minerals, in "X-ray identification and crystal structures of clay minerals" (Edited by Brown, G.) 393-445.
- MERING, J. (1949): L'interférence des rayons-X dans les systèmes à stratification désordonnée. *Acta Cryst.*, 3, 371-377.
- OBERC, J. (1966): *Geologia krystaliniku Wzgórz Strzelińskich*. *Studia Geologica Polonica*, XX.
- OINIMA, K., HAYASHI, H. (1965): Infrared study of mixed - layer clay minerals. *Am. Mineral.*, 50, 1213-1227.
- REYNOLDS, R.C., HOWER, J. (1970): The nature of interlayering in mixed - layer illite-montmorillonites. *Clays and Clay Minerals*, 18, 25-36.
- ROSS, M. (1968): X-ray diffraction effects by non-ideal crystals of biotite muscovite, montmorillonite, mixed clays, graphite, and periclase, *Zeitschrift für Kristallographie*, 126, 80-97.
- RUSSELL, J.D., CRUZ, M. WHITE, J.L., BAILEY, G.W., PAYNE, R., POPE, J.D. Jr., ROSALEY, J.I. (1968): Mode of chemical degradation of striazines by montmorillonite, *Science*, 160, 1340-1342.
- SCHULTZ, L.G., SHEPARD, A.O., BLACKMON, P.D., STARKEY, H.C. (1971): Mixed-layer kaolinite-montmorillonite from the Yucatan Peninsula, Mexico. *Clays and Clay Minerals*, 19, 137-150.

- SHIMOYAMA, A., JOHNS, W.D., SUDO, T. (1969): Montmorillonite kaolin clay in acid clay deposits from Japan. Proc. Intern. Clay Conference, Tokyo, Japan, 1, 225-233.
- SUDO, T., HAYASHI, H. (1956): A Randomly interstratified kaolin-montmorillonite in acid clay deposits in Japan, Nature, 178, 1115-1116.
- SZPILA, K., WIEWIÓRA, A., GADOMSKI, M. (1972): Preliminary investigation of kaolinite-smectite from Jegłowa, Lower Silesia. Bull. Acad. Polon. Sci., Série Sci. Terre, 20, 19-24.
- WIEWIÓRA, A. (1971): A mixed-layer kaolinite-smectite from Lower Silesia, Poland. Clays and Clay Minerals, 19, 415-416.

## CORRELATION BETWEEN THE HYDROXYL STRETCHING BANDS AND THE CHEMICAL COMPOSITION OF TRIOCTAHEDRAL MICAS

J.M. Rousseaux, C. Gomez Laverde, Y. Nathan, P.G. Rouxhet  
Laboratoire de Physico-Chimie Minérale, Université Catholique de  
Louvain, de Croylaan 42, 3030  
Heverlee, Belgium

**ABSTRACT.** - The integrated parallel absorption coefficient of the OH stretching bands and the hydroxyl content have been determined for a series of 14 biotites and 22 phlogopites. Correlations with the chemical composition allowed to estimate the absorption coefficient per hydroxyl for N and I bands respectively and to propose new assignments for V bands of biotites. The absorption coefficient of the latter allows to detect the presence of an appreciable amount of octahedral aluminium.

### INTRODUCTION

The observation of the hydroxyl stretching bands of silicates is often applied for elucidating crystallochemical features of these minerals or describing their behaviour under various conditions. The information is usually provided through qualitative comparison of spectra, band shape interpretation or relative intensity measurements. However in some instances the measurement of absorption coefficient, although not straightforward, could be valuable by allowing a real quantification of the observations or characterizing various types of hydroxyls by an appropriate parameter.

It has been described before how to practically determine a reliable absorption coefficient for the OH stretching bands of micas (Rouxhet, 1970). This was called integrated parallel absorption coefficient K. The term integrated means that its value was deduced from the band area; the term parallel is used because the effect of orientation of hydroxyls was taken account, the coefficient being

the true absorption coefficient of a system where the electric vector of the radiation would be parallel to the direction of all hydroxyl groups. The so determined coefficient is proportional to the concentration of hydroxyls responsible for the band. The proportionality factor is only related to the effective charge and mass of the oscillators, it does not depend neither on the frequency or the width of the band nor on the orientation of molecular groups in the crystal.

In the present paper the data of the quantitative interpretation of OH stretching bands are reported for a collection of 14 biotites and 22 phlogopites. These data and other characteristics of the spectra will then be correlated with the chemical composition of the minerals.

The samples are described and their complete chemical analysis reported in the paper by Rousseaux et al. Comparison of the structural formulae with the diagram of octahedral composition given by Foster (1960) shows that phlogopites cover a representative range of  $R^{3+} + R^{4+}$  contents, but have all a low  $Fe^{2+}$  content. There are 4  $Mg^{2+}$  biotites with a low  $R^{3+}$  content and 10  $Fe^{2+}$  biotites.

## EXPERIMENTAL PROCEDURE

### Infrared data

The spectra were recorded with a Beckman IR 12 spectrograph, set in conditions suitable for recording quantitatively the shape of the bands in absorbance. The light was polarized by a Beckman AgCl plates polarizer, placed before the mirror focusing the light on the thermocouple and thereby affecting both the reference and the sample beam.

The samples were cleaved plates of about 1 by 1 cm; their thickness was expressed in  $mg/cm^2$ . When necessary the interference fringes were reduced by cleaving the plate in two parts which were maintained slightly out of parallelism. The sample holder is similar to the one used by Rouxhet (1970) but of greater dimension; it was placed directly in the sample beam.

### Weight loss curves

Thermogravimetric curves were recorded for biotites; the use of a RG Cahn electrobalance allowed to detect weight changes of 0.02 % with samples of about 300 mg. The samples were platelets of about 2 by 10 mm. The heating program allowed to reach 400°C in 2 hours, with a subsequent temperature rise of 30°C per hour. As the atmospheric pressure provoked oscillations, a pressure of about 200 torr of oxygen was maintained in the system. In order to avoid electrostatic perturbations an alumina tube was preferred to a fused silica tube.

## RESULTS AND DISCUSSION

The phlogopites show the typical N and I pleochroic bands (Vedder, 1964) due to hydroxyls about perpendicular to the ab plane and located respectively close to 3 divalent ( $R^{2+}R^{2+}R^{2+}$ ) and 2 divalent + 1 trivalent octahedral cations ( $R^{2+}R^{2+}R^{3+}$ ). Upon decreasing the angle between the polarization direction and the  $c^*$  axis, the relative increase of the integrated intensity is not significantly different for the N and for the I bands.

For the biotites studied the N and I bands are not separated because of the presence of  $Fe^{2+}$  ions in appreciable amount (Wilkins, 1967). The centre of gravity of the resulting band shifts approximately from 3700 to 3655  $cm^{-1}$  as the atomic ratio

$$\frac{Fe^{2+}}{Mg^{2+} + Fe^{2+}}$$

changes from 0.3 to 0.7. The V bands, due to hydroxyls associated with an octahedral vacancy, will be described later in details.

The integrated parallel absorption coefficient  $K$  has been determined on one hand for N and I bands together, and on the other hand for V bands, using methods described by Rouxhet (1970). It has been checked again that for both biotites and phlogopites the intensity of the N-I bands is independent of the orientation of the polarization plane with respect to the a and b axis. By measuring interference fringes near the absorption bands it has also been verified that 1.6 is a satisfactory value for the refractive index. For all biotites the integrated area used for V bands was the average between the minimum and maximum values observed when rotating the polarization vector in the ab plane; the  $K$  coefficient was estimated by using of relation (6) of that paper. Among the phlogopites, a few had a V band of very low intensity; the values obtained for the absorption coefficient are not reported because they lack in accuracy and are of no further use for the present work.

The volumetric measurement of the total hydroxyl content of micas has been described by Rouxhet (1970) and Rousseaux et al. The TGA curves of biotites show a fairly well defined plateau after a loss of 0.01-0.05% attributed to molecular water. The subsequent step was attributed to the loss of V hydroxyls by Vedder & Wilkins (1969). As already observed by these authors the temperature of the step varies from 550° to 850°C, being progressively higher for samples showing a smaller weight loss. The appearance of a plateau or a clear inflection point after the loss of V hydroxyls is due to the loss of other hydroxyls being combined with an oxidation process; it is not observed if the TGA curve is recorded under vacuum. Therefore the TGA curve should be considered as providing only an estimation of the V hydroxyl content.

The results obtained are in agreement with those obtained previously through static weight loss curves (Rouxhet, 1970). The N + I hydroxyl content of biotites is calculated by difference between V hydroxyl and total hydroxyl contents.

The values obtained for the integrated parallel absorption coefficient K and the hydroxyl content are reported in Table I and Table II for phlogopites and biotites respectively. Fig. 1 illustrates the linear relationship between the two parameters.

Table I. Data for phlogopites: Integrated parallel absorption coefficient K (wavenumber  $\text{mg}^{-1} \text{cm}^2$ ), hydroxyl content (%  $\text{H}_2\text{O}$ ), ratio of the integrated absorbance of bands I and N ( $A_I/A_N$ ).

	K	% $\text{H}_2\text{O}$	$A_I/A_N$		K	% $\text{H}_2\text{O}$	$A_I/A_N$
P <sub>1</sub>	43.0	3.59	0.52	P <sub>14</sub>	33.2	2.35	0.51
P <sub>2</sub>	51.5	4.02	0.54	P <sub>15</sub>	26.8	1.95	0.35
P <sub>3</sub>	35.3	3.02	0.30	P <sub>16</sub>	21.2	1.87	0.44
P <sub>4</sub>	42.4	2.59	0.60	P <sub>17</sub>	26.2	2.03	0.42
P <sub>5</sub>	26.6	2.17	0.28	P <sub>18</sub>	12.2	1.20	0.15
P <sub>6</sub>	27.0	1.96	0.30	P <sub>19</sub>	26.2	1.82	0.52
P <sub>8</sub>	32.6	2.60	0.50	P <sub>20</sub>	12.6	1.26	0.23
P <sub>9</sub>	34.0	2.73	0.66	P <sub>22</sub>	30.0	2.12	0.69
P <sub>10</sub>	31.7	2.89	0.42	P <sub>23</sub>	33.1	3.50	0.0
P <sub>11</sub>	28.7	2.42	0.30	P <sub>24</sub>	42.4	3.02	0.59
P <sub>12</sub>	42.0	2.32	0.78				

#### N and I bands

A comparison of the results for the N+I bands of phlogopites and biotites in Fig. 1 shows that using the integrated absorbance allows comparing the absorption coefficient of bands having a different shape. The dispersion of dots is of course partially due to a rather low accuracy, however it is worth investigating about its possible significance.

For phlogopites the separate measurement of N and I band areas is rather straightforward and was performed on various spectra of each sample. On the other hand the ratio of the number of

Table 2: Data for biotites: content of the main octahedral cations (ions per three octahedral sites); integrated parallel absorption coefficient K of V and N-I bands (wavenumber  $\text{mg}^{-1} \text{cm}^2$ ) and corresponding hydroxyl content (%  $\text{H}_2\text{O}$ )

	Octahedral cations					V bands		N-I bands	
	$\text{Al}^{3+}$	$\text{Ti}^{4+}$	$\text{Fe}^{3+}$	$\text{Fe}^{2+}$	$\text{Mg}^{2+}$	K	% $\text{H}_2\text{O}$	K	% $\text{H}_2\text{O}$
B11	0.60	0.13	0.17	1.24	0.46	21.5	0.30	25.2	1.92
B13	0.51	0.14	0.21	1.27	0.57	24.3	0.27	27.5	1.19
B5	0.38	0.25	0.10	1.36	0.76	25.1	0.36	39.4	2.32
B3	0.27	0.20	0.15	1.31	0.86	24.3	0.49	37.0	2.49
B1	0.25	0.17	0.09	1.26	1.08	22.7	0.36	40.9	2.91
B7	0.00	0.16	0.03	1.15	1.52	2.0	0.12	16.4	1.58
B8	0.09	0.17	0.04	0.75	1.90	2.8	0.19	17.2	1.18
B10	0.04	0.13	0.09	1.04	1.60	2.6	0.15	15.1	1.42
B12	0.05	0.13	0.09	1.04	1.53	2.1	0.14	13.2	1.46
B6	0.02	0.18	0.18	1.42	1.15	2.1	0.19	18.5	1.67
B9	0.05	0.21	0.23	1.41	1.05	5.6	0.30	19.8	2.03
B4	0.08	0.17	0.20	1.48	0.93	4.2	0.25	25.0	2.21
B2	0.06	0.15	0.25	1.44	1.05	4.0	0.26	27.1	1.95
B14	0.09	0.13	0.18	1.44	1.02	3.5	0.28	29.7	2.19

sites I and N may be estimated from the chemical analysis by the expression  $3X/Y$  (Vedder, 1964), where Y is the number of divalent ions ( $\text{Mg}^{2+}$ ,  $\text{Fe}^{2+}$ ,  $\text{Mn}^{2+}$ ) per three octahedral sites. In our calculations X was taken as the number of  $\text{Al}^{3+} + \text{Fe}^{3+} + \text{Ti}^{4+}$  ions per three octahedral sites.

Figure 2 shows the correlation between the ratio of integrated absorbances ( $A_I/A_N$ ) and the ratio of number of sites; the slope is about 1.95. It is noteworthy that considering the  $\text{Al}^{3+}$  ions alone for calculating X would give a graph with about the same slope but with a intercept of about 0.2. If it is considered that the vicinity of two trivalent cations is improbable, the ratio of the number of

sites may be estimated by

$$\frac{X}{Y-2} \quad \text{or} \quad \frac{X}{1-X}$$

A graph similar to Fig. 2 is then obtained with a slightly higher dispersion and a slope of about 1.6.

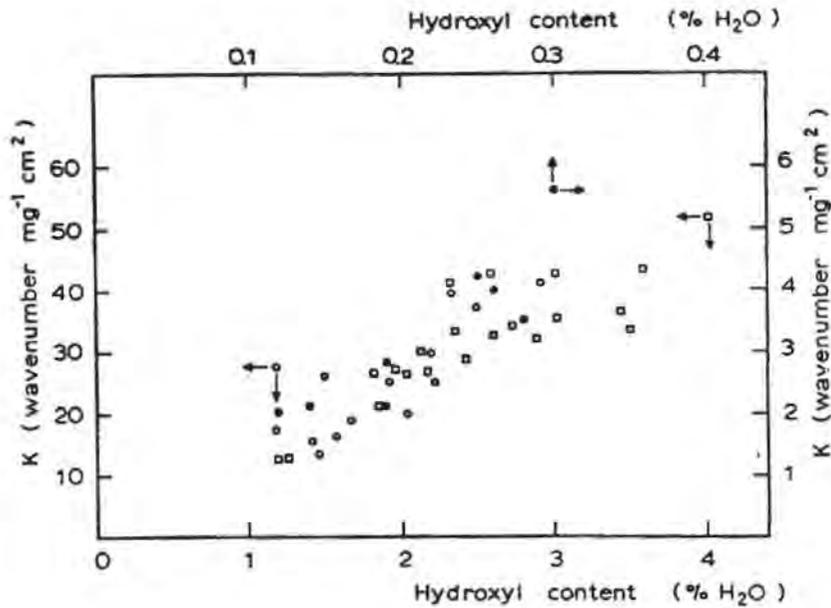


Figure 1. Correlation between the integrated parallel absorption coefficient  $K$  and the hydroxyl content;

- N-I bands of phlogopites; ○ N-I bands of biotites;
- V bands of biotites.

From these data it is concluded that the absorption coefficient per hydroxyl would be about 1.8 times higher on I than on N sites. Complementary information is provided by the values of the bulk absorption coefficient per hydroxyl  $k$ ; this is given in wavenumber  $(\mu\text{mole OH})^{-1} \text{ cm}^2$  if calculated by the expression

$$\frac{K \times 0.9}{\% \text{ H}_2\text{O}}$$

Figure 3 shows the correlation between  $k$  and

$$\left(\frac{Y}{3X} + 1\right)^{-1}$$

which is an estimation of the proportion of I sites. According to the

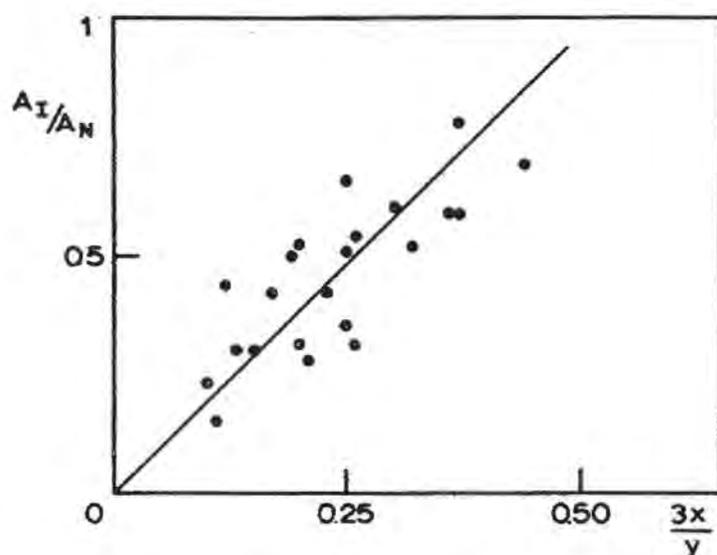


Figure 2. Correlation for phlogopites between the ratio of the area of bands I and N ( $A_I/A_N$ ) and the ratio of hydroxyl sites I and N estimated from chemical analysis.

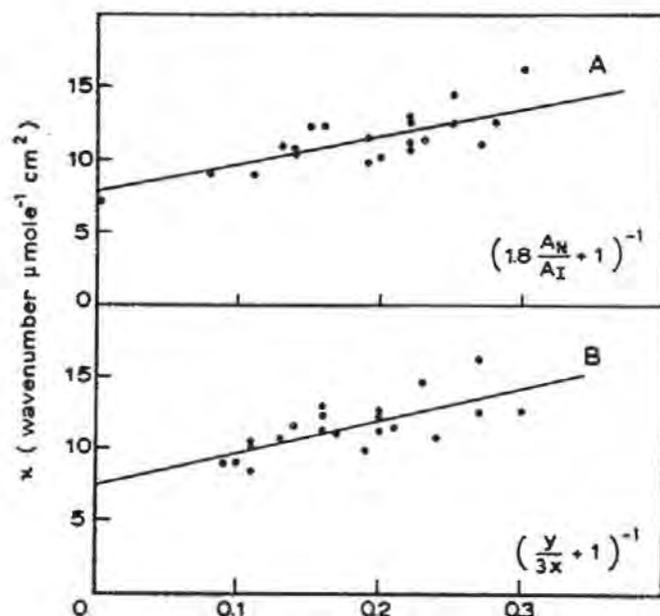


Figure 3. Correlation for phlogopites between the bulk parallel absorption coefficient per hydroxyl K and the proportion of I hydroxyl sites estimated A - from infrared data (correlation coefficient: 0.74; intercept: 7.9, slope: 19.1); B - from chemical analysis (correlation coefficient: 0.71, intercept: 7.6, slope: 21.8).

method used for calculating the structural formulae (Rousseaux et al., errors in hydroxyl content measurement affect the last expression in the same direction as  $k$ . Therefore the proportion of I sites has also been estimated by the expression  $(1.8 A_N/A_I + 1)^{-1}$ , which is only depending on infrared data; the corresponding correlation is illustrated by Fig. 3A. In both graphs the dot of sample P21 was deleted because this has a high Li content.

The intercept of the graphs in Fig. 3 shows that the parallel absorption coefficient per hydroxyl N is close to 8 wavenumber  $(\mu\text{mole})^{-1} \text{ cm}^2$ . It is interesting to note that a value of about 7 may be calculated from data obtained for two amphiboles (Rouxhet et al., 1972). The slopes obtained for the same graphs are given in the legend of Fig. 3. Although the precision is very low, they suggest that  $k$  may be 3-4 times higher for I than for N hydroxyls.

At present it is not possible to refine these estimations. It should also be kept in mind that they are based on the assumption that the distribution of hydroxyls is random among N-I sites. If there is some preferred association of the excess oxygen ions with I sites, the ratio  $k_I/k_N$  must be higher than indicated above. No further precision can be obtained by utilizing the data obtained for biotites.

By the use of a curve analyser, it has been attempted to decompose the spectra into individual components  $N_A$  ( $\text{Mg}^{2+} \text{Mg}^{2+} \text{Mg}^{2+}$ ),  $N_B$  ( $\text{Mg}^{2+} \text{Mg}^{2+} \text{Fe}^{2+}$ ),  $N_C$  ( $\text{Mg}^{2+} \text{Fe}^{2+} \text{Fe}^{2+}$ ) etc., as described by Wilkins (1967). However it was found that the method is not applicable to studying the possibility of ordering of octahedral cations or preferential association of hydroxyl, fluorine or excess oxygen ions with some octahedral environments. The spectra of 12 phlogopites, containing no more than 0.07  $\text{Fe}^{2+}$  ions per three octahedral sites provided the following characteristics for  $N_A$  ( $\text{Mg}^{2+} \text{Mg}^{2+} \text{Mg}^{2+}$ ) and  $I_A$  ( $\text{Mg}^{2+} \text{Mg}^{2+} \text{R}^{3-4+}$ ) bands:

$N_A$  : position  $3712 \pm 2 \text{ cm}^{-1}$ , half band width  $25 \pm 2 \text{ cm}^{-1}$   
 $I_A$  : position  $3669 \pm 1 \text{ cm}^{-1}$ , half band width  $36 \pm 4 \text{ cm}^{-1}$

### V bands

Figure 1 shows that the absorption coefficient per V hydroxyl observed for 9 biotites is about the same as for N-I hydroxyls of biotites and phlogopites; at present this coincidence cannot be discussed further. However it is quite striking that 5 biotites show very much higher values for  $k$ , so much that it is not even necessary to know the corresponding hydroxyl content to identify them.

Spectra representative of the various samples studied are given in Fig. 4. The two curves reported for each sample correspond to the two extremes observed when rotating the polarization direction in the ab plane; all of them were recorded at normal incidence. In Table II ordering and grouping the samples were done according

to the characteristics of the V bands and fit nicely differences in the chemical composition. In particular it appears clearly that the biotites with a high  $k$  value have an octahedral aluminum content not lower than 0.25 per 3 sites.

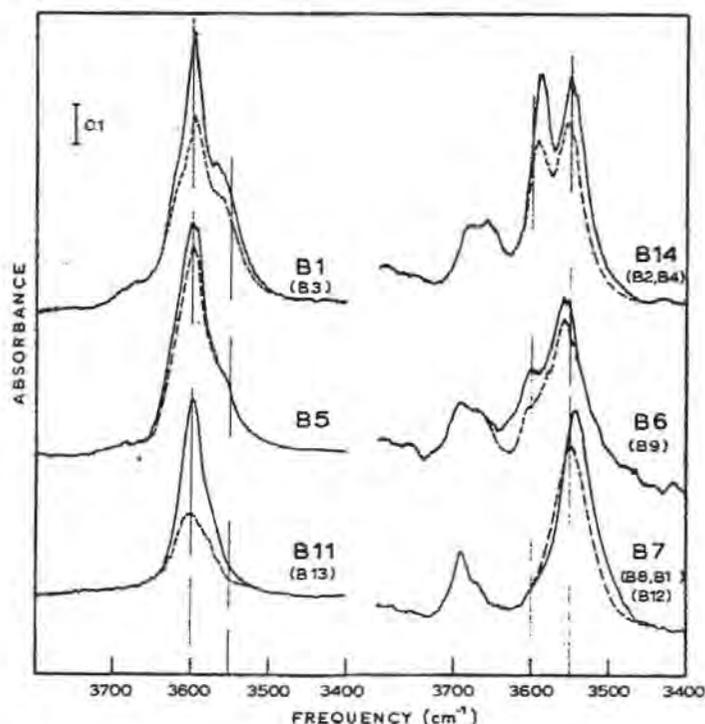


Figure 4. Hydroxyl stretching bands at normal incidence of the indicated biotites, also representative for the samples indicated between brackets. The two curves correspond to the extremes observed when the polarization vector is rotated in the  $ab$  plane.

These biotites show one band around  $3590\text{--}3600\text{ cm}^{-1}$ . No other band is observed for sample B11; as the  $\text{Al}^{\text{VI}}$  content decreases a shoulder develops at about  $3560\text{ cm}^{-1}$  and is quite clear for samples B1 and B3. Muscovites are also characterized by an absorption coefficient per hydroxyl considerably higher than those observed for N-I hydroxyls of trioctahedral micas (Rouxhet, 1970). Therefore it is concluded that V hydroxyls in Al rich biotites are bound to two octahedral cations having a charge higher than 2. The band at  $3600\text{ cm}^{-1}$  may then be attributed to hydroxyls located on  $\text{Al}^{3+}\text{Al}^{3+}\text{V}$  sites. The  $3560\text{ cm}^{-1}$  component would presumably be due to  $\text{Al}^{3+}\text{Fe}^{3+}\text{V}$  or  $\text{Al}^{3+}\text{Ti}^{4+}\text{V}$  environments.

The two samples having a very high  $\text{Al}^{\text{VI}}$  content show a well marked variation of band intensity when the polarization direction is rotated in the  $ab$  plane. The observed dichroic ratio is about 2 for B11 and 2.9 for B13 while it is about 1.3 for B5, B3 and B1. A

high dichroic ratio indicates that the octahedral vacancies are distributed in a fairly ordered way.

For Mg biotites only one band is observed around  $3550\text{ cm}^{-1}$ . The Fe biotites B4, B2 and B14 show two bands of about equal height respectively at  $3590$  and  $3550\text{-}3560\text{ cm}^{-1}$  while for samples B6 and B9 the  $3590\text{ cm}^{-1}$  component appears only as a shoulder. A comparison of the octahedral layer compositions of the three groups of samples shows that the  $3590\text{ cm}^{-1}$  component increases when the  $\text{Fe}^{3+}$  content increases with respect to  $\text{Ti}^{4+}$ . Therefore this component must be due to hydroxyls located on  $\text{R}^{2+}\text{Fe}^{3+}\text{V}$  sites while the  $3550$  component would possibly correspond to  $\text{R}^{2+}\text{Ti}^{4+}\text{V}$  environments.

These biotites show dichroic ratios of 1 to 1.4. However for the Mg rich samples the position of the band at  $3550\text{ cm}^{-1}$  is appreciably altered when the polarization vector is rotated in the ab plane. This peculiar behavior may be explained by the presence of various components due to hydroxyls located for instance on  $\text{Fe}^{2+}\text{Ti}^{4+}\text{V}$  and  $\text{Mg}^{2+}\text{Ti}^{4+}\text{V}$  sites and having different pleochroic properties. It has been indeed reported by Hogg and Meads (1970) that the  $\text{Fe}^{2+}$  ions occupy preferentially the more symmetric octahedral sites.

The band at  $3620\text{ cm}^{-1}$  reported by Vedder (1964) and Farmer et al. (1967, 1971) is not observed for the biotites studied here. However it appears clearly among the V bands a few phlogopites.

## CONCLUSIONS

The reported data show that the quantitative use of hydroxyl stretching bands is feasible and can lead to interesting data.

The parallel absorption coefficient per hydroxyl located near three divalent octahedral cations was found to be 8 wavenumber  $(\mu\text{mole})^{-1}\text{ cm}^2$ . The substitution of a divalent by a tri or tetravalent ion makes this coefficient to be higher by a factor which may be of the order of 1.8 to 4.

Comparison of infrared data with chemical composition allowed to propose new tentative assignments for V bands of biotites. High values of the parallel absorption coefficient per hydroxyl are thought to indicate the association of hydroxyls with  $\text{R}^{3+}\text{R}^{3+}\text{V}$  or  $\text{R}^{3+}\text{R}^{4+}\text{V}$  sites.

Pleochroic measurements have indicated an ordered distribution of octahedral vacancies in samples having 0.5-0.6 Al ions per three octahedral sites.

## ACKNOWLEDGEMENTS

J.M. Rousseaux was supported by the "Institut pour l'Encouragement de la Recherche Scientifique dans l'Industrie et l'Agriculture" and C. Gomez Laverde by the "Office de Coopération pour le Développement". Y.Nathan was on a leave of absence from the Geological Survey of Israel, supported by the Israel-Belgium Cultural Relations Agreement. P.G. Rouxhet was a research fellow of the "Fonds National de la Recherche Scientifique".

## REFERENCES

- FARMER, V.C., RUSSEL, J.D., AHLRICHS, J.L. and VELDE, B. (1967): Vibrations du groupe hydroxyle dans les silicates en couches. Bull. Groupe Franc. Argiles 19-2, 5-10.
- FARMER, V.C., RUSSEL, J.D., Mc. HARDY, W.J., NEWMAN, A.C.D., AHLRICHS, J.L. and RIMSAITE, J.Y. (1971): Evidence for loss of protons and octahedral iron from oxidized biotites and vermiculites. Min. Mag. 38, 121-137.
- FOSTER, M.D. (1960): Interpretation of the composition of trioctahedral micas. U.S. Geolog. Survey Prof. Paper 354-B.
- HOGG, C.S. and MEADS, R.E. (1970): The Mössbauer spectra of several micas and related minerals. Min. Mag. 37, 606-614.
- ROUSSEAU, J.M., VIELVOYE, L.A., ROUXHET, P.G. and HERBILLON, A.J.: The vermiculitization of trioctahedral micas: correlations between the K level and the chemical composition. To be published.
- ROUXHET, P.G. (1970): Hydroxyl stretching bands in micas: A quantitative interpretation. Clay Miner. 8, 375-388.
- ROUXHET, P.G. GILLARD, J.L. and FRIPIAT, J.J. (1972): Thermal decomposition of amosite, crocidolite and biotite. Min. Mag. 36, 325-333.
- VEDDER, W. (1964): Correlations between infrared spectrum and chemical composition of mica. Amer. Min. 49, 736-768.
- VEDDER, W. and WILKINS, R.T.W. (1969): Dehydroxylation and rehydroxylation, oxidation and reduction of micas. Amer. Miner., 54, 482-509.
- WILKINS, R.W.T. (1967): The hydroxyl-stretching region of the biotite mica spectrum. Min. Mag. 36, 325-333.



# LE SPECTRE INFRAROUGE DES BIOTITES: VIBRATIONS D'ÉLONGATION BASSE FRÉQUENCE DES OH DU RESEAU

J. Chaussidon

Institut National de la Recherche Agronomique  
Station d'Agronomie - C.N.R.A. - 78 - Versailles - France

**ABSTRACT.** - The infrared absorption of stretching vibrations of structural dioctahedral OH was studied with polarized radiation in the case of five biotites; crystals were rotated around the normal to ab plane. Four samples are obviously dichroic with a frequency of the maximum absorption which varies according to the polarization, parallel to a or to b axis. These results are interpreted by considering that measured absorption is the sum of two elementary absorptions due respectively to OH in  $C_{2/m}$  or  $C_2$  symmetry. The quantitative composition rule of those absorptions depends on the polytype and implies that " $C_{2/m}$ " OH have a maximum absorption frequency higher than " $C_2$ " OH, which seems supported by an estimation of two OH dipoles interaction at the octahedral vacancy.

## INTRODUCTION

Des deux massifs d'absorption infrarouge correspondant aux vibrations d'élongation des OH de constitution des biotites, le massif basse fréquence dû aux OH appartenant à une structure localement dioctaédrique est le moins bien connu.

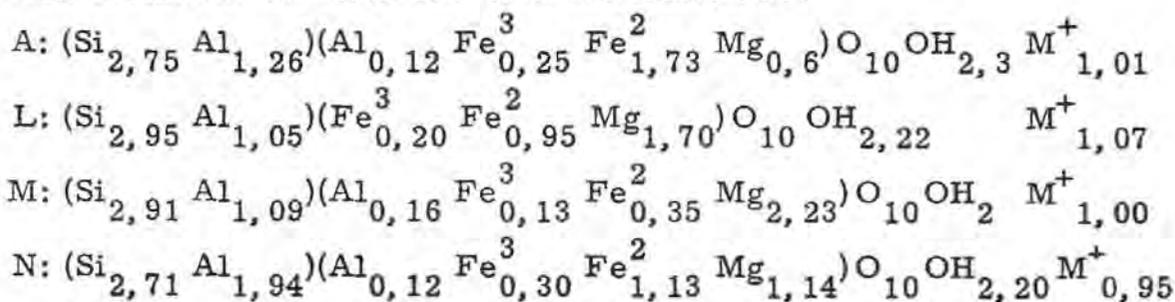
Dans un travail déjà ancien, VEDDER (VEDDER et al. 1963) avait pu déterminer avec précision l'orientation de la projection du moment de transition de l'hydroxyle sur le plan a b dans le cas de la muscovite. Ce minéral présente en effet un très fort dichroïsme d'absorption selon que la lumière est polarisée parallèlement à l'axe a ou à l'axe b; de plus, la structure de la muscovite est relativement simple et le nombre des polytypes différents les plus souvent

rencontrés est réduit. Le spectre de la muscovite dans la région 2000 - 4000  $\text{cm}^{-1}$  ne montre qu'une bande à une fréquence qui ne varie pas avec l'orientation des axes par rapport au vecteur électrique, et qui reste pratiquement la même quel que soit l'échantillon.

Dans le cas des biotites en général, le spectre change d'un échantillon à l'autre. Plusieurs maxima d'absorption peuvent être observés, les fréquences en sont variables et le dichroïsme dans le plan a b peut être nul ou assez fort. Ceci tient à la variété des cations présents en couche octaédrique et à l'existence signalée d'une façon assez courante d'au moins quatre polytypes simples différents, 1 M, 2 M 1, 2 M 2 et 3 T. Enfin, le taux d'occupation souvent élevé de la couche octaédrique, implique que la présence de grands domaines à structure ordonnée comme dans le cas de la muscovite soit assez peu probable, et qu'il faille tenir compte simultanément des deux structures hydroxyliques dioctaédriques possibles, correspondant aux groupes de symétrie de la maille C 2/m et C 2.

## PARTIE EXPERIMENTALE

Cinq biotites ont été étudiées. L'échantillon B ("Biotite de Bancroft" fournie par WARDS) n'a pas été analysée chimiquement. Les formules structurales sont les suivantes:



Les spectres ont été enregistrés sur un spectrophotomètre Beckman IR 12 équipé d'un polariseur à lames de Ag Cl disposé dans l'optique aussi près que possible du thermocouple, juste avant la fente de sortie. Les échantillons étaient soit munis d'un diaphragme circulaire de 6 mm de diamètre et éclairés par le faisceau normal, soit examinés dans le dispositif condenseur de faisceau. Aucune différence n'a été observée entre ces deux techniques. Les mesures étaient effectuées sur un tour complet autour de la normale au plan ab, de  $10^\circ$  en  $10^\circ$ , en incidence normale.

## RESULTATS EXPERIMENTAUX

Ils sont résumés par les Figs. 1 à 5.

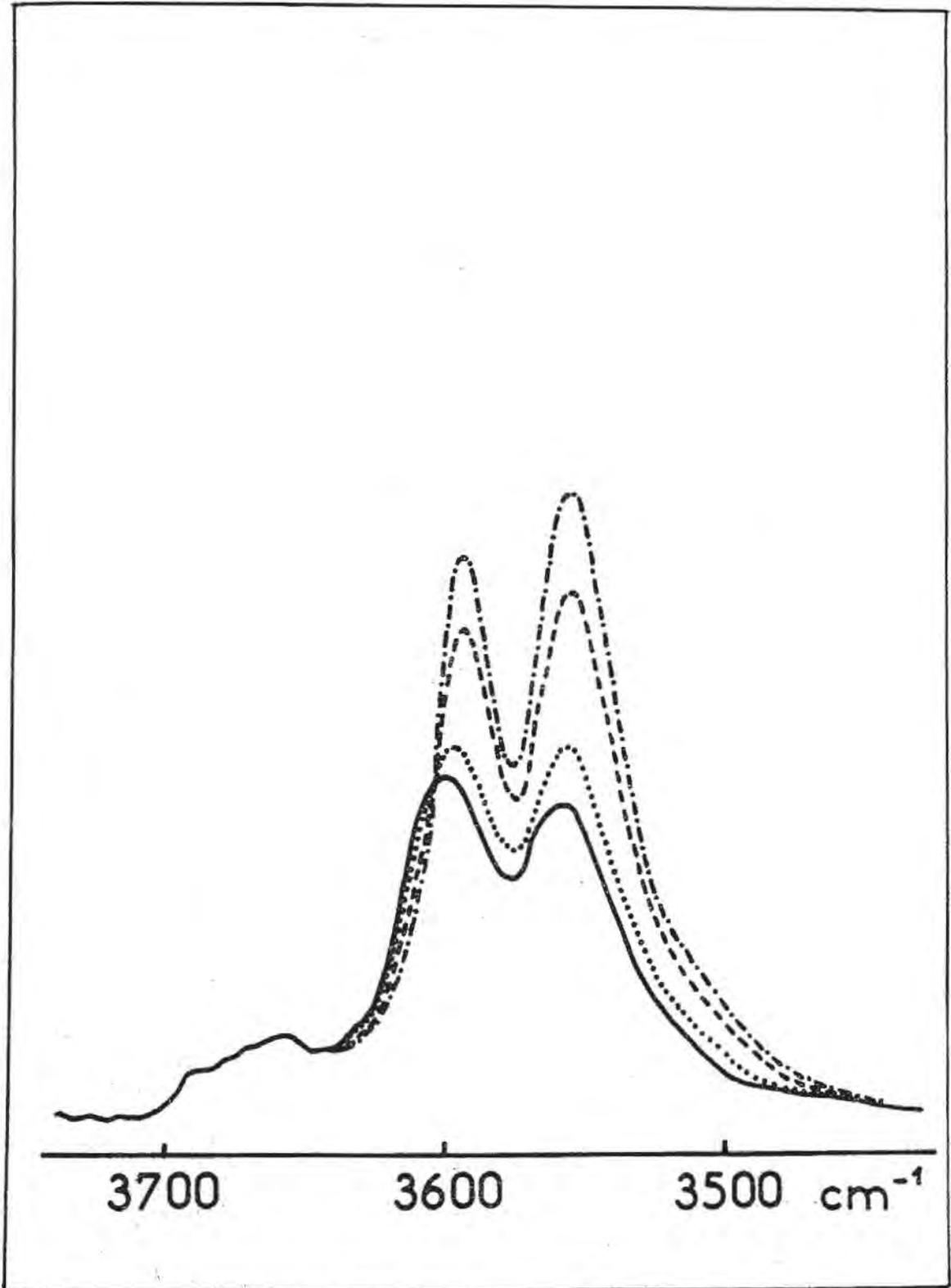


Figure 1. Spectre de la biotite A.  
 Les différents tracés correspondent à 4 valeurs de l'angle  $\theta$  entre le vecteur électrique et l'axe a: -.-.-:  $\theta = 0^\circ$ ; ----:  $\theta = 30^\circ$ ; .....:  $\theta = 60^\circ$ ; ———:  $\theta = 90^\circ$ .

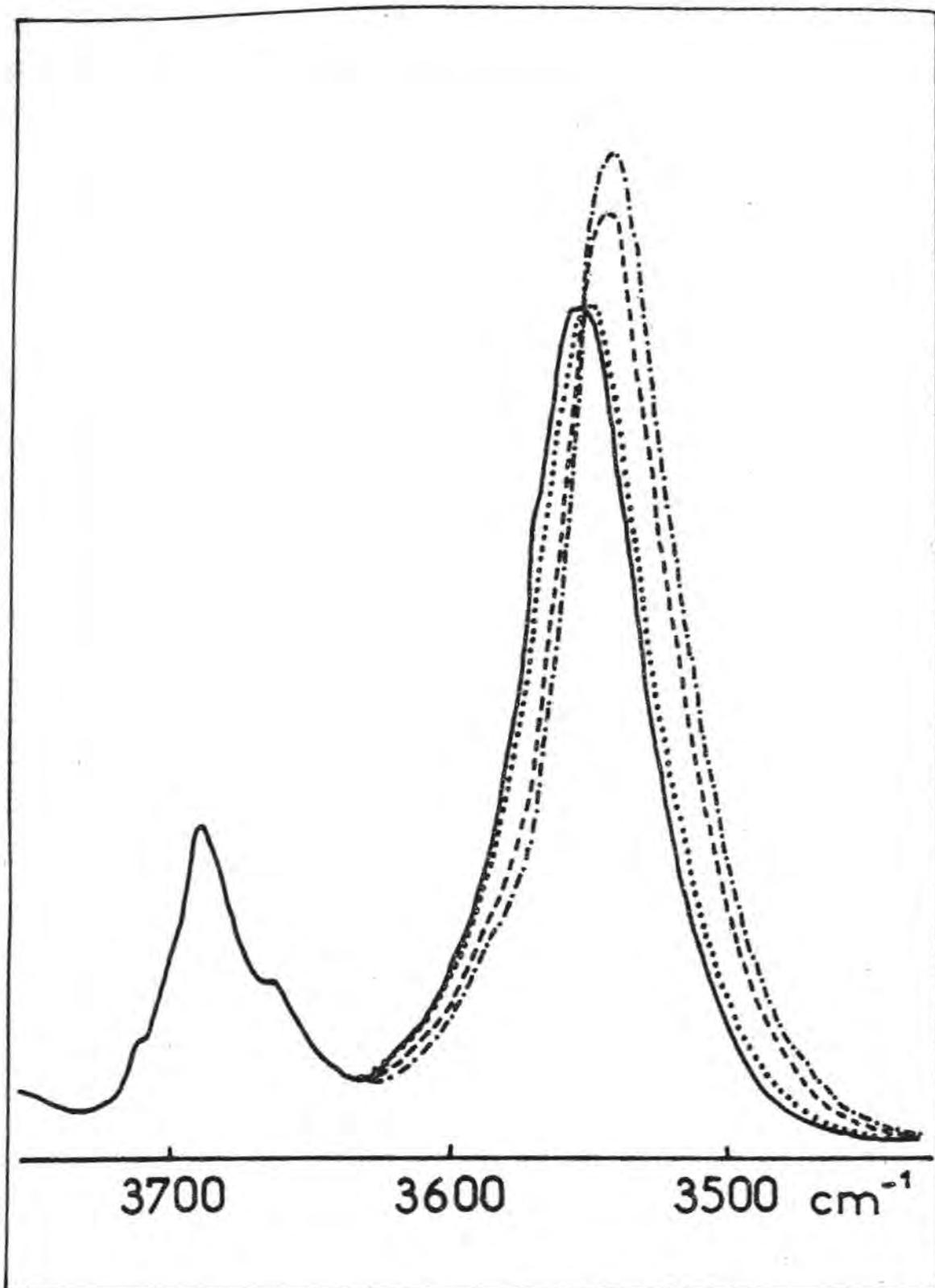


Figure 2. Spectre de la biotite B. Môme signification des tracés que sur la Fig. 1.

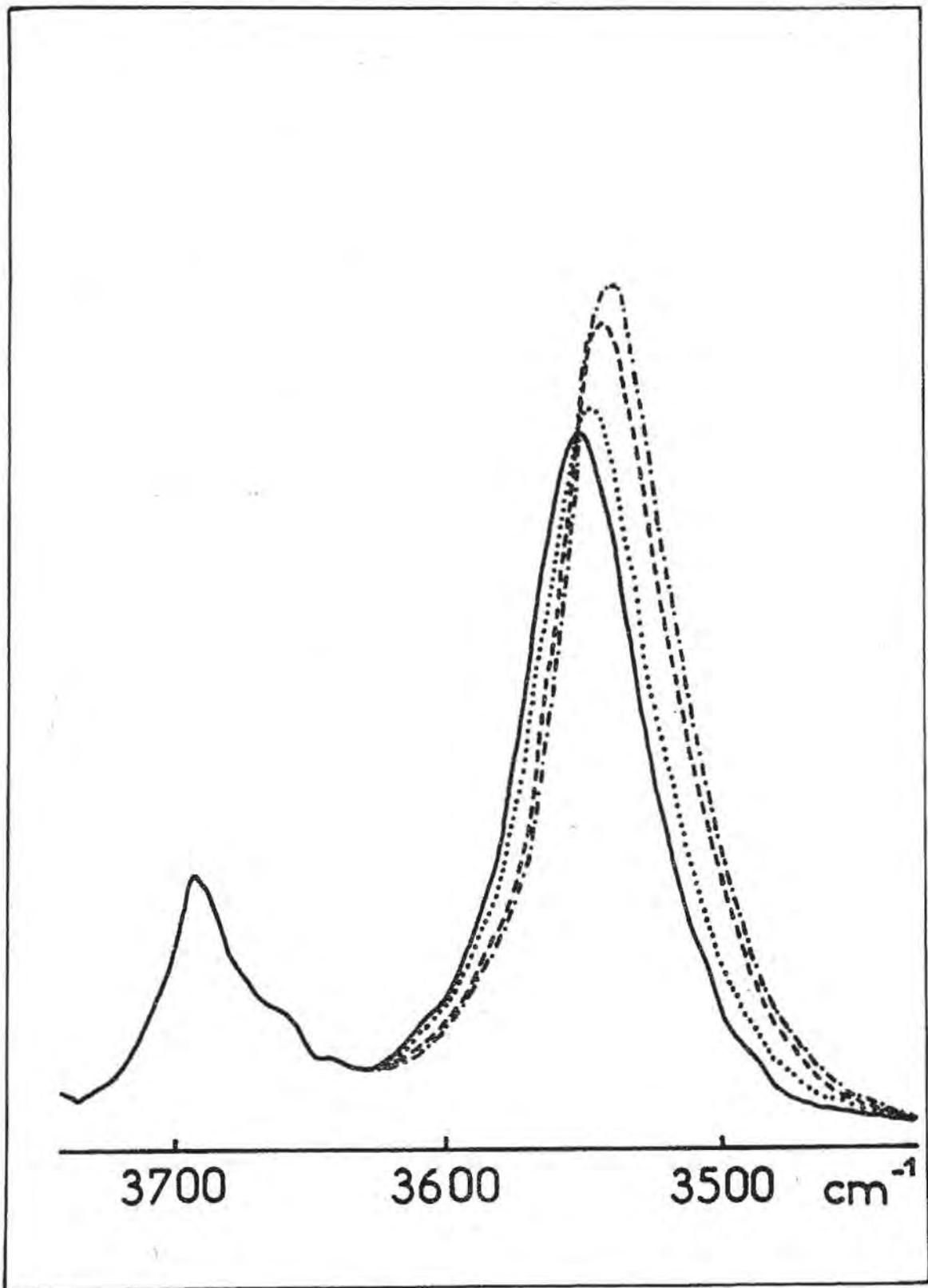


Figure 3. Spectre de la biotite L. Môme signification des tracés que sur la Fig. 1.

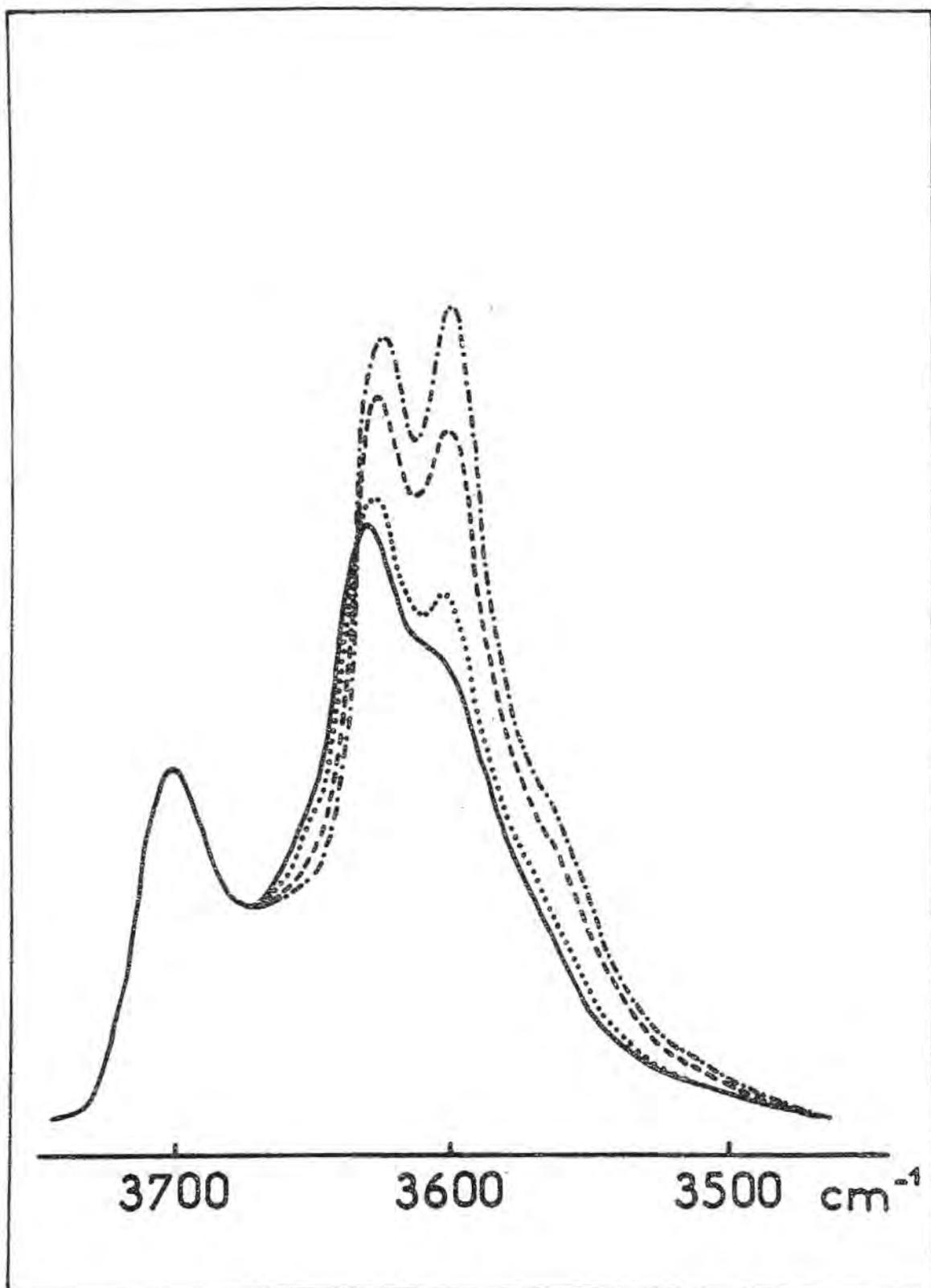


Figure 4. Spectre de la biotite M. Même signification des tracés que sur la Fig. 1.

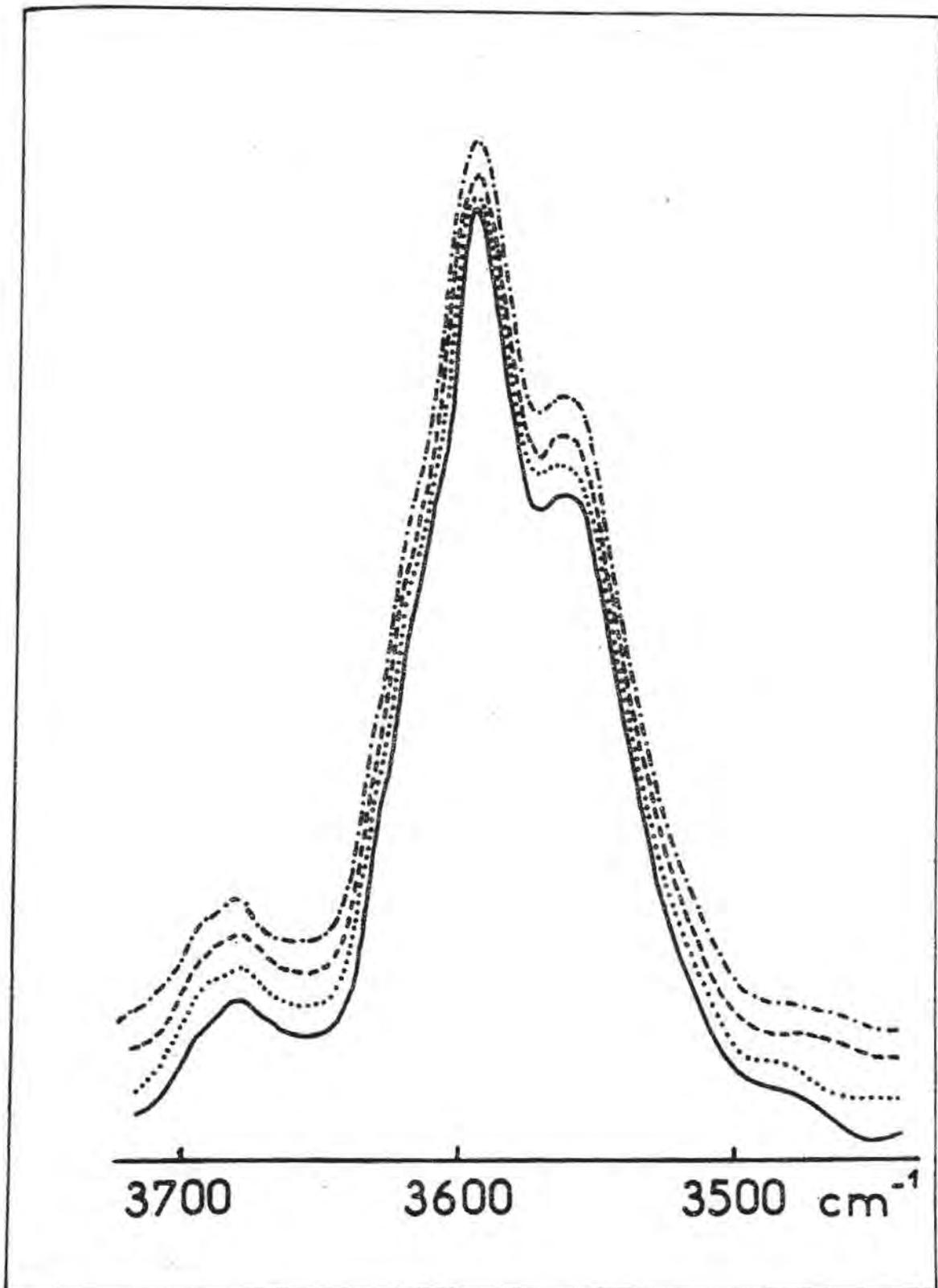


Figure 5. Spectre de la biotite N. Môme signification des tracés que sur la Fig. 1.

Des cinq échantillons étudiés, seule la biotite N n'est pas dichroïque. Les quatre autres sont dichroïques à des degrés divers, mais ont toutes les caractéristiques communes suivantes:

1. L'absorption intégrée en polarisation parallèle à l'axe a est plus grande qu'en polarisation parallèle à l'axe b.
2. La fréquence des maxima apparents dérive vers les basses fréquences quand on passe de la polarisation parallèle à l'axe b à la polarisation parallèle à l'axe a.
3. Toutes les courbes se coupent en un point isosbestique.

On peut noter au passage que les points 1 et 2 avaient été observés par VEDDER (VEDDER et al. 1969) sur une biotite ("Madagascar Amber W # 4") assez similaire à notre échantillon M.

Lorsqu'on porte la densité optique à une fréquence donnée en fonction de l'angle existant entre un axe du minéral et le vecteur électrique, on obtient - sauf à la fréquence du point isosbestique évidemment - une sinusoïde dont la période est de  $180^\circ$  et dont l'amplitude et la phase varient avec la fréquence choisie.

## DISCUSSION

L'existence ou l'absence de dichroïsme est à rattacher au polytype. Il est clair en effet qu'un polytype 3 T ne peut être dichroïque, alors que les formes 1 M, 2 M 1 et 2 M 2 le sont. Ce problème a déjà été étudié par FRIPIAT (FRIPIAT et al. 1965) qui toutefois n'a pas observé de dérive dans la fréquence des maxima d'absorption; la faible variation des absorptions intégrées selon la polarisation a été considérée par ces auteurs comme l'indice d'une répartition statistique équivalente des projections des moments sur le plan ab, le long de trois directions faisant entre elles un angle de  $120^\circ$ . Ce modèle est identique à celui fourni par un polytype 3 T.

Dans nos expériences, l'existence de deux fréquences limites et celle d'un point isosbestique indiquent, qu'à une fréquence donnée, l'absorption est la somme de deux absorptions élémentaires en quadrature. Nous avons fait l'hypothèse que la fréquence des OH en symétrie "C 2/m" était différente de celle des OH en symétrie "C 2" (voir Fig. 6), et l'on a appelé A 1 la projection sur le plan ab du moment "C 2/m" et A 2 celle du moment "C 2".

Dans ces conditions, en admettant une répartition statistique des lacunes et en retenant pour les polytypes 1 M, 2 M 1 et 2 M 2 une structure idéale (voir Fig. 6), les absorptions Aa et Ab respectivement en polarisation parallèle à l'axe a et à l'axe b sont données dans le Tableau I.

Si l'on résout ces équations en A 1 et A 2 en prenant pour Aa et Ab les valeurs expérimentales à chaque fréquence, on obtient pour les fréquences centrales  $\nu_0$  des bandes A 1 et A 2 le clas-

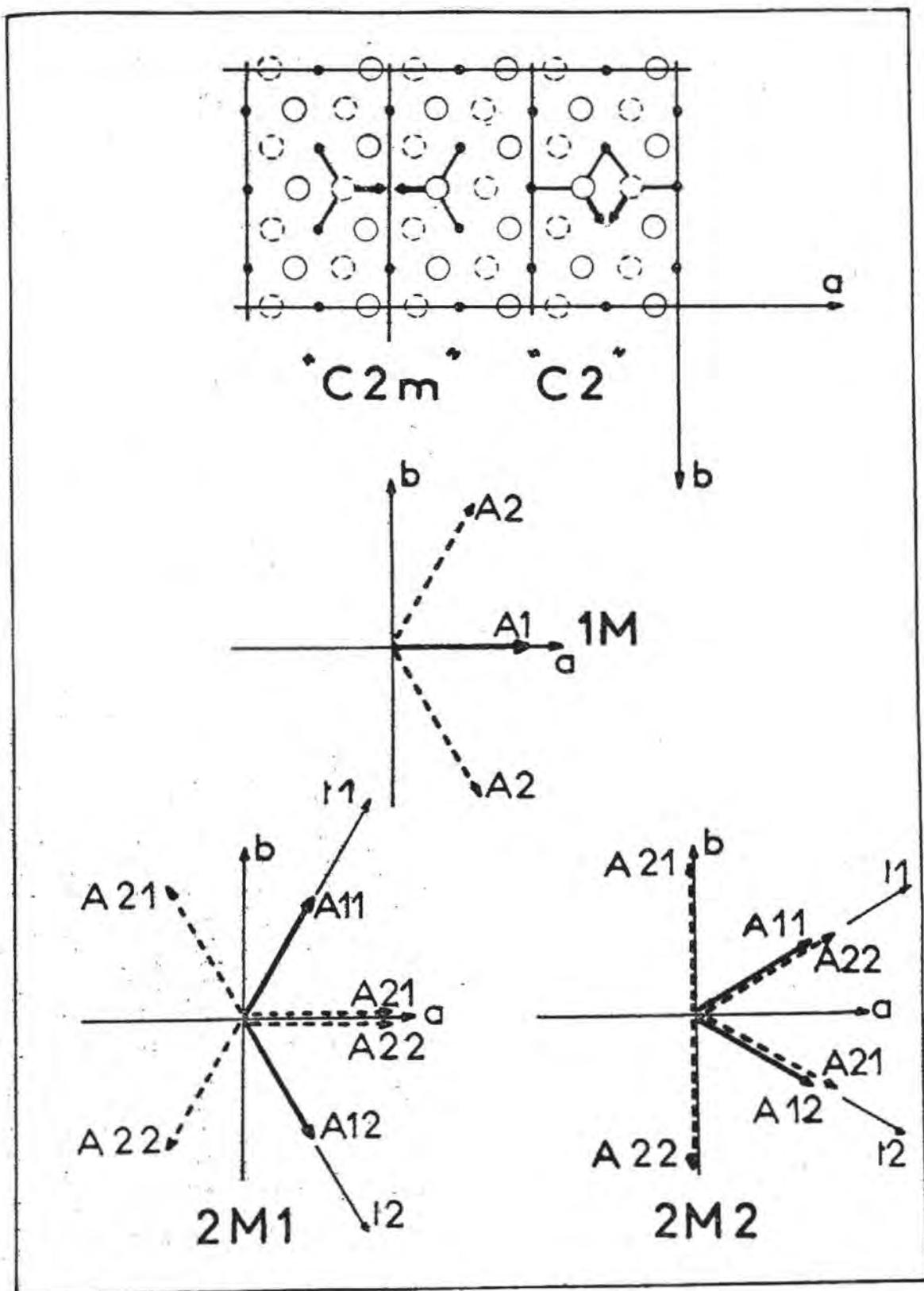


Figure 6. Représentation schématique des deux orientations possibles des OH dioctaédriques et des projections des moments sur le plan  $a b$  pour 3 polytypes différents.

sement suivant:

Polytype 1 M	$\nu_0 A 1 < \nu_0 A 2$
Polytype 2 M 2	$\nu_0 A 1 < \nu_0 A 2$
Polytype 2 M 1	$\nu_0 A 1 > \nu_0 A 2$

Si l'on calcule l'interaction dipole-dipole pour deux OH en symétrie "C 2/m" ou "C 2", on constate que la composante du champ d'un des OH dans la direction de l'autre est plus intense dans le cas "C 2" que dans le cas "C 2/m". Dans le cadre théorique très simple où nous nous sommes placés, ce résultat reste qualitativement vrai quelles que soient les distances interatomiques choisies à l'intérieur des différentes valeurs citées dans la littérature. L'incertitude existant sur ces dernières et la simplification du modèle rendent extrêmement hasardeuse l'interprétation quantitative de la perturbation. Par contre, il semble plausible de considérer qualitativement que la fréquence  $\nu_0 A 1$  soit supérieure à la fréquence  $\nu_0 A 2$ , ce qui amène à retenir, pour les micas dichroïques étudiés, la structure polytype 2 M 1.

Tableau I

Polytype	A a	A b
1 M	$A 1 + 2 A 2 \cos^2 60$	$2 A 2 \sin^2 60$
2 M 1	$2 A 1 \cos^2 60 + A 2(1 + \cos^2 60)$	$2 A 1 \sin^2 60 + A 2 \sin^2 60$
2 M 2	$2 A 1 \cos^2 30 + A 2 \cos^2 30$	$2 A 1 \sin^2 30 + A 2(1 + \sin^2 30)$

Le calcul effectué avec les formules appropriées du Tableau I amène à tracer dans le cas des biotites B et L des bandes A 1 et A 2 dissymétriques; de plus, la bande A 1 a dans la zone basse fréquence une absorption légèrement négative. On a donc cherché à ajuster numériquement la valeur des angles fixant la direction des projections A 1 et A 2.

Les valeurs suivantes:

$$\begin{aligned} \text{angle entre A 11 et b} &= 25^\circ \\ \text{angle entre A 21 et } t_1 &= 68^\circ \end{aligned}$$

font disparaître les anomalies signalées ci-dessus et confèrent aux deux bandes A 1 et A 2 un profil à très peu près symétrique, une hauteur au maximum équivalente et une fonction génératrice à peu près identique. La Fig. 7 donne un exemple de ce genre de résultat.

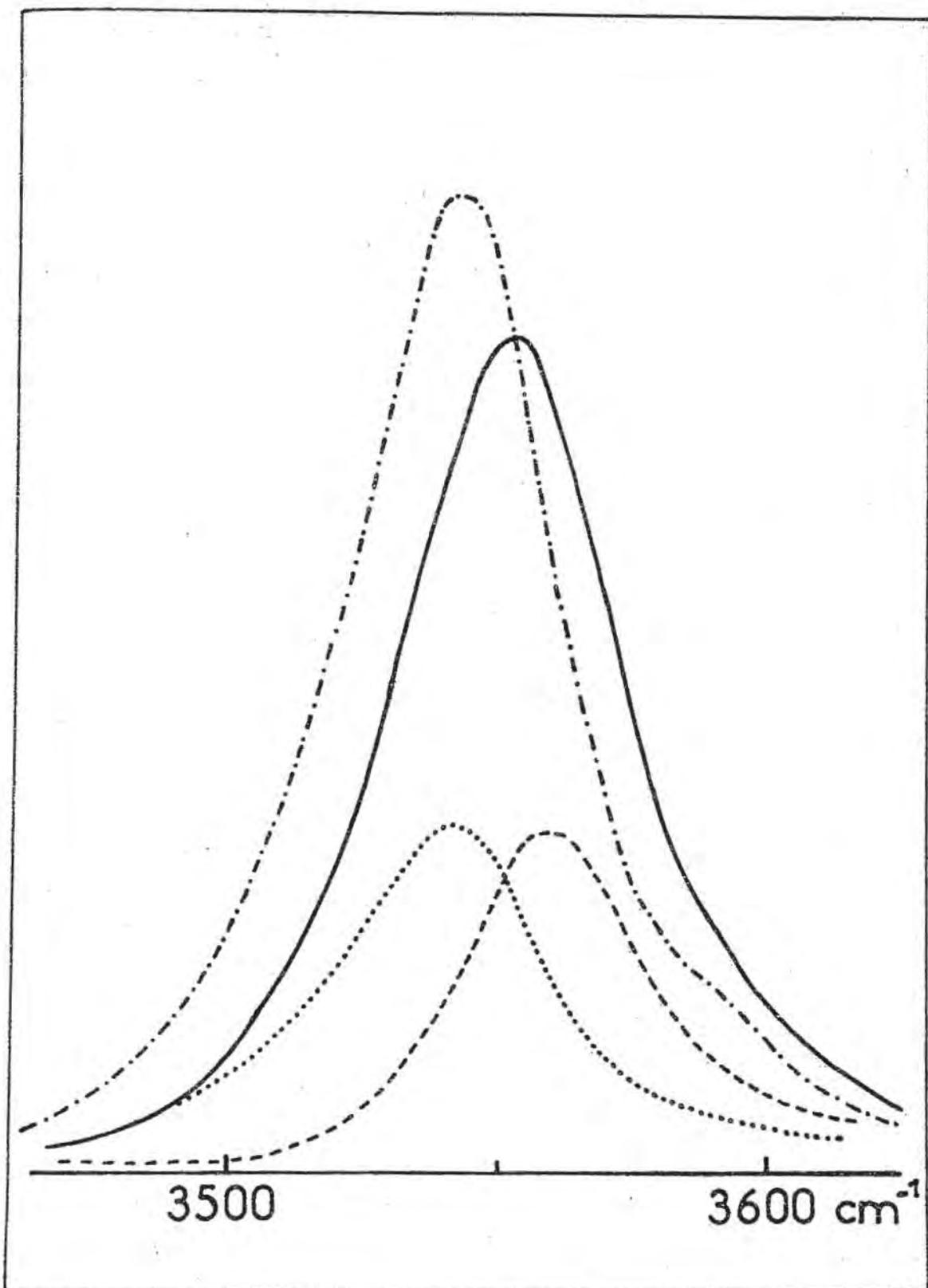


Figure 7. Biotite B. - . - . -: spectre pour  $\theta = 0^\circ$ ; —: spectre pour  $\theta = 90^\circ$ ; .....: bande A 2; - - - -: bande A 1.

Nous n'attachons aucune signification particulière à ces corrections. Elles intègrent en effet toutes les erreurs expérimentales et les écarts éventuels entre la structure réelle du mica et la structure théorique. Nous n'avons pas tenu compte notamment de la déformation que peut induire la rotation des tétraèdres sur la couche octaédrique.

Les fréquences centrales  $\nu_{\text{O}} \text{ A } 1$  et  $\nu_{\text{O}} \text{ A } 2$  sont données dans le Tableau II pour les trois biotites A, B et L: dans ces trois échantillons en effet, les bandes haute fréquence des hydroxyles dressés sur le plan ab n'interfèrent que très peu avec les bandes basse fréquence, ce qui évite une correction aléatoire. Dans le cas de la biotite A, les deux couples de valeurs fournies correspondent aux deux maxima résolus.

Tableau II

Biotite	$\nu_{\text{O}} \text{ A } 1$ (cm <sup>-1</sup> )	$\nu_{\text{O}} \text{ A } 2$ (cm <sup>-1</sup> )	$\nu_{\text{O}} \text{ A } 1 - \nu_{\text{O}} \text{ A } 2$ (cm <sup>-1</sup> )
A	$\left\{ \begin{array}{l} 3571 \\ 3609 \end{array} \right.$	$\left\{ \begin{array}{l} 3554 \\ 3593 \end{array} \right.$	$\left\{ \begin{array}{l} 17 \\ 16 \end{array} \right.$
B	3559	3541	18
L	3558	3542	16

La comparaison des Fig. 1 et 4 aux Figs. 2 et 3 met en évidence une différence marquée de l'intensité du dichroïsme et l'on doit s'attendre alors à ce que les bandes A 1 et A 2 n'aient pas la même intensité; c'est ce que montre effectivement le calcul. Les bandes A 1 et A 2 ont, comme les spectres expérimentaux, plusieurs maxima résolus, et l'on est en droit de penser que ce contour spectral apparemment simple recouvre en fait l'existence d'un système de bandes compliqué, ce qui n'est pas surprenant compte tenu des travaux de FARMER (FARMER et al 1967, FARMER et al 1971) sur les minéraux dioctaédriques. Dans ce cas, il est probable que selon le couple de cations voisins de la lacune, les OH de type C 2/m ou C 2 n'ont pas une probabilité équivalente. Toutefois, si l'on considère que la fréquence centrale des bandes A 1 est supérieure à celle des bandes A 2, on n'est conduit à introduire dans les formules du Tableau I qu'un coefficient différent de 1 pour les termes en A 1 et A 2.

## CONCLUSION

En plus de la variabilité bien connue des fréquences des bandes basse fréquence des OH des biotites due au grand nombre des environnements cationiques octaédriques possible, il apparaît qu'un facteur de variabilité supplémentaire soit à rechercher, pour chaque OH lié à deux cations donnés, dans l'existence de deux fréquences d'absorption différentes liées au type de la lacune. Si pour un échantillon examiné à l'état de poudre fine dispersée dans une matrice saline cet effet n'est pas sensible, par contre dès que la taille des cristaux devient importante, ce facteur peut jouer en créant une dispersion apparente des résultats. Si l'interprétation que nous en donnons est correcte, cet effet peut être mis à profit pour distinguer le polytype auquel appartient le mica, au moins dans les cas simples qui sont les plus fréquemment rencontrés.

## REMERCIEMENTS

Nous tenons à remercier Mme E. HUARD pour la collaboration technique qu'elle nous a apportée.

## REFERENCES

- FARMER V.C., RUSSELL J.D., AHLRICHS J.L., VELDE B. (1967): Vibrations du groupe hydroxyle dans les silicates en couche. Bull. Gr. Fr. des Argiles 19 (2), 5-9.
- FARMER V.C., RUSSELL J.D., Mc HARDY W.J., NEWMAN A.C.D., AHLRICHS J.L., RIMSAITE J.Y.H. (1971): Evidence for loss of protons and octahedral iron from oxidized biotites and vermiculites. Mineral. Mag. 38 (294) 121-137.
- FRIPIAT J.J., ROUXHET P., JACOBS H. (1965): Proton delocalization in micas. Amer. Mineral. 50, 1937-1958.
- VEDDER W., Mc DONALD R.S. (1963): Vibrations of the OH ions in muscovite. J. Chem. Phys. 38 n 7, 1583-1590.
- VEDDER W., WILKINS R.W.T. (1969): Dehydroxylation and rehydroxylation, oxidation and reduction of micas. Amer. Mineral. 54, 482-509.



DEPROTONATION OF NONTRONITE RESULTING FROM  
CHEMICAL REDUCTION OF STRUCTURAL FERRIC IRON\*

C. B. Roth and R. J. Tullock

Department of Agronomy, Purdue University  
Lafayette, Indiana 47907

**ABSTRACT.** - Chemical reduction of structural iron in a nontronite-D<sub>2</sub>O suspension at room temperature and pressure resulted in the total replacement of structural hydroxyls with deuterioxylys. Reduction of the nontronite in H<sub>2</sub>O brought about a net decrease in the total quantity of hydroxyl groups present but subsequent air oxidation restored the OH content to that found in the original untreated nontronite. It is proposed that chemical reduction of iron in nontronite involves electron migration into the structure with the simultaneous formation of H<sub>2</sub>O from condensation of two structural hydroxyl groups. This free water diffuses out of the structure and is followed by protonation of an oxygen.

Slight proton-deuteron exchange was observed with mild hydrothermal treatment of nontronite-D<sub>2</sub>O suspensions at 100°C, however, complete exchange was accomplished by hydrothermal treatment at 150°C. Hydroxyl exchange of deuterated nontronite did not proceed at room temperature by washing the sample with water or by repeated flushing with water vapor in a vacuum cell at low pressure (< 10 torr). Complete deuteration of nontronite by hydrothermal techniques allowed the replacement of structural deuterioxylys to be studied using hydrogen containing reagents such as H<sub>2</sub>O<sub>2</sub>, N<sub>2</sub>H<sub>4</sub> or H<sub>2</sub>O.

---

\*Journal Paper \_\_\_\_\_, Purdue University, Agricultural Experiment Station, Lafayette, Indiana. Contribution from the Department of Agronomy.

## INTRODUCTION

Oxidation and reduction reactions play an important role in the weathering of soil minerals. The ease with which iron in nontronite can be reduced and oxidized makes it an ideal material in which to study structural changes associated with reduction and oxidation reactions in clay minerals. Changes in the valence state of structural iron brings about hydroxide-oxide conversions in hydroxylated silicates (Addison and Sharp, 1962, 1963; Vedder and Wilkins, 1969; Farmer *et al.*, 1971) which can be followed easily with the use of deuterium and infrared spectroscopy. The deprotonation or protonation of nontronite, resulting from reduction and oxidation of structural iron, was followed by infrared spectroscopy.

## MATERIALS AND METHODS

Nontronite (Wards No. H-33a, Wards Scientific Establishment, Rochester, NY) was sodium saturated with NaCl. The excess salt was removed by centrifugation and dialysis until a negative chloride test ( $\text{AgNO}_3$ ) was obtained. The  $< 2\mu$  fraction was separated by sedimentation. The original Na-saturated nontronite contained structural ferric iron in octahedral positions coordinated with oxygens and hydroxyls and will be designated in this paper as N-OH<sub>x</sub>. Complete deuteration of the nontronite was accomplished by reacting a nontronite-D<sub>2</sub>O suspension in a hydrothermal bomb at 150°C for 18 hours. The deuterated nontronite will be designated N-OD<sub>x</sub>. Partial deuteration of nontronite was accomplished by placing samples of a nontronite-D<sub>2</sub>O suspension in a 100°C bath for time periods up to 24 hours. Reduction of structural ferric iron was accomplished by the addition of either granular Na<sub>2</sub>S<sub>2</sub>O<sub>4</sub> (0.5 mg/mg clay) to a nontronite suspension or by placing the dried nontronite film approximately 3 cm above the liquid surface of freshly dispensed anhydrous hydrazine. The reduced samples will be designated either as N-OH<sub>r</sub> or N-OD<sub>r</sub> indicating either structural hydroxyls or deuterioxyls and reduced iron. Oxidation of the reduced nontronite was accomplished by adding 5 ml of 15% H<sub>2</sub>O<sub>2</sub> to approximately 30 mg of reduced clay in suspension or by exposing the dried film to air at room temperature or 100°C. Infrared spectra of films resulting from the deposition of suspensions on either rolled silver chloride (Harshaw Chemical Co., Cleveland, Ohio) or Irtran-2 (Eastman Kodak, Rochester, NY) windows were recorded on a Perkin-Elmer 421 spectrophotometer.

## RESULTS AND DISCUSSION

The infrared spectra of the original and the hydrothermally deuterated nontronite ( $N-OH_x$  and  $N-OD_x$ ) are shown in Fig. 1. The absorption for the OH stretch ( $3560\text{ cm}^{-1}$ ) and the OD stretch ( $2630\text{ cm}^{-1}$ ) are separated by a factor of 1.355 indicating the net reaction in the hydrothermal bomb at  $150^\circ\text{C}$  for 18 hours was a simple D for H exchange in the Na saturated nontronite. Substitution of D for H in isolated OH ions theoretically decreases the intensity of the stretching band by a factor of 1.887 which is related to the reduced masses of the OH and OD groups (Vedder and Wilkins, 1969). The frequency of the infrared absorption band associated with Fe-OH bending is reduced from  $810\text{ cm}^{-1}$  to  $595\text{ cm}^{-1}$  by complete deuteration of the nontronite structure (Fig. 1). Other structural changes, if any, were not detected by infrared analysis. Very little deuterium for hydrogen exchange was detected in a nontronite ( $N-OH_x$ )- $D_2O$  suspension equilibrated at room temperature for 2 weeks. The  $N-OD_x$  was stable in a  $H_2O$  suspension, as a dried film exposed to the at-

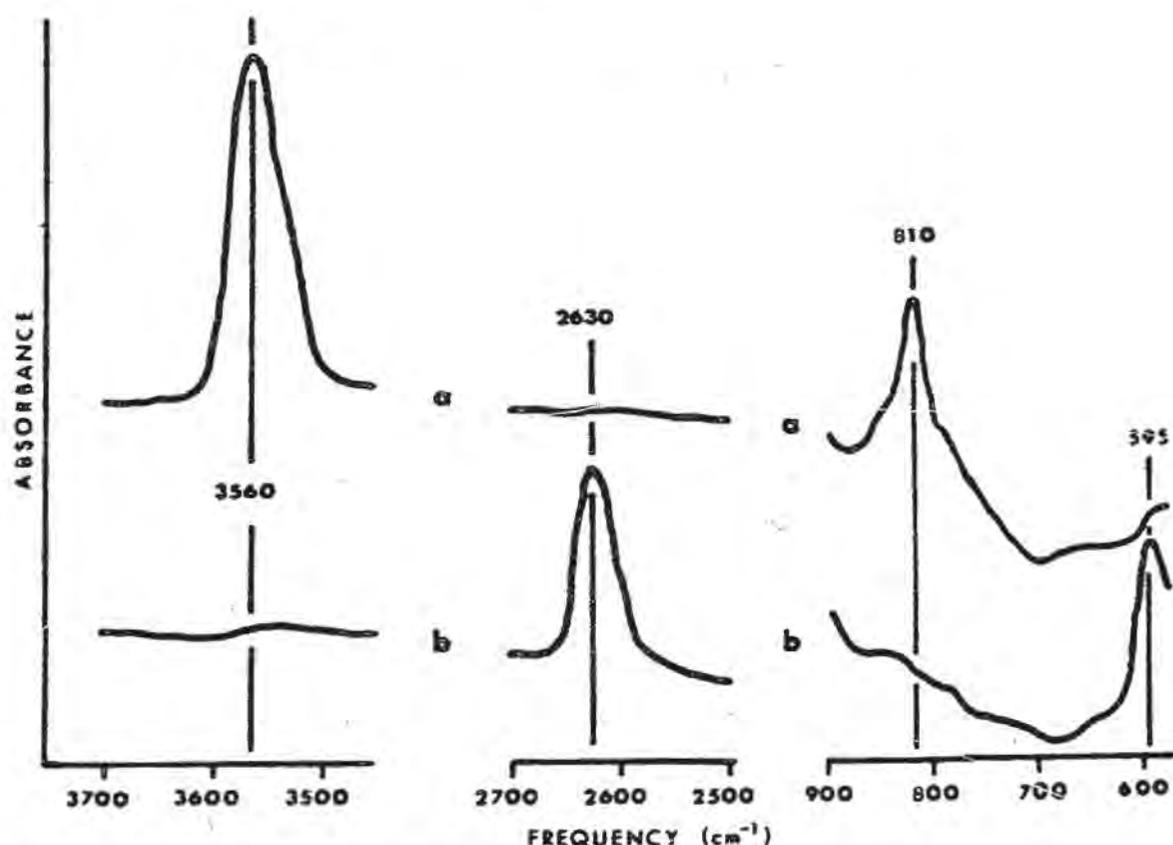


Figure 1. IR absorption spectra of sodium saturated nontronite (a) original,  $N-OH_x$ , and (b) completely deuterated,  $N-OD_x$ , by hydrothermal bomb treatment at  $150^\circ\text{C}$  for 18 hours.

mosphere or as a dried film exposed to repeated evacuation and flushing with H<sub>2</sub>O vapor.

A nontronite (N-OH<sub>x</sub>)-D<sub>2</sub>O suspension heated to 100°C for only 15 minutes resulted in measurable D for H exchange (Fig. 2). The increased D for H replacement with heating time is shown by the reduction in intensity of the 3560 cm<sup>-1</sup> band of OH stretch and the simultaneous increase in the 2630 cm<sup>-1</sup> band of OD stretch. The absorption ratios (OH/OD) indicate approximately 30 percent D for H exchange when nontronite, N-OH<sub>x</sub>, in D<sub>2</sub>O was heated at 100°C for 24 hours (Fig. 2). Although the extent of transformation of an OH mineral to the analogous OD form varies extensively both between and within clay mineral groups, the expanding layer silicates were shown by Russell, Farmer and Velde (1970) to be susceptible to a more complete exchange in less time than other groups of clay minerals. Complete deuteration of saponite, hectorite, vermiculite and montmorillonite was possible with three, one-hour treatments

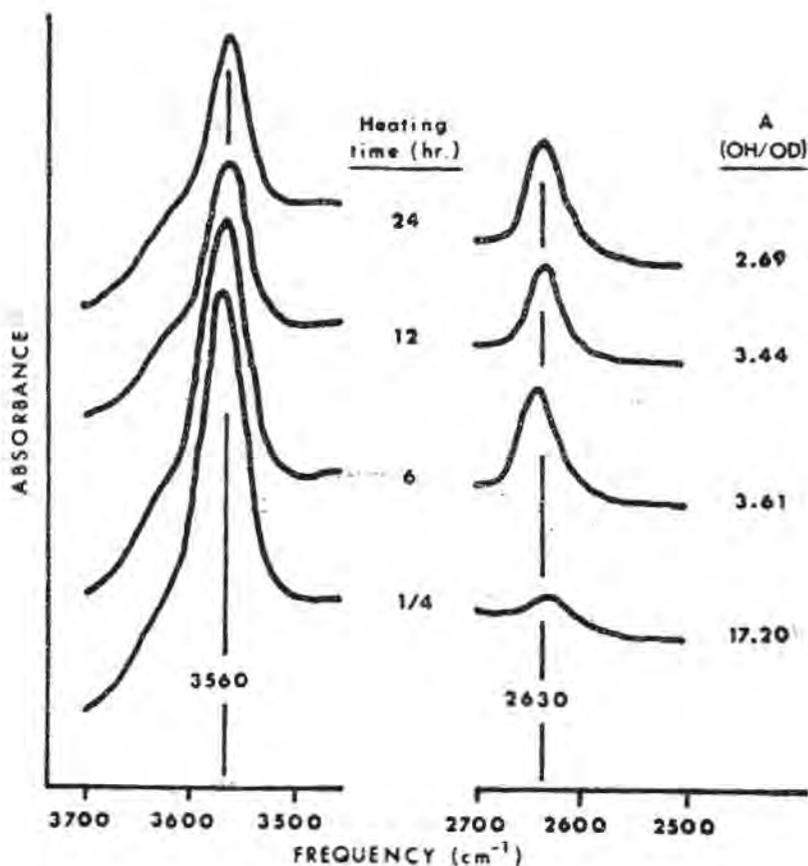


Figure 2. IR absorption spectra of sodium saturated nontronite, N-OH<sub>x</sub>, in D<sub>2</sub>O suspension heated at 100°C for the time specified (hours), with the measured absorbance ratio (A) for OH/OD stretch.

at 350°C (Russell et al., 1970). The previous authors noted in their paper the sharp contrast of their results with those of Roy and Roy (1957), who reported less than 50 percent D for H conversion of a montmorillonite after 3 days heating at 370°C and about 1.4 kb pressure. Vedder and Wilkins (1969) reported that as much as 700 hours was required to 80% deuterate a thin sample of muscovite at very high temperature and pressure (600°C and 5 bars). The nontronite used in this study was deuterated hydrothermally at lower temperature and pressure than have been reported for most layer silicates.

Complete exchange of structural hydroxyls in nontronite, N-OH<sub>x</sub>, with deuterioxylys accompanied reduction of the structural ferric iron with Na<sub>2</sub>S<sub>2</sub>O<sub>4</sub> in D<sub>2</sub>O at room temperature (Fig. 3b). Similarly, reduction of deuterated nontronite, N-OD<sub>x</sub>, in H<sub>2</sub>O was accompanied by a complete exchange of H for D (Fig. 3a). Oxidation of the reduced nontronite (N-OH<sub>x</sub> reduced in D<sub>2</sub>O to form N-OD<sub>r</sub>) with 15 percent H<sub>2</sub>O<sub>2</sub> in H<sub>2</sub>O at 25°C resulted in both hydroxylys and deuterioxylys in the structure (Fig. 3c).

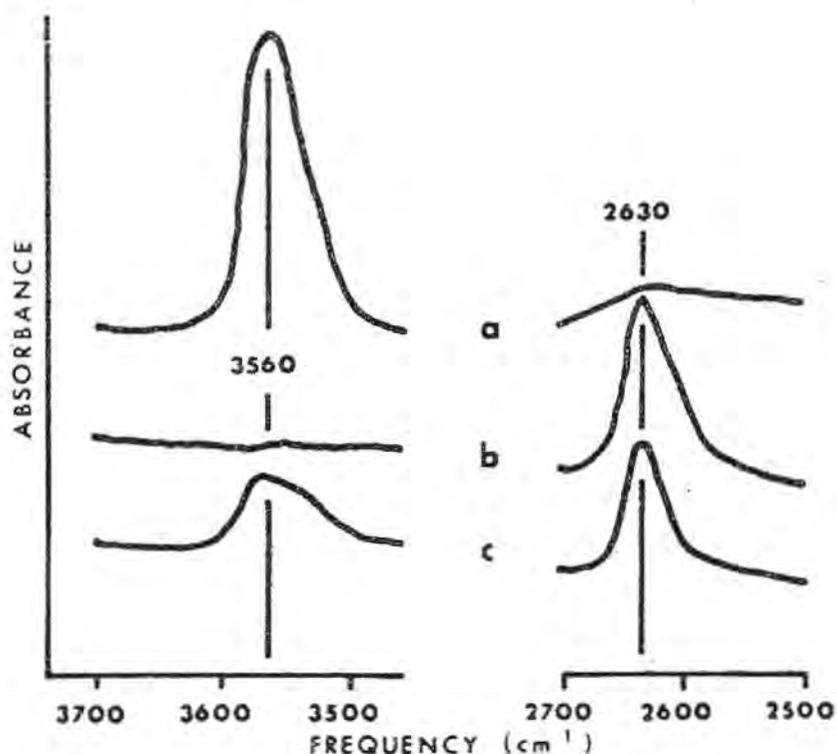


Figure 3. IR absorption spectra of air dried sodium saturated nontronite (a) deuterated nontronite, N-OD<sub>x</sub>, reduced in H<sub>2</sub>O with Na<sub>2</sub>S<sub>2</sub>O<sub>4</sub>, (b) original nontronite, N-OH<sub>x</sub>, reduced in D<sub>2</sub>O with Na<sub>2</sub>S<sub>2</sub>O<sub>4</sub> and (c) reduced nontronite used in b after oxidation with H<sub>2</sub>O<sub>2</sub> in H<sub>2</sub>O.

Reduction of nontronite,  $N-OH_x$ , with  $Na_2S_2O_4$  in  $H_2O$  decreased the absorption frequency for the structural OH from  $3560\text{ cm}^{-1}$  (Fig. 1a) to  $3540\text{ cm}^{-1}$  (Fig. 4a). Partial oxidation of the reduced nontronite,  $N-OH_r$ , increased the OH stretch frequency to approximately  $3550\text{ cm}^{-1}$  (Fig. 4b) while further oxidation, accomplished by heating the sample in air at  $100^\circ\text{C}$  for 48 hours, restored the frequency to its original value of  $3560\text{ cm}^{-1}$  (Fig. 4c). The decrease in the infrared absorption frequency when nontronite,  $N-OH_x$ , is reduced in  $H_2O$  is consistent with the results for OH associated with  $Fe^{2+}$ ,  $Fe^{3+}$  octahedral cations (Farmer et al., 1967). Ferrous-ferric iron analysis of the reduced nontronite suggested  $Fe^{2+}$ ,  $Fe^{3+}$  OH groups were formed rather than  $Fe^{2+}$ ,  $Fe^{2+}$ ; OH groups (Roth et al., 1969). The increases in absorbance due to OH stretching (Fig. 4), and OH bending (Fig. 5d, e, f) with oxidation of

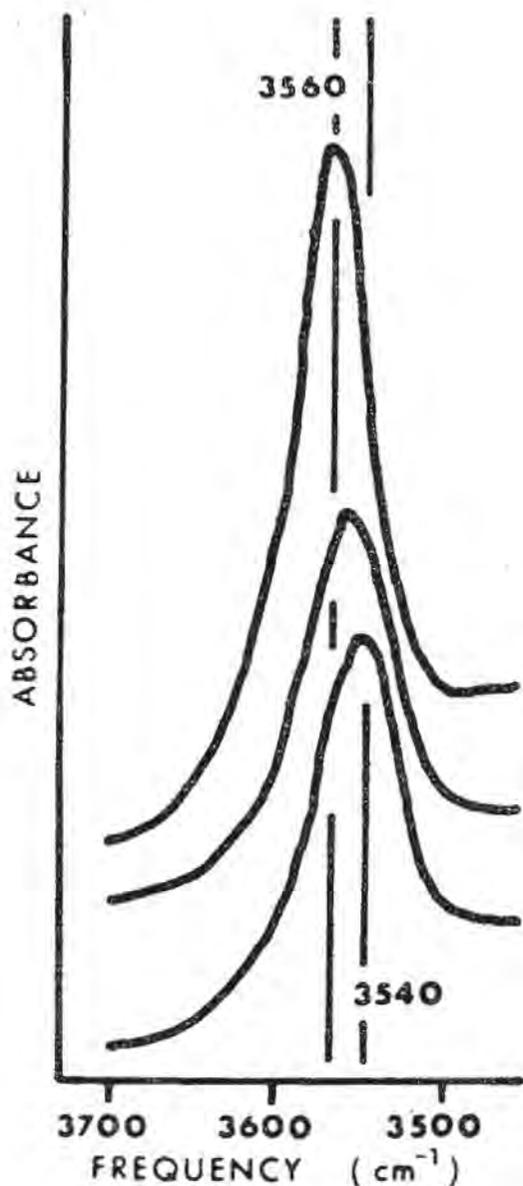


Figure 4. IR absorption spectra of a sodium saturated nontronite,  $N-OH_x$ , sample (a) reduced in  $H_2O$  with  $Na_2S_2O_4$  and dried in an oxygen free atmosphere (b) subsequently oxidized in air at  $25^\circ\text{C}$  for 48 hours and (c) oxidized further in air at  $100^\circ\text{C}$  for 48 hours

of reduced nontronite shows more hydroxide associated with the oxidized sample. Although some increased OH stretching absorption could result from a change, on oxidation of  $\text{Fe}^{2+}$  to  $\text{Fe}^{3+}$ , in the inclination angle of the hydroxyl with respect to the plane of the octahedral layer (Alrichs, et al., 1965), the increased absorption due to HO-Fe bending,  $810 \text{ cm}^{-1}$ , can only be accounted for by an increase in OH content after oxidation of the reduced nontronite.

As indicated by a comparison of Figs. 5(a) and 5(b), the deuteroxyl sites in deuterated nontronite,  $\text{N-OD}_x$ , are relatively unavailable to exchange with the protons of  $\text{NH}_3$  vapor. Essentially complete H for D exchange occurred when air dried deuterated nontronite,  $\text{N-OD}_x$ , was exposed to, and reduced by, gaseous  $\text{N}_2\text{H}_4$  as indicated by the increase in intensity of the band at  $810 \text{ cm}^{-1}$  attributed to

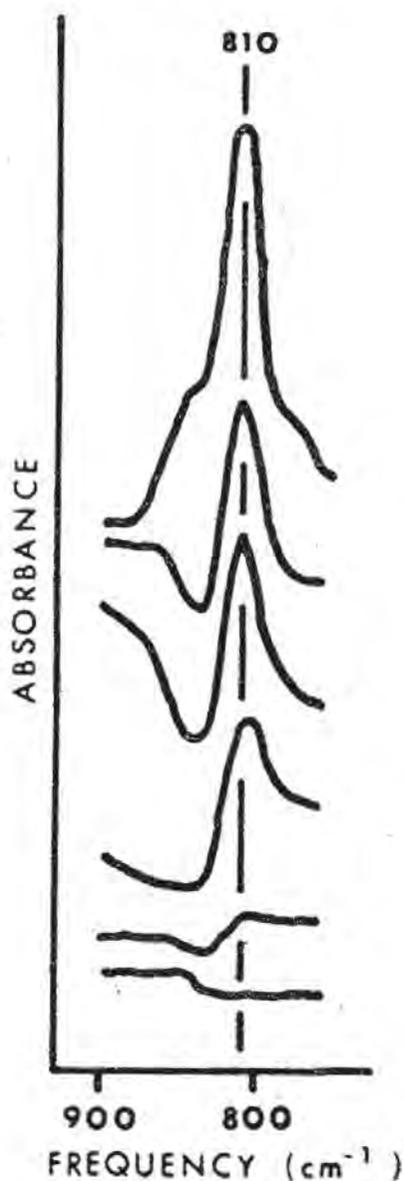


Figure 5. IR absorption spectra of sodium saturated nontronite: (a) deuterated,  $\text{N-OD}_x$ , (b) deuterated,  $\text{N-OD}_x$ , and exposed to  $\text{NH}_3$  vapor, (c) deuterated,  $\text{N-OD}_x$ , and exposed to  $\text{N}_2\text{H}_4$  vapor, (d, e and f) same samples as in Fig. 4a, b and c, respectively,

the bending mode of the HO-Fe bond (Fig. 5c). Therefore, reduction of structural iron in nontronite was accompanied by the exchange of structural protons even in the absence of excess H<sub>2</sub>O. The 595 cm<sup>-1</sup> band associated with the bending mode of the DO-Fe bond could not be observed since the sample in Fig. 5c was run on Irtran-2 because of the potentially explosive mixture of hydrazine and AgCl.

In summary, the following observations have been made concerning reduction of structural iron in nontronite:

1. Hydroxyls in nontronite are relatively stable to exchange at room temperature.

2. Reduction of nontronite decreases the structural OH content.

3. Reduction of nontronite brings about complete exchange of structural hydrogens.

4. Oxidation of reduced nontronite restores the original OH content without complete exchange of structural hydrogens.

It is proposed that chemical reduction of iron in the dioctahedral mineral nontronite involves a migration of an electron to the ferric iron with the simultaneous formation of H<sub>2</sub>O from condensation of two structural hydroxide groups. This water molecule is free to diffuse and leaves the nontronite structure. The oxygen of the "oxide" group resulting from the condensation reaction is then protonated. This sequence of reactions would account for the complete exchange of structural hydrogens when nontronite is reduced (Fig. 3), and for the reduction in the quantity of OH groups present in the reduced sample (Fig. 4). In keeping with the observations of Roth et al. (1969), no change in cation exchange capacity would occur. Oxidation of the reduced nontronite would require only the migration of a hydroxyl group into the structure simultaneous with the transfer of an electron in the opposite direction. Thus, there would not be complete exchange of structural hydroxyls (Fig. 3c) and the quantity of OH groups would increase with oxidation (Fig. 4).

In micas the ferrous iron which occupied the larger octahedral positions, i.e., the octahedrons in which the hydroxyl groups are in trans positions instead of cis positions, was preferentially oxidized under natural weathering (Yussoglou et al., 1972). One-half of the iron in nontronite occupies the larger (trans) octahedral position (Dr. N. J. Yussoglou, personal communication). Therefore, it is thought that, in nontronite, the iron which occupies the larger octahedrons would preferentially undergo reduction-oxidation reactions.

#### ACKNOWLEDGEMENT

The authors would like to extend a special thanks to Dr. Joe L. White for his helpful suggestions and discussions throughout the course of this study.

## REFERENCES

- ADDISON, W. E. and SHARP, J. H. (1962): A mechanism for the oxidation of ferrous iron in hydroxylated silicates. *Clay Minerals Bull.* 5, 73-79.
- ADDISON, W. E. and SHARP, J. H. (1963): Redox behavior of iron in hydroxylated silicates. *Clays Clay Minerals* 11, 95-104.
- AHLRICH, J. L., RUSSELL, J. D., HARTE, R. D. and WIESMILLER, R. A. (1965): Infrared spectroscopy of clay mineral systems. *Proc. Indiana Academy Sci. for 1965.* 75, 247-255.
- FARMER, V. C., RUSSELL, J. D., AHLRICH, J. L. and VELDE, B. (1967): Vibration du groupe hydroxyle dans les silicates en couches. *Bull. Grpe. Fr. Argiles.* 19, 5-10.
- FARMER, V. C., RUSSELL, J. D., MCHARDY, W. J., NEWMAN, A. C. D., AHLRICH, J. L. and RIMSAITE, J. Y. H. (1971): Evidence for loss of protons and octahedral iron from oxidized biotites and vermiculites. *Mineralogical Mag.* 38, 121-137.
- ROTH, C. B., JACKSON, M. L. and SYERS, J. K. (1969): Deferation effect on structural ferrous-ferric iron ratio and CEC of vermiculites and soils. *Clays Clay Minerals.* 17, 253-264.
- ROY, D. M. and ROY, R. (1957): Hydrogen-deuterium exchange in clays and problems in the assignment of infra-red frequencies in the hydroxyl region. *Geochimia et Cosmochimica Acta.* 11, 72-85.
- RUSSEL, J. D., FARMER, V. C. and VELDE, B. (1970): Replacement of OH by OD in layer silicates and identification of the vibrations of these groups in infrared spectra. *Mineralogical Mag.* 37, 869-879.
- VEDDER, W. and WILKINS, R. W. (1969): Dehydroxylation and rehydroxylation, oxidation and reduction of micas. *Am. Mineralogist* 54, 482-509.
- YASSOGLOU, N. J., NOBELI, C. COSTICAS, A. and SIMOPOULOS, A.: Weathering of micas in two soils in northern Greece evaluated by Mossbauer and conventional techniques. *Soil Sci. Soc. Am. Proc.* 36, (In press).



# ANALYSE STRUCTURALE DE LA SEPIOLITE A PARTIR DES DONNEES DE LA DIFFRACTION ELECTRONIQUE

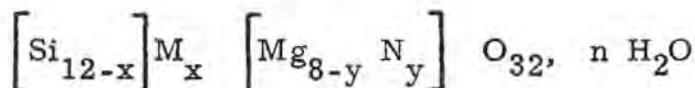
M. Rautureau, C. Tchoubar et J. Méring

Laboratoire de Cristallographie, U.E.R. de Sciences  
Centre de Recherche sur les Solides  
à Organisation Cristalline Imparfaite  
C.N.R.S. - 45 - ORLEANS 02 - FRANCE

**ABSTRACT.** - Fourier analysis of electron diffraction intensities from single crystals of sepiolite have lead to certain improvements with respect to the crystal structure proposed by Brauner and Preisinger. Electron density projection on (010) and (100) show, firstly, the existence of an additional atom in coordinates  $y/b = 0.250$  and  $z/c = 0.750$ , and secondly, that tetrahedral layers are displaced by a translation of  $z/c = 0.017$  parallel to the  $c$  axis.

## INTRODUCTION

Les sépiolites constituent un groupe de phyllosilicates dont la formule générale, d'après les analyses de Caillère (1933), peut être écrite:



$M_x$  et  $N_y$  représentant des substitutions isomorphiques, différentes suivant l'origine du minéral.

Les premières analyses structurales de la sépiolite ont été effectuées par Nagy et Bradley (1955), d'une part, et par Brauner et Preisinger (1956) d'autre part. Ces différents auteurs ont proposé des modèles structuraux assez semblables pour lesquels le monocristal de sépiolite est constitué de rubans disposés en quinconce,

chaque ruban étant une portion de feuillet 2:1 trioctaédrique (une section normale à l'allongement d'un monocristal est schématisée sur la Fig. 1; l'axe c est pris suivant la direction d'allongement).

Brauner et Preisinger ont trouvé que la sépiolite a une maille orthorhombique de groupe spatial Pncn, ce qui a été confirmé ensuite par plusieurs auteurs (Brindley, 1959; Zvyagin, 1967; Martín-Vivaldi et Robertson, 1971).

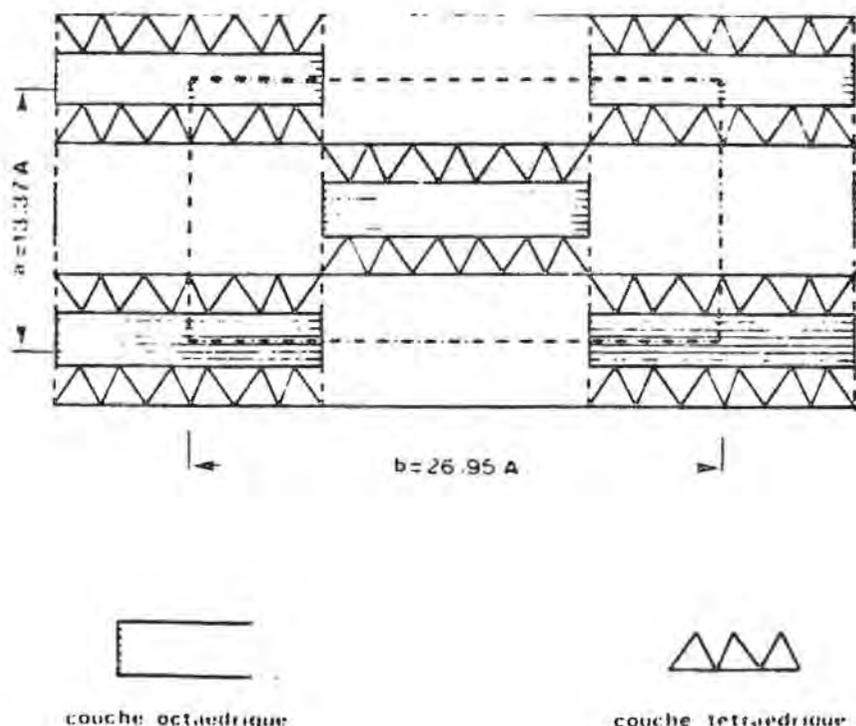
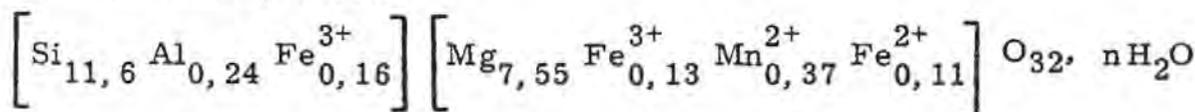


Figure 1. Schème structural de la sépiolite. Section normal à l'axe C.

Toutefois, les structures proposées étaient basées sur les résultats obtenus par diffraction des rayons X, or la nature même de la sépiolite, minéral à la fois microcristallisé et à texture fibreuse, ne permet pas, dans ces conditions une analyse structurale précise.

De ce fait, il nous a semblé nécessaire de reprendre l'analyse structurale des sépiolites en utilisant le microscope électronique qui, seul, permet l'obtention de diagrammes de monocristaux isolés de très faibles dimensions. Nous avons effectué ce travail sur la sépiolite d'Ampanrandava (Madagascar) qui semble être la forme la plus parfaite de ce groupe de phyllosilicates et dont la formule chimique est:



## ETUDE MORPHOLOGIQUE PRELIMINAIRE

Afin de choisir les monocristaux exploitables par les méthodes d'analyse de Fourier, nous avons d'abord effectué une étude morphologique en microscopie électronique par transmission reliant systématiquement l'aspect des cristaux à leur diagramme de diffraction (Rautureau et Tchoubar, 1972).

Cette étude a montré que la sépiolite présente deux aspects caractéristiques:

1. D'une part on observe des particules très fines, sans aucune texture visible (voir Fig. 4) d'épaisseur toujours voisine de 150 Å (mesurée par ombrage Pt-C) pour une largeur moyenne d'environ 300 Å et une longueur dépassant généralement quelques microns.

De telles particules conduisent toujours à un diagramme de monocristal qui, compte tenu du groupe spatial Pncn et des paramètres de la maille de la sépiolite, correspond dans la plupart des cas aux réflexions  $0Kl$ , avec  $k + l = 2n$  (voir Fig. 2): ceci indique que ces particules s'orientent préférentiellement avec la face (100) parallèle à la membrane-support. Cependant il est également possible d'obtenir, à partir de tels monocristaux, des diagrammes correspondant aux réflexions  $h0l$  (voir Fig. 3) qui sont dûs à des particules orientées avec la face (010) perpendiculaire au faisceau d'électrons.

2. D'autre part, on observe des particules qui présentent une striation parallèle à leur axe d'allongement, donnant une morphologie de fibre. De tels cristaux ont des dimensions variables mais toujours nettement supérieures aux dimensions des particules homogènes: leur largeur et leur épaisseur peuvent atteindre 5.000 Å pour une longueur de quelques dizaines de microns. L'ombrage au Pt-C montre que ces cristaux présentent une succession de surépaisseurs délimitant des sillons parallèles à l'axe d'allongement (voir Fig. 5). De telles particules striées conduisent à des diagrammes plus ou moins caractéristiques de fibres, avec une désorientation azimuthale plus ou moins prononcée.

Dans la suite du travail nous n'avons donc utilisé que les diagrammes obtenus à partir des particules ne présentant aucune texture qui constituent les monocristaux élémentaires. Le caractère monocristallin de telles particules peut d'ailleurs être confirmé en microscopie à haute résolution en visualisant directement les plans réticulaires par la méthode d'interférence à deux ou plusieurs faisceaux. Ainsi, la Fig. 6 montre, dans une particule homogène, l'arrangement parfaitement régulier des plans (020), visualisés en faisant interférer les réflexions 000 et 020. De même, la Fig. 7 montre l'interférence de la réflexion 000 avec les réflexions 020, 040, 060, et, d'autre part, de la réflexion 000 avec la réflexion 031.

## ANALYSE STRUCTURALE

Les méthodes d'analyse de Fourier ont été appliquées successivement aux diagrammes de monocristaux présentant les réflexions 0Kl (Rautereau, Tchoubar et Méring, 1972) et aux diagrammes présentant les réflexions h0 .

Le microscope utilisé était équipé d'un porte objet inclinable permettant de rattraper les défauts d'orientation de chaque particule par rapport au faisceau d'électrons.

Enfin, la mesure des intensités des réflexions a été effectuée à partir de clichés photographiques à l'aide d'un microdensitomètre à balayage (flying spot) permettant d'obtenir l'intensité intégrée pour chaque réflexion.

En utilisant les intensités des réflexions 0Kl et h0l nous avons successivement effectué les projections de Fourier des atomes de la maille de sépiolite sur le plan (100) et sur le plan (010). Le modèle structural qui nous a servi de point de départ était le modèle proposé par Brauner et Preisinger. Les projections effectuées correspondaient soit à l'ensemble des atomes de la maille, soit à la contribution partielle de certains atomes de la maille, permettant ainsi leur localisation (méthode des séries différences).

L'examen comparatif des différentes projections obtenues a permis de constater plusieurs différences avec le modèle proposé par Brauner et Preisinger.

1. Un atome a été mis en évidence aux coordonnées  $y/b = 0,250$  et  $z/c = 0,750$ . Cette position était inoccupée dans le modèle de Brauner et Preisinger. Il s'agit vraisemblablement du transfert d'un atome d'une position possible à une autre, plutôt que d'une erreur dans les analyses chimiques. Ceci conduit à prévoir une révision probable de la formule structurale de la sépiolite, notamment en ce qui concerne la localisation des substitutions isomorphiques, sans pour cela remettre en cause les données de l'analyse élémentaire.

2. Par ailleurs, on constate que les couches tétraédriques occupent une position relative différente de celle indiquée par Brauner et Preisinger. Par rapport au modèle de ces auteurs il est nécessaire de faire glisser chaque couche tétraédrique parallèlement à elle-même de  $z/c = 0,017$ . Ce déplacement a lieu dans un sens tel qu'il conduit à une diminution du décalage relatif des deux couches tétraédriques d'un même feuillet 2:1.

3. La projection de Fourier sur le plan (010); correspondant à la contribution des seuls atomes des couches tétraédriques, a montré qu'il faut également revoir la position des oxygènes de chaque couche tétraédrique.

Les oxygènes constituant le plan de base d'une couche tétraédrique doivent être glissés de  $\frac{x}{a} = 0,010$  vers l'extérieur du feuillet tandis que les oxygènes de sommet des tétraèdres (couche octaé-

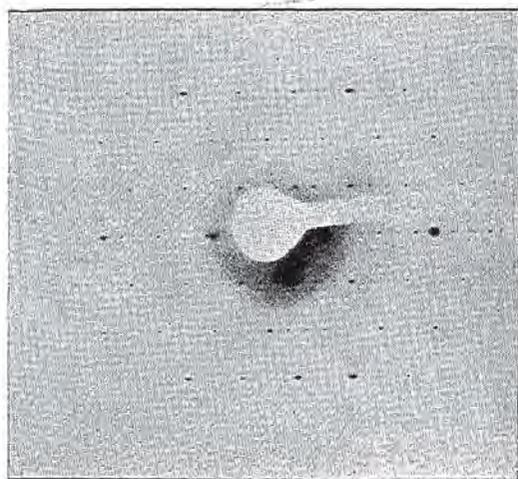


Fig. 2. Diagramme de diffraction d'électrons d'une particule de sepiolite avec orientation préférentielle. Plan [100] perpendiculaire au faisceau des électrons.

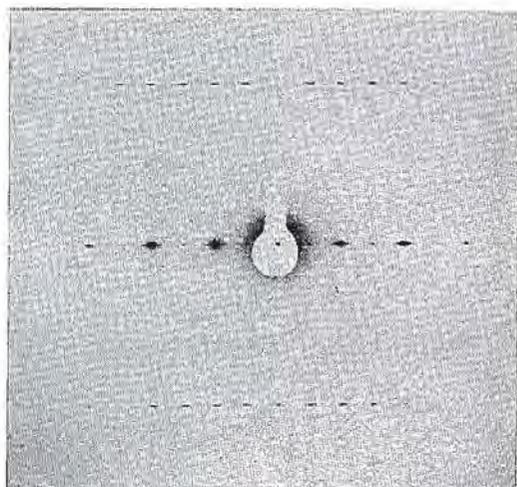


Fig. 3. Diagramme de diffraction d'électrons d'une particule de sepiolite avec orientation préférentielle. Plan [010] perpendiculaire au faisceau des électrons.

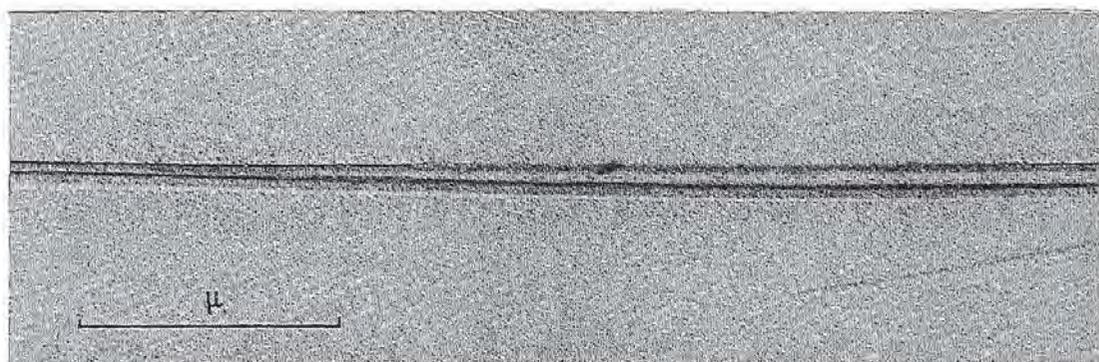


Fig. 4. Microphotographie d'une particule de sepiolite d'Ampandrandava (Madagascar). Ombrage de Pt-C. Cristal sans aucune texture visible.

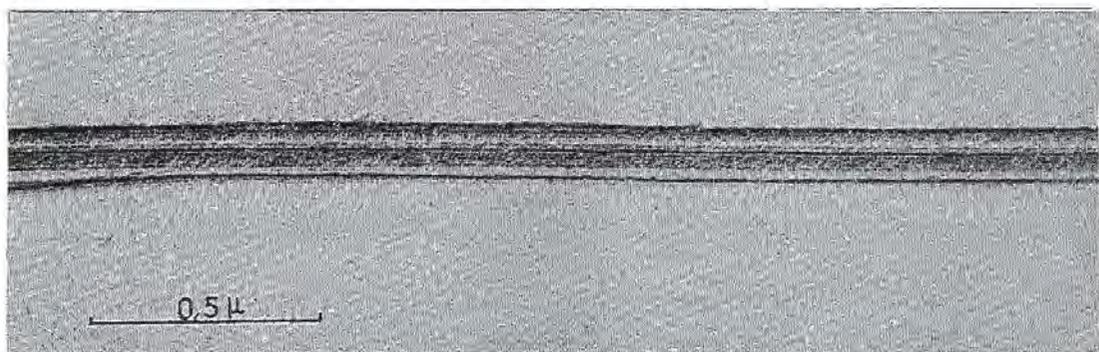


Fig. 5. Microphotographie d'une fibre du même material, montrant une striation parallèle à la direction d'allongement.



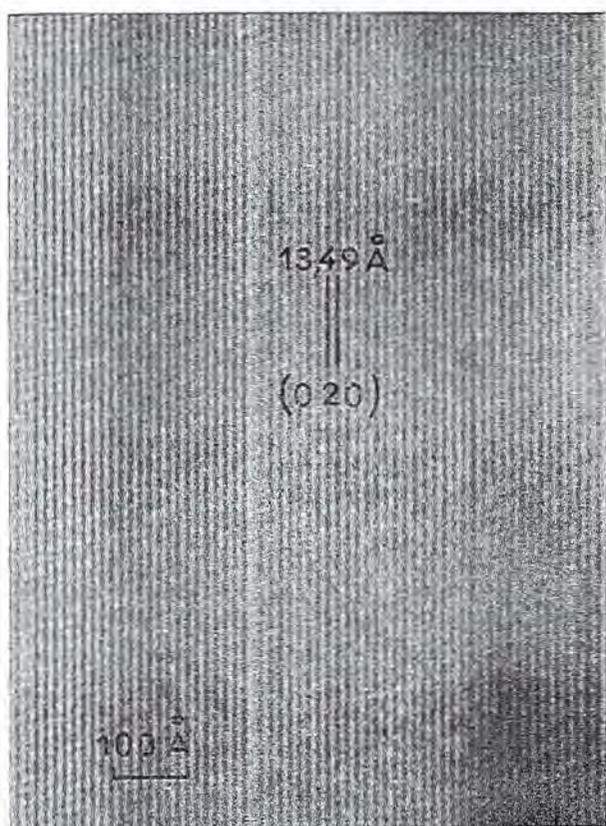


Fig. 6. Microphotographie d'haute résolution d'une particule de sepiolite obtenue par la méthode d'interférence du faisceau multiple. La disposition parfaitement régulière des plans 020 indique le caractère microcristallin de la particule.

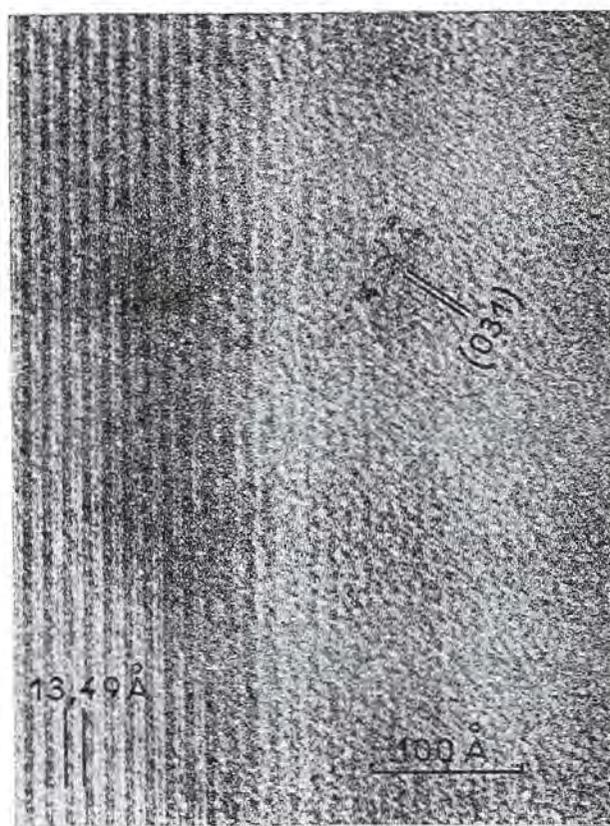


Fig. 7. Microphotographie d'haute résolution montrant l'interférence de la réflexion 000 avec autres réflexions.



drique) doivent être glissés de la même quantité vers la couche octaédrique.

La Fig. 8 montre la projection de Fourier, sur le plan (100), du potentiel correspondant à l'ensemble des atomes contenus dans un quart de maille de sépiolite (la projection présente un plan-miroir à  $y/b = 0,250$ ). Les lignes fermées sont des courbes équipotentielles présentant un écart entre elles de 100 unités arbitraires. Nous avons indiqué, sur cette figure, la position des atomes de silicium, d'oxygène et de l'eau de cristallisation. Les traits pleins et pointillés relient les positions, sur la projection, des atomes de silicium de chaque couche tétraédrique. Le retournement d'une couche tétraédrique, conduisant à la quinconce des éléments de feuillet 2:1, s'effectue autour des oxygènes marqués O'. Enfin la flèche simple indique la position qui était inoccupée dans le modèle de Brauner et Preisinger.

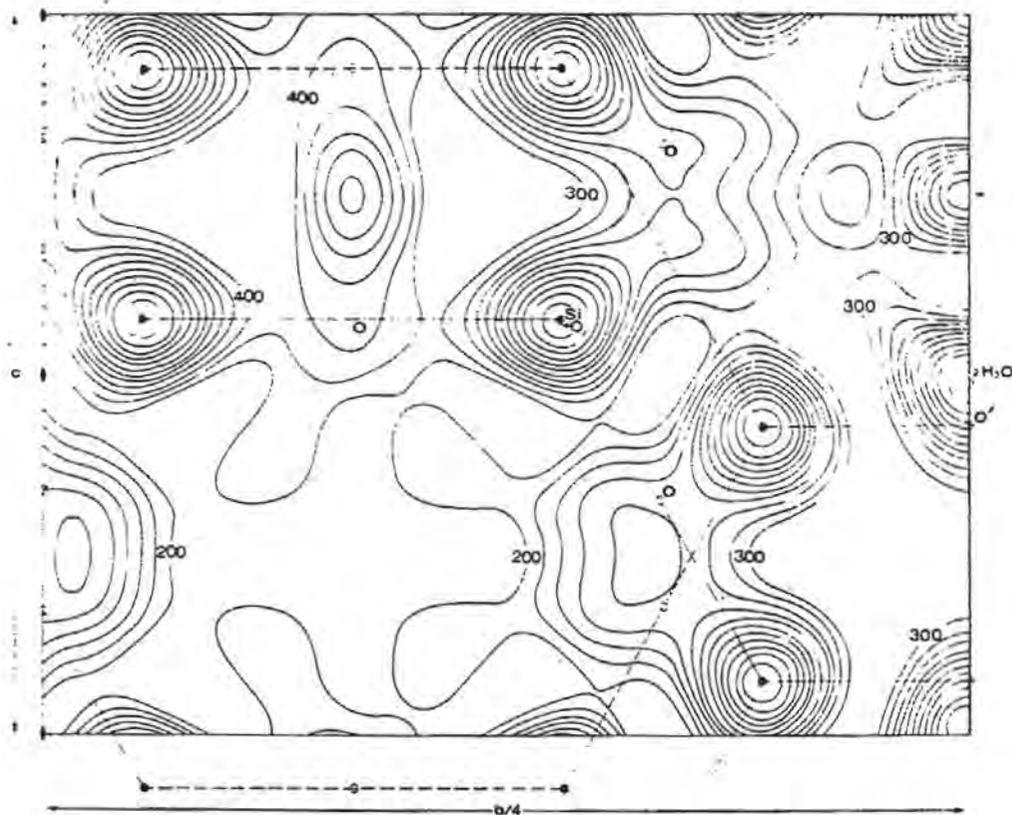


Figure 8. Projection de Fourier sur le plan (100). Lignes équipotentielles prises à intervalles de 100 unités arbitraires. On indique les positions des atomes de Si, O et H<sub>2</sub>O de cristallisation. La flèche indique la présence d'un atome en position non occupée dans la structure de Brauner et Preisinger.

La Fig. 9 donne la projection de Fourier, sur le plan (010), du potentiel correspondant à l'ensemble des atomes contenus dans une demi-maille. Un plan-miroir existe à  $\frac{x}{a} = 0,250$  et la figure a été dessinée de façon à montrer la projection, sur le plan (010), d'un feuillet 2:1 complet. Ici encore l'écart entre les courbes équipotentielles est de 100 unités arbitraires. Enfin, nous avons représenté en trait plein les projections des tétraédres, tandis que des traits pointillés délimitent les cavités octaédriques. Il faut remarquer que, sur cette figure, la présence d'un atome en position  $y/b = 0,250$   $z/c = 0,750$  n'est pas décelable car le pic de potentiel correspondant coïncide avec les projections des magnésiums de la couche octaédrique.

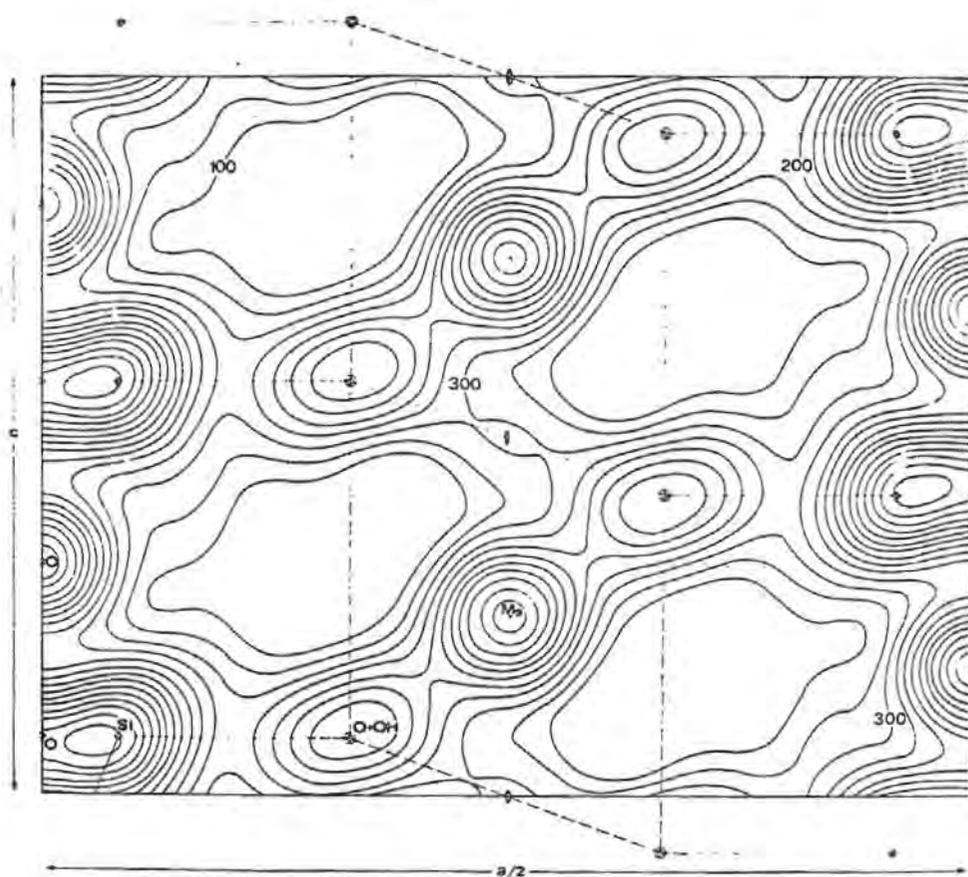


Figure 9. Projection de Fourier sur le plan (010). Sur cette projection la présence d'un nouveau atome en position  $y/b = 0,250$ ,  $z/c = 0,750$  n'est pas détectable pour coïncider avec la projection des Mg de la couche octaédrique.

## CONCLUSIONS

L'analyse de Fourier des diagrammes de monocristaux de sépiolite conduit à confirmer, dans sa forme générale, la structure proposée par Brauner et Preisinger.

Notre analyse montre toutefois qu'il est nécessaire d'apporter quelques retouches au modèle proposé par ces auteurs. Ces modifications conduisent à un accord plus satisfaisant entre les valeurs des intensités mesurées et calculées.

## REMERCIEMENTS

Nous remercions Mademoiselle S. Caillère, Professeur au Muséum d'Histoire Naturelle de Paris à qui nous devons les échantillons de sépiolite d'Ampanrandava et qui a eu l'amabilité de refaire l'analyse chimique de ce minéral dans le cadre de notre travail.

Les calculs et les traçages des projections de Fourier ont été effectués à l'aide de l'ordinateur du centre de calculs du Groupe de Recherches Ionosphériques, Laboratoire C.N.R.S. à Orléans.

## BIBLIOGRAPHIE

- BRAUNER, K. et PREISINGER, A. (1956): Struktur und Entstehung des sepioliths. *Tschermaks min. petr. Mitt.* 6, 120-140.
- BRINDLEY, G.W. (1959): X Ray and electron diffraction data for sepiolite. *Amer. Miner.* 44, 495-500.
- CAILLERE, S. (1933): Sur une sépiolite fibreuse de Madagascar. *C.R. Ac. Sc. Paris.* 196, 416-417.
- MARTIN-VIVALDI, J.L. et ROBERTSON, R.H.S. (1971): The electron optical investigation of Clays, J.A. Gard editor, *Mineralogical Society, London*, 3, 255-275.
- NAGY, B. et BRADLEY, W.F. (1955): The structural scheme of sepiolite. *Amer. Miner.* 40, 885-892.
- RAUTUREAU, M. et TCHOUBAR, C. (1972): Etude morphologique de la sépiolite par microscopie électronique. *J. Microscopie*, 14, sous presse.
- RAUTUREAU, M. TCHOUBAR, C. et MERING, J. (1972): Analyse structurale de la sépiolite par microdiffraction électronique. *C.R. Ac. Sc. Paris.* 274, 269-271.
- ZVYAGIN, B.B. (1967): *Electron Diffraction Analysis of Clay mineral structures*, Plenum Press, New-York.



TRIANGULAR DIAGRAMS IN USE OF A SURVEY  
OF CRYSTAL CHEMISTRY OF CHLORITES

K. Oinuma,

Natural Science Laboratory, Toyo University,  
Tokyo, Japan,

S. Shimoda and T. Sudo

Geological and Mineralogical Institute,  
Faculty of Science, Tokyo University of Education,  
Tokyo, Japan.

ABSTRACT. - The diagrams were made by the following ways: The ideal general formula of chlorites was given as the ferrous form  $(Mg_{6-x-y-3d/2}Fe''_yAl_{x+d})(Si_{4-x}Al_x)O_{10}(OH)_8$ , where "d" is the parameter of the dioctahedral nature. c-parameter was represented by the value of one chlorite species for one set of diagrams. Dispersion correction was applied for the atomic scattering factor of Fe by the values of  $\Delta f'$  and  $\Delta f''$  as listed in the International Tables for X-ray Crystallography.

About 24 diagrams were made which are different from one another according to the difference of the following factors: (a) Lorentz-polarization factors, (b) combinations of basal reflections, (c) c-parameters and (d) atomic scattering factors. Although differences among diagrams being due to (c) and (d) are not serious for the purpose of a survey of crystal chemistry of chlorites, we can still choose a set of diagrams which show the values showing the best degree of agreement with the observed values obtained from the four test specimens: (A) Fe-rich, (B) Fe-Mg-rich, (C) Mg-rich and (D) Al-rich chlorites.

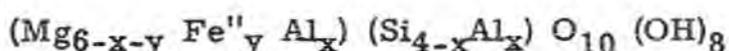
Values of samples A, B and C fall near the line showing equal distribution of cations in the two different octahedral sheets, and that of sample D falls in the domain showing asymmetric distribution, that is di.-tri. type. Chlorites occurring in Recent marine sediments and in a wall-rock-alteration-halo and some aluminium-rich chlorites were studied referring to the diagrams.

## INTRODUCTION

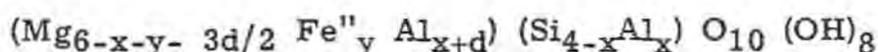
Relations between chemical compositions and relative intensities of basal reflections of chlorites were studied by Brown (1955), Brindley and Gillery (1956), Schoen (1962) and Peruk (1964). The general principle of the present study is in accord with those of the earlier works. Here we show the diagrams to be used for survey of crystal chemistry of chlorites of various modes of occurrence.

## DIAGRAMS

The structural formula of the completely trioctahedral (tri.-tri.) type is as follows:



This formula may approach to the completely dioctahedral (di.-di.) type by the substitution as  $1.5 \text{ Mg} \approx 1 \text{ Al}$ ,



The ways to make the present diagrams are as follows:

1. Cations as Si, Al and Mg are close to one another with regard to the atomic scattering factors particularly in the range of small values of  $\sin \theta/\lambda$ . The factor of Si was used for (Si, Al) in the tetrahedral site. The factors of (Mg, Al) in trioctahedral arrangement and Al in dioctahedral arrangement were represented by the factors of Mg and Al respectively.

2. Diagrams were made for Cu-K $\alpha$  radiation. Dispersion correction was applied for the atomic scattering factor of Fe by the values of  $\Delta f'$  and  $\Delta f''$  listed in International Tables (Lonsdale, et al., 1962).

3. C-parameter gradually varies along with the change of chemical compositions. The basal spacing largely depends upon the amount of Al in the tetrahedral site (Brindley and Gillery, 1956; Hey, 1954), and furthermore the correction terms due to the other atoms as iron and manganese were proposed by Hey (1954). However in Fe''-Mg chlorites as well as Al-chlorites, the value  $d(001)$  does not show noticeable deviation from a straight line relating  $x$  and  $d(001)$ . As indicated by Brindley and Gillery (1956) increasing ferric iron tends to make plotted points slightly deviate from the straight line. Conclusively variations of c-parameters would give a negligible influence on relative intensities of low order reflections.

4. Ferric irons may be included in the chlorite lattice as a primary form (ortho-chlorite) or as a secondary oxidized form

(leptochlorite). The total iron in the formula assigned from the diagram may be represented by the ferrous form.

Twenty-four diagrams were made, which are grouped as follows:

1. Two kinds of diagrams were made, one has three components of  $I(14\text{\AA})$ -- $I(7\text{\AA})$ -- $I(4.7\text{\AA})$  and the other has three components of  $I(7\text{\AA})$ -- $I(4.7\text{\AA})$ -- $I(3.5\text{\AA})$ .

2. Each of the above three component diagrams were grouped into two; one is random powder and the other oriented powder.

3. Each of the diagrams in (2) is further modified according to the different c-parameters used.

4. Scattering factors were used as atomic or ionic scattering factors or their average values. These factors were referred to International Tables (Lonsdale, et al., 1962) except of  $O^{2-}$  which was given in Internationale Tabellen (Harmann, 1935).

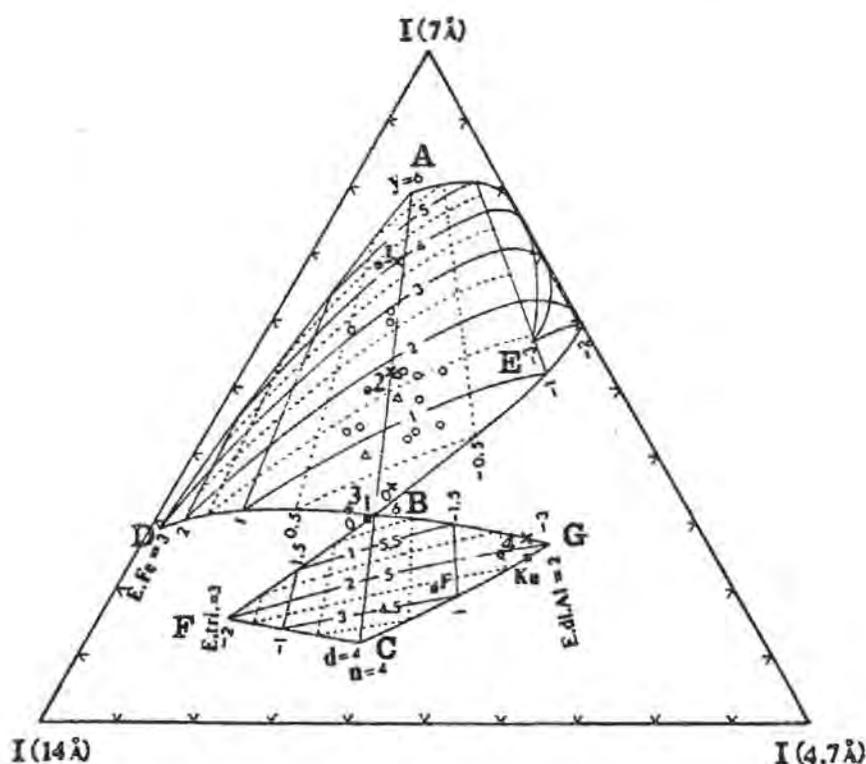


Figure 1.  $I(14\text{\AA})$ - $I(7\text{\AA})$ - $I(4.7\text{\AA})$  triangle diagram  
(Powdered specimens with random orientation)

- : standard specimens (packed into an aluminium holder)
- x: standard specimens (on glass slide)
- Δ: chlorite in Recent marine sediments of the Pacific Ocean
- : chlorite in hydrothermal alteration areas of the Tateishi ore body of the Kamikita mine
- : Al-rich chlorite

Sample numbers and letters correspond to those in the text.

A diagram is selected and shown in Fig. 1. This diagram was made by using the c-parameter of Brown and Bailey (1962) and the scattering factors for atoms. The triangle diagrams, I(14Å) - I(7Å) I(4.7Å), is composed of left and right wings joined by a straight line, A-B-C. Plotted points on this line show equal distribution of octahedral cations between the octahedral site in the silicate layer and in the hydroxyl layer. The range of A-B represents the completely tri-octahedral type, and the range of B-C represents the series from tri. - tri. type (at B) toward di. - di. type (at C) through tri. - di. (or di. - tri.) type. The numerals shown along the line A-B show y-value. The y-value may show not only the amount of ferrous iron but the total amounts of Fe, Mn and Cr, because they have similar atomic scattering factors. The numerals shown along the line B-C represent the total number of cations (n) and the amount of Al of the dioctahedral arrangement (d). The area ADBE represents the range of the chemical composition of Mg-Fe rich chlorites and the area BFCG represents the chemical composition of Al-rich chlorites. The left wing of the area ADBE shows the range of excess Fe in the silicate layer, and its right wing represents the range of excess Fe in the hydroxyl layer. The left wing BFC represents the range of excess Al of the dioctahedral arrangement in the hydroxyl layer and the right wing represents the range of excess Al of the dioctahedral arrangement in the silicate layer.

In the diagram, "E. Fe" shows the number of Fe, Mn and Cr in the silicate layer minus the number of Fe, Mn and Cr in the hydroxyl layer. "E. di. Al" shows the number of Al of the dioctahedral arrangement in the silicate layer minus the number of Al of the dioctahedral arrangement in the hydroxyl layer and "E. tri." shows the number of (Mg, Al) of the trioctahedral arrangement in the silicate layer minus the number of (Mg, Al) of the trioctahedral arrangement in the hydroxyl layer.

The same symbols as above are used in the I(7Å) -- I(4.7Å) - I(3.5Å) triangle diagrams.

## EVALUATION OF THE DIAGRAMS

Twenty-four diagrams are largely modified from one another according to the difference in Lorentz-polarization factors used and slightly modified from one another according to the difference in c-parameters and atomic scattering factors.

On account of various assumptions taken in the preparation of these diagrams, moderate degree of agreement would be anticipated between structural formulas obtained from these diagrams and those calculated directly from chemical compositions. Therefore there is no clear way to select the most suitable diagram except referring to the data for some standard chlorite specimens.

We selected four standard chlorite samples on the series Fe-Mg-Al chlorites (Table I). These samples were finely pulverized and packed into an aluminium holder as random powder as possible. Peak intensities were obtained by measuring heights of peaks, which were corrected by the slit system used. The structural formulas of these standard samples of chlorites were estimated on all prepared diagrams and compared with the formulas calculated directly from the chemical compositions. It is shown that these values were shown to be closer to each other on the diagram made with the c-parameter of Brown and Bailey (1962) and the scattering factors of atoms (Fig. 1) than on the other diagrams. Therefore we selected the diagram to be usable for the purpose of survey of crystal chemistry of chlorites.

## APPLICATION

### 1. Chlorites in Recent marine sediments.

Plots of the chlorites in Recent marine sediments studied in our laboratory are all shown in the area of Mg-Fe chlorite and close to the AB-line.

### 2. Wall rock alteration around the ore, Tateishi ore body of the Kamikita mine.

The ore body occurs replacing rhyolite or rhyolitic tuffs along irregular fissures. One adit, about 500 meters in length, has cut rhyolite from the central ore body outward. It has been made clear that clay mineral and non-clay mineral components as well as some trace elements show clear correlative changes along with distances from the central ore body (to be published elsewhere). Chlorite occurs as one of the principal alteration products. The results are given in Fig. 1, which brings out the fact that the amount of iron in chlorite increases on going outward from the central ore body.

### 3. Aluminium-rich chlorites.

Crystallochemical data for Al-rich chlorite has been accumulated recently, and some of them were summarized up by Eggleston and Bailey (1967) and some additional Japanese data are shown in Table I.

We have noticed occurrence of chlorite with unequal distribution of octahedral cations. When dioctahedral montmorillonite is chloritized in the course of sedimentation or diagenetic processes by fixation of magnesium in the interlayer region, chlorite with unequal distribution of octahedral cations would be formed. There may be some cases where the difference between equal or unequal distributions of octahedral cations is due to the difference

of origin of chlorite. Chlorite with unequal distribution of octahedral cations would be expected to be found in chlorite in Recent marine sediments. However the chlorite of Recent marine sediments in the Pacific Ocean studied in our laboratory are close to those with equal distribution.

Table I. Chemical compositions of chlorite used for evaluation of the diagrams and aluminium rich chlorite from Japan.

Sample No.	1	2	3	4	F	Ku	I
SiO <sub>2</sub>	22.24%	25.76%	29.07%	35.63%	39.01%	37.27%	35.64%
TiO <sub>2</sub>	-	-	0.32	-	0.47	0.30	0.12
Al <sub>2</sub> O <sub>3</sub>	17.05	21.26	21.82	34.87	32.15	35.45	27.89
Fe <sub>2</sub> O <sub>3</sub>	13.38	6.75	0.82	5.01	0.90	0.48	2.52
FeO	26.26	14.60	3.67	0.43	0.10		
MnO	5.42	-	-	0.05	-	none	0.10
MgO	4.10	18.64	29.90	8.63	10.14	10.66	18.95
CaO	tr.	0.90	0.19	1.13	0.54	0.41	0.10
Na <sub>2</sub> O	-	-	tr.	0.24	0.10	0.30	0.67
K <sub>2</sub> O	-	-	tr.	0.46	1.52	2.50	1.51
H <sub>2</sub> O(+)	10.05	10.33	10.76	12.24	14.15 (lg. loss)	11.00	11.24
H <sub>2</sub> O(-)	0.98	1.32	2.76	1.91		2.18	1.53
Total	99.48	99.56	99.32	100.60	99.50 (S: 0.42)	100.65	100.27
d(001)	14.8Å	14.25Å	14.22Å	14.18Å	14.28Å	14.31Å	14.37Å
x*	1.6	1.1	1.1				
b <sub>0</sub>	9.35Å	9.29Å	9.22Å	9.054Å	9.048Å	9.066Å	9.186Å
y**	3.8	2.2	0.3				
y <sup>+</sup>	4.3	1.7	0.2				
n <sup>+</sup>				4.95	4.65	4.86	5.95
d <sup>+</sup>				2.1	2.7	2.28	0.1
E. Fe +	0.3	0.2	0.2				
E. di. Al <sup>+</sup>				1.46	0.73	1.72	
E. tri. <sup>+</sup>				-2.19	-1.095	-2.58	
Impurity	-	-	-	Mixed-layer	Illite Quartz Pyrite	Illite	Illite

\* Calculated from d(001)

\*\* Obtained from b-parameter

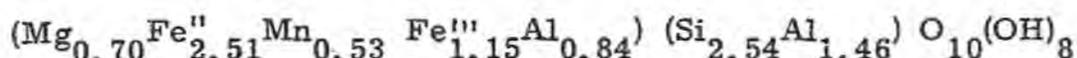
+ Read from the diagram

E. tri. = - E. di. A. x 3/2

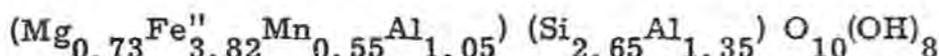
Notes of Table I.

1. Iron-rich chlorite, manganiferrous thuringite (Sudo, 1953)

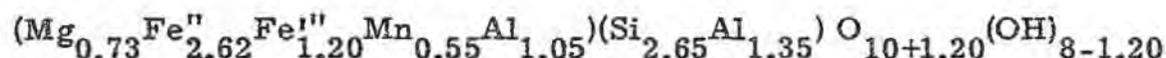
When this chlorite is essentially orthochlorite, the structural formula is as follows:



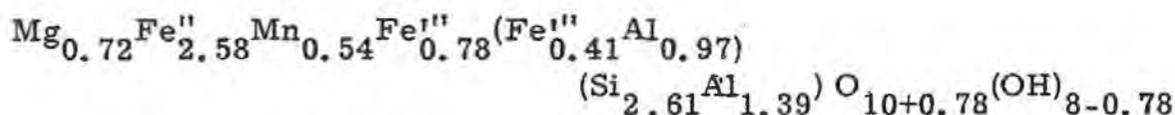
When the completely ferrous form of this chlorite is primary, its structural formula may be given as follows:



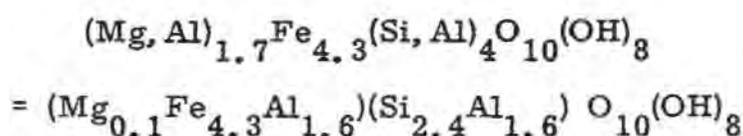
When ferric iron has entirely been derived from ferrous oxidation of ferrous ions, the structural formula of the oxidized chlorite may be written as follows:



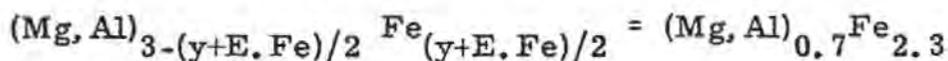
When a part (z) of ferric iron is primary and the other part (z') has been derived from ferrous iron by oxidation, the structural formula may be given as follows:



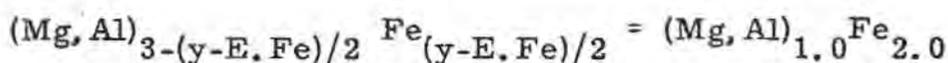
From the diagram, the structural formula may be given as follows:



The cations in the octahedral site in the silicate layer is



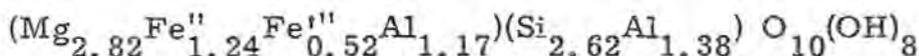
and the cations in the octahedral site in the hydroxyl layer is



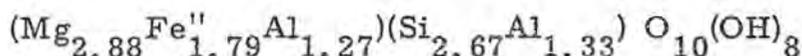
2. Mg-Fe chlorite from the Hitachi mine (Sato and Sudo, 1956)

When this ferric iron is entirely primary replacing aluminium

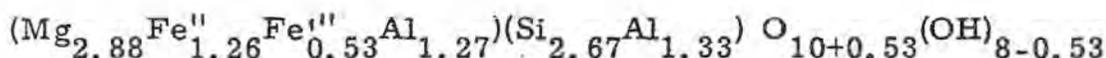
ions, the structural formula may be written as follows:



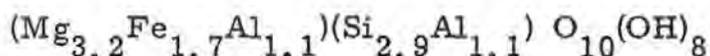
When the completely ferrous unoxidized form of this chlorite is primary, the structural formula may be represented as follows:



When ferric iron has entirely been derived from ferrous iron, the structural formula may be given as follows:

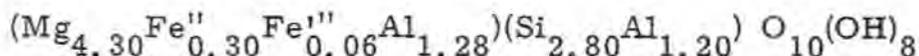


The structural formula may be read from the diagram as follows:

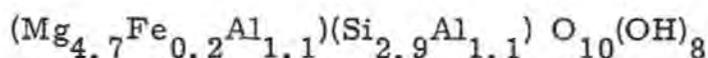


3. Mg-chlorite from the Wanibuchi mine (Satamoto and Sudo, 1956)

The structural formula is as follows:

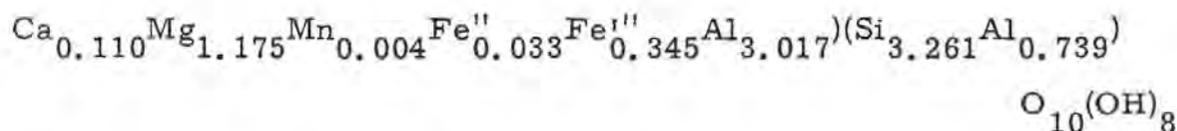


From the diagram, the structural formula may be given as follows:



4. Al-rich chlorite from the Kamikita mine (Hayashi and Oinuma, 1964)

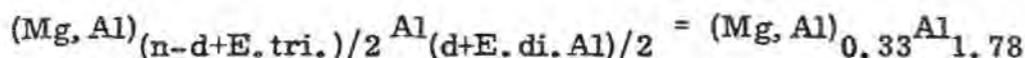
The structural formula is as follows:



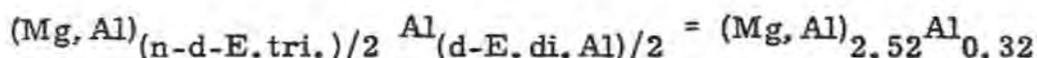
where  $n = 4.684$ . X-ray intensity is closer to di. (silicate layer) --tri. (hydroxyl layer) (Sudo and Sato, 1966), and  $n$ -value is subdivided as tri. part: 2.052 and di. part: 2.632.

From the diagram, cations in the octahedral site in the sili-

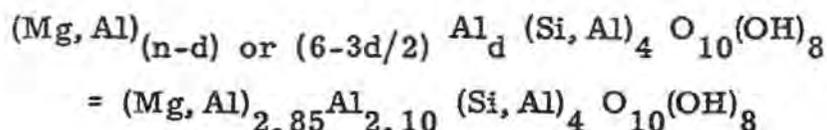
cate layer is



and the cations in the octahedral site in the hydroxyl layer is

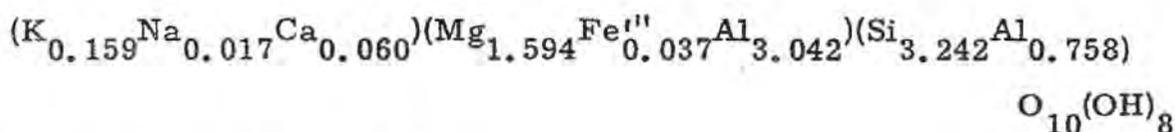


The structural formula may be written as follows:



F. Al-rich chlorite from the Furutobe mine (Tsukahara, 1964)

The following formula was obtained from the chemical composition obtained after subtracting the amounts of impurities from the chemical composition in the column F.



(n = 4.909 and d = 2.284)

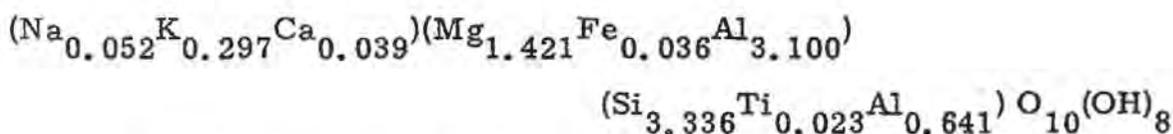
From the diagram, the following formulas are obtained.

The cations in the silicate layer:  $(\text{Mg, Al})_{0.43} \text{Al}_{1.72} (\text{Si, Al})_4$

The cations in the hydroxyl layer;  $(\text{Mg, Al})_{1.52} \text{Al}_{0.98}$

The structural formula:  $(\text{Mg, Al})_{1.95} \text{Al}_{2.70} (\text{Si, Al})_4 \text{O}_{10}(\text{OH})_8$

Ku. Al-rich chlorite from the Kurosowa mine (Suzuki, unpublished)



From the diagram, the following formulas are obtained.

The cations in the silicate layer:  $(\text{Mg, Al})_{0.00} \text{Al}_{2.00} (\text{Si, Al})_4$

The cations in the hydroxyl layer:  $(\text{Mg, Al})_{2.58} \text{Al}_{0.28}$

The structural formula:  $(\text{Mg, Al})_{2.58} \text{Al}_{2.28} (\text{Si, Al})_4 \text{O}_{10} (\text{OH})_8$

I. Al-rich chlorite from the Iwami mine (Shimoda, unpublished)

$(\text{Na}_{0.119} \text{K}_{0.176} \text{Ca}_{0.010}) (\text{Mg}_{2.586} \text{Fe}_{0.193} \text{Mn}_{0.008} \text{Al}_{2.280})$   
 $(\text{Si}_{3.262} \text{Ti}_{0.009} \text{Al}_{0.729}) \text{O}_{10} (\text{OH})_8$

From the diagram the following formula is obtained.

The structural formula:  $(\text{Mg, Al})_{5.85} \text{Al}_{0.10} (\text{Si, Al})_4 \text{O}_{10} (\text{OH})_8$

### REFERENCES

- BAILEY, S.W. and TYLER, S.A. (1960): Clay minerals associated with the Kake Superior iron ores. *Econ. Geol.* 55, 150-175.
- BRAMMALL, A., LEECH, J.G.C. and BANNISTER, F.A. (1937): The paragenesis of cookeite and hydromuscovite associated with gold at Ogofau, Carmarthenshire. *Mineral. Mag.* 24, 507-521.
- BRINDLEY, G.W. (1961): Chlorite minerals, In: *X-ray Identification and Crystal Structures of Clay Minerals*, G. Brown editor, Chap. VI, 242-296, Mineralogical Society, London.
- BRINDLEY, G.W. and GILLERY, F.H. (1956): X-ray identification of chlorite species. *Amer. Mineral.* 41, 169-186.
- BRINDLEY, G.W. and ROBINSON, K. (1951): The chlorite minerals. In: *X-ray identification and Crystal Structures of clay Minerals* G. Brown editor, Ch. VI, 173-198, Mineralogical Society, London.
- BROWN, G. (1955): The effect of isomorphous substitutions on the intensities of (001) reflections of mica-and chlorite-type structures. *Mineral. Mag.* 30, 657-665.
- BROWN, G. and BAILEY, S.W. (1962): Chlorite polytypism: I. Regular and semi-random one-layer structures. *Amer. Mineral.* 47, 819-850.
- BRYDON, J.E., CLARK, J.S. and OSBORNE, V. (1962): Dioctahedral chlorite. *Can. Mineral.* 6, 595-609.
- CAILLÈRE, S., HÉNIN S. and POBEGUIN, T. (1962): Presence d'un nouveau type de chlorite dans les "bauxites" de Saint-Paul-de-Fenouillet (Pyrenees-Orientales). *C.R.Acad. Sci. Paris.* 254, 1657-1658.
- EGGLESTON, R.A. and BAILEY, S.W. (1967): Structural Aspects of dioctahedral chlorite. *Amer. Mineral.* 52, 673-689.
- FRENZEL, G. and SCHEMBRA, F.W. (1965): Ein dioktaedrischer Chlorit vom Kaiserbachtal (Südpfalz), *Neues Jahrb. Min. Monatsh.* 108-114.
- HARMANN, C. (1935): In: *Internationale Tabelle zur Bestimmung*

- von Kristallstrukturen, 2, Gebrüder Borntraeger, Berlin.
- HEY, M.H. (1954): A new review of the chlorites, *Minerl. Mag.* 30, 277-292.
- LONSDALE, K. MACGILLAVRY, C.H. and RICK, G.D. (1962): In: *International Tables for X-ray Crystallography*, 3, Physical and chemical tables, 1-362, Kynoch Press, Birmingham, England.
- MÜLLER, G. (1961): Vorläufige Mitteilung über ein neues dioctaedisches Phyllosilikat der Chlorit-Gruppe. *Neues Jahrb. Minerl., Monats.* 5, 112-120.
- MÜLLER, G. (1963): Zur Kenntniss di-oktaedrischer Vierschicht-Phyllosilikate (Sudoit-Reihe der Sudoit-Chlorit-Gruppe). *Proc. Int. Clay Conf.*, Stockholm. I, 121-130.
- PETRUK, W. (1964): Determination of the heavy atom content in chlorite by means of the X-ray diffractometer. *Mineral.* 49, 61-71.
- SAKAMOTO, T. and SUDO, T. (1956): Magnesium-rich chlorite from the Wanibuchi mine, Shimane Prefecture. *Miner. Jour.* 1, 348-358.
- SATO, H. and SUDO, T. (1956): Chlorite from the Hitachi mine, Ibaragi Prefecture. *Mineral. Jour.* 1, 395-397.
- SCHOEN, R. (1962): Semi-quantitative analysis of chlorites by X-ray diffraction. *Amer. Mineral.* 47, 1384-1392.
- SUDO, T. (1943): On some low temperature hydrous silicates found in Japan. *Bull. Chem. Soc. Japan.* 18, 281-329.
- SUDO, T. and SATO, M. (1966): Dioctahedral chlorite. *Proc. Int. Clay Conf.*, Jerusalem, Israel. 1, 33-39.
- TSUKAHARA, N. (1964): Dioctahedral chlorite from the Furutobe mine, Akita Prefecture, Japan. *Clay Science.* 2, 56-75.



# REACTION AT LOW TEMPERATURES BETWEEN KAOLIN AND LITHIUM CARBONATE

A. Garcia Verduch and J.S. Moya Corral

Instituto de Cerámica y Vidrio  
Carretera de Madrid a Valencia, Km. 24,300  
Arganda del Rey (Madrid), Spain

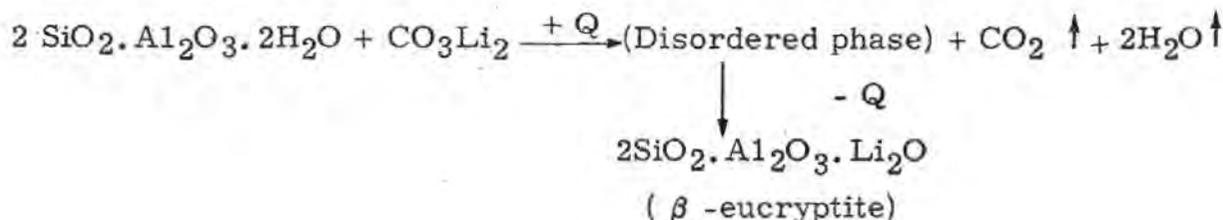
ABSTRACT. - The reactions which occur in 1:1 mol mixtures kaolin- $\text{CO}_3\text{Li}_2$  and metakaolin- $\text{CO}_3\text{Li}_2$  have been investigated by X-ray diffraction analysis, DTA, TGA and DTG. Infrared spectroscopy has also been used to study the reactions in the 1:1 mol mixture kaolin- $\text{CO}_3\text{Li}_2$ .

The mathematical treatment of Freeman-Carroll has been applied to the experimental TGA and DTG data in order to calculate the activation energies for the decomposition of  $\text{CO}_3\text{Li}_2$  in the reactions: kaolin- $\text{CO}_3\text{Li}_2$  ( $E_1^*$ ) and metakaolin- $\text{CO}_3\text{Li}_2$  ( $E_2^*$ ). The following values have been obtained:  $E_1^* = 17,1$  Kcal/mol and  $E_2^* = 24,8$  Kcal/mol.

The experimental results can be explained by assuming that the reaction between kaolin and  $\text{CO}_3\text{Li}_2$  takes place by direct interaction of both reactants through a mechanism of counterdiffusion of  $\text{Li}^+$  and  $\text{H}^+$  ions, while the reaction between metakaolin and  $\text{CO}_3\text{Li}_2$  proceeds by simultaneous diffusion of  $\text{O}^-$  and  $2 \text{Li}^+$  ions.

## INTRODUCTION

In the kaolin-lithium carbonate system, the reactions take place according to the following sequence;



The reaction between both components goes through an intermediate stage in which a disordered, metastable phase is formed. This amorphous phase, when heated at a rate of 25°C/min. (as in DTA), transforms itself at about 750°C into the lithium silicoaluminates ( $\beta$ -eucryptite) through a process of recrystallization.

The formation of the crystalline phase  $\beta$ -eucryptite takes place at considerably lower temperatures when heated for long periods. The present authors (1970) have observed signs of  $\beta$ -eucryptite development in kaolin-lithium carbonate mixtures heated for 210 hours at temperatures as low as 500°C.

According to Y. Kubo and T. Yamabe (1969), the reaction processes in the kaolin-alkali carbonate (Li, Na, K) systems, consist of three stages: decomposition of kaolin and alkali carbonate, reaction of the decomposed products to give an intermediate phase, and its subsequent transformation into a stable phase. The major difference between the three series lies in the degree of structural continuity from metakaolin to the most stable product, via an intermediate phase, as revealed by X-ray and electron diffraction studies.

The reaction processes are interpreted by Y. Kubo and T. Yamabe in terms of the structures of metakaolin and the alkali aluminosilicate products, by assuming a mechanism which involves simultaneous diffusion of alkali and oxygen ions in the metakaolin structure.

The purpose of this investigation has been to elucidate the mechanism of the reaction between kaolin and lithium carbonate at low temperatures, prior to the formation of the stable crystalline  $\beta$ -eucryptite phase, which is the final product of the reaction.

Attention will be placed on two main points: a) Reactivity of kaolin and metakaolin with lithium carbonate, and b) Ionic diffusion mechanisms in both systems.

## EXPERIMENTAL

The following materials have been used: a) Lithium carbonate, reagent grade; b) Fraction less than 2  $\mu$  of a well crystallized kaolinite, extracted from a kaolin from Lage (Spain). The fraction used has the following wt % composition: SiO<sub>2</sub>, 45,72; Al<sub>2</sub>O<sub>3</sub>, 38,29; Fe<sub>2</sub>O<sub>3</sub>, 0,23; CaO, 0,18; MgO, 0,08; Na<sub>2</sub>O, 0,10; K<sub>2</sub>O, 0,09; loss on ignition, 14,47; c) Metakaolin prepared by heating the above fine fraction of Lage kaolin to 550°C during 48 hours.

The 1:1 mol mixtures of kaolin-CO<sub>3</sub>Li<sub>2</sub> and metakaolin-CO<sub>3</sub>Li<sub>2</sub> were prepared according to the following scheme: a) Preliminary mixing of the powder materials with a small amount of distilled water performed in an agate mortar. b) Drying of the mixtures at

110°C during 24 hours. c) Final mixing of the powder suspended in acetone in a small agate ball mill, during 5 hours.

From the mixtures thus prepared, pellets of 1 cm. diameter were pressed.

The pellets of the above mixtures were heated in air to 365°C for periods ranging from 4 to 250 hours.

The reactions in the 1:1 mol mixture kaolin- $\text{CO}_3\text{Li}_2$  were followed by X-ray diffraction analysis, infrared spectroscopy, DTA, TGA and DTG.

The reactions in the 1:1 mol mixture metakaolin- $\text{CO}_3\text{Li}_2$  were followed by X-ray diffraction analysis, DTA, TGA and DTG.

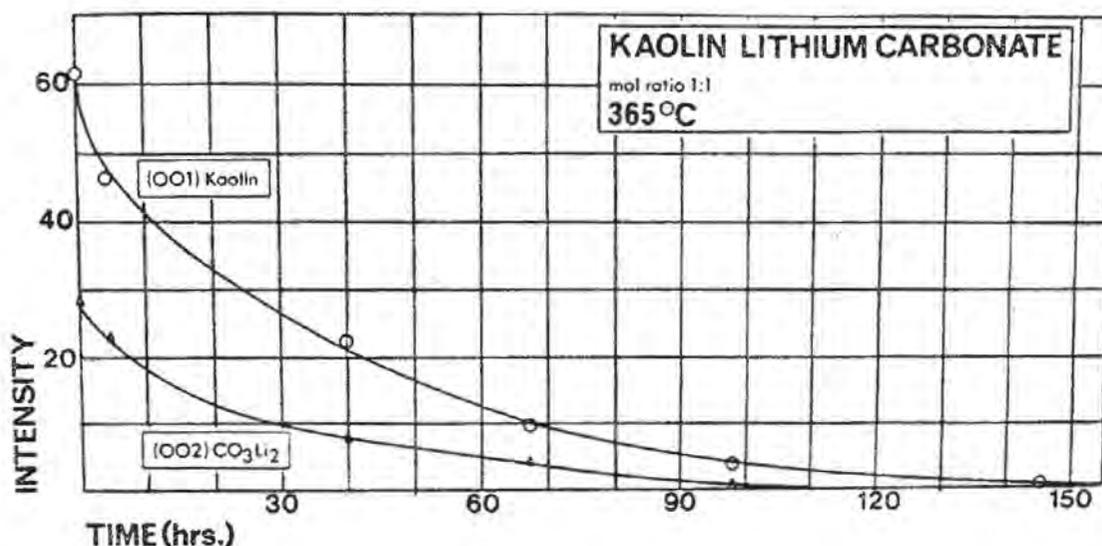


Fig. 1. - X-ray diffraction peak intensities vs. heating time at 365°C.

## RESULTS

### A. X-ray diffraction analysis

Figure 1 shows a plot of the intensities corresponding to the (001) plane of kaolinite and to the (002) plane of lithium carbonate, against the time of heating at a constant temperature of 365°C. It is evident from these results that both crystalline lattices are gradually destroyed at such a low temperature, to form a disordered phase which is amorphous to X-rays. Kaolinite alone does not show appreciable signs of decomposition when heated at 400°C during 70 hours (Fig. 6). Lithium carbonate alone decomposes at an appreciable rate when heated above 700°C (A. García Verduch and J.S. Moya Corral (1970)).

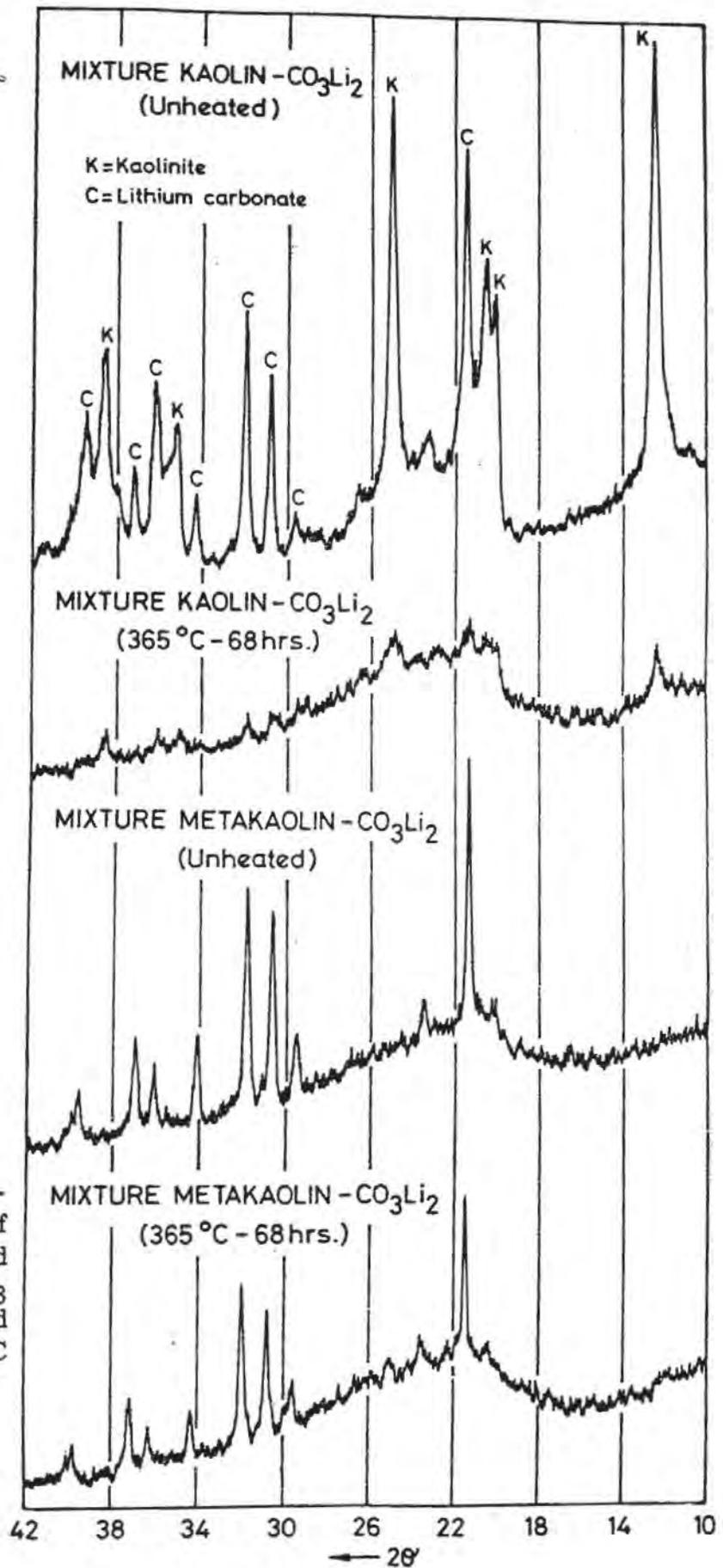


Fig. 2. - X-ray diffraction patterns of kaolin -  $\text{Li}_2\text{CO}_3$  and metakaolin -  $\text{Li}_2\text{CO}_3$  mixtures, unheated and heated at  $365^\circ\text{C}$  for 68 hours.

With the aim of exploring the existence of a different reactivity of kaolin and metakaolin against lithium carbonate, a single heating was made of the two mixtures at a temperature of 365°C - 68 hours. The result of this experiment can be seen in Fig. 2, where the X-ray diffraction patterns of both heated mixtures are compared with the patterns of the unheated mixtures. In such conditions, the lithium carbonate has reacted almost to completion with the kaolin, while the metakaolin has caused only a partial reaction.

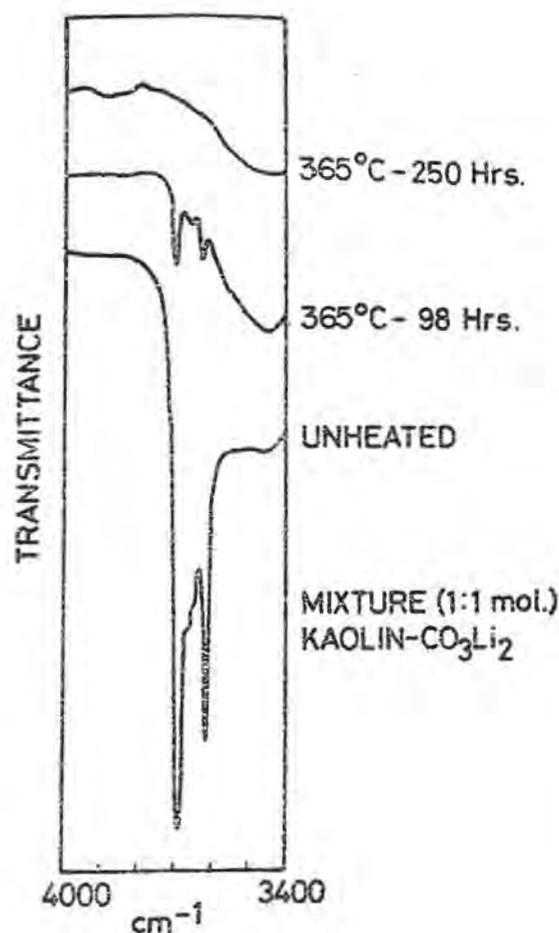


Fig. 3. - Infrared spectra of the 1:1 mol. kaolin-Li<sub>2</sub>CO<sub>3</sub> mixture, unheated and heated at 365°C for 98 and 250 hours.

### B. Infrared spectroscopy

The mixture 1:1 mol of kaolin and lithium carbonate, both unheated and heated at 365°C for different periods, has been analyzed by infrared spectroscopy. In Fig. 3 only the OH valence bands of kaolinite are showed. The gradual shortening of these valence bands can be taken as an indication that the reaction between kaolinite and lithium carbonate proceeds with a simultaneous loss of OH water.

### C. Thermal analysis

The DTA, TGA and DTG of the 1:1 mol mixtures of kaolin and metakaolin with lithium carbonate have been performed using a Mettler instrument. The results are shown in Fig. 4.

The DTA of the mixture kaolin- $\text{CO}_3\text{Li}_2$  shows an important endothermal effect at  $550^\circ\text{C}$ , corresponding to the main reaction between both components to form the disordered phase. This reaction seems to proceed almost entirely in the solid state, even at the heating rate used in the experiment ( $25^\circ\text{C}/\text{min.}$ ). At  $730^\circ\text{C}$ , a rather complex exothermal effect is observed. This stepwise behavior in the evolution of heat seems to indicate that the formation of the crystalline phase  $\beta$ -eucryptite is a complex phenomenon which takes place through several energy states. Finally, at  $1.400^\circ\text{C}$ , a sharp endothermal effect indicates the melting of the  $\beta$ -eucryptite.

The thermal behavior of the mixture metakaolin- $\text{CO}_3\text{Li}_2$  is also shown in Fig. 4. The first impression one gets from the observation of this DTA curve is that the thermal effects occur at higher temperatures than in the kaolin- $\text{CO}_3\text{Li}_2$  system. The first endothermal effect at  $610^\circ\text{C}$  may correspond to the beginning of the reaction in solid state. The TGA and DTG indicate that only a small amount of matter reacts at this stage. The second endothermal effect which is observed at  $700^\circ\text{C}$  is very sharp. The TGA and DTG show that within this temperature range, a fast loss of weight takes place. Both observations support the view that a large quantity of matter reacts in the presence of a liquid phase, which in this case is the lithium carbonate. The exothermal effect at about  $800^\circ\text{C}$  is smaller and more continuous than the one in the other system. This may indicate that in the case of metakaolin, at a heating rate of  $25^\circ\text{C}/\text{min.}$ , the reaction between both components takes place at a temperature high enough to overlap with the process of recrystallization of  $\beta$ -eucryptite.

### DISCUSSION

From the experimental data given by TGA and DTG, it has been possible to elaborate the diagram of Freeman-Carroll (1958) for the decomposition of  $\text{CO}_3\text{Li}_2$  when it reacts both with kaolin and with metakaolin. In this diagram, the values of

$$\frac{\Delta \log \frac{dW}{dt}}{\Delta \log W_r}$$

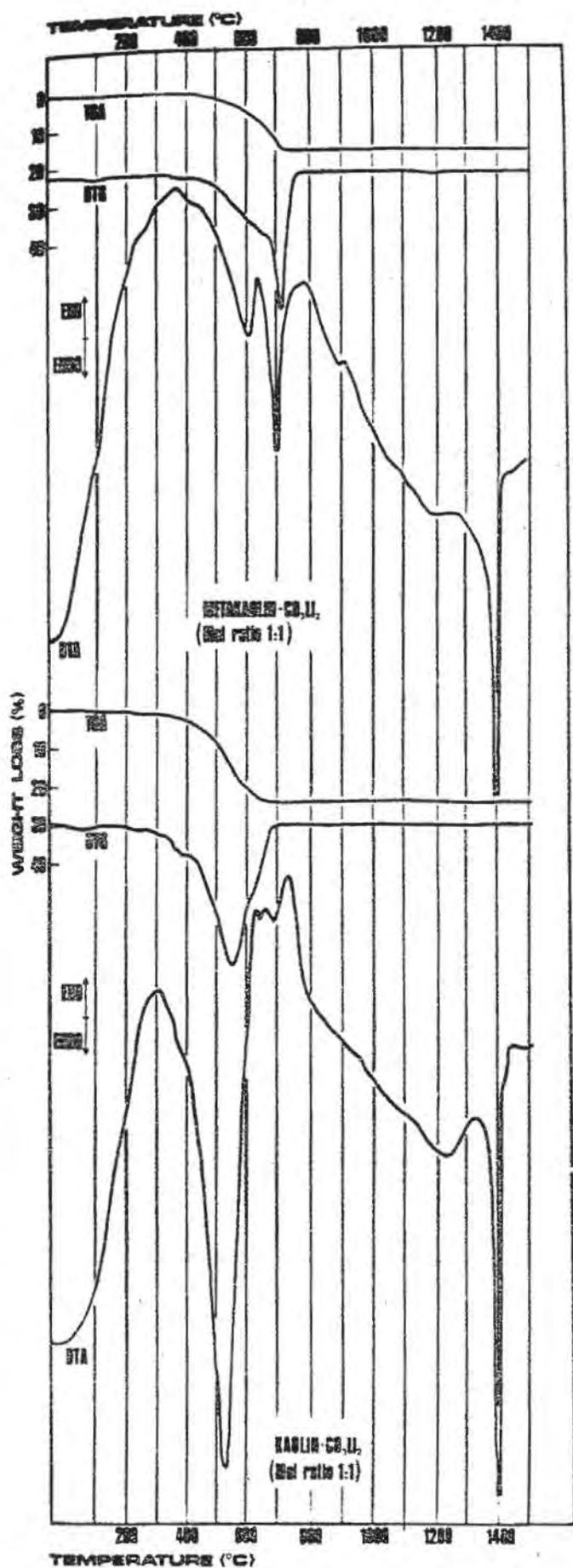


Fig. 4. - TGA, DTG and DTA curves of 1:1 mol. kaolin-Li<sub>2</sub>CO<sub>3</sub> and metakaolin-Li<sub>2</sub>CO<sub>3</sub> mixtures.

are plotted against

$$\frac{\Delta (T^{-1})}{\Delta \log W_r}$$

(Fig. 5) where:

$W$  = Total weight loss ( $\text{CO}_2$ ) at the time  $t$

$W_c$  = Weight loss at completion of reaction

$W_r = W_c - W$

$T$  = Absolute temperature

Tables I and II present the data required for the calculation of the activation energy of decomposition of  $\text{CO}_3\text{Li}_2$  in both reactions. The measured weight losses are within 1,5% of the theoretical values.

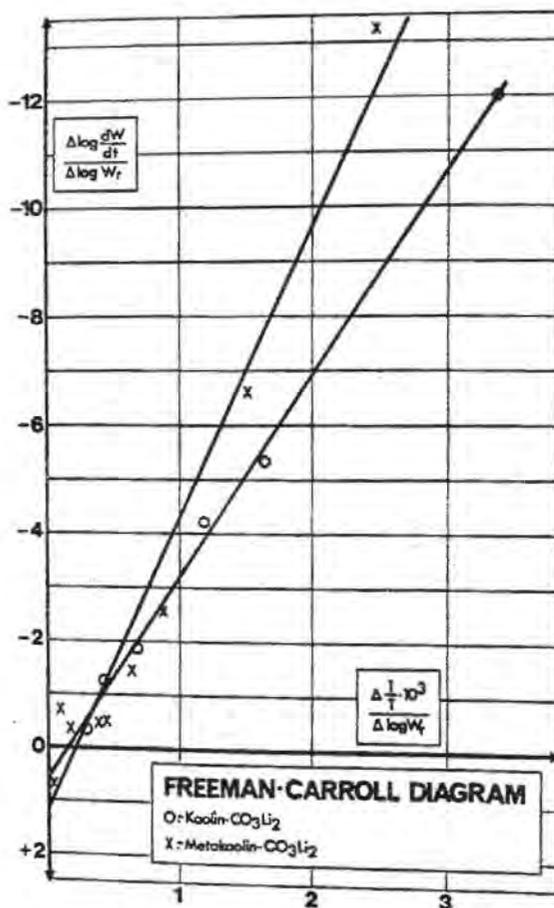


Fig. 5. - Freeman - Carroll diagram for kaolin -  $\text{Li}_2\text{CO}_3$  and metakaolin- $\text{Li}_2\text{CO}_3$  mixtures.

Table I

KAOLIN-CO<sub>3</sub>Li<sub>2</sub>

T °C	T °K	$\frac{1}{T} \cdot 10^3$	W <sub>CO<sub>2</sub></sub> %	W <sub>r</sub> CO <sub>2</sub>	log W <sub>r</sub> CO <sub>2</sub>	$\frac{dW_{CO_2}}{dt}$	$\log \frac{dW_{CO_2}}{dt}$	$\Delta \frac{1}{T} \cdot 10^6$	$\Delta \log W_r CO_2$	$\Delta \log \frac{dW_{CO_2}}{dt}$	$\frac{\Delta \frac{1}{T} \cdot 10^3}{\Delta \log W_r CO_2}$	$\frac{\Delta \log \frac{dW_{CO_2}}{dt}}{\Delta \log W_r CO_2}$
425	698	1,4326	2,123	11,130	1,0530	2,370	0,3747	49,5	0,0306	-0,1630	1,61	-5,32
450	723	1,3831	2,722	10,531	1,0224	3,450	0,5378	46,2	0,0388	-0,1620	1,18	-4,16
475	748	1,3369	3,624	9,829	0,9835	5,010	0,6998	43,3	0,0646	-0,1255	0,67	-1,94
500	773	1,2936	4,955	8,298	0,9189	6,690	0,8254	40,5	0,0959	-0,1130	0,42	-1,17
525	798	1,2531	6,600	6,653	0,8230	8,680	0,9385	38,1	0,1243	-0,0571	0,30	-0,45
550	823	1,2150	8,256	4,997	0,6987	9,900	0,9956					

W<sub>T</sub> = 13,252 %

Table II

METAKAOLIN-CO<sub>3</sub>Li<sub>2</sub>

T °C	T °K	$\frac{1}{T} \cdot 10^3$	W %	W <sub>r</sub>	log W <sub>r</sub>	$\frac{dW}{dt}$	$\log \frac{dW}{dt}$	$\Delta \frac{1}{T} \cdot 10^6$	$\Delta \log W_r$	$\Delta \log \frac{dW}{dt}$	$\frac{\Delta \frac{1}{T} \cdot 10^3}{\Delta \log W_r}$	$\frac{\Delta \log \frac{dW}{dt}}{\Delta \log W_r}$
500	773	1,2936	2,196	13,804	1,1400	1,800	0,2552	40,5	0,0163	-0,2157	2,48	-13,22
525	798	1,2531	2,705	13,295	1,1236	2,940	0,4683	38,1	0,0250	-0,1661	1,52	-6,62
550	823	1,2150	3,450	12,549	1,0986	4,310	0,6344	36,8	0,0424	-0,1125	0,86	-2,65
575	848	1,1792	4,619	11,381	1,0561	5,585	0,7470	33,8	0,0519	-0,0744	0,65	-1,43
600	873	1,1454	5,901	10,099	1,0042	6,645	0,8224	31,9	0,0803	-0,0431	0,39	-0,53
625	898	1,1135	7,607	8,393	0,9239	7,510	0,8756	30,1	0,0800	-0,0401	0,37	-0,50
650	923	1,0834	9,019	6,981	0,8439	8,235	0,9156	28,6	0,1466	-0,0579	0,19	-0,39
675	948	1,0548	11,019	4,981	0,6973	9,410	0,9736	27,1	0,3714	-0,2730	0,07	-0,73
700	973	1,0277	13,882	2,118	0,3259	17,645	1,2466	25,7	0,5685	0,4115	0,04	0,72
725	998	1,0020	15,423	0,577	0,7574-1	6,840	0,8353					

W<sub>T</sub> = 16 %

The slope of the straight lines is equal to

$$\frac{E^*}{2,3 R}$$

where R is the gas constant and E\* is the activation energy.

From the slope of the straight lines, the activation energies for the decomposition of CO<sub>3</sub>Li<sub>2</sub> in the reactions: kaolin + CO<sub>3</sub>Li<sub>2</sub> (E<sub>1</sub>\*) and metakaolin + CO<sub>3</sub>Li<sub>2</sub> (E<sub>2</sub>\*) have been calculated.

E<sub>1</sub>\* = 17,1 Kcal/mol; E<sub>2</sub>\* = 24,8 Kcal/mol.

These values demonstrate that the kaolin is more apt than the metakaolin to react with the CO<sub>3</sub>Li<sub>2</sub>.

If the reaction between kaolin and CO<sub>3</sub>Li<sub>2</sub> should proceed in two separate steps, i.e. decomposition of kaolin and CO<sub>3</sub>Li<sub>2</sub> and reaction of the products of decomposition, as has been stated by Y. Kubo and T. Yamabe (1969), the reaction mechanism would be the

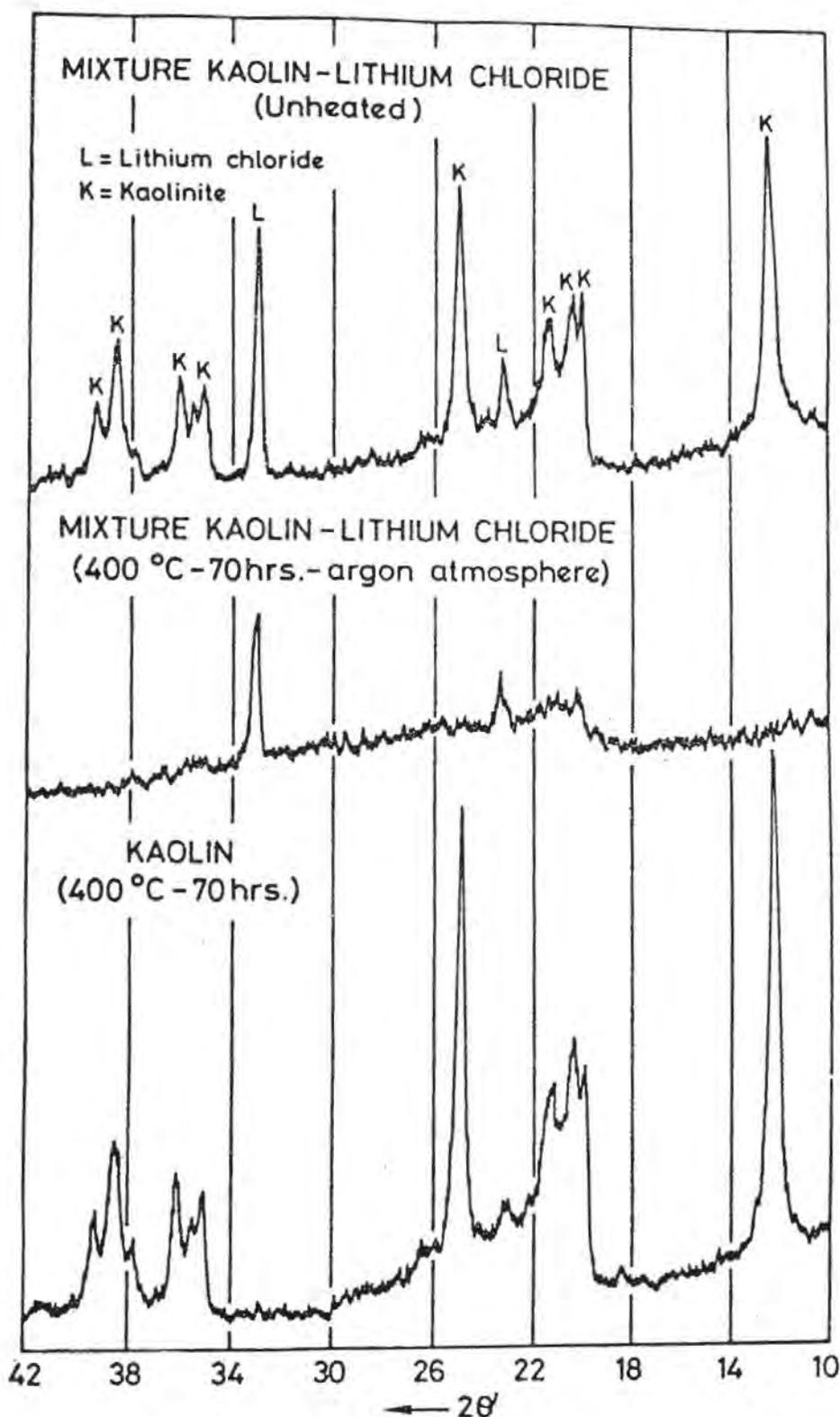


Fig. 6. - X-ray diffraction patterns of 1:1 mol. kaolin-LiCl mixture, unheated and heated at 400°C for 70 hours (argon atmosphere). The X-ray diffraction pattern of kaolin heated at 400°C for 70 hours has been included for comparison.

same whether kaolin or metakaolin should be taken as the starting material. The fact that along the present investigation marked differences in behavior have been observed, lead us to think that two entirely different mechanisms prevail for kaolin and for metakaolin.

The reaction between metakaolin and  $\text{CO}_3\text{Li}_2$  to form a disordered phase, takes place by addition of  $\text{Li}_2\text{O}$  to the anhydrous silicoaluminate network. In the case of kaolin, where constitutional water is present, the reaction proceeds by substitution of  $\text{Li}_2\text{O}$  by  $\text{H}_2\text{O}$ . Thinking in terms of ionic diffusion, the mechanism for metakaolin should involve a simultaneous diffusion of  $\text{O}^- + 2 \text{Li}^+$ . In the case of kaolin, the  $\text{O}^-$  is not required to diffuse, but only  $\text{Li}^+$  and  $\text{H}^+$  need to move in counterdiffusion through the  $\text{OH}^-$  layer of the kaolinite lattice. This second mechanism is more favored from the energetic point of view, due to the higher mobility of the  $\text{H}^+$  ions against the  $\text{O}^-$  ions.

The rate of decomposition of  $\text{CO}_3\text{Li}_2$  at such low temperatures is independent on the rate of intake of  $\text{Li}^+$  ions by the network of the silicoaluminate. The different activation energies in both systems seem to substantiate the existence of the two diffusion mechanisms already described.

In order to give evidence of the mechanism of reaction in the case of kaolin ( $\text{H}^+ \rightleftharpoons \text{Li}^+$ ), a 1:1 mol mixture of kaolin + lithium chloride (with a slight excess of lithium chloride) has been heated at  $400^\circ\text{C}$  for 70 hours in an argon atmosphere. The absence of oxygen both in the reacting salt and in the atmosphere, excludes its participation in the reaction, leaving only the possibility of counterdiffusion of  $\text{Li}^+$  and  $\text{H}^+$  mechanism. Under such conditions, it has been observed (Fig. 6) that the reaction proceeds to completion. In Fig. 6 is also shown an X-ray diffraction pattern of the kaolinite subjected to the same thermal treatment in air. It does not show any appreciable sign of dehydroxilation.

In conclusion, it can be said that the reaction between kaolinite and lithium carbonate to form a disordered phase, takes place by direct interaction between both reactants through a mechanism of counterdiffusion of  $\text{Li}^+$  and  $\text{H}^+$  ions.

## REFERENCES

- FREEMAN, E.S. and CARROLL, B. (1958); The application of thermoanalytical techniques to reaction kinetics. The thermogravimetric evaluation of the kinetics of the decomposition of calcium oxalate monohydrate. *Jour. Phys. Chem.*, 62, 4, 394-397.
- GARCIA VERDUCH, A. and MOYA CORRAL, J.S. (1970); Formación de eucryptita a partir de caolin y carbonato de litio. *Bol. Soc. Esp. Cerám.*, 9, 6, 697-720.

KUBO, Y. and YAMABE, T. (1969); Mechanism of solid state reactions between kaolin and alkali (lithium, sodium and potassium) carbonates. 1969 International Clay Conference, Tokyo. Japan, pp. 915-922.

## FORMATION OF $\beta$ -SPODUMENE BY SOLID STATE REACTION BETWEEN PYROPHYLLITE AND LITHIUM CARBONATE

Shigekazu Udagawa, Hiroyuki Ikawa and Kazuyori Urabe

Department of Inorganic Materials Engineering,  
Tokyo Institute of Technology, Tokyo, Japan

ABSTRACT. - A formation of  $\beta$ -spodumene by solid state reaction between pyrophyllite and lithium carbonate was studied by X-ray powder diffraction and single crystal X-ray techniques. The reaction process was summarized as follows: Starting mixture  $\rightarrow$  Intermediate phase  $\rightarrow$  Silica O  $\rightarrow$   $\beta$ -Spodumene. It was revealed from the single-crystal X-ray study that an intermediate phase appears just before the formation of silica O and is poorly oriented with respect to the original pyrophyllite. The intermediate phase is markedly similar to silica O, and its structure may be a disordered silica O type structure. The structural continuity is partly maintained only at an early stage of the reaction and is destroyed at a later stage of the reaction.

### INTRODUCTION

Since  $\beta$ -spodumene and its  $\text{SiO}_2$  solid solutions are of great technological interest because of their low thermal expansion. Many studies on this compound have been made in terms of ceramic science and technology. Most intensive efforts have been focussed on phase equilibrium studies and thermal expansion behaviors of  $\beta$ -spodumene compositions (Roy et al., 1949, 1950; Smoke, 1950; Hummel, 1951; Skinner, 1960; Ostertag, 1968). However, little work has been done on the solid state reaction to form  $\beta$ -spodumene, and up till now, no study on the formation of  $\beta$ -spodumene by the solid state reaction between pyrophyllite and lithium carbonate has been made.

Extensive studies on the solid state reaction between kaolin and alkali (lithium, sodium and potassium) carbonates (Kubo et al., 1966, 1967, 1968, 1969) may have some relevance to the reaction relating to this study.

In the present paper, the reaction process in the system pyrophyllite-lithium carbonate was studied by powder X-ray diffraction and single-crystal X-ray techniques, and its reaction mechanism was discussed from the structural point of view.

## MATERIALS

**Natural pyrophyllite:** A natural pyrophyllite used in this investigation was obtained from Suzaka, Nagano Prefecture, Japan, from which a powdered pyrophyllite of  $< 5\mu$  was prepared by water-elutriation. X-ray diagrams indicate monoclinic pyrophyllite with a trace of quartz.

**Synthetic pyrophyllite:** Pyrophyllite crystals used for the investigation of the reaction mechanism were synthesized as a pseudomorph after vermiculite under hydrothermal condition. 50 mg of vermiculite flakes (0.2 ~ 1 mm in size) and 100 mg of quartz powders were sealed with 1 ml of  $AlCl_3$  solutions in a silver tube. And it was reacted in a hydrothermal test-tube-type reactor at  $450^\circ \sim 550^\circ C$  and  $500\text{ kg/cm}^2$  for 50 ~ 100 hrs. Pyrophyllite crystals 0.2 ~ 1 mm in size were separated from a residual quartz and other reaction products by decantation.

X-ray single-crystal methods were applied to the synthetic pyrophyllite in order to obtain its structural informations. X-ray oscillation and Weissenberg photographs are indexed from the following lattice parameters: Monoclinic;  $a = 5.14$ ,  $b = 8.94$ ,  $c = 18.40\text{ \AA}$ ,  $\beta = 100^\circ$ . The synthetic pyrophyllite shows strong preferred orientation along its crystal axes and, in consequence, is considered to be a well ordered aggregate which could be regarded as equivalent to a single crystal. Fig. 1(A) shows a rotation photograph about the a-axis (See Fig. 1).

**Lithium carbonate:** An E.P. reagent-grade lithium carbonate ( $Li_2CO_3$ ) was used for making the starting mixture of pyrophyllite- $Li_2CO_3$  system.

## EXPERIMENTAL PROCEDURES

1. Solid state reaction between powdered pyrophyllite and lithium carbonate.

An equimolar mixture of powdered pyrophyllite- $Li_2CO_3$  system was made homogeneous by ethanol wet grinding in an agate mortar

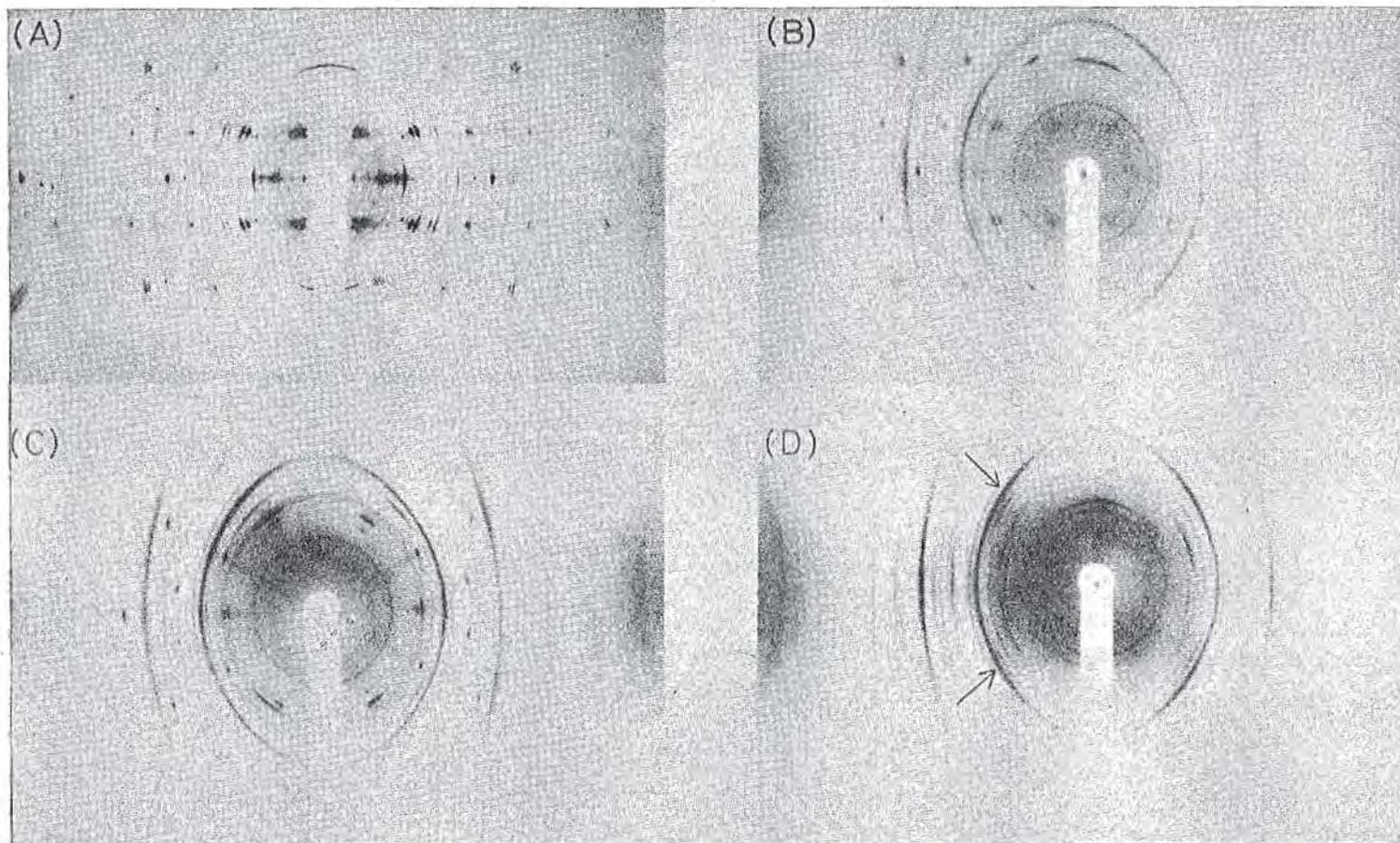


Figure 1. X-ray single-crystal photographs. (A) Rotation photograph about the a-axis of synthetic pyrophyllite, and oscillation photographs of the product obtained at 580°C for 3 days: (B) a-axis oscillation, (C) b-axis oscillation, and (D)  $c^*$  oscillation.



and homogeneity was checked by X-ray diffraction. Small pellets, diameter 10 mm, and thickness approximately 3 mm, were pressed at 300 kg/cm<sup>2</sup>, and were fired in platinum envelopes in an electric furnace at a given temperature between 400° and 1300°C for 2 hrs., and then cooled in air. The reaction products were identified by means of X-ray diffractometer records taken with CuK $\alpha$  radiation and scanning speeds 1° (2 $\theta$ )/min. (or occasionally 1/4°(2 $\theta$ )/min.).

2. Solid state reaction between synthetic pyrophyllite crystal and lithium carbonate.

In order to clarify the reaction mechanism, further investigation of the reaction between synthetic pyrophyllite crystal and lithium carbonate was made using single crystal X-ray techniques. A large number of crystals of synthetic pyrophyllite mentioned above were packed into a gold tube with a large amount of lithium carbonate powders and were heated at 580°C for 3 days in an electric furnace. The reaction products were pseudomorphs after pyrophyllite, not significantly changed in general appearance. X-ray rotation and oscillation photographs were made of the pseudomorphs to find what phases would be present, and what preferred orientation, if any, each phase would possess. Some reaction products mentioned above were again heated at 870°C for various lengths of time, and the resulting pseudomorphs were studied by X-ray single-crystal methods. Unfiltered copper radiation was used for X-ray single-crystal experiments.

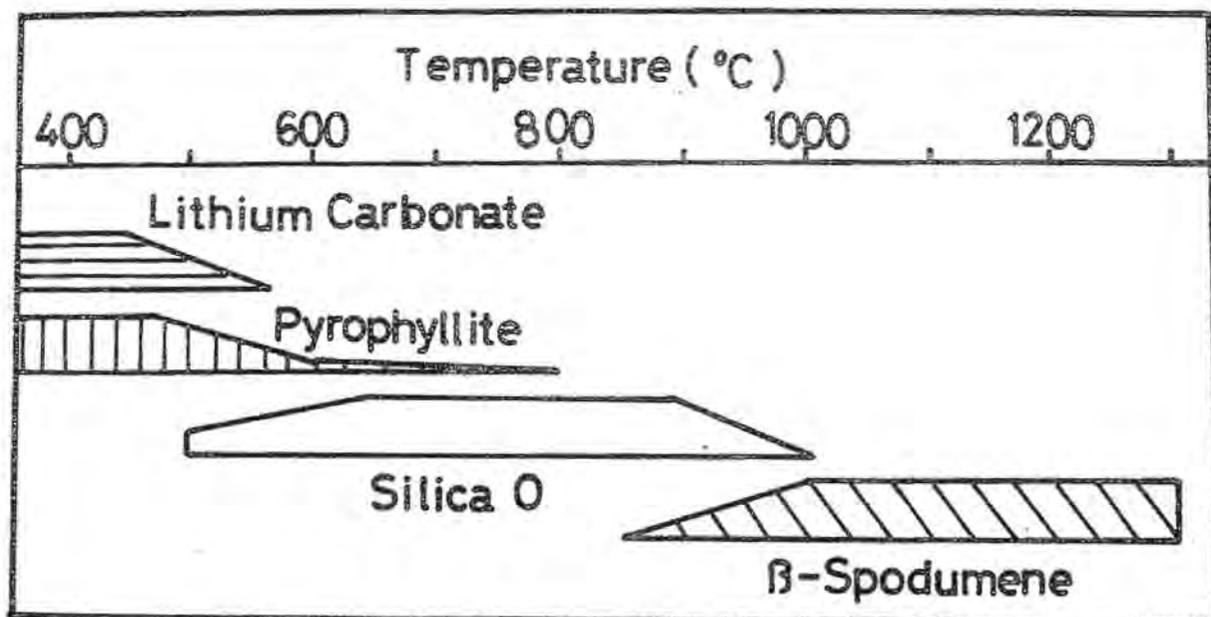


Figure 2. Schematic representation of the over-all process of the reaction between powdered pyrophyllite and lithium carbonate.

## EXPERIMENTAL RESULTS AND DISCUSSION

1. The reaction process in the powdered pyrophyllite-lithium carbonate system.

The over-all process on the reaction between powdered pyrophyllite and  $\text{Li}_2\text{CO}_3$  was examined by powder X-ray diffraction techniques, and the result is displayed schematically in Fig. 2 (See Fig. 2). The mixture of powdered pyrophyllite and lithium carbonate began to decompose at about  $460^\circ\text{C}$ , and a phase with high quartz type structure first appeared at  $500^\circ\text{C}$  and increased its amount up to  $800^\circ\text{C}$  with the increase of temperature. The phases having a structure essentially the same as that of high quartz ( $\beta$ -quartz) have been designated by Roy (1959) as silica O. And, unlike  $\beta$ -quartz, the phases are stable or at least metastable at room temperature. The formation of silica O generally occurs in silicate containing aluminum and lithium.

The phase mentioned above could be identified as silica O by its powder X-ray diffraction pattern which shows good agreement with those of silica O and negative  $\beta$ -spodumene described by Roy et al (1959) (See Table 1). Roy, Roy and Osborn (1950) and Henglein (1956) showed that in the composition of spodumene ( $\text{Li}_2\text{O}:\text{Al}_2\text{O}_3:4\text{SiO}_2$ ) the crystalline phase with  $\beta$ -eucryptite type structure ( $\beta$ -quartz type structure) is often formed. It is, therefore, not surprising that silica O is formed in the pyrophyllite-lithium carbonate system.

Table I. X-ray data for the intermediate phase and silica O formed from pyrophyllite- $\text{Li}_2\text{CO}_3$  system.

hkl	silica O (Roy 1959)				Natural Pyro.		Synthetic Pyrophyllite					
	SiO <sub>2</sub> richest high-quartz		SiO <sub>2</sub> poorest $\beta$ -eucryptite		800°C 2 hrs.		580°C 3 days		870°C 15 min.		870°C 90 min.	
	d Å	I/I <sub>0</sub>	d Å	I/I <sub>0</sub>	d Å	I/I <sub>0</sub>	d Å	I	d Å	I	d Å	I
100	4.32	40	4.55	22	4.54	30	4.5	w	4.6	w	4.5	w
101	3.38	100	3.53	100	3.49	100	3.47	s	3.49	vs	3.48	vs
110	2.498	10	2.621	10	2.62	10					2.69	vw
102	2.303	5	2.384	3	2.34	5			2.37	m	2.36	m
200	2.165	18	2.274	9	2.27	10					2.26	vw
201	2.013	12	2.105	8	2.09	10					2.08	vw
							1.98	s	1.98	m	1.97	m
112	1.842	60	1.914	38	1.888	40	1.89	w	1.88	w	1.89	w
202	1.696	3	1.763	3	1.745	3						
211	1.568	25	1.643	24	1.634	15			1.63	vw	1.65	vw
300					1.508	2			1.51	vw	1.49	vw
212	1.404	20	1.463	11	1.451	10						
203	1.393	35	1.441	16	1.418	20	1.41	m	1.40	m	1.40	m

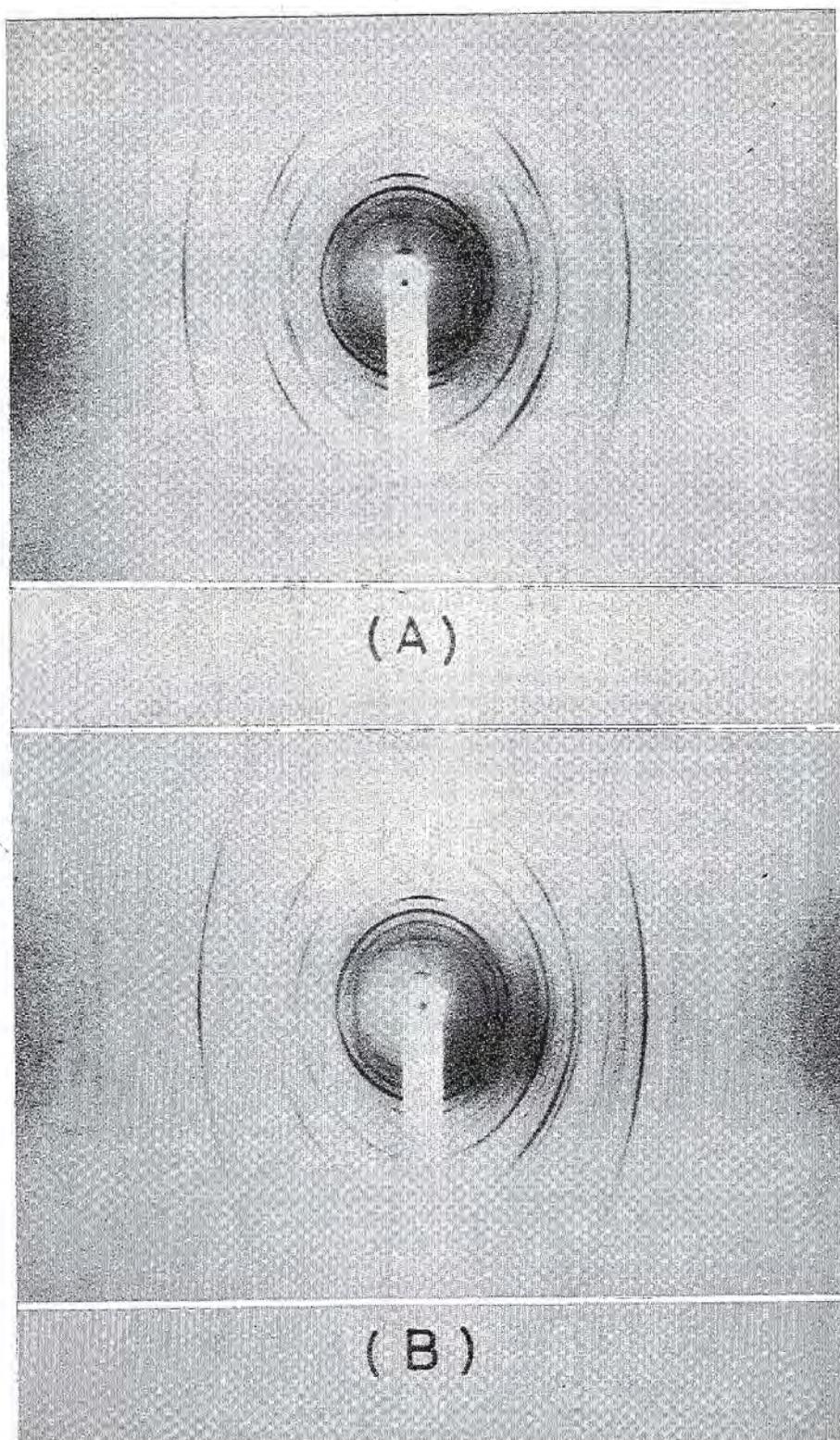


Figure 3. Oscillation photographs of the products obtained at 870°C for various length of time: (A) for 15 min., (B) for 90 min. (oscillation around  $c^*$ ).



The amount of silica O began to decrease at about 850°C, but, on the other hand,  $\beta$ -spodumene started to form at this temperature and developed at the expense of silica O.

2. The reaction between synthetic pyrophyllite crystal and lithium carbonate.

In order to interpret the reaction process, further investigations were made using single-crystal X-ray techniques. Oscillation photographs of the products reacted at 580°C for 3 days were taken about the a- and b- axes of the original pyrophyllite and about  $c^*$ , the direction normal to the (001) cleavage plane, and they are shown in Figs. 1(B), (C) and (D). As shown in Figs. 1(B) ~ (D), oscillation diagrams generally consist of diffused spots of pyrophyllite anhydride and Debye-Scherrer rings, and some streaks along Debye-Scherrer rings as indicated by the arrows in photographs, are also observed. In particular, these streaks are observed clearly in oscillation photographs about  $c^*$ .

The crystal used for previous experiments was demounted from the specimen holder, heated at 870°C for a certain length of time and again mounted to obtain oscillation diagrams. Figs. 3(A) and (B) show oscillation photographs around  $c^*$  of the product obtained at 870°C for 15 min. and at 870°C for 90 min. respectively, in which diffused arcs of pyrophyllite anhydride and Debye-Scherrer rings were again observed (See Fig. 3).  $d$ -spacings obtained from above-mentioned photographs with those of silica O are also listed in Table I.

As obvious in Table I, the reflections of the products heated at about 580°C agree approximately with those of silica O except a reflection of  $d = 1.98 \text{ \AA}$ . The  $1.98 \text{ \AA}$  reflection decreases in intensity with the increase of temperature and time, and it finally disappears. With the decrease of intensity of  $1.98 \text{ \AA}$  reflection, streaks along Debye-Scherrer rings of silica O have become faint, and the rings have finally become completely smooth. Judging from these experimental results, the product obtained at about 580°C is considered to be an intermediate phase developed just before the formation of silica O, and it is poorly oriented with respect to the original pyrophyllite structure. The intermediate phase mentioned above is markedly similar to silica O, and in view of the features of X-ray reflections shown in photographs, its structure may be a disordered silica O type structure.

Oscillation photograph around  $c^*$  of the product obtained at 870°C for 5 hrs. shows smooth Debye-Scherrer rings of silica O together with a faint residual pattern from pyrophyllite anhydride, and a very faint powder pattern of  $\beta$ -spodumene is just discernible without orientation effects.

3. Mechanism of the formation of an intermediate phase.

Oscillation photographs around  $c^*$  show the periodicity of  $5.0 \pm 0.5 \text{ \AA}$ , but streaky features of the reflection preclude exact measurements. It may be supposed that this periodicity corresponds to the repeat distance along a-axis ( $a = 5.23 \text{ \AA}$ ) and/or that along

c-axis ( $c = 5.45 \text{ \AA}$ ) of silica O.

X-ray single-crystal studies show that, in the reaction sequence to form silica O with subsequent formation of  $\beta$ -spodumene, an intermediate phase with a disordered silica O type structure is formed directly from pyrophyllite anhydride.

The structure of pyrophyllite anhydride has not yet been worked out in detail. However, Nakahira et al (1964) showed that there is little change in the entire structural scheme at the stage of dehydroxylation to form an anhydrous phase and only lattice distortion takes place to some extent.

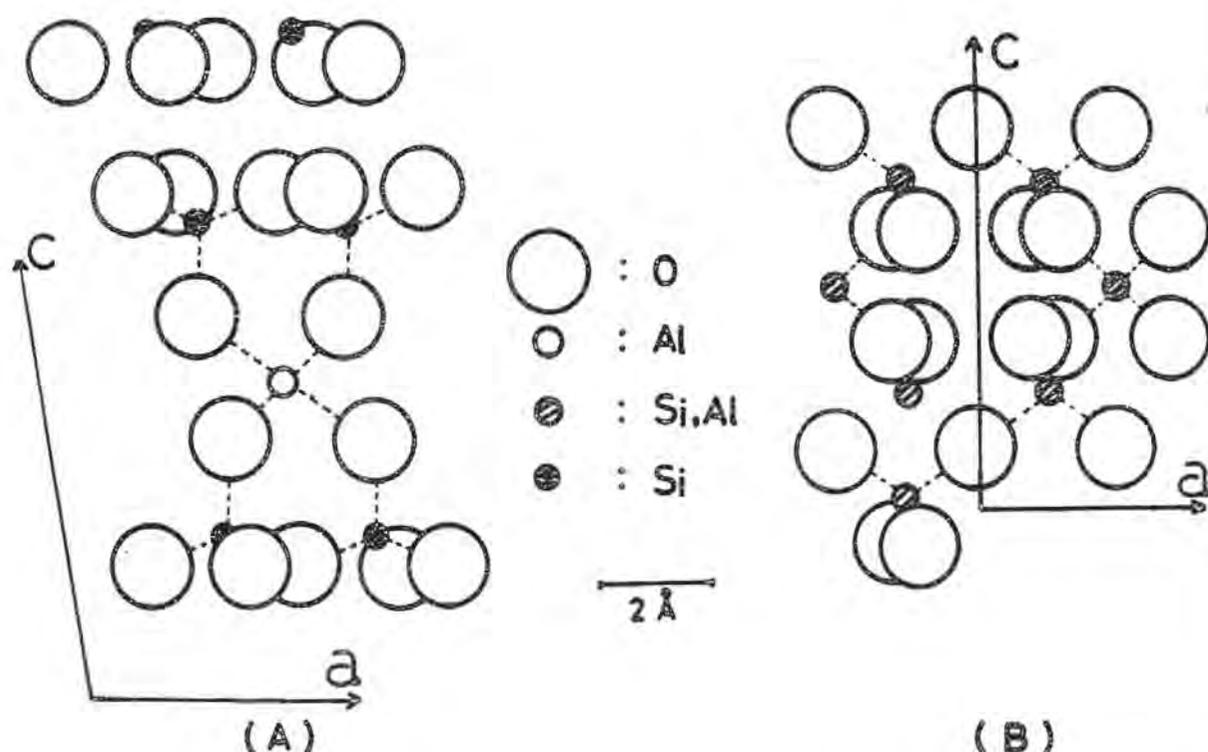


Figure 4. Schematic representation of (A) the structure of pyrophyllite and (B) that of silica O in which Li ions are neglected.

Therefore, much attention will be directed toward the structure of both the starting pyrophyllite and the product phase silica O. A schematic representation of the structures of pyrophyllite and silica O is given in Fig. 4. In the structure of pyrophyllite, the (001) cleavage plane is a close-packed oxygen layer, and the layer sequence along  $c^*$  is  $-\text{Si}-\text{O}..-\text{O}-\text{Si}-(\text{O},\text{OH})-\text{Al}-(\text{O},\text{OH})-\text{Si}-\text{O}..-\text{O}-\text{Si}-$ . In the structure of silica O, the plane normal to the c-axis is an oxygen layer, and the layer sequence along c-axis is  $..-\text{O}-\text{Si}(\text{Al})-\text{O}-\text{Si}(\text{Al})-\text{O}..$  if lithium ions are neglected. This layer sequence is similar to that along c of pyrophyllite (See Fig. 4). From the relation bet-

ween the oxygen layers of two crystals mentioned above, it may be assumed that, in the early stage of the reaction, a large amount of an intermediate phase is formed with the weak orientation relationship of its c-axis parallel to the  $c^*$  direction of pyrophyllite. And this might be the reason why, in oscillation photographs around  $c^*$ , streaky reflections appear along Debye-Scherrer rings of silica O.

With the increase of temperature, the intermediate phase transforms to silica O with subsequent formation of  $\beta$ -spodumene. This reaction process might be the diffusion process of cations such as  $Si^{4+}$ ,  $Al^{3+}$  and  $Li^+$  into the oxygen framework of silica type. Moreover, the structural continuity is destroyed at this stage of the reactions. This could be attributed to dissimilarity between the structure of pyrophyllite and those of higher temperature phases such as silica O and  $\beta$ -spodumene.

#### REFERENCES

- HENGLEIN, E. (1956): Zur Kenntnis der Hochtemperatur-Modifikation von Lithium-Aluminium-Silikaten. Fortschr. Mineral. 34, 40-43.
- HUMMEL, F.A. (1951): Thermal Expansion Properties of Some Synthetic Lithia Materials. J. Am. Ceram. Soc. 8, 235-239.
- KUBO, Y., YAMAGUCHI, G. and KASAHARA, K. (1966): Inverted phase relation in the formation of nepheline and carnegieite from the system kaolinite-sodium carbonate. Am. Mineralogist. 51, 516-521.
- KUBO, Y., YAMAGUCHI, G. and KASAHARA, K. (1967): Reaction process to form nepheline-carnegieite minerals from various starting materials. Mineral. J. (Tokyo), 5, 213-223.
- KUBO, Y., YAMAGUCHI, G. and KASAHARA, K. (1968): Kinetic and electron optical studies of the reaction processes between kaolinite and sodium carbonate. Am. Mineralogist. 53, 917-928.
- KUBO Y. and YAMABE, T. (1969): Mechanism of solid state reactions between kaolin and alkali (lithium, sodium and potassium) carbonates. Proc. Int. Clay Conf., Tokyo. 1. 915-922.
- NAKAHIRA, M. and KATO, T. (1964): Thermal transformations of pyrophyllite and talc as revealed by X-ray and electron diffraction studies. Clays Clay Miner., Proc. 12th Nat. Conf. 21-27.
- OSTERTAG, W., FISCHER, G.R. and WILLIAMS, J.P. (1968): Thermal expansion of synthetic  $\beta$ -spodumene and  $\beta$ -spodumene-silica solid solutions. J. Am. Ceram. Soc. 51, 651-654.
- ROY, R. and OSBORN, E.F. (1949): The system lithium metasilicate-spodumene-silica. J. Am. Chem. Soc. 71, 2086-2095.
- ROY, R., ROY, D.M. and OSBORN, E.F. (1950): Compositional and stability relationships among the lithium Aluminosilicates: eucryptite spodumene, and petalite. J. Am. Ceram. Soc. 33, 152-159.

ROY, R. (1959): Silica O, a new common form of silica. Z. Krist. 111, 185-189.

SKINNER, B.J. and EVANS, H.T., JR. (1960): Crystal chemistry of  $\beta$ -spodumene solid solutions on the join  $\text{Li}_2\text{O}-\text{Al}_2\text{O}_3-\text{SiO}_2$ . Am. J. Sci., Bradley Vol. 258A, 312-324.

SMOKE, E.J. (1951): Ceramic compositions having negative linear expansion. J. Am. Ceram. Soc. 34, 87-90.

## ADDITIONAL CONTRIBUTION

### INFRARED STUDY OF ATTAPULGITE AND HCl TREATED ATTAPULGITE

Efraim Mendelovici

Instituto de Investigación Química, Facultad de Farmacia,  
Universidad de los Andes, Merida, Venezuela.

**ABSTRACT.** - Infrared absorption spectra show important changes in the positions and form of the absorption bands of a film of attapulgite after it has been pumped out. An attempt to differentiate among some of the multiple frequencies due to OH groups is based on the information obtained from the dehydration and deuteration experiments. The  $1198\text{ cm}^{-1}$  shoulder, characteristic of attapulgite, is assigned to a Si-O vibration. When attapulgite is refluxed with HCl 6N for 5 hours the octahedral layer is dissolved. The acid attack causes the disappearance of the Si-O-Si absorption bands from attapulgite giving rise to a characteristic vibration at  $1090\text{ cm}^{-1}$ , as well as another absorption at  $960\text{ cm}^{-1}$ . The latter indicates the presence of silanol groups.

### INTRODUCTION

The infrared spectra of attapulgite or palygorskite have been reported by Gonzalez García et al. (1956) and by Otsuka et al. (1968). Also, infrared studies of heated attapulgite have been published (Ovcharenko, 1966; Hayashi et al., 1969; Taracevich, 1970).

The object of this work is to present additional information on the behaviour of attapulgite when evacuated. Moreover, some interpretations regarding the frequencies of the OH groups are based on isotopic exchange experiments.

Another aspect of this work deals with the modifications of attapulgite upon HCl attack. Infrared spectra of HCl treated attapulgite have not been previously reported.

## EXPERIMENTAL

### Materials

The material examined in this study was the 43 Georgia attapulgite as supplied by Ward's Natural Science Establishment. The cation exchange capacity is given as 30 milliequivalents per 100 g. This material was suspended in water and that finer than 2 microns fraction siphoned off. A portion of this fraction was saturated with  $\text{Ca}^{2+}$  by washing three times with the 1N chloride salt and centrifuging. Excess salt was removed by washing with distilled water until a  $\text{AgNO}_3$  test showed negative for  $\text{Cl}^-$ . Unless otherwise indicated the term "attapulgite" employed henceforth will refer to the above prepared sample.

### Dehydration

Thin self supporting films (2-3 mg./ $\text{cm}^2$  thickness) for the infrared study were prepared by drying an aqueous suspension of attapulgite of adequate density in aluminium foil dishes. The suspensions were dispersed for 3 minutes by ultrasonic vibration before drying.

The resulting films were mounted in an evacuable brass cell fitted with NaCl windows for the dehydration and deuteration experiments. The vacuum inside the cell after pumping out for 30 minutes was about  $25 \times 10^{-3}$  mm. Hg. The cell could be heated to  $100^\circ\text{C}$  by calibrated thermistors.

### Deuteration

Isotopic exchange of hydrogen with deuterium was carried out at  $20^\circ\text{C}$  (room temperature) and at  $100^\circ\text{C}$ . In the latter case the procedure was: admission of anhydrous  $\text{D}_2\text{O}$  in contact with the film, evacuation of the cell and repetition of this process 6 to 7 times during one hour, while the cell was heated at  $100^\circ\text{C}$ .

Infrared spectra ( $4000\text{-}600\text{ cm}^{-1}$ ) were recorded on a Beckman IR7, double beam spectrophotometer fitted with NaCl prism and gratings. The films were always oriented normal to the incident beam.

HCl treatment 1.00 g of Georgia attapulgite was ground to colloidal size and transferred to a 250 ml. round bottomed flask. Then 70 cc. of hydrochloric acid (Merck) was added followed by 70 cc. distilled water. Two such mixtures were refluxed for 5 and 9 hours. After each period the solid was separated and washed until free of  $\text{Cl}^-$  and then dried in the oven.

For the infrared study, 1% transparent discs of the dry sample were prepared using potassium bromide of spectroscopic gra-

de. An evacuable die was used for the preparation of the discs.

The infrared spectra of these discs were recorded using a Perkin-Elmer 621, double beam spectrophotometer.

## RESULTS AND DISCUSSION

### Dehydration

The spectra shown in Fig. 1 reflect the changes in the absorption bands of a film of attapulgite, after it is evacuated at ambient beam temperature. Thus, the vibrations at 915 and 1198  $\text{cm}^{-1}$  virtually disappear as a new absorption at 930  $\text{cm}^{-1}$  becomes evident. The large and dissymmetric band at 1655-1660  $\text{cm}^{-1}$  becomes sharp and symmetrical about a maximum at 1625  $\text{cm}^{-1}$  (Figs. 1 and 2). Simultaneously the 3330, 3400, 3555 and 3595  $\text{cm}^{-1}$  absorption bands are removed; the last two being shifted to 3520 and 3570  $\text{cm}^{-1}$  respectively. The intensity of the 3625  $\text{cm}^{-1}$  absorption band is increased. The spectra in Fig. 2 which cover the stretching and deformation regions of the OH vibrations, show also the partial and complete rehydration of a film of attapulgite after evacuation and heating at 50 and 100°C. It can be easily seen that after total rehydration - by leaving the film in contact with atmospheric moisture during the night at 20°C (ambient temperature) - the original absorptions of attapulgite are completely regenerated (Fig. 2, d).

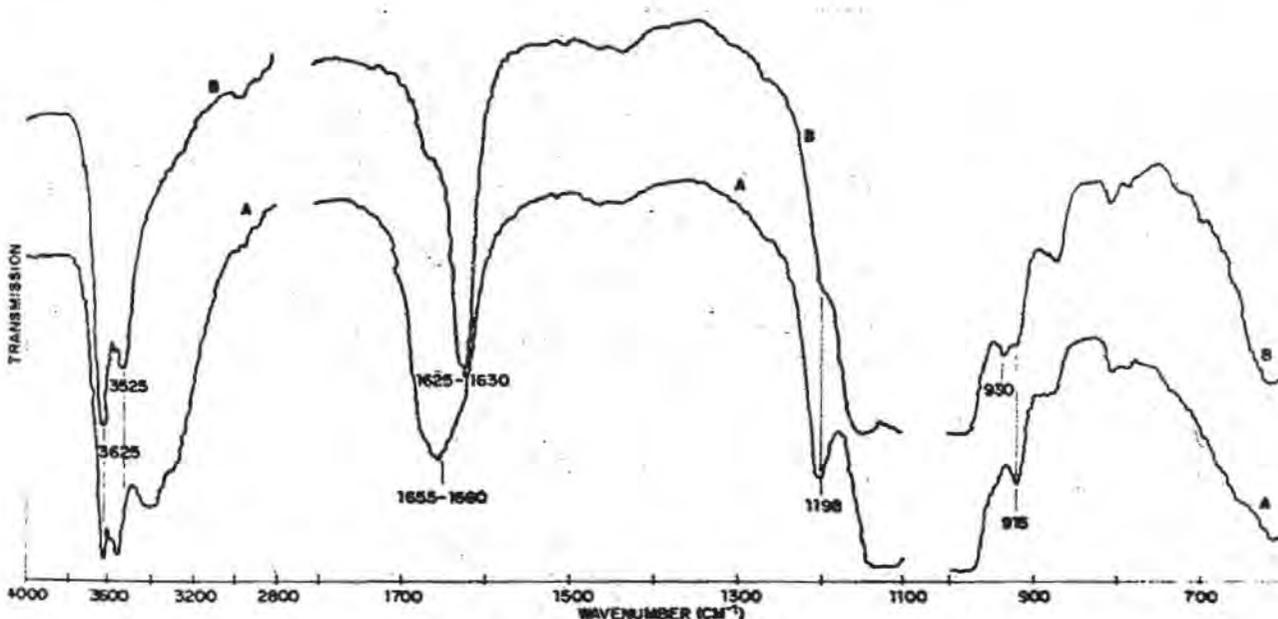


Figure 1. Infrared spectra (600-4000  $\text{cm}^{-1}$ ) of: (A) attapulgite at ambient beam temperature; (B) after evacuation at ambient beam temperature for 30 min.

In the absence of evacuation the same results are not obtained. Thereby when attapulgite was heated only, the absorption bands did not show any major modification until the temperature reached 400°C. Similar results have been reported by Hayashi et al. (1969), on heating palygorskite at atmospheric pressure.

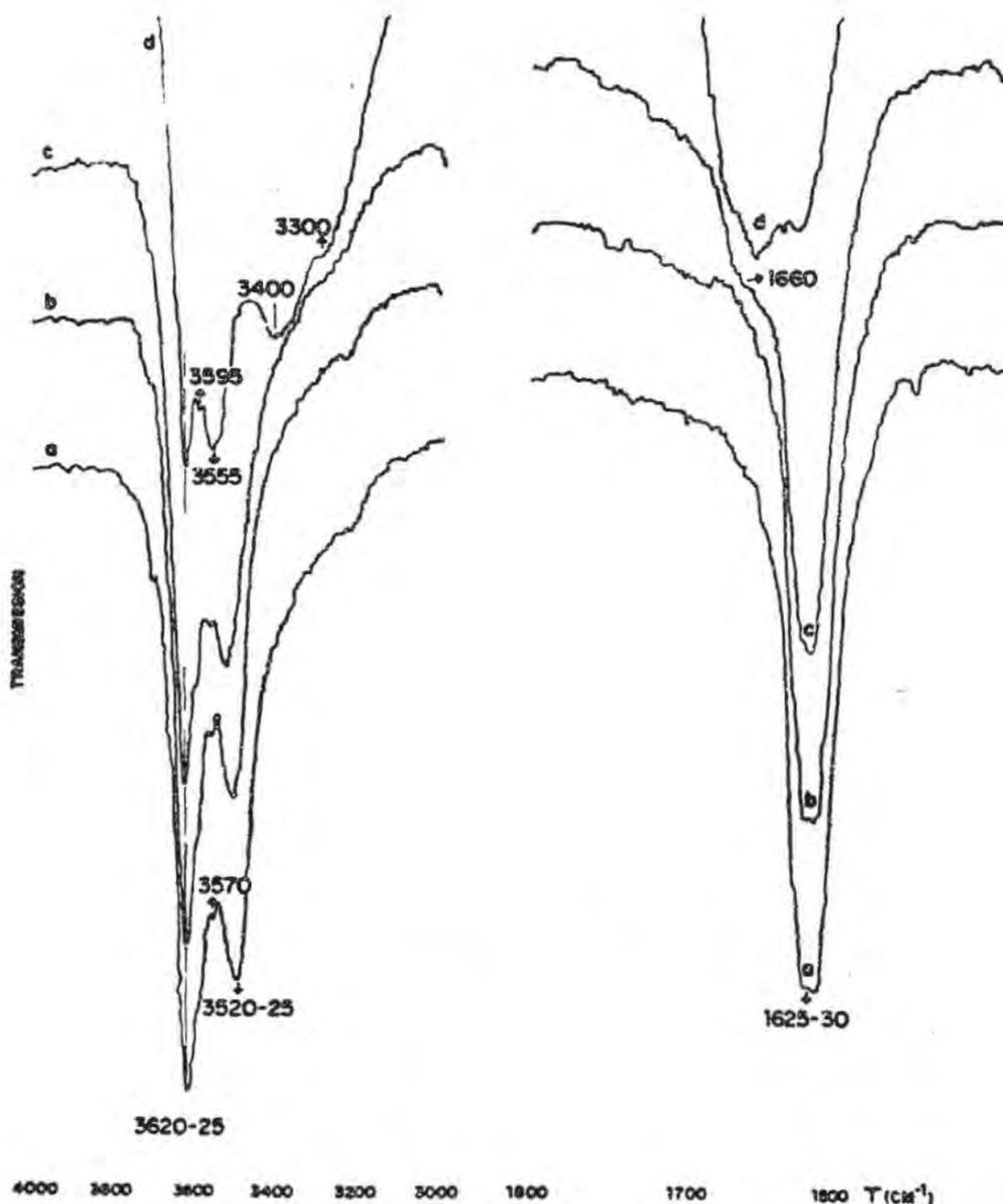


Figure 2. Infrared spectra of attapulgite after: (a) evacuation at 50°C, (b) evacuation at 100°C, (c) partial rehydration at room temperature, (d) total rehydration at room (ambient) temperature.

## Deuteration

Exchange with  $D_2O$  at  $100^\circ C$  has reduced by 80% the intensities of the 1625 and  $3525\text{ cm}^{-1}$  absorption bands, shifting them to 1217 and  $2595\text{ cm}^{-1}$  respectively (Fig. 3). The intensity of the  $3625\text{ cm}^{-1}$  band is only slightly diminished; its corresponding deuterioxy appears as a weak shoulder at  $2672\text{ cm}^{-1}$ . The weak peak at  $3730\text{ cm}^{-1}$  on the evacuated attapulgite (Fig. 3, A) is also affected by deuteration; its counterpart may be observed at  $2760\text{ cm}^{-1}$ . The isotopic ratios of frequencies OH:OD for the 1625, 3525, 3625 and  $3730\text{ cm}^{-1}$  vibrations are 1.34, 1.35, 1.35 and 1.35 respectively.

Rehydration of the above deuterated films, by leaving them in contact with atmospheric water for 3 hours, leads to the reappearance of the original frequencies of attapulgite, including that at  $3730\text{ cm}^{-1}$ .

The source of the sharp and intensive peak at  $2705\text{ cm}^{-1}$  can not be clearly established in this work. The greater multiplicity of components in the OD region when isotopic exchange takes place in some silicates, may be due to many causes. One reason may be the improved resolution in the OD region, where new combination

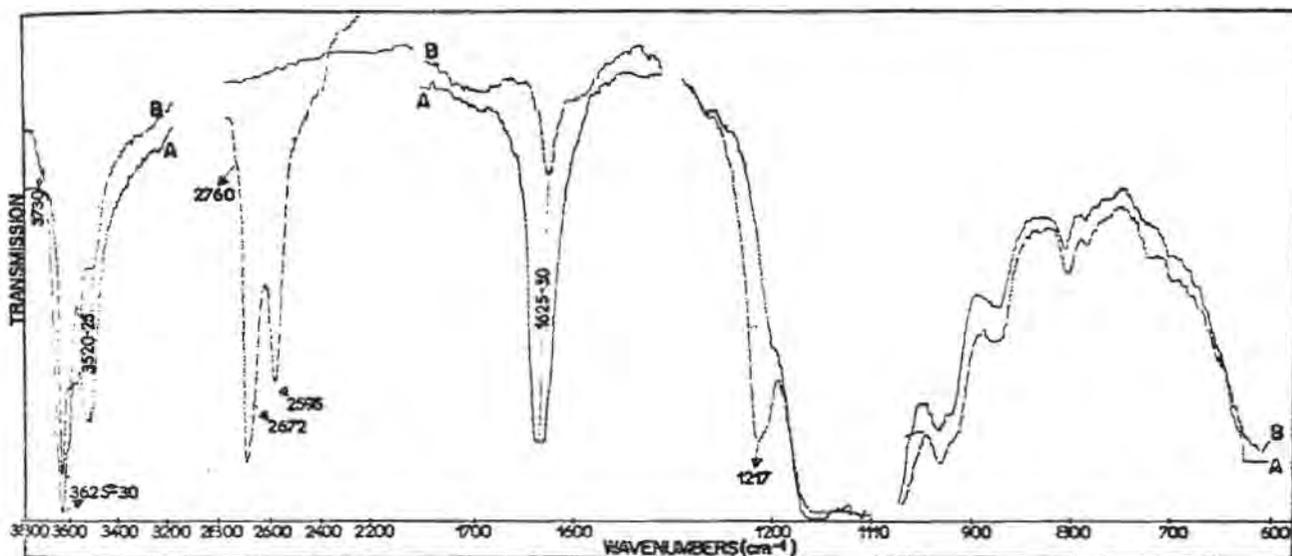


Figure 3. Infrared spectra of attapulgite after: (A) evacuation at  $100^\circ C$ , (B) deuteration at  $100^\circ C$ .

bands can result. On the other hand, coupling and decoupling between OD vibrations and hydrogen bonding of the OH groups may influence the positions of the frequencies.

Physically adsorbed water was removed from attapulgite by evacuation or by evacuation and heating, as is shown by the di-

sappearance of the  $3400\text{ cm}^{-1}$  frequency (Fig. 1 and 2). This frequency can be ascribed to the stretching modes of vibration of associated water molecules.

The disappearance of the  $3400\text{ cm}^{-1}$  frequency is matched by the shifting of the  $3555\text{ cm}^{-1}$  band to  $3525\text{ cm}^{-1}$ . At the same time the H-O-H deformation band at  $1660\text{ cm}^{-1}$  is shifted to a lower frequency at  $1625\text{ cm}^{-1}$ . This may suggest that energetically different hydrogen bondings are involved. The fact that the bands at  $3525$  and  $1625\text{ cm}^{-1}$  are affected by deuteration in a parallel manner (Fig. 3) indicates that they could arise from the same source.

From the continued presence of the  $3625\text{ cm}^{-1}$  absorption after the disappearance of the  $3555$  and  $3400\text{ cm}^{-1}$  bands upon dehydration, it seems that the species responsible for this vibration are different to those associated with the other absorption bands observed in the  $3000\text{-}4000\text{ cm}^{-1}$  region; while from the deuteration results we can conclude that the OH absorbing at  $3625\text{ cm}^{-1}$  must be located in inaccessible positions in attapulgite minerals.

The presence of the absorption at  $3625\text{ cm}^{-1}$  in the  $\text{H}_2\text{O}$  system of Mg-saponite has been interpreted by Farmer and Russel (1971) as corresponding to bonds to uncharged surface oxygens. Frequencies below  $3625\text{ cm}^{-1}$  are assigned to hydrogen bonding to the oxygen of Si-O-Si linkage and the lower frequency components to water - water bonds and H-bonds to the oxygen of Al-O-Si linkages.

According to Farmer and Russel (1971) when saponite and other trioctahedral layer silicates are evacuated, the chains of water molecules are shortened, leading to a trihydrate configuration, which might be responsible for a reduction in the effective symmetry in the silicate lattice and the cause of perturbation of the Si-O vibrations. A similar interpretation would explain the disappearance of the  $1198\text{ cm}^{-1}$  band - assigned to a stretching Si-O vibration in attapulgite - when this silicate is evacuated (Fig. 1). Since the frequency at  $1198\text{ cm}^{-1}$  has not been reported for any other clay silicate is evacuated (Fig. 1). Since the frequency at  $1198\text{ cm}^{-1}$  has not been reported for any other clay silicate it appears to be characteristic of attapulgite.

Absorption bands at  $1200\text{ cm}^{-1}$  arising from silicon - oxygen bonds, have been mentioned by Fripiat et al. (1963) in silica gel prepared from ethyl ortosilicate and by Benesi and Jones (1959) in amorphous forms of silica.

The shoulder marked at  $3730\text{ cm}^{-1}$  in attapulgite (Fig. 3, A) could be due to the presence of silica impurity as it has been shown e.g. in rutile by Jones and Hockey (1971). On the other hand absorption bands at  $3740\text{ cm}^{-1}$  have been mentioned by Angell and Schaffer (1965) in zeolites and by Cannings (1968) in sepiolite, being ascribed in both cases to Si-OH vibrations.

## HCl treatment

The ir spectra of Georgia attapulgite which has been refluxed for 5 and 9 hours with HCl 6N (Fig. 4) show that as the absorption band at  $915\text{ cm}^{-1}$  is removed, characteristic vibrations appear at 800 and  $955\text{--}60\text{ cm}^{-1}$ . The latter has been attributed to the Si-O-H angle deformation vibration (Fripiat et al., 1963).

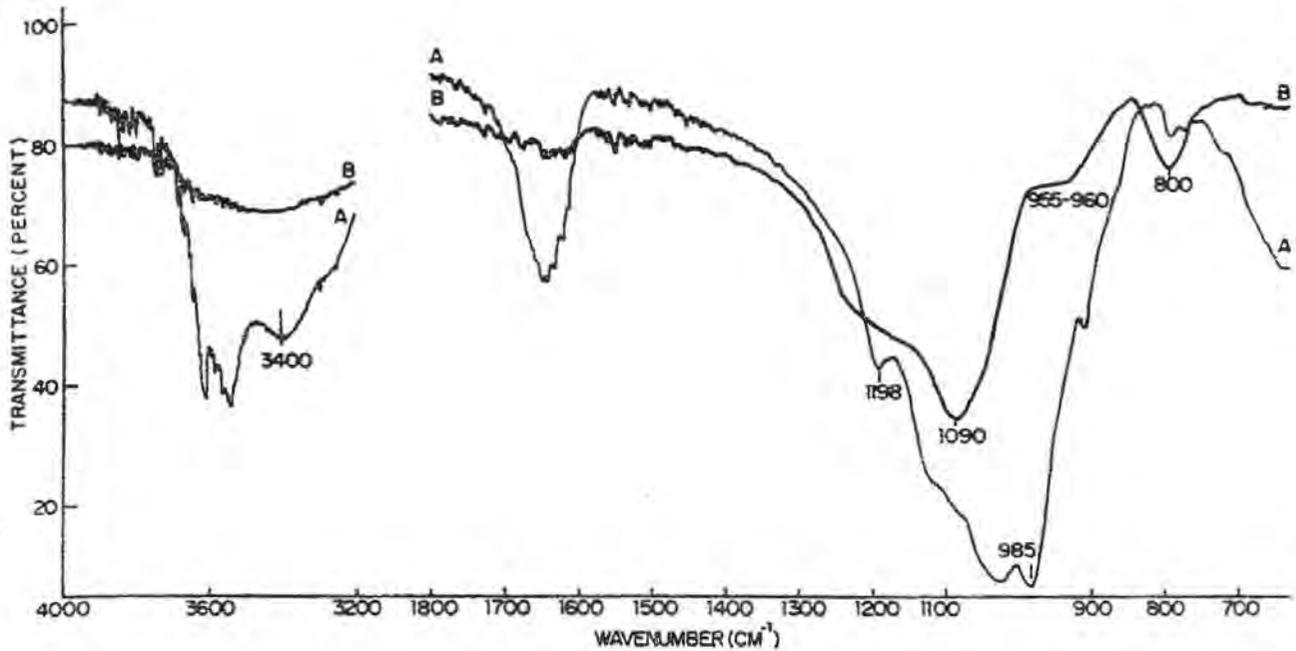


Figure 4. Infrared spectra of discs of: (A) Georgia attapulgite, (B) after 5 or 9 hours boiling with HCl 1:1.

Absorptions at 800 and  $970\text{ cm}^{-1}$  have been also reported by Gastuche (1963) in HCl treated biotite and at  $960\text{ cm}^{-1}$  by Fripiat and Mendelovici (1968) in HCl treated chrysotile. Thus, the  $960\text{ cm}^{-1}$  vibration in HCl treated attapulgite must arise from silanol groups. Moreover the large band at  $1660\text{ cm}^{-1}$  in attapulgite is considerably reduced upon the HCl treatment, whereas the OH stretching vibrations are substituted by a very broad band covering the OH stretching region.

After 5 hours of acid attack the dissolution of the octahedral layer is inferred from the development observed in the absorption bands due to Si-O vibrations in attapulgite. Thus, the set of absorptions at 985, 1030 and at  $1198\text{ cm}^{-1}$  is converted into one characteristic band at  $1090\text{ cm}^{-1}$  (Fig. 4). Similar results have been observed in HCl modified chrysotile by Fripiat and Mendelovici (1968).

Studying the HCl modification of palygorskites both by X-ray and D.T.A., Nathan (1968) also concluded that a strong acid attack dissolves completely the octahedral layer of this silicate.

#### ACKNOWLEDGEMENTS

The author wishes to express his gratitude to Professor M.M. Mortland from the Soil Sciences Dept. Michigan State University at East Lansing, for his guidance. To Dr. Myles Keogh from the Natural Products Division of this Institute for helping in the preparation of the manuscript and to Dr. W. Hertl for spectra recorded on the 621 Perkin-Elmer Spectrophotometer.

#### REFERENCES

- ANGELL, C.L. and SCHAFFER, P.C. (1965): Infrared spectroscopic investigations of zeolite and adsorbed molecules. *J. Phys. Chem.* 69, 3463-3470.
- BENESI, H.C. and JONES, A.C. (1959): An infrared study of the water - silica gel system. *J. Phys. Chem.* 63, 179-182.
- CANNINGS, F.R. (1968): An infrared study of hydroxyl groups on sepiolite. *J. Phys. Chem.* 72, 1072-1074.
- FARMER, V.C. and RUSSEL, J.D. (1971): Interlayer complexes in layer silicates. *Trans. Faraday Soc.* 67, 2737-2749.
- FRIPIAT, J.J., LEONARD, A. and BARAKE, N. (1963): Relation entre la structure et texture des gels de silice. *Bull. Soc. Chim.* 1, 122-140.
- FRIPIAT, J.J. and MENDELOVICI, E. (1968): Derivés organiques des silicates. I. -Le derive methyle du chrysotile. *Bull. Soc. Chim.* 2, 483-492.
- GASTUCHE, M.C. (1963): Kinetics and dissolution of Biotite. I. Interfacial rate process followed by optical measurement of the white silica rim. *Proc. 1963 Int. Clay Conf., Stockholm* 1, 67-75.
- GONZALEZ GARCIA, S., BEUTELSPACHER, H. and FLAIG, W. (1956): Espectroscopía infrarroja de arcillas y minerales estructuralmente análogos. *An. Real Soc. Esp. Fis. Quim.* 52 B, 369.
- HAYASHI, H., OTSUKA, R. and IMAI, N. (1969): Infrared study of sepiolite and palygorskite on heating. *Amer. Mineral.* 53, 1613-1624.
- JONES, P. and HOCKEY, J.A. (1971): Infrared studies of rutile surfaces. Part 1. *Trans. Faraday Soc.* 67, 2669-2678.
- NATHAN, Y. (1968): Dissolution of palygorskite by hydrochloric acid. *Israel J. Chem.* 6, 275-283.
- OTSUKA, R., HAYASHI, H. and SHIMODA, S. (1968): Infrared ab-

sorption spectra of sepiolite and palygorskite. Mem. Sch. Sci. Eng., Waseda Univ. 32, 13-24.

OVCHARENKO, F.D. (1966): The regulation of colloid chemical properties of clay minerals. Proc. 1966 Int. Clay Conf., Jerusalem, 1, 199-310.

TARACEVICH, Yu. I. (1970): Spectral study of the thermal dehydration of palygorskite. Dokl. Akad. Nauk. Ukr. SSSR 32, 938-942; quoted in Chem. Ab. 74, 34203 m (1971).



S E C T I O N II

CLAY MINERAL GENESIS AND SYNTHESIS



## CHAIRMAN'S INTRODUCTION

### DATA AND TENDENCIES OF RECENT YEARS IN THE FIELD "GENESIS AND SYNTHESIS OF CLAYS AND CLAY MINERALS"

Georges Millot

The geochemical cycle of clay minerals includes three stages: a) The weathering zone where clay minerals are neoformed; b) the sedimentation zone wherein clay minerals are carried and eventually transformed; c) the diagenesis zone where clay minerals are transformed and then disappear. One must emphasize that the term "diagenesis" clearly defined in the last century must be understood in its proper meaning. It corresponds to the crust's zone located between sedimentation and metamorphism. The modification of the clay mineral lattice under the environment's influence is called a transformation and not a diagenesis. Taking the term "diagenesis" in the meaning of transformation is a misinterpretation in the geological language.

I shall review the improvements of the last years in the study of clay genesis in the area of Weatherings (I), Sediments (II), Diagenesis (III), Experimental Syntheses (IV) and Thermodynamic explanations (V).

The corresponding bibliography involves some hundred of references which are to find in several scientific periodicals and especially in Clay minerals, Clays and clay minerals, Clay Science and Bulletin du Groupe Français des Argiles. It is impossible here to mention all these studies. I shall only present the scientific tendencies and the possible orientation of researches.

#### I GENESIS OF CLAY MINERALS IN THE WEATHERING ZONE

Among the three mechanisms originating clay minerals - heritage, transformations and neoformation - the weathering zone is at first characterized by neoformation and secondarily by transformations.

### 1. Gels

An appreciable improvement was performed in the study of amorphous materials found in weathered products and soils. First, because the processes of extraction and analysis of amorphous materials, silica, alumina and iron sesquioxides, made important progresses. And then, because the direct study is made possible by new techniques such as infrared rays. This results in three expositions:

a) The study of gels during weathering: inside minerals, on the edges of minerals, in aggregates and weathered products: that is seeking the relations between the nature of gels and the type of neoformed clay minerals.

b) The study of andosols has considerably progressed (allophanes, imogolite). There is a promising way in the study of the relations between allophanes and organic matter acting as stabilizing of amorphous materials. Its destruction would induce crystalline neoformations.

c) The study of iron sesquioxides made important progresses. Relations between nature of sesquioxides, color of soils and pedogenetic mechanisms rise. Analyses and experimentations must be pursued in that way.

### 2. Gibbsite and kaolinitic soils

The inventory of the possibilities observed in nature can be completed: gibbsite or kaolinite directly originating from the weathered silicate; gibbsite or kaolinite born from gels; gibbsite crystallized from solutions; kaolinite obtained by silicification of gibbsite etc... Each case is different and corresponds to different equilibria likely to be interpreted by thermodynamic models. On another hand, nature shows logical series, such as allophane, halloysite, disordered kaolinite, ordered kaolinite. These series testify the transition from disorder to order and seem to necessitate successive recrystallizations rather than unlikely thermodynamic transformations.

### 3. Montmorillonitic soils

Montmorillonites take an increasing place in weatherings. They characterize a double tropical belt around the globe, on both sides of an equatorial belt. These montmorillonites are alumino-ferromagnesian. Their composition is very variable and the relation between composition and genesis still deserves some study. These montmorillonites can directly be neoformed by authigenesis from crystals in the way of weathering. They can also originate from the transformations of micas, chlorites or illites, or crystallize from solutions. All these cases and the thermodynamic mechanisms of their formation are still to be studied.

#### 4. Attapulgitic and sepiolitic soils

Under humid climates, attapulgite and sepiolite are hydrolyzed. But in arid soils, characterized by calcareous crusts, attapulgite and sepiolite can be neofomed. Several cases have just been described in the world. The mechanism of these neoformations has to be defined.

#### 5. Vertical and oblique dynamics

The weathering of rocks and minerals presents a vertical component. Rain enters the profile and induces hydrolyses and genesis of clay minerals. But soil solutions are also migrating laterally in weathering mantles, from upstream towards downstream countries. The migrating ions are fixed in the landscapes as by a chromatographic mechanism. Ferruginous, calcareous, sulfated and saline crusts follow each other. As for silicates, kaolinite, montmorillonite, attapulgite, sepiolite and finally Na silicates or silico-aluminates (magadiite, kenyaite, kanemite, mordenite, etc...) succeed one another.

The genesis of clay minerals and silicates in weathered products and soils uses autochthonous ions (hydrolysis) and allochthonous ones (oblique migration). The geochemistry of these different possibilities must be looked upon in every case.

## II GENESIS OF CLAY MINERALS IN THE SEDIMENTATION ZONE

In the sedimentation zone, the typical mechanism explaining the origin of clay minerals is heritage: sedimentary clay minerals are usually allogenetic and detrital. But transformations may occur in particular environments and also neoformations in concentrated geochemical environments. The study of recent sediments necessarily includes early diagenesis lying in the reactions between minerals and connate waters of sediment.

### 1. Present-day sedimentation. Oceanography

The large inventory of the distributions of clay minerals in lakes, estuaries and oceans is well advanced. The great oceanographic campaigns have shown the distribution of clay minerals in the present-day sediments of the globe, from the arctic and antarctic poles to the equator. Great zones stand out: detrital minerals, non weathered illites and chlorites in polar countries; minerals of the chemical weatherings, i.e. montmorillonite and kaolinite in tropical and equatorial countries; montmorillonite in the countries where volcanism intervenes.

The continuation of this large inventory will be welcome, but now, more accurate and precise measurements on particular sedimentary environments are undertaken.

Relation clay minerals - subaquatic magmatic irruptions. In the countries of the globe, where subaquatic magmatic irruptions occur, subaquatic alterations can give rise to particular minerals, such as serpentine, attapulgite, zeolites etc...

Relation clay minerals - organic matter. The environments rich in organic matter, i.e. euxenic, sapropelic environments are acting upon clay minerals and this action is differential. Dissolution or transformation phenomena and possible neoformations must be studied.

Relation clay minerals - siliceous organisms. A sea rich in silicate particles can provide siliceous faunas and floras. Silica is stocked in the sedimentary deposit. But after deposition, silica can be released again and feeds silicate transformations or neoformations. So, the role of Diatoms and Radiolarias in clay mineralogy is a subject to carry on.

Relation clay minerals - metals. After their deposition, clay minerals can transform by capture of major or trace elements. Here can be mentioned the studies on the genesis of glauconites by Fe and K capture, on clay minerals unusually enriched in minor elements, on oolitic ores and on subaquatic manganese ores. Many studies are in process and must be carried on.

Variations in clay minerals according to time. Subaquatic cores are brought back by oceanographic ships. The study of clay minerals can develop in three ways: a) study of variations in the course of sedimentation, reference horizons, current variations; b) study in a monotonous sedimentation of the climatic variations occurring on continent; c) study of early diagenesis in environments concentrated enough. Clay mineralogy can be modified by reactions with connate waters. The study of the cores must make allowance for these three possibilities.

## 2. Ancient sediments

The clay petrography of ancient sediments includes diagenesis. But under the veil of diagenesis, clay petrography reveals numerous typical characters of sediments. The inventory of clay minerals in sediments is carried on. In 1950, we disposed of some thousands of measurements and nowadays we have several hundreds of thousands of data. The work develops in three directions.

Tectonic reconstructions. The most often detrital clay minerals are the reflection of the composition of the continents which provided them. Clay petrography is an important factor of the paleogeographic reconstructions in ancient series.

Climatic reconstructions. The most often detrital clay minerals are the reflection of the continental weatherings which provided them. During the periods of appeased tectonics, clay minerals are an important tool for climatic reconstructions.

Reconstructions of chemical environments. In sedimentary ba-

sins where ionic concentrations increase, clay minerals evolve by transformation or appear by neof ormation. Clay minerals are tools for the reconstruction of phosphatic and hypersiliceous environments, glauconitic sediments, magnesian, sulfated or saliferous deposits.

Every sedimentary formation can be explained according to different points of view. As the case may be, this point of view be geodynamic, paleoclimatic or geochemical.

### 3. Isotopic geochemistry and geochronology

The application of isotopic geochronology to clay minerals first began by measurements on glauconies. Nowadays, the improvement of methods allows us to study common clay samples. When sediments go dry and become rocks, ionic exchanges between crystals and interstitial water stop. The medium gets closed. If there is no new event taking place - metamorphism, granitization, hydrothermal inflows - isotopic dating is possible. Nowadays, several laboratories give us data on clay sediments by Rb/Sr and K/A methods.

Azoic formations are numerous on the surface of the globe and especially Lower, Middle and Upper Precambrian sedimentary deposits. The whole represents 1.5 milliard of years. Isotopic dating applied to clays will allow us to determine the age of the sedimentary overlying beds of old shields, about which we have no information for more than hundred millions of years. Moreover, if an anchimetamorphism or an epimetamorphism or a geochemical event affects these great sedimentary series it is the age of the metamorphism or of the secondary event which is determined. In general, there is no other mean available to date these phenomena.

## III DIAGENESIS ZONE AND TRANSITION TOWARDS METAMORPHISM

In different countries of the globe, the study of the evolution of clay minerals during diagenesis has just be brought to end. Many samples collected on the surface or in deep boreholes provided the matter to study. We learnt the crystallochemical transformations of clay minerals: disappearance of kaolinite and montmorillonite, organization of irregular then regular mixed layers such as allevardite and corrensite leading to the typical minerals of tardive diagenesis, illite and chlorite.

Then we get to anchizone in which are found illite and chlorite, pyrophyllite, paragonite, chloritoid etc... If metamorphism takes a larger place, mica and chlorite size increases. These micas usually are phengites.

The crystallochemical mechanisms of diagenesis have been reconstructed. Nowadays, we know that the mineralogical transformations of diagenesis are the same as those of weathering but of opposite direction. The progressive tetracoordination of aluminum in micaceous lattices is the symmetrical process of progressive hexacoordination of aluminum during weathering up to the types of kaolinite and gibbsite. The play of K, Na, Mg, Fe cations is also symmetrical: entering the lattices by diagenesis and escaping from them by weathering.

The applications of the techniques of clay petrography to the diagenesis and epimetamorphism zones must nowadays become general. It will supply to geologists many informations about the thousands of meters of shales neglected up to now.

#### IV SYNTHESSES AND EXPERIMENTAL WEATHERINGS

In hydrothermal conditions, syntheses give us numerous models of superficial silicate genetic conditions. We succeeded in the synthesis of sepiolite and various montmorillonites. Synthesis tests including a large proportion of heavy metals (Cu, Ni, Cr) can define the conditions of pH and relative concentrations allowing to aid the bonding between cations and  $\text{Si(OH)}_4$ . The conditions must offer a cation less stable in its hydroxide than in the octahedral cavity of silicate.

The synthesis of kaolinite is the most worrying for the investigators. In spite of its frequency in natural weatherings, its laboratory synthesis remains delicate. A series of artifices is used to induce the activation of alumina offered to dilute silica solutions. Organic complexes may play this role. Grinding promotes the reaction. Mineral acids are more efficient by forming Al cations able to orderly polycondense with  $\text{Si(OH)}_4$ . Other techniques induce the formation of intermediary badly crystallized structures supplying alumina, active for the reaction of kaolinite synthesis. It is important to carry on the tests up to synthesis models reflecting the two following mechanisms frequent in nature; intervention of organic matters and action of acid and desaturated media.

The experimental weatherings of rocks and minerals have been carried on. The role of the weathering of trioctahedral micas appeared very important in the granite disintegration. The study of the weathering of these micas has employed several laboratories. The mechanism of hydrolysis of interlayer K ions has been shown as well as the process of oxidation of octahedral ferrous iron accompanied by an increase of interlayer spacings. This is the phenomenon of vermiculitization, which is the first stage of natural

weatherings. Then, different experimentations in various conditions of pH and cation concentration give models similar to the different destinies of micas in various types of natural weathering.

Syntheses and experimental weatherings must be carried on by mimicking as much as possible the natural conditions and especially the geochemical conditions of the surface.

## V THERMODYNAMIC MODELS

Clay minerals are typical of the hydrosphere. As they appear in weathering zone, sedimentation zone, diagenesis zone, they are in equilibrium with solutions and other present minerals. If these clay minerals are displaced from an environment to another, they become unbalanced but they tend to take a new equilibrium in their new environment.

These equilibria between clay minerals, solutions and present minerals are multivariable. To define the role of a factor such as pH, concentration in silica, magnesium etc..., the others must be fixed. And models are necessary for reasoning: these are equilibrium diagrams. Several thermodynamic diagrams have just been realized. These diagrams allow us to foresee the succession of minerals occurring when the concentrations in hydrogen and different cations vary in a given environment. As soon as data are obtained in the nature, thermodynamic models can be adjusted to the cases observed. In the study of syntheses or experimental weatherings as well as in the study of natural weatherings and transformations, thermodynamic models are a valuable tool for investigators.

## CONCLUSIONS

The tendencies I take for the most important in the future researches on clay mineral genesis and synthesis in the superficial geochemistry are the following:

1. Intervention of organic chemistry and biochemistry. The behavior of silica, alumina and iron sesquioxides mostly depends on organic matters occurring at the surface. Several laboratories must resolutely make organic chemistry intervene in their studies.

2. Study of natural solutions and thermodynamic models. The studies on clay mineral genesis began by the study of the minerals themselves. When they appear, they are in equilibrium with solutions and these equilibria can be calculated. The studies on clay

mineral genesis must use at the same time natural data, models of experimental syntheses and thermodynamic models.

3. Isotopic geochemistry. The components of clay minerals hold stable or radioactive isotopes. Their study begins and must be carried on in order to better understand their genesis and to date the last phenomenon having contracted their lattice.

# CONTRIBUTION A LA CONNAISSANCE DE LA SYNTHÈSE DES KAOLINS

B. Siffert

Centre de Recherches sur la Physico-Chimie des  
Surfaces Solides  
24, Avenue du Pdt Kennedy  
68 - Mulhouse - France

R. Wey

Ecole Supérieure de Chimie  
3, rue A. Werner  
68 - Mulhouse - France

## INTRODUCTION

Les conditions de genèse des minéraux argileux ont été précisées en 1948 par G. Millot. Cet auteur a pu établir des corrélations entre les conditions du dépôt géologique et le type de minéral argileux formé. Il a montré, en particulier, que les minéraux argileux de la famille du kaolin se forment dans des milieux acides, pauvres en cations.

Leur genèse a lieu, aussi bien dans les conditions ordinaires de température et de pression du milieu supergène que dans les conditions hydrothermales.

La reproduction de ces phyllites au laboratoire dépend de la nature des matériaux de départ utilisés et surtout des conditions de température et de pression.

Les premiers essais de synthèse de kaolinite eurent lieu en milieu hydrothermal entre 200 et 400°C, dans des conditions telles que les vitesses de réaction soient suffisamment élevées (Noll, 1930 à 1936; Norton, 1939, 1941; Ewell et Insley, 1935; Roy, 1951, 1953). Le minéral prend naissance aussi bien par recristallisation de gels mixtes silice-alumine (Fripiat, de Kimpe et Herbillon, 1966; de Kimpe, Gastuche et Brindley, 1961; Rayner, 1961; Roy et Osborn, 1954; Grubb, 1968; Hénin et Caillère, 1957; Siffert, 1962) que par altération ou attaque d'autres phyllites ou minéraux tels les felds-

paths (Badger et Ally, 1935; Brindley et Radoslovich, 1956; Lagache, Wyart et Sabatier, 1963; Oberlin et Tchoubar, 1963, 1965; Schwarz et Trageser, 1935; Pedro, 1958, 1960, 1961; Trichet, 1969; Tsuzuki et Mitzutani, 1969), le quartz, les oxydes ou hydroxydes cristallisés de l'aluminium (Oberlin et Couty, 1970; Siffert et Dennefeld, 1971; Dennefeld, 1970; Roy et Osborn, 1954).

Pour induire la cristallisation, certains auteurs ont ensemencé la masse amorphe. Dans ces conditions, les résultats obtenus sont forcément ambigus.

D'autres, comme de Kimpe, Fripiat et Herbillon (1966) ont étudié l'influence des ions alcalins sur la recristallisation des gels. Selon Oberlin et Tchoubar (1963), la kaolinite semble se former à partir de boehmite mal cristallisée prenant naissance à la surface du feldspath altéré. Les particules de boehmite constitueraient des centres actifs susceptibles de fixer les molécules  $\text{Si(OH)}_4$  de la solution. La kaolinite précipiterait ensuite sur le feldspath par polymérisation des monomères ainsi formés. En traitant directement une boehmite bipériodique (pseudo-boehmite) par une solution saturée en silice, Oberlin et Couty (1970) enregistrent un résultat identique.

Ces divers travaux en milieu hydrothermal montrent qu'il est possible d'utiliser comme source de silice et d'alumine différentes formes solides plus ou moins organisées. Il est remarquable de noter que tous ces essais ont été effectués en présence d'acides. Ces synthèses mettent aussi en évidence la nécessité d'opérer à une température supérieure ou égale à  $175^\circ\text{C}$  pour voir apparaître la kaolinite.

Cependant, l'étude du milieu naturel montre, sans contestation possible, que la kaolinite se forme à température ordinaire. Mais, toutes les tentatives de transformation de solides cristallisés (brucite, hydrargillite, etc.) en présence de silice dans les conditions ordinaires de température et de pression ont échoué (Harrison, 1933; Hénin et Caillère, 1953 à 1963; Pedro et Berrier, 1968; Siffert, 1962). Il en est de même des études de recristallisation de gels mixtes silice-alumine (Caillère et Hénin, 1954; Siffert, 1962).

La seule voie possible, préconisée par Correns dès 1939, semble être la méthode des solutions diluées. Correns et ses collaborateurs (1961) avaient observé que l'altération des feldspaths par des sources chaudes acides, laissait autour du cristal une couche gélifiée de silice et d'alumine pouvant se dissoudre dans la solution; ils envisagent la formation des argiles par recombinaison des ions dans la solution.

En appliquant cette méthode, Caillère, Hénin et leurs collaborateurs (1948 à 1963) ont, en effet, réussi à synthétiser à température ordinaire la presque totalité des phyllites, exception faite, des argiles purement alumineuses. Ils proposèrent le mécanisme suivant:

Les minéraux argileux se formeraient par fixation de la silice sur une couche d'hydroxyde présentant une amorce de structure phylliteuse.

Ils attribuent leur échec dans la préparation des phyllites alumineuses au fait que l'aluminium précipite simultanément sous formes de différents hydroxydes, empêchant ainsi le greffage de la silice.

D'autres auteurs attribuent cette difficulté à la dualité des coordinences que présente l'aluminium (4 et 6). Ainsi, Fripiat et ses collaborateurs ont été amenés à penser que la difficulté de la synthèse de la kaolinite serait liée au fait qu'un gel aluminique prend spontanément un caractère pseudo-boehmitique et non gibbsitique. Rappelons, cependant, que l'aluminium présente la même coordinence aussi bien dans la boehmite, la gibbsite que dans le kaolin.

Roy et Osborn (1954) pensent qu'il faut atteindre le seuil de transformation de la gibbsite en boehmite pour que la réaction avec la silice ait lieu. D'après ces auteurs, la destruction du réseau de la gibbsite favoriserait l'apparition d'une phase alumineuse pouvant réagir avec la silice.

Siffert (1962) attribue les échecs des synthèses de la kaolinite à basse température au comportement particulier du cation  $Al^{3+}$  en solution.

Il avance deux raisons essentielles:

La forte hydratation de l'ion  $Al^{3+}$

Son insolubilité dans la gamme des pH favorables à la formation de la kaolinite.

Nous discuterons, dans ce travail, les conséquences qui en résultent pour la synthèse de la kaolinite et les possibilités de remédier à ces difficultés.

## HYDRATATION DU CATION ALUMINIUM

Le cation  $Al^{3+}$  possède à la fois une charge électrique élevée et un faible rayon ionique, ce qui se traduit par une énergie d'hydratation considérable. Il exerce sur les molécules d'eau un effet de polarisation électrique important et présente, de ce fait, un caractère acide accru. Son indice d'hydratation (nombre de molécules d'eau contenues dans la sphère d'hydratation) est deux fois plus grand que celui du magnésium (Harvey et Porter, 1967). A basse température, cette coquille de molécules d'eau empêche la réaction avec la silice.

Lorsqu'on atteint 175°C en milieu hydrothermal, limite inférieure de formation de la kaolinite, il semble que cette couche d'eau soit éliminée, du moins, peut-on admettre que la mobilité des molécules d'eau devient suffisante pour permettre à la silice d'accéder aux atomes d'aluminium. Cette température limite de 175°C peut

être rapprochée de celle de 120°C pour les ions alcalins. En effet, dans un travail sur l'échange des ions alcalins dans la vermiculite sous pression de vapeur d'eau, Wey, Wurtz et Siffert (1970) ont constaté que les cations alcalins présentaient vis-à-vis de l'échangeur un comportement identique à partir de 120°C. Pour expliquer leurs résultats, les auteurs ont été obligés d'admettre que les cations perdaient leur eau d'hydratation à partir de cette température. Par analogie, on peut penser que cette limite se situe aux environs de 175°C pour le cation  $Al^{3+}$ .

## INSOLUBILITE DE L'ION ALUMINIUM

La chimie de l'aluminium en solution est gouvernée par l'insolubilité de cet ion dans un large intervalle de pH. Un simple calcul, faisant appel au produit de solubilité de l'hydroxyde, montre que la silice est environ cent millions de fois plus soluble que l'alumine à pH 7. Ce déséquilibre en faveur de la silice perturbe considérablement une réaction possible entre l'aluminium et la silice. Il provoque le plus souvent un dépôt superficiel de silice sur les composés alumineux rendant toute réaction ultérieure impossible. Ainsi, Dennefeld (1970) a pu montrer dans une étude quantitative sur la transformation hydrothermale de la gibbsite en boehmite que la réaction était considérablement ralentie en présence de silice. Il admet un blocage des sites réactifs de la gibbsite et la formation d'un alumino-silicate superficiel amorphe.

En réalité, le déséquilibre entre l'aluminium et la silice en solution n'est qu'apparent. L'aluminium présente, en effet, une solubilité beaucoup plus élevée si l'on fait appel aux autres formes que l'ion  $Al^{3+}$ . Suivant les conditions de pH, on peut obtenir toute une série de polycations condensés du type  $Al[Al_2(OH)_5]_n^{(n+3)+}$  (Biedermann, 1956; Kohlschütter et Hantelmann, 1941) ou encore des cations  $[Al_6(OH)_{15}]^{3+}$  et  $[Al_8(OH)_{20}]^{4+}$  (Stumm et Morgan, 1962). Les moins condensés de ces cations sont solubles; si la condensation croît, on passe insensiblement aux hauts polymères colloïdaux insolubles.

Si ces polycations se lient à la silice, ils n'engendrent point de kaolin, mais des gels. Siffert (1962) a pu le montrer en étudiant l'interaction de divers cations aluminium provenant de sels ordinaires (chlorure, sulfate, aluminate) avec une solution saturée en silice monomoléculaire.

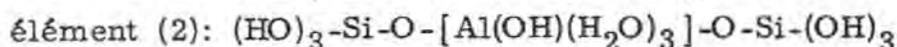
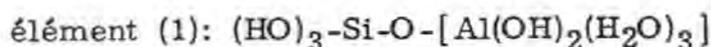
## SYNTHESES DE LA KAOLINITE A BASSE TEMPERATURE

Pour augmenter la solubilité de l'aluminium vis-à-vis de la silice, pour éviter l'eau d'hydratation et la formation de polycations,

plusieurs voies sont possibles. Nous en avons retenues deux:

1. La décomposition rapide d'un complexe oxalique de l'aluminium dans une solution saturée en silice monomoléculaire.
2. L'attaque et le broyage de la gibbsite avant traitement avec la silice amorphe.

1. En décomposant au sein d'une solution saturée en silice monomoléculaire (120 à 140 mg  $\text{SiO}_2/1$ ) de l'oxalate d'aluminium, Siffert et Wey (1961), Siffert (1962) ont obtenu un protokaolin. En faisant varier le rapport  $\text{Al}^{3+}/\text{C}_2\text{O}_4^{2-}$ , on déplace le pH de coprécipitation silice-alumine vers la valeur moyenne où la silice peut réagir en tant qu'acide avec un ion aluminium basique. Cependant, l'emploi de l'anion oxalique  $[\text{Al}(\text{C}_2\text{O}_4)_3]^{3-}$  a surtout permis de préparer des ions aluminium débarassés de leur couche d'eau d'hydratation, celle-ci étant remplacée par des ions oxalate dont l'élimination favorise la combinaison Si-Al (échange de ligandes). Mais, il apparaît à travers ce mécanisme que l'on peut obtenir instantanément une quantité importante de cations basiques du type  $[\text{Al}(\text{H}_2\text{O})_5\text{OH}]^{2+}$  et  $[\text{Al}(\text{H}_2\text{O})_4(\text{OH})_2]^+$ . Ces ions en se combinant à la silice formeraient des éléments que l'on peut schématiser de la façon suivante:



La condensation de ces éléments conduirait, soit au feuillet tétraèdre-octaèdre du type kaolin dans le premier cas (Fig. 1), soit au feuillet tétraèdre-octaèdre-tétraèdre dans le deuxième cas (Fig. 2). Evidemment, un tel mécanisme exige l'élimination des molécules d'eau portées par les atomes d'aluminium et celle des hydroxyles des atomes de silicium. Comme cette condensation est plus ou moins parfaite, il n'est pas étonnant de précipiter dans ces conditions, un produit homogène, mais imparfaitement cristallisé (protokaolin).

Récemment, Linares et Huertas (1970) ont enregistré un résultat tout à fait identique en remplaçant l'anion oxalique par un complexe soluble entre l'aluminium et les acides fulviques.

2. Un autre moyen pour abaisser la température de synthèse de la kaolinite consiste à faire réagir une gibbsite broyée et de la silice amorphe en présence d'acides complexants. Ainsi, Dennefeld, Siffert et Wey (1970), Siffert et Dennefeld (1971) ont étudié la transformation hydrothermale de la gibbsite en boehmite en présence de silice amorphe. En partant d'une gibbsite broyée, ils ont réussi à former la kaolinite à  $135^\circ\text{C}$  dans un temps relativement court (7 jours). Le broyage peut augmenter les défauts à la surface de la gibbsite et favoriser la dissolution de l'aluminium.

En traitant cet hydroxyde non broyé, en présence d'acide oxalique ou sulfurique, on arrive encore à synthétiser la phyllite à

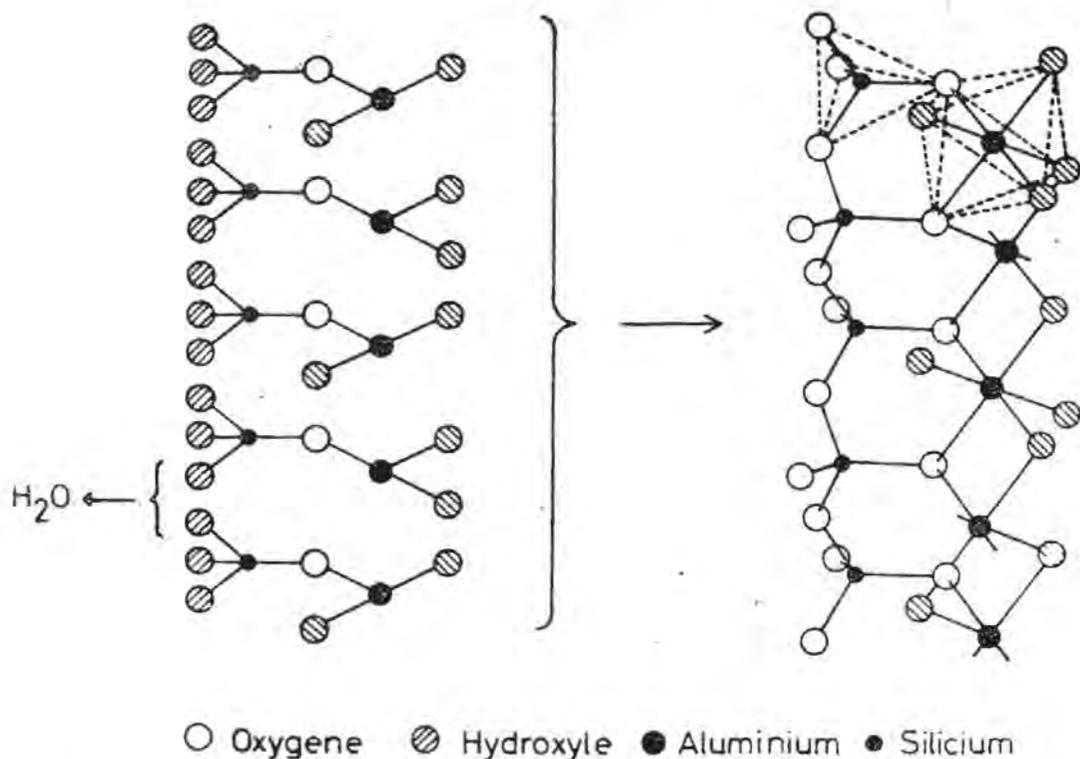


Figure 1. Polymérisation des éléments du type (1) et formation des feuillets tétraèdre-octaèdre d'un minéral de type kaolinique.

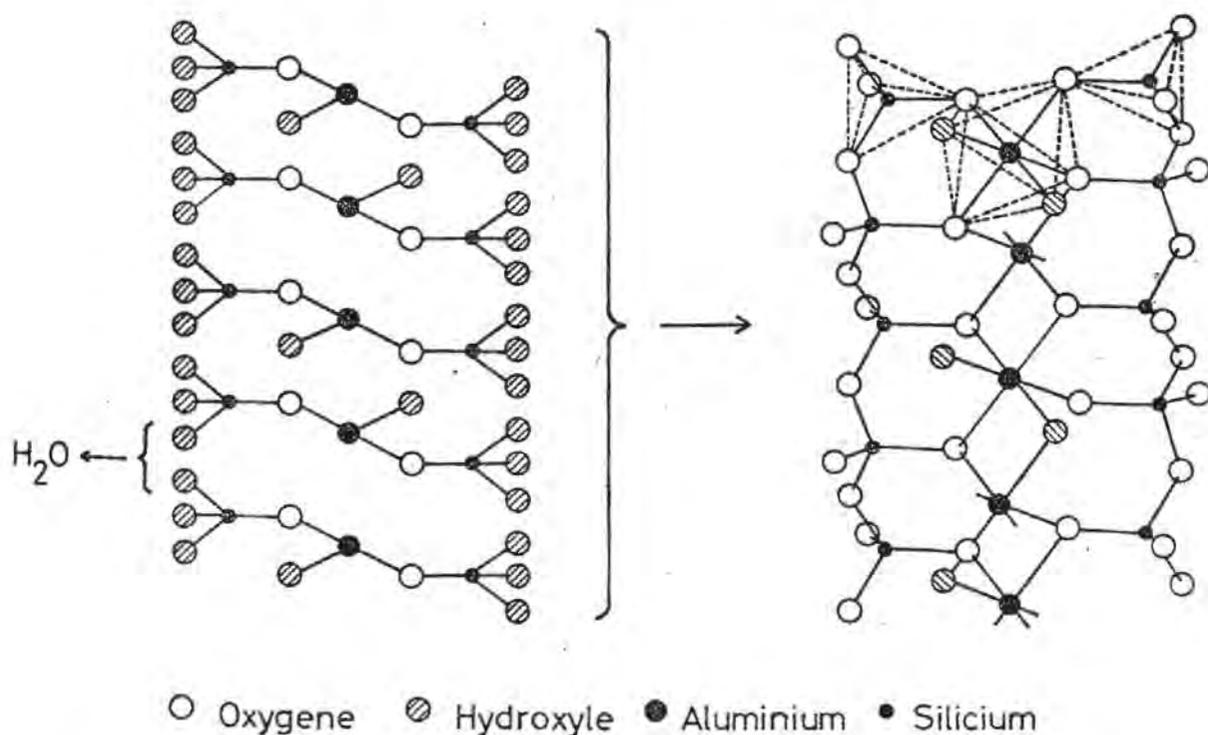


Figure 2. Polymérisation des éléments du type (2) et formation des feuillets tétraèdre-octaèdre-tétraèdre d'un minéral alumineux de type montmorillonitique.

135°C. Mais, ce n'est qu'en conjuguant l'effet du broyage et l'action complexante (ou dissolvante) des acides que l'on arrive à abaisser la température de synthèse à 115°C, température inférieure à celle nécessaire pour transformer la gibbsite en boehmite (125°C).

Toutefois, parmi les acides utilisés, seul l'acide sulfurique permet d'obtenir la phyllite alumineuse bien cristallisée à 115°C. En opérant dans les mêmes conditions mais en présence d'acide chlorhydrique, la kaolinite ne cristallise qu'au-dessus de 150°C.

A concentration égale, l'acide sulfurique produit, par conséquent, une "activation" de la gibbsite nettement supérieure à celle de l'acide chlorhydrique.

Sur la Fig. 3, nous comparons les quantités de kaolinite formée à 175°C en fonction du rapport  $H^+/Al^{3+}$ . On constate que la quantité optimale de kaolinite est obtenue pour le rapport  $H^+/Al^{3+}$  égal à 0,8 en présence d'acide chlorhydrique, tandis qu'avec l'acide sulfurique, ce rapport est de 0,1.

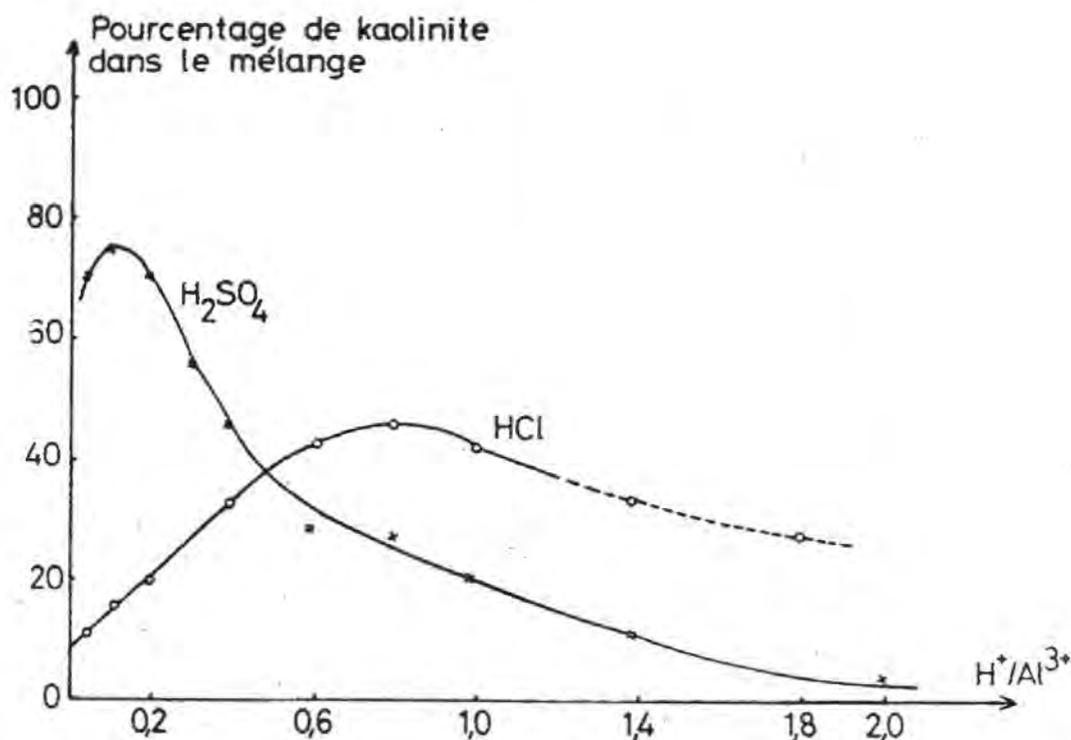


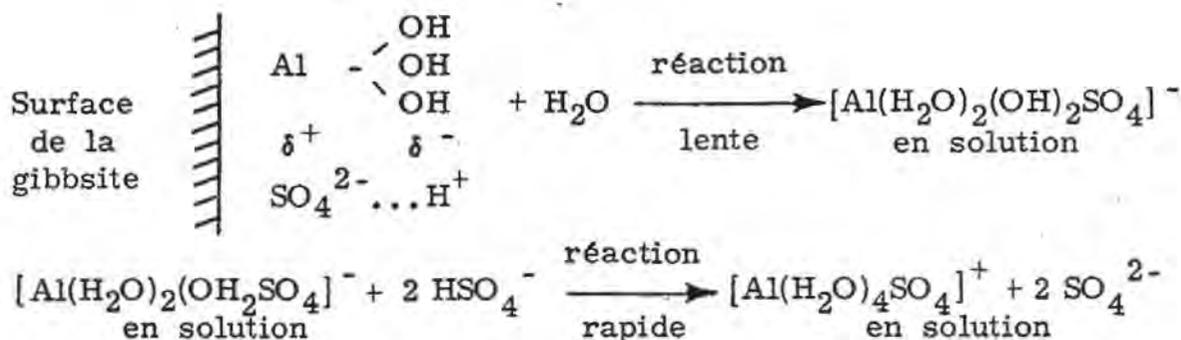
Figure 3. Influence du rapport  $H^+/Al^{3+}$  sur la synthèse de la kaolinite.

Comparaison des résultats en présence de HCl et de  $H_2SO_4$  (175°C - 7 jours).

Ceci semble indiquer que "l'activation" de la gibbsite n'est pas uniquement liée à la concentration protonique du milieu. L'anion de l'acide joue un rôle. Il interviendrait directement dans la dis-

solution de l'aluminium en permettant, par exemple, la formation de cations complexes d'aluminium, contenant comme ligandes des hydroxyles et des sulfates.

On rejoint ainsi les conclusions de Packter et Dhillon (1969) sur la cinétique de dissolution de la gibbsite par les acides minéraux. Selon ces auteurs, la réaction de dissolution en présence d'acide sulfurique s'effectuerait par une double interaction dipolaire entre les sites Al-OH de la surface de la gibbsite et des paires d'ions ( $H^+ \dots SO_4^{2-}$ ) adsorbés:



Ainsi, les acides donnant le plus facilement des cations basiques se révèlent les plus efficaces pour la synthèse de la kaolinite.

Il existe certainement dans la nature des kaolinites qui doivent leur formation à la décomposition de complexes organiques de l'aluminium. Mais toutes les kaolinites ne sont pas d'origine pédologique.

De même, on connaît des kaolinites mélangées à de l'alunite (sulfate basique d'aluminium de formule  $KAl_3(OH)_6(SO_4)_2$ ). Dennefeld et Siffert (1970) ont d'ailleurs préparé un peu de kaolinite à 70°C. par percolation d'une solution saturée en silice monomoléculaire (120 mg/l  $SiO_2$ ) sur un sulfate basique d'aluminium synthétique, de formule  $(H_3O) Al_3(OH)_6(SO_4)_2$ . Mais ces gisements sont également limités.

Il nous apparaît, de plus en plus, que le seul anion suffisamment abondant à la surface du globe et qui puisse complexer l'aluminium soit la silice.

Récemment, Schenk (1969) étudiait la cinétique de précipitation de l'aluminium à 25°C en présence de silice; il a pu mettre en évidence la formation de complexes silicoalumineux solubles.

Nous reproduisons sur la Fig. 4 les résultats enregistrés par Schenk pour la réaction d'hydrolyse d'une solution d'aluminium de concentration  $10^{-5}$  mole/litre. On constate que l'alumine précipite pour les faibles teneurs en silice. Mais dès que la concentration atteint  $7,5 \times 10^{-4}$  mole/litre, l'aluminium reste en solution. Schenk pense qu'il se forme des complexes silicoalumineux identiques à ceux décrits par Weber et Stumm (1965) pour l'ion ferrique  $Fe^{3+}$ .

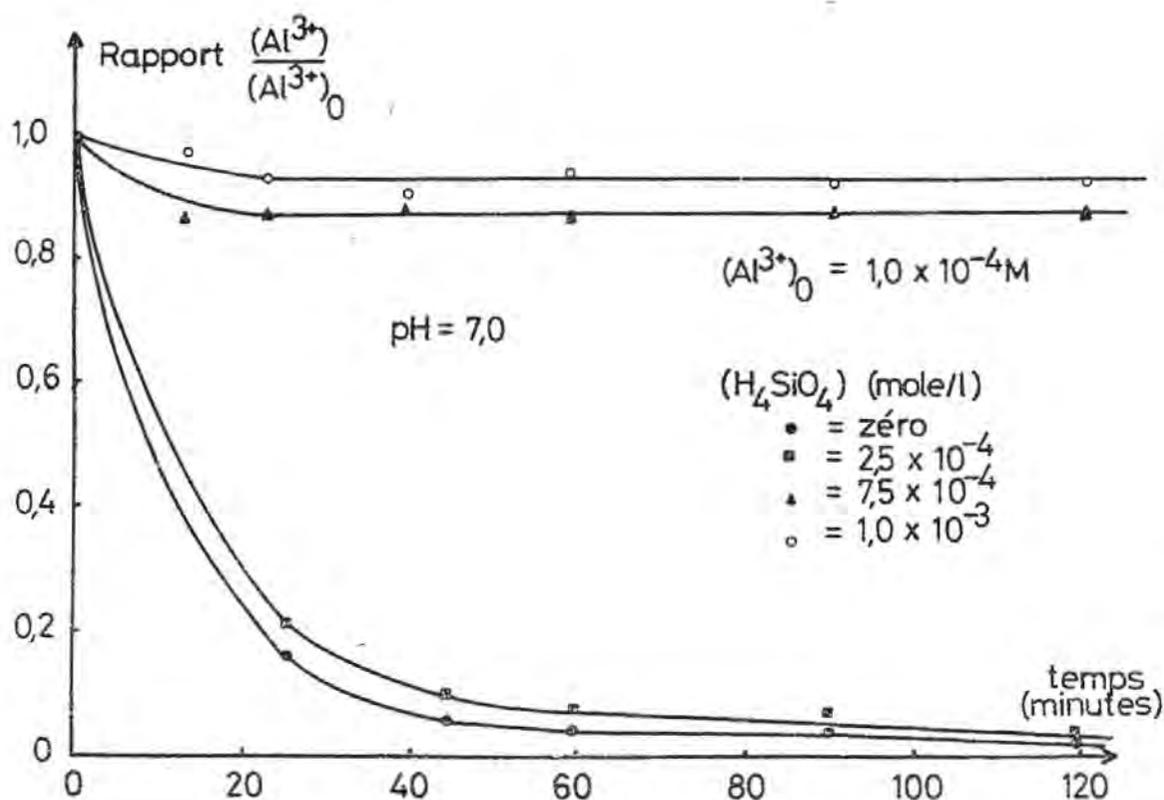


Figure 4. Précipitation de l'aluminium en présence de silice (selon Schenk)

Selon cet auteur, il faut une concentration en silice environ cinq fois plus élevée que celle de l'aluminium pour voir apparaître de tels complexes.

Nous avons repris les expériences de Schenk et essayé de déterminer avec plus de précision le rapport silice/alumine de ces complexes.

#### MODE OPERATOIRE

Dans une série d'erlenmeyers de capacité 1 litre, nous avons introduit successivement un volume constant d'une solution de silice monomoléculaire, de volumes croissants d'une solution de chlorure d'aluminium ( $AlCl_3, 6 H_2O$ ), quelques millilitres de soude concentrée pour ajuster le pH vers 6,8, puis de l'eau distillée pour compléter à un litre de solution.

Deux concentrations en silice ont été utilisées:

pour la série I :  $[H_4SiO_4]_0 = 5,42 \times 10^{-4}$  mole/litre

pour la série II:  $[H_4SiO_4]_0 = 2,9 \times 10^{-4}$  mole/litre

La concentration en aluminium variant au sein de chaque série entre  $2,45 \times 10^{-4}$  et  $9,61 \times 10^{-4}$  mole/litre.

Après un repos d'un mois et demi à température ordinaire, nous avons filtré les solutions sur membranes "Millipore" de diamètre des pores égal à 250 A et dosé la silice et l'aluminium par colorimétrie.

Sur les Fig. 5 et 6, nous avons porté les variations des rapports  $[Al^{3+}]/[Al^{3+}]_0$  et  $[H_4SiO_4]/[H_4SiO_4]_0$  en fonction du logarithme de la concentration initiale en aluminium:

$[Al^{3+}]_0$  et  $[H_4SiO_4]_0$  étant les concentrations initiales en aluminium et silice

$[Al^{3+}]$  et  $[H_4SiO_4]$ , les concentrations après réaction.

On observe, comme pour les essais de Schenk, une solubilisation importante de l'aluminium, fonction de la teneur en silice; elle est maximum pour la concentration initiale en aluminium voisine de  $10^{-4}$  mole/litre (Fig. 5).

En utilisant les données fournies par les courbes de la Fig. 6, nous avons déterminé pour les deux séries d'essais le rapport  $SiO_2/Al_2O_3$  des complexes silicoalumineux. Pour ce faire, nous avons admis que toute la silice et tout l'aluminium se trouvent combinés

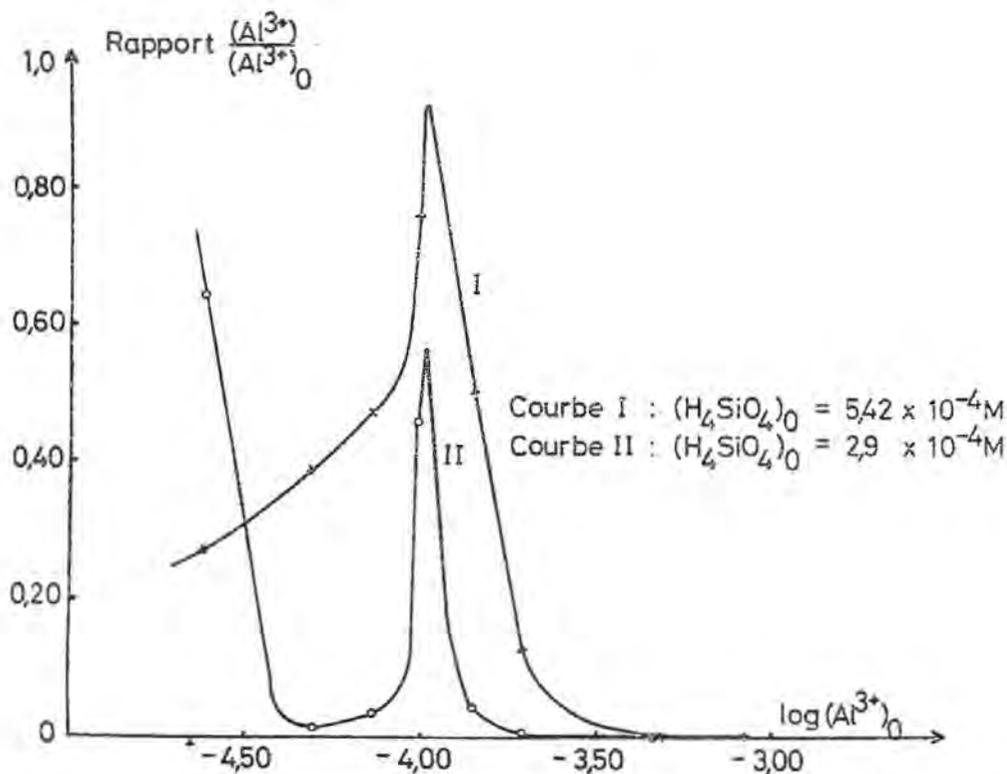


Figure 5. Solubilisation de l'aluminium par la silice en fonction du logarithme de la concentration initiale en aluminium - pH =  $6,82 \pm 0,2$ , température ordinaire.

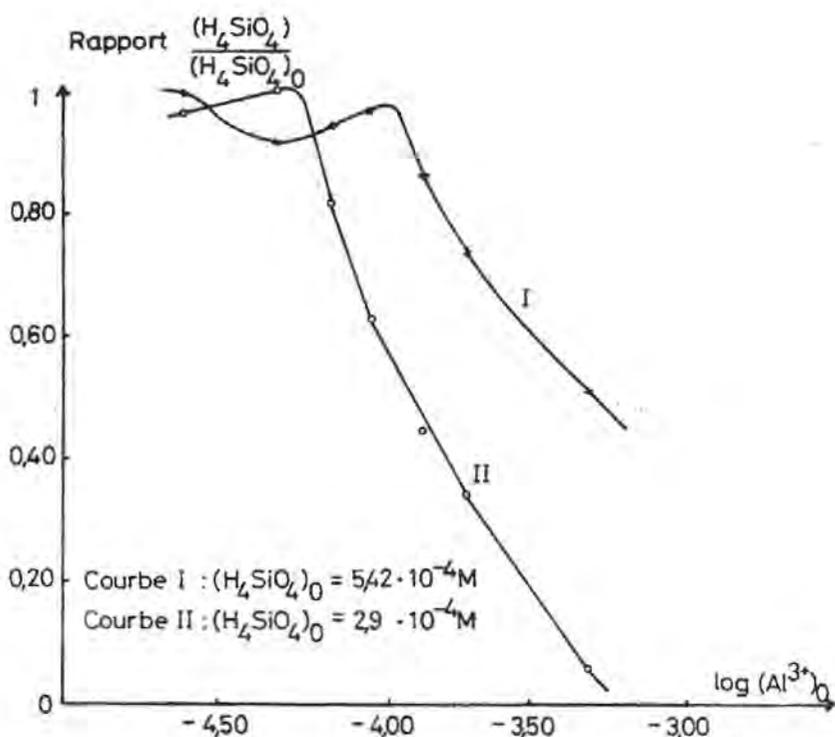


Figure 6. Variation du rapport  $(H_4SiO_4)/(H_4SiO_4)_0$  en fonction du logarithme de la concentration initiale en aluminium - pH = 6,82 ± 0,2, température ordinaire.

à l'état de complexes. En effet, aucun précipité ne s'est formé dans les solutions pour lesquelles les rapports  $[H_4SiO_4]/[H_4SiO_4]_0$  sont maximum, c'est-à-dire pour les solutions dont les concentrations initiales en aluminium sont de  $1,01 \times 10^{-4}$  et  $5,76 \times 10^{-5}$  mole par litre.

Un calcul simple montre alors que le rapport  $SiO_2/Al_2O_3$  est égal à 6,12 pour la première série d'essais et 5,95 pour la seconde. La valeur de ce rapport indiquerait que nous sommes en présence d'unités de complexes formés par six atomes de silicium et deux atomes d'aluminium. Elle permet également d'avancer l'hypothèse que nos complexes pourraient être constitués par des assemblages en "anneaux" à six tétraèdres de silice  $Si(OH)_4$ , liés chimiquement aux deux atomes d'aluminium, chaque "élément" formant déjà une amorce de feuillet phylliteux.

Il reste évidemment à définir les conditions de polymérisation ou d'association de tels "éléments", Harder (1970) nous donne une première indication. Ce chercheur a, en effet, réussi à synthétiser un fire-clay à 20°C en laissant vieillir une solution  $3,3 \times 10^{-4}$  molaire en silice et  $1,76 \times 10^{-4}$  molaire en aluminium vers pH 4,5 et 5 pendant 3 mois, c'est-à-dire exactement dans les conditions de concentrations définies ci-dessus. En dehors de ces limites, on

peut penser que la polymérisation des complexes sera désordonné avec pour conséquence une précipitation de gel mixte amorphe (Siffert, 1962; Harder, 1970). Remarquons que les cycles à six tétraèdres de silice semblent conservés lors de la précipitation du gel. En effet, la bande d'absorption en lumière infrarouge vers  $800\text{ cm}^{-1}$  que l'on observe pour tous les gels de silice et même pour les verres serait attribuable aux vibrations "en anneaux" des tétraèdres de silice (Matossi, 1949).

## CONCLUSION

La formation de la kaolinite nécessite donc la mise en solution simultanée de la silice et de l'aluminium. Pour pallier à l'insolubilité de cette dernière, on doit envisager sa solubilisation sous forme d'ions complexes minéraux ou organiques.

Il apparaît que la silice peut dans certaines conditions de pH et de concentration provoquer elle-même de tels complexes aluminium solubles.

C'est certainement dans ce domaine, encore peu exploré, de la chimie des solutions diluées que réside la clef de la genèse la plus commune de la kaolinite supergène.

## BIBLIOGRAPHIE

- BIEDERMANN, G. et BROSSET, C. (1954): In: Inorganic Polymer Chemistry, F. Gimblett, Butterworths, London 1963.
- BRINDLEY, G.W. et RADOSLOVICH, E.W. (1955): X-Ray studies of the alteration of soda feldspar. *Clays and Clay minerals*, 4, 330-336.
- CORRENS, C.W. (1961): Observations sur la formation et la transformation des minéraux argileux lors de la décomposition des basaltes. *Coll. Int. C.N.R.S.*, 105, 109-116.
- DE KIMPE, C., GASTUCHE, M.C. et BRINDLEY, G.W. (1961): Ionic coordination in alumino-silicic gels in relation to clay mineral formation. *Am. Miner.*, 49, 1370-1381.
- DENNEFELD, F. (1970): Contribution à la synthèse des phyllites alumineuses du type kaolin. Thèse, Strasbourg.
- DENNEFELD, F., SIFFERT, B. et WEY, R. (1970): Etude de l'influence des complexants de l'aluminium et du broyage des hydroxydes d'aluminium sur la formation hydrothermale de la kaolinite. *Bull. Gr. Fr. Argiles*, 22, 179-190.
- EWELL, R.H. et INSLEY, H. (1935): Hydrothermal Synthesis of Kaolinite, dickite, Beidellite and Nontronite. *J. Res. Natl. Bur. Std.*, 15, 173-186.

- FRIPIAT, J.J., DE KIMPE, C. et HERBILLON, A. (1966): Synthesis of analcite and clay minerals in relation to the reactivity of the starting materials. Proc. Int. Clay Conf., 1, 109-119.
- GRUBB, P.L.C. (1968): Phase changes in aged sesqui oxide gels and some analogies with katamorphic processes. C.S.I.R.O. Division of Applied Mineralogy, Melbourne, Aust. 30-51.
- HARDER, H. (1970): Kaolinite-Synthese bei niedrigen Temperaturen. Naturwissenschaften, 57 Jg, Heft 4, 193.
- HERVEY, K.B. et PORTER, G.B. (1967): Introduction to physical inorganic chemistry, Addison-Wesley Publ. Comp., U.S.A.
- HENIN, S. et CAILLERE, S. (1961): Vue d'ensemble sur le problème de la synthèse des minéraux phylliteux à basse température. Coll. Int. C.N.R.S., 105, 31-43 (revue bibliographique des travaux de ces auteurs).
- KOHLSCHÜTTER, H.W. et HANTELMANN, P. (1941): Basische aluminium-chloride. Z. anorg. allgem. Chem., 248, 319-344.
- LAGACHE, M., WYART, J. et SABATIER, G. (1963): Sur la formation de la kaolinite par altération de l'albite à 200°C en présence de CO<sub>2</sub>. C.R. Acad. Sc. Paris, 256, 2501-2503.
- LINARES, J. et HUERTAS, F. (1971): Minéral synthesis at ambient temperature. I. Preliminary study. Bol. Geol. Minero., 82 (1), 77-86.
- MATOSSI, F. (1949): In: Encyclopedia of Physics, S. Flügge, Light and matter. II, 26, 839-841.
- MILLOT, G. (1948): Relations entre la constitution et la genèse des roches sédimentaires argileuses. Géol. Appl. Prosp. Min., 11, n° 2, 3 et 4.
- NOLL, W. (1935): Mineralbildung im System Al<sub>2</sub>O<sub>3</sub>-SiO<sub>2</sub>-H<sub>2</sub>O. Neues Jahrb. Mine. Geol. Beilage, A 70, 65-115.
- NORTON, F.H. (1941): Formation hydrothermale des minéraux argileux au laboratoire. Am. Miner. 26, n° 1, 1-17.
- OBERLIN, A. et TCHOUBAR, C. (1965): Formation de kaolinite par altération de l'albite. Bull. Gr. Fr. Argiles, 18, 13, 49-51.
- OBERLIN, A. et COUTY, R. (1970): Conditions of kaolinite formation during alteration of some silicates by water at 200°C. Clays and Clay Min., 18, 347-355.
- PACKTER, A. et DHILLON, H.S. (1969): Therheterogenous reaction of gibbsite powder with aqueous inorganic acid solutions; kinetics and mechanisms. J. Chem. Soc., A-17, 2588-2592.
- PEDRO, G. (1958 à 1961): Genèse des minéraux argileux par évolution des matériaux amorphes provenant de l'altération de diverses roches. C.R. Acad. Sc. Paris, 250, 1697-1699.
- PEDRO, G. et BERRIER, J. (1968): Etude de la silicification expérimentale de la brucite Mg(OH)<sub>2</sub>. C.R. Acad. Sc. Paris, 266, 2369-2371.
- RAYNER, J.H. (1961): An examination of the rate of formation of kaolinite from a coprecipitated silica gel. Coll. Int. C.N.R.S., 105, 123-127.

- ROY, R. et OSBORN, E.F. (1954): Studies in the system  $\text{Al}_2\text{O}_3\text{-SiO}_2\text{-H}_2\text{O}$ . Am. Inst. Min. and Metallurg. Eng., ST-Louis, 76.
- SCHENK, J.E. (1969): Interaction of monomeric silica with iron, manganese and aluminium in aqueous solution. Ph. D., Univ. Michigan.
- SCHWARZ, R. et TRAGESER, G. (1935): Über die Synthese des Pyrophyllit. Z. Anorg. Allgem. Chem., 225, 142-150.
- SIFFERT, B. (1962): Quelques réactions de la silice en solution: la formation des argiles. Mem. Carte Géol. Als. Lorr., 21, 1-86.
- SIFFERT, B. et WEY, R. (1961): Sur la synthèse de la kaolinite à température ordinaire. C.R. Acad. Sc. Paris, 254, 1460-1462.
- SIFFERT, B. et DENNEFELD, F. (1971): Etude de l'influence des acides minéraux forts sur la synthèse de la kaolinite à partir du mélange gibbsite-silice amorphe. Bull. Gr. Fr. Argiles, 23, 91-106.
- STUMM, W. et MORGAN, J.J. (1962): Chemical aspects of coagulation. J. Amer. Water Works Assu., 54, 971.
- TRICHET, J. (1969): Contribution à l'étude de l'altération expérimentale des verres volcaniques. Thèse n° A.O.-3149, Paris.
- TSUZUKI, Y. et MIZUTANI, S. (1969): Kinetics of hydrothermal alteration of sericite and its application to the study of alteration zoning. Proc. Int. Clay Min. Tokyo, 1, 513-522.
- WEBER, W.J. et STUMM, W. (1965): Formation of a silicato-Iron (III) Complex in aqueous solution. J. Inorg. Nucl. Chem., 27, 237-239.
- WEY, R., WURTZ, M. et SIFFERT, B. (1970): Etude de l'échange de cations monovalents sur vermiculite à 300°C à l'aide d'un autoclave à circulation continue de liquide. Bull. Soc. Chim. France, 6, 2078-2083.

## A CONTRIBUTION TO THE SYNTHESIS OF KAOLINITE (\*)

A. La Iglesia-Fernández and J.L. Martín-Vivaldi

Departamento de Cristalografía y Mineralogía, Facultad de Ciencias, Universidad de Madrid, España.

Instituto "Lucás Mallada". C.S.I.C. Madrid, España.

**ABSTRACT.** - Kaolinite was not synthesized at room temperature from solutions that only contained aluminum ions and monomer silica. The precipitate obtained when modifying the pH did not contain kaolinite and it was not formed by treatment in autoclave at a temperature of 132°C and 2 atm. pressure for 180 h., even in the presence of fulvic acids.

The synthesis of kaolinite succeeded when silica-aluminum ions solutions contain also fulvic acids, if concentration of monomer silica was maintained below its limit of solubility. Crystallization went better as dilution was increased, but in all cases an amorphous phase was present. This amorphous phase was transformed into kaolinite by treatment in an autoclave at 132°C and 2 atm., when the precipitate was suspended in a solution of fulvic acids. When treatment was done in pure water no transformation occurred.

The synthesis of kaolinite occurred with less activation energy at pH far from ca. pH=6 (specially at pH=4-), that is, when working far from the pH region of minimum solubility gibbsite, mainly in the low pH side. In this pH region the kaolinite shows also a minimum of solubility against a dilute solution of fulvic acids.

The precipitate obtained at pH=4 was the richest in kaolinite, which has a good crystallinity and behaves against DMSO as an ordered T polytype.

All above results prove the effectiveness of fulvic acids in the kaolinite synthesis both from solution and from gels with a pre-kaolinic structure. They also show that the synthesis of kaolinite is certainly a coprecipitation of silica and aluminum ions, which is impeded when reaching the minimum solubility of gibbsite and kaolinite.

---

(\*) This study is part of the La Iglesia-Fernandez's Ph. D. Thesis to be submitted to the Universidad Complutense de Madrid, under the supervision of Prof. Martín-Vivaldi.

## INTRODUCTION

Kaolinite was synthesized under hydrothermal conditions by NORTON, (1939-1941) and ROY, (1961), among others. CAILLERE and col. (1956-1961) suggested that clay minerals are formed by fixation of a silica tetrahedral layer on a hydroxal octahedral one. They succeeded in synthesizing several phyllosilicates at room temperature but failed in the synthesis of kaolinite. They attribute this failure to the possibility of the aluminum ion being exa or tetracoordinated.

FRIPIAT and col. (1961) working on the ageing of silica-alumina gel came to the conclusion that this ageing increased the rigidity of the silica layers, and through X-ray fluorescence they showed that gel formation at low pH facilitates the aluminum exa-coordination.

WEY and SIFFERT (1961) suggested the presence of organic molecules as an exa coordinating agent for aluminum. They succeeded in the synthesis of kaolinite at room temperature by using the oxalic complex of aluminum against monomer silica. They explain this formation in a similar way to that of a basic salt (SIF-FERT-1962). They continued their researches using different organic acids (citric, tartaric, salicylic) and inorganic ones (Hydrochloric and sulfuric), and so confirmed former ideas about the necessity of a pre-gibbsitic structure for the achievement of the kaolinite synthesis.

LINARES and HUERTAS (1971 a and b) succeeded too in synthesizing kaolinite at room temperature, with fulvic acid as catalyst, using molar ratios  $\text{SiO}_2/\text{Al}_2\text{O}_3$  above 1 and under pH conditions from 3 up to 9. The influence of fulvic acid in the synthesis is not fully analyzed.

Certainly the understanding of the catalytic action of fulvic acid is a very complex one, because, even knowing for certain (MARTIN and REEVE 1960, SCHNITZER and SKINNER-1963 and WRIGHT and SCHNITZER-1963) the exa coordination of aluminum by fulvic acids, these are a very complex mixture (KONONOVA-1964) of substances going from simple aminoacids up to those of a very complex structure and high molecular weight.

As the detailed action of fulvic acids in the kaolinite synthesis is not known as well as the influence of initial dissolution concentration and pH on the kinetics of the process and on the characteristics of the kaolinite obtained, the present researches have been initiated with the aim of contributing to a deeper knowledge of the synthesis of this phyllo-silicate.

## EXPERIMENTAL

For the extraction of the fulvic fraction a peat from Padul (Granada) was used, after the method described by SCHNITZER and SKINNER (1963). By colorimetry, the calculated concentration of fulvic acid solution was 0,392 g/l.

For kaolinite synthesis a solution at different concentrations with monomer silica, aluminum, chlorite and fulvic acid, were used, adjusting pH from 4 up to 8, keeping reaction vessels in the dark for periods of 40 and 60 days at room temperature. The precipitates obtained were studied by X-ray diffraction, electron microscopy and electron diffraction.

The kaolinite formation was followed measuring the pH as well as determining the amount of kaolinite through X-ray diffraction. The results of autoclave treatments of precipitates were also studied. At the same time a study of the solubility of kaolinite in fulvic acid solutions was carried out.

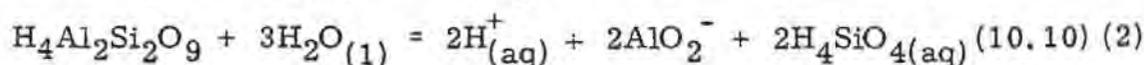
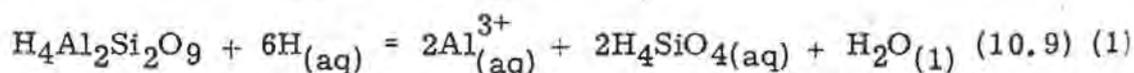
### 1. Influence of the monomer silica concentration

During our first experiments, the kaolinite did not crystallize using silica concentration near its solubility limit (140-150 ppm). In previous tests it was observed by X-ray that the formation of kaolinite was higher the lower was silica concentration; to prove these facts the following experiments were planned: a) Two systems at pH 4 and 4,6 containing 70 ppm of  $\text{SiO}_2$  and 35 ppm of  $\text{Al}_2\text{O}_3$  ( $\text{SiO}_2/\text{Al}_2\text{O}_3 = 3,3$ ) and fulvic acid with a concentration of 0,157 g/l (40%). b) Four systems at pH 3,3; 4,0; 4,7 and 5,0 containing 35 ppm of  $\text{SiO}_2$  and 17,5 ppm of  $\text{Al}_2\text{O}_3$  and fulvic acid with a concentration of 0,078 g/l. After a hundred days time the pH and silica concentration was measured in every system. Table I summarizes the results obtained.

These results show clearly that the amount of precipitated silica and thus the kaolinite formed is higher when using lower concentrations. After that, in further synthesis, very dilute solutions were used as far as was possible, though an extreme dilution would oblige one to handle large volumes in order to obtain amounts of kaolinite which could be easily handled.

### 2. Influence of pH and fulvic acid concentration

As the catalytic action of fulvic acid in the kaolinite synthesis should be a complex one, we planned two kinds of experiments on the basis of GARREL's equations.



First, by dissolution of kaolinite, following the path of the reaction, measuring the equilibrium pH as well as determining the  $\text{SiO}_2$  that goes into solution. Second, by reaction between monomer silica and aluminum ions, a) following the process by measurements of pH, and b) through the amount of formed kaolinite.

2.1. Kaolinite solubility. - Kaolinite was suspended into a solution of fulvic acids at two different concentration. Every experience was carried out at several pH values. The amount of soved silica as well as of pH were determined after 40 days.

Table I

pH initial	pH equil.	initial conc. $\text{SiO}_2$ ppm	equil. conc. $\text{SiO}_2$ ppm
4,0	4,3	70	50
4,6	4,8	70	47
3,3	3,8	35	23
4,0	4,3	35	20
4,7	4,7	35	20
5,0	5,0	35	20

Table II

SOLUBILITY OF KAOLINITE IN SOLUTIONS OF FULVIS ACIDS

10% Fulvic Acid			40% Fulvic Acid		
pH ini.	pH equi.	$\text{SiO}_2$ equi.	pH ini.	pH equi.	$\text{SiO}_2$ equi.
3,95	4,9	35 ppm	4,0	4,55	39 ppm
5,0	5,32	34	5,0	5,24	38
6,2	6,0	34	5,9	5,8	39
7,0	6,8	35	7,0	6,8	40
8,0	7,3	37	8,0	7,42	43

It may be observed (Table II) that the initially low pH increases and medium/high pH, decreases, as the reaction proceeds. This behaviour agrees with the two proposed equations, depending on the type of aluminum ion as a function of pH.

A graphic representation of pH (as absolute values) gives two parabolas with minima calculated at ca. pH=6. (Fig. 1).

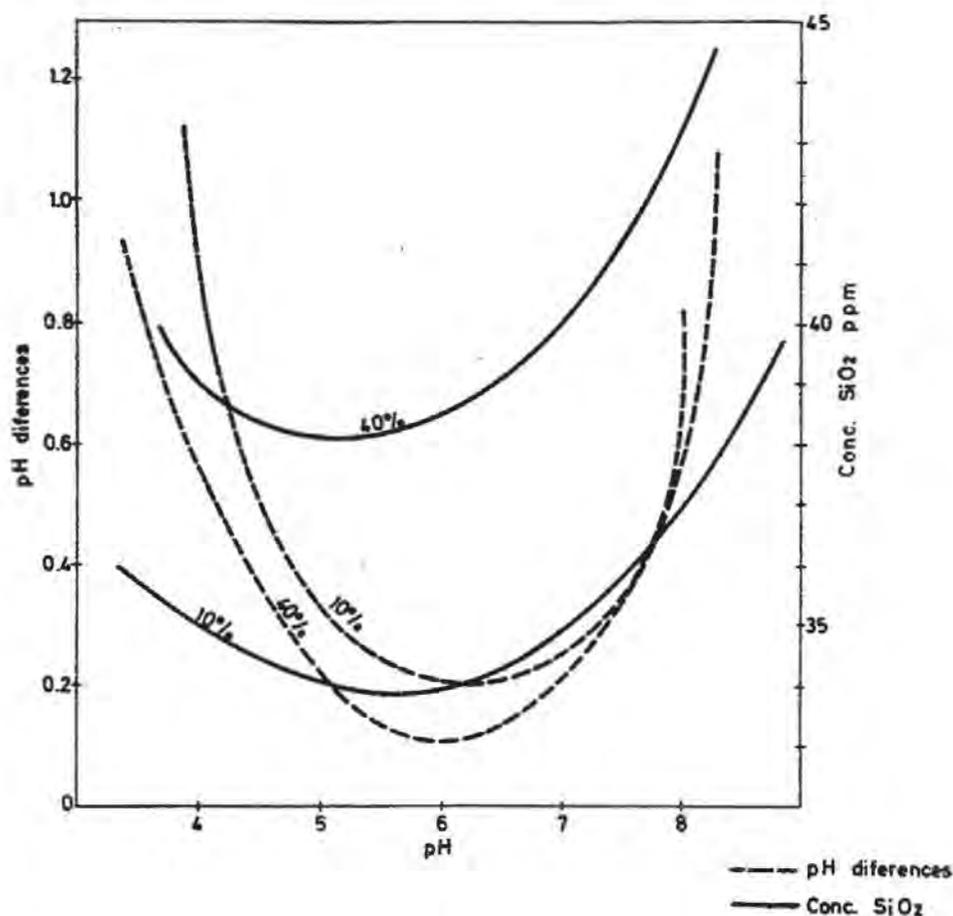


Figure 1. Curves showing pH and SiO<sub>2</sub> in solution, as a function of starting pH, when kaolinite is treated with a fulvic acids solution, at 60°C during 40 days.

In fact, when the reaction happens at the lower pH, equation (1) is followed: then the H<sup>+</sup> must go down to a smaller extent the closer we are to the equilibrium pH. When the system is settled at the beginning at higher pH values, equation (2) should be followed with a similar but reversed behaviour.

The existence of minima in the curves of pH suggests that the minimum of kaolinite solubility is around pH=6. This fact is confirmed by representing the monomer silica in solution as a function of pH.

If we compare the above curve with that of the solubility of gibbsite (ROBERSON-1969) (Fig. 1) it is observed that both minima are in the region of pH=6. It seems then to be confirmed that the minimum of solubility of kaolinite accords with the minimum of gibbsite solubility, which seems to mean that in the reversed process, -synthesis-, the gibbsite precipitation may play an important role in the kaolinite precipitation.

The relative position for both sets of curves also confirm the efficiency of the catalyst, that is, dissolution goes easier the higher is the concentration of fulvic acids.

2.2. Kaolinite synthesis. - A) in all experiments the solutions contained 100 ppm of  $\text{SiO}_2$  and 70 ppm of  $\text{Al}_2\text{O}_3$ , with the following

### TEMPERATURE 18°C

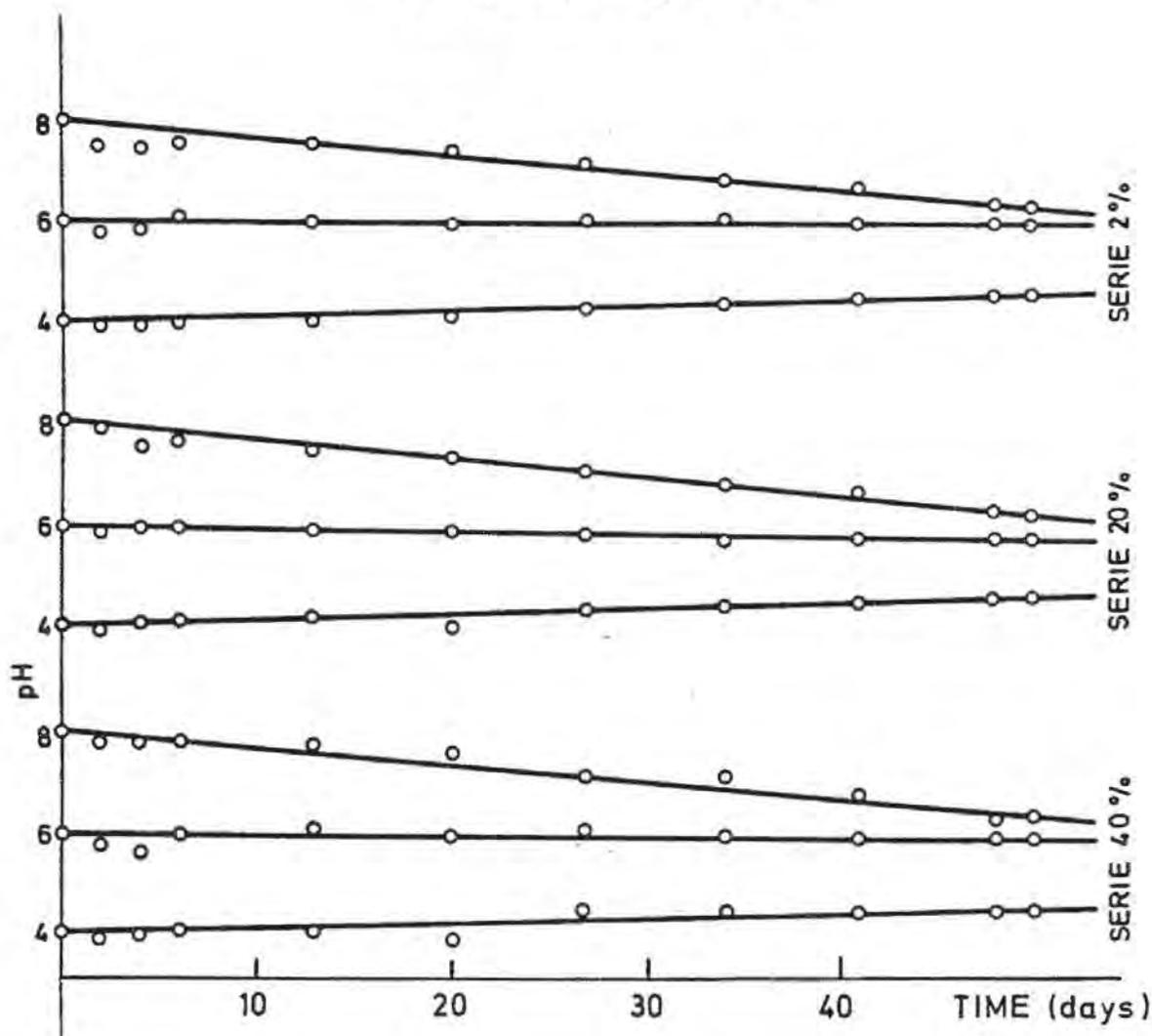


Figure 2. PH modification of the mather solution in kaolinite synthesis as a function of time.

concentrations of fulvic acids: 0,0078 g/l; 0,078 g/l and 0,157 g/l. For every one of each we operated at 18°C, 60°C and 97°C to study the activation energy of the reaction.

The reaction was followed by measuring the pH; these values could be influenced by the dissociation of fulvic acids but, as this will represent a constant value, we can compare the relative rate of reaction for different pH values and concentrations of the catalyst. Reaction flasks were kept away from air and light; deionized and deaerated water has been employed and dry nitrogen was passed through during measurement.

We may observe (Fig. 2) that in experiments at low pH values, these go up as the reaction proceeds, and that the opposite occurs in experiments at medium and high pH values, in accordance with SIFFERT's results (1970), but not in accordance with those obtained by LINARES and HUERTAS (1971), in similar experiments, as they always got a lowering of pH values.

Table III

CONSTANT FOR THE RATE OF REACTION AFTER  
pH MEASUREMENTS

Catalyst Conc.	pH Initial	Rate Constants - Days <sup>-1</sup>		
		18°C	60°C	97°C
2% 0,0078 g/l	4	1,16 10 <sup>-2</sup>	5,09 10 <sup>-2</sup>	1,54 10 <sup>-1</sup>
	6	-1,54 10 <sup>-3</sup>	-2,24 10 <sup>-2</sup>	5,37 10 <sup>-2</sup>
	8	-3,12 10 <sup>-2</sup>	-2,96 10 <sup>-1</sup>	-6,89 10 <sup>-1</sup>
20% 0,078 g/l	4	1,06 10 <sup>-2</sup>	4,89 10 <sup>-2</sup>	1,17 10 <sup>-1</sup>
	6	-5,98 10 <sup>-3</sup>	-2,71 10 <sup>-2</sup>	-7,10 10 <sup>-2</sup>
	8	-2,43 10 <sup>-2</sup>	-1,75 10 <sup>-1</sup>	-3,79 10 <sup>-1</sup>
40% 0,157 g/l	4	1,03 10 <sup>-2</sup>	4,32 10 <sup>-2</sup>	1,18 10 <sup>-1</sup>
	6	-2,06 10 <sup>-3</sup>	-2,71 10 <sup>-3</sup>	-3,40 10 <sup>-2</sup>
	8	-3,16 10 <sup>-2</sup>	-1,10 10 <sup>-1</sup>	-2,83 10 <sup>-1</sup>
100% 0,392 g/l	4	4,05 10 <sup>-2</sup>	1,43 10 <sup>-2</sup>	5,01 10 <sup>-2</sup>
	6	-1,05 10 <sup>-3</sup>	-4,98 10 <sup>-3</sup>	-2,66 10 <sup>-2</sup>
	8	-1,93 10 <sup>-2</sup>	-6,65 10 <sup>-2</sup>	-2,49 10 <sup>-1</sup>

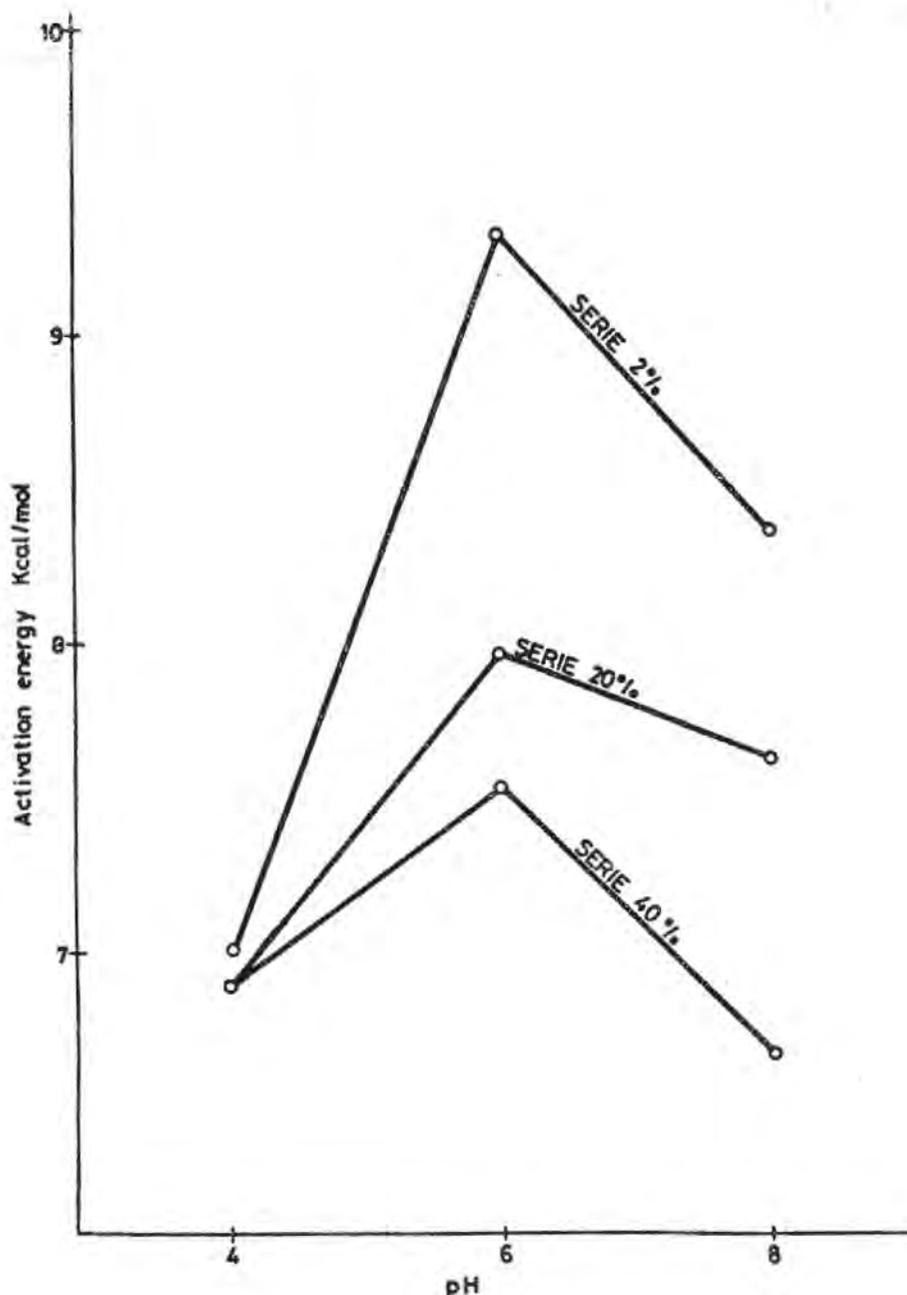


Figure 3. Activation energies in the synthesis of kaolinite, calculated from rate of reaction plotted as a function as starting pH.

If the two equations given by GARRELS were strictly followed, pH variation could be expected with different sign after initial pH, but in fact just with the opposite senses as these obtained by SIF-FERT and ourselves.

Probably, given equation cannot be strictly applied, on account both of the existence of gels and of the complex behaviour of fulvic acids. Table III contains the constant for the rate of reaction. From then on, the activation energies of the reaction have been cal-

culates by means of Arrhenius equation:

$$K = Ae^{-\frac{E_a}{Rt}}$$

Figure 3 represents the activation energies as a function of the initial pH. Curves show a maximum at pH=6 for any concentration of the catalyst. On those pH in which the activation energies are high, the active action of the catalyst is obvious. pH 4 must be so favourable for the synthesis that there is practically no influence of the catalyst.

The presence of a maximum of pH 6 seems to be incongruent with the fact that kaolinite and gibbsite have a maximum of insolubility at that pH value. A reasonable explanation could be to suppose that, just on account of this minimum of solubility for gibbsite, this must tend to crystallize as an independent phase, avoiding good coprecipitation of aluminum with silica, to give kaolinite. The kaolinite formed at this pH must be through condensation of silica on "proto-gibbsite". That is, the kaolinite synthesis occurs at low pH as a reaction between ion whilst around pH=6 the reaction is a reaction of gels, which require a higher activation energy.

B) The process of synthesis has also been studied by means of the amount of kaolinite formed and its crystallinity. The employed solutions contained 100 ppm SiO<sub>2</sub>, 50 ppm Al<sub>2</sub>O<sub>3</sub> (SiO<sub>2</sub>/Al<sub>2</sub>O<sub>3</sub> = 3,40) and 0,078 g/l of fulvic acids (20%); pH were adjusted to the values: 3; 4; 4, 6; 5; 6 and 7 leaving the system for a period of 65 days at room temperature and measuring the pH at the end of this period of time. pH variations have followed the same path as that in the above mentioned experiments.

The precipitates were studied by X-ray diffraction once dried at room temperature as well as after being laid them under 132°C and 2 atm pressure in an autoclave.

pH were in both cases the same as those employed in the synthesis. The period of time in the autoclave was always of 30 h., with sampling at 5, 15 and 30 h. Fig. 4 shows the X-ray diffraction diagram of samples after 30 h. in the autoclave.

In order to get an idea of the degree of order in the kaolinite obtained, the pH 4 precipitate was selected because of the relatively great amount of this precipitate and of the good quality of its X-ray diffraction diagram. As the diagram, owing to the operative method, showed a high degree of orientation, we turned to study the degree of ordering by its behaviour in an atmosphere saturated with DMSO at 60°C for 30 and 50 h. The values obtained for  $R=I_{11}/I_7$  were of 4 and 10,6 respectively, a result which accords with those of MARTIN-VIVALDI and col. (1970). The kaolinite behaves as a T polytype, even close to a dickite.

To determine the amount of kaolinite in the precipitate, it was

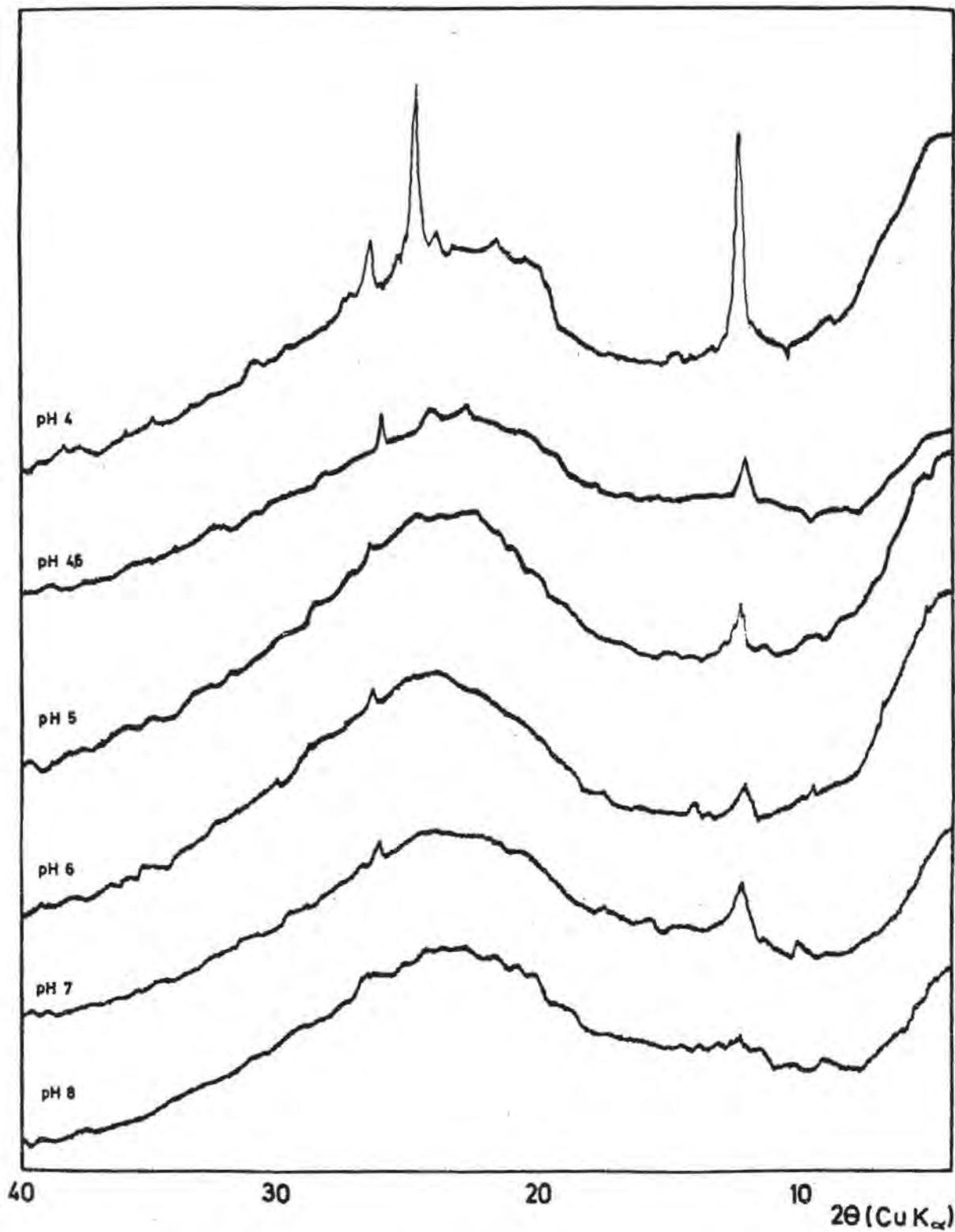


Figure 4. X-ray diffractogram (oriented aggregated) of precipitates obtained in the synthesis of kaolinite after treatment in autoclave during 30 h. at 132°C an 2 atm.

mixed with illite as internal standard. Using the ratio  $I_{001 \text{ kaol.}} / I_{001 \text{ illite}} = 2$ , the calculated percentage of kaolinite for the three series of experiments are shown in Table IV.

The highest amount of kaolinite was obtained at pH=4, whilst at the remaining pH the amount of kaolinite were very low, even the quality of precipitates were higher. Despite the fact that figures of this group are variable and low, the greatest ones belong to the

Table IV

KAOLINITE PERCENTAGE AFTER TREATMENT OF PRECIPITATE IN AN AUTOCLAVE IN SUSPENSION WITH FULVIC ACIDS

pH	0 Hours without the autoclave	5 Hours	15 Hours	30 Hours
4,0	22,5	29	36,5	38,0
4,6	3,3	4,6	4,25	6,0
5,0	3,2	6,0	7,2	9,4
6,0	1,6	4,0	4,6	5,5
7,0	5,2	7,0	8,9	11,7

After treatment in an autoclave without fulvic acids

pH	0 Hours	5 Hours	15 Hours	30 Hours
4,0	22,5	19,5	20,3	19,5
4,6	3,3	2,5	2,6	3,9
5,0	3,2	3,3	3,3	3,0
6,0	1,6	3,7	4,0	3,1
7,0	5,2	6,6	6,6	5,7

highest pH. These facts agree with our results after the calculation of activation energies: kaolinite is synthesized better as pH is far from that of minimum solubility of gibbsite and kaolinite. Results of treatments in an autoclave in the presence of fulvic acids, that is, in similar conditions as in the synthesis at room temperature, show that the amount of kaolinite increases as function of the time of treatment. Anyhow the rise in the amount of kaolinite, from the initial precipitate to that after 5 h. treatment, is greater as less

kaolinite was initially present. This suggests the existence of allophanic gels, or very disordered kaolinite on which the thermal treatment is very effective.

The total percentage for the increase in kaolinite, after 30 h. treatment follows in a similar way, with a strong rise for samples prepared at pH=6.

Treatment of precipitates in aqueous solution shows no formation of kaolinite. We may mention in this respect that precipitates obtained in the absence of fulvic acids did not contain kaolinite, even after treatment in an autoclave in solution of fulvic acids.

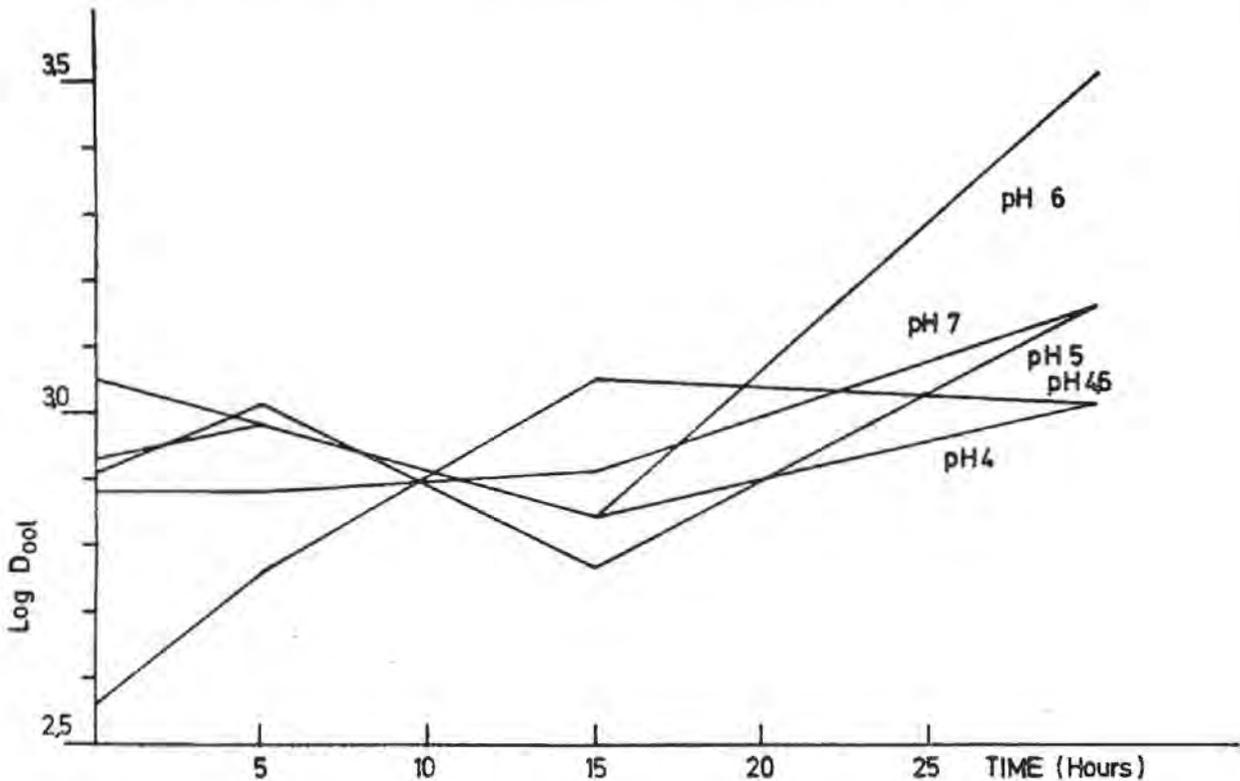


Figure 5. Graphical plot of the calculated average size of kaolinite crystals as a function of time of treatment in an autoclave (132°C and 2 atm.) in an aqueous suspension.

All those facts point out the necessity of a catalyst not only in order to synthesize kaolinite from silica and aluminum solution at room temperature, but also with allophanic gels which do not have a "pre-kaolinitic" structure.

The action of treatment in an autoclave has also been studied by measuring the average size of crystals and analyzing their X-ray diffraction diagrams. The width of reflexion at half their height was used (KLUG and ALEXANDER-1954; FAYOS and SALVADOR-1971) correcting for diffractometer (ALEXANDER-1954).

As Fig. 5 and 6 show, the average size of particles grow in all experiments when treated in water. On the other hand, on ave-

rage, the size of crystals is not modified when treated in a solution of fulvic acids. Crystals prepared at pH=4 show a singular behaviour, as neither of the two treatments modified the crystals.

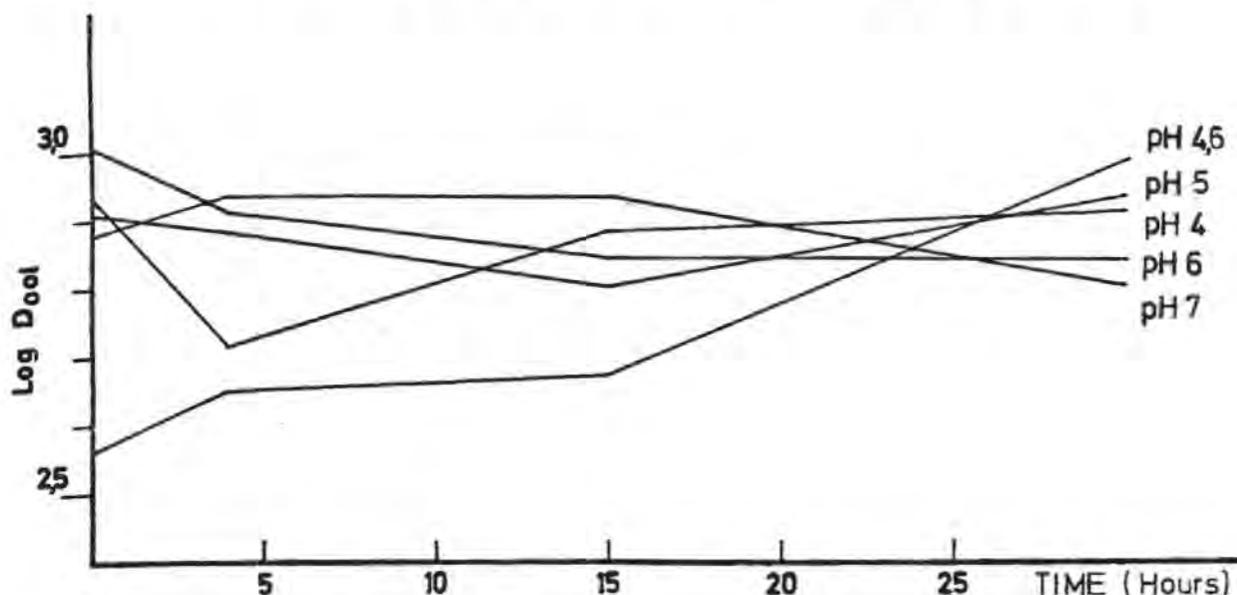


Figure 6. Same as Fig. 5 but for crystals treated in a fulvic acids solution.

The observation of some precipitates under the electron microscope (Figs. 7 a and b), shows a low perfection of crystals for those prepared both at pH 4 and 6, but their size is lower for the latter one. Their crystallinity is good, as deduced from their microdiffraction, for those prepared at pH=4. Figs. 8 a, b and c show crystals obtained at this pH after treatment in an autoclave for periods of 5, 15 and 30 h. Microphotography as well as microdiffraction show clearly the improvement of crystals as a function of the time of treatment.

#### REFERENCES

- CAILLERE, S. et HENIN, M.S. (1961): Vues d'ensemble sur le problème de la synthèse des minéraux phylliteux a basse température. *Genèse et Synthèse des Argiles*. Coll. du C.N.R.S. N° 105, 31-43.
- DENNEFELD, F., SIFFERT, B. et WEY, R. (1970): Etude de l'influence des complexantes de l'aluminium et du broyage des hydroxides d'aluminium sur la formation hydrothermal de la kaolinite. *Bull. Group Fran. Argiles*. XXII, 179-190.
- DUPUIS, T. (1971): Caracterization par analyse thermique diferentielle des complexes de Al avec les acides fulviques et humiques. *Thermal Analysis*. 3, 281-288.

- FAYOS, J. and SALVADOR, P. (1971): A systematic approximate method for determination of structure factors from a powder diffractogram and its application to the solution of the structure of metavariscite. *J. Appl. Cryst.* 4, 159-163.
- GARRELS, R.M. and CHRIST, C.L. (1965): *Solutions minerals and equilibria*. H. and R. New York.
- KLUG, H.P. and ALEXANDER, L.E. (1954): *X-ray diffraction procedures*. John Wiley and sons. Inc. New York.
- KONONOVA, M.M. (1966): *Soil organic matter*. Pergamon Press.
- LINARES, J. and HUERTAS, F. (1971): Kaolinite synthese at room temperature. *Science*. 171, 896-897.
- LINARES, J. y HUERTAS, F. (1971): Síntesis de minerales a temperatura ordinaria. 1.- Estudio preliminar. *Bol. Geol. y Min.* LXXXII-I, 77-86.
- MARTIN, A.E. and REEVE, R. (1960): Chemical studies of pozzolic illuvial horizons. *Soil. Sci.* 11, 369-381.
- MARTIN POZAS, J.M. (1969): Tesis Doctoral. Universidad de Granada.
- MARTIN VIVALDI, J.L., POZZUOLI, A. e MATTIAS, P. (1971): Nota preliminare sull'espandibilita de alcuni minerali laminari. A.T.T.I. del 1º Congresso Nazionale, Gruppo Italiano dell'A.I.P.E.A.
- NORTON, F.H. (1939): Hydrothermal formations of clays minerals in laboratory. Part. I. *Am. Min.* 24, 1-17.
- ROBERSON, C.E. and HEM, J.D. (1969): Solubility of aluminium in the presence of hydroxide, fluoride, and sulfate. *Geol. Surv. Watter-Supply. Paper* 1827-C.
- ROY, R. (1961): The preparation and properties of synthetic clay minerals. *Genese et Synthèse des Argiles. Bul. C.N.R.S. N° 105*, 83-98.
- SIFFERT, B. (1962): Quelques reactions de la silice en solution: la formation des argiles. *Mem. Serv. de la Carte Geol. D'Alsace et Lorraine*.
- SIFFERT, B. et DENNEFELD, F. (1971): Etude de l'influence des acides minéraux fort sur la synthèse de la kaolinite a partir de mélange gibsita silice amorphe. *Boll. Groupe Français des Argiles. XXXIII*, 92-106.
- SCHNITZER, M. and SKINNER, S. (1963): Organo-Metallic, interactions in soil. *Soil Sci.* 96-102.
- WEY, R. et SIFFERT, B. (1961): Reactions de la silice monomoléculaire en solution avec les ions Al et Mg. *Genèse et Synthèse des Argiles. Coll. du C. N.R.S. N° 105*, 11-24.
- WRIGHT, J.R. and SCHNITZER, M. (1963): Matalo-Organic interaction associated with pozzolization. *Soil Science Society Proceedings*. 171-176.

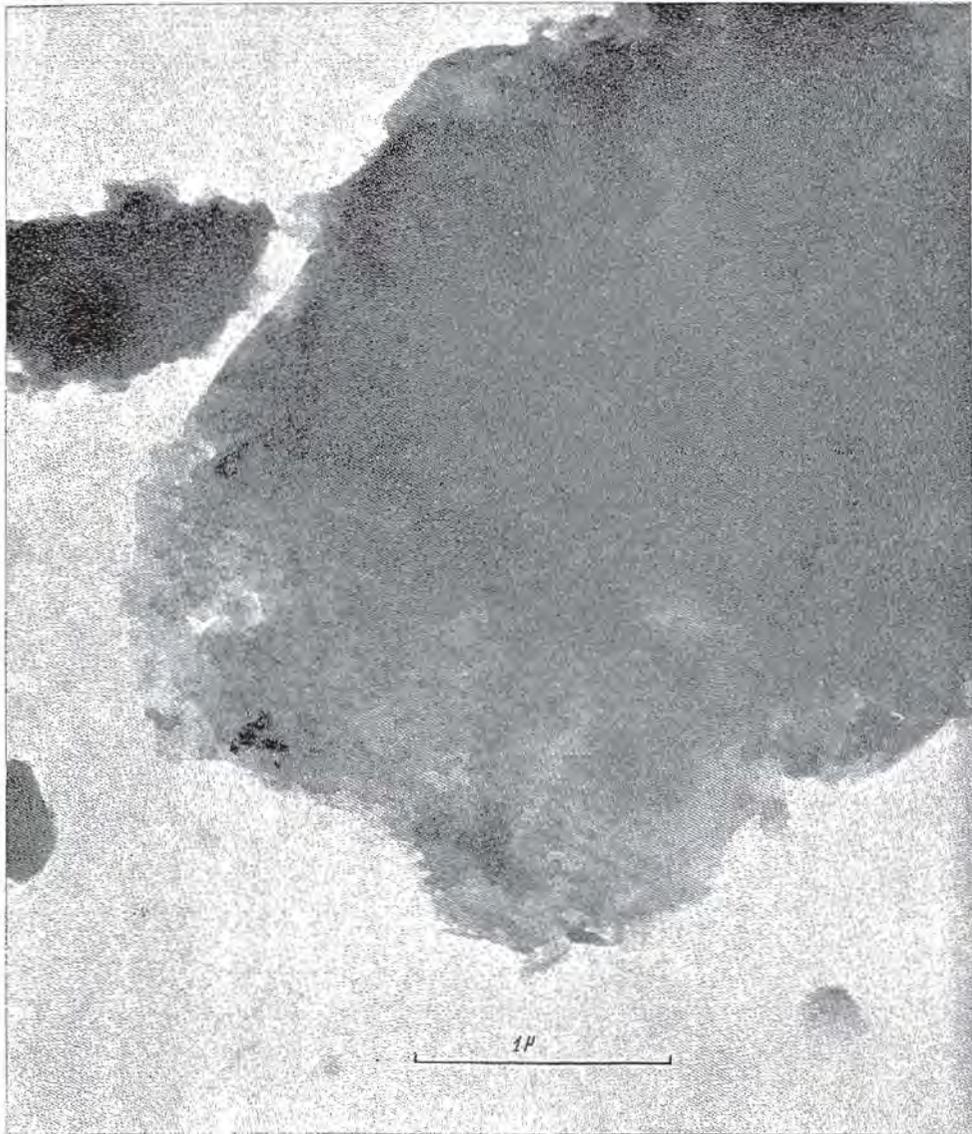


Figure 7. a) Microphotograph and microdiffraction of precipitate obtained at  $\text{pH} = 4$  left 60 days at room temperature against the mother solution.



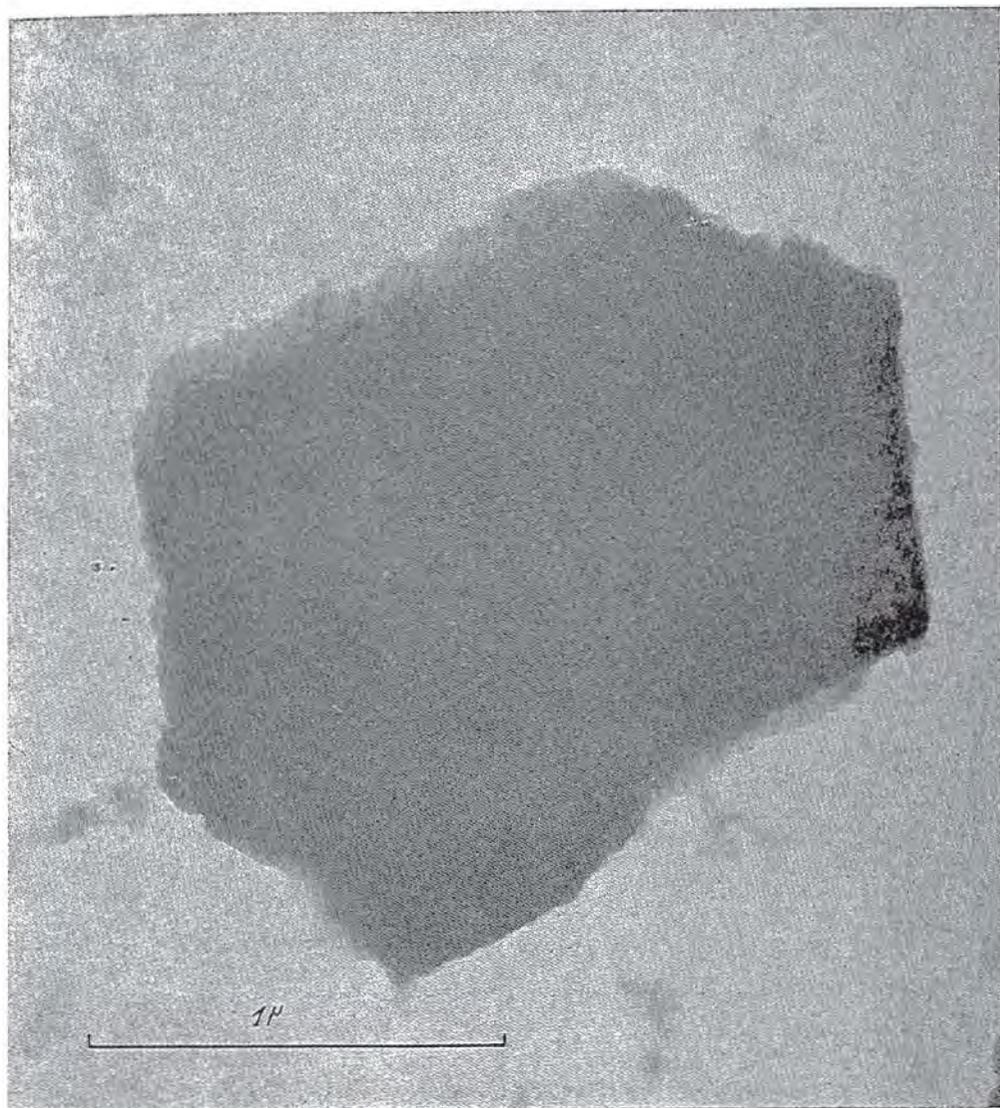


Figure 7. b) Microphotograph of precipitate at  $\text{pH} = 6$ , left as a).





Figure 8. a) Microphotograph of precipitate both obtained and treated in autoclave at PH = 4 in a fulvic acids solution. (Treated 5 h.)



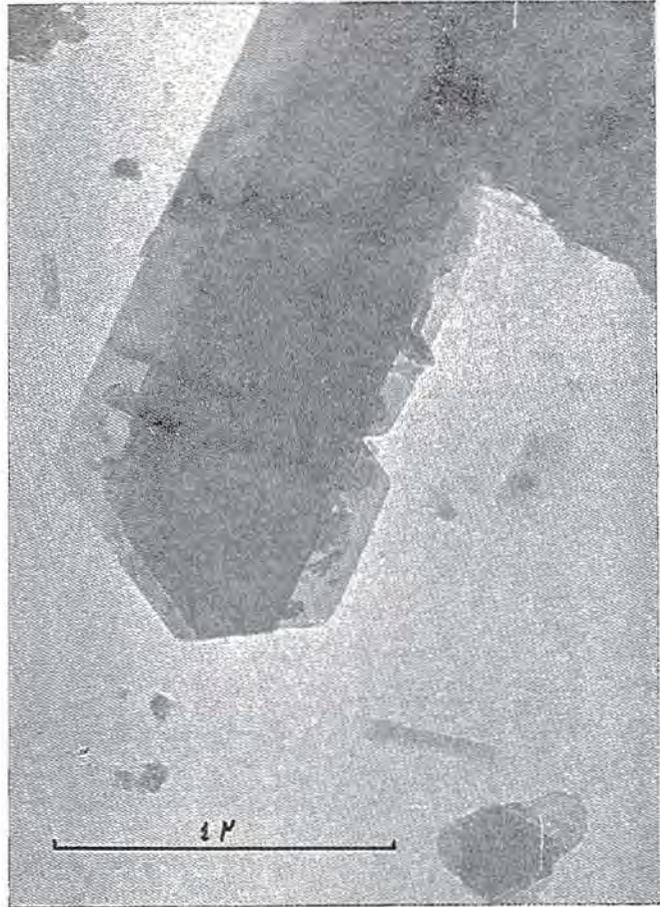


Figure 8. b) Same as a),  
treated 15 h. with its mi-  
crodiffraction.



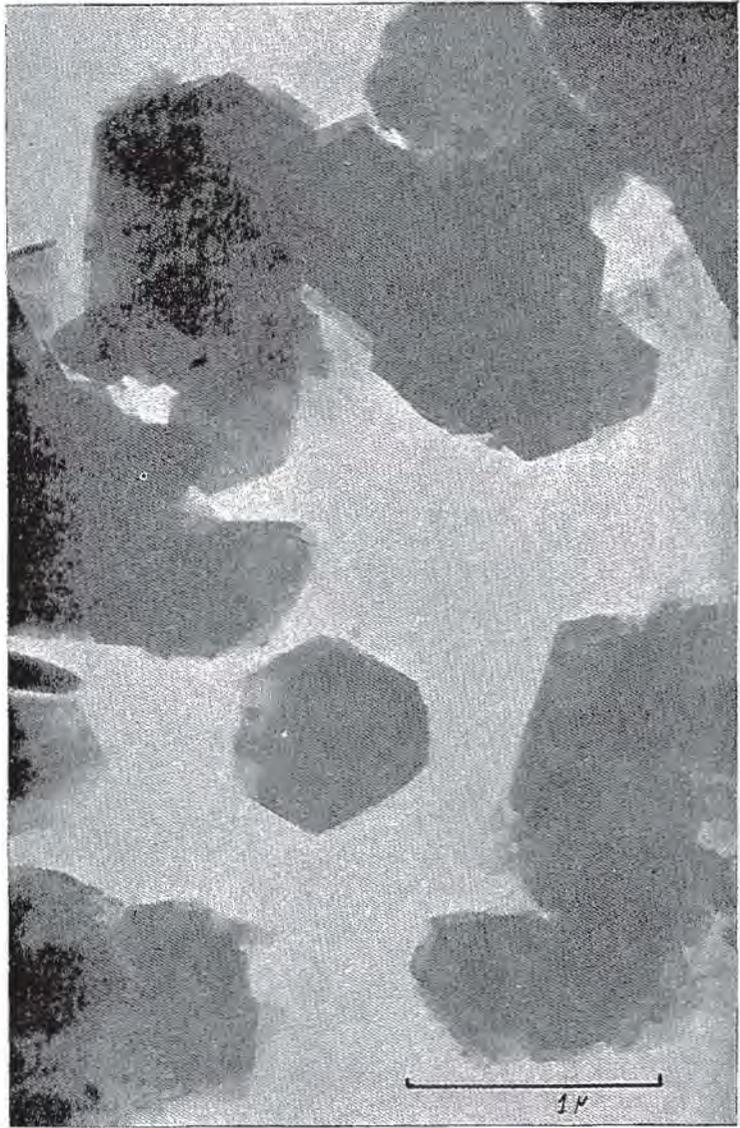


Figure 8. c) Same as b),  
treated 30 h.



# IMPORTANCE OF THE SILICA SUBTRACTION PROCESS DURING THE HYDROTHERMAL KAOLINITIZATION OF AMORPHOUS SILICO-ALUMINAS

L. Rodrique\*, G. Poncelet\*\* and A. Herbillon\*

Laboratoire de Physico-Chimie Minérale, Institut des Sciences  
de la Terre, de Croylan 42, 3030 Heverlee, Belgium

**ABSTRACT.**- Amorphous aluminosilicates of various compositions were hydrothermally aged in hydrochloric acid solution (pH 0.1 or 4.8) and distilled water, under different conditions of temperature and pressure. The results of X-ray analysis and electron microscopy allow to specify the conditions of kaolinite formation with respect to several experimental factors namely chemical composition of the starting material, acidity of the solution and aging temperature. Considering the structural features of the silico-aluminic gels, it is suggested that the depolymerized state of the Al which is observed when the starting material is rich in silica, is an important factor of success for the kaolinite synthesis. The results suggest also that the clay microcrystals are obtained through a progressive arrangement of "rows" of O-Si-O-Al-OH chains rather than by a silicification of a poorly crystallized aluminic support. The formation of these rows would be favored when the mechanism leading to the formation of kaolinite is that implying a subtraction of silica.

## INTRODUCTION

Kaolinite genesis is most generally considered as the result of a "neof ormation by subtraction" of silica namely (Milot, 1964), whereas some examples, undoubtedly less frequent, show the kaolinitization as the result of an addition process of silica onto an aluminous support (Delvigne, 1965). The gross chemical balance,

---

\* The University of Louvain and M.R.A.C. (Tervuren)

\*\* The University of Louvain

however, does not allow to propose a growth mechanism for the phyllite, and several authors (Tchoubar, 1965; Oberlin and Couty, 1970) have shown that, during the hydrothermal alteration of a silicate mineral, the kaolin formation was the result of an addition of silica on an activated aluminic phase.

Laboratory syntheses conducted in order to specify the conditions and the mechanisms of formation of this mineral, generally involve a hydrothermal treatment of a starting material in which the stoichiometric ratio Al:Si of kaolinite is already realized (De Kimpe et al., 1964; Poncelet and Brindley, 1967; Oberlin and Couty, 1970; Dennefeld et al., 1970; De Kimpe and Fripiat, 1968). Such situation, from the chemical balance viewpoint, allows neither the subtraction nor the addition of silica to occur as in nature. Another prerequisite condition to kaolin formation concerns the importance of the hexacoordinated state of aluminum in the starting materials (De Kimpe et al., 1964; Dennefeld et al., 1970; Linares and Huer-tas, 1971).

The present study, which constitutes a prolongement of the work of De Kimpe (1967), aims to specify the hydrothermal evolution of amorphous silico-aluminas with various  $\text{Al}_2\text{O}_3/\text{Al}_2\text{O}_3 + \text{SiO}_2$  ratios under different pH conditions, favoring a higher solubility of silica or of alumina. The silico-aluminic gels were those used in the structural studies of Léonard et al. (1964), Cloos et al. (1968, 1969); these gels are characterized by varying  $\text{Al}^{\text{IV}}$  and  $\text{Al}^{\text{VI}}$  contents.

In the composition range  $0 < \text{Al}_2\text{O}_3/\text{Al}_2\text{O}_3 + \text{SiO}_2 \leq 0.4$ , about 50 per cent of the total aluminum content appears as fourfold coordinated; as the total aluminum content is increased, the relative  $\text{Al}_{\text{app}}^{\text{IV}}$  content is rapidly decreasing.

## EXPERIMENTAL

### A. Preparation of the starting materials

Pure gels with variable  $\text{Al}_2\text{O}_3/\text{Al}_2\text{O}_3 + \text{SiO}_2$  weight ratios have been prepared by slow cohydrolysis of the required quantities of ethylsilicate and aluminum isopropoxide, following the experimental procedure described by Léonard et al. (1964). The main feature of this procedure is that it provides gels free of cationic and anionic impurities.

The following weight ratios were realized: 100, 89, 72, 60, 48.5, 31.5 and 24 %  $\text{Al}_2\text{O}_3/\text{Al}_2\text{O}_3 + \text{SiO}_2$ . These gels were X-ray amorphous except for the first two ratios which contain mixtures of bayerite and pseudoboehmite.

## B. Hydrothermal treatment and examination of the products

Gold tubes containing about 300 mg of solid and 4 ml of liquid were reacted (in most cases during 7 days) in a stainless steel autoclave that was heated in a cylindrical furnace. Solutions of different acidities were used: N HCl, 0.1 N HCl, solution of pH 4.8 and distilled water. The experiments were performed at temperatures ranging from 175 to 250°C ( $\pm 2^\circ\text{C}$ ) and the pressure was the saturating water pressure at the corresponding temperature.

After treatment the products were washed with distilled water by centrifugation, dried at 60°C, ground, and finally dried again at 105°C. All the reacted products were examined with a Philips X-ray diffractometer using Ni-filtered Cu K $\alpha$  radiation and a Geiger detector. Some products were also examined with an AEI, type EM6G electron microscope. The preparations were realized by deposition of a drop of suspension of the ultrasonically dispersed sample on a grid covered with a carbon film. No further shadowing was made.

## C. Results and interpretation

### X-Ray diffraction

The results of the hydrothermal experiments conducted at 175°C are given in Table 1. Regardless of the acidity of the initial solution or the composition of the starting gel, kaolinite is not synthesized. Under these conditions, boehmite and pseudo-boehmite are generally produced from the gels high in alumina; amorphous sub-

TABLE 1. EXPERIMENTS PERFORMED IN GOLD TUBES DURING 7 DAYS AT 175°C - 8.8 atm. ( $\pm$  300 mg AMORPHOUS ALUMINO-SILICIC GELS IN PRESENCE OF 4 ml ACID OR NEUTRAL SOLUTION). X-RAY RESULTS

Chemical composition Al <sub>2</sub> O <sub>3</sub> /Al <sub>2</sub> O <sub>3</sub> + SiO <sub>2</sub> of the starting material (%)	Nature of the solution			
	N HCl	10 <sup>-1</sup> N HCl	HCl pH 4.8	H <sub>2</sub> O
100.0	B	B	B	B
89.0	B	B	Psb	Psb
72.0	B	B	Psb	Psb
60.0	Psb	Psb	Poor Psb	Poor Psb
48.5	Am	Poor Psb	Poor Psb	Poor Psb
31.5	Am	Poor Psb	Am	Am
24.0	Am	Am	Am	Am

B, boehmite; Psb, pseudoboehmite; Am, amorphous phase.

tances are obtained from the silica- rich gels. It appears that low pH values (0 and 1) favor the formation of well-crystallized boehmite from gels with high alumina contents.

These results are in good agreement with the structural schema of similar silico-aluminas proposed by Cloos et al. (1969): the hydrothermal treatment results in the appearance of an individualized aluminic phase, crystalline or pseudocrystalline, as soon as the initial gel has a higher polymerized  $Al^{VI}$  content than the Al content involved in the tetrahedral network of the nucleus, i. e. from a  $Al_2O_3/Al_2O_3 + SiO_2$  ratio of  $\sim 0.4$  or higher. In other words, hydrothermal treatment favor the crystallization of aluminum hydroxide, on the one hand, and enriches the residual noncrystalline phase in silica, on the other hand.

Table 2 contains the results obtained from the experiments performed at 200°C. The results are similar to those reported at 175°C in the runs made at pH 0 and pH 1: depending upon the composition of the gels, boehmite, pseudoboehmite or amorphous products are formed. When a solution of pH 4.8 or distilled water is used, kaolinite is produced from gels containing 31.5 and 24%  $Al_2O_3$ .

TABLE 2. EXPERIMENTS PERFORMED IN GOLD TUBES DURING 7 DAYS AT 200°C - 15.3 atm. ( $\pm$  300 mg AMORPHOUS ALUMINO-SILICIC GELS IN PRESENCE OF 4 ml ACID OR NEUTRAL SOLUTION). X-RAY RESULTS

Chemical composition $Al_2O_3/Al_2O_3 + SiO_2$ of the starting material (%)	Nature of the solution			
	N HCl	$10^{-1}$ N HCl	HCl pH 4.8	H <sub>2</sub> O
100.0	B	B	B	B
89.0	B	B	Psb	Psb
72.0	B	Psb	Psb	Psb
60.0	Psb	Psb	Psb	Psb
48.5	Poor Psb	Poor Psb	Poor Psb	Poor Psb
31.5	Am	Poor Psb	Poorly crystallized Kte	Well-crystallized Kte
24.0	Am (+ Psb)	Am	Am (+ Kte)	Well-crystallized Kte

B, boehmite; Psb, pseudoboehmite; Am, amorphous phase; Kte, kaolinite

All other conditions being equal, it is not the gel with the initial composition similar to the theoretical composition of kaolinite which most readily leads to the formation of this mineral. When

the initial composition and experimental conditions do not favor segregation and concentration of the aluminum into a separate aluminic phase, kaolinite appears in the reacted products. In contrast, when aluminum solubility is enhanced (at low pH values), part of it demixes into pseudoboehmite whereas the other part remains integrated in an amorphous compound. By analogy with an open system in which the removal of the most soluble element would be effected, the kaolinitization observed here may be assimilated to a synthesis by subtraction of silica.

At 220°C (Table 3), the conditions under which kaolinite is formed are extended. For the solutions at pH 4.8 and 7, the domain of existence of kaolinite includes the gel with an  $Al_2O_3/Al_2O_3 + SiO_2$  ratio equal to 48.5%, a composition which allows synthesis to take place without gain or loss of silica. No formation of kaolinite is observed in strongly acid solutions; the results are very similar to those obtained at 175° and 200°C.

TABLE 3. EXPERIMENTS PERFORMED IN GOLD TUBES DURING 7 DAYS AT 220°C - 22.9 atm. ( $\pm$  300 mg AMORPHOUS ALUMINO-SILICIC GELS IN PRESENCE OF 4 ml ACID OR NEUTRAL SOLUTION). X-RAY RESULTS

Chemical composition $Al_2O_3/Al_2O_3 + SiO_2$ of the starting material (%)	Nature of the solution			
	N HCl	$10^{-1}$ N HCl	HCl pH 4.8	H <sub>2</sub> O
100.0	B	B	B	B
89.0	B	B	B	Psb
72.0	B	Psb	Psb	Psb
60.0	Psb	Poor Psb	Psb	Psb
48.5	Poor Psb	Poor Psb	Poorly crystallized Kte	Poorly crystallized Kte
31.5	Am	Poor Psb	Well-crystallized Kte	Well-crystallized Kte
24.0	Am	Am	Poorly crystallized Kte	Poorly crystallized Kte

B, boehmite; Psb, pseudoboehmite; Am, amorphous phase; Kte, kaolinite

At 250°C (Table 4) the favourable influence of the temperature coefficient on the reaction clearly appears, since, as it can be seen, kaolinite is synthesized over the entire pH range investigated. With solutions of initial pH 4.8 and 7, clay synthesis occurs just as it does at 220°C, when the  $Al_2O_3/Al_2O_3 + SiO_2$  ratio of the starting gel is lower or equal to the ratio present in kaolinite. In

strongly acid solutions, kaolinite is obtained even when the silica content is lower than in kaolin, but in this case, it coexists with the demixed alumina phase, which, as seen at 175°C, is favored in such a medium. This tendency to demixion is even observed (at least in N HCl solution) for gels with lower Al<sub>2</sub>O<sub>3</sub> contents, and there also, kaolinite and crystalline aluminum hydroxide are present together.

TABLE 4. EXPERIMENTS PERFORMED IN GOLD TUBES DURING 7 DAYS AT 250°C - 39.2 atm. (+ 300 mg AMORPHOUS ALUMINO-SILICIC GELS IN PRESENCE OF 4 ml ACID OR NEUTRAL SOLUTION). X-RAY RESULTS

Chemical composition Al <sub>2</sub> O <sub>3</sub> /Al <sub>2</sub> O <sub>3</sub> + SiO <sub>2</sub> of the starting material (%)	Nature of the solution			
	N HCl	10 <sup>-1</sup> N HCl	HCl pH 4.8	H <sub>2</sub> O
100.0	B	B	B	B
89.0	B	B	B	B
72.0	B	B	Psb	Psb
60.0	B + poorly crystal- lized Kte	Psb + poorly crystal- lized Kte	Psb	Psb
48.5	B + well-crystal- lized Kte	Well-crystallized Kte	Very well crystal- lized Kte	Very well crystal- lized Kte
31.5	Poorly crystallized Kte (+ B)	Am (+ Psb)	Well-crystallized Kte	Well-crystallized Kte
24.0	Am (+ Psb)	Am (+ Kte)	Poorly crystal- lized Kte	Poorly crystal- lized Kte

B, boehmite; Psb, pseudoboehmite; Am, amorphous phase; Kte, kaolinite.

The general trends of the results presented in Tables 1 to 4 allow grouping of the data obtained for N HCl and 0.1 N HCl solutions on the one hand, and those obtained for the more neutral solutions (pH 4.8 and 7); the set of conditions resulting in the synthesis of kaolinite may be represented as in Table 5.

It appears that the synthesis of kaolinite is promoted by the presence of excess silica or the presence of aluminum in fourfold coordination in the starting gels. As a consequence, if one considers the gross balance of the transformation gel → kaolinite, the obtainment of this mineral by a process of silica subtraction is accomplished within a wider range of temperature and composition than its formation involving a process of silica addition (or aluminum subtraction); this latter situation is realized only twice within the set of experimental conditions used here.

From the balance viewpoint, the transformation of a system with 48.5% alumina can hardly be accounted for by one or the other

process; but if, in this case, aluminum is demixed before kaolinite appears (by example, in strong acid medium), it is clear that the synthesis of kaolinite will then be the result of a process involving the subtraction of silica.

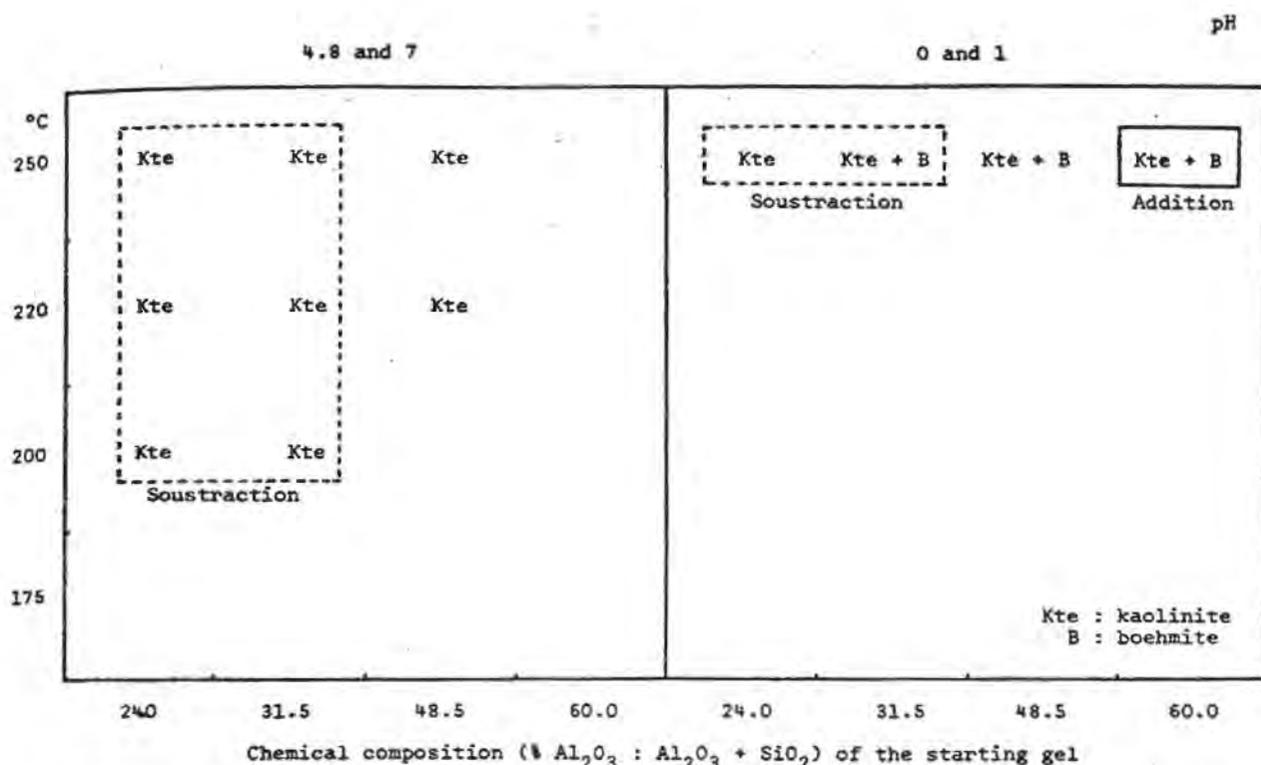


**TABLE 5.** SCHEMATIC REPRESENTATION OF THE EXISTENCE CONDITIONS FOR KAOLINITE SYNTHESIZED BY HYDROTHERMAL AGING OF ALUMINO-SILICIC GELS OF VARIOUS COMPOSITIONS, DURING 7 DAYS UNDER DIFFERENT pH AND TEMPERATURE CONDITIONS. X-RAY RESULTS.

Electron microscopy and diffraction have been used by several authors (Tchoubar, 1965; Oberlin and Couty, 1970) to put in evidence the existence of a poorly defined intermediate phase (pseudoboehmite) during the genesis of aluminous phyllites. In our experiments, and particularly if only the evolution of compounds with equal or lower aluminum content than that existing in kaolinite are taken into consideration, there is no experimental evidence of an activated phase of pseudoboehmitic nature as a precursor required for the formation of kaolinite.

On the contrary, the mineral appears for the first time at the expenses of materials which show no tendency to evolve into boehmite. This is confirmed by a long duration experiment (15 days) at 175°C in neutral medium with the 31.5%  $Al_2O_3$  gel (Fig. 1). Kaolinite is found after 15 days and no trace of boehmite is detected in the course of this experiment. A similar observation is made in a study of the transformation kinetics carried out in the same conditions at 200°C (Fig. 2).

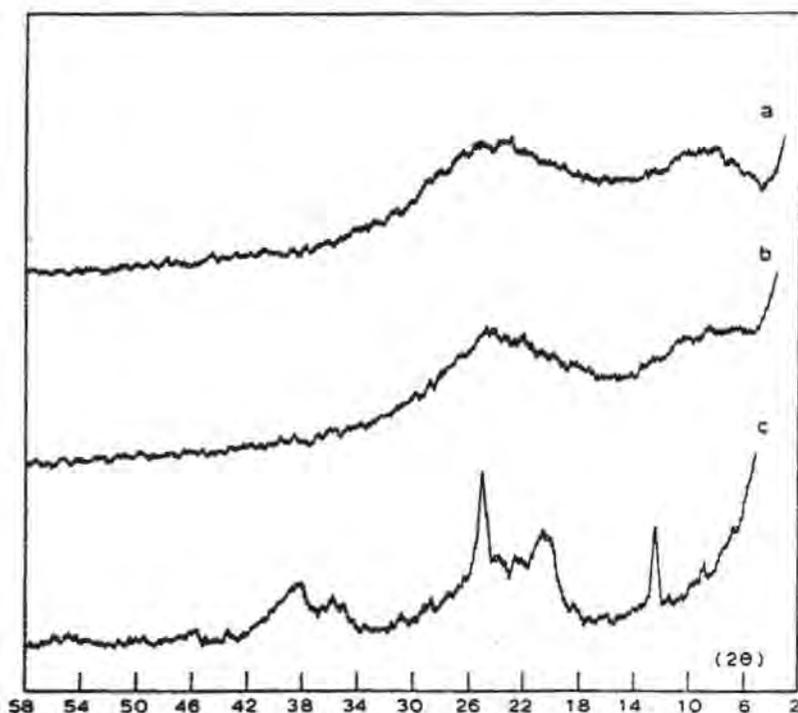


Figure 1. X-ray diffraction patterns showing transformation of the gel containing 31.5%  $\text{Al}_2\text{O}_3/\text{Al}_2\text{O}_3 + \text{SiO}_2$  aged at  $175^\circ\text{C}$  under neutral conditions: (a) starting material; (b) after 7 days; (c) after 15 days.

Consequently, a microscopic examination has been performed on samples from which, on the basis of chemical balance, kaolinization was achieved through a process of silica subtraction (i. e. the gels with initial  $\text{Al}_2\text{O}_3$  content  $\leq 48.5\%$ ) in order to confirm the X-ray data.

### Morphological study

The characteristic facies of the examined samples are collected in Fig. 3-10. The kaolin mineral appears as thin filaments and crumpled membranes (bidimensional kaolinite - see, for example Fig. 3), as pseudo-hexagonal plates (Fig. 4, 5, 9 and 10) or as laths or particles resembling halloysite (Fig. 6). At the end of a systematic examination of these samples, it is rather striking to notice how rarely kaolinite appears as nice well-shaped pseudo-hexagonal crystals even when the X-ray diffraction traces indicate the presence of a well-crystallized kaolinite.

In many products obtained with a neutral or a pH 4.8 solution, i. e. in the acidity range in which kaolinitization is achieved the most easily, variable quantities of spherical particles are observed. These particles (of variable size, between 2,000 and 10,000 Å)

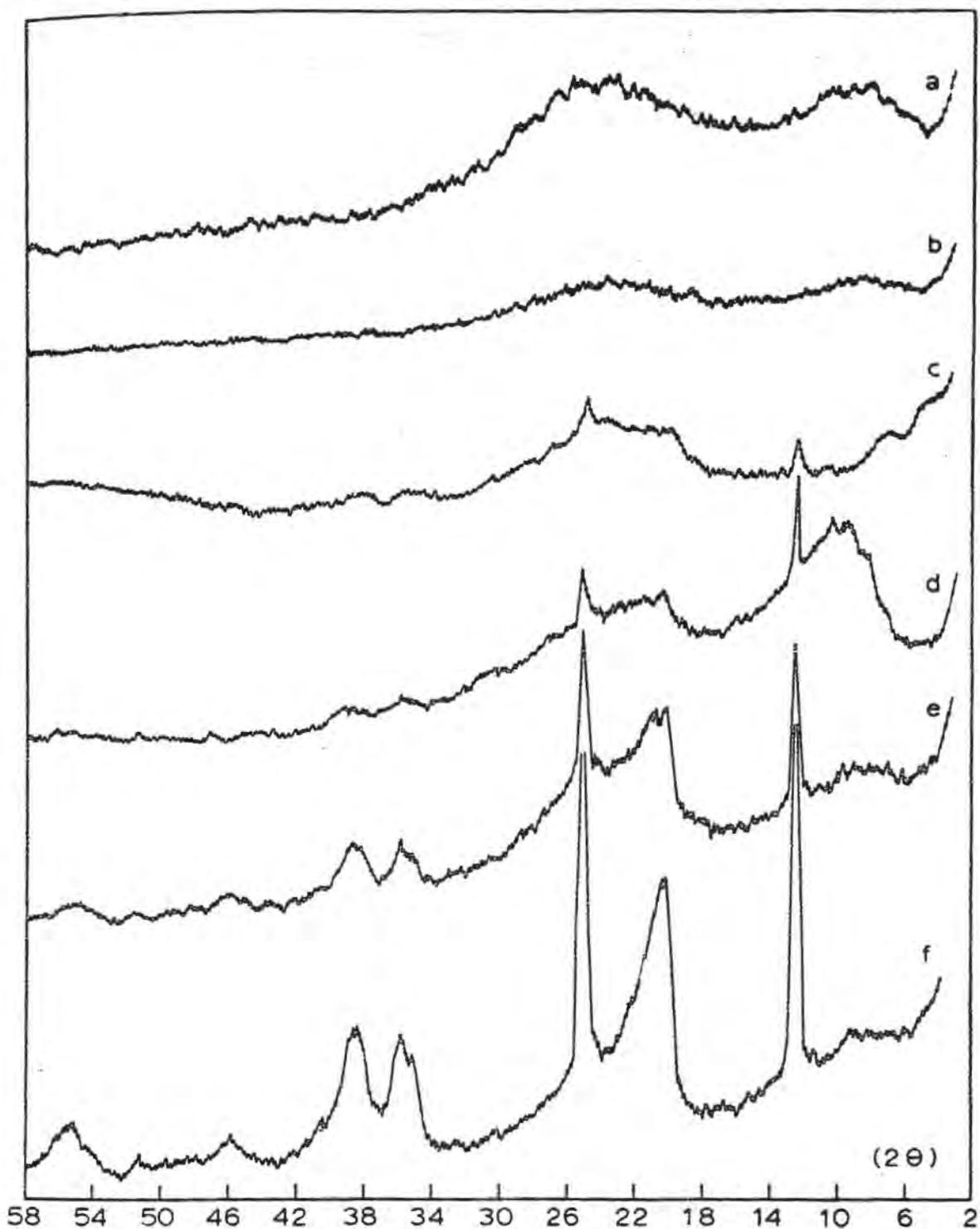


Figure 2. X-ray diffraction patterns showing transformations of the gel containing 31.5%  $\text{Al}_2\text{O}_3/\text{Al}_2\text{O}_3 + \text{SiO}_2$  aged at  $200^\circ\text{C}$  under neutral conditions: (a) starting material; (b) after 1 day; (c) after 3 days; (d) after 4 days; (e) after 5 days; (f) after 7 days.

were not found in the starting materials. They present clear morphological analogies with allophanes observed in soils developed from vitreous parent materials (Sudo, 1959; Siffermann and Millot, 1968) or with the spherical particles observed by Trichet (1969) in an experimental alteration of volcanic glasses (Trichet and Svoronos, 1968; Trichet and Sella, 1968). Within the limit of the results collected at the present time, it can be seen that those "balls" formed during the hydrothermal treatment, do not appear in the syntheses conducted in strongly acidic conditions, even when kaolinite is detected by X-rays.

The microscopic observation shows that the kaolinite genesis takes place, at least partially, at the expenses of the elements constituting these particles. This is clearly shown by Fig. 5 in which crystalline flakes with a kaolinitic facies are in contact with such globular particles. These latter would then constitute active centers in the genesis of the clay.

In the light of Tchoubar's (1965) and Trichet's (1969) results, the initial step may be seen as the transformation of these allophane-like particles into thin filaments of kaolin (see Fig. 3, 4 and 7-9); these filaments would evolve into crumpled membranes (Fig. 3 and 4) which would further develop in laths and tridimensional plates of kaolinite (see particularly Figs. 12 and 13).

It is also interesting to point out that similar particles studied by Trichet (1969) and which contain, besides silica and alumina, alkali or alkaline-earth elements, may experimentally evolve into clay minerals of the montmorillonite and kaolinite groups on the one hand, and towards hydrated aluminum oxides, on the other hand. Trichet and Sella (1968) report also that, whatever the origin of the glass, those spherical particles are rich in silica ( $\text{Al}_2\text{O}_3/\text{Al}_2\text{O}_3 + \text{SiO}_2$  ratio between 0.2 and 0.4). In our experiments, they appear only when silica-rich gels are used as starting materials.

## GENERAL DISCUSSION

The experimental results permit a more precise evaluation of the conditions governing the formation of aluminous clay minerals during the hydrothermal aging of amorphous silico-aluminas. They show that genesis of kaolin minerals is the easiest when the starting gels are characterized by a high silica content. The importance of the subtraction of silica, as shown by the chemical balance is supported by the fact that synthesis is favored in conditions which realize neutrality, i.e. where silica is more mobile than aluminum. The X-ray diffraction observations and the electron microscopic examination do not support the view that the birth of kaolinite follows a mechanism of addition of silica onto an aluminic support.

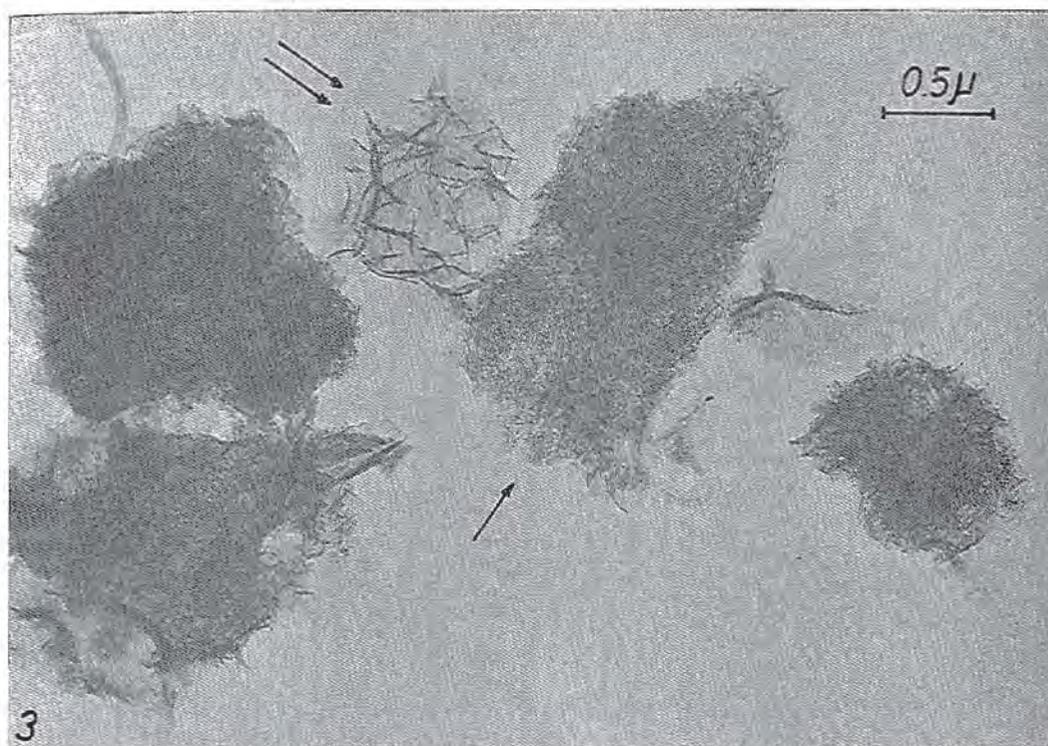


Figure 3. Thin filaments (single arrow) and crumpled membranes (double arrow) of kaolinite observed after aging a gel with 48.5 %  $\text{Al}_2\text{O}_3$  at  $200^\circ\text{C}$  during 7 days under neutral conditions.  $\times 36,500$ .

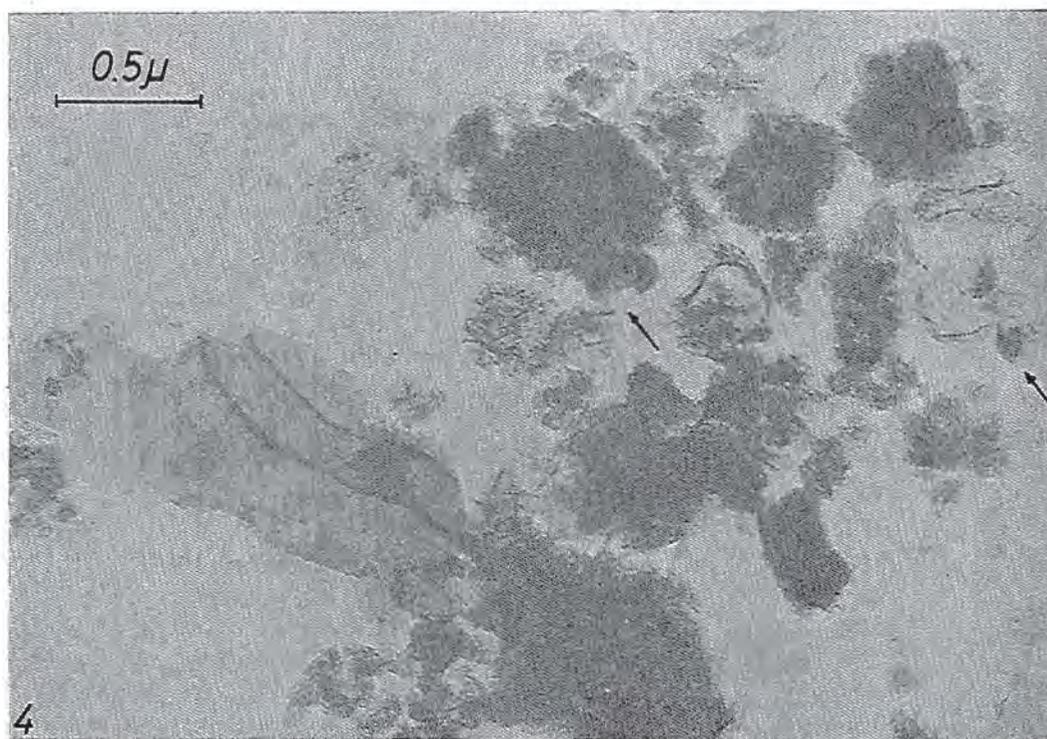


Figure 4. Globular particles (see arrows), filaments and crumpled membranes, and pseudo-hexagonal crystals of kaolinite found in the product obtained from a gel with a 31.5 %  $\text{Al}_2\text{O}_3$  content aged at  $200^\circ\text{C}$  during 7 days under neutral conditions.  $\times 46,000$ .



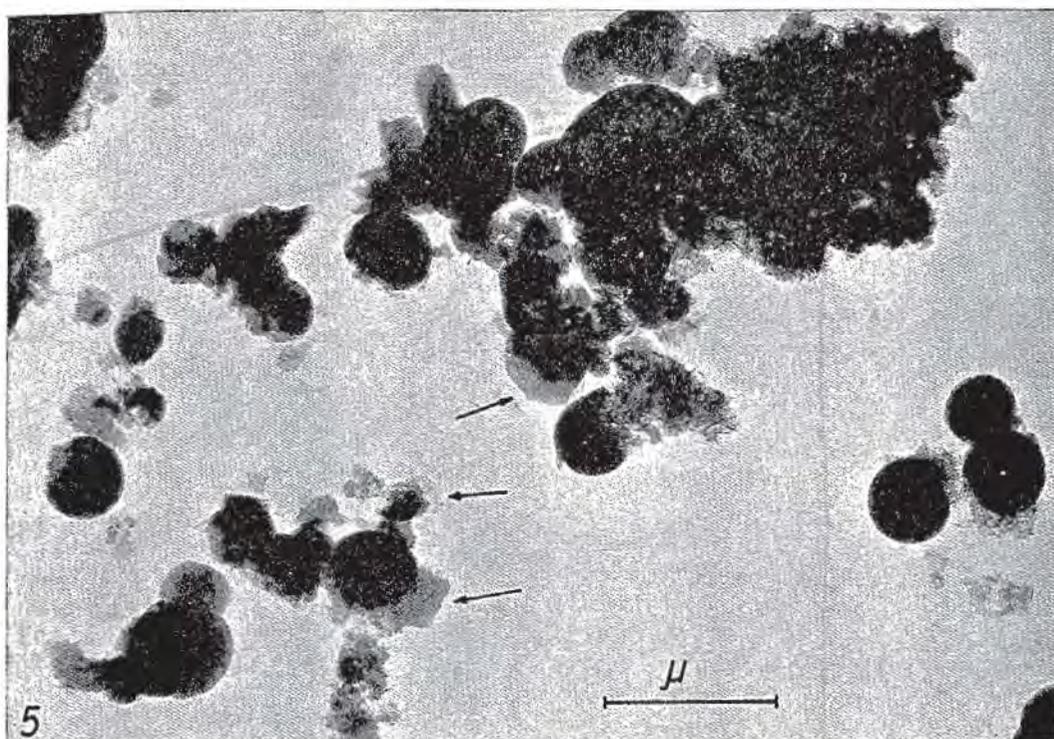


Figure 5. Small plates of kaolinite (see arrow) developing in contact with globular particles (gel with a 48.5 %  $\text{Al}_2\text{O}_3$  content aged at 220° C during 7 days under neutral conditions).  $\times 27,500$ .

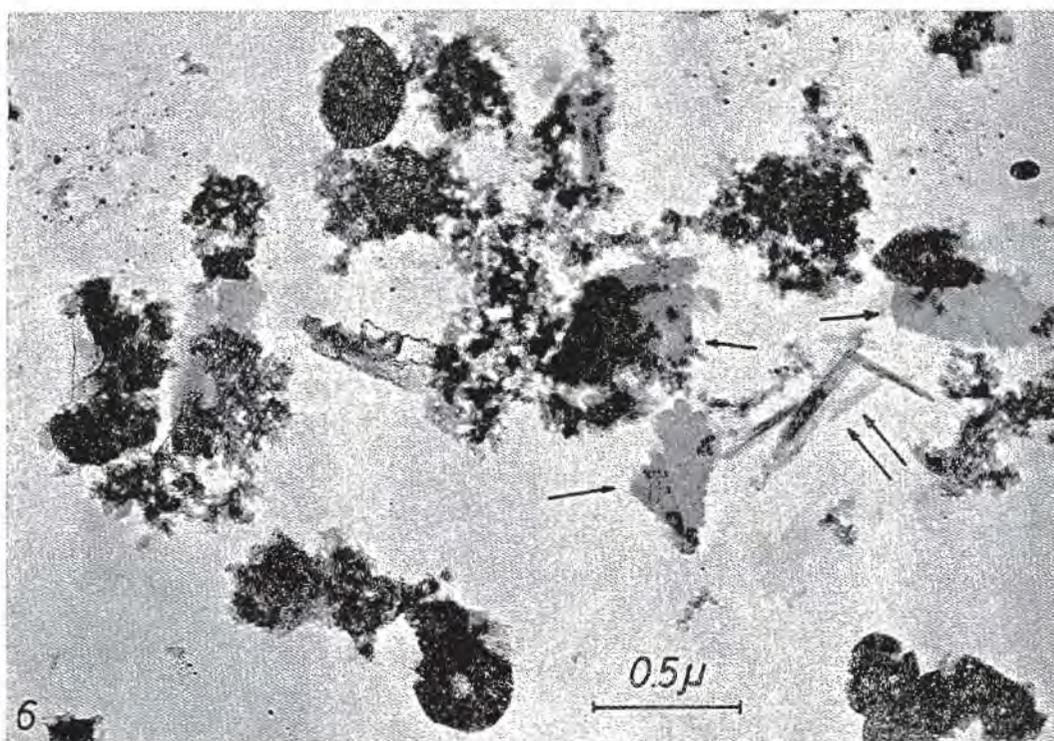


Figure 6. Spherical particles, small crystals of kaolinite (single arrows) and halloysite-like material (double arrow) observed in the sample obtained from a gel with a 31.5 %  $\text{Al}_2\text{O}_3$  content aged at 250° C during 7 days under neutral conditions.  $\times 47,000$ .



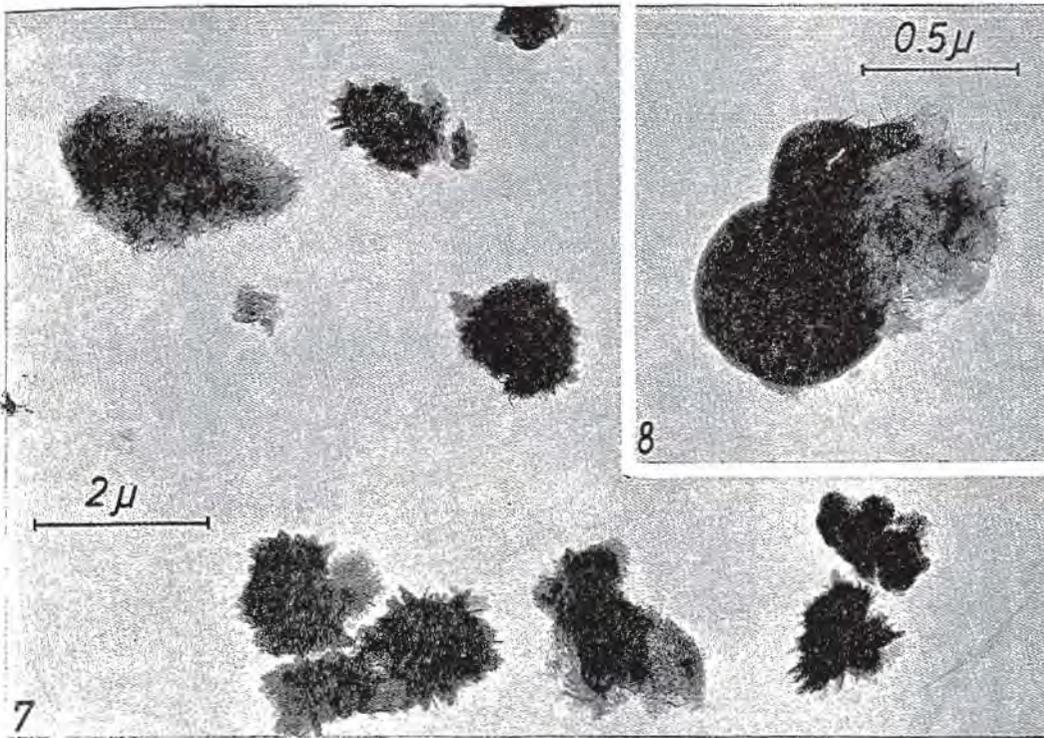


Figure 7. General aspect of the transformation of spherical particles in filaments and tri-dimensional laths or plates of kaolinite (gel with a 48.5 %  $\text{Al}_2\text{O}_3$  content aged at 220° C during 7 days under HCl pH 4.8 conditions).  $\times 14,000$ .

Figure 8. Evolution of filaments and membranes of kaolinite in contact with globular particles (gel with a 48.5 %  $\text{Al}_2\text{O}_3$  content aged at 220° C during 7 days under neutral conditions).  $\times 50,000$ .

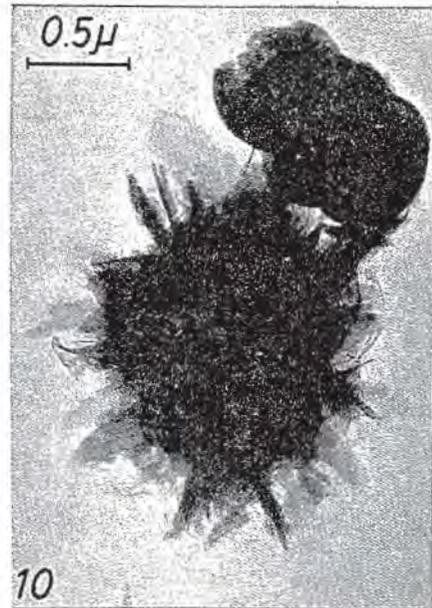
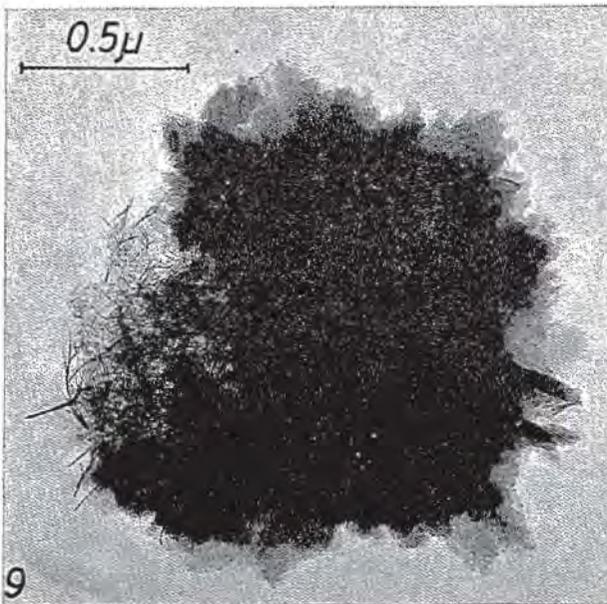


Figure 9. Filaments and small crystals of kaolinite in way of formation observed in the product formed from a gel with a 48.5 %  $\text{Al}_2\text{O}_3$  content aged at 220° C during 7 days under HCl pH 4.8 conditions.  $\times 53,500$ .

Figure 10. Globular particles and laths or plates of kaolinite in way of formation observed after aging a gel with a 31.5 %  $\text{Al}_2\text{O}_3$  content at 220° C during 7 days under HCl pH 4.8 conditions.  $\times 32,500$ .



As shown by Cloos et al. (1969), the gels with a chemical composition  $\text{Al}_2\text{O}_3/\text{Al}_2\text{O}_3 + \text{SiO}_2 \leq 0.4$  are characterized by a high  $\text{Al}^{\text{IV}}/\text{Al}^{\text{VI}}$  ratio (near unity). This shows that the fourfold coordination in our starting material does not inhibit the formation of kaolinite. It is also worthy of note that in these gels,  $\text{Al}^{\text{VI}}$  saturating the exchange sites is only slightly polymerized whenever the  $\text{Al}^{\text{IV}}/\text{Al}^{\text{VI}}$  ratio is high. This unpolymerized state, as well for  $\text{Al}^{\text{VI}}$  as for  $\text{Al}^{\text{IV}}$  isolated in the silica network, seems to constitute a far more important synthesis factor than the initial coordination state of this element.

It appears, thus, that if kaolinite is to be formed without passing through an activated intermediate such as pseudoboehmite, i. e. at low temperature, the main phenomenon to be avoided is a preliminary step in which Al would condense as a poorly crystallized support. This can be achieved by aging a starting material in which Al is depolymerized, under conditions ensuring insolubility of aluminum and hence favoring the probability of binding of alumina with silica rather than the probability of association of alumina with itself. From this standpoint, the starting gel with a yield of 30%  $\text{Al}_2\text{O}_3$  is certainly the most favourable starting material, as confirmed by the success obtained in the formation of kaolinite at 175°C.

The results suggest that the formation of kaolinite at the expenses of O-Si-O-Al-OH chains (whose further juxtaposition would lead to the development of aluminous phyllites) requires an activation energy lower than the silicification of a poorly crystalline aluminic support. This observation is in agreement with the conclusions drawn by De Kimpe and Fripiat (1968) from a study on the hydrothermal kaolinitization from  $\text{H}_3\text{O}^+$ -zeolites. The formation of these preliminary rows would be favored in the absence of a process leading towards aluminium hydroxide crystallization; one can also believe that this inhibiting process would tend to be absent when synthesis is the result of a silica subtraction.

Whatever the mechanism of the crystalline growth of kaolinite, the good agreement between our results and what is observed under natural conditions should be pointed out.

Indeed, the parallelism between the data relative to the crystallization of the gel with the 30%  $\text{Al}_2\text{O}_3$  content and the observation made by Delvigne and Martin (1970) on the kaolinitization of a feldspar through an amorphous phase rich in silica is rather noteworthy.

In both cases, the simplest mechanism leading to the formation of kaolinite is that implying a subtraction of silica.

## ACKNOWLEDGEMENTS

The authors wish to thank Professor J.J. Fripiat, Professor St. Arnaud and Professor P. Cloos for interesting discussions. The technical assistance of Messers L. Vielvoye and M. Genet is gratefully acknowledged.

## REFERENCES

- CLOOS, P., HERBILLON, A. and ECHEVERRIA, J. (1968): Allophane - like synthetic silico-aluminas. Phosphate adsorption and availability: Trans. 9th Intern. Congr. Soil Sci. II, 733-743.
- CLOOS, P., LEONARD, A.J., MOREAU, J.P., HERBILLON, A. and FRIPIAT, J.J. (1969): Structural organization in amorphous silico-aluminas. *Clays and Clay Minerals*, 17, 279-287.
- DE KIMPE, C.R. (1967): Hydrothermal aging of synthetic aluminosilicate gels. *Clay Minerals*, 7, 203-214.
- DE KIMPE, C.R. and FRIPIAT, J.J. (1968): Kaolinite crystallization from H-exchanged zeolites. *Amer. Min.*, 53, 216-230.
- DE KIMPE, C.R., GASTUCHE, M.C. and BRINDLEY, G.W. (1964): Low-temperature syntheses of kaolin minerals. *Amer. Mineral.* 49, 1-16.
- DELVIGNE, J. (1965): Pédogenèse en zone tropicale. I. La formation des minéraux secondaires en milieu ferrallitique. Ph.D. Thesis, Louvain, Fac. Sciences, 177 p.
- DELVIGNE, J. et MARTIN, H. (1970): Analyse à la microsonde électronique de l'altération d'un plagioclase en kaolinite par l'intermédiaire d'une phase amorphe. *Cah. ORSTOM, Sér. Géol. II*, 2, 259-295
- DENNEFELD, F., SIFFERT, B. et WEY, R. (1970): Etude de l'influence des complexants de l'aluminium et du broyage des hydroxydes d'aluminium sur la formation hydrothermale de la kaolinite. *Bull. Groupe Franç. Argiles*, t. 22, 179-190.
- LEONARD, A., SUZUKI, Sho, FRIPIAT, J.J. and DE KIMPE, C. (1964): Structure and properties of amorphous silico-aluminas - I. Structure from X-ray fluorescence spectroscopy and I.R. spectroscopy. *J. Phys. Chem.* 68, 2608-2617.
- LINARES, J. and HUERTAS, F. (1971): Kaolinite: synthesis at room temperature. *Science*, 171, 896-897.
- MILLOT, G. (1964): *Géologie des argiles*. Paris, Masson, 499 p.
- OBERLIN, A. and COUTY, R. (1970): Conditions of kaolinite formation during alteration of some silicates by water at 200°C. *Clays and Clay Minerals*, 18, 347-356.
- PONCELET, G. and BRINDLEY, G.W. (1967): Experimental forma-

- tion of kaolinite from montmorillonite at low temperature. Amer. Mineral. 52, 1161-1173.
- SIEFFERMANN, G. et MILLOT, G. (1968): L'halloysite des sols jeunes sur basaltes récents du centre Cameroun. Bull. Groupe Franç. Argiles, 20, 25-39.
- SUDO, T. (1959): Mineralogical study on clays of Japan. Maruzen Co., Ltd., Tokyo, 328 p.
- TCHOUBAR, C. (1965): Formation de la kaolinite à partir d'albite altérée par l'eau à 220°C. Etude en microscopie et diffraction électroniques. Bull. Soc. Franç. Minér. Crist., 88, 483-518.
- TRICHET, J. (1969): Contribution à l'étude de l'altération expérimentale des verres volcaniques. Ph.D. Thesis, Paris, 232 p.
- TRICHET, J. et SELLA, C. (1968): Etude de la structure des verres volcaniques. Relation avec leur mode de formation et d'altération. C.R. Acad. Sc. Paris, t. 267, 1084-1086.
- TRICHET, J. et SVORONOS, D.R. (1968): Etude des premiers stades d'altération d'un verre volcanique. C.R. Acad. Sc. Paris, t. 266, 1207-1209.



GEOCHEMICAL EVOLUTION OF CLAY MINERALS  
IN THE WEATHERED PRODUCTS AND SOILS  
OF MEDITERRANEAN CLIMATES

Hélène Paquet and Georges Millot

Institut de Géologie, Université Louis Pasteur, Strasbourg, France

**ABSTRACT.** - The geochemical evolution of clay minerals under mediterranean climates was principally studied in fersiallitic soils and brown isohumic soils from Morocco, Lebanon, Greece and South France.

The authors point out the different mechanisms governing this evolution.

INTRODUCTION

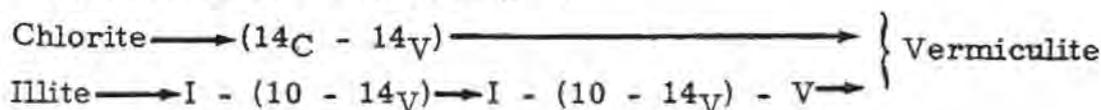
The evolution of clay minerals in the weathered products and soils of mediterranean countries was studied in collaboration with A. Ruellan in the case of Morocco, M. Lamouroux in the case of Lebanon, J.R. Desaunettes in the case of Greece and P.P. Bottner in the case of South France. In every country, weathered products and soils were studied according to the variations in landscapes and climates. This pointed out the influence of drainage, mean annual rainfall and largeness of dry season. The detailed description of landscapes, weathered products, soils and mechanisms can be found in the following papers: MOROCCO: Millot et al. (1969), Paquet et al. (1969), Ruellan (1971); LEBANON: Lamouroux et al. (1967), Lamouroux (1971), Lamouroux et al. (1972); GREECE: Desaunettes (1971); SOUTH FRANCE: Bottner (1971), Paquet and Bottner (1972).

## I DEGRADATION OF THE COMMON CLAY MINERALS (Illite and chlorite). VERMICULITIZATION

In Morocco, the Bni Sassene Mountains are characterized by fersiallitic soils formed on Secondary flyshs or limestones under a mean annual rainfall between 600 and 1 200 mm. The common clay minerals, i.e. illite and chlorite are transformed into illite-vermiculite. In the Mounts of Lebanon, the calcareous massives give rise to fersiallitic soils: when mean annual rainfall exceeds 1 000 mm, illite transforms into vermiculite with the intermediary stage of illite-vermiculite mixed layers. In Greece, the fersiallitic soils developed on sandstones and shales and the podzolic soils formed on granites show the same evolution up to vermiculite (good drainage, mean annual rainfall higher than 1 000 mm). In the South France, in the fersiallitic soils formed from the Secondary hard limestones of Vercors, illite and chlorite evolve by successive stages toward vermiculite, which is found in the leached podzolic soils; the mean annual rainfall is between 1 000 and 2 000 mm.

The general view is the following. In the well-drained fersiallitic or podzolic soils, under a mean annual rainfall higher than 800 mm, illites and chlorites inherited from parent rocks are subject to a partial hydrolysis leading to illite-vermiculite mixed layers then to vermiculite itself. Chlorite is more vulnerable than illite so that its degradation temporarily protects the latter; then the two minerals evolve together and in a convergent way toward vermiculite. This is the mechanism of the transformation into vermiculite or vermiculitization which was often described (Jackson et al. 1959, 1965; Gjems, 1960, 1967; Camez, 1962; Millot et al., 1965; Tardy, 1969, etc.).

The process is the following(\*):



## II DEGRADATION - AGGRADATION OF COMMON CLAY MINERALS (Illite and chlorite). MONTMORILLONITIZATION

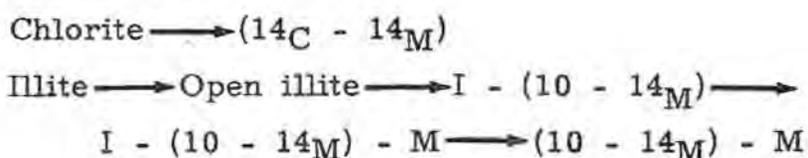
When drainage and mean annual rainfall decrease, the degradation of clay minerals by means of leaching of soluble ions goes on but the amount of silica increases in solutions. Silica is fixed by clay minerals. Illite and chlorite are transformed into mixed layers of illite-montmorillonite type.

(\*) See Lucas' nomenclature in Lucas (1962).

In Morocco, on the flanks of mountains, at a lower altitude, and under a mean annual rainfall between 400 and 500 mm, the fersiallitic soils show a strong calcareous accumulation and the inherited illite is degraded and gives rise to illite-montmorillonite mixed layers. In Lebanon, when mean annual rainfall is lower than 1 000 mm, the illite-montmorillonite mixed layers are found in the badly drained karstic pockets, in the hydrated brown soils of the mountains and in the red soils of the piedmonts, where the drainage is slower. In Greece, in fersiallitic soils developed from calcareous or basic rocks, illite and chlorite transform into "swelling mixed layers", when drainage is slower and mean annual rainfall is lower. In Languedoc (South France), where more calcic fersiallitic soils take place, a tendency to montmorillonitization can be pointed out, in the form of the stage I - (10 - 14<sub>M</sub>).

In these cases, the interstitial solutions circulating around the clay minerals are desaturated in the most soluble ions such as potassium, magnesium and iron, but relatively saturated in silica, as compared with TOT lattices. This results in the mixed transformation phenomena called "degradation - aggradation" by Tardy (1969) and Paquet (1970).

The process is the following:



### III AGGRADATION OF ILLITE

In the semi-arid or arid lowlands, the solutions brought during the humid season get concentrated during the dry season. In Morocco, in the Triffa or Zebra Plains, it is noted that illite is less open and mixed layers occur less abundantly in the "isohumic" soils than in the material which gave rise to them. And this takes place so much as climates are more arid. The confined environments allow the ions to enter again the illitic structures, which became better crystallized as shown by X-ray diagrams, and electron microscope. This is the phenomenon of transformation by aggradation.

### IV NEOFORMATION OF MONTMORILLONITE

When coming to the badly watered and badly drained lowlands, where a humid season bringing ions in solution alternates with a dry season concentrating the latter, we can point out the authigenesis of montmorillonite.

In Morocco, the neoformation of montmorillonite was not observed in the Triffa and Zebra Plains. But in the Bekaa Plain (Lebanon), the red soils on the piedmonts show a very poor drainage, strong calcareous crusts and the large predominance of well crystallized montmorillonite in the clay fraction. The ions originating from the hydrolyses on highlands have migrated towards the plain, where they are concentrating during the dry season, giving rise to authigenic montmorillonites. These montmorillonites are to be added to the badly crystallized ones originating from the transformation of illites. This mechanism of montmorillonite authigenesis is obvious and very important during the weathering of basalts in Lebanon: the hydrolysis of basaltic glasses directly provides the ions necessary to neoformations; these neoformed montmorillonites are magnesio-ferriferous (Paquet, 1970). Likewise in Greece, the direct neoformation of montmorillonite can be observed from crystalline rocks rich in alkaline-earthly ions, such as andesites and ophiolites.

#### V NEOFORMATION OF ATTAPULGITE

In arid plains, where very thick calcareous encrustations and crusts are found, a new clay mineral takes place: attapulgite. In Morocco, in the calcareous encrustations and crusts occurring in the chesnut soils of the Triffa Plain and in the brown soils of the Zebra Plain, attapulgite represents 100% of the clay fraction. In Lebanon, in the northern part of the Bekaa Plain, calcareous encrustations and crusts provide the same results. Nor in Morocco neither in Lebanon, is attapulgite present in the rocks of highlands or in the soils of mountains or hills. Thus, it is impossible for this clay mineral to be inherited: it is neoformed in situ.

The problem of soil attapulgitic clarifies. It was shown that attapulgite is unstable in soils when mean annual rainfall exceeds 300 mm: in fact, attapulgite gets hydrolysed and gives rise to montmorillonite (Barshad et al., 1956; Paquet, 1961; Yaalon et al., 1966; Garcia Rodriguez et al., 1967; Paquet et al., 1969; Paquet, 1970). The same phenomenon was observed as for sepiolite (Sanchez Camazano and Garcia Rodriguez, 1971). In contrast, in desertic climates, attapulgite was several times described in soils (see references in Paquet, 1970). But often this clay mineral was already present in parent rocks, so it must be considered as inherited and not as neoformed. The neoformation, however seemed to be likely in Irak (Al Rawi and Sys, 1967) and connected to the formation of calcareous crusts in New-Mexico (Vanden Heuvel, 1966). Here it is proved that attapulgite is neoformed under arid climates in calcareous encrustations and crusts of steppe soils.

## VI CONCLUSION

The mediterranean landscapes show a very large scope in the evolution of clay minerals.

1. Under a mean annual rainfall of some 1 000 mm and with a good drainage, common clay minerals, illite and chlorite evolve by subtraction, giving rise to illite-vermiculite mixed layers, then to vermiculite. This is the degradation towards vermiculite.

2. Under a mean annual rainfall about 500 mm, and with a poorer drainage, illite and chlorite evolve by subtraction (soluble ions) and addition (silica), giving way to illite-montmorillonite mixed layers. This is the degradatio-aggradation towards montmorillonite.

3. Under a mean annual rainfall lower than 300 mm, illites tend to contract and mixed layers to reconstruct by fixation of ions previously lost. This is the phenomenon of aggradation.

4. Under a mean annual rainfall of some 300 to 500 mm, in the lowlands where humid seasons alternate with dry seasons, the ions brought during humid season get concentrated during dry season and authigenesis of montmorillonite takes place. This is the neoformation of montmorillonite.

5. Under arid climates, in the lowlands where mean annual rainfall is lower than 300 mm and where thick calcareous crusts take place, attapulgitic is neofomed and its amount represents 100% of the clay fraction in the crusts. This is the neoformation of attapulgitic.

In summary, the leaching environment of highlands induces the transformation of silicates by subtraction or degradation. In contrast, in lowlands wherein the ions originating from the hydrolyses of highlands are brought and where the environment is confined, silicates evolve by addition: the mechanisms are aggradation and neoformation.

## REFERENCES

- AL RAWI, G.J. and SYS, C. (1967): A comparative study between Euphrates and Tigris sediments in the Mesopotamian flood plain. *Pédologie*, Gand 17, 187-211.
- BARSHAD, I., HALEVY, E., GOLD, H.A. and HAGIN, J. (1956): Clay minerals in some limestone soils from Israël. *Soil.Sci.* 81, 423-437.
- BOTTNER, P. (1971): La pédogenèse sur roches mères calcaires dans une séquence bioclimatique méditerranéo-alpine du Sud de la France. Thèse Sci. Montpellier, ronéo, 296p. et Mém. Serv. Carte géol. Als. Lorr., France (in press).
- CAMEZ, T. (1962): Etude sur l'évolution des minéraux argileux dans les sols des régions tempérées. Mém. Serv. Carte géol. Als. Lorr., France 20, 90 p.

- DESAUNETTES, J.R. (1971): Sols rouges fersiallitiques sur micaschistes en Grèce. *Science du Sol* 2, 37-49.
- GARCIA RODRIGUEZ, A., FORTEZA BONNIN, J., SANCHEZ CAMAZANO, Ma. and MARTIN PATINO, Ma.Ta. (1967): Estudio de suelos de la Armuna, comarca castellana de suelos mediterráneos. *C.R. Conf. Sols Médit.*, Madrid 1966, 107-126.
- GJEMS, O. (1960): Some notes on clay minerals in podzol profiles in Fennoscandia. *Clay Min. Bull.* 4, 203-209.
- GJEMS, O. (1967): Studies on clay mineral formation in soil profiles in Scandinavia. *Medd. Norsk Skogforssøksvesen* 81, XXI-4, 303-415.
- X JACKSON, M.L. (1959): Frequency distribution of clay minerals in major great soil groups as related to the factors of soil formation. *Clays and Clay Minerals* (6th Nat. Conf., 1957), 133-143.
- ✓ JACKSON, M.L. (1965): Clay transformation in soil genesis during the Quaternary. *Soil Sci.* 99, 15-22.
- LAMOUREUX, M., PAQUET, H., PINTA, M. and MILLOT, G. (1967): Notes préliminaires sur les minéraux argileux des altérations et des sols méditerranéens du Liban. *Bull. Serv. Carte géol. Als. Lorr.*, France 20, 277-292.
- LAMOUREUX, M. (1971): Etude des sols formés sur roches carbonatées. Pédogenèse fersiallitique au Liban. Thèse Sci. Strasbourg et Mém. Serv. Carte géol. Als. Lorr., France (in press).
- LAMOUREUX, M., PAQUET, H. and MILLOT, G. (1972): Evolution des minéraux argileux dans les sols du Liban. *Pédologie*, Gand (in press).
- LUCAS, J. (1962): La transformation des minéraux argileux dans la sédimentation. Etudes sur les argiles du Trias. Mém. Serv. Carte géol. Als. Lorr., France 23, 202 p.
- ✓ MILLOT, G., LUCAS, J. and PAQUET, H. (1965): Evolution géochimique par dégradation et aggradation des minéraux argileux dans l'hydrosphère. *Geol. Rundsch.* 55, 1-20.
- MILLOT, G., PAQUET, H. and RUELLAN, A. (1969): Néof ormation de l'attapulгите dans les sols à carapaces calcaires de la Basse Moulouya (Maroc oriental). *C.R. Acad. Sci. Paris*, 268-D, 2771-2774.
- PAQUET, H. (1961): Etude de la fraction argileuse de quelques sols d'Afrique. Thèse 3<sup>e</sup> cycle Strasbourg, ronéo, 30 p.
- PAQUET, H., RUELLAN, A., TARDY, Y. and MILLOT, G. (1969): Géochimie d'un bassin versant au Maroc oriental. Evolution des argiles dans les sols des montagnes et des plaines de la Basse Moulouya. *C.R. Acad. Sci. Paris* 269-D, 1839-1842.
- PAQUET, H. (1970): Evolution géochimique des minéraux argileux dans les altérations et les sols des climats méditerranéens et tropicaux à saisons contrastées. Thèse Sci. Strasbourg, 1969 et Mém. Serv. Carte géol. Als. Lorr., France 30, 212 p.
- PAQUET, H. and BOTTNER, P. (1972): La pédogenèse sur roches mères calcaires tendres sous les étages bioclimatiques montagnard,

subalpin et alpin dans les Préalpes françaises du Sud. *Science du Sol* (in press).

RUELLAN, A. (1971): Contribution à la connaissance des sols des régions méditerranéennes. Les sols à profil calcaire différencié des plaines de la Basse Moulouya (Maroc oriental). Thèse Sci. Strasbourg 1970 et Mém. O.R.S.T.O.M. 54, 302 p.

SANCHEZ CAMAZANO, M. and GARCIA RODRIGUEZ, A. (1971): Atapulgita y sepiolita en suelos sobre sedimentos calizos de Salamanca, España. *An. Edaf. y Agrobio.* 30, 357-373.

TARDY, Y. (1969): Géochimie des altérations. Etude des arènes et des eaux de quelques massifs cristallins d'Europe et d'Afrique. Thèse Sci. Strasbourg et Mém. Ser. Carte géol Als. Lorr., France 31, 199 p.

VANDEN HEUVEL, R.C. (1966): The occurrence of sepiolite and attapulgite in the calcareous zone of a soil near Las Cruces, New Mexico. *Clays and Clay Minerals* (13rd Nat. Conf., 1964), 193-207.

YAALON, D.H., NATHAN, Y., KOYUMDJISKY, H. and DAN, J. (1966): Weathering and catenary differentiation of clay minerals in soils on various parent materials in Israël. *Intern. Clay Conf. Jerusalem* 1, 187-198.



## DISTRIBUTION AND GENESIS OF IMOGOLITE IN VOLCANIC ASH SOILS OF NORTHERN KANTO, JAPAN

S. Aomine and C. Mizota

Faculty of Agriculture, Kyushu University, Fukuoka, Japan

**ABSTRACT.** - The pattern of the occurrence of imogolite was investigated on volcanic ash soils in the Northern Kanto Plain. Imogolite occurs as networks of fibre-like particles covering soil grains or filling interstices in the soils. It coexists always with allophane, and very often with gibbsite, but never with halloysite. Imogolite is mostly scarce in the A<sub>1</sub>-horizon of the soils and increases down the profile to a layer in the B or C-horizon, then rapidly decreases with depth and finally disappears. Halloysite, if any, occurs in further deep layers.

The concentration of Si in the soil solution is small in imogolite-rich layers compared with in halloysite-present layers, but larger than in gibbsite-rich layers. Imogolite appears to be formed from Al and Si ions in the moisture regime on the surface of soil grains or in the interstice of the soils, being its constituents supplied through percolating water.

### INTRODUCTION

Since the name of imogolite was given to a fibre-like mineral discovered in Ando soils from Japan (Yoshinaga and Aomine, 1962) the mineral has been reported in weathered pyroclastic materials from various parts of Japan and also from West Germany (Jaritz, 1967), Chile (Besoain, 1969; Aomine et al., to be published), and Papua (Greenland et al., 1969). Sieffermann and Milot (1969) presented a photograph of imogolite in Andosols developed from recent basaltic rocks in Cameroon, and more recently Wada et al. (to be published) found imogolite in saprolite of basalt in Maui, Hawaii. Imogolite seems to be of a unique structure (Wada

and Yoshinaga, 1968; Russell et al., 1969; Wade et al., 1970) and to be closely genetically related to allophane (Yoshinaga and Aomine, 1962; Wada, 1967) and to gibbsite (Yoshinaga and Yamaguchi, 1970).

The present paper discusses the genesis of imogolite in pyroclastic materials, presenting the results of an investigation on the distribution of imogolite in Ando soils in the Northern Kanto Plain.

## EXPERIMENTAL

A field survey was carried out in an area of about 36 x 45 km<sup>2</sup> around Utsunomiya (139°55'E, 36°33'N), where four beds of pumice (from above, Shichihonzakura, Imaichi, Kanuma and Maoka have intervened the profiles of Ando soil. Since imogolite is present as gel-like films in the pumice beds, if any, the mineral can be detected macroscopically in the beds without difficulty. And the occurrence of halloysite in the pumice beds is easily noticed with its appearance of grayish color and stickyness. Sixty samples were collected from 9 profiles shown in Fig. 1.

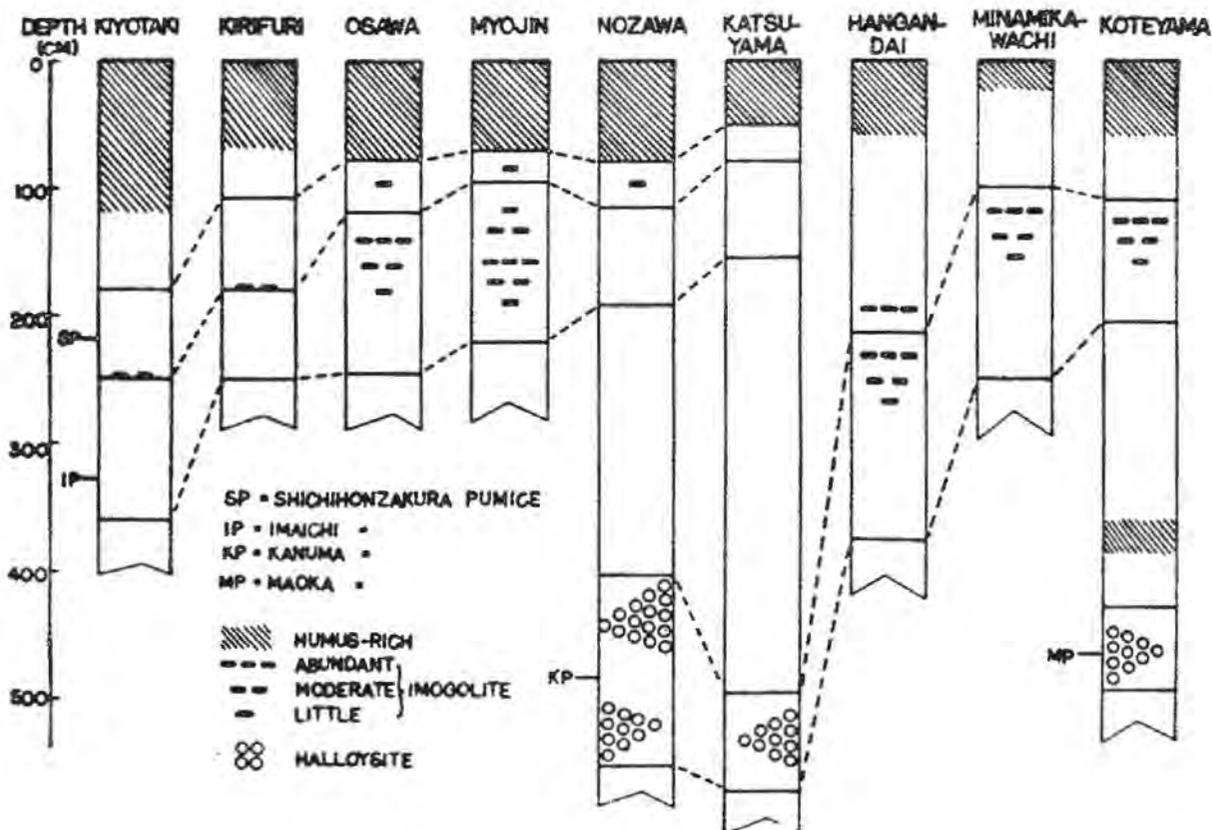


Figure 1. Diagrams of sampling soil profiles.

A quantitative determination of imogolite and gibbsite contents was made by differential thermal analysis, measuring the area of the endothermic peaks at 420 and 300°C, characteristic to respective minerals. The differential thermal analysis was carried out at a heating rate of 20°C/min. in a nitrogen atmosphere, using air-dried, untreated samples and a Thermoflex of Rigakudenki Co. Imogolite was determined by this method as low as 2% on the basis of oven-dried original sample. The samples containing imogolite below this limit were, prior to the analysis, treated to concentrate it by the removal of organic matter and coarse fraction. The removal of allophane for this purpose would be preferable to others for allophanic soils. This method will be reported in a separate paper.

## RESULTS AND DISCUSSION

The Shichihonzakura pumice bed almost always lies on the Imaichi pumice bed in the northern part of the area under survey (Fig. 1). The occurrence of imogolite in this bed appears anomalous, being present or absent even within a small area.

Imogolite also occurs anomalously in the Imaichi pumice. In some places, the mineral is most abundant in the upper part of the bed, decreasing with depth, whilst in other places, it occurs most abundantly in the middle part of the bed. At particular places, Kiyotaki and Kirifuri, the abundant film of imogolite can be observed in the boundary zone of about 5 cm thick, of the Shichihonzakura and Imaichi beds.

The Kanuma pumice bed is covered with an Ando soil which tends thin toward the east and the south. In the northern part of the area, the Ando soil is moreover covered with the Imaichi pumice, the Shichihonzakura pumice and another Ando soil successively. Thus, weathering conditions in the Kanuma pumice bed should be different with places from the north to the south as well as from the west to the east. In this connection, it is noticeable that the imogolite film can be seen only in the Kanuma pumice underlain by the surface Ando soil and that halloysite is detected in the same pumice below the Imaichi pumice bed. For example, halloysite patches are observed in the Kanuma pumice at Nozawa, Katsuyama and Myojin, while imogolite films are abundant in the same pumice at Hangandai and Minamikawachi (Fig. 1).

The Maoka pumice bed is found at a depth of about 400 cm in the eastern part of the area, being covered successively with a buried Ando soil, the Kanuma pumice and the surface Ando soil. Its major clay minerals are allophane and halloysite, resembling the Kanuma pumice bed below the Imaichi pumice.

The imogolite film is not uniformly distributed in the profile of the Kanuma pumice bed. The film is generally most abundant in

the upper part of the bed and decreases with depth as shown in Fig. 1 and Table I. Where the film is abundant, weathering of pumice grains is more advanced. A similar relationship can be seen between the amount of the film and the weathering degree in the Shichihonzakura pumice. The films occur exclusively covering the surface of weathered pumice grains or filling interstices in the bed, as described by Wada and Matsubara (1968) for the Kitakami pumice. Some unweathered andesitic rock fragments covered with imogolite films were found in the pumice beds examined, indicating that the films developed on the fragments being the constituents or units of imogolite transported from other parts. It is also to be noted that the layer of maximal imogolite lies below that of maximal gibbsite in the Hangandai profile, suggesting a general weathering trend from imogolite to gibbsite under the condition of this profile.

The imogolite film was found also in weathered volcanic ash materials, although the size of film was smaller and thinner than that in the pumices. It suggests that the networks and bundles of imogolite fibres, often observed in the electron micrographs of the clay fraction of volcanic ash soils, are very likely to be the pieces of imogolite film.

Table I. Contents of imogolite, gibbsite and halloysite of samples

Depth	Im	Gb	Hl	Depth	Im	Gb	Hl	Depth	Im	Gb	Hl
(cm)	(%)	(%)		(cm)	(%)	(%)		(cm)	(%)	(%)	
Myojin			Hangandai				Katsuyama				
0-70	0	0	-	0-60	1.8	1.0	-	0-50	0	0	-
70-95*	<1	0	-	60-90	2.2	9.8	-	50-80*	0	0	-
95-125∩	<1	0	-	90-120	3.8	7.0	-	80-155∩	0	0	-
140-170∩	8	1.8	-	120-150	7.0	1.4	-	155-185	0	0	++
190-220∩	0	0	-	150-180	8.0	0.8	-	195-225	0	0	++
Osawa			180-210	13.0	0	-	235-265	0	0	++	
0-80	0	0	-	210-230#	4.0	0	-	315-345	0	0	++
80-120*	<1	0	-	270-290#	<1	0	-	355-385	0	0	++
120-160∩	4	12.4	-	350-390#	0	0	-	395-425	0	0	++
160-210∩	<1	4.8	-					440-490	0	0	++
210-245∩	0	0.2	-					490-565#	0	0	+++

\* Shichihonzakura pumice, ∩ Imaichi pumice, # Kanuma pumice, Im = imogolite, Gb = gibbsite, Hl = halloysite, - absent, ++ moderate, +++ abundant.

Table I shows the contents of imogolite, gibbsite and halloysite in several samples. As shown in the table, the presence of imogolite is in a close relation with the presence of gibbsite but not with halloysite. Gibbsite occurs as aggregates mostly of silt to fine sand size fraction in the Imaichi pumice. A part of them are embedded in the film of imogolite and others cluster on the film. It may appear that these two minerals have been formed concurrently, alternately or successively in the interstices of the pumice bed. However, it is very unlikely that imogolite and gibbsite different in nature from each other are formed at the same time from the same solution. They might be formed alternately or successively according to conditions in the moisture regime of the interstice, which would be fluctuated or changed with the weather, weathering stage, deposition of new pyroclastic materials on the surface of the soil, and so on. It is noticeable that imogolite and/or gibbsite are not present in the inner part of pumice grains but in the outside of the grains. Here, an assumption that Al is mobile in the soils is needed for elucidation of the formation of imogolite and gibbsite in the interstice of the soils. Eswaran and De Coninck (1971) interpreted the gibbsite formation in voids of basaltic rocks on the assumption that liberated alumina which was perhaps in a gel stage, was mobile and could be transported. This interpretation could be employed to the formation of imogolite and gibbsite in the Ando soil, although no evidence has been obtained on the movement of aluminum in the Ando soil.

The samples of pumice as well as volcanic ash containing imogolite do not have halloysite. Halloysite occurs in deeper horizons than imogolite and/or gibbsite. It suggests that halloysite develops in volcanic ashes and pumices through a weathering course different from that for imogolite or gibbsite. The weathering course hereupon depends on conditions such as precipitation, temperature, water permeability, reaction of the soil and the concentration of Si ions in the soil solution.

As shown in Fig. 1, the Kanuma pumice is covered with an Ando soil of which parent materials are very likely to be of the same origin in every part of the area under survey. The mineralogical composition of the fine sand of the Ando soil at Hangandai (0 to 210 cm depth) actually resembles that of the buried Ando soil at Katsuyama (355 to 490 cm depth), indicating the same origin of parent materials of both the soils. It would be worthy to compare clay minerals, soil reaction, and soluble Si content of these samples, in order to consider the relation between the soil condition and the weathering course. The content of soluble Si is evidently low in the soil solution of the Hangandai soil against the Katsuyama soil irrespective of soil pH (Table II). Al-vermiculite, imogolite and gibbsite are predominant in the former soil contrasting the dominance of halloysite and vermiculite in the latter soil (Fig. 2), although a considerable amount of allophane is common to both the soils. A

low concentration of Si ions would mean the predominance of reactive Al for the allophanic soil. Provided that imogolite and gibbsite are formed from respective constituent ions in the moisture regime of the soil, a soil solution low in Si would be favorable to the formation of these Al-rich minerals.

Table II. Si in soil solution, pH of n-KCl soil suspension (1:2.5) and molar ratio of silica to alumina of allophanic clays less than  $0.2 \mu$

Depth	pH	Si	Depth	Si	SiO <sub>2</sub> /Al <sub>2</sub> O <sub>3</sub>
(cm)		(ppm)	(cm)	(ppm)	
Hangandai			Myojin		
0-60	5.1	37	140-170§	7	1.14
90-120	5.8	29	190-220§	25	1.56
120-150	5.5	45	Hangandai		
180-210	5.6	52	210-230#	54	1.42
Katsuyama			270-290#	63	1.67
155-185	5.1	63	350-370#	88	1.90
235-265	5.4	95	Minamikawachi		
315-345	5.3	68	100-130#	22	1.41
395-425	5.4	86	220-250#	52	1.59
			Nozawa		
			400-500#	61	1.71

§ Imaichi pumice, # Kanuma pumice.

Soil solution was prepared from the suspension of fresh samples (soil: 0.05M-NaCl = 1:5, pumice: distilled water = 1:5).

As already mentioned, the film of imogolite is confined to the surface of grains or voids of the pyroclastic materials, and no imogolite has been found within the grains. Weathered pumice grains themselves are composed of predominant allophane of which molar ratio of silica to alumina is in direct proportion to the concentration of Si ions in the soil solution as shown in Table II. The correlation coefficient between these two values was  $+0.96 \pm 0.02$ . Allophane, X-amorphous Al-silicates various in the molar ratio of silica to alumina, is an intermediary product chiefly from glass in the weathering course of pyroclastic materials under a humid climate. Allophane of which components, Al and Si ions, are highly reactive, is apt to release and adsorb Si ions being dependent upon the Si con-

centration in the soil solution. Thus, allophane may develop into gibbsite ( $\text{Si}/\text{Al} = 0$ ) under desilication and also into halloysite ( $\text{Si}/\text{Al} = 1$ ) under resilication. Either of these crystalline minerals or both are always found in old Ando soils.

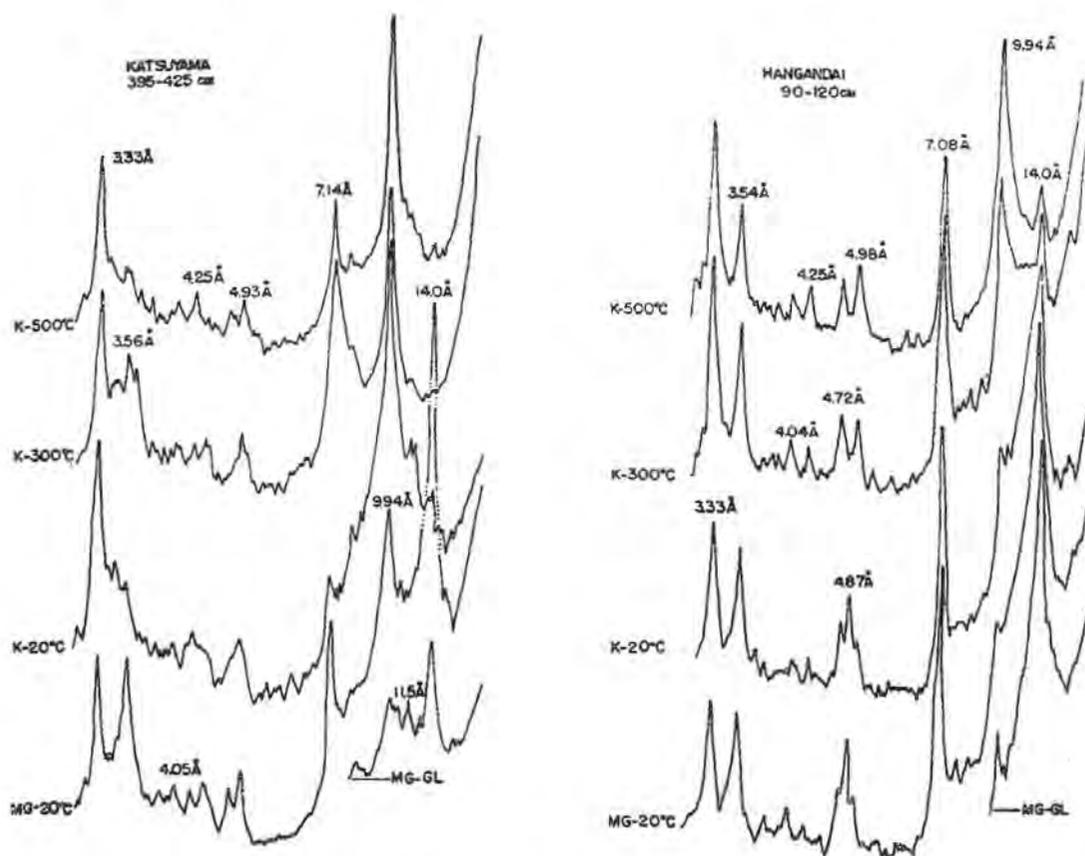


Fig. 2. X-ray diffraction patterns of  $2 \mu$  clays (parallel orientation) MG-GL: Mg-saturated and glycerol-solvated, MG-20°C: Mg-saturated and air-dried at 20°C, K-20°C: K-saturated and air-dried at 20°C, K-300°C: K-saturated and oven-heated at 300°C, K-500°C: K-saturated and oven-heated at 500°C.

Imogolite occurs neither in very young Ando soils nor in old ones but in somewhat young Ando soils, suggesting to be a metastable mineral of an intermediate  $\text{Si}/\text{Al}$  (0.5). The pattern of the occurrence of imogolite films in the soils suggests that imogolite is formed from Al and Si ions in the moisture regime on the surface of grains or in voids of the soils, being constituent ions supplied through percolating water. A large non-capillary porosity, an ample supply of Al ions and water, and a suitable concentration

of Si ions in the soil solution would be necessary for the formation of imogolite in the soil. Such conditions are often provided in comparatively upper layers of young Ando soils under humid climates. The environment of gibbsite formation appears to be very similar to that for imogolite, excepting a more low concentration of Si ions in the soil solution.

#### REFERENCES

- AOMINE, S., INOUE, A. and MIZOTA, C.: Imogolite of Chilean volcanic ash soils. (to be published).
- BESOAIN M., E. (1969): Imogolite in volcanic ash soils of Chile. *Geoderma*. 2, 151-169.
- ESWARAN, H. and DE CONINCK, F. (1971): Clay mineral formations and transformations in basaltic soils in tropical environments. *Pedologie*. 21, 181-210.
- GREENLAND, D.J., WADA, K. and HAMBLIN, A. (1969): Imogolite in a volcanic ash soil from Papua. *Australian J. Sci.* 32, 56-58.
- JARITZ, G. (1967): Ein Vorkommen von Imogolit in Bimsboeden Westdeutschlands. *Z. Pflanzenernaehr. Dueng. Bodenk.* 117, 65-77.
- RUSSELL, J.D., MCHARDY, W.J. and FRASER, A.R. (1969): Imogolite: a unique aluminosilicate. *Clay Minerals*, 8, 87-99.
- SIEFFERMANN, G. and MILLOT, G. (1969): Equatorial and tropical weathering of recent basalts from Cameroon: allophane, halloysite, metahalloysite, kaolinite and gibbsite. *Proc. Intern. Clay Conf.* 1969, Tokyo. 1, 417-430.
- WADA, K. (1967): A structure scheme of soil allophane. *Am. Mineralogist*. 52, 670-708.
- WADA, K. and MATSUBARA, I. (1968): Differential formation of allophane, "imogolite", and gibbsite in the Kitakami pumice bed. *Trans. 9th Intern. Congr. Soil Sci.*, Adelaide. 3, 123-131.
- WADA, K. and YOSHINAGA, N. (1968): The structure of "imogolite". *Am. Mineralogist*. 54, 50-71.
- WADA, K., YOSHINAGA, N., YOTSUMOTO, H., IBE, K. and AIDA, S. (1970): High resolution electron micrographs of imogolite. *Clay Minerals*. 8, 487-489.
- WADA, K., HENMI, T., YOSHINAGA, N. and PATTERSON, S.H.: Imogolite and allophane formed in saprolite of basalt on Maui, Hawaii. (to be published).
- YOSHINAGA, N. and AOMINE, S. (1962): Imogolite in some Ando soils. *Soil Sci. Plant Nutri.* (Tokyo). 8, 114-121.
- YOSHINAGA, N. and YAMAGUCHI, M. (1970): Occurrence of imogolite as gel film in the pumice and scoria beds of western and central Honshu and Hokkaido. *Soil Sci. Plant Nutr.* (Tokyo). 16, 215-223.

## CLAY MINERALOGY OF SOILS ON ULTRABASIC ROCKS FROM SABAH, BORNEO

H. Eswaran and C. Sys

Geological Institute, University of Ghent,  
Rozier 44, Ghent, Belgium

**ABSTRACT.** - The clay mineralogy of an Inceptisol, Alfisol and an Oxisol formed on Ultrabasic rocks has been studied with different techniques in order to evaluate the mineral transformations ensuing. The Inceptisol, with a clay mineral association of nontronite and kaolinite, shows no changes with depth. In the Alfisol, the rock has weathered to produce nontronite, chlorite and kaolinite; destruction of the 2:1 minerals results in a relative accumulation of kaolinite and goethite in the surface horizons. In both the profiles, significant amounts of amorphous silica are present. The saprolite zone of the Oxisol has antigorite, talc, nontronite and traces of kaolinite and goethite. In the oxic horizon, however, goethite forms more than 50%, gibbsite about 20% and the remaining clay is kaolinite and traces of nontronite. Amorphous silica forms about 10% in the saprolite zone, is absent in the oxic horizon and small amounts are present in the Al-B1 horizons.

Studying the clay mineral composition and distribution, it has been concluded that these are mainly due to the physiographic position of the profiles which determines the amount and rate of water percolating down the profiles. In the saprolite zone nontronite is being formed; the absence of saponite is explained in terms of the competitive effect of iron. The magnesium is partly employed for the formation of chlorite. In the oxic stage of weathering, the 2:1 clays and perhaps also the kaolinite is being destroyed, the aluminum crystallizes as gibbsite, the iron as goethite, the titanium as rutile and silica is lost by leaching. The soil clay is thus dominated by oxides or oxyhydrates.

## INTRODUCTION

Soils on Ultrabasic rocks being derived from magnesium minerals or alteration products thereof are characteristically the most easily weathered in the tropics. Compared to other parent materials of similar age or even older, these soils are impoverished of their nutrients much more easily and rapidly and further due to the nature of the parent material, they also tend to accumulate trace elements (nickel, chromium and cobalt) in significant quantities and sometimes of the order of a few percent (Soane et al., 1959; Schellmann, 1964). Such properties make these soils undesirable for agricultural practises and as such form one of the problematic soils of the humid tropics.

From a point of view of soil genesis, these soils are very interesting. The parent material has an unique mineralogical association unlike most other residual parent materials where feldspars tend to dominate and influence the weathering products. The objective of this study is to contribute to the mineralogical transformations ensuing during the genesis of these soils.

## MATERIALS AND METHODS

The soils were sampled from the State of Sabah of Malaysia. Profile characteristics and micromorphological studies of these soils will be given elsewhere. The rocks are essentially early Pleistocene formations; petrographically, the original rock was perhaps medium-grained and harzburgitic in composition prior to serpentinisation. There are relicts of orthopyroxene, olivine and minor amounts of chromium spinel (picotite). The serpentine minerals are antigorite and chrysotile.

Soil formation on this parent material is mainly a function of the physiographic position. Profile M14, an Inceptisol has been sampled on a relatively steep slope of the ridge. The second profile, Profile M5 an Alfisol, is on a more undulating to flat landscape. The serpentinised rock lies unconformably on hard andesite and due to the impervious andesitic rock below, water percolation through the profile is retarded. Consequently, the lower horizons of these soils are not impoverished of bases. The third profile, R1 an Oxisol, is present on a very flat excessively drained ridge.

The soils were sampled according to pedogenetic horizons. Where the horizons recognized in the field were deep, more than one sample per horizon was taken. Clays ( $< 2\mu$ ) were separated after removal of organic matter with hydrogen peroxide, using a 2% solution of sodium carbonate for dispersion and a 2% solution of hydrochloric acid for flocculation.

The clays were studied first with X-ray diffraction using a Philips instrument with a Cu K $\alpha$  cathode. Free iron oxides were removed with the citrate-dithionite-bicarbonate method of MEHRA et al., (1960) and amorphous materials by the technique proposed by HASHIMOTO et al., (1960). In the latter technique the sodium hydroxide was replaced by potassium hydroxide as finely crystalline minerals tended to be dissolved by the former and less by the latter. X-ray diffraction was performed after each dissolution analysis. The clays were also subjected to thermal analysis using a Du Pont T.G.A., D.T.A. Thermal analyser. As an inert gas was not available, these thermal analyses were performed in air. The iron free clays were also studied with the transmission electron microscope. The scanning electron microscope was also employed for the transformation studies. Some of the clays were also studied with infra-red spectroscopy(\*). The infra-red analysis has been employed only to confirm the observations made with the other techniques. Total analysis on the clays were performed according to the method of PRUDEN et al. (1969). Cation exchange capacity was done by saturating the clay with ammonia and determining the absorbed ammonia by micro-Kjeldahl distillation.

Semi-quantitative estimates of the various clay minerals were made by the procedure of allocation (Jackson, 1965) based on the different analysis performed on the clays.

## RESULTS AND DISCUSSION

### 1. Characterisation and estimation of clay minerals

The X-ray diffractograms of the untreated clays are given in Fig. 1. The presence of kaolinite has been confirmed by thermal analysis and also by the dimethyl-sulfoxide test of GARCIA et al. (1965) where the 7.2 Å peak of kaolinite shifts to 11 Å upon treatment. Nontronite has been confirmed by the Li test of GREENEKELLY (1955) and by infra-red spectroscopic studies of KBr pressed discs. In the latter, nontronite shows a hydroxyl stretching vibration at 3564 cm<sup>-1</sup> and hydroxyl bending vibration at 848 cm<sup>-1</sup>.

The total analysis of the clays is given in Table I where the sample numbers, depth and horizons are also given. In Table II, the free iron content, cation exchange capacity and molar ratios are given. Based on these analysis and the other thermal and differential dissolution analysis, semi-quantitative estimates of the clay mineral composition has been made and the results are given in Table III.

---

(\*) The authors are very grateful to Dr. V.C. FARMER and the Maucaulay Soil Research Institute for the facilities provided to the senior author for the infra-red spectroscopic studies.

Table I. Total chemical composition of the clays. All data expressed as percent

Sample No.	Horizon	Depth (cm)	SiO <sub>2</sub>	Al <sub>2</sub> O <sub>3</sub>	Fe <sub>2</sub> O <sub>3</sub>	TiO <sub>2</sub>	CaO	MgO	MnO	P <sub>2</sub> O <sub>5</sub>	K <sub>2</sub> O	Na <sub>2</sub> O	H <sub>2</sub> O	H <sub>2</sub> O + Total
<u>Inceptisol</u>														
B2441	A <sub>1</sub>	0-18	45.57	20.59	14.52	1.69	1.20	2.42	0.18	0.17	0.08	0.75	2.22	11.53 100.92
B2442	(B)	18-48	47.01	20.34	12.76	1.45	1.41	2.31	0.06	0.06	0.16	0.58	2.47	12.41 101.02
B2443	C	48-80	46.53	13.07	13.38	1.41	0.68	2.43	0.07	0.03	0.22	0.69	2.13	11.91 100.32
<u>Alfisol</u>														
B2422	A <sub>1</sub>	0-19	30.01	18.98	29.34	2.61	0.14	0.79	0.58	0.57	0.03	0.09	3.14	14.17 100.54
B2423	B <sub>1</sub>	19-38	29.59	20.28	27.92	2.13	0.31	0.81	0.34	0.48	0.03	0.26	2.96	15.84 100.96
B2424	B <sub>2t</sub>	38-54	30.86	18.55	26.76	1.70	0.31	1.04	0.21	0.37	0.02	0.18	2.53	16.91 99.44
B2425	B <sub>3</sub>	54-105	37.35	11.84	31.18	0.90	0.23	1.64	0.22	0.32	0.02	0.23	3.04	15.07 102.04
B2427	BC	105-130	39.14	11.44	29.34	0.73	0.12	1.93	0.15	0.26	0.02	0.20	2.87	13.80 100.00
B2428	C	130-145	41.87	8.19	22.34	0.56	0.19	4.83	0.13	0.23	0.03	0.19	4.18	16.12 98.86
B2430	CR	145+	45.12	6.59	20.92	0.41	0.27	5.00	0.08	0.23	0.03	0.22	4.01	16.47 99.35
<u>Oxisol</u>														
B3110	A <sub>1</sub>	0-5	10.48	17.66	51.93	0.79	0.13	0.35	0.32	0.39	0.05	0.08	2.38	17.28 101.84
B3111	B <sub>1</sub>	5-14	8.18	18.14	54.32	0.80	0.05	0.54	0.30	0.48	0.02	0.12	2.21	15.67 100.83
B3112	B <sub>21, ox</sub>	14-40	7.70	18.14	52.88	0.77	0.10	0.34	0.29	0.23	0.03	0.03	2.64	18.36 101.51
B3113	B <sub>22, ox</sub>	40-87	6.77	19.02	54.32	0.83	0.01	0.30	0.22	0.36	0.03	0.03	2.48	16.84 101.21
B3114	B <sub>23, ox</sub>	87-100	6.28	19.11	56.33	0.85	0.01	0.23	0.22	0.25	0.04	0.07	1.70	14.55 99.64
B3115	B <sub>24, ox</sub>	100-160	7.40	17.42	56.75	0.97	0.01	0.21	0.30	0.36	0.02	0.10	2.52	12.84 99.00
B3116	B <sub>3</sub>	At 600 cm	31.59	13.24	34.71	0.35	0.20	5.56	0.16	0.25	0.01	0.32	2.87	10.74 100.00
B3117	CR	At 700 cm	37.28	13.12	24.93	0.35	0.70	7.92	0.15	0.17	0.02	0.44	1.98	11.54 98.60

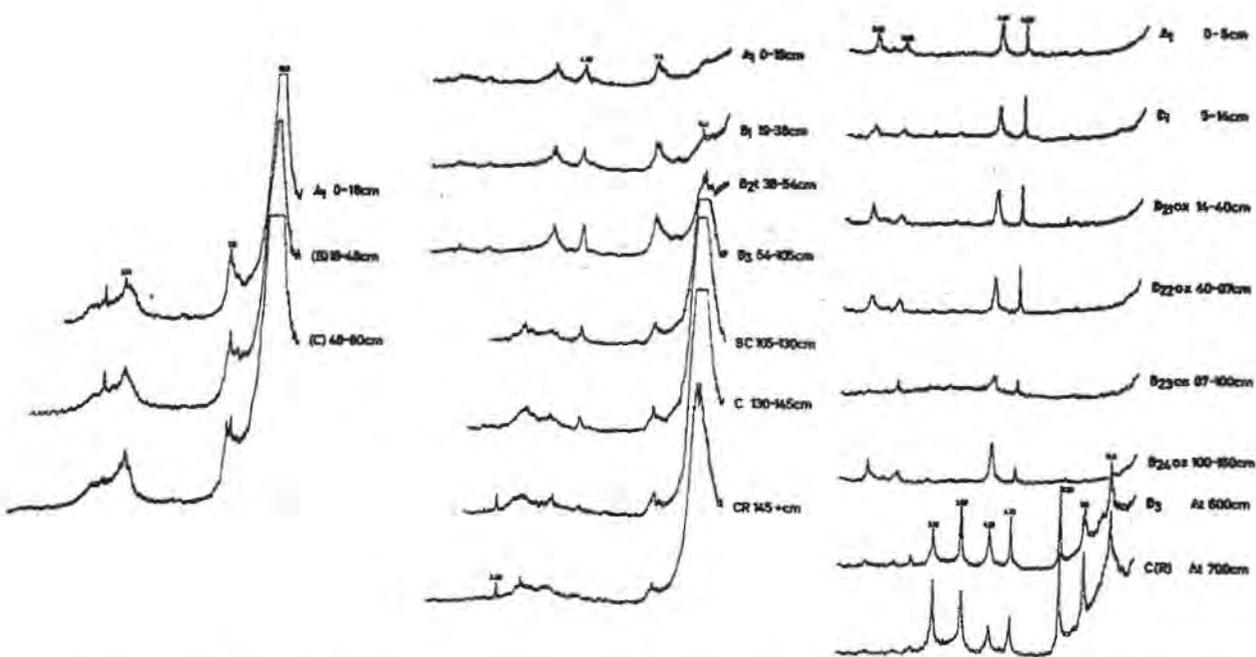


Figure 1. X-ray diffractograms of the untreated clays. From left to right, Inceptisol, Alfisol and Oxisol.

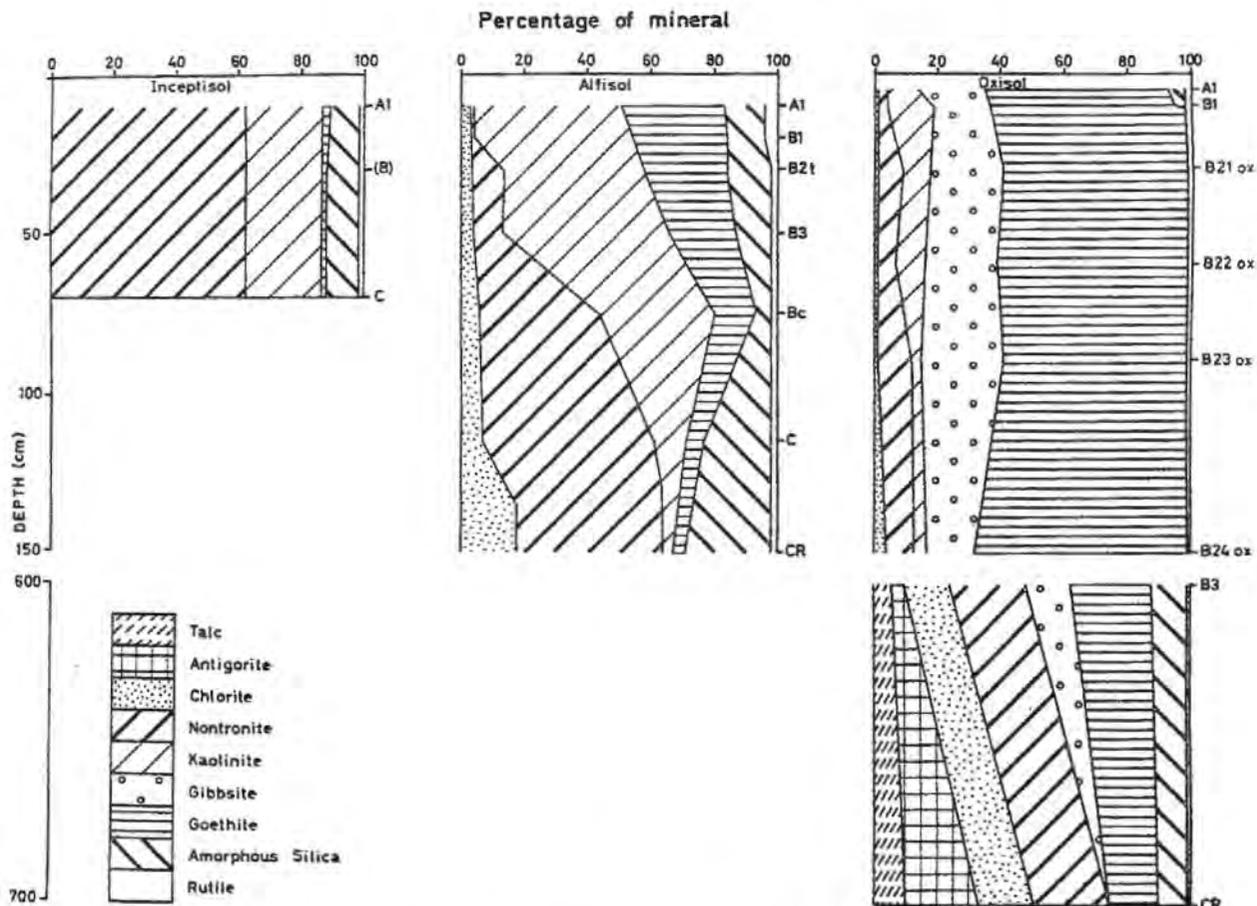


Figure 2. Distribution of clay minerals as a function of depth.

Table II. Free iron, CEC and molar ratios of the clays

Sample No.	Free iron % Fe <sub>2</sub> O <sub>3</sub>	CEC M. eq. 100 g. clay	Molar ratios		
			SiO <sub>2</sub> /Al <sub>2</sub> O <sub>3</sub>	SiO <sub>2</sub> /R <sub>2</sub> O <sub>3</sub>	SiO <sub>2</sub> /MgO
<u>Inceptisol</u>					
B2441	4.08	85.2	3.76	2.59	12.63
B2442	3.38	85.6	3.92	2.80	13.65
B2443	3.03	86.4	3.79	2.69	12.85
<u>Alfisol</u>					
B2422	29.17	30.6	2.68	1.35	25.49
B2423	27.58	32.4	2.48	1.32	24.51
B2424	23.72	48.4	2.82	1.47	19.91
B2425	19.14	56.8	5.35	2.00	15.28
B2427	12.17	65.2	5.81	2.20	13.61
B2428	7.64	74.3	8.68	3.16	5.82
B2430	6.24	80.6	11.62	3.84	6.05
<u>Oxisol</u>					
B3110	51.07	3.2	1.01	0.35	20.09
B3111	53.58	3.8	0.77	0.26	10.16
B3112	50.28	3.6	0.72	0.25	15.19
B3113	52.30	4.2	0.60	0.21	15.14
B3114	52.73	8.4	0.56	0.19	18.32
B3115	52.72	13.6	0.72	0.23	23.64
B3116	25.83	18.3	4.05	1.51	3.81
B3117	17.27	30.2	4.82	2.18	3.16

Table III, and Fig. 2 show that the clays from the three horizons of the Inceptisol are quite similar, with 62% nontronite and 24% kaolinite. There is about 10% amorphous material which is essentially unallocated silica. The amount of free iron is low and the allocated goethite is about 2%. The CEC of the clays is about 85 m.eq. per 100 g.

In the Alfisol, there are distinct changes as a function of depth. The silica-alumina ratio drops from 11 to about 3 indicating an extensive desilicification in the surface horizon. There is a four fold increase in the silica-magnesium ratio due to a considerable loss of magnesium. The sesquioxidic enrichment in the surface horizon is illustrated by the decrease in the silica-sesquioxide ratio. These changes are due to changes in the clay mineral composition. In the CR horizon, nontronite predominates with minor amounts of chlorite

and kaolinite. The nontronite shows a gradual increase with depth though the change from A1-B1 horizons to the B2t is rather abrupt. This is attributed partly to a absolute accumulation of nontronite in the B2t horizon by vertical translocation and also to a destruction of the mineral in the top soil. The changes in unallocated silica (referred to here as amorphous silica) as a depth function is interesting. There appears to be a minimum amount in the BC horizon. The amount of amorphous silica is also higher than in the clays of the Inceptisol. The high amount in the surface horizon is perhaps due to destruction of the 2:1 clays. Most of the silica and alumina released upon weathering recombine to form kaolinite; some

Table III. Percentage allocated mineralogical composition of the clays. Ta = Talc; Ant. = Antigorite; Chl. = Chlorite; Nont. = Nontronite; K. = Kaolinite; Gib. = Gibbsite; Goe. = Goethite; Amor. = Amorphous silica; R. = Rutile.

Sample No.	Ta.	Ant.	Chl.	Nont.	K.	Gib.	Goe.	Amor.	R
<u>Inceptisol</u>									
B2441	0	0	0	62	24	0	3	9	2
B2442	0	0	0	62	24	0	2	10	2
B2443	0	0	0	62	24	0	2	10	2
<u>Alfisol</u>									
B2422	0	0	3	1	47	0	32	13	4
B2423	0	0	3	1	50	0	30	12	4
B2424	0	0	4	10	44	0	26	14	2
B2425	0	0	6	38	22	0	21	11	2
B2426	0	0	7	54	19	0	13	5	2
B2428	0	0	18	46	7	0	6	21	2
B2430	0	0	18	46	3	0	4	27	2
<u>Oxisol</u>									
B3110	0	0	1	3	10	21	58	5	2
B3111	0	0	1	3	15	18	59	3	2
B3112	0	0	1	8	9	23	56	0	1
B3113	0	0	1	6	9	23	58	0	1
B3114	0	0	1	11	3	26	59	0	1
B3115	1	1	1	12	4	22	58	0	1
B3116	6	4	14	24	1	14	27	10	1
B3117	10	23	18	23	0	0	16	10	1

of it is being translocated down the profile whilst the remaining is retained as amorphous gels. The increase in the lower horizons could be attributed to translocation. The CEC shows a progressive increase with depth.

In the Oxisol (Table II), the changes as a function of depth are much more severe. The silica-alumina ratio decreases ten fold from the CR horizon to the oxic horizon but there is a slight increase again towards the surface. The silica-magnesium ratio increases from 3 to 21 and this is due to a decrease in magnesium content from about 8 percent to less than 0.3. Accumulation of iron and aluminum in the oxic horizon causes a marked decrease in the silica-sesquioxide ratios. The cation-exchange capacity (Table II) shows a ten fold decrease from 30 to 3 m.eq. per 100 g. clay. These changes are due to the changes in the mineralogical composition (Fig. 2 and Table III). The CR horizon comprises an association of talc, antigorite, nontronite, chlorite and some goethite. In contrast, in the oxic horizon, only traces of 2:1 silicate clays are present; goethite forms more than 50% of the clay fraction, gibbsite about 20 percent and only minor amounts of kaolinite are present. Amorphous silica is completely absent in the oxic horizon but about 5 percent is present in the A1 and 10 percent in the B3 and CR horizons. Another interesting feature is the slight decrease of gibbsite in the A1 and B1 and increase of kaolinite and amorphous silica in these horizons. This perhaps points to a silicification of gibbsite in the A1 horizon.

## 2. Morphology of the minerals

The clay minerals encountered have been studied with the transmission electron microscope (TEM). The morphology confirmed to the established forms of these minerals (BEUTELSPACHER and VAN DER MAREL, 1968). One exception is the nontronite which does not show a tubular or lath-shaped form as has been reported in literature. These iron-rich montmorillonite minerals or nontronite as termed here are platy with diffuse and curled up edges.

The soil material has also been studied with the scanning electron microscope (SEM). In Fig. 3, the lath-shaped antigorite crystals are to be seen. The laths are arranged to form a platy structure and the plates show a face to face stacking arrangement. Weathering results in a buckling of the plates and the laths (Fig. 3, b). The products of weathering cannot be evaluated. Booklets of talc can also be observed (Fig. 4, a) in different parts of the fracture surface of the CR horizon of the Oxisol. Fig. 4, b shows the alteration of talc. Nontronite appears to form epitactically on the talc crystals. The morphology of the nontronite is observed in the soil material of the C horizon of the Alfisol (Fig. 5). The crystal aggregates have a typical fold on the surface; the edges are diffuse and the surface smooth. No tubular or lath-shaped forms were pre-

sent in any of the profiles. The kaolinite in the Alfisol and Oxisol profiles is generally fine ( $<1\mu$ ) and frequently present as clumps cemented together by the iron oxyhydrates. The goethite crystals in the Oxisol are also too fine to be resolved by the SEM.

### 3. Discussion

The three soils employed in this study represent three stages of weathering on ultrabasic rocks in the humid tropics: Inceptisol (recent stage of weathering), Alfisol (intermediate stage of weathering) and Oxisol (ultimate stage of weathering). The different weathering stages and consequently, clay mineral suites, in these three profiles are primarily due to the physiographic positions of the soils. The recent soils are located on rather steep slopes, water runoff is greater than percolation and consequently leaching is minimal. Clay formation is thus taking place in an environment rich in bases. The Alfisol has a substratum of hard andesitic rock at a depth of 2,5 m. and as a result the lower part of the profile has an environment resembling that of the recent soil. The upper part is however impoverished of bases. The Oxisol is an excessively drained soil on a plateau-like landscape. Leaching is intense and the environment is thus acid.

As observed by WILDEMAN et al. (1968), one of the initial products of weathering is nontronite or iron rich montmorillonite. The rock in this study has about 32% MgO and one could anticipate the formation of saponite. This should be specifically so for the clays of the Inceptisol and Alfisol. Concluding from the present study and that of WILDEMAN et al. (1968), a possible explanation is that weathering of the serpentine minerals also liberates large quantities of iron and in such a situation nontronite is formed in preference to saponite. In these soils however, a greater loss of magnesium is also ensuing through leaching.

WILDEMAN et al. (1968, b) have shown experimentally that magnesium is easily lost by leaching and this is more pronounced in CO<sub>2</sub> containing water. Consequently, the loss of magnesium and the competitive effect of iron is resulting in the formation of nontronite and not saponite. This competitive effect may be more important than a simple capacity and intensity factor suggested by YAALON (1970) and so needs further investigation.

Part of the magnesium that remains is perhaps going into the formation of chlorite. The chlorite (ripidolite) is not present in the Inceptisol but present in small amounts in the Alfisol and the lower part of the Oxisol. Total analysis of the clay of the Inceptisol showed about two percent magnesium but no chlorite has been observed with any of the analytical techniques.

In the solum of the Alfisol, chlorite and nontronite are subject to destruction. The destruction of these minerals liberate silica, alumina and iron. In the Alfisol, kaolinite is formed in large

amounts; during this process, all the alumina is being utilized, while excess silica is mostly lost from the profile. Some of it remains as perhaps amorphous silica gels. This is only a hypothesis and cannot be substantiated. During the allocation of minerals there is always excess silica and water which could not be allocated and so has been indicated in the text as amorphous silica. WILDEMAN et al. (1968) encountered the same problem and they have associated the excess water to the excess silica, as has been done here, but do not mention in what form this could exist in the soil. The excess silica is obvious by preventing the formation of gibbsite as is evidenced by its absence in the Alfisol profile.

The iron released by the destruction of the 2:1 silicate minerals is partly present as amorphous oxyhydrates and as goethite. For convenience, all the iron has been allocated to goethite.

In the solum of the Oxisol, the weathering intensity is so high that removal of silica is as rapid as that of magnesium. Consequently all the silica that is available crystallises as kaolinite; the excess alumina crystallises as gibbsite and the iron as goethite. Amorphous silica is however present in significant quantities in the B3 and CR horizons and this maintains the silica potential necessary to retard destruction of nontronite. About five percent of amorphous silica is also present in the A1-B1 horizons. Compared to the oxic horizon, the A1-B1 horizons have a slightly higher kaolinite content and lower gibbsite content. This seems to suggest a silicification of gibbsite leading to the formation of kaolinite a hypothesis proposed by HARRISON (1933). The present authors contribute to this hypothesis and suggest that the source of silica for this process is from the decomposition of organic matter.

## CONCLUSION

The three profiles represent three pedo-environments and each is characterized by a suite of clay minerals. The pedogenetic horizons represent micro-environments having properties different from the overlying or underlying horizons. In this study, an attempt is made to characterize each of these micro-environments in terms of the clay mineral associations. In the Oxisol for example, the A1 and B1 horizons differ from the oxic horizon by slight silicification of gibbsite. In the oxic horizon the alumino-silicate minerals are being destroyed and the clay is attaining an oxide or oxyhydrate state, i.e. all the aluminum is present as gibbsite, all the iron as goethite or amorphous oxyhydrates, the titanium as rutile and the silica is leached out.

In the Inceptisol environment, silicate clay synthesis is active and this is predominantly 2:1 clays. In the Alfisol, the surface ho-



Figure 3. a) SEM photograph of soil material with Antigorite.  $\times 10,000$ .

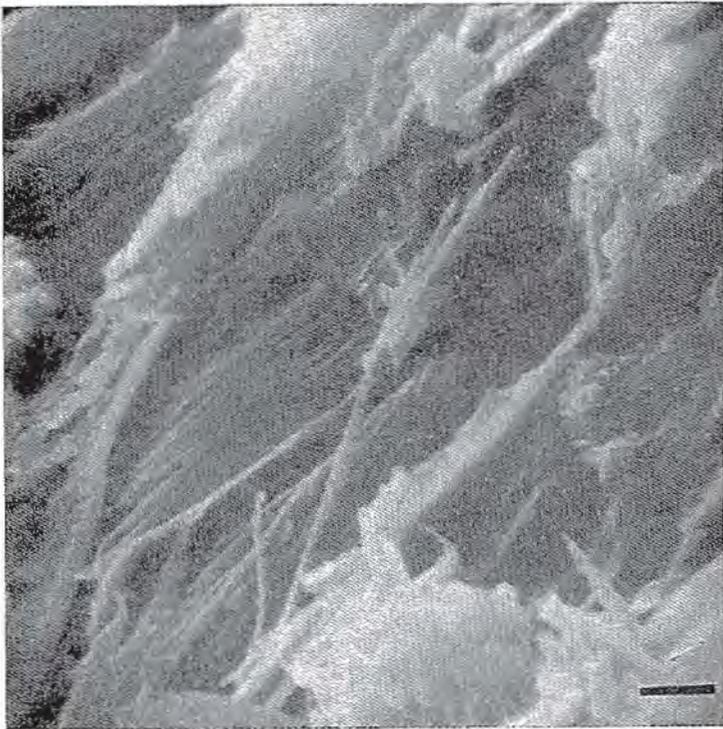


Figure 3. b) An initial stage in the weathering of Antigorite.  $\times 10,000$ .  
Sample from CR horizon of Oxisol.





Figure 4. a) SEM photograph of talc.  $\times 10,000$ .

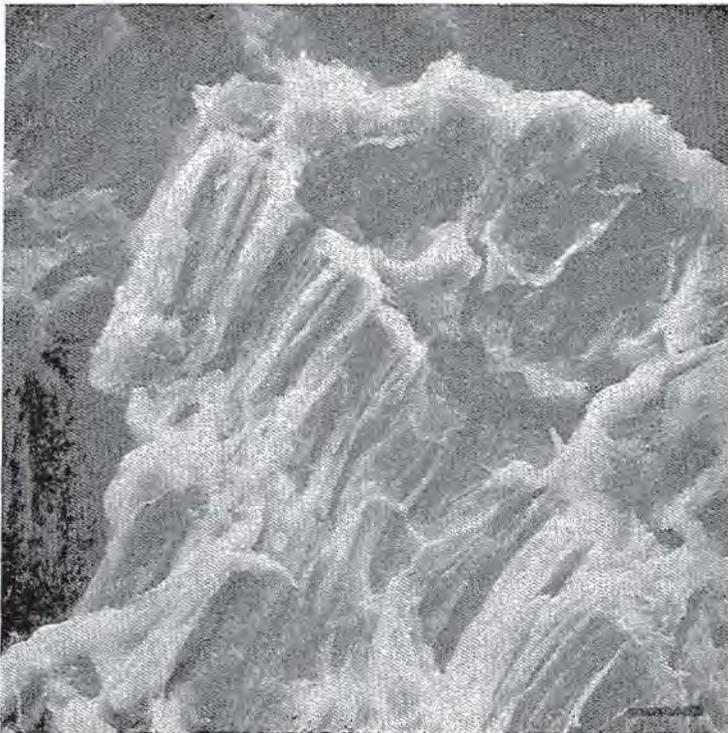


Figure 4. b) Nontronite is present epitactically on talc.  $\times 10,000$ .  
CR horizon of Oxisol.





Figure 5. SEM photograph of matrix of C horizon of Alfisol showing the presence of Nontronite.  $\times 2,500$ .



horizons have an environment conducive to destruction of the 2:1 silicate clays whilst in the subsurface horizons such destructive mechanisms are retarded.

Considering the pattern of transformations in the three profiles, it is evident that the trend is the same but the intensities are different. From this study, the following generalizations can be made.

1. Magnesium is lost much more rapidly than silica during the genesis of these soils.

2. Any remaining magnesium participates in chlorite formation rather than saponite and this is partly because of the competitive effect of iron which is also present in large quantities.

3. The iron enters the silicate lattice to form nontronite and formation of this mineral continues as long as the silica potential is high enough.

4. In slightly acid environments, the 2:1 silicate clays are destroyed; the released iron crystallizes as goethite or remains as amorphous iron oxyhydrate. The silica combines with alumina to form kaolinite and if insufficient alumina is present, the silica is present as amorphous gels or leached out in the profile.

5. In more acid environments, the kaolinite is also being destroyed; silica is leached out and excess alumina crystallizes as gibbsite.

6. If a source of silica is present as from decomposition of organic matter, silicification of gibbsite may occur in the surface horizons.

#### ACKNOWLEDGEMENTS

The authors wish to acknowledge a grant provided by the Ministry of Foreign Affairs, Belgium, which enabled us to undertake the study of the soils of Sabah. We are also very grateful to the Director and members of staff of the Department of Agriculture, Sabah, for their cooperation.

The assistance of Prof. Dr. R. TAVERNIER and our colleagues is appreciated. We wish to thank Miss M. DUCHENE who performed most of the analytical work.

#### REFERENCES

- BEUTELSPACHER, H., and H.W. VAN DER MAREL (1968): Atlas of electron microscopy of clay minerals and their admixtures. Elsevier publ. Co. Amsterdam. 333 pp.
- GARCIA, G.S. and CAMAZANO, S.M. (1965): Adsorption complexes

- of clay minerals with dimethyl-sulfoxide. *Ann. Edafol, Agrobiol.* 24: 495-520. *Soils. Fert.* 29: 2969.
- GREENE-KELLY, R. (1955): Dehydration of the montmorillonite minerals. *Mineral. Mag.* 30, 604-15.
- HARRISON, J.B. (1933): The katamorphism of igneous rocks under humid tropical conditions. Imp. Bureau of Soil Science, Rothamsted Exp. Station, England.
- HASHIMOTO, I. and M.L. JACKSON (1960): Rapid dissolution of allophane and kaolinite-halloysite after dehydration. *Clays and clay minerals* 7, 102-103.
- JACKSON, M.L. (1965): Soil chemical analysis - advanced course. 2nd printing. Published by the author.
- MEHRA, O.P. and JACKSON, M.L. (1960): Iron oxide removal from soils and clays by a dithionite-citrate system buffered with sodium bicarbonate. *Clays and clay minerals*, 7, 317-342.
- PRUDEN, G. and KING, H.G.C. (1969): A scheme of semi-micro analysis for the major elements in clay minerals based on modifications to conventional methods of silicate analysis. *Clay Minerals* 8, 1-13.
- SCHELLMAN, W. (1964): Zur lateritischen Verwitterung von Serpentin. *Geol. Jahrb.* 81, 645-678 (English abstract).
- SOANE, B.D. and SAUNDER, D.H. (1959): Nickel and chromium toxicity of serpentine soils in southern Rhodesia. *Soil Sci.* 88, 322-330.
- WILDEMAN, W.E., M.L. JACKSON and L.D. WHITTIG (1968): Iron-rich montmorillonite formation in soils derived from Serpentine. *Soil Sci. Soc. Amer. Proc.* 32, 787-794.
- WILDEMAN, W.E., M.L. JACKSON and L.D. WHITTIG (1968, b): Serpentine rock dissolution as a function of CO<sub>2</sub> pressure in aqueous solution. *Amer. Mineral.* 53, 1252-1263.
- YAALON, D.H. (1970): On high-iron montmorillonites: Discussion of the "significance of magnesium and iron in montmorillonite formation from basic igneous rocks". *Soil Sci.* 110, 74-76.

ORIGIN AND SPECIFIC STRUCTURAL FEATURES OF CLAY  
MINERALS FROM THE LATERITIC BAUXITES  
IN THE EUROPEAN PART OF THE U.S.S.R.

A. P. Nikitina and B. B. Zvyagin

Academy of Sciences of the U.S.S.R., Moscow, U.S.S.R.

ABSTRACT

Mineral and chemical composition of Lower Carboniferous Lateritic bauxites have been studied, with results allowing two genetic complexes or assemblages of clay minerals to be identified in these bauxites presenting the upper weathering crust zone in phyllite shales. The first genetic complex is composed of the residual minerals which were formed in the course of laterite type weathering, the second one is made up of epigenetic minerals superimposed on bauxites under changed reductive conditions associated with the effect of swampy-lagoonal waters during the pre-transgressive stage of the Lower Carboniferous sea, as well as underground water activity after the bauxites were overlaid by the sedimentary cover.

Kaolinite is the most widespread in the first genetic complex while the dioctahedral  $2M_1$  type mica is much less common. The mixed-layered (chlorite-vermiculite, biotite-montmorillonite) minerals which are composing the lower zones of the weathering crust's profile have not been traced here, owing to the fact of being decayed. In the second genetic complex chamosites are widely distributed, occurred mainly in two generations reflecting the successive stages of their evolution, and together with them, kaolinite (resilicificated) is found.

Identification and structural characteristics of minerals have been made mainly from texture electron diffraction patterns obtained on a high-voltage electronograph at  $V = 350$  kv.

Kaolinites -both residual and epigenetic- are triclinic with an ordered structure, especially the epigenetic one. As chemical analysis has shown the residual kaolinite, unlike the epigenetic one, contains usually notable amounts (up to 1.5%) of  $TiO_2$ , which does corroborate its genetic relation with the weathering crust.

Chamosites of both generations are trioctahedral serpentine-like layer silicates with a semi-random structure. They represent, mostly, some combinations of the monoclinic and orthogonal polytypes in various proportions (structural types A and B, after Zvyagin). In some instances the structural type B does not make its appearance.

Thermographic survey in nitrogen, differently from usual one in oxygen, has revealed two extra effects at 780 and 830° which, for a case of mixture with other clay minerals, does facilitate the diagnostic of chamosites in bauxites. The chemical composition of chamosites is rather unstable. Its dependence on the environments which existed at the time of their formation has been established.

Chamosites of earlier generation were formed without any important amounts either of silica or magnesium being carried in and, therefore, they are richer in aluminium than the later generated chamosites.

All data on chemical components introduced in or carried away from the matter of interest being accounted for, enables us to suggest the following succession in time for those processes which are answerable for the formation of minerals belonging to the second genetic complex: 1) chamotization I, accompanied by the  $Fe^{3+}$  transition into  $Fe^{2+}$ , migration of alumina and a rather insignificant amount of silica being carried in; 2) decoloration of bauxites of  $Fe^{2+}$  evacuation, presumably in the form of complex organic compounds, which improved the quality of bauxites; 3) chamotization II and kaolinization which proceeded with high amounts of silica being washed into the top of bauxites, this deteriorating their quality. Widely distributed epigenetically superimposed minerals are characteristic of bauxite-bearing formations from the Lower Carboniferous Stage.

The establishment of genetic assemblages of clay minerals allows to interpret the origin of bauxites and predict their quality.

## PHASE EQUILIBRIA FOR DIOCTAHEDRAL EXPANDABLE PHASES IN SEDIMENTS AND SEDIMENTARY ROCKS

B. Velde

Laboratoire de Pétrographie  
Université de Paris VI  
9, quai Saint-Bernard - Paris Ve - France

**ABSTRACT.** - It is necessary to establish chemical inter-relations under various geological environments in order to understand the transformations and occurrence of clay minerals. Through a combination of chemical data for the phases concerned and judicious use of available pertinent experimental studies, it is sometimes possible to determine the conditions which are critical to the existence or non-existence of a phase in a given environment. Sepiolite and palygorskite are notable examples.

Combined information using chemical analyses of 19 well characterized illites, 91 montmorillonites and 84 mixed layered dioctahedral minerals from the literature and the results of hydrothermal experimentation on natural and synthetic clay minerals has been used to delineate the major phase relations between these phases, kaolinite and chlorites.

The fully expandable ("montmorillonite") phases form a large compositional range which isolates kaolinite from illite at low temperatures and pressures (sedimentation and early compaction). The following assemblages appear, kaolinite-montmorillonite; mixed layered-illite. Early diagenesis (burial) necessitates the formation of two series of mixed layered minerals, beidellite-illite and montmorillonite-illite. The assemblages kaolinite-beidellite, mixed layered-illite and kaolinite-montmorillonite, mixed layered-illite are dependent upon the existence of a kaolinite-illite tie-line which necessitates the separation of the two types of expandable phases beidellite and montmorillonite.

Addition of chlorite, of variable Mg/Fe content, allows a fourth phase to appear among the phyllosilicates thus completing the census of the most common clay minerals in sedimentary rocks. Through correlation with information from deep bore holes, it is also possible to predict the critical assemblages in the evolution of a series of sediments undergoing burial and thus estimate the pressure - temperature conditions which they have experienced.

## INTRODUCTION

Among the most common clay minerals found in sediments and sedimentary rocks one finds illite, montmorillonites, mixed layered dioctahedral phases, chlorite and kaolinite. It is in fact frequent to find illite, an expanding phase, chlorite and kaolinite in the same rock. What permits four phyllosilicate phases to be commonly associated and what does this mean in terms of the phase equilibria in clay mineral systems?.

If we consider the origin of these minerals it is fairly well established now that the largest part of illite found in such rocks is of diagenetic origin (Dunoyer de Segonzac, 1969) and that kaolinite is most commonly formed as a weathering product or formed diagenetically (Millot, 1964). Montmorillonite and mixed layered phases appear to be present in sedimentary rocks in a regular manner according to the geothermal gradient which they experience and independently of their age (Perry and Hower, 1969; Steiner, 1968; Muffler and White, 1969; Iijima and Utada, 1970; Browne and Ellis, 1970; Dunoyer de Segonzac, 1969; Van Moort, 1971). They thus appear to be responsive to specific physical conditions imposed upon them and would therefore be unlikely to be present as metastable phases in sedimentary rocks. Chlorite occurrence poses a more delicate problem since it is frequently found as a detrital phase in sedimentary materials, but is also known to form on the ocean bottom (Porrenga, 1967 a, b) in estuaries (Rohrlich et al., 1969) and as a product of diagenesis (Millot, 1964). Let us for the moment postpone the analysis of chlorite stability and concentrate upon illite, kaolinite and the expanding phases.

## NATURAL MINERAL COMPOSITIONS

In considering the compositions of natural minerals, one must initially devise a convenient method of comparing between the various compositions through a simplification of the ten or so common chemical components found in the minerals. This can be done as a first approximation by grouping the divalent transition elements plus magnesium ( $3R^{2+}$ ), the trivalent ions  $Al^{3+}$  and  $Fe^{3+}$  ( $2R^{3+}$ ) and the alkaline earth and alkali elements combined with a trivalent ion ( $M^+R^{3+}$ ).  $SiO_2$ ,  $H_2O$  and  $TiO_2$  are considered to be unimportant to the analysis either by their great or insignificant abundance in sediments and sedimentary rocks.

The term  $3R^{2+}$  is used because divalent transition elements and magnesium are present in phyllosilicates in about this number when end-member minerals are formed (talc, phlogopite, serpentine). The same is true for the  $2R^{3+}$  term (kaolinite, pyrophyllite).

$M^+R^{3+}$  is near the ratio of these ions present in micas and feldspars, at least to a first approximation (this excludes the celadonite - glauconite micas which do not enter the considerations here).

Using these elements as coordinates in a triangular plot, the composition of kaolinite forms the  $2R^{3+}$  pole and chlorite is found between this and the  $3R^{2+}$  extreme (Fig. 1). Illite\* forms a compact

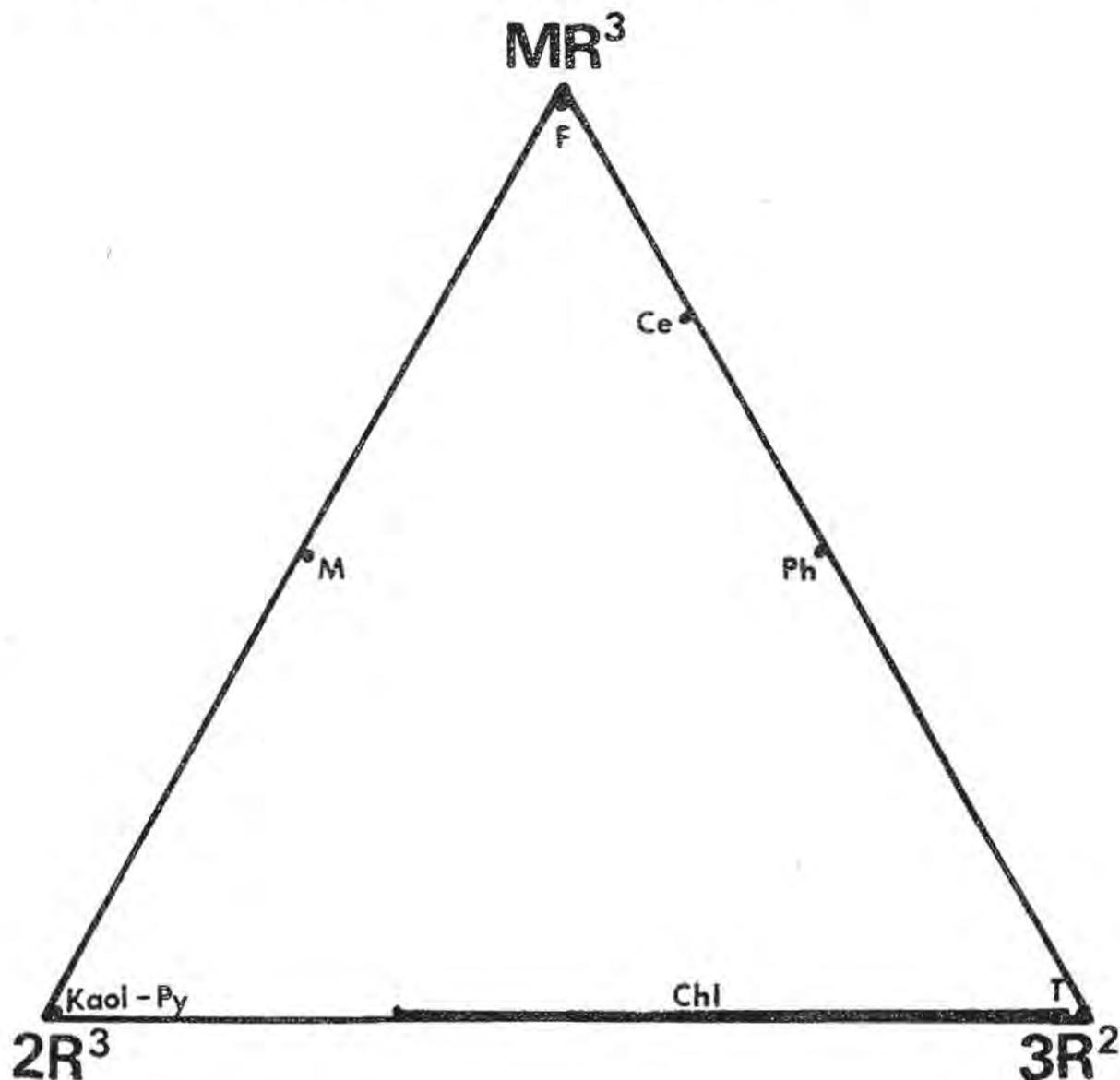


Figure 1. Representation of the ideal compositions of some major phyllosilicate phases in the  $M^+R^3 - 2R^3 - 3R^2$  coordinates.

M = muscovite, paragonite; P = phlogopite; Py = pyrophyllite; Kaol = kaolinite; T = talc; Chl = chlorite, 14 or aluminous 7 Å polymorphs; Ce = celadonite; F = feldspar.

\*See appendix for the references and the norms used to select the chemical analyses used.

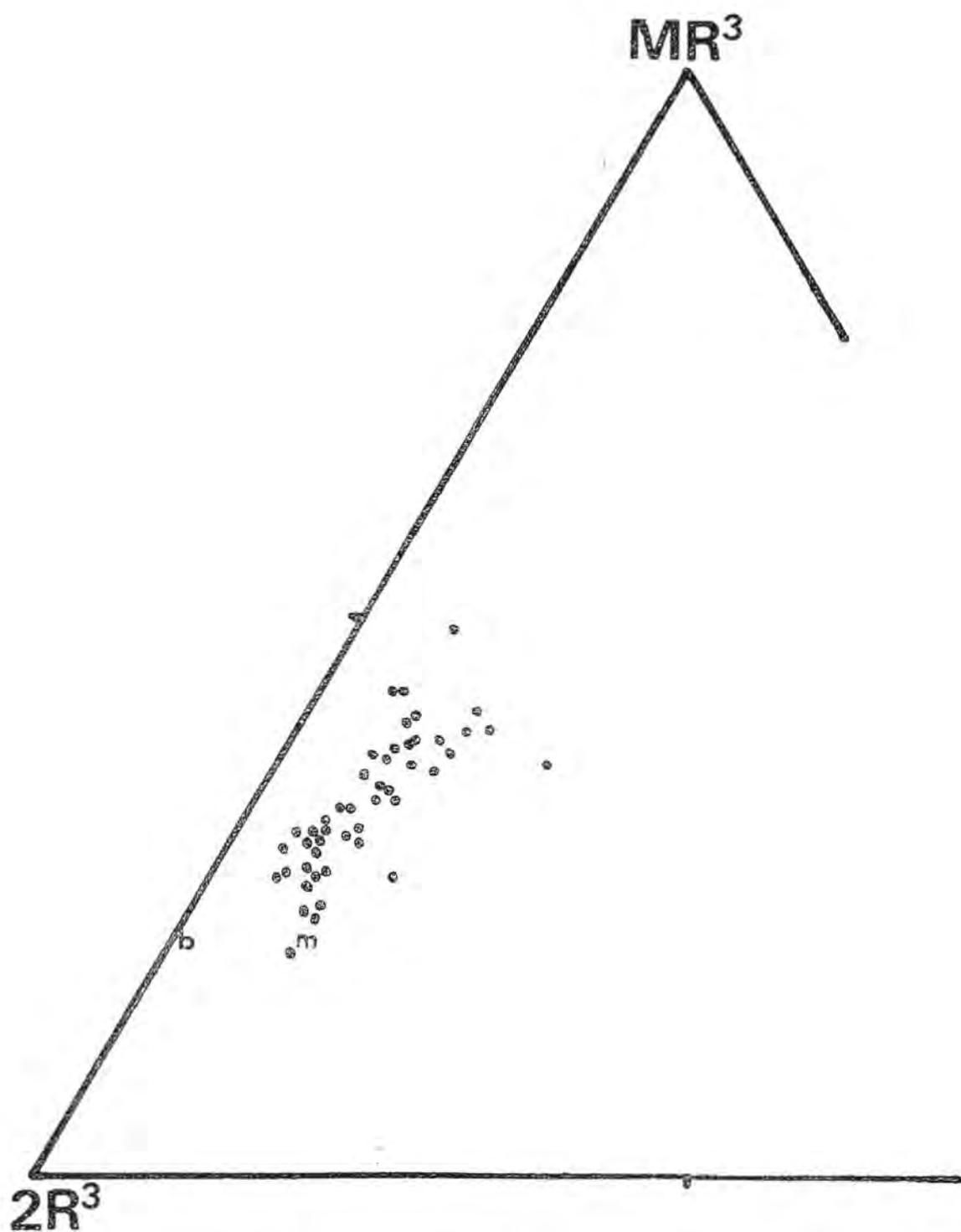


Figure 2. Chemical compositions of natural fully expandable dioctahedral montmorillonites in the  $M^+R^3 - 3R^2 - 2R^3$  coordinates.  
 b = beidellite; m = montmorillonite.

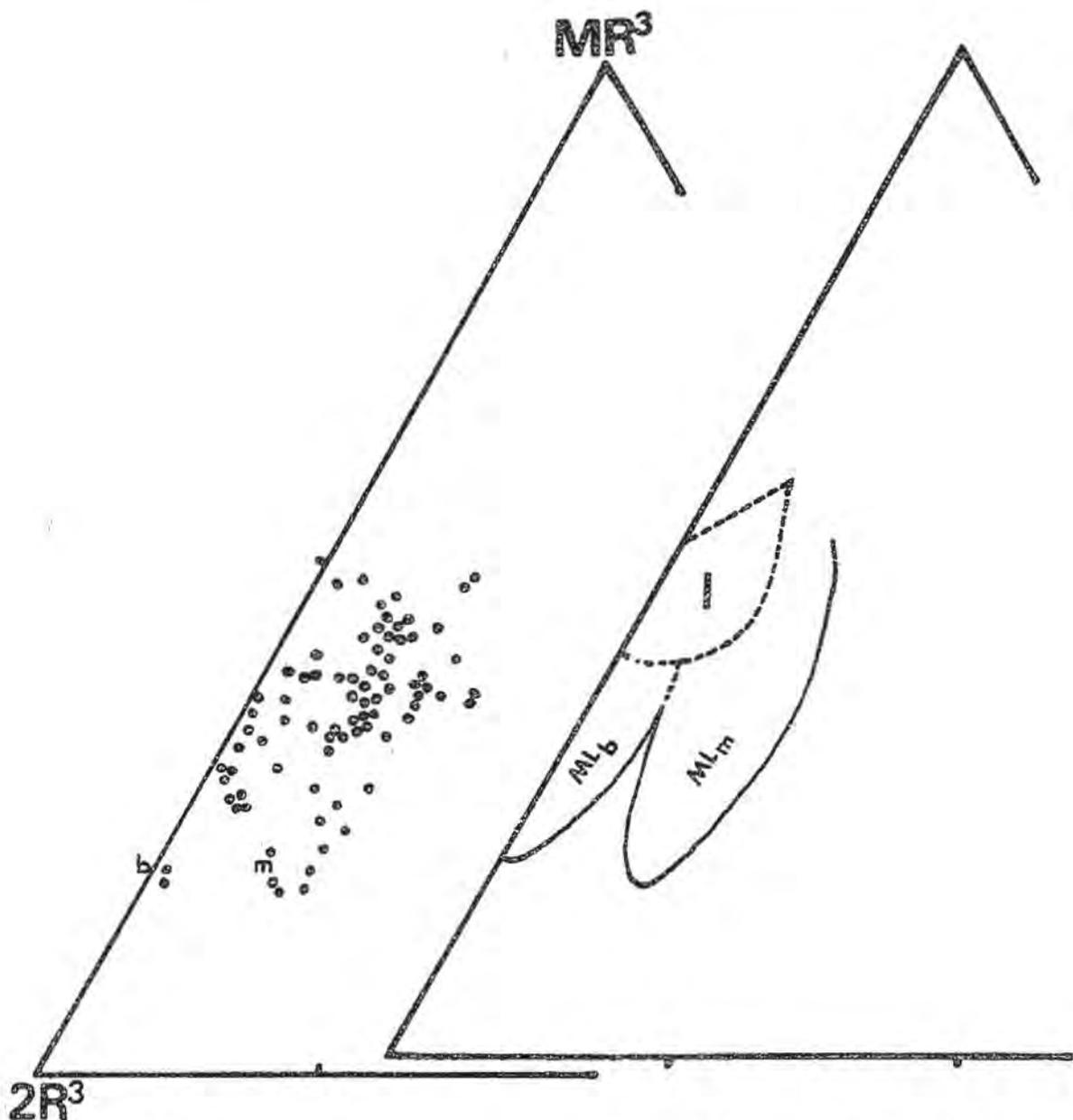


Figure 3. Chemical compositions of natural mixed layered expandable phases (natural) in the  $M^+R^3 - 2R^3 - 3R^2$  coordinates. I. = illite;  $ML_b$  = mixed layered beidellite series;  $ML_m$  = mixed layered montmorillonite series.

grouping near the mid-point of the  $2R^3$  and  $M^+R^3$  side of the triangle. Dioctahedral montmorillonites form a scatter of points between the ideal compositions of beidellite (b) and montmorillonite (m) and that of dioctahedral mica (Fig. 2). Mixed layered minerals appear to form a more coherent series of compositions which can be interpreted to represent mixtures of montmorillonites (of ideal compositions) and illites (Fig. 3). Two series are discerned, that between illite and beidellite /  $M_{0.3}^+(R^{3+})_2(Si_{3.7}Al_{0.3})O_{10}(OH)_2 \cdot nH_2O$  / and illite - montmorillonite /  $M_{0.3}^+(R_{1.7}^{3+}R_{0.3}^{2+})Si_4O_{10}(OH)_2 \cdot nH_2O$  . /

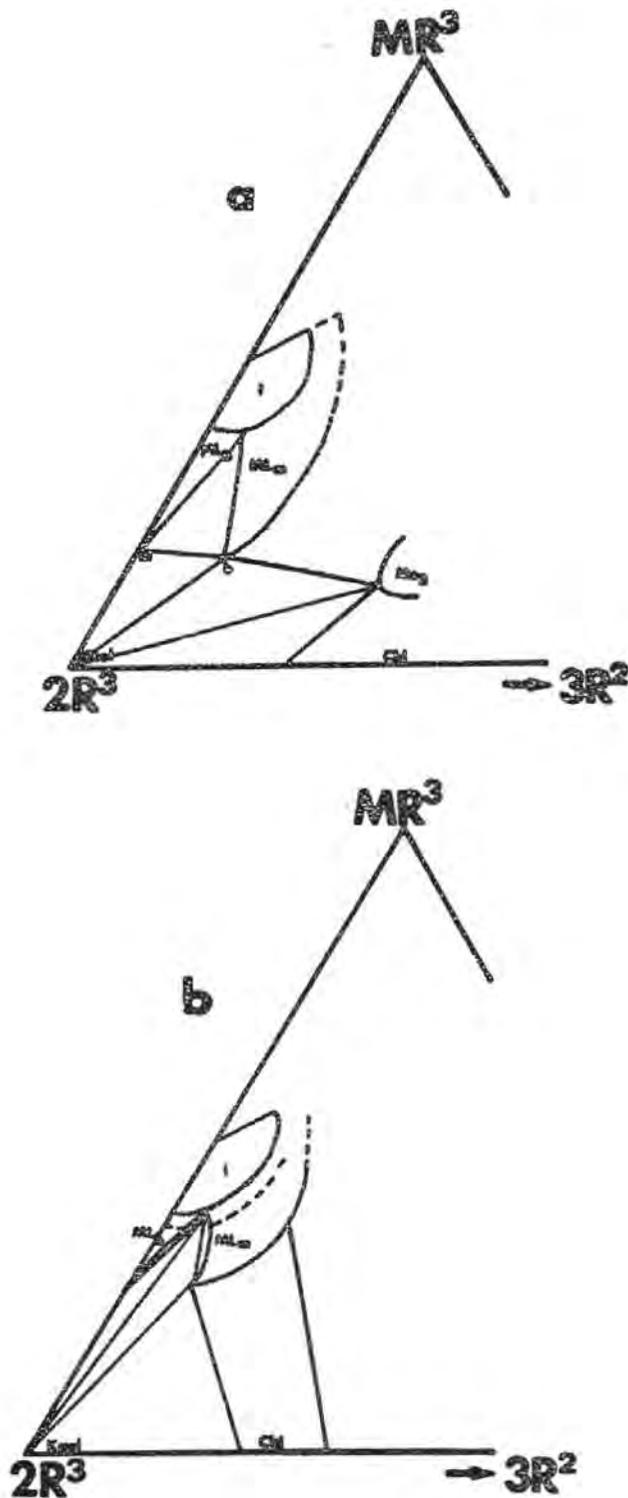


Figure 4. Proposed phase relations for the expanding and mica-like dioctahedral phases:

a) low temperatures (less than 100°C) paragenesis I

b) moderate temperatures (100 - 200°C) paragenesis II.

Kaol = kaolinite; ML = mixed layered illite beidellite or illite-montmorillonite; Mo<sub>3</sub> = trioctahedral expandable phases; Chl = chlorite;

I = illite, b = beidellite, m = montmorillonite (dioctahedral).

One must remember here that certain errors are likely to arise from somewhat uncritical use of the raw data such as misassignment of Mg in interlayer positions (which would be  $M^+R^{3+}$ ) to an octahedrally coordinated position ( $3R^{2+}$ ), an effect discussed by Foster (1953) concerning montmorillonites. Despite certain inadequacies the trends of the compositions seem to be evident in the figure.

If we consider the montmorillonites or fully expandable phases as a whole, and don't pose too many questions about the large range of interlayer charge which ranges from 0.3 to near 0.7, they can be considered to be intermediate in bulk composition between the two mixed layered series. This most probably means that the two montmorillonites, beidellite and montmorillonite, are joined by a compositional tie-line, that is they can coexist in the same rock or sediment and those materials found in nature and analyzed as montmorillonite are most often mixtures of the two types, indistinguishable to present means of identification. Fig. 4a indicates probable relations between the phases of interest when these fully expandable dioctahedral minerals are present. The montmorillonite tie-line gives the kaolinite - two montmorillonite three-phase field and the series of mixed layered phases joined by tie-lines (shaded area in the figure). We will call this paragenesis I.

The second series of relations which interest us are those of the two mixed layered mineral series. Since natural single phase compositions are isolated into two distinct groups, it is possible to deduce that a bulk composition lying in between the two series would produce a phase other than a mixed layered phase and thus not be analyzed as such. This eliminates the possibility of the mixed layered - mixed layered tie-lines and necessitates one which isolates the two series. This can be effected by the joining of kaolinite to illite or another  $M^+R^{3+}$  -rich phase. Looking again at the compositions of mixed layered phases, it is apparent that the area near illite could be occupied by a continuous mineral solid solution between the beidellite and montmorillonite mixed layered series. These compositions correspond roughly to those of allevardite or allevardite - like minerals with from 50 to, more commonly, 30% expanding layers in regular interstratification.

We might note here that the mineral name rectorite - considered by Brown and Weir (1963) to be equivalent and to supercede allevardite, is a sodic beidellite mineral with 50% expanding layers. Natural, ordered, mixed layered phases found in sedimentary rocks tend more commonly to be potassic and montmorillonitic, such as the type allevardite (Brindley, 1956). They will also contain not 50 but 35 - 30% expanding layers (Hower and Mowatt, 1966). Such minerals hold a rather special place in the development of mixed layered mineral systems under varying conditions of pressure and temperature as we will see later.

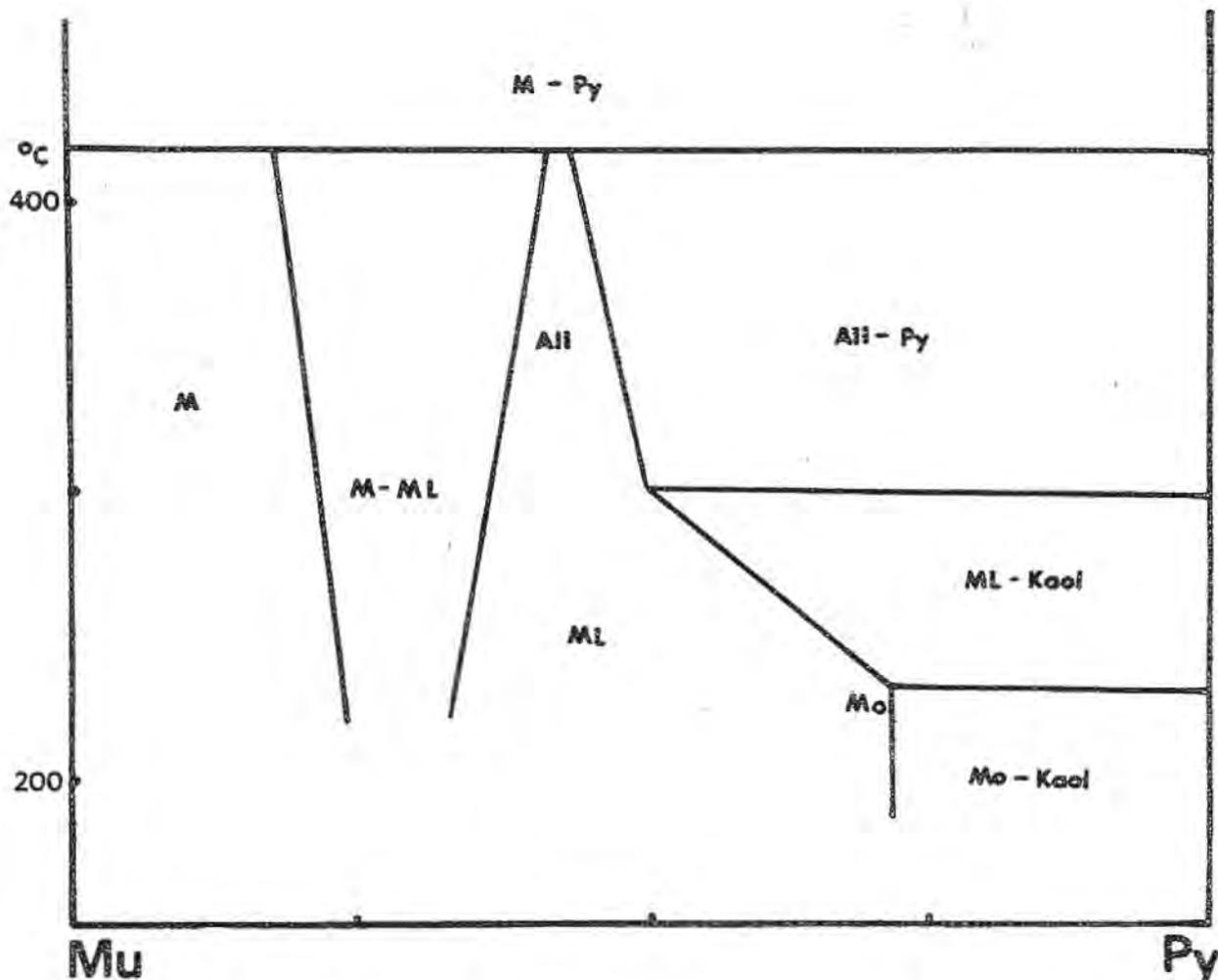


Figure 5. Phases found between the compositions muscovite - pyrophyllite at 2Kb pressure (after Velde, 1969). M = mica (tending to an illite like phase) ML = random mixed layered phase, All = allavardite-like phase; Mo = fully expandable phase.

### Experimental studies

Experiments on the muscovite-pyrophyllite compositional series give a certain understanding of the phase relations within a mica expandable mineral series. In this case we can consider the experimental system analogous to the illite - beidellite sequences forming the lower half of the left hand side of the triangular plot (Fig. 1). The phases produced at 2Kb total pressure and 250°C - 450°C are shown in Fig. 5. Three points are important - the gap in solid solution (continuous mixed layering) which increases between illite and a mixed layered phase as temperature increases. Also important is the fact that the phase containing expanding layers stable at highest temperatures contains about 35% montmorillonite and tends to be ordered in the experiments. It can be assimilated to the natural al-

leopardite - like phases found in sequences of deeply buried rocks. The third relation of interest is that kaolinite, or pyrophyllite does not coexist with the mica - like phases (illite in natural systems). Thus when expandable phases are present, the illite - kaolinite association is not stable. This is more or less apparent from the compositions of natural phases shown in Fig. 3.

If the illite-beidellite series can be accounted for and a kaolinite-potassic of  $M^+Al$  tie-line valid above the stability of montmorillonites how is the illite - montmorillonite association so common in sediments and sedimentary rocks to be accounted for?. We can only surmise the precise phase relations at the moment since no pertinent data is available for the bulk compositions lying between muscovite and chlorite, those which would produce the assemblages containing montmorillonite-mixed layered phases. However the experiments reported by Velde and Brusewitz (1972) on natural minerals in this series indicate a similar behavior to that of muscovite-beidellite mixed layered minerals. This information combined with the chemical compositions of the natural minerals leads one to believe that the two series of interlayered phases are analogous. However, since the montmorillonites contain important quantities of divalent iron and magnesium, it can be expected that temperatures of mineral reaction will be lower than those of the aluminous illite-beidellite types. Thus the formation of the ordered alleopardite-like phase and subsequent production of chlorite would occur at lower temperatures than the crystallization of pyrophyllite for example. It is also possible that the aluminous expanding phases will be stable when only illite-chlorite are present for the ferromagnesian compositions.

### General phase relations

From the above it is possible to deduce that kaolinite will coexist with the phase containing the greatest amount of expandable layers possible and also with chlorite. As we have proposed, kaolinite should coexist with an  $M^+R^{3+}$  - rich phase forming a tie-line between the two series of mixed layered minerals. We will suppose that this phase is illite, the mineral most commonly associated with kaolinite in sedimentary rocks. We will suppose further that this illite can coexist stably with a highly expandable phase, also a common occurrence in nature.

What then does this give with respect to the two compositional series of expanding minerals in the  $3R^{2+} - 2R^{3+} - M^+R^{3+}$  system?. Fig. 4b shows the resulting phase relations which are implicit from the above analysis. This will be called facies II. The points plotted for the mixed layered minerals do not really permit one to define with rigour the exact compositional fields of the mineral species. This is especially true since the spacial relations are very restricted, a poor analysis giving one or two percent alumina too much

would displace a mixed layered mineral from one series to another. Because of geometrical necessity, the expanding mineral series are figured as being accurate, thus permitting a series of illite-mixed layered mineral tie-lines. The only justification for such a tie-line is the very common association of illite, mixed layered and kaolinite minerals in sedimentary rocks. Since all of these minerals are of low temperature origin (weathering or diagenetic), we suppose that they will not be frequently present as metastable phases because they are at or near their conditions of formation. The argument made to substantiate this statement is that, if a phase has a field of stability under geologic conditions and if its presence is known not to be a function of time (at least on the scale of several tens of millions of years) and finally if it is known to exist in varying geologic environments, i.e. the process involved in its formation is varied, it will in frequently be present as a metastable phase compared to its surrounding mineral assemblage.

Thus the phase relations of Fig. 4 indicate the chemical composition of natural minerals and the common assemblages found in sedimentary rocks. They show an expandability between 90-30%. However there has been a major improvement in our understanding of clay mineral paragenesis - we can see from the figure that the kaolinite-bearing assemblages will contain the mixed layered phase with the highest expandability possible given the P-T conditions of formation. As we have seen in Fig. 5, this expandability is a function of temperature at constant pressure for the potassic beidellitic series. Thus kaolinitic assemblages will be important in describing the evolution of a series of sedimentary rocks.

The last paragenesis is represented by the formation of the allevardite-like phase which can coexist with kaolinite and illite over a considerable P-T range. We assume the development of beidellite and montmorillonite interlayered series are parallel, certainly an inaccuracy, but for lack of better data this convenience must be accepted. Concerning most sedimentary rocks, their bulk compositions are such that they will be in the montmorillonite-chlorite-illite series rather than beidellitic, and as a result we will let our attention center on these minerals.

This leaves the problem of the common association of chlorite with the three phases discussed above. As we can see in Fig. 4, using the generalized coordinates ( $R^{2+} = Mg + Fe^{2+}$ ) chlorite cannot coexist stably with three other phases. However its very common occurrence with these clays in sedimentary rocks and its appearance under experimental conditions (Velde and Brusewitz; 1972) as a reaction product produced in the process of decreasing the amount of expandable material present suggest that chlorite could be a stable phase in a four phyllosilicate assemblage. If we consider the known compositions of clay minerals, we find that compared to those thus far discussed, chlorite is or can assumed to be iron-rich relative to the others.

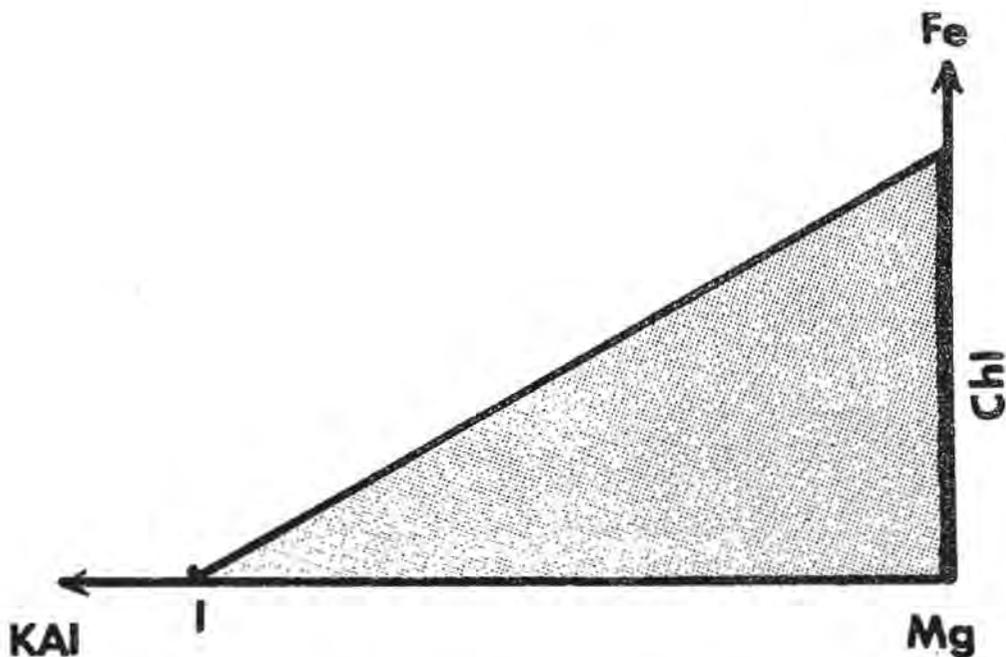
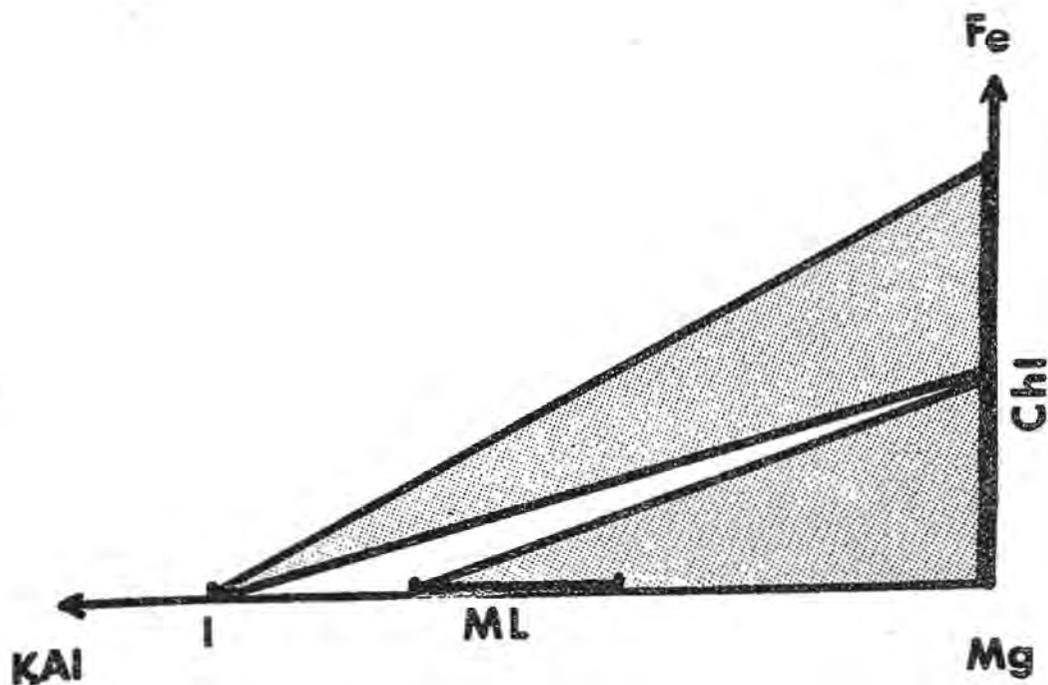


Figure 6. Possible phase relations in systems with variable  $\text{Fe}^{2+}$  content. chl = chlorite; ML = mixed layered illite-montmorillonites; I = illite.

mixed layered phase stable above  
 mixed layered phase unstable below.

The direct chemical evidence for this statement is largely lacking. However, X-ray data reported in the literature and information of the author strongly suggest that chlorites from sedimentary rocks - especially those in illite - chlorite assemblages, are predominantly iron-bearing. This is based upon the calculations of diffraction reflections (Brindley and Gillery, 1956) which indicate iron predominance when the 14 Å reflection is significantly of less intensity than the 7 Å reflection. Thus the octahedrally coordinated ionic site has  $Fe > Mg + Al$ .

One can readily suspect that the phase which concentrates a specific element can be produced solely due to a high total concentration of this element in a rock. Accordingly, one must take this element into consideration in any analysis of the phases present and the causes of their presence. Let us suppose then that chlorite is the only phase to contain highly variable quantities of Fe - Mg among the clay minerals mentioned here. Fig. 6 shows the probable relations between chlorites, illite and expandable phases. If total iron concentrations are high, chlorite will appear early in a series of rocks of a given  $M^+R^{3+} - (2R^{3+} - 3R^{2+})$  ratio. Otherwise it will be absent as long as the mixed layered mineral of this composition is stable. It might be mentioned that the composition of the chlorite stable with illite and the mixed layered mineral will be a function of the P-T conditions of its formation, that is its Mg/Fe ratio and  $R^{2+}/R^{3+}$  ratio as well. Because many assemblages contain several phyllosilicate phases, this composition will be little dependent upon the bulk composition of the rock and more so upon the physical conditions of formation. Thus chlorite compositions (relative Mg-Fe-Al proportions) should be good indications of the conditions under which a clay mineral assemblage has been formed. Unfortunately, we have little reliable information at present on chlorite compositions from multiphase assemblages in sedimentary rocks. However it seems that this would be a fruitful direction for future research.

If we look back at Figs. 4 and 6, most of the common clay mineral assemblages found in rocks can be explained as well as the variation from one sample to another in a closely spaced sequence. Aluminous rocks such as those found in hydrothermal alterations of granites will contain the kaolinite-beidellite series of assemblages. Illite represent either  $M^+R^{3+}$  - rich or high temperature conditions of formation: intermediate compositions, common in many sediments result in kaolinite parageneses. Magnesian iron-rich rocks will contain chlorite-mixed layered assemblages and possibly trioctahedral expanding phases such as vermiculite or corrensite.

#### P-T conditions and "diagenetic" mineral assemblages

As has been stated in the opening section, expanding phases behave in a rather regular manner as depth increases in a sequence of sediments or rocks bearing clay minerals. The most impor-

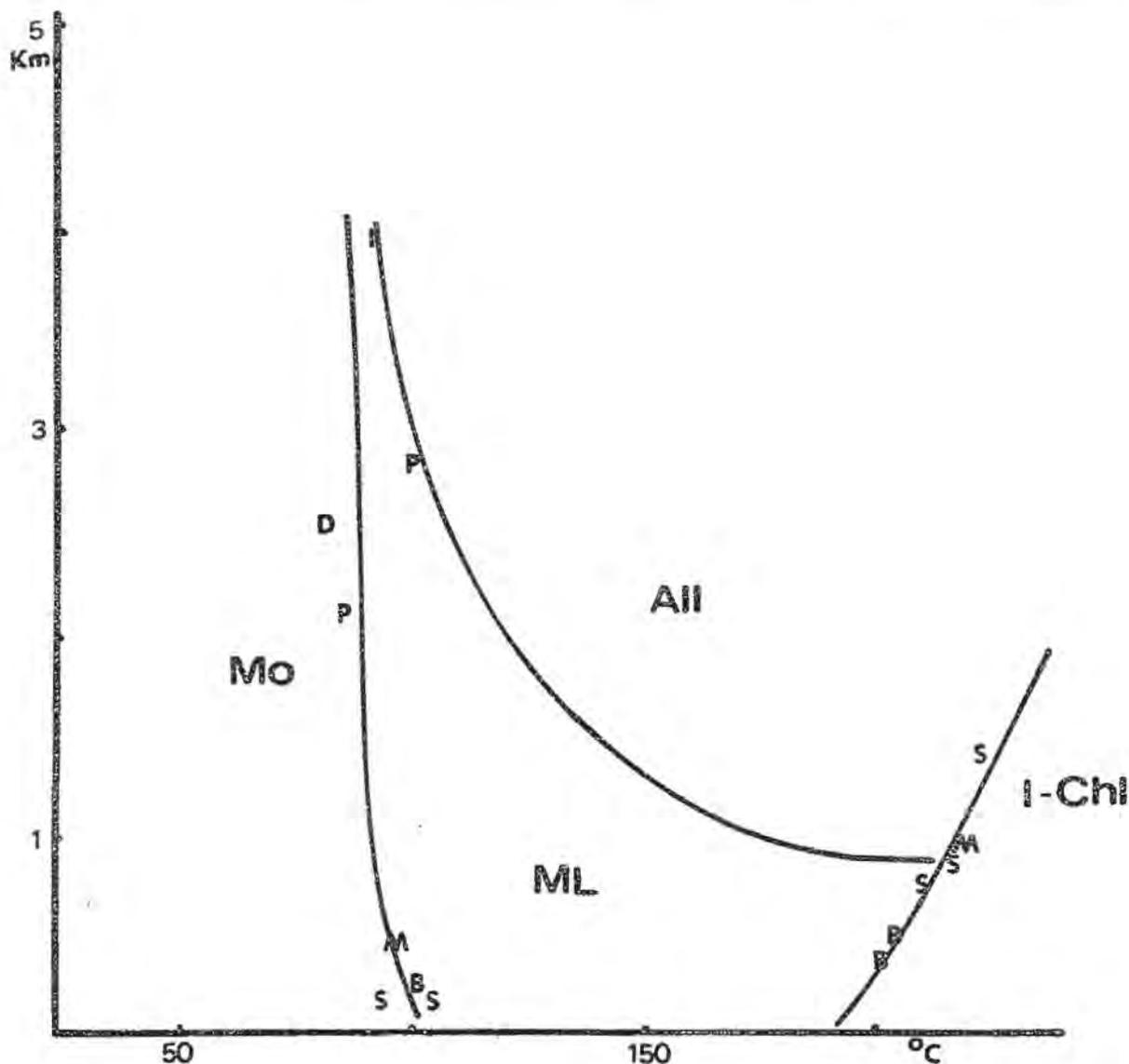


Figure 7. Depth - temperature plot of natural mineral assemblages for the fully expandable phases (Mo), random, 30 - 80% mixed layered (ML) and random or, more frequently ordered 30% mixed layered (All) minerals. Data from Steiner (1968) S, Muffler and White (1969) M, Perry and Hower (1969) P, Iijima (1970) I, Browne and Ellis (1970) B, and Dunoyer de Segonzac (1969) D.

I - C = illite, chlorite paragenesis. Tertiary or younger sediments are represented in these studies.

tant change is the maximum expandability of the mixed layered phase (which should be accompanied by kaolinite if our analysis is correct). The maximum expandability can be correlated with pressure and temperature, the data from the literature is shown in Fig. 7. Careful consideration of the key mineral assemblages which give a maximum expandability of the mixed layered phases will allow a series of rocks to be placed on a paleogeothermal gradient using Figs. 4 and 7.

It is probable that still better information can be gained through a knowledge of compositional-pressure, temperature relations for chlorites which will allow a greater precision in this schema. It is believed that the outline given here can be used to better interpret clay mineral assemblages found in sediments and sedimentary rocks and will serve as a basis for further interpretations of chemical information and experimental data dealing with clay minerals.

## SOURCES OF MINERAL CHEMICAL ANALYSES

### Diocahedral montmorillonites

Alietti and Alietti (1962); Anderson and Reynolds (1966)  
Early (1953); Foster (1953); Koster (1960); Schultz (1969)  
Stringham and Taylor (1950); Walker et. al. (1967)

### Diocahedral mixed layered

Ball (1968); Bonorino (1959); Brown and Weir (1963); Cole (1966)  
Hower and Mowatt (1966); Kodama (1966); Schultz (1969)  
Steiner (1968); Tomita, et .al. (1969); Weaver (1956)

### Illites

Gabis (1963); Gaudette, et .al. (1966); Hower and Mowatt (1966)  
Mackenzie (1957)

### Chlorites

data compiled by Velde (1973)

## REFERENCES

- ALIETTI, A., and ALIETTI, L. (1962); Su due diversi tipi di montmorillonite riconosciuti nella bentonite di gemmano (Forli). *Periodo. Min.*, 31, 261-86.
- ANDERSON, D.M. and REYNOLDS, R.C. (1966): Umiat bentonite: an unusual montmorillonite from Umiat, Alaska. *Amer. Min.*, 51, 1443-56.
- BALL, D.F. (1968): Interstratified illitic clay in Ordovician ash from Conyay, North Wales. *Clay Min.*, 7, 363-6.
- BONORINO, F.G. (1959): Hydrothermal alteration in the Front Fange mineral belt, Colorado. *Bull. Geol. Soc. Ame.*, 70, 53-90.
- BRINDLEY, G.W., and GILLERY, F.H. (1956): X-ray identification of chlorite species. *Amer. Min.*, 41, 169-186.
- BRINDLEY, G.W. (1956): Alleverdite, a swelling double-layer mica mineral *Amer. Min.* 41, 91-103.

- BROWN, G., and WEIR, A.H. (1963): The identity of rectorite and alleverdite. *Ist Int. Clay Conf. Proceed.*, 27-36.
- BROWNE, D.R.L., and ELLIS, A.J. (1970): The Ohaki-Broadlands hydrothermal area New Zealand: mineralogy and related geochemistry. *Amer. Journ. Sci.*, 269, 97-131.
- COLE, W.E. (1966): A study of a long-spacing mica-like mineral. *Clay. Min.* 6, 261-81.
- DUNOYER de SEGONZAC, G. (1969): Les minéraux argileux dans la diagenèse, passage au métamorphisme. *Ser Carte Géol. Als-Lorraine* 29, 320 p.
- EARLEY, J.W., OSTHAUS, B.B., and MINLE, I.H. (1953); Purification and properties of montmorillonite. *Amer. Min.* 38, 707-24.
- FOSTER, M.D. (1953): Geochemical studies of clay minerals: II. Relation between substitution and swelling in montmorillonite. *Amer. Min.* 38, 994-1006.
- GABIS, V. (1963): Etude minéralogique et géochimique de la série sédimentaire oligocène du Velay. *Bull. Soc. fr. min. Crist.* 86, 315-54.
- GAUDETTE, H.E., EADES, J.L., and GRIM, R.E. (1966): The nature of illite. *Clays and Clay Min.* 13, 33-48.
- HOWER, J., and MOWATT, T.C. (1966): The mineralogy of illites and mixed-layer illite/montmorillonites. *Amer. Min.* 51, 825-854.
- IJIMA, A. and UTADA, M. (1970): Present day zeolitic diagenesis of the Neogene geosynclinal deposits in the Niigata Oil field, Japan. *Ame. Chem. Soc. 2nd Int. Zeolite Conf.*, 548-554.
- KODAMA, H. (1966): The nature of the component layers of Rectorite. *Amer. Min.* 51, 1035-55.
- KÖSTER, H.M. (1960): Nontronit und Picotit and dem Basalt des Ölberges bei Hundsanzen, Westerwald. *Beiträger für Min. Petr.* 7, 71-5.
- MACKENZIE, R.C. (1957): The illite in some old Red Sandstone soils and sediments. *Min. Mag.* 31, 681-7.
- MILLOT, G. (1964): *Géologie des Argiles*. Masson & Cie., Paris.
- van MOORT, J.C. (1971): A comparative study of the diagenetic alteration of clay minerals in Mesozoic shales from Papua, New Guinea, and in Tertiary shales from Louisiana, U.S.A. *Clays and Clay Min* 19, 1-20.
- MUFFLER, L.J.P., and WHITE, D.E. (1969): Active metamorphism of Upper Cenozoic sediments in the Salton Sea Geothermal field and the Salton Trough, Southeastern California. *Bull. Geol. Soc. Ame.* 80, 157-82.
- PORRENGA, D.H. (1967a): Clay Mineralogy and geochemistry of of recent marine sediments in tropical areas. Thesis, University of Amsterdam.
- PORRENGA, D.H. (1967b): Glauconite and chamosite as depth indicators in the marine environment. *Marine Geol.* 5, 495-501.
- ROHRLICH, V., PRICE, N.B., and CALVERT, S.E. (1969): Chamosite in recent sediments of Loch Etive Scotland. *Journ. Sed.*

Petr. 39, 624-31.

SCHOEN, R., and WHITE, D.E. (1965): Hydrothermal alteration in GS - 3 and Econ. Geol. 60, 1411-21.

SHULTZ, L.G. (1969): Lithium and potassium absorption, dehydroxylation temperature, and structural water content of aluminous smectites. Clays and Clay Min. 17, 115-49.

STEINER, A. (1968): Clay minerals in hydrothermally altered rocks at Wairakei, New Zealand. Clays and Clay Min. 16, 193-213.

STRINGHAM, B., and TAYLOR, A. (1950): Nontronite at Bingham, Utah. Amer. Min. 35, 1060-66.

TOMITA, K., and YAMASHITA, H., OBA, N. (1969): An interstratified mineral found in altered andesite. Journ. Jap. Assoc. Min. Pet. Econ. Geol. 61, 25-34.

VELDE, B., and BRUZEWITZ, A.M. (1972): Transformation of natural clay minerals at elevated temperatures and pressures. Geol. För Forsh. (in press).

VELDE, B.: Phase equilibria studies in the system  $MgO-Al_2O_3-SiO_2-H_2O$ : Chlorites and associated minerals. Min. Mag. (In press).

WALKER, T.R., RIBBE, P.H., and HONEA, R.M. (1967): Geochemistry of hornblende alteration in Pliocene red beds Baha California, Mexico. Bull. Geol. Soc. Ame. 78, 1055-60.

WEAVER, C.E. (1956): Mineralogy of the middle Devonian Tioga K-bentonite. Amer. Min. 41, 359-62.

## CLAY MINERALOGY OF BOTTOM SEDIMENTS IN THE ADRIATIC SEA

F. Veniale, F. Soggetti, B. Pigorini, A. Dal Negro and A. Adami

Instituto di Mineralogia, Petrografia e Geochimica  
Università di Pavia (Italy)

**ABSTRACT.** - The study covers the clay fraction of about 180 samples of bottom sediments from the Adriatic Sea cored in the area of the paleodelta shelf of the Po river.

The distribution of heavy and light minerals in the sand fraction, and the grain-size patterns led to state source(s) and dispersion of these sediments, pointing out a mainly longitudinal dispersion pattern. Radiocarbon-dating determinations of shelly tests have established ages ranging from about 15,000 years, for fossil organisms near the shelf edge of the paleodelta, to about 4,000 years in the northern shelf close to the present Po delta. These results are in agreement with the trend of the paleodelta regression corresponding to the Pleistocene-Holocene marine transgression.

Montmorillonite and kaolinite are generally decreasing shore → open-basinward in the transversal profiles, and with a trend present delta → paleodelta edge in the longitudinal ones, whereas chlorite is increasing in the same directions. Vermiculite is absent in the nearshore sediments, appearing only off-shore and decreasing seaward. No significant variations have been observed for illite.

The clay minerals distribution indicates mainly a differential mechanic sorting and/or flocculation(?), both in transversal and longitudinal profiles. The controverse behaviour of chlorite, and the presence of low amounts of mixed-layer minerals, not detected in the fluvial sediments discharged into the Adriatic basin, might suggest the possibility of regeneration (aggradation) of some detrital clay minerals under the influence of the marine environment. An alternative interpretation of the chlorite pattern, decreasing from the paleodelta edge (older sediments) toward the present delta (younger sediments), may be a variation of its sedimentation rate, depending on change occurred in the source area(s) and/or transport conditions of the terrigenous materials during the paleodelta regression.

## INTRODUCTION

The Adriatic Sea is an oblong land-locked basin bordered on the western side by the Apennines and on the eastern side by the Dinaric chain. The northern part is filled up to shelf-level, the southern part is the deepest, formed by an abyssal plain up to 1,216 m deep. The two portions are separated between Pescara and Sebenik by the "middle Adriatic fossa", lying at a depth of about 270-280 m.

The oblong morphology of the Adriatic basin has been the purpose of sedimentological research by many authors. Sources and dispersion of the late Pleistocene and Holocene deposits have been investigated by Pigorini (1967, 1968).

Recent sedimentation in the Adriatic Sea reflects the different environments of the northern shelf and of the southern "fossa".

The uneven continental shelf is covered by sediments supplied mostly by the Po river. Modern sedimentation has given rise to a mud and sandy-mud prodelta, off the Po delta, to a nearshore strip of fine sand and to an off-shore belt of mud (see Fig. 1-A). A coastal sediment zone facing Venice represents detrital contributions of the Adige and other Venetian rivers. The remaining part of the shelf is covered by regressive relict sands deposited by the Pleistocene Po, which during the sea level lowering of the post-Monastirian regression (corresponding with the last Würm-glaciation) advanced its deltaic system to the present-day shelf edge off Pescara.

Radiocarbon-dating determinations (Marino and Pigorini, 1969) chiefly agree with this hypothesis: age regression ranges from about 15,000 years B.P. (= Before Present) for fossil organisms near the shelf edge, to about 4,000 years B.P. in the northern part of the shelf near the present Po delta.

The principal source of the shelf sediments is the Pleistocene-Holocene Po basin, which supplied unstable heavy minerals suites derived from igneous and metamorphic rocks of the central and western parts of the Alpine chain (see Fig. 1-A). In the southern "fossa" mud deposition is predominant. Pleistocene bathyal sands are ascribed to the Ofanto-Vulture area of the southern Apennines, and to the volcanic ashes from Vulture, Vesuvius and other volcanoes of the central and southern Italy.

A predominantly longitudinal dispersion has been ascertained for shelf sediments, throughout the Pleistocene-Holocene history of the Po basin. Sedimentary supply is lateral and dispersion is predominantly transversal in the southern deeper part of the Adriatic Sea (see Fig. 2).

A summary of sedimentological data on the Adriatic Sea has been supplied by van Straaten (1970). For a review of the bibliography on Adriatic Sea refer to the above mentioned Authors. Other papers are mainly concerned with restricted areas (von Rad et al.,

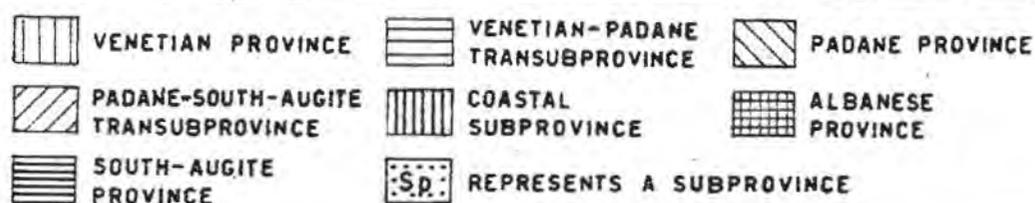
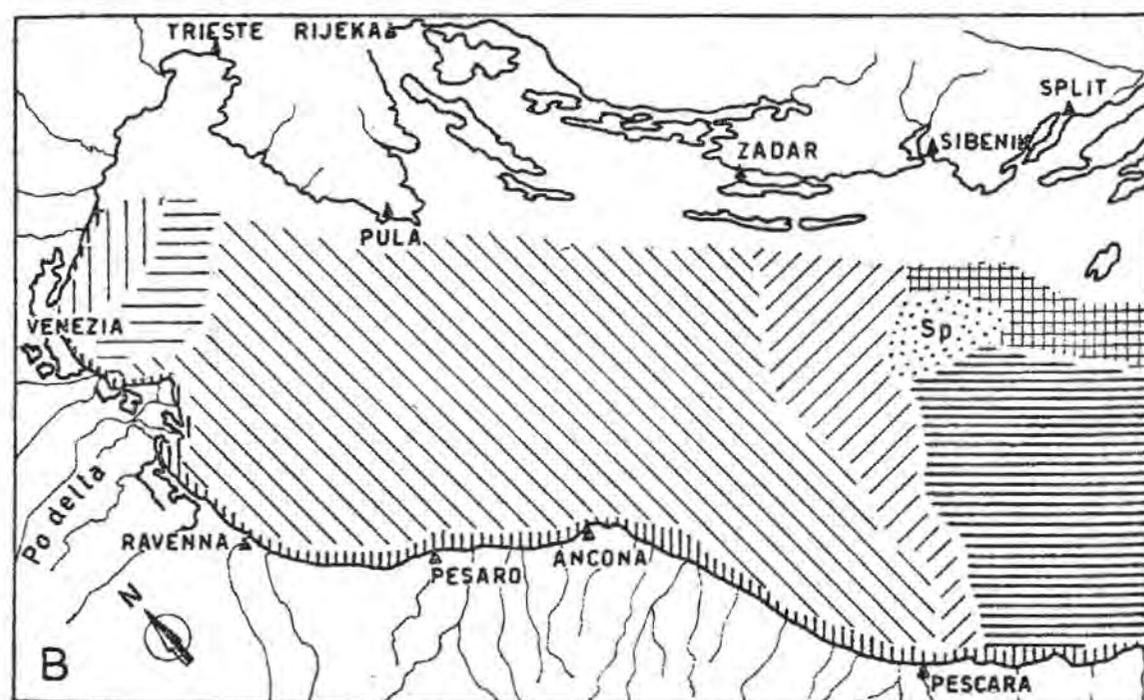
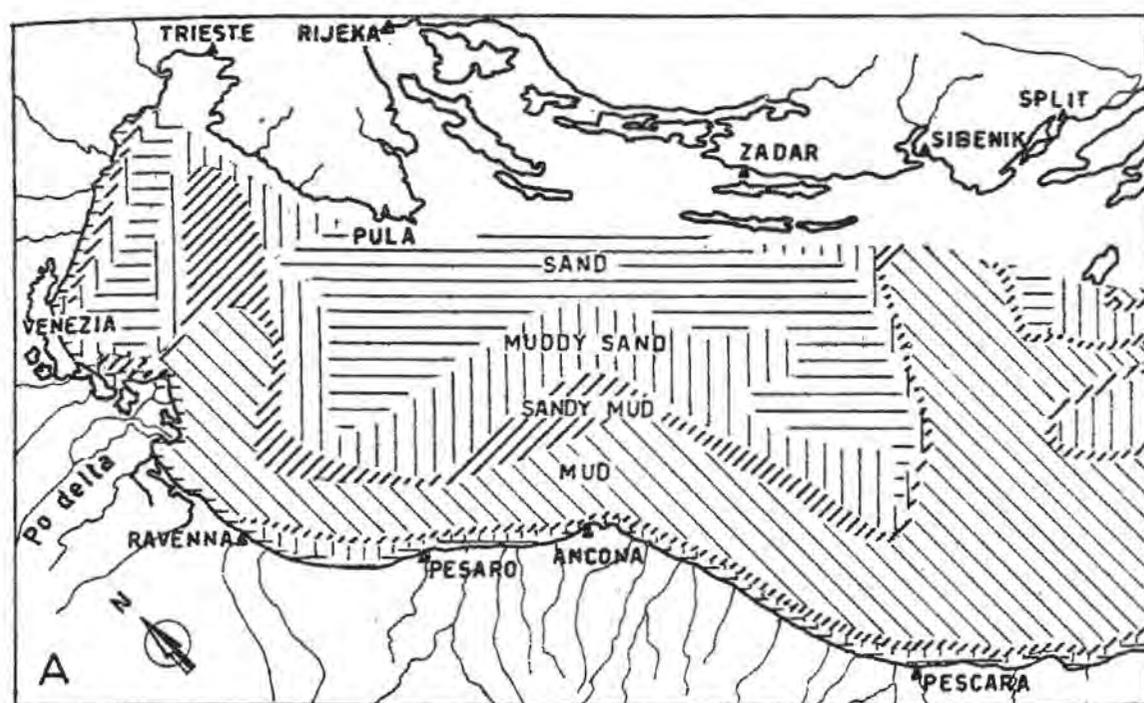


Figure 1. A) Generalized distribution of grain-size types of sediments, and B) of heavy mineral provinces in the paleodelta area of the Adriatic Sea.

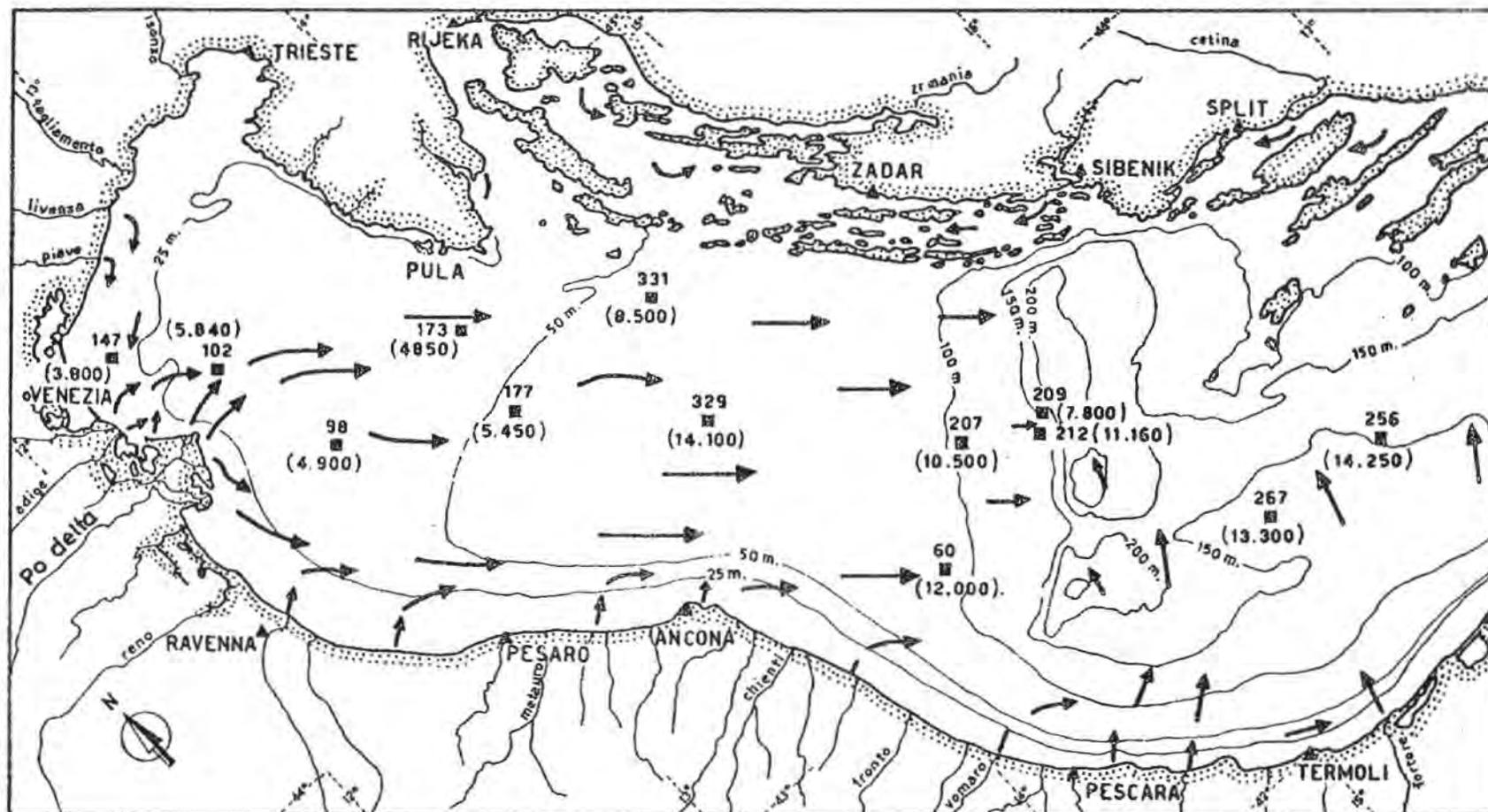


Figure 2. Dispersion pattern of recent sediments, and their radiocarbon ages (years B.P.) in the Adriatic Sea; furthermore, schematic bathymetry of the basin.

1970; Hesse et al., 1971; Angeli et al., 1970; Rizzini and Veggiani, 1969; Zezza, 1969).

The present paper is mainly concerned with the clay mineral distribution in the northern shelf area of the Po paleodelta; further investigations are in progress regarding the southern "fossa" of the Adriatic basin.

## EXPERIMENTAL

The materials of study were collected on two 1962 cruises with the fishing boat "Nuovo San Pio" from Pescara and on board of the "Horizon" ship from Scripps Institution of Oceanography (La Jolla, California-USA). During these expeditions bottom samples were taken at 360 localities from the whole length of the Adriatic Sea.

Sedimentological data from these samples have been already published by Pigorini (1968) and van Straaten (1970).

Figure 3 shows the sample location map of the zone investigated (Po paleodelta area), with indication of the samples selected as most representative for the study of the clay fraction.

The original bottom sediment samples were repeatedly washed with distilled water to remove marine salts. The fraction  $< 2 \mu$  was isolated from the rest of the sample by allowing the material  $> 2 \mu$  to settle out of suspension (about 25 grams of washed sample were placed in a beaker with 600 ml water and allowed to settle out of the upper 5 cm of each dispersion after 4 hours).

Standard X-ray diffraction techniques were used to identify the clay minerals. Oriented aggregates of the clay fraction were prepared by settling and drying at the room temperature and humidity of the laboratory about 1 ml of the fine suspension on glass slides. Mineral identification was further facilitated by vapour pressure glycolation (the clay mounts were allowed to remain for 1 hour at 60°C in an ethylene glycol atmosphere, after Burton, 1955), and by heating for 2 hours at 550°C in a calibrated muffle furnace.

The untreated and treated slides were then analysed by X-ray diffraction, and the diffractometric traces were carried out on duplicate samples, using Cu Ni filtered radiation of a Philips PW 1010 unit at a setting of  $10^3$  cps, multiplier 1 and ratemeter 2, with KV 40 and mA 20; the scanning speed used was  $1^\circ 2\theta$  per minute with a chart speed of 60 cm per hour.

Clay minerals were identified on the basis of several peaks, but the reflection from the (001) plane and its shifting when subjected to the various standard treatments was considered characteristic; namely 7.15 Å for kaolinite, 10 Å for illite (without attempt to

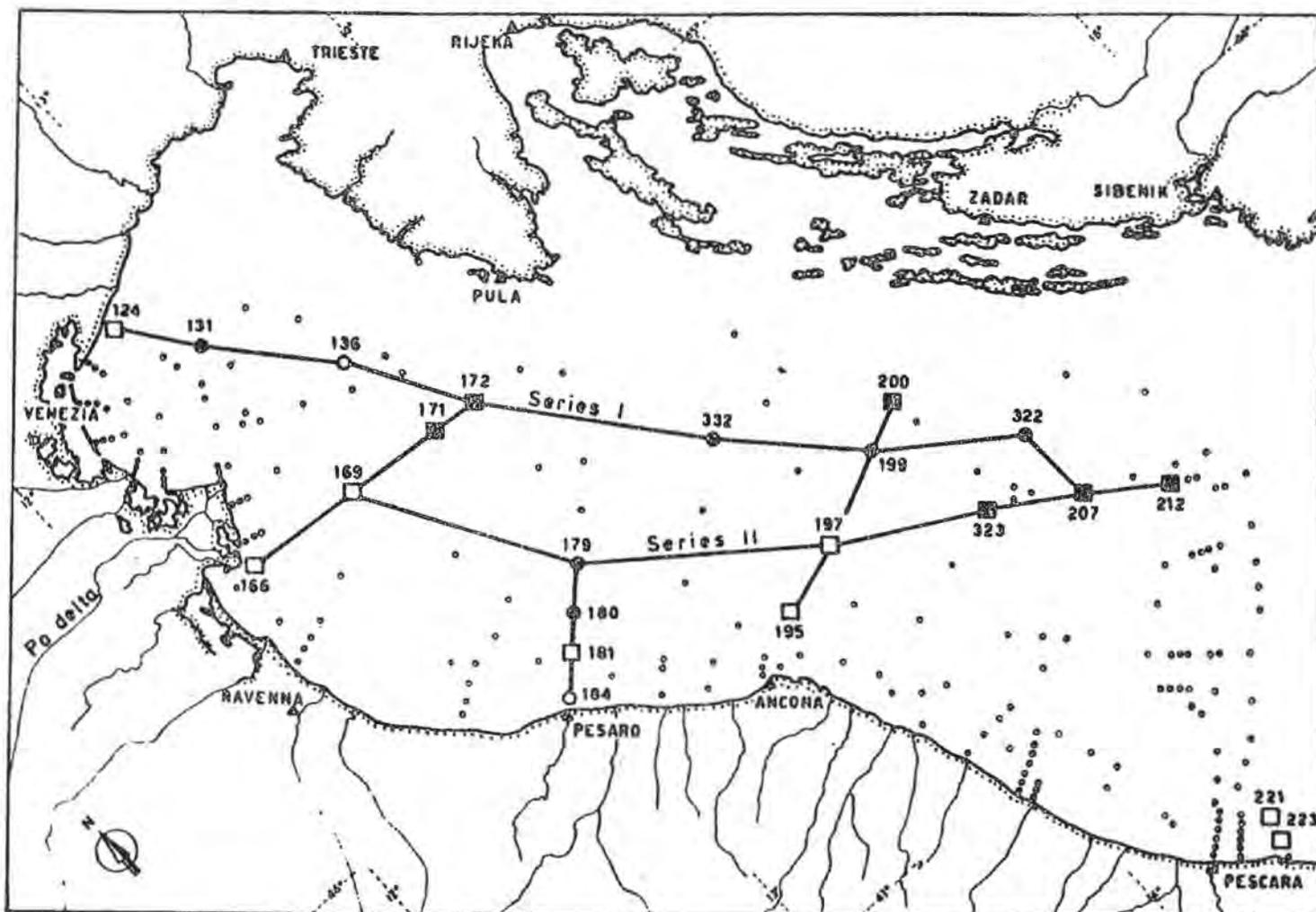


Figure 3. Position of core stations, and of the most representative samples selected for X-ray investigation, with indication of their grain-size type (■ sand, ● muddy sand, ○ sandy mud, □ mud).

distinguish the different micas), 14 Å for chlorite and 17 Å (upon glycolation) for montmorillonite; for a swelling < 17 Å it was assumed the mineral to be probably vermiculite (see scheme in Fig. 4).

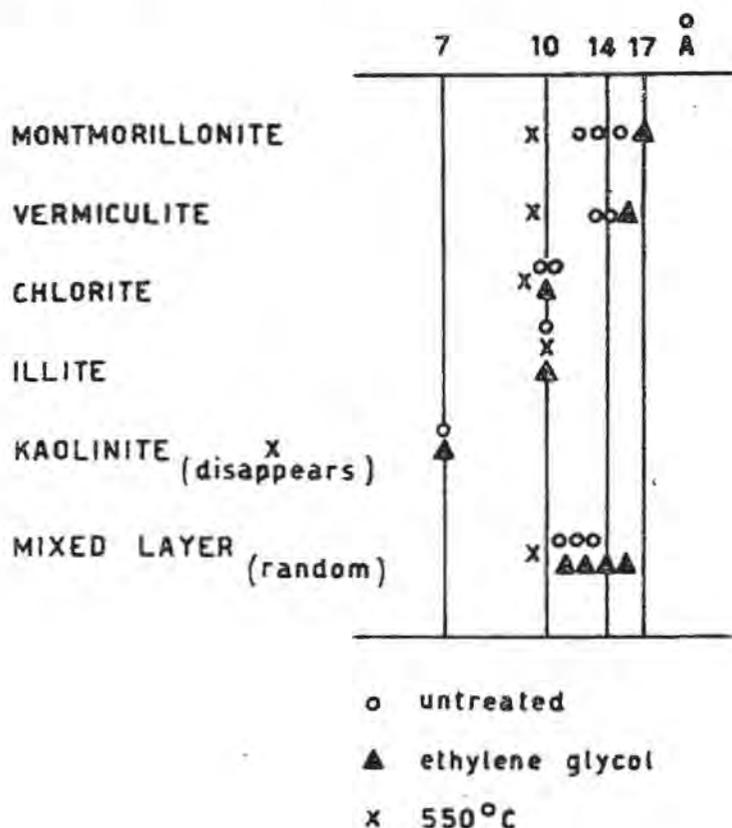


Figure 4. Diagram illustrating the shift of the (001) X-ray diffraction peak taken as characteristic for the different clay minerals, when untreated, glycolated and heated.

To express semi-quantitatively (van der Marel, 1966) the relative amount of each clay mineral component, a modification of the methods of Schulz (1960) and Biscaye (1965) was used: the maximum peak height of the (001) reflection of each mineral and two additional peak height measurements taken at 0.4° 2θ intervals on either side of the maximum peak height were summed. We have found that this method of measuring peak intensity is rapid and correlates very well with measurements of peak area. To compensate for the effects of low angle X-ray scattering, the intensity of the 17 Å glycolated montmorillonite peak was divided by 3 when compared to (001) illite peak intensity; to reduce the effect of the (002) chlorite peak, the (001) kaolinite peak intensity was divided by 2 or some other factor in proportion to the relative intensities of the reflections at 3.57 Å (= 002 of kaolinite) and 3.54 Å (= 004 of chlorite). The intensity measurement of each clay mineral was expressed as

a mutual percentage of the total (100 ratio); the precision or reproducibility of the procedure of analysis is  $\pm 5$  to  $\pm 10\%$ , the higher values being usually found in the case of smectite. Other mineral components as quartz, feldspars, carbonates, amorphous phases, and so on, are not considered in this investigation.

## RESULTS OF X-RAY DIFFRACTION ANALYSIS

The most representative among the 180 samples investigated are shown in Fig. 3. Some longitudinal and transversal profile series have been selected in order to check up dispersion, transport, trend(s) of sedimentation, and/or transformations occurred in the basin environment. Furthermore, these samples were selected belonging to different sedimentary petrological provinces and granulometric classification.

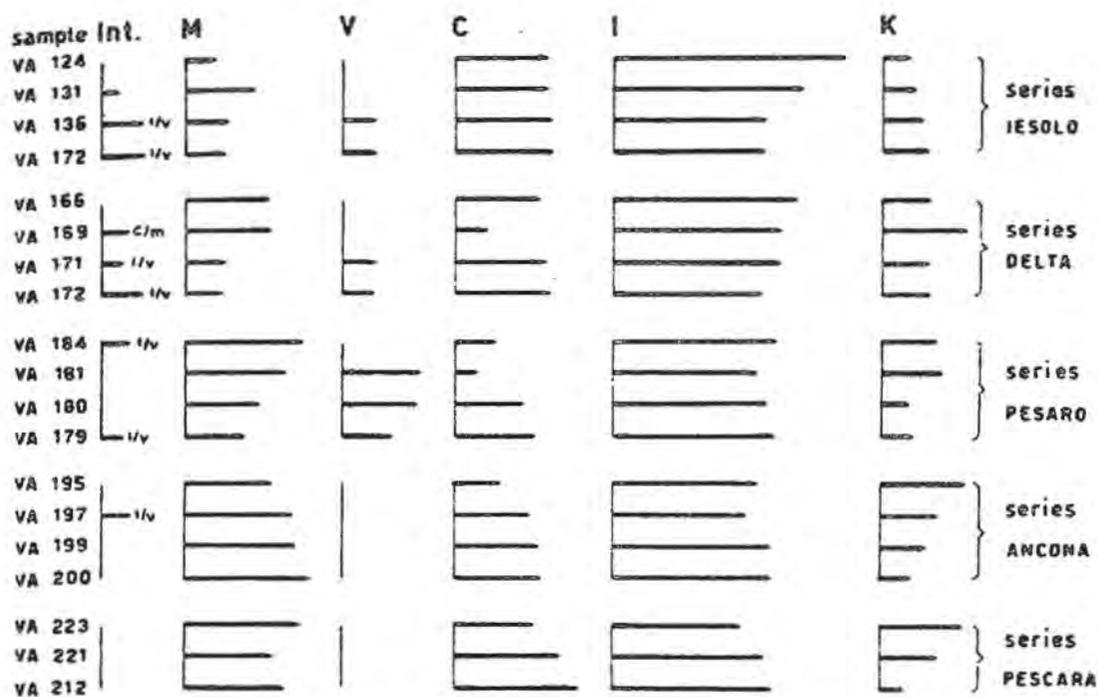
X-ray diffractograms showed that the clay fraction of the bottom sediments in the Po paleodelta area of the Adriatic Sea consists of a mixture of illite, montmorillonite, chlorite, kaolinite, vermiculite(?) and mixed-layer clay minerals (see Fig. 5).

The most abundant clay mineral is illite (30-40%, rarely up to 50%), without significant variations both in transversal and longitudinal profile series; the only exception is the Iesolo series, where a decrease in the content of this mineral is observed near-shore  $\rightarrow$  open-seaward.

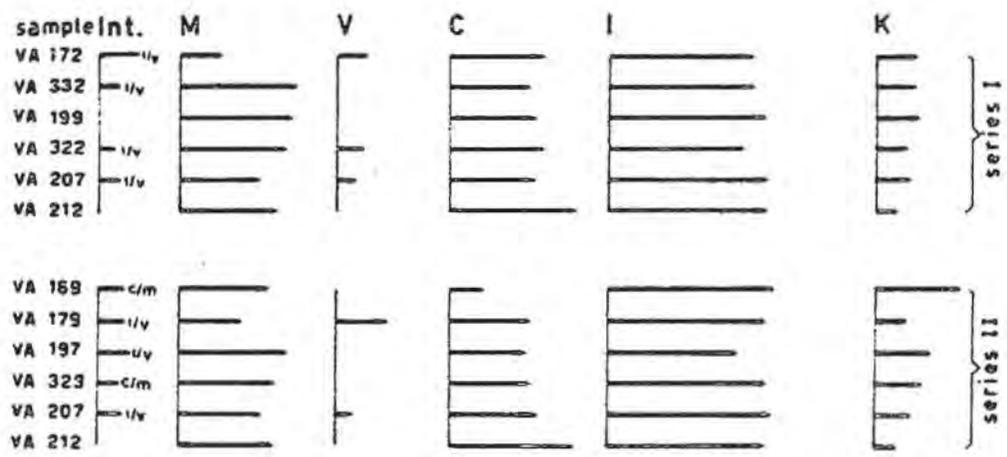
Montmorillonite and chlorite are also relatively abundant (up to 20-30%), but their distribution is quite different from that of illite. Montmorillonite is generally decreasing shore  $\rightarrow$  open-basinward in the transversal profiles, with the exception of the Ancona series; some discrepancies observed in the dispersal of montmorillonite are probably the result of long-shore currents. Chlorite, instead, is increasing in the same directions. Along the longitudinal series montmorillonite is decreasing with a trend present delta  $\rightarrow$  paleodelta edge, whereas the contrary is true for chlorite.

Kaolinite is less abundant (10-20%) and decreasing near-shore  $\rightarrow$  open-seaward, and present delta  $\rightarrow$  paleodelta edge.

Vermiculite and mixed-layers are subordinate (10% or less, except the Pesaro series). Vermiculite is absent in the near-shore sediments, appearing only off-shore and decreasing seaward; the mixed-layer clay minerals seem to be increasing in the same direction of the transversal profiles (see, for instance, the Iesolo and Delta series).



**TRANSVERSAL SERIES**



**LONGITUDINAL SERIES**

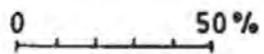


Figure 5. Semi-quantitative representation of the clay mineral composition of the fraction  $< 2 \mu$  of selected samples belonging to several transversal and longitudinal profile series in the Po paleodelta area (see Fig. 3). Int = interstratification (mixed-layer), M = montmorillonite, V = vermiculite, C = chlorite, I = illite, K = kaolinite.

## DISCUSSION

The under  $2 \mu$  size fraction of marine sediments has appeared attractive for the study of indicators of source areas of the terrigenous discharges, of the influence of the marine environment on the mineralogical composition of the detrital clays, and of the sedimentological aspects of the basin investigated.

A large number of papers on the clay mineralogy of marine sediments have been published; a literature survey is referred to some comprehensive publications (Millot, 1964; Parham, 1966; Porenga, 1967; Griffin et al., 1968; Rateev et al., 1969; Keller, 1970).

The clay fraction of surface sediments of the Mediterranean Sea have been recently investigated by Chamley (1971) and Venkatarathnam et al. (1971); refer to the literature reviewed in these papers, and see also Tomadin (1971). In the eastern area six clay mineral assemblages have been distinguished, which have distinctive sources and their dispersal reflects different agents of transport. A Nile assemblage with very high amounts of well-crystallized smectite (>50%) and 15-25% kaolinite is found on the eastern Nile cone and within the eastern Levantine basin. Its distribution has resulted from the dispersal by the easterly directed surface water currents which form part of the counter-clockwise gyre in the eastern Mediterranean Sea. The Levantine intermediate water has transported from the southeast Aegean Sea on to the Mediterranean ridge southeast of Crete a southeast Aegean assemblage characterized by 40-60% well-crystallized smectite and higher contents of chlorite and illite than in the Nile assemblage. A kaolinite-rich assemblage (20% - > 30% kaolinite), coinciding with high carbonate values, occurs on the western section of the Mediterranean ridge and to some extent in the western Nile cone, as a consequence of transport by wind from North Africa. The restriction of Kithira and Messina assemblages (illite- and chlorite-rich assemblages) to deep parts of the Ionian basin is chiefly due to water movements involved in deep circulation. A Sicilian assemblage with 20- > 30% kaolinite and 30-50% smectite in the westernmost part of the Ionian basin south of Sicily, has mainly resulted from the dispersal by easterly moving surface waters from the western Mediterranean Sea.

Only little is known, however, about the clay mineralogy of the Adriatic Sea sediments, the only study being that of Damiani et al. (1964) reporting the results of X-ray diffraction analyses on the clay fraction of five cores from the bottom of the "meso-Adriatic fossa". The clay minerals in these samples appear to be mainly detrital; the montmorillonite only could be derived by alteration of volcanic materials.

Very suitable for our investigations has been the study of Quakernaat (1968) on the distribution of clay minerals in recent fluvia-

tile sediments along the Italian west (Tyrrhenian) and east (Adriatic) coasts. Along the Adriatic coast, between Chioggia and Lesina, the river sediments contain high-charge vermiculite, 20-40% illite, 30-40% high-charge smectite and about 10% kaolinite.

The clay mineralogy of bottom sediments in the Po paleodelta area of the Adriatic Sea, as determined by us, show that montmorillonite and kaolinite are generally decreasing shore → open-basinward in the transversal profiles, and with similar trend in the direction present delta → paleodelta edge in the longitudinal series. Chlorite is increasing in the same directions. Vermiculite is absent in the near-shore sediments, appearing only off-shore and decreasing seaward. No significant variations have been observed for illite.

Such a clay mineral distribution indicates mainly a differential mechanic sorting and/or flocculation(?), both in transversal and longitudinal profiles. The controverse behaviour of chlorite, and the presence of low amounts of mixed-layer minerals, not detected in the fluvial sediments discharged into Adriatic basin, might suggest the possibility of regeneration (aggradation) of some detrital clay minerals under the influence of the marine environment. An alternative interpretation of the chlorite pattern, decreasing from the paleodelta edge (older sediments) toward the present delta (younger sediments), may be a variation of its sedimentation rate, depending on changes occurred in the source areas and/or transport conditions of the terrigenous materials during the paleodelta regression.

#### REFERENCES

- ANGEELI, A., RIZZINI, A. and VEGGIANI, A. (1970): I sedimenti recenti della costa adriatica romagnola. Mineralogia e stratigrafia del sottosuolo ravennate. Boll. Camera C.I.A.A. Forlì, 24, 5-64.
- BISCAYE, P.E. (1965): Mineralogy and sedimentation of recent deep-sea clay in the Atlantic Ocean and adjacent seas and oceand. Bull. Geol. Soc. Amer., 76, 803-832.
- BURTON, G.D. (1965): Vapor pressure glycolation of oriented clay minerals. Amer. Miner., 40, 124-126.
- CHAMLEY, H. (1971): Recherches sur la sédimentation argileuse en Méditerranée. Thèse Univ. Aix-Marseille, 401 pp.
- DAMIANI, A., FAVRETTO, L. and MORELLI, G.L. (1964): Le argille della fossa mesoadriatica. Arch. Oceanogr. Limnol., 13, 187-196.
- GRIFFIN, J.J., WINDOM, H and GOLDBERG, E.D. (1968): The distribution of clay minerals in the World Ocean. Deep-Sea Research, 15, 433-459.

- HESSE, R., RAD, von, U. and FABRICIUS, F.H. (1971): Holocene sedimentation in the strait of Otranto between the Adriatic and Ionian Seas (Mediterranean). *Marine Geol.*, 10, 293-355.
- KELLER, W.D. (1970): Environmental aspects of clay minerals. *Journ. Sed. Petrol.*, 40, 788-813.
- MAREL, van der, H.W. (1966): Quantitative analysis of clay minerals and their admixtures. *Contr. Mineral. Petro.*, 21, 96-138.
- MARINO, C.M. and FIGORINI, B. (1969): Datazione dei sedimenti recenti del Mare Adriatico col metodo del radio-carbonio. *Atti Soc. Ital. Sci. Nat.*, 109, 469-484.
- MILLOT, G. (1964): *Geologie des argiles*. Masson, Paris.
- PARHAM, W.E. (1966): Lateral variations of clay mineral assemblages in modern and ancient sediments. *Proc. Internatl. Clay Conf. Jerusalem*, 1, 135-145.
- FIGORINI, B. (1967): Aspetti sedimentologici del Mare Adriatico. *Mem. Soc. Ital. Sci. Nat.*, 16, 131-200.
- FIGORINI, B. (1968): Sources and dispersion of recent sediments of the Adriatic Sea. *Marine Geol.*, 6, 187-229.
- PORRENGA, D.H. (1967): Clay mineralogy and geochemistry of recent marine sediments in tropical areas. Thesis, Univ. Amsterdam, 145 pp.
- QUAKERNAAT, J. (1968): X-ray analyses of clay minerals in some recent fluvial sediments along the coasts of central Italy. Thesis, Univ. Amsterdam, 105 pp.
- RAD, von, U., SIGL, W. and OELTZSCHNER, H. (1970): Bodenströmungen und Sedimenttransport im Golf von Manfredonia (Italien, Südadria). *Geol. Rundsch.*, 60, 145-164.
- RATEEV, M.A., GORBUNOVA, Z.N., LISITZKYN, A.P. and NOSOV, G.L. (1969): The distribution of clay minerals in the oceans. *Sedimentology*, 13, 21-43.
- RIZZINI, A. and VEGGIANI, A. (1969): Studio della distribuzione delle sabbie a mezzo dei minerali pesanti. Litorale adriatico tra Ravenna e Fano. *Boll. Camera C.I.A.A. Forlì*, 23, 45-75.
- SCHULZ, L.G. (1960): Quantitative X-ray determinations of some aluminous clay minerals in rocks. *Clays Clay Miner.*, 7, 216-224.
- STRAATEN, van, L.M.J.U. (1970): Holocene and late-Pleistocene sedimentation in the Adriatic Sea. *Geol. Rundsch.*, 60, 106-131.
- TOMADIN, L. (1971): I minerali argillosi nei sedimenti recenti di tre monti sottomarini del Mare Tirreno. *Atti 1º Congr. Naz. Gruppo Ital. A.I.P.E.A.*, 35-42.
- VENKATATHNAM, K. and RYAN, W.B.F. (1971): Dispersal patterns of clay minerals in the sediments of the eastern Mediterranean Sea. *Marine Geol.*, 11, 261-282.
- ZEZZA, F. (1969): Interpretazione idrodinamica delle strutture sedimentarie nei depositi di spiaggia del litorale adriatico della Puglia. *Geol. Appl. Idrogeol.*, 4, 47-61.

## DISTRIBUTION OF CLAY MINERALS IN THE SPANISH TRIASSIC SEDIMENTARY BASINS(\*)

M.A. Caballero and J.L. Martín Vivaldi

Departamento de Cristalografía y Mineralogía, Facultad de Ciencias,  
Universidad Complutense, Madrid, Spain.  
Instituto de Geología Económica e Instituto "Lucas Mallada"  
del C.S.I.C., Madrid, Spain.

**ABSTRACT.** - The present paper is a detailed study of the distribution of clay minerals in four Spanish Triassic sedimentary basins. It was found that this distribution depends not only on the geomorphology of the area of origin, on the climate and on the quantity of ions in the basin, but that compartmentalisation of the substrata and the type of rocks to be found in the area of origin are also important determinant factors.

### INTRODUCTION

The fine fraction both of the Germanic and of the Alpine facies of the Spanish Triassic sediments has been studied by numerous authors: Martín Vivaldi and Mac Ewan (1957); Martín Vivaldi and Rodríguez Gallego (1961); Lucas (1962); Dorronsoro, González and Martín Vivaldi (1967); Krum (1969); Marfil (1971); González, Fenoll Hachali and Martín Vivaldi (1971); Caballero and López Aguayo (1972).

---

(\*) This study is part of the Caballero's Ph. D. Thesis to be submitted to the Universidad Complutense de Madrid, under the supervision of Prof. Martín-Vivaldi.

Previous studies dealt only with partial aspects of the problem. The present paper is intended to be a study of different Spanish basins, analysing the variations in their mineralogy, from the basins of the north of Spain, by way of those in the centre, to those of the south of Spain, the results of which will be possible to compare with those obtained in the French and in the Moroccan Triassic by Lucas (1962).

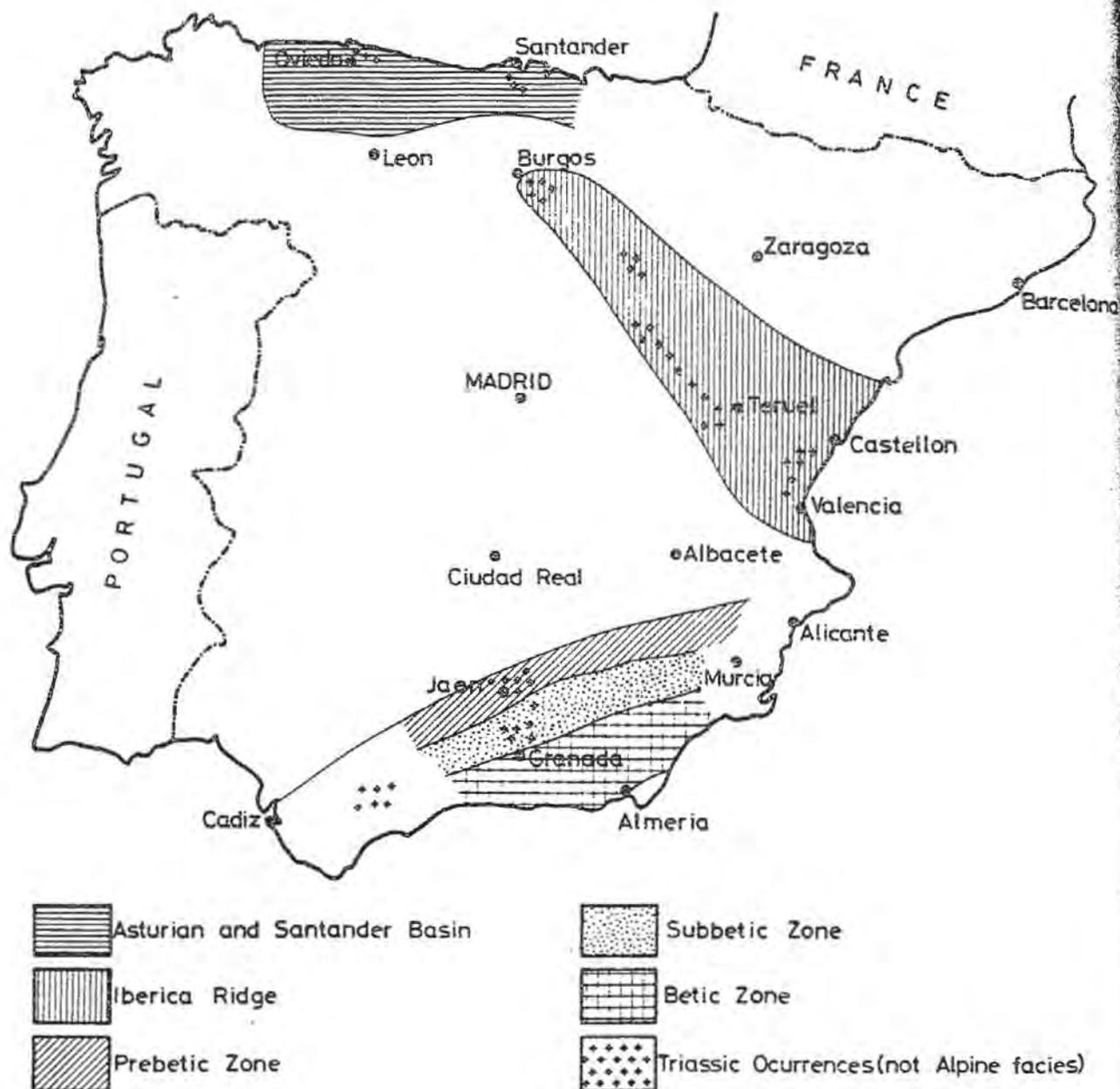


Figure 1. Geographical setting of the four Triassic sedimentary basins studied.

## GEOGRAPHICAL AND GEOLOGICAL SETTING

The four sedimentary basins studied are schematically represented in Fig. 1 which indicates approximately the position of the Triassic outcrops within them.

### Triassic Asturian Basin

The Triassic outcrops of the Asturian basin run from south of Cabo Peñas as far as Ribadesella, reaching their maximum extension in the area of Villaviciosa.

The series begins with some sand marl materials which are termed Permo-Triassic, since their precise age is difficult to establish. The Triassic series properly speaking comprises a belt of sandstones and conglomerates which can be up to 100 m. thick. Above them lie some metres of marl, clay marls and limestone marls possibly attributable to the Muschelkalk, and finally the upper strata of the series comprise marls and red clays intercalated with beds of gypsum and bipyramidal quartzes which belong to the Keuper and which have a mean thickness of 200 m.

### Iberian Ridge

The Iberian Ridge is bounded on the north-east by the Ebro depression, on the south-east by the Tajo basin and on the south by the Betic Ranges.

Within this zone the Triassic is very fully developed, and now here in the Iberian peninsula does it attain a greater extension.

The Buntsandstein is composed of basal conglomerates of brecciated type and of conglomerates interbedded with sandstones and clays.

The Muschelkalk is largely composed of dolomitic limestones, limestones and marls.

The Keuper has a typically Germanic facies, being composed of variegated clays and marls, interbedded at frequent intervals with gypsums and salts.

### Prebetic Zone

The Prebetic zone constitutes the most outlying sector of the Betic ranges, being bounded on the north by the Central Tableland, on the north-east by the Iberian Ridge, on the east by the Guadalquivir depression and on the south by the Subbetic Zone.

In this zone, the Buntsandstein is composed of basal conglomerate interbedded with sand. Calcareous levels interbedded with marl make up the Muschelkalk, while the Keuper is basically of clay marl, interbedded at frequent intervals with gypsums.

## Subbetic Zone

The Subbetic Zone includes the most southerly Triassic outcrops of Germanic facies in the Iberian Peninsula, and it is bounded on the north by the Prebetic Zone and on the south by the Betic zone where the Triassic has an Alpine character.

In the Subbetic Zone only the Keuper is well developed, the Muschelkalk only appears at certain points and there in small thicknesses. The Buntsandstein does not appear at all, or at least up to the present time no materials have been found which are clearly attributable to this stage.

The Keuper, of a typically Germanic facies, is composed of variegated clays interbedded with gypsums, which are sometimes massive, and at certain points there may be interbeddings of sand.

To establish good stratigraphic columns in this zone is very difficult owing to the intense diastrophism to which these materials have been subjected, accentuated by their high levels of plasticity.

## EXPERIMENTAL METHODS

The fraction  $< 2 \mu$  was extracted, using "Calgon" as a dispersing agent, and was subsequently studied by means of x-ray diffraction, by D.T.A. and by electron microscope. For the x-ray diffraction a Philips diffractometer and  $\text{Cu K}\alpha$  radiation was used. The D.T.A. reading were obtained by a Deltatherm apparatus, model D-200, and electron microscopy was carried out with a Philips microscope, model M-300.

The quantitative estimates were arrived at by homogenising the complex exchange with magnesium acetate and by arbitrarily assigning to all the minerals an identical reflectance. Thus although the percentages are not accurate they are comparable one with another.

## EXPERIMENTAL RESULTS

### Asturian Basin

Table I shows the range of values for the mineralogical composition of the fine fractions of the Triassic in the Asturian Basin. It will be seen from this that the Permo-Triassic is fundamentally illitic. Kaolinite appears in some series, generally in those nearest the edges of the basin. Chlorite can in specific series reach relatively high values (40%), the material being of low crystallinity.

At particular points in the basin and in the upper strata there appear fairly regular interstratifieds of chlorite-montmorillonite,

Table I

Mineralogical composition range for fine size of Triassic Asturian Basin

	I	K	C	M	V	$14_C-14_M$	S	$10_I-14_C$
Permotriassic	100 - 60	5 (x)	40 - 0	-	-	40 - 0 (x)	-	-
Lower Keuper	30 - 10	-	20 - 10	-	-	80 - 60	-	-
Upper Keuper	30 - 10	5 (x)	90 - 70	70 - 20	(x)	-	30 - 10 (xx)	10 - 5 (x)

I = Illite; K = Kaolinite; C = Chlorite; M = Montmorillonite; V = Vermiculite;  $14_C - 14_M$  = Interstratified chlorite-montmorillonite; S = Sepiolite;  $10_I - 14_C$  = Interstratified mica-chlorite; (x) = Sporadic or lons localized zones; (xx) = not frequent

and these may be associated with chlorite of a crystallinity higher than that found in the lower strata of the Permo-Triassic.

The Lower Keuper is characterised by a lower percentage of illite; chlorites are not very abundant but there is on the other hand a high percentage of interstratifieds of chlorite-montmorillonite type.

The Upper Keuper shows a clear predominance of chlorite over the remaining minerals, and these are chlorites of high crystallinity, the crystal being of hexagonal habit, similar to those described by Lucas (1962) and of rhombic habit, similar to those described by Alonso and Marfil (1970); Fig. 2 shows one of these chlorites of rhombic morphology.

The study made by x-ray diffraction to calculate the degree of asymmetry, in accordance with Petruk's method of calculation (1964) gave a figure of 0.3, which indicates a very low content of heavy atoms in the octahedral layer.

This fact and the similarity between D.T.A. curves obtained by us and those given by Caillere and Henin (1957) for penninite, leads us to think that we have here a fundamentally magnesian chlorite of the penninite-clinoclone variety.

Very sporadically and at very localised points in some series, minerals like kaolinite, vermiculite and mica-chlorite interstratifieds may appear, but always in low proportions.

Infrequently and in very specific and localised areas of the basin, not necessarily in the centre, montmorillonite and sepiolite are found, the percentage of the latter rising towards the top of the formation.

### Iberian Ridge

Table II shows the mineralogical composition of the Triassic of the Iberian Ridge.

It can be deduced from this that the Muschelkalk is basically illitic with small quantities of chlorite.

The Lower Keuper shows a smaller quantity of illite while the amount of chlorite rises and there are some interstratifieds. In the most illitic areas kaolinite may be found.

The Middle Keuper is characterised by a conspicuous increase in interstratifieds and a reduction in the amount of illite.

The Upper Keuper shows a high concentration of interstratifieds, the chlorite being well crystallised and even showing a rhombic morphology.

At some points in the basin close to areas which emerged during the Keuper, small percentages of kaolinite and even large quantities of montmorillonite may be found next to the illite and the interstratifieds.

Table II

Mineralogical composition range for fine size of Triassic

## IBERICA RIDGE

	I	K	C	M	$^{14}_C-^{14}_M$
Muschelkalk	100 - 75	-	25 - 0	-	-
Lower Keuper	60 - 50	5 (x)	30 - 20	-	20 - 10
Medium Keuper	30 - 20	-	30 - 20	-	60 - 40
Upper Keuper	30 - 20	5 (x)	20 - 10	40 - 20 (x)	60 - 40

(Symbols see Table I)

Prebetic Zone

(Table III). In the Prebetic zone both the Buntsandstein and the Muschelkalk are stages in which illite and chlorite predominate though the latter not in a very high proportion. In the Upper Muschelkalk interstratifieds of chlorite-montmorillonite type are found next to the illite and chlorite.

In the Keuper the illitic nature of the basin remains, but the percentage of montmorillonite rises in relation to the lower stages. In series at a distance from the border of the basin the illitic character of this stage diminishes noticeably (30%), as does the amount of montmorillonite (10%-20%). On the other hand the quantity of interstratifieds at 14 A rises.

Subbetic Zone

(Table IV). The Keuper of the subbetic zone is characterised by its high illite content and also by the constant presence of chlorite, in the majority of cases in a high percentage, the chlorites being in general well crystallised in hexagonal or rhombic habits. Associated with these minerals and in saline facies an interstratifieds of chlorite and swelling chlorite. Also, sepiolite is found in some very localised sectors.

Table III

Mineralogical composition range for fine size of Triassic

## PREBETIC ZONE

	I	K	C	M	$10_I-14_C$	$14_C-14_M$
Buntsandstein	100 - 80	5	20 - 10	-	5	-
Muschelkalk	100 - 80	5 (x)	10 - 5	20 - 10	-	20 - 10
Keuper	100 - 30	5 (x)	20 - 10	40 - 10	10 - 5	50 - 40 (x)

(Symbols see Table I)

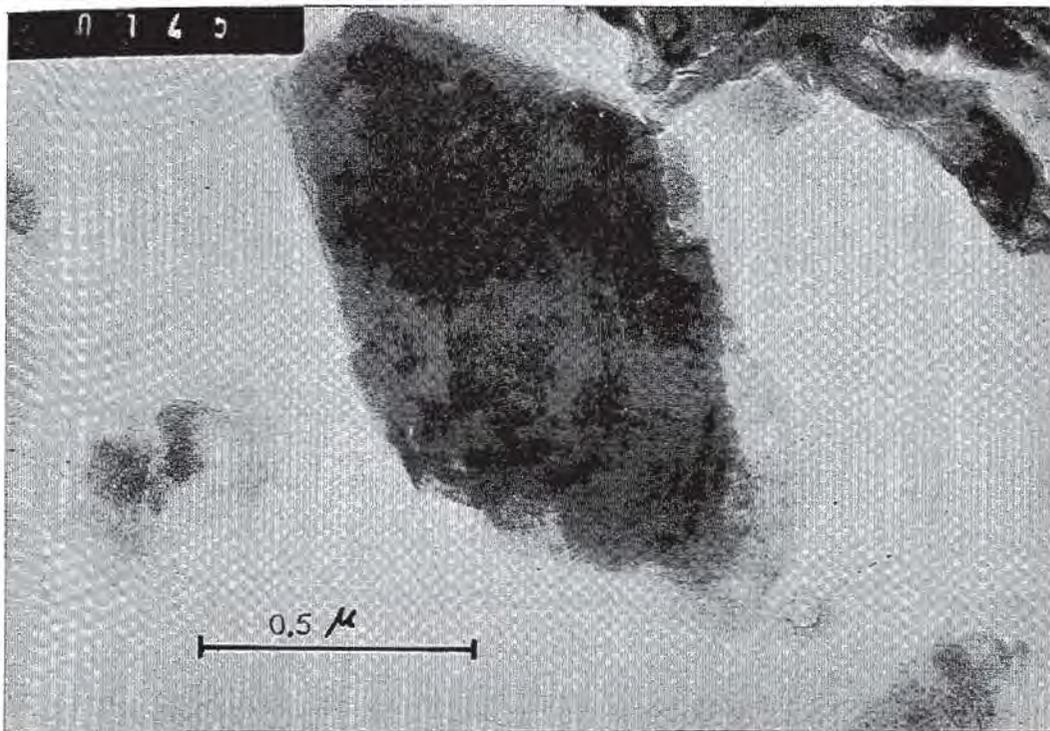


Fig. 2 Triassic chlorite of rhombic habit.



Table IV

Mineralogical composition range for fine size of Keuper

## SUBBETIC ZONE

Minerals	%
Illite	80 - 70
Chlorite	50 - 20
Kaolinite	X
Sepiolite	(xx)
$^{14}C - ^{14}SC$	20 - 10

$^{14}C - ^{14}SC$  = Interstratified Chlorite-Swelling chlorite.

In the Subbetic Zone of the Betic ranges it is very difficult to speak of proximity to or distance from coastlines for the Triassic, since it is almost entirely allochthonous or diapiric in character, and to fix its original position is in the majority of cases an arduous task and one whose results are somewhat hypothetical.

## DISCUSSION AND CONCLUSIONS

A preliminary analysis of the results set out above indubitably points to a schema of mineral distribution similar to that given by Lucas (1962) and Millot (1964) for Triassic basins. That is to say, some lower strata which are clearly detrital and in which illite is in the majority, followed by strata less detrital in character in which interstratifieds are the most abundant minerals, and finally essentially argilloceous strata with numerous saline facies in which illite appears less than other minerals, with chlorites and even neoformed minerals being the most abundant.

According to the authors previously cited this sequence does not hold good only in the vertical plane but is accentuated as we approach the center of the basin, when the detrital influences are less and where also the quantity of ions in solution is greater. From a chronological point of view the detrital strata (illite, poorly crystallised chlorite). Would correspond in general to a Buntsandstein-Lower Muschelkalk period; the strata with abundant interstratifieds to an Upper Muschelkalk-Lower Keuper period and the strata of neoformed minerals (sepiolite) and well crystallised chlorites to a Middle-Upper Keuper period.

A more rigorous analysis of the data we have obtained leads us to believe that the schema postulated above is correct as a large scale generalisation, but that it is not wholly applicable to each particular basin, since the sedimentation within each of the basins is not only determined by the geomorphological conditions of the zones of emergence, by the quantity of ions in the basin, or by climatic factor; rather the nature of the rocks in the area of origin and the compartmentalised structure of the basins are very decisive and important for the distribution of clay minerals in Triassic sedimentary basins.

Thus, the Asturian Basin examined in outline offers a clear example of how detrital minerals are abundant in the lower Triassic. Illite is very abundant, and there is Kaolinite and poorly crystallised chlorite. Interstratified are present in the greatest quantities in the middle to upper Triassic, and well crystallised chlorites (rejuvenated?, neoformed?, transformed?) are the most abundant minerals in the Upper Triassic.

Nevertheless it can be seen that, even in the Permo-Triassic, in certain sectors of the basin transformation must have occurred frequently; interstratified are found in quantities up to 40%, which indicates that even during a period of fundamentally detrital sedimentation, in certain sector the quantity of ions was sufficiently great to begin the scarring of the inherited degraded networks, with the subsequent appearance of the interstratified structures.

During the sedimentation of the Upper Triassic there must have been areas in which the alkalinity and the ions present were suitable for the neoformation of montmorillonite and sepiolite. Nevertheless these areas not necessarily be found in the interior of the basin; if the compartmentalisation of the basin were sufficient, such conditions could be found even close to the border.

In the Iberian Ridge a reduction in illite is also found between the Muschelkalk and the Keuper at the same time as interstratified minerals and well crystallised chlorites increase in number. But in some series montmorillonites and kaolinites appear in proximity to zones of emergence, which leads us to consider that they are possibly detrital in character or even that the compartmentalisation of the basin and the alkalinity were sufficient for the neoformation of smectites.

The paleogeographical data of Sánchez de la Torre and Agueda (1970) indicate clearly that the distances between the points at which we have found montmorillonite and the coast do not exceed 20 Km., and at the same time they confirm that the basin is highly compartmentalised with numerous ridges and hollows. These facts can lead one to conclude either that the montmorillonite was inherited or that it was neoformed or both at once.

In the Prebetic Zone we find a distribution similar to that of the Iberian Ridge. The series nearest to the zones of emergence, which in this case form the Central Tableland, are very rich in illite, and the proportions of montmorillonite can reach a high percentage, with kaolinite usually being present. As we move southwards, towards the interior, interstratifieds become more abundant and the detrital character becomes less pronounced, although not a great deal less so, yet montmorillonite continues to be present in lower percentages. This would confirm the hypothesis that in areas relatively close to the coasts inherited montmorillonite may be found, and that at the same time, if the basin is compartmentalised, conditions can be produced suitable for aggradation (appearance of interstratified).

In the Subbetic Zone it is difficult, as we have said, to establish the original position of Triassic materials, yet it is right to suppose that these sediments are further offshore than those of the Prebetic Zone, a fact confirmed by their less detrital character in relation to the Prebetic Zone (reduction in the percentage of illite) and also by the fact that the chlorites found are of a magnesian type, of good crystallinity and excellent morphology, which suggests that they are the result of transformation. At the same time the very localised presence of sepiolite and kaolinite means that there must exist in the basin areas of high alkalinity and ionic concentration in which the neoformation of sepiolite is possible, and areas near sector of emergence, in the interior of the basin, capable of receiving kaolinite formed in a non-marine environment, since we find it difficult to accept, as Krum accepts (1969), that kaolinite may be formed in marine conditions, since the washing necessary for the formation of this mineral can only be produced with difficulty in basins like those with which we are dealing even in the areas nearest to the coast.

Finally, in view of the facts above, we must assume that the distribution of clay minerals in Triassic basins, at least those in Spain, is determined by the following considerations:

a) The compartmentalisation of the basin, which can bring about conditions of alkalinity and ionic concentration at any point in the basin, and not necessarily in the centre of it.

b) Even during the Lower Triassic compartmentalisation of the basin can influence ionic conditions sufficiently for the occurrence of aggradation to be possible.

c) The climatic conditions during the Triassic must have diffe-

rent from place to place and not been uniform as Lucas assumed (1962) since we have found the mineralogy to differ between the north and south of the Peninsula.

d) Montmorillonite is a mineral frequently found in the Middle-Upper Triassic, and can be either inherited or neoformed.

e) Illite generally diminishes from the Lower to the Upper Triassic, although in border series close to continental zones very high values may be attained even in the Upper Triassic.

#### REFERENCES

- ALONSO, J. and MARFIL, R. (1970): Morfología de las cloritas triásicas, Reunión Hispano-Belga de Minerales de la Arcilla. Madrid pp 215-218.
- CABALLERO, M.A. and LOPEZ AGUAYO, F. (1972): Ambientes genéticos de los minerales de la arcilla en cuencas sedimentarias Triásicas y Wealdenses españolas, VI Reunión Grup. Español Sed. (Granada). (in preense).
- CAILLERE, S. and HENIN, S. (1957): The Chlorite and Serpentine minerals. Cap. VIII of The Differential Thermal Investigation of Clays, Mackenzie Edit. Mineralogical Society London.
- DORRONSORO, C., GONZALEZ MARTINEZ, J. and MARTIN VIVALDI, J.L. (1967): Nota sobre la mineralogía del Trias bético y subbético, VII Inter. Sed. Cong. Edimburg(not publisher).
- GONZALEZ MARTINEZ, J., FENOLL HACH-ALI, P. and MARTIN VIVALDI, J.L. (1970): Estudio mineralógico de niveles arcillosos del Trias Alpujarride, Bol. Geol. Min. LXXXI-VI. pp 620-629.
- KRUM, M. (1969): A scheme of clay mineral stability in sediments, based on clay mineral distribution in Triassic sediments of Europe, 1969 Inter. Clay Conf. Tokyo, Japan, pp 313-324.
- LUCAS, J. (1962): Le transformation des mineraux argileux dans le sedimentation. Etudes sur les argiles du Trias. Mem. Serv. Carte Geol. d'Alcase et de Lorraine. nº 23.
- MARTIN VIVALDI, J.L. and MAC EWAN, D. (1957): Triassic chlorites from the Jura and the Catalan coastal Range, Clay Min. Bull. vol 3. pp 177-183.
- MARTIN VIVALDI, J.L. and RODRIGUEZ GALLEG0, M. (1961): Some problems in the identification of clay minerals in mixtures by x-ray Diffraction I. Chlorite-Kaolinite mixtures, Clay Min. Bull. vol. 4 pp 288-292.
- MILLOT, G. (1964): Geologie des argiles, Mason et Cie. Edit. Paris.
- PETRUK, W. (1964): Determination of the heavy atom content in chlorite by means of the x-ray diffractometer. Amer. Min.vol 19 pp 61-71.
- SANCHEZ DE LA TORRE, L. and AGUEDA, J. (1970): Paleogeografía del triásico en el sector occidental de la Cordillera Ibérica, Est. Geol. vol XXVI pp 423-430.

# CLAY MINERAL PROVINCES IN EUROPEAN MALM

W.M. Bausch

Mineralogisches Institut der Universität Erlangen  
Erlangen, Germany

## ABSTRACT

Clay mineral distribution in sediments of Upper Jurassic were investigated in most parts of Europe. Only the insoluble residues of limestones were selected, for the following reasons:

- a) similar sedimentary conditions.
- b) preservation effect of lime matrix.

The clay mineral distribution in this geologic period was not homogeneous. There are found five "clay mineral provinces".

1. Kaolinite-illite province on the epicontinental shelf of France, Germany and part of the Balkans.
2. Two chlorite-albite provinces in marginal regions of the Tethys geosyncline (south-east of France and eastern Betic chains).
3. Chlorite province in Lower Saxony basin.
4. Muscovite province in Iberian peninsula.
5. Illite-mixed-layer province (free of kaolinite) in the Tethys geosyncline.

The clay mineral assemblages demonstrate the integrated weathering conditions on the surrounding denudated land masses. Only in few cases influences of sedimentary conditions (semi-salinar conditions in the Lower Saxony basin) or local influences (high relief energy on the Iberian peninsula) are visible.

Kaolinite forms under tropical weathering conditions, and not under conditions of limestone sedimentation. Therefore the kaolinite-illite ratio may be used for paleoclimatic conclusions.

Widespread similar trends of this ratio in the succession Oxfordian-Kimmeridgian-Tithonian stages may be interpreted as climatic changes.

There are some indications that illite is formed from mixed-layer minerals in early stages of diagenesis.



CRYSTALLOCHEMICAL HETEROGENEITY OF GLAUCONITE AS  
DEPENDING ON THE CONDITIONS OF ITS FORMATION  
AND POSTSEDIMENTARY CHANGE

V.D. Shutov, M.Ya. Katz, V.A. Drits, A.L. Sokolova  
Geological Institute, USSR Academy of Sciences,  
Moscow, USSR

G.A. Kazakov

Institute for Geochemistry and Analytical Chemistry,  
USSR Academy of Sciences, Moscow, USSR

ABSTRACT. - A method for the study of the crystallochemical heterogeneity of "monomineral" glauconite samples is proposed. The experimental investigation of glauconites of various geological age with this method and the analysis of published data made it possible to suggest a scheme of the process of formation of glauconite and its postsedimentary evolution.

INTRODUCTION

Numerous studies have been devoted to glauconite (Hendricks, Ross, 1941; Smulikowski, 1954; Burst, 1958; Hower, 1961; Millot, 1964; Foster, 1969; Nikolaeva, 1971; and others); however, the genesis of this mineral and its postsedimentary evolution remain largely obscure and require further investigation.

This paper proposes a method for analysis of the crystallochemical non-uniformity of glauconite. The method has been applied to obtain new data on the sedimentary conditions of the formation of glauconite and on the chemical evolution of its composition during epigenesis (deep diagenesis). The results of the investigation of the crystallochemical heterogeneity of "monomineral" glauconite samples

enabled a more rational analysis of the interrelations between the chemical composition and the geological age of glauconite using published data for that purposes.

Only one characteristic morphogenetic type of glauconite was chosen for the object of study its globules in the sandy and aleuritic rocks of various geological age, predominantly developed in platform and, to a lesser extent, in miogeosyncline areas.

## DESCRIPTION OF METHOD

A "monomineral" glauconite sample, extracted from the rock with the aid of an electromagnetic isodynamic separator, was divided into different density fractions in a heavy liquid column with a stepwise change of density. The sample was placed at the bottom of the column. Through a capillary tube inserted from the top down to the bottom of the column ever heavier liquids (mixture of bromoform and dimethylformamide) were supplied to form a discrete series of layers, each 2-3 cm high. The layer density increased up the column with a step of  $0.020 \pm 0.001 \text{ g/cm}^3$ . (The density of "working" liquids was controlled by calibrated bench marks). In order to reduce the influence of porosity of the mineral grains, the sample was left to stay for two hours in the lightest "working" liquid. To extract the grains of different density concentrated in the strata at the juncture of the adjacent liquids these were pumped out together with the grains from the top of the column. Each fraction of the sample was weighed. Then a histogram of the density distribution of the grains was plotted. X-ray and electron diffraction were used to establish for every fraction the polytype, degree of structural order, presence of mixed-layer structures, etc. For some of the fractions the complete or partial chemical composition was determined. About 50 glauconite samples were studied in this manner.

## EXPERIMENTAL

Figure 1 shows most characteristic histograms for glauconites of different age and the major features of the individual fractions, such as the values of  $d$ ,  $\text{K}_2\text{O}$  content and the chemical composition. For shortage of space we cannot discuss in this paper the finer structural differences of various fractions manifested in the directed changes of the shape and intensity of basal reflections, degree of structural order, etc.

A typical feature of recent glauconites is the fact that their grain density varies in an exceptionally wide range between 2.3 and  $2.8 \text{ g/cm}^3$ . With the increasing density of the globules a directed

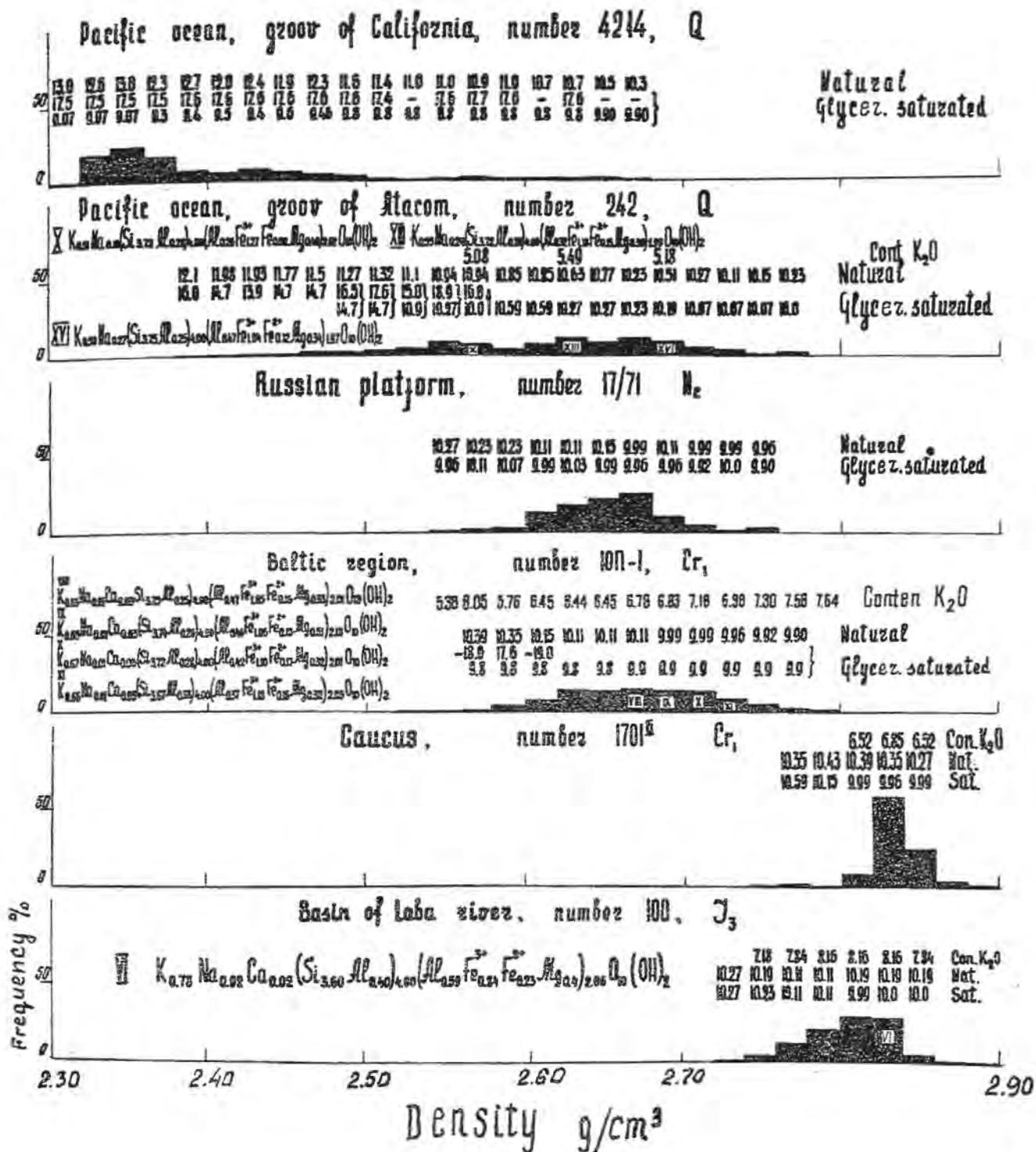


Figure 1 a.

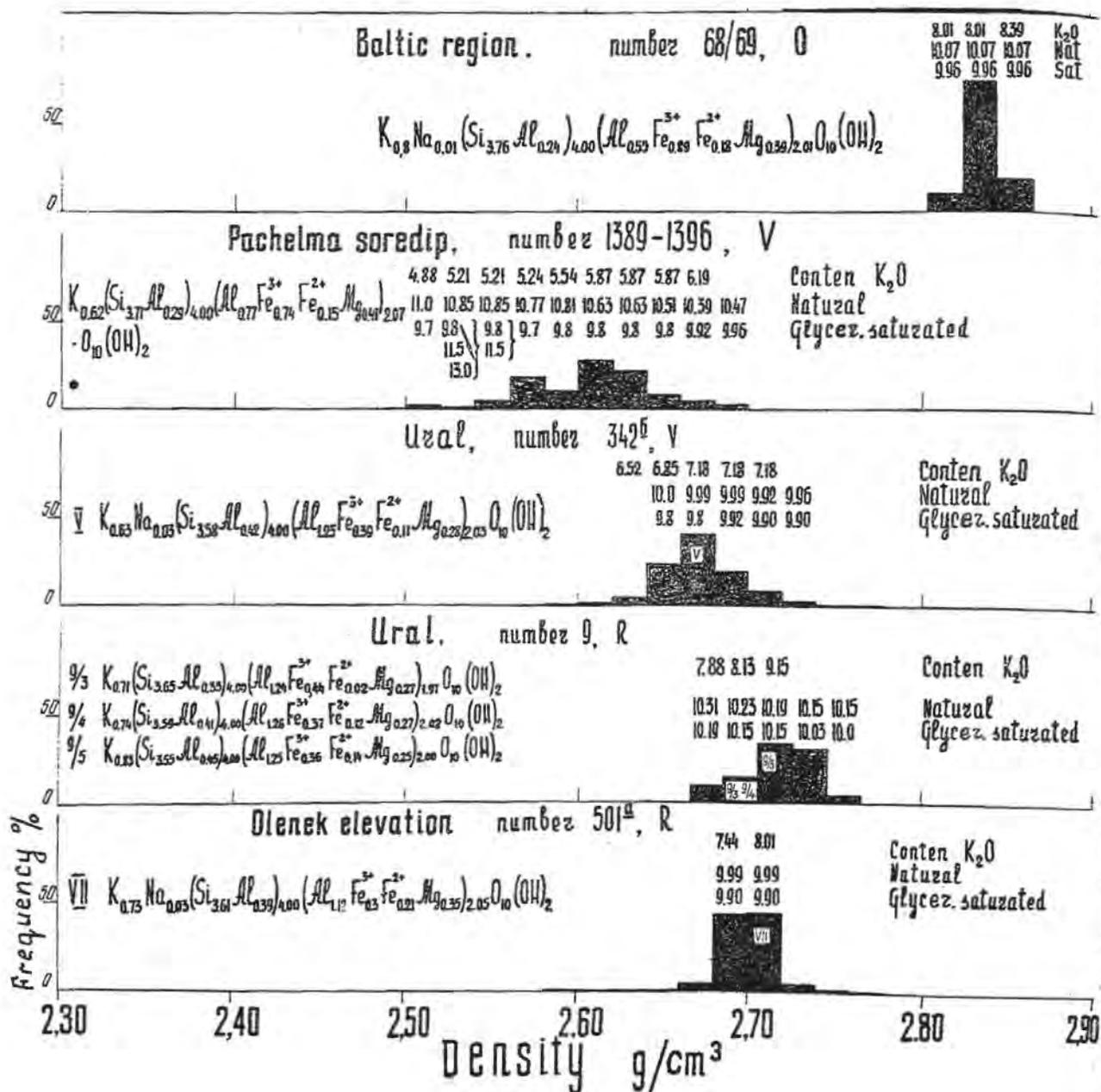


Figure 1 b.

structural change is observed—from montmorillonite through a series of mixed-layer structures to glauconite containing practically no swelling layers (Fig. 1, samples 4214 and 242). Sample 242 from the Atakomsk Trench with the glycerine complex forms 14 Å layers which is connected with the limit saturation of the montmorillonite interlayers with K cations. After heating, the layers are contracted to 10 Å. The main factor determining the density fractionation of recent glauconite grains is the number of swelling interlayers (see Fig. 1, the structural formulas of the fractions of Sample 242).

For Tertiary and Cretaceous glauconites, the density range of the fractions is considerably narrowed, largely because of the absence of the lightest fractions. This is due to the disappearance of montmorillonite (e.g., in Sample ЮП-1 it is present only as relics) and the essential decrease of the number of swelling layers in mixed-layer structures. However, as the facial environments vary in a broad range between dispersed and concentrated processes of formation of glauconite globules, the grain density accordingly varies in either a relatively narrow (e.g., Sample 1701) or broad range (e.g. Sample ЮП-1). The heterogeneity of samples for this mineral group depends both on the number of swelling layers and on the variation of the cation composition of the glauconites. For example, in Sample ЮП-1, the growth of the grain density is accompanied by a decrease of the number of swelling layers and an increase of K, Fe<sup>3+</sup> and Al<sub>IV</sub> content. The glauconites of the Early Mesozoic and Paleozoic horizons are characterized by an even narrower density spectrum confined within the range of 2.80 - 2.85 g/cm<sup>3</sup>, due to the extremely concentrated process of the glauconite formation in the samples studied. The glauconite fractions have practically constant composition, contain no swelling layers and are marked by a high structural order (modification 1 M). (Fig. 1, Samples 68/69 and 100).

The studied glauconites of the Pre-Cambrian (Vendian) complex are characterized as a rule by more distended histograms of grain density distribution (as compared with the preceding glauconite group) and a general shift of the histogram towards lesser density values. This is particularly clear in the case of the glauconites of the platform units (Fig. 1, Sample 1389-1396). In the lightest fractions of these samples, a low K<sub>2</sub>O content and a relatively greater number of 14 Å layers swelling under glycerine saturation are observed. The glauconites of the miogeosyncline zones have a more uniform composition (Fig. 1, Sample 342), the swelling layers being observed only in the lightest fractions. In the both cases, the composition of the glauconites is characterized by a higher Al<sup>3+</sup> content. In turn, the oldest Riphean (Sinian) glauconites were found to have a narrow histogram around 2.7 g/cm<sup>3</sup>, high K<sub>2</sub>O (up to 9%) and Al<sub>2</sub>O<sub>3</sub> (up to 20%) content, practical absence of mixed-layer phases, and extremely high structural order. Data for Sample 9 (Fig. 1) indicate that K and Al contents grow with the increasing fraction density.

The data give convincing evidence of heterogeneity within so-called "monomineral" samples. It is the greatest for recent glauconites. This heterogeneity of glauconites has been found clearly to decline with increasing geological age. A high content of  $Fe^{3+}$  cations in octahedra of Tertiary and Cretaceous glauconite structures is also typical. Conversely, the increase of the geological age leads to a growth of  $Al^{3+}$ . The greatest structural order is, *ceteris paribus*, peculiar of the fractions having the greatest  $K_2O$  content.

These regularities suggest that in analyzing the interrelations between the composition, formation conditions and the geological age it would be wrong to disregard the heterogeneity of glauconites and to conduct their comparative studies without first subdividing them into groups. Therefore, published chemical analyses of glauconites (see "References" for the list of authors whose data on glauconites have been used) were divided into four groups according to  $K_2O$  content. Only the chemical analyses of globular glauconites extracted from sandy and aleuritic rocks were treated.

Figure 2 gives the distribution of the figurative points in the coordinates system  $Al_{\Sigma} (Al_{VI} + Al_{IV}) - Fe_{VI}^{3+} - \Sigma R_{VI}^{2+}$ . In the first group of samples ( $K_2O > 8\%$ ), the fields occupied by recent and Tertiary, Cretaceous, Paleozoic and Pre-Cambrian glauconites are clearly discernible. A consecutive shift of the fields towards greater  $Al_{\Sigma}$  is observed with the increase of age.

The same tendency is also traceable in the second and third groups, although the fields are not clearly delimitable, because the composition of glauconites of each age broadly varies either towards greater or smaller  $Fe^{3+}$  content.

The fourth group of samples ( $K_2O < 6\%$ ) contains glauconites mostly of a "young" age, including Cr. A complete overlapping of the fields of glauconites of different ages is typical of this group. Its major distinction from the preceding groups is that it contains the greatest number of Al-enriched "young" glauconites.

Figure 3 shows the dependence between  $Al_{IV}$  and the Fe-content of octahedra of all glauconites of different age. It is obvious that with an increasing geological age one can observe a shifting of the composition of glauconites towards lesser Fe-content up to pseudomorphoses of illite on glauconite; a tendency towards greater  $Al_{IV}$  with the "ageing" of glauconite is observable.

Figure 4 shows the dependence of  $Al_{VI}$  on  $Fe_{VI}^{3+}$  for four glauconite groups distinguished by  $K_2O$  content. Within each group the samples are divided into subgroups by  $Al_{IV}^{3+}$  content. The diagram is characterized by the following features:

1.  $Al_{VI} - Fe_{VI}^{3+}$  substitution grows within each of the subgroups with the increasing geological age.

2. Within each group it is possible to distinguish zones having a certain range of  $Al_{IV}$  content, in which a majority of the samples is concentrated (Fig. 4). In passing over from the first to the fourth

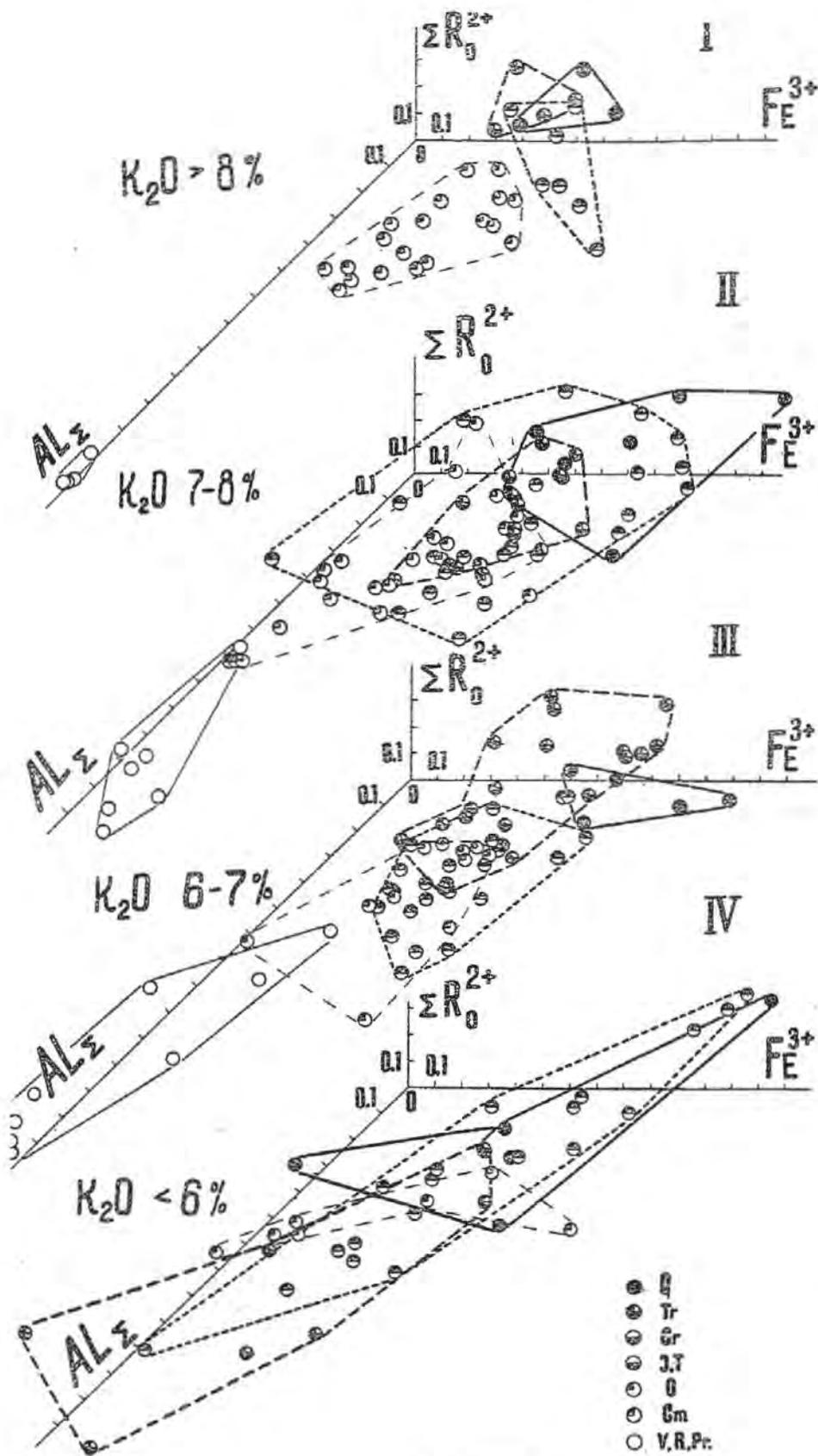


Figure 2.

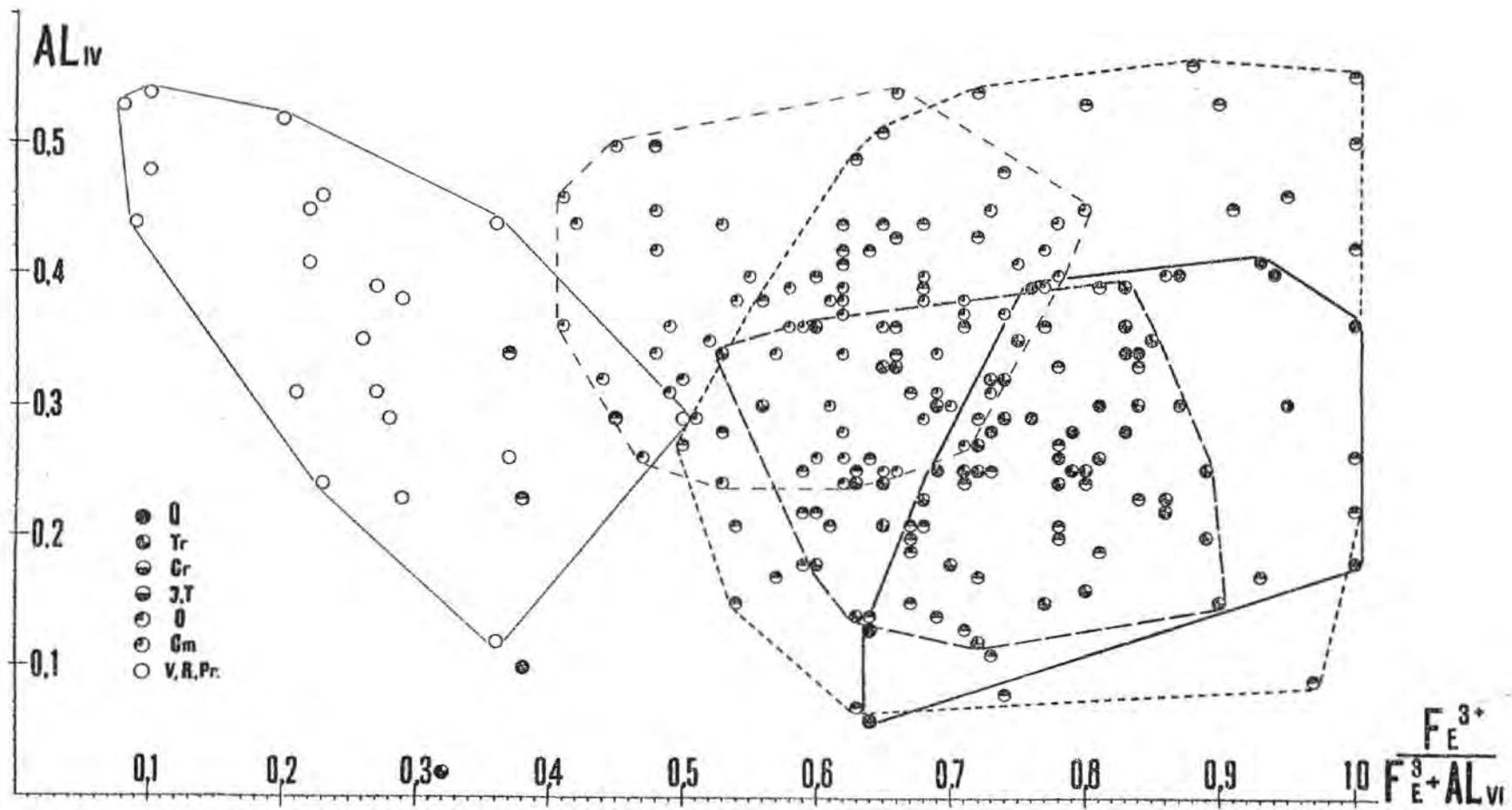


Figure 3.

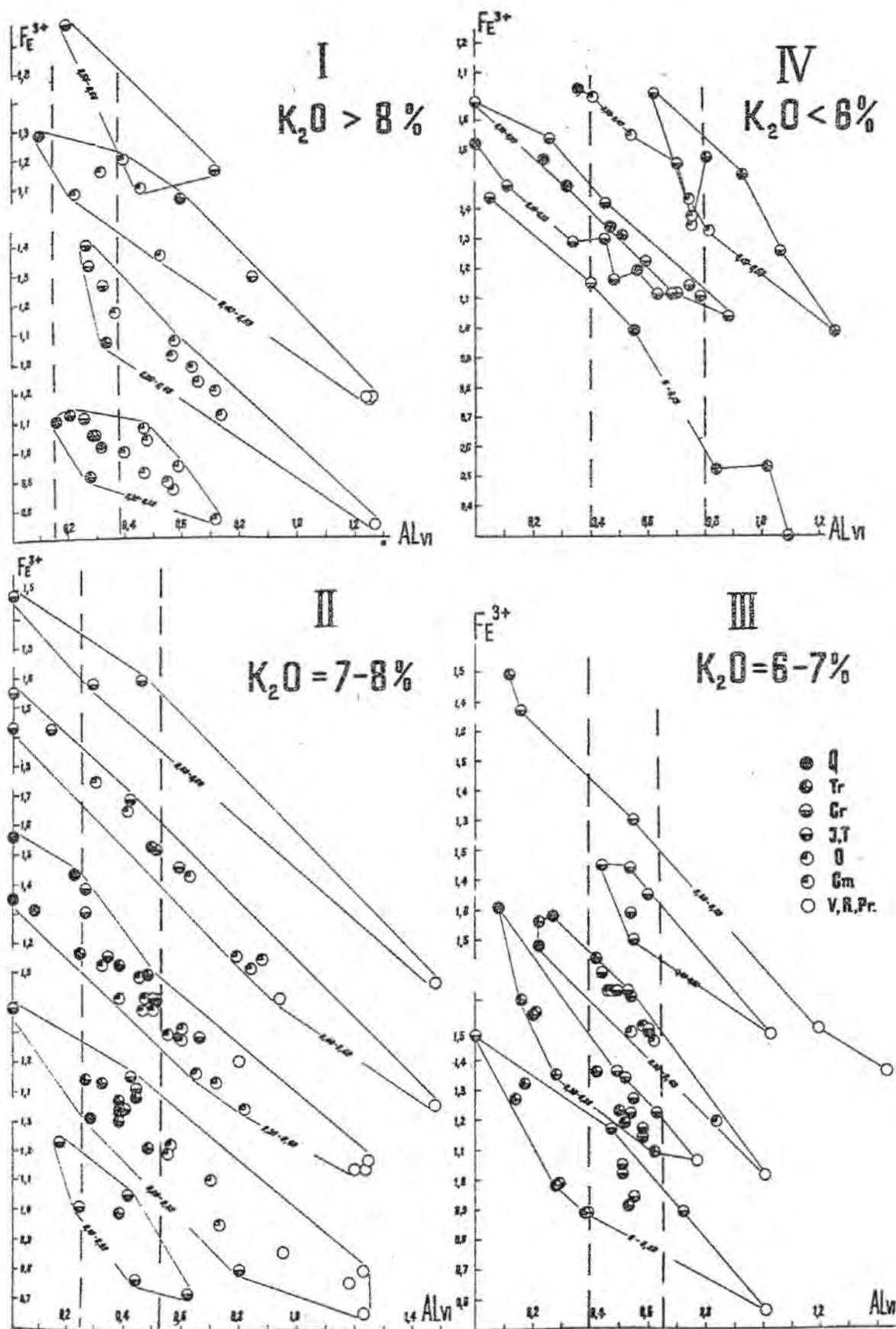


Figure 4.

group, the average  $Al_{IV}$  content of each zone consecutively grows. An "ageing" of glauconites takes place with the increasing  $Al_{IV}$  within the vertical zone of each group indicated by dotted lines (Fig. 4). As a rule, this trend is violated in the upmost parts of the zones, i. e. in case of the maximum  $Al_{IV}$  content, and "younger" glauconites again appear. We believe that their appearance is due not to the typical process of glauconitization, but rather to its development through transformation of biotite, muscovite, etc., inheriting the high tetrahedral charge of the latter.

3. Passing from the first to the fourth group, one observes a gradual decline of the lower limit down to which Al-for-Si substitution is possible in the group in question. In the first group the minimal value of  $Al_{IV}$  is 0.2 - 0.3; in the second one, it is 0.1 - 0.2; third, 0 - 0.2; and fourth, 0 - 0.1.

## DISCUSSION

We shall now discuss the general scheme of formation and post-sedimentary change of globular glauconite. As has been unambiguously indicated by the experimental data of the study of recent and Cretaceous glauconites, montmorillonite was the primary material for their formation. The character of the primary montmorillonite has been found to depend on the type of the associating terrigenous material and to vary from Fe-montmorillonite (nontronite) (Sample 242) and Fe-Al-montmorillonite (Sample 4214) to the predominantly Al montmorillonite (Sample 107-1). The former is connected with an abundance of phemic mineral fragments and basic effusives, while the latter associates with pure quartzose clastics. To a certain extent, glauconite inherits the features of primary montmorillonite. The most heterogeneous "young" glauconites of the fourth group (Fig. 2, 4) are represented both by predominantly Fe- and predominantly Al-varieties. Low Al-for-Si substitution in tetrahedra of a majority of contemporary glauconites of the fourth group, paralleled by a wide variations of octahedral composition, also emphasizes the "cognition" of glauconite with montmorillonites of various initial compositions.

That glauconite mostly was formed on montmorillonite seems logical since the latter appeared at the earliest stages of the formation of marine sandy silt in the presence of the minimal concentrations of the necessary elements, first of all Si and Al. In the conditions of low concentrations of K, montmorillonite functions as its efficient accumulator. Direct formations of glauconite, on the other hand, requires concentrated K solutions, which do not occur in normal marine environments.

The transformation of nontronite into glauconite through a series of mixed-layer structures takes place rather easily, since the

size of the octahedral network is such that K cations being fixed in the nontronite interlayers virtually do not affect the a and b parameters of the unit cell.

However, it seems that, in nature, glauconite can be formed also from initial Al-montmorillonite. Thus far it remains unclear whether in this case a preliminary "nontronitization" of the initial montmorillonite takes place, followed by its subsequent transformation into glauconite, or, conversely, if the supply of K leads to the Fe<sub>VI</sub>-for-Al<sub>VI</sub> substitution in octahedra. In the latter case the supply and fixation of K in Al-montmorillonite for the most part occurs in every second layer (Shutov et al., 1969). Such formation of mixed-layer structures perhaps causes a state of tension in individual layers, since the tetrahedral networks adjacent to the K-saturated interlayer must be more distended as compared with the tetrahedral networks of the same layers adjacent to the hydrated interlayers. The state of tension in the individual layers can be "eliminated" by Fe<sub>VI</sub>-for-Al<sub>VI</sub> substitution and the corresponding increase of the size of octahedral networks and the whole layer.

The process of penetration, accumulation and fixation of K cations and the parallel increase of Fe<sub>VI</sub> cations and decrease of Al<sub>VI</sub> cations in octahedra constitutes the essence of the typical sedimentary-diagenetic glauconitization.

Apparently, Al cations moved out of octahedra again took part in the formation of montmorillonite at the surface of the globule, which was again filled with K and Fe; Al was again moved out to form the new montmorillonite cover of the globule, and so forth. The kinetics of this mechanism of globule formation was described by Zumpe (1971). Figs. 7, 8 of his paper clearly show a Fe and K impoverishment and Si enrichment of the surface boundary of the globule.

The above scheme of the process of glauconite formation is corroborated by the published data on chemical composition of glauconites. For the glauconites of the recent stage, characterized by a general uplift of the continents and supply of polymictic phemic material to the basin, the initial stage of formation was Fe- or Fe-Al-montmorillonites. In the Tertiary epoch, largely characterized by a greater penneplenization of the continent and supply of weathered and (or) acid pyroclastic material to the basin, evidently the primary material was montmorillonite of a predominantly Al composition. Accordingly, Fig. 3 distinguishes for group IV two fields "tending" toward greater Fe-content in the case of recent glauconites and greater Al-content in the case of Tertiary glauconites.

The stage of the glauconite formation can take place with different velocities, depending on various facial environments, concentrations and supplies of the primary "building" material. At this stage there is no direct correlation between the geological age and the completion of the glauconitization process. For instance, Miocene glauconite (Fig. 1, Sample 17/71) was formed quickly and com-

pletely, whereas Cretaceous (Fig. 1, Sample KOT -1) and even older Vendian glauconite (Fig. 1, Sample 1389) recorded the successive stages of the glauconitization process with the relics of the initial montmorillonite phase.

The posterior stages of the postsedimentary transformation of glauconite, on the one hand, consisted in its maturation, i.e. in increase of  $Al_{IV}$  with the "ageing" of glauconite (See bottom-to-top the vertical columns bounded by dotted lines, Fig. 4).

On the other hand, with the growing geological age, "illitization" of glauconite was taking place. It was connected with its recrystallization, during which  $Fe^{3+}$  cations were removed from the structure and the octahedral positions were occupied by Al cations. This process is widespread in the epigenetic change of layer silicates (Fig. 4).

It is not impossible, however, that in the "oldest" epochs (R, P<sub>2</sub>), characterized by poor organics, formation of glauconites primarily enriched in  $Al_{VI}$  also took place, as suggested by Nikolaeva (1971).

#### REFERENCES

- BARANOVA, N.M. (1961): On glauconite in Sarmatian deposits of the Southern slope of the Ukrainian crystalline shield. *Voprosy mineralogii osad. obraz.* 6. Lvov University. [In Russian].
- BENTON, K. and KASPER, M. (1965): Notes on the mineralogy and origin of glauconite. *Journal Sediment. Petrol.*, 35, 155-161.
- BURST, J. (1958): Mineral heterogeneity in glauconite pellets. *Amer. Miner.*, 43, 481-497.
- DOULLET Ph., ODIN, G.S. (1968): Etude chimique et minéralogique de grains de glauconite provenant des formations crétacées et tertiaires du Bassin de Paris. *Bull. Groupe Fran. Argiles*, 20, 13-24.
- FENOSHINA, U.I. (1961): Glauconites from the Lower Torton deposits of the Luben Veliky Spa. *Voprosy mineralogii osadoch. obrazov.* 6. Lvov University. [In Russian].
- FOSTER, M. (1969): Studies of celadonite and glauconite. *Geol. Sur. Prof. Pap.* 614-F, Washington.
- GORBUNOVA, L.I. (1961): Glauconite from the Lower Permian deposits of the Northeastern Caucasus. *Voprosy mineralogii osad. obrazov.* 6. Lvov University. [In Russian].
- HENDRICKS, S.B., and POSS, C.S. (1941): Chemical composition and genesis of glauconite. *Amer. Miner.*, 26, 683-708.
- HOWER, J. Jr. (1961): Some factors concerning the nature and origin of glauconite. *Amer. Miner.*, 46, 313-334.

- LAZARENKO, E.K. (1969): Mineralogy of the Podol Region. Lvov University. [In Russian].
- LANGER-KUZNYAROVA, L., LAZARENKO, E.K., and FENOSHINA, U.I. (1963): On Mineralogy of Ordovician glauconite. Mineral. sb. Lvov. geol. obshchestva, 17, 2. [In Russian].
- MILLOT, G. (1964): Geologie des Argiles. Paris.
- NASIDZE, G.I. (1966): On mineralogy of Georgian glauconites. Soobshcheniya AN Gruz SSR, 44, 2. [In Russian].
- NIKOLAEVA, I.V. (1971): Minerals of the glauconite group and the evolution of their chemical composition. Problemy obschei i regional'noi geologii, 320-335. Novosibirsk. [In Russian].
- NIKOLAEVA, I., KOVALEVA, L.T. and SUKHARENKO, A.V. (1971): Evolution of the chemical composition and classification of the minerals of the glauconite group. Glaukonit v sovremennykh nizhnepaleozoiskikh i dokembriiskikh otlozheniyakh. "Nauka". [In Russian].
- SHUTOV, V.D., DRITS, V.A. and SAKHAROV, B.A. (1969): On the mechanism of postsedimentary transformation of montmorillonite into hydromica. Proc. Inter. Clay Conf., 1, 523-533.
- SMULIKOWSKI, K. (1954): The problem of glauconite. Archiwum. Mineralogiczne Polska Akad Nauk 18, 21-120.
- ZUMPE, H.H. (1971): Microstructure in Cenomanian glauconite from Isle of Wight. England Miner. Mag., 38, 215-224.



# GENETIC TYPES AND PARAGENETIC ASSOCIATIONS OF MINERALS OF THE CORRENSITE GROUP

A. G. Kossovskaya

Institute of Geology. Academy of Sciences. Moscow. U.S.S.R.

## ABSTRACT

A comparative study has been carried out of corrensite-type mixed-layer minerals, which are wide-spread in evaporitic deposits, in the terrigene rocks that underwent deep epigenesis and in post-magmatically altered basalts. A parallel analysis was made of minerals, in paragenesis with which corrensites occur in the above geological environments.

In evaporitic complexes the chlorite-smectite mixed-layer minerals are mostly confined to gypseous terrigene-chemogenic rocks. The number of swelling and non-swelling interlayers in mixed-layer minerals to a great extent depends on the permeability of the surrounding medium. The corrensite minerals frequently occur in association with chlorites, Fe-illites, trioctahedral smectites and zeolites (analcime). In low-permeability rocks corrensite is replaced by chlorite. In limestones, peculiar "defective" chlorites were found, in which  $d_{001}$  consecutively decrease with the increase of  $t^{\circ}\text{C}$ . The predominant development of Fe-illites takes places in dolomitic rocks. The formation of corrensite in those conditions is handicapped by the fact that Mg accumulates mostly in dolomite. A characteristic feature of clay minerals of evaporitic deposits, and in particular corrensite, is a low content of  $\text{Fe}^{+2}$ , which is connected with the absence of organic material, and, consequently, of a reduction medium. The crystallochemical characteristics of the authigenic clay minerals of evaporitic deposits are wholly determined by the chemical properties of the medium and are practically independent of the nature of the clastic material that was supplied to the basin. This genetic type of corrensite and its paragenesis can be referred to as faecal-syngenetic.

The second genetic type of corrensite is wide-spread in cavities of variolitic basalts, chlorite and smectite occur in association with corrensite. By their structural features such corrensites

are similar to the mixed-layer minerals of the terrigene-evaporitic complexes, but they differ from the latter by a high content of  $\text{Fe}^{2+}$  as well as  $\text{Mg}^{2+}$ . In this case the genetic type of corrensite and its paragenesis is determined by a medium rich in ferretic elements, and it can be called post-magmatic.

In terrigene rocks that underwent deep epigenetic change and are enriched in ferretic minerals, a peculiar mixed-layer mineral also occurs with  $d_{001} = 28 \text{ \AA}$ . In its structure chlorite and vermiculite-like layers are alternating. The composition of these minerals is similar to that of the corrensite from basalts, but greatly differs from the first two corrensites by the structural features and, in particular, by the absence of the swelling effect in "labile" interlayers. The peculiarity of this mineral is due to the hampered water exchange of the surrounding medium. This genetic type of corrensite and its paragenesis (chlorite, illite and laumontite) can be referred to as epigenetic.

For all the three genetic types of corrensite found in the U.S.S.R. their crystallochemical formulae and structural-mineralogical characteristics are given.

# GENESIS AND THERMODYNAMIC STABILITY OF DIOCTAHEDRAL AND TRIOCTAHEDRAL MIXED-LAYER MINERALS IN SEDIMENTARY ROCKS

S.G. Sarkisyan and D.D. Kotelnikov

The Institute of Geology and Exploitation of Combustible  
Fuels, Moscow (U.S.S.R.)

**ABSTRACT.** - The study of clay minerals shows that mixed-layer minerals are often present in sedimentary rocks. They are mainly represented not only by disordered montmorillonite-hydromica mixed-layer clay minerals of a dioctahedral type but also by ones of a trioctahedral type (chlorite-montmorillonite and chlorite-vermiculite), which are often present in the form of ordered varieties.

Each of these mixed-layer formations exerts different influence on reservoir properties of the rocks due to the amount of swelling layers.

Dioctahedral mixed-layer minerals deteriorate the quality of caprocks. On the contrary the presence of trioctahedral mixed-layer minerals has a positive effect on the resistance of the rocks to oil and gas migration.

The presence of trioctahedral mixed-layer minerals in reservoir rocks decreases their porosity and permeability. On the contrary the presence of dioctahedral mixed-layer minerals provides favourable reservoir properties to sandstones and siltstones.

## INTRODUCTION

Numerous investigations show that mixed-layer minerals are often present in sedimentary rocks. They are mainly represented by variously interstratified swelling (montmorillonite) and non-swelling (hydromica) 2:1 layers of a dioctahedral type, as well as by interstratification of 2:1 swelling layers and 2:2 non-swelling layers of either dioctahedral or trioctahedral type.

In recent sediments and in relatively young shallow formations the amount of swelling layers in mixed-layer minerals exceeds 50 per cent, in some cases about 100 per cent (Fig. 1). According to the investigations made by Reynolds (1967), the mixed-layer minerals of this type (Fig. 1) are represented by typically disordered montmorillonite-hydromica varieties with montmorillonite layers dominating.

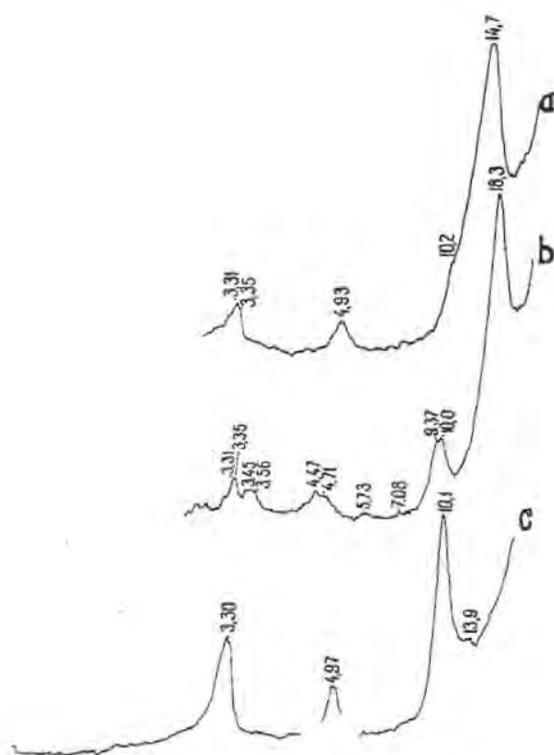


Figure 1. Diffractometer curves of less than 0.001 mm fraction of silty vitroclastic tuff of the Upper Coniacian-Lower Santonian age of the Minor (Small) Caucasus. Disordered montmorillonite-hydromica mixed-layer formation, containing 80 per cent of swelling and 20 per cent of non-swelling layers with a chlorite admixture: a) Initial sample, b) ethylenglycol saturated sample, c) sample heated at 550°C for 2 hours.

#### POSTSEDIMENTATIONAL ALTERATIONS OF CLAY MINERALS

After deposition of the sediments the undergo postsedimentational alteration to the extent of increasing depth and temperature. During the epigenetic stage the swelling layers undergo dehydration including montmorillonite of a volcanic origin (Fig. 2, sample 1).

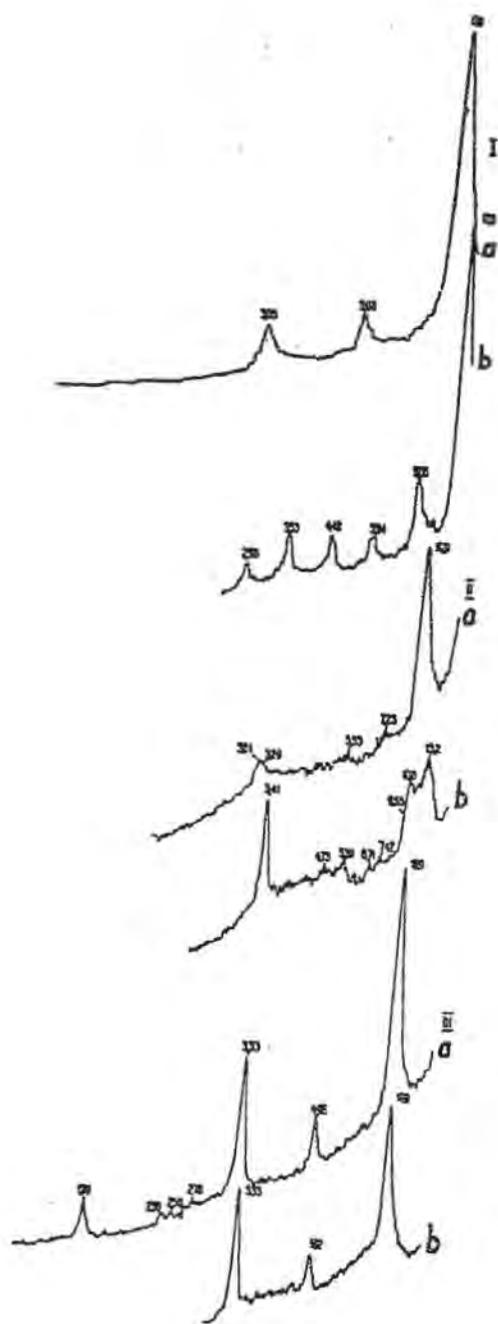


Figure 2. Diffractometer curves of a less than 0.001 mm fraction of volcanic and sedimentary rocks:

- I. Ca - Montmorillonite, floridine clay, Eocene, Georgia;
  - II. Disordered montmorillonite-hydromica mixed-layer formation containing 30 per cent of swelling and 70 per cent of non-swelling layers with a chlorite admixture. Tuff sandstone, Upper Albian, Minor (Small) Caucasus;
  - III. Disordered montmorillonite-hydromica mixed-layer formation containing less than 10 per cent of swelling layers; argillite, Eifellian, Pripyat'depression. Byelorussia.
- a) Initial sample; b) glycerine saturated.

As a result of this, disordered mixed-layer minerals occur, which contain about 30 per cent of swelling layers (Fig. 2, sample II) or even less (Fig. 2, sample III). Dehydration of the clay minerals occurs in three separate stages as reported by J. Burst (1969).

It should be noted that instability of an ordered structure consisting of 50 per cent swelling and 50 per cent of non-swelling layers is a distinguishing feature of mixed-layer minerals of a dioctahedral type in sedimentary rocks.

The limits of alteration of swelling minerals (Fig. 2, sample 1) into less hydrated forms (Fig. 2, samples II and III) lie at different depths and depend on the age and burial depth and also on the genetic nature of the swelling layers.

A relationship between the age of the rocks and the degree of their alteration was reported by Kopeliovich, Kossovskaya and Shutov (1961) for different regions of the USSR. New available data were recently obtained by Lebedeva (1971) for the Western Siberian lowland and Russian platform. This investigator showed that the amount of swelling layers decreases with the depth of the subsidence and that the dehydration of clays occurs respectively in the interval of 300 - 350 meters.

#### NEOFORMED DISORDERED MIXED-LAYER MINERALS OF A DIOCTAHEDRAL TYPE

Disordered montmorillonite-hydromica 2:1 mixed-layer clay minerals of a dioctahedral type are widely spread in sediments of open seas and oceans, i. e. in sediments of transgressive aquatoria, which are characterized by normal salinity (35%). As far as the genetic nature is concerned, mixed-layer clay minerals of this type may be related according to Weaver (1958, 1959) either to degradation of hydromica, by loss of part of cations, mainly interlayer  $K^+$ , or to adsorption of cations by montmorillonite of a volcanic origin ( $K^+$  by the interlayer spaces and  $Al^{3+}$  by silicate layers of the structure respectively). The process of cation adsorption occurs not only at the interlayer space but also within the silicate layers. This process of aggradation and degradation was named according to Lucas (1962) transformation.

The aggradation rate of 2:1 structure depends on the value of the interlayer charges. Degraded hydromicas which have lost only  $K^+$  are characterized by high interlayer charges. Therefore, due to the so called "structural memory" (Grim, Bradley, 1955), they are capable of very rapid reconstruction of the initial properties. Opposite to this, montmorillonites of a volcanic origin, in which replacement of  $Si^{4+}$  by  $Al^{3+}$  in tetrahedrons is lower than in hydromica structures, have relatively low layer charges (0.25 to 0.6 units). In this connection their aggradation is slower than that of

hydromicas. Similar is the behaviour of highly degraded hydromicas (Kotelnikov and Solodkova, 1971).

The reduction of the amount of swelling layers in sedimentary rocks with depth is more intensified due to higher geothermal gradient and greater dislocation of the deposits (Burst, 1969; Sarkisyan and Kotelnikov, 1971).

#### NEOFORMED ORDERED MIXED-LAYER CLAY MINERALS OF A TRIOCTAHEDRAL TYPE

Sedimentary rocks contain not only dioctahedral mixed-layer minerals but also ones of a trioctahedral type (chlorite-montmorillonite and chlorite-vermiculite), which are often present in the form of ordered varieties (Fig. 3, samples I and II).

If we consider the higher interlayer charges of vermiculite (0.6 to 0.9 units) and compare them with the charges of the montmorillonite we shall come to the conclusion that the formation of mixed-layer minerals with different swelling layers should take place in different conditions. For instance, according to the experimental data reported by Vyart and Sabatier (1969) chlorite-montmorillonite mixed-layer minerals may be formed due to increasing temperature from dioctahedral montmorillonite or illite in the presence of  $MgCO_3$  and  $CaCl_2$ , respectively.

Development of chlorite-montmorillonite in some areas of Western Europe and Africa is confined to evaporite basins as reported by Lippman (1954), Millot (1964) and other investigators.

The analysis of the geological and geochemical conditions for the occurrence of chlorite-montmorillonite mixed-layer formations also indicates their relation with the weathering products of the volcanic glass as well as with  $Mg^{2+}$  carbonates. For instance, chlorite-montmorillonite mixed-layer formation studied by Postnikova and Kotelnikov (1969) were found in dark argillites containing volcanic glass remains and large dolomite rhombohedrons. Chlorite-montmorillonite mixed-layer minerals related to the weathering of volcanic rocks were found in other regions of the USSR.

Reliably identified chlorite-vermiculite was also found among the weathering and hydrothermal products of crystalline rocks (Drits and Kossovskaya, 1963; Johnson, 1964; Gradusov and Chizhikova, 1968; Teodorovich, Kotelnikov and Akayeva, 1969; Sedson, Pedro, Robert and Dejon, 1969; Akayeva and Kotelnikov, 1970; Melnikov and Sidorenko, 1968; Gradusov and Lazareva, 1970; Heyas, 1970). For instance, Sedson et al. (1969) established that a chlorite-vermiculite mineral has been formed as a result of biotite alteration. Melnikov and Sidorenko (1968) reported about neof ormation of chlorite-vermiculite structures due to hypersthene alteration. Gradusov

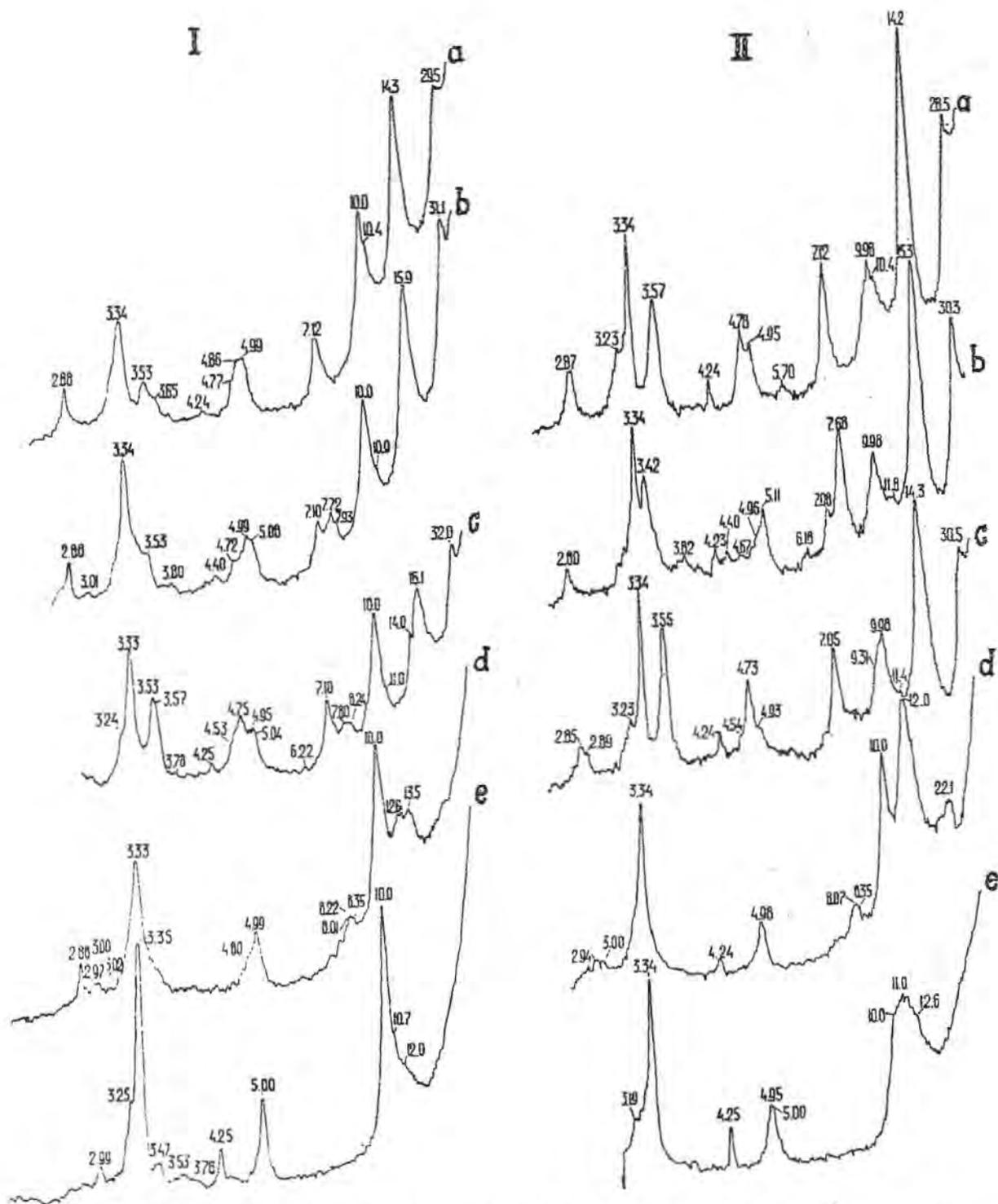


Figure 3. Diffractometer curves of a less than 0.001 mm fraction of sedimentary rocks:  
 I. Ordered chlorite-montmorillonite, argillite, Late Precambrian, Yenisey ridge, East Siberia;  
 II. Ordered chlorite-vermiculite, calcareous tuff pellite. Upper Coniacian - Lower Santonian, Minor (Small) Caucasus. The samples contain an admixture of montmorillonite-hydromica mixed-layer formation containing 10 per cent (I) and 25 per cent (II) of swelling and 90 and 75 per cent of non-swelling layers, respectively. Chlorite admixture.  
 a) Initial sample; b) ethylenglycol saturated sample; c) glycerine saturated sample; d) sample heated at 600°C for 2 hours; e) sample treated with a 10 per cent solution of warm HCl (80°C).

and Lazareva (1970) found that chlorite-vermiculite mixed-layer minerals were formed due to replacement of plagioclase and hornblende.

As it is well known the trioctahedral minerals are not stable in the hypergenesis zone, i.e. in an open system (Mac Ewan, 1948). Therefore the chlorite-vermiculite minerals as discussed above are related to a fairly low intensity of weathering of the rocks containing the components necessary for the formation of such structures. In accordance with the investigations made by Kotelnikov and Akayeva (1971), mixed-layer chlorite-vermiculite formations are found in sedimentary rocks which contain an admixture of endogenic (volcanic) material. These formations are related to the intensive alteration of plagioclase, biotite, hornblende and augite, which are present in the Cretaceous sedimentary-volcanic series of the Minor (Small) Caucasus.

It should be noted that the necessary condition for formation and future preservation of trioctahedral structures of clay minerals in sedimentary rocks is the presence of a closed system in which, the cations are not removed from the medium (Razxmova, 1971). Therefore, mixed-layer trioctahedral formations in sedimentary rocks are generally confined to fine-grained rocks, i.e. clayey and clayey-carbonate rocks. Under such conditions, the cations which are released in the process of decomposition of dark coloured minerals are not removed from the system but are redistributed with the formation of the layer silicates and minerals of other groups. The observed higher degree of dehydration of hydromica which is often associated with trioctahedral mixed-layer minerals indicates the process of redistribution of cations, including  $K^+$  (Viar and Sabatier, 1969). And at the same time the rocks composed of dioctahedral 2:1 structures contain a large amount of swelling layers.

An important property of ordered mixed-layer formations of a trioctahedral type is the wide range of thermodynamic conditions under which they remain stable in sedimentary rocks. For instance, the study of the Earth's crust in different regions of the USSR has shown that ordered mixed-layer minerals of a trioctahedral type are present in the sedimentary-volcanic rocks in all stratigraphic subdivisions. In Paleozoic deposits ordered mixed-layer structures of a trioctahedral type were found at depths up to 3600 meters. At these depths the mixed-layer dioctahedral minerals which are associated with the trioctahedral type contain less than 10 per cent of swelling layers.

The absence of mixed-layer dioctahedral minerals with a large content of swelling layers at greater depths can be explained by water loss from the interlayer spaces by the effect of a high geostatic pressure and particularly at high temperature.

On the contrary the interlayer water in mixed-layer trioctahedral structures is more connate (X-ray identification and Structures..., 1961). Therefore, they preserve 50 per cent of swelling layers at high pressures and temperatures.

## CONCLUSIONS

Different thermodynamic stability of dioctahedral and trioctahedral mixed-layer formations in sedimentary rocks indicates the physical properties of deeply buried rocks, in particular, their caprock capacity and reservoir properties. Thus, the presence of trioctahedral mixed-layer minerals in clayey caprocks, which contain interlayer connate-water have a positive effect on the resistance of the rocks to oil and gas migration. At the same time, dioctahedral mixed-layer minerals which are easily dehydrated due to fairly weak thermodynamic effects deteriorate the quality of caprock because of a larger amount of open micropores and the reduction of rock plasticity. Similarly, swelling clay minerals which at great depth may be only trioctahedral mixed-layer minerals decrease porosity and permeability of reservoir rocks. On the contrary, a small amount of swelling layers in dioctahedral mixed-layer minerals found at great depth provides the preservation of favourable properties of sandstones and siltstones necessary for oil and gas production.

## REFERENCES

- AKAYEVA, V.P., KOTELNIKOV, D.D. (1970): Mixed-layer formations in clayey rocks of the Cretaceous formations of the northeast and east of the Small Caucasus. *Doklady Acad. Nauk USSR*, v. 193, N 6, p. 1380-1383.
- BURST, J.F. (1969): Diagenesis of Gulf Coast clayey sediments and its possible relation to petroleum migration. *Bull. Amer. Assoc. Petrol. Geologists*, v. 53, N 11, p. 73-93.
- DRITS, V.A., KOSOVSKAYA, A.G. (1963): Sangarite - a new agrillaceous mineral with a regular mixed-layer structure. *Doklady Acad. Nauk. USSR*, v. 151, N 4, p. 934-938.
- GRADUSOV, B.P., LAZAREVA, V.M. (1970): Mixed-layer formations in Upper Eocene deposits of East Georgia. In book: "Clays, their mineralog. properties and practical significance", Moscow, "Nauka", p. 58-63.
- GRADUSOV, B.P., CHIZHIKOVA, N.P. (1968): Methods of determining the mobile interlayer interval in ordered trioctahedral mixed-layer forms of chlorite and labile 2:1 packets. *Lithology and mineral resources*, N 5, p. 124-127.
- GRIM, R.E., BRADLEY, W.F. (1955): Structural implications in diagenesis. *Geol. Rundsch.*, Bd. 43, S. 469-474.
- HEYAS, J.B. (1970): Polytypism of chlorite in sedimentary rocks. *Clays and clay minerals*, t. 18, p. 285-306.
- JOHNSON, L.J. (1964): Occurrence of a regularly interstratified

chlorite-vermiculite as a weathering product of chlorite in a soil. *Mineralogist*, 1964, v. 49, N 5/6, p. 556-572.

KOPELIOVICH, A.V., KOSOVSKAYA, A.G., SHUTOV, V.D. (1961): Some features of epigenesis of terrigenous formations of platform and geosynclinal areas. *Izvestia Acad. Nauk. USSR, ser. geol.*, N 6, p. 18-31.

KOTELNIKOV, D.D., AKAYEVA, V.P. (1971): Clay minerals of sedimentary-volcanic formations of the Cretaceous geosyncline of the Minor (Small) Caucasus. In Collection: ... "Study and use of Clays". Proceedings of the 9th Session of the All-Union Commission on study and use of clays, Minsk, "Nauka i Tekhnika", p. 56-59.

KOTELNIKOV, D.D., SOLODKOVA, N.A. (1971): Conditions of accumulation of Late Precambrian deposits of the Teya and Chapa river basins (the Yenisey ridge). *Doklady Acad. Nauk USSR*, v. 199 N 3, p. 688-691.

LEBEDEVA, G.V. (1971): Epigenetic zoning of the Jurassic and Cretaceous clay rocks of the West Siberian Lowland. In Collection: "Study and use of clays". Proceedings of the 9th Session of the All-Union Commission on study and use of clays, Minsk, "Nauka i Tekhnika", p. 76-78.

LIPPMAN, F. (1954): Über einen Keuperton von Zaisersweiher bei Manelbronn, Heidelberg. *Beitr. Mineral u. Petrogr.*, Bd. 4, H. 1/2, S. 130-134.

LUCAS, J. (1962): La transformation des minéraux argileux dans la sédimentation. Etude sur les argiles du Trias. *Mem. Serv. Carte Geol. "D'Alsace-Lorraine"*, N 23, 202 pp.

MacEWAN, D.M.C. (1948): Les minéraux argileux de quelques sols écossais, Verres et Sillic. *Industr.*, v. 13, N 1, p. 41-46.

MELNIKOV, V.S., SIDORENKO, E.F. (1968): Unknown vermiculite from the Pridnestrovie area. *Mineral. Collection of Lvov University*, v. 22, N 3, p. 264-270.

MILLOT, G. (1964): Géologie des Argiles (altérations, sédimentologie, géochimie), Paris, 494 pp. Russian translation, Moscow, "Mir", 1968, 359 pp.

POSTNIKOVA, I.E., KOTELNIKOV, D.D. (1969): New information on volcanic activity in Late Precambrian deposits of the Irkutsk amphitheatre. *Doklady Acad. Nauk USSR*, v. 186, N 5, p. 1146-1149.

RAZUMOVA, V.N. (1971): Hydrothermal montmorillonite clays as source rocks of crust weathering of the Black Sea coast of Adzharia. *Bull. of the Moscow Society of Naturalists, ser. geol.*, v. 76 part 46, N 1, 86-100.

REYNOLDS, R.C. Jr. (1967): Interstratified clay systems: calculation of the total one-dimensional diffraction function. *Amer. Mineralogist*, v. 52, p. 661-672.

SARKISYAN, S.G., KOTELNIKOV, D.D. (1971): Clay minerals and problems of petroleum geology. Moscow, "Nedra", 182 pp.

SEDDON, F.K., PEDRO, G., ROBERT, M., DEJON, J. (1969): Sur l'évolution des biotites et la formation d'intergrades à 14 Å (vermiculite-chlorite) dans les arènes granitiques de Tazily (massif de Luzy, Morvape meridional). C.R. Acad. Sci., Ser. D, v. 268, N 15, p. 1901-1904.

TEODOROVICH, G.I., KOTELNIKOV, D.D., AKAYEVA, V.P. (1969). On the genesis of bentonites and mixed-layer forms in the Cretaceous deposits of the Minor (Small) Caucasus. Lithology and mineral resources, N 4, p. 71-85.

VYART, J., SABATIER, G. (1969): Reproduction des argiles et des ophites du Keuper. Russian translation in book: "Problems of petrology and genetic mineralogy". Moscow, "Nedra", v. 1, p. 136-143.

WEAVER, Cj. E. (1958): The effects and geologic significance of potassium "fixation" by expandable clay minerals derived from muscovite, biotite, chlorite and volcanic material. Amer. Mineralogist, v. 43, N 9/10, p. 839-861.

WEAVER, Ch. E. (1959): The clay petrology in sediments. Clays and clay minerals. Proc. 6th Nat. Conf. California August 19-23, 1957. London, Pergamon Press, p. 154-187.

X-ray identification and Crystal Structures of Clay Minerals. Edited by G. Brown, London, 1961. Russian translation, 1965, Moscow, pp. 599.

# GENESIS OF CHLORITE, VERMICULITE, SERPENTINE, TALC, AND SECONDARY OXIDES IN ULTRABASIC ROCKS

J. Rimsaite

Geological Survey of Canada, Ottawa, Canada

**ABSTRACT.** - Secondary chlorite, vermiculite, serpentine and oxides replace primary olivine, phlogopite and spinel, and have been observed in all ultrabasic rocks before their disintegration in clastic sediments under weathering conditions. Relative proportions of primary and secondary minerals were estimated in two hundred ultrabasic rocks under a petrographic microscope and secondary minerals were identified by x-ray diffraction analysis. Selected primary minerals and their alteration products were studied by electron microprobe to determine chemical changes that take place during hydration of the primary minerals in the host rock.

It was found that all these rocks are partly to completely altered to serpentines and that the alteration of the phlogopite follows serpentinization of the olivine and alteration of the spinel. Serpentinization of the olivine depends on the circulation and nature of aqueous solutions and proceeds through the following phases: thin serpentine veinlets "s-1" form in olivine fractures probably at high temperature due to water and hydroxyl released from the mica during emplacement of the ultrabasic rock. These veinlets serve as channels for aqueous solutions and usually contain opaque oxides of elements removed from the lattice of host olivine. The aqueous solutions from the "s-1" veinlets penetrate remnant olivine "islands" which alter first to a fine-grained, almost isotropic serpentine "s-2" and later recrystallize to a fibrous serpentine "s-3" with a prominent "hour-glass" texture. Serpentine rims "s-4", probably deuteric, crystallize around olivine, adjacent to fine-grained groundmass and are genetically related to bright-green chlorite rims which surround primary phlogopite. Interstitial or groundmass serpentine includes speckles "s-5", platy "s-6" and acicular "s-7" varieties and is associated with magnetite grains and other oxides. The vein serpentine, in addition to speckled and platy varieties, contains fibres stretched along the walls "s-8", and colloform, ribbon-like aggregates "s-9" which grade into fibres "s-10" elongated perpendicular

to vein walls. The vein serpentine forms from ions removed from the primary minerals, as well as those introduced from outer sources, and it is commonly associated with hydroxides and carbonates.

The phlogopite and spinel are unstable in the interstitial and vein serpentine "s-5" to "s-10", and, at the initial phase of alteration, contain contorted veinlets of serpentine. The phlogopite alters to chlorite, vermiculite and talc. More complex reactions between anions and cations removed from the primary minerals with those introduced from outer source through fractures result in crystallization of nickeliferous goethite, jarosite, diverse carbonates, secondary micas and chlorite.

The question proposed for discussion is: how these fine-grained secondary minerals in ultrabasic rocks can be distinguished from those which form in sediments under weathering conditions?.

## INTRODUCTION

Mineral genesis is one of the most interesting fields of clay mineralogy. Studies of mineral genesis include laboratory experiments on chemical decomposition of igneous and metamorphic minerals, mineral synthesis, and research on clay mineral occurrences in sediments. Problems in laboratory studies arise from the time factor and the difficulty of reproducing natural environmental conditions, whereas in a sediment there may be insufficient data on primary source of clay minerals. To learn more about chemical and genetic relationship between primary and secondary minerals, and natural processes of alteration, this study is based on electron probe microanalyses of primary minerals and their alteration products in thin polished sections.

The serpentinized ultrabasic rocks from Canadian nickel and other mineral deposits provide an excellent material for the genetic studies of alteration products in relation to the primary minerals. When olivine alters to serpentine (chlorite), and phlogopite to vermiculite and talc, the ratio of (Mg, Fe) O to  $\text{SiO}_2$  decreases as shown in Fig. 1. This chemical change can take place either by the preferential loss of (Mg, Fe) O from the lattice, or by addition of  $\text{SiO}_2$ . These changes are considered in the study of serpentinization.

The objectives of this paper are to provide examples of diverse mineral alterations in parent rocks before their disintegration in clastic sediments, to propose genetic classification of serpentines, and to discuss chemical and genetic relationships between the primary olivine and phlogopite and their alteration products: chlorite, serpentine, vermiculite, talc and secondary oxides.

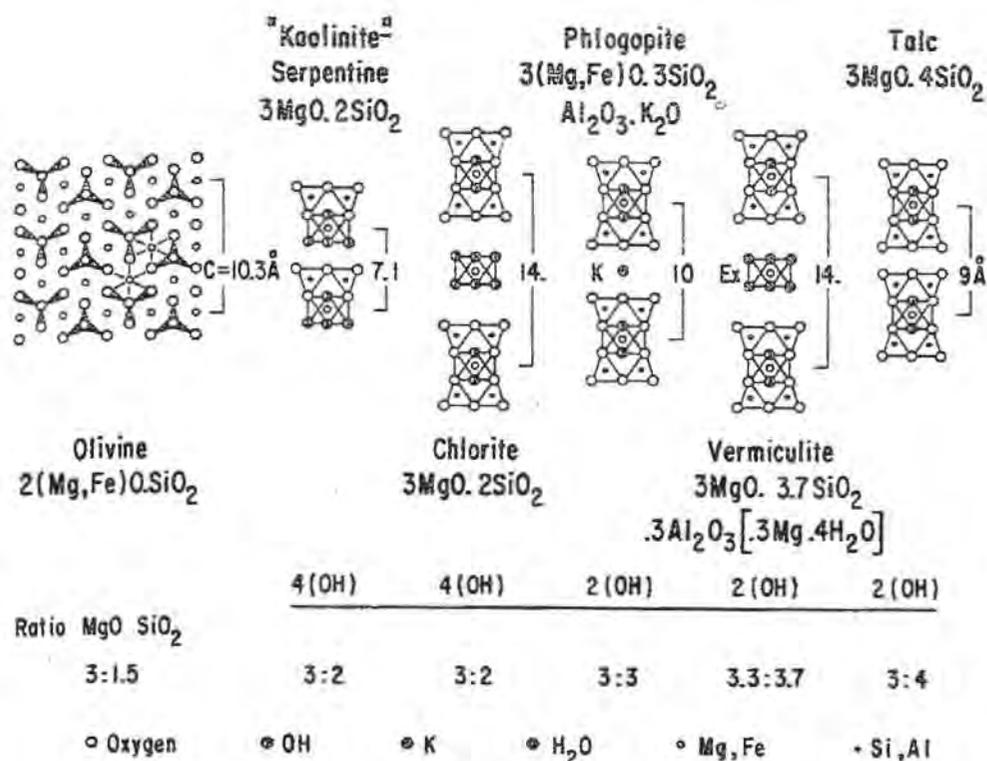


Figure 1. Diagrammatic representation of structural and chemical changes during alteration of olivine and phlogopite to serpentine, chlorite, vermiculite and talc.

More detailed descriptions of serpentines and their structures from specific Canadian localities are given by Aumento (1970), Coats (1968) and in the other publications quoted by these authors.

## SPECIMENS AND EXPERIMENTAL PROCEDURES

The textural relationships between the primary minerals and their alteration products were studied in thin sections of 200 ultra-basic rocks, mainly from Canadian chromium and nickel deposits (Figs. 2 to 7). Chemical changes during alteration of olivine, phlogopite and spinel were determined by electron probe microanalyses on selected fresh and altered portions of the grain in thin polished sections. X-ray scanning pictures were used to show distribution of elements in an altered area (Fig. 8), and quantitative analyses were made by point counting (Tables I and II). The interlayer alkalis, K, Rb, Sr, were determined by x-ray spectrography in phlogopite and related vermiculite and talc concentrates (Table III).

DTA and TG analyses were made on 200 mg serpentine concentrates to determine their thermal stability and impurities, and to distinguish between "strongly adsorbed" water and water of crystallization. Alteration products, impurities, and new anhydrous phases in heated serpentines were determined by M. Bonardi and G. Pringle using an x-ray powder camera. Selected DTA, TG and XRD charts of serpentines and talc are reproduced in Fig. 9, and the relationship between the x-ray intensity ratio of the fourth basal reflection of vermiculite to the third basal reflection of phlogopite and potassium content of the mica is shown in Fig. 10. Chemical analyses for  $\text{Fe}_2\text{O}_3$ ,  $\text{FeO}$ ,  $\text{H}_2\text{O}$ , F and Cl in primary minerals and in their alteration products continue.

### ALTERATION OF OLIVINE AND GENESIS OF SERPENTINES

Olivine phenocrysts crystallize early at high temperature and become unstable after the emplacement of the ultrabasic rock near the surface of the earth's crust. The Mg-rich olivine alters to serpentine by losing about 15%  $\text{MgO}$ , and olivine containing 16%  $\text{FeO}$  loses both iron and magnesium (Table I). The olivine contains more nickel than the related serpentine veinlets "s-1" and less silica than deuteric serpentine rims "s-4". The serpentines are classified on the basis of their origin, mode of occurrence, sequence of crystallization and textures into three groups (Fig. 2) and ten following types;

Group I : residual serpentines, pseudomorph after olivine and other phenocrysts:

"s-1", veinlets along fractures, cutting host olivine into polygonal fragments (Fig. 2 "O");

"s-2", serpentized olivine fragments (islands) between veinlets "s-1" (Fig. 3);

"s-3", serpentine "s-2" recrystallized to birefringent fibres with a prominent "hour-glass" texture (Fig. 4);

"s-4", deuteric serpentine rims surrounding olivine and spinel (Figs. 3 and 15).

Group II : groundmass serpentine, in part residual, pseudomorph after primary constituents of the groundmass, and in part forming from ions liberated from phenocrysts:

"s-5", fine-grained, speckled serpentine with low birefringence (Fig. 6);

"s-6", small plates with low to moderate birefringence (Fig. 6);

"s-7", acicular and flaky serpentine with moderate birefringence (recrystallized "s-5 & 6", Fig. 7).

Group III: vein serpentines forming from ions removed from primary minerals, phenocrysts and groundmass, with or without additional ions from the outer source:

"s-8", glassy crusts and aggregates stretched parallel to the vein walls (Fig. 6);

"s-9", colloform, ribbon-like aggregates with moderate birefringence (Fig. 6), grading to

"s-10", fibrous serpentine, elongated perpendicular to the vein walls.

Table I

Electron probe analysis of olivine and serpentine  
(Analyst G.R. Lachance)

Specimen	SiO <sub>2</sub> %	Al <sub>2</sub> O <sub>3</sub> %	Total Fe as Fe <sub>2</sub> O <sub>3</sub> %	MgO %	MnO %	Ni %
1*. Olivine, Fo 90	41.	0.0	7.0	51.7	0.1	0.2
"s-1" veinlets	38.4	0.0	9.2	34.5	0.3	0.0
"s-4" rims	42.6	0.0	6.1	35.8	0.3	0.0
2. Olivine, Fo 77	40.5	0.0	16.	42.5	0.2	0.1
"s-1" veinlets	36.	0.1	13.	38.9	0.0	0.0
"s-4" rims	42.	0.0	7.4	41.0	0.2	0.0
3. Serpentine "s-2"	37.4	0.2	18.0	27.3	0.2	0.0
"s-4" rims	39.3	0.4	8.0	34.7	0.1	0.8
4. Serpentine "s-5, 6, 7"***	25.	15.2	22.	21.4	0.1	0.0
"s-10" green fibres	25.	15.4	22.	20.2	0.1	0.0
chlorite, recrystallized	25.	15.4	26.	17.	0.2	0.0

\*Numbers refer to host rocks and to the authors of pertinent geological publications: 1, kimberlite (Lee and Lawrence, 1968); 2, peridotite, Renzy Lake Ni-deposit (Forrester, 1957); 3, Serpentinite, Werner Lake Ni-deposit (Carlson, 1958); 4, Serpentinite Manitoba Nickel Belt (Zurbrigg, 1963).

\*\*Analyses of three groundmass serpentines "s-5, 6, 7" are very similar.

The serpentines are associated with very fine-grained opaque minerals, and coarser-grained magnetite and sulphides. Some of the secondary minerals have been identified as oxides, hydroxides, and hydrous carbonates, but some are too small for positive iden-

tification and probably consist of native metals and their alloys (Fig. 8, distribution of Ni). Application of electron probe microanalyses for studies of the fine-grained secondary minerals is very effective, and new species have been discovered, such as muscoxite by Jambor (1969).

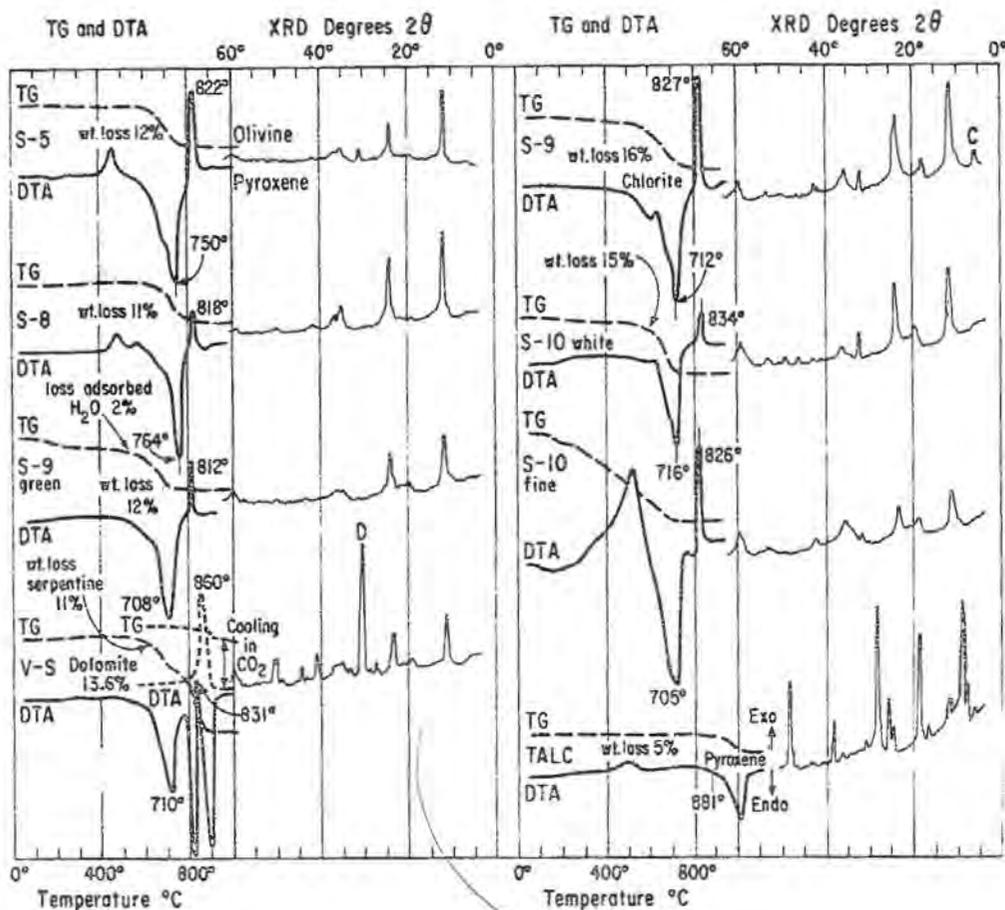


Figure 9. DTA, TG and XRD charts of serpentine and talc. Vein serpentine "V-S" contains dolomite and calcite, DTA and TG analyses by R.H. Lake of the Mines Branch.

DTA and TG analyses indicate that the serpentines contain different hydroxyl and water contents which are released at diverse temperatures (Fig. 9). Serpentines "s-1", "s-4", "s-9" and "s-10" have about 2 per cent of "strongly adsorbed" water and appear to be potential carriers of aqueous solutions in the host rock. It is important to point out the effect of sample preparation on the apparent water content of the serpentine. Specimens crushed in a plastic ballcrusher have up to seven per cent adsorbed water (Fig. 9, specimen "s-10"-fine). The glassy and striated serpentine "s-8" appears to be hydroxyl-deficient, and probably has lost some water due to pressure and shearing. DTA and TG curves of such serpen-

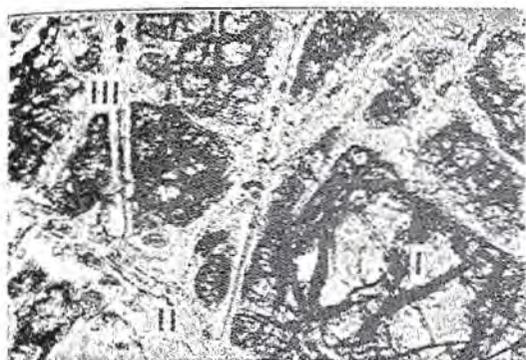


Figure 2. Ultrabasic rock with three groups of serpentine: I, pseudomorphs after olivine; II, groundmass serpentine; III, vein serpentine.  $\times 45$ .

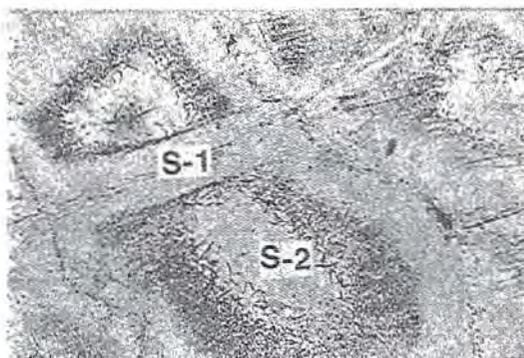


Figure 3. Serpentine pseudomorphs after olivine: «s-1» along olivine fractures; «s-2» replaces remnant olivine «islands».  $\times 500$ .



Figure 4. Serpentine veinlets «s-1» and «s-3» fibres with «hour-glass» texture.  $\times 500$ , + N.

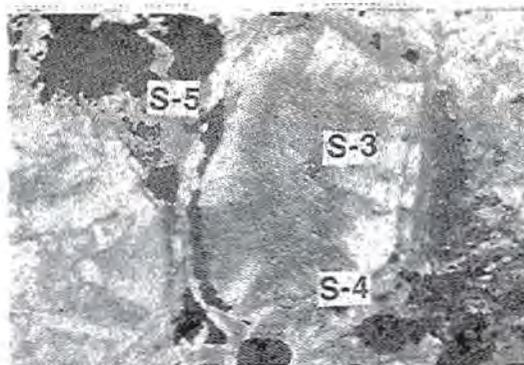


Figure 5. Serpentine «s-3» replacing olivine with prominent rims «s-4» in groundmass serpentine «s-5».  $\times 100$ , + N.



Figure 6. Groundmass serpentine «s-6» with vein serpentines «s-8» and «s-9».  $\times 45$ .

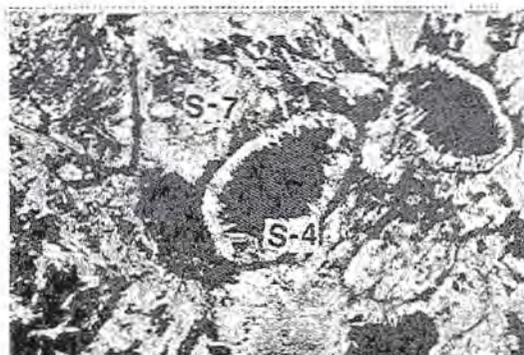


Figure 7. Olivine replaced by magnetite (black) with serpentine rims «s-4» in acicular serpentine «s-7».  $\times 45$ .



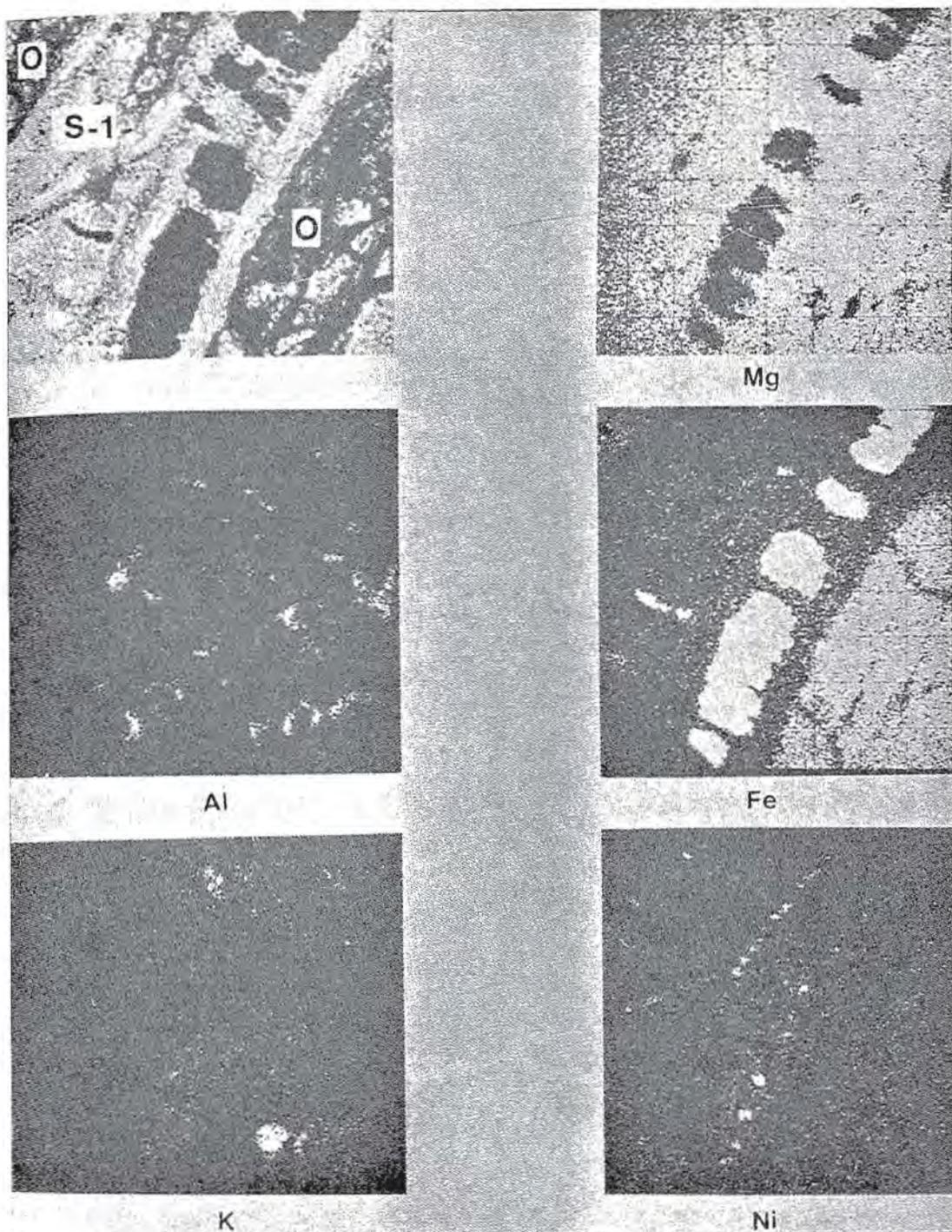


Figure 8. Upper left: photomicrograph of serpentine «s-1» with secondary oxides in olivine «O», and x-ray scanning pictures for Mg, Al, Fe, K and Ni. Scanning area 150 × 150 microns. Electron probe analysis by A. G. Plant.



tines indicate higher temperatures of dehydration (above 750°C, Fig. 9). It is important to point out that anhydrous phases of the serpentines are olivine and pyroxene, and those of talc only pyroxene, because of the relative increase of  $\text{SiO}_2$  in the alteration products. In metamorphosed serpentinites "s-1" veinlets are replaced by talc, and "s-2" serpentine by pyroxene, which suggests that "s-1" veinlets contained originally more water than serpentine "s-2". Depending on the quantity and nature of penetrating aqueous solutions, and on the stage of serpentization, serpentinites consist either of several serpentine types retaining the original olivine texture, or are replaced by massive groundmass or vein serpentine. The latter lose the peridotite texture. The distribution of secondary oxides and opaque minerals also depends on aqueous solutions penetrating the rock. They either remain in host minerals or are removed by aqueous solutions and redeposited away from the original source. The redeposited Mg, Ni and Cr can reach sufficient concentration to form ore deposits.

#### ALTERATION OF PHLOGOPITE AND ITS RELATION TO VERMICULITE AND CHLORITE

In ultrabasic rocks phlogopite is an early-crystallizing mineral. It is cogenetic with olivine but less abundant. Phlogopite crystallizes at high temperatures as Mg-rich silicate, but with decreasing temperature, when residual magma becomes depleted of magnesium and relatively enriched in iron and silica, mica continues to grow as dark biotite. The biotite frequently forms rims around phlogopite or long bands between [001] cleavage planes of the host (Fig. 11). When K and Al become consumed during early phases of crystallization, phlogopite phenocrysts continue growing as bright-green iron-rich chlorite (Table II). The chlorite rims contain more silica and iron, and less alumina than the phlogopite. They are believed to be cogenetic with the deuteric serpentine rims "s-4". In altered rocks, serpentine penetrates phlogopite along the fractures. Such serpentine veinlets contain more  $\text{SiO}_2$ , Fe and Mg, and less Al, Cr, Ti, Ni and K than the host mica (Table II). The initial phase of mica alteration begins with losses of interlayer cations and titania, which usually remains within the parent mica as exsolved rutile needles (Fig. 12 and 13). The ratio of  $(\text{Mg, Fe})\text{O}$  to  $\text{SiO}_2$  in micas and associated chlorites and vermiculites depends on alumina content which replaces silica. With the exception of chlorites from "metaperidotite" (Fig. 14 and Table II), the chloritized micas lose about 90% of their original alumina and gain some magnesia and iron. Phlogopite alters to vermiculite first along the margins and cleavage planes, thus consisting of altered and fresh layers and patches. The vermiculitic margins commonly appear speckled and lose

Table II

Electron probe analysis of phlogopite and associated chlorite, spinel, serpentine and goethite (Analyst G.R. Lachance)

Specimen	SiO <sub>2</sub> %	Al <sub>2</sub> O <sub>3</sub> %	TiO <sub>2</sub> %	Cr <sub>2</sub> O <sub>3</sub> %	Total Fe as Fe <sub>2</sub> O <sub>3</sub> %	MgO %	Ni %	K <sub>2</sub> O %
1* Phlogopite	39.	18.5	3.1	1.5	4.6	29.8	0.1	9.6
serpentine veinlet	40.	0.8	0.1	0.0	5.4	43.7	0.0	0.4
2. Phlogopite	39.	14.2	1.1	0.1	7.5	24.	0.0	9.0
altered portion	37.	13.2	0.7	0.0	8.2	25.2	0.0	6.2
chlorite rim	45.	1.4	0.1	0.0	16.5	30.2	0.0	0.2
3. Phlogopite	37.2	17.1	0.4	0.3	7.	27.1	0.1	6.4
chlorite	26.4	20.8	0.0	0.2	5.	36.0	0.0	0.0
spinel	0.0	40.8	0.1	16.7	25.	9.2	0.1	0.0
goethite	6.4	0.1	0.0	0.0	76.3	0.2	0.7	0.0
4. Phlogopite	37.6	17.8	0.7	0.7	3.4	28.1	0.1	7.3
green margin	37.1	13.7	0.6	0.5	6.4	29.0	0.1	6.3
chlorite rim	37.9	1.2	0.0	0.0	5.5	44.5	0.0	0.0
4m. Phlogopite (Fig. 14"p")	38.6	19.1	0.6	0.2	5.6	23.6	0.0	8.3
green margin "g"	38.4	17.1	0.6	0.2	7.8	25.7	0.0	6.9
chlorite "c"	26.1	21.8	0.0	0.2	7.4	30.9	0.0	0.0

\*Numbers refer to the same rocks as in Table I.

Table III

X-ray spectrographic analysis of phlogopite, associated vermiculite and talc, and of secondary mica-talc-serpentine aggregates (Analyst J. Gravel)

	Phlogopite*	Vermiculite	Talc	Phlogopite Fig. 15**	Aggregate "a"	Aggregate Fig. 6
Total Fe as Fe <sub>2</sub> O <sub>3</sub>	5.4	4.5	1.5	4.1	9.7	6.7
K <sub>2</sub> O %	9.0	3.2	0.0	8.6	1.7	3.
Rb ppm	750	300	< 30	410	290	200
Sr ppm	110	30	< 30	< 30	30	30

\*Stanleyville, Vermiculite mine (Hoadley, 1960).

\*\*Werner Lake Ni-deposit (Carlson, 1958).

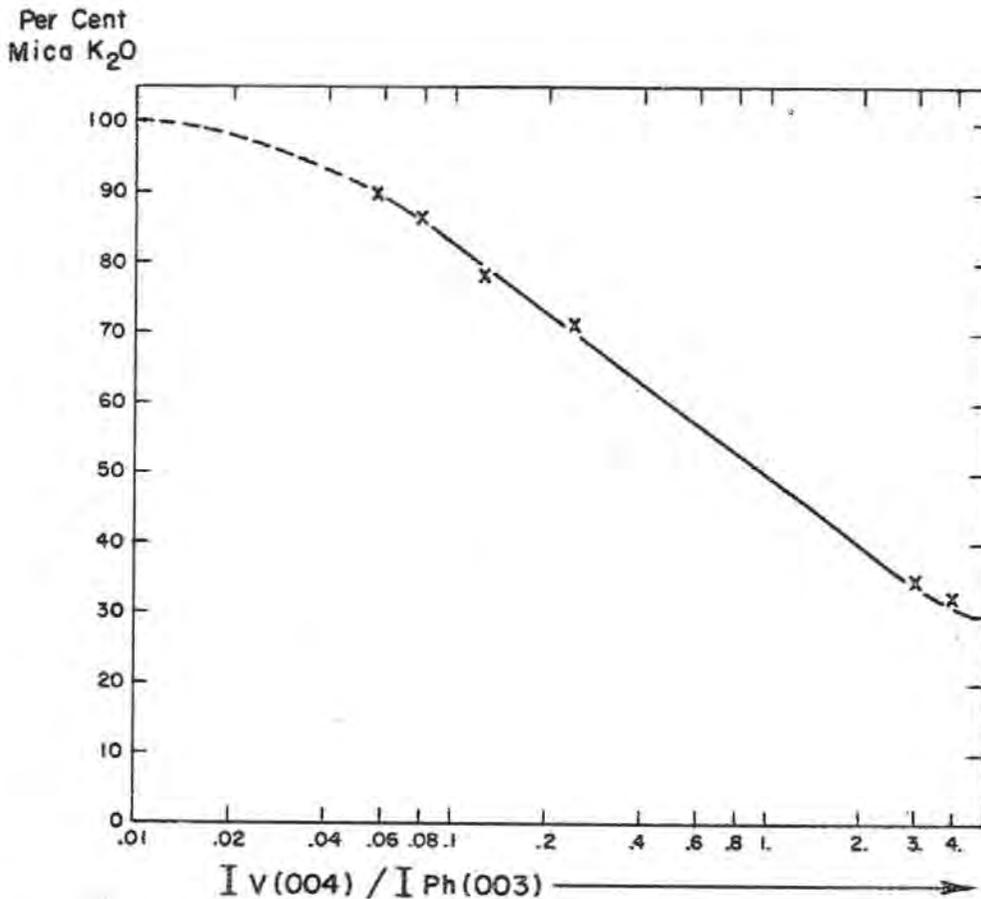


Figure 10. Relationship between x-ray intensity ratio of the fourth basal reflection of vermiculite to the third basal reflection of phlogopite and potassium content of the mica. Nickel-filtered Cu radiation; 45 kV, 16 mA.

refrignce and birefringence (Fig. 12, "V" specks). The fresh remnants of phlogopite in vermiculite and vice versa can be determined quantitatively by x-ray diffractometer (Fig. 10). With advancing stages of alteration, phlogopite loses similar proportions of K and Rb, and somewhat more Sr (Table III). Along the faults and shearing zones, the deformed vermiculite loses its interlayer water and alters to fibrous talc. During its alteration to vermiculite and talc, the phlogopite also loses some iron (Table III).

#### SECONDARY MINERALS RESULTING FROM REACTIONS BETWEEN IONS RELEASED FROM PRIMARY MINERALS AND THOSE INTRODUCED FROM OUTER SOURCES

The alkalis released from phlogopite, and Mg and Fe lost from the olivine and minerals of the groundmass react to form fine-grained mica-serpentine-talc aggregates. These aggregates replace serpentinized olivine grains, retaining the original texture (Fig. 15). Former serpentine veinlets "s-1" are replaced by talc (Fig. 16). The aggregates contain different proportions of K, Rb and Sr, and more iron than the associated phlogopite (Table III). Small secondary mica flakes form also in serpentine veinlets "s-1" and in olivine fractures (K distribution in Fig. 8). Relatively high alumina content in the massive groundmass serpentine also results from the complex reactions between ions released from minerals in the host rock and those introduced by aqueous solutions from outer sources. The relatively high nickel content of bright green serpentine "s-4" is also a result of complex reactions between decomposing Ni-pyrrhotite and silicates. Secondary oxides and hydroxides crystallize in an oxidizing environment also from decomposing sulphides and silicates. Minerals identified include: nickelliferous goethite (Table II), jarosite, muskoxite, hematite and magnetite. Secondary minerals forming with addition of Ca and CO<sub>2</sub> are stichtite, coalingite, magnesite, dolomite and calcite. These carbonates and epidote replace preferentially certain serpentine types, and thus some altered rocks retain peridotite texture after severe chemical alteration.

#### SUMMARY AND CONCLUSIONS

Textural and chemical relationships between primary minerals and their alteration products have been studied under a petrographic microscope and by electron microprobe. Serpentes have been classified on the basis of their origin, sequence of crystallization and textures into three groups and ten types. It was found that olivine

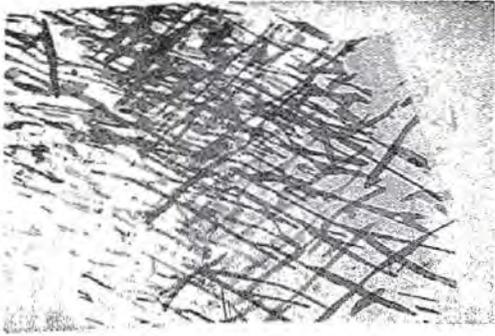


Figure 11. Secondary biotite (dark bands) between [001] cleavage planes of phlogopite.  $\times 100$ .

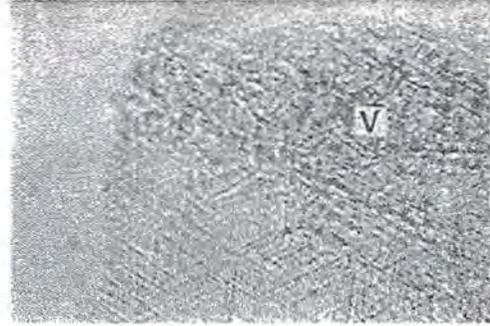


Figure 12. Exsolved rutile needles in phlogopite that alters to vermiculite «v» along the edges.  $\times 100$ .

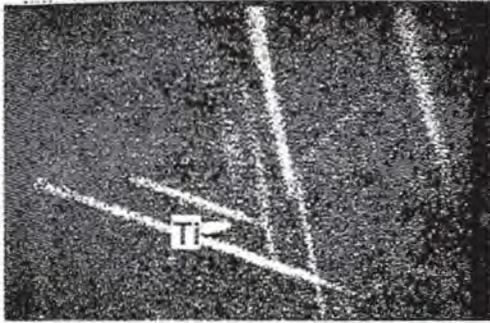


Figure 13. X-ray scanning picture for Ti showing distribution of rutile in mica. Scanning area  $160 \times 100$  microns. Electron probe analysis by G. R. Lachance.

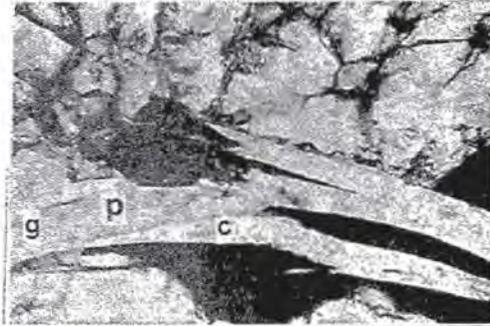


Figure 14. Phlogopite «p» with green margin «g» and chlorite bands «c» in «metaperidotite».  $\times 100$ .

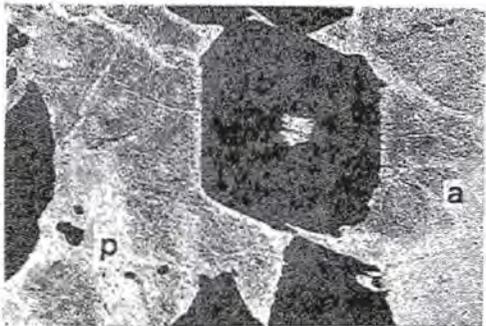


Figure 15. Spinel (black) with serpentine rims «s» in phlogopite groundmass «p» with phlogopite-serpentine-talc aggregates «a».  $\times 100$ .

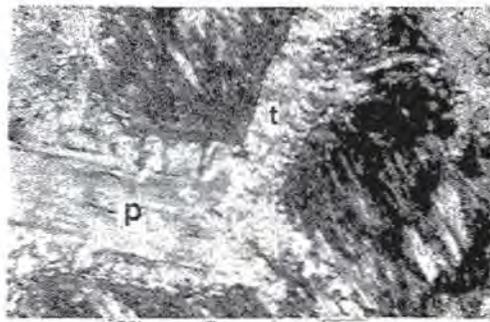


Figure 16. Phlogopite «p» partly replaced by talc «t» in phlogopite-serpentine-talc aggregates.  $\times 500$



alters to serpentine by losing Mg and Fe, whereas phlogopite alters to vermiculite and chlorite by losing alkalis, titania and usually alumina. In the rocks examined, talc forms from serpentine and vermiculite by dehydration. Chlorite also crystallizes from serpentine during low grade metamorphism. The removed ions from altered primary minerals either crystallize in the parent mineral and rock, or can be removed by aqueous solutions away from the source and redeposited to form secondary Mg, Fe and Ni deposits.

The proposed future research includes:

1. Additional electron probe microanalyses on fresh and altered portions of the same grain.
2. Determinations of FeO, Fe<sub>2</sub>O<sub>3</sub>, H<sub>2</sub>O, F, and Cl in fresh and altered portions.
3. Laboratory experiments on further alteration of partly altered minerals.
4. Studies of the effect of alkalis released from phlogopite on the removal of silicates and their replacement by sulphides and oxides.

#### ACKNOWLEDGEMENTS

The author wishes to thank R.H. Lake of the Mines Branch for DTA and TG experiments; G.R. Lachance and A.G. Plant for electron probe studies; M. Bonardi and G. Pringle for x-ray identification of minerals and anhydrous phases, and J. Gravel for x-ray spectrographic analyses.

#### REFERENCES

- AUMENTO, F. (1970): Serpentine mineralogy of ultrabasic intrusions in Canada and on the Mid-Atlantic Ridge. Geol. Surv., Canada, Paper 69-53.
- CARLSON, H.D. (1958): Geology of the Werner Lake - Rex Lake area. Ontario Dept. of Mines. Rep. 66, pt. 4.
- COATS, C.J.A. (1968): Serpentine minerals from Manitoba. Can. Mineralog. 9, 322-347.
- FORRESTER, M.Q.R. (1957): The Lake Renzy Nickel deposit, Pontiac County, Quebec. M. Sc. thesis, University of Western Ontario, London, Ontario, Canada.
- HOADLEY, J.W. (1960): Mica deposits of Canada. Geol. Surv., Canada, EGS No. 19.
- JAMBOR, J.L. (1969): Muscovite, a new hydrous magnesian ferric iron oxide from the Muskox intrusion, Northwest Territories, Canada.

Amer. Miner. 54, 684-696.

LEE, H.A. and LAWRENCE, D.E. (1968): A new occurrence of kimberlite in Gauthier Twp., Ontario. Geol. Surv., Canada, Paper 68-22.

ZURBRIGG, H.F. (1963): Thompson Mine geology. Bull. Can. Inst. Mining. Met. 56, 451-460.

## SOME ASPECTS OF STRUCTURAL TRANSFORMATIONS OF CLAY MINERALS UNDER HYDROTHERMAL CONDITIONS

Frank-Kamenetskij V., N. Kotov, E. Goilo, G. Klotchkova.

Department of Crystallography and Laboratory of High Pressure  
and Temperature. Geological Faculty, Institute of Earth Crust,  
Leningrad University, Leningrad. USSR.

**ABSTRACT.** - By investigation of processes of regional epigenesis-initial metamorphism is very important to model the processes of the structural alterations of the solid phases of clay minerals under hydrothermal conditions. In this connection there were carried out some experiments under high P-T parameters ( $P_{H_2O} = 1-2$  kbar, 200-700°C) mainly with dioctahedral layered silicates (kaolinite, dickite, metahalloysite, montmorillonite, palygorskite, sepiolite). The character of new-formed intermediate and final phases mainly depends on the contents of the original materials and upon the type of the mineralizator added. The peculiarity of their crystalline structure is defined to the great extend by the structure of the initial material, which is inherited in the process of solid state transformational reactions with the participation of the vaporous phase.

It is important to examine the relations of structural and thermodynamic factors in clay alteration by investigation of clay minerals used as typomorphic indicators of environment properties. On the basis only of natural observations it is practically impossible to do this and, for that purpose, model experiments are of great importance. In this connection the crystallochemical exploration of structural and phases transformations in clay minerals under concrete conditions, close those of epigenesis and initial metamorphism, was the aim of this work that was carried out during the course of last years.

When the experiment parameters were chosen, it are taken into account: structural properties of initial minerals (kaolinite, dickite, metahalloysite, montmorillonoids, sepiolite, palygorskyte), their widespread occurrence, and also the fact, that the most important properties of chemical composition and mineral structure were already formed by previous processes during syn- and diagenesis,

partially by katagenesis and initial metamorphism. In rock lithification these minerals undergo the influence of temperature up to 100-300°C and pressure up to 7-10 kbar often in presence of mineralized pore solutions, that, on data of hydrogeochemical explorations, contain for the most part K, Na, Ca, Mg, Cl, SO<sub>4</sub>, CO<sub>3</sub> ions (Valyashko, 1958).

## THE PRINCIPAL FEATURES OF PHASE TRANSFORMATIONS

The methodical modes and the material based on facts concerning the transformations of kaolinite group minerals, montmorillonites, sepiolite and palygorskyte in hydrothermal pure and chloride solutions of K, Na, Ca, Mg ( $P_{H_2O} = 1-2$  kbar, 100-500°C, exposition from 3 hours to 10 days) were already repeatedly discussed (Frank-Kamenetskij et al., 1966-1971; Kotov, Shitov, 1971; Tomashenko et al., 1971).

The high temperatures in this experiments did not prevent to make apparent the phaseous relations of the clay minerals, containing hydroxyl, as far as the high pressure was made by H<sub>2</sub>O - vapours. The combination of high pressure of water and temperature has allowed in these experiments to create the reactions, typical for low temperatured unstable natural processes of kata- and metagenesis, metasomatose etc. Short expositions of experiments allowed to follow the intermediate synthetic phases on the way to the syntheses of final stable products, that are observed in natural conditions and to show their principal features.

Bellow is given only the principal necessary information about phase relationships for some parameters of experiments (Figs. 1, 2).

As it is evident from Figs. 1, 2, a special role of swelling threegraded structures, as intermediate metastable phases is revealed, and as well, that the character of the final phases depends on the composition of the original material and the type of additions - mineralizators. Schematically the ways of alterations of clay minerals in the light of those experiments, are given in Table I.

The transformation prevails over all the other processes (Fig. 3), that is connected with the succession of the structure motives within the basis, polytype modification, the type of octahedral distributions, layers, tetrahedral and octahedral nets.

The phases of nontransforming origin are not shown on the scheme (Table I). Considering this scheme we must note the following main features:

1. New formations of layered silicates are limited within dioctahedral and trioctahedral structures.
2. The transformations as a rule occur by stages, usually through the smectites of montmorillonitic or beidellitic type, and the

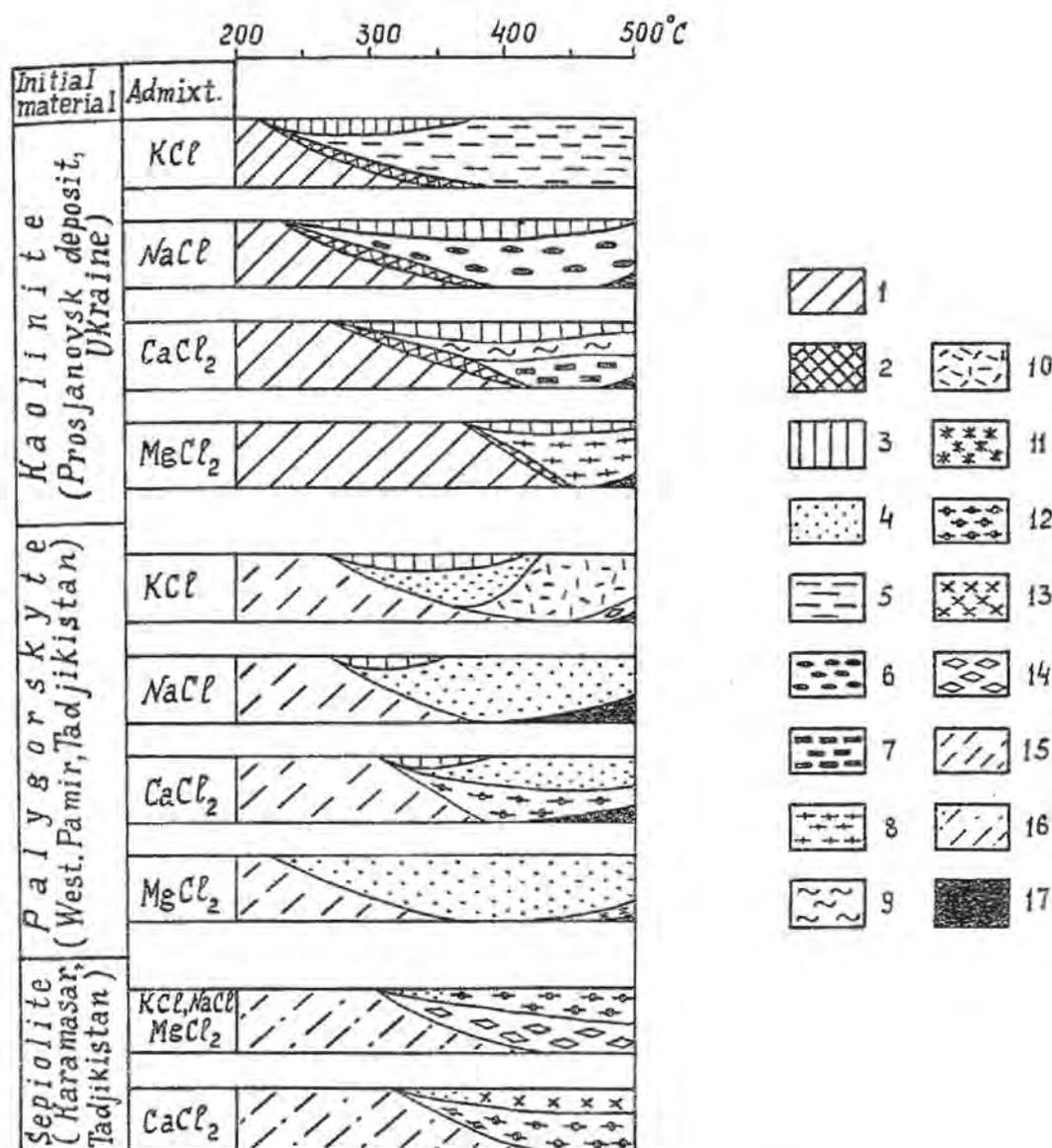


Figure 1. Phase transformations of some silicates in presence of chloride solutions ( $P_{H_2O} = 1$  kbar, 200-500°C, 22-44 hrs., concentration of salts-3-6 gram per litre).

1. Kaolinite, 2. disordered kaolinite, 3. dioctahedral montmorillonite, 4. trioctahedral montmorillonite, 5. K-hydromica, 6. Na-hydromica, 7. monolayered hexagonal analogue of anortite, 8. tosudite, 9. rectorite, 10. disordered mixed-layered mica-montmorillonite, 11. disordered mixed-layered chlorite-montmorillonite, 12. talc, 13. tremolite, 14.  $SiO_2$ , 15. palygorskite, 16. sepiolite, 17. solid admixtures/ x - andalusite in experiments with kaolinite; quartz + biotite + K-feldspar (with K), albite + nepheline (with Na), quartz + anortite + tremolite (with Ca), talc + quartz (with Mg) - in experiments with palygorskite/.

Borders and fields of phase distribution on x-ray data.

final results depend on the smectite structure (a position of Al in the fourfold or a sixfold coordination).

3. In hydrothermal conditions at relatively low temperatures, when diffusive and transforming processes dominate, the synthesis of the final stable products after original layered structures, follows the formation of regular and non-regular mixed-layered phases, the existing conditions of which are within the wide range of pressure-temperature parameters.

4. The mutual disposition of fields of smectites, mixed layered and final stable newly formed phases, picking out in the scheme, reflects the main features of consecutive structural-typomorphic alterations of clay minerals with variations of temperature.

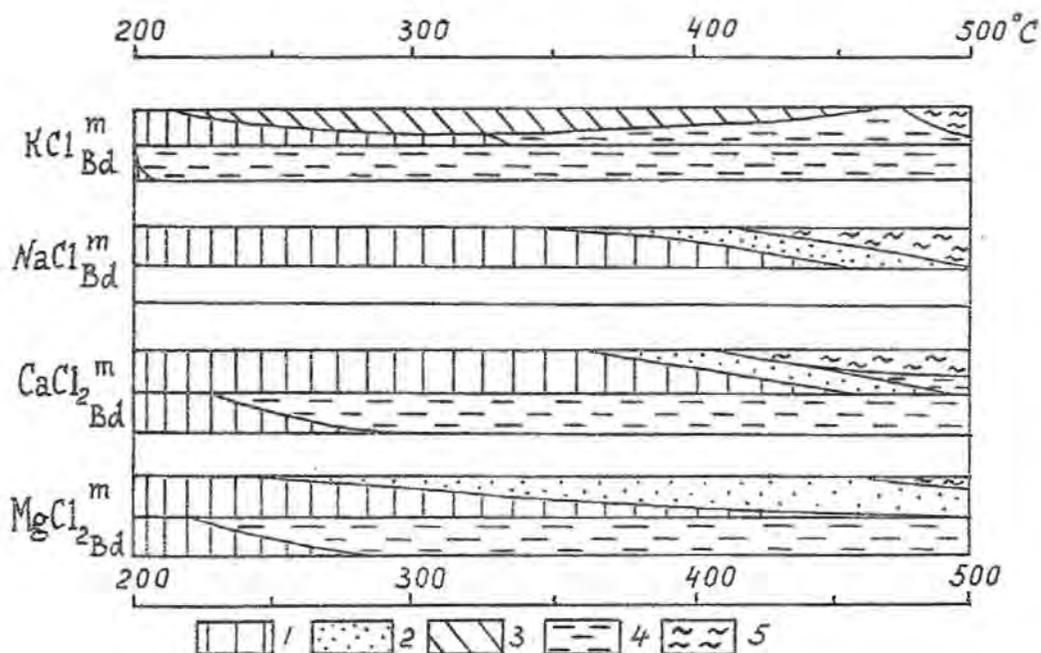


Figure 2. Phase transformations of dioctahedral montmorillonite and beidellite in hydrothermal conditions ( $P_{H_2O} = 900 \text{ kg/cm}^2$ , 200-500°C, 3-24 hrs.).

1. Initial materials, 2. trioctahedral montmorillonite, 3. partly ordered mica-montmorillonite, 4. final phases: mica (with K, Na), rectorite (with Ca), tosudite (with Mg), 5. feldspars; sanidine (with K), albite (with Na), anortite (with Ca).

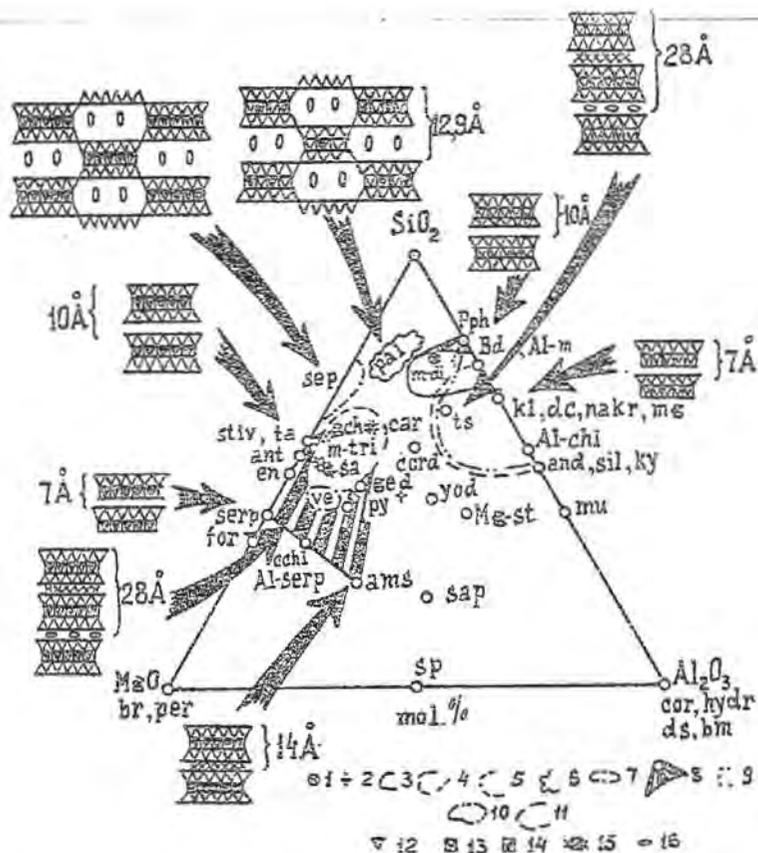
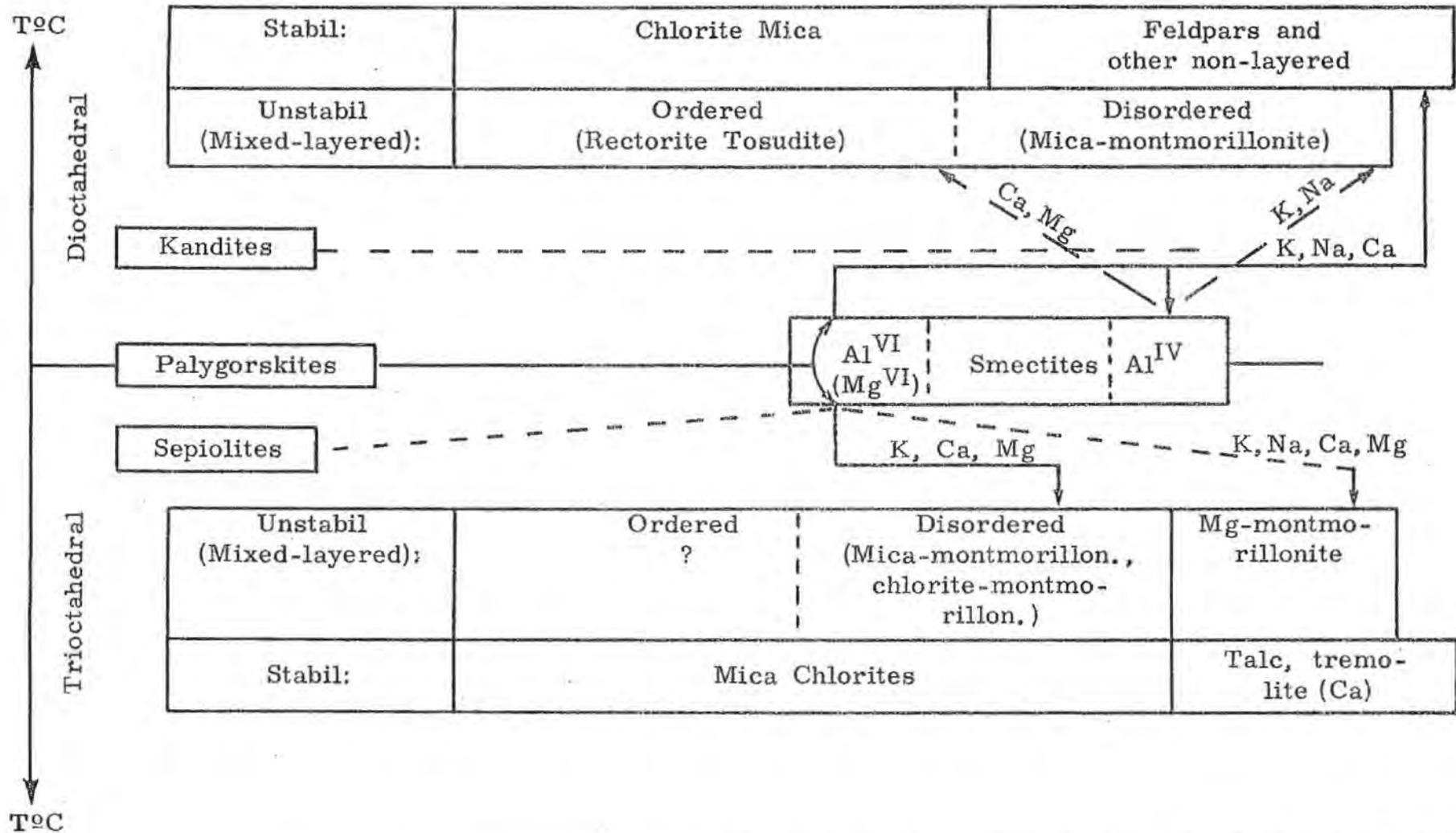


Figure 3. Composition of some stable and metastable silicated and general structural trends of layered and pseudolayered phases. Phases:

1. Montmorillonite (Askangel deposit, Georgia), 2. Al-chlorite enriched with Mg (by Eggleston and Bailey, 1967), 3. field of dioctahedral montmorillonite compositions, 4. the same for trioctahedral, 5. compositions of sepiolites, 6. palygorskites, 7. vermiculites, 8. mixed-layered mica- and talc-montmorillonites and chlorite-montmorillonites, 9. mixed-layered pyrophyllite-beidellite-Al-montmorillonite, 10. mixed-layered pyrophyllite-Al-chlorite, 11. mixed-layered beidellite-Al-montmorillonite-Al-chlorite. Fragments of structures: 12. tetrahedrons, 13. octahedrons (di), 14. octahedrons (thri), 15. brucite interlayer, 16. exchange ions and molecules of  $H_2O$ . Abbreviations: sep-sepiolite, pal - palygorskite, m-di-dioctahedral montmorillonites, m - tri - the same trioctahedral, pph - pyrophyllite, bd - beidellite, Al-m-Al-montmorillonite, Kl - kaolinite, dc - dickite, nacr - nacrite, mg - metahalloysite, ts - tosudite, Al-chl - Al-chlorite, and - andalusite, sil - sillimanite, Ky - kyanite, mu - mullite, cor - corundum, hydr - hydrargillite, ds - diaspore, bm - boehmite, sp - spinel, sap - sapphirine, Mg-st-Mg-stauroilite, Yod-yoderite, cord - cordierite, car - cardenite, gch - gchasulite, sa - saponite, ta - talc, stiv - stivensite, ant - antophyllite, en - enstatite, ve - vermiculites, ged - gedrite, py - pyrope, serp - serpentine, chl - clinochlore, Al - serp - Al - serpentine, ams - amesite, for - forsterite, br - brucite, per - periclase.

Table I

## Schematic Relations in the Transformation of Clay Minerals



## Some peculiarity of transformation reactions

Looking at the scheme (Table I) one must take into account, that the structures of newly formed phases depend on the structural peculiarities of the initial material: the structures are inherited in the process of solid state transformational reactions and essentially, influence on energetics, in particular on the temperature of the reactions. Solid state transformational reactions, investigated in this work are shown in the Table II. The reactions are divided into two categories: without and with the changing of composition. The category I includes structural reactions that lead to order-disorder homogeneous layers. These defects of structures were made by the stress with was typical for upper part of crust for wash-out and folding region. In the same category there must be placed, unstudied in present article, reactions of the polytypes - polymorphs formations and those with the alteration of atoms order in the layer. The category 2 with alteration of composition includes phases reactions widespread in nature among clay minerals.

All reactions were classified on degree of inheritance of structure on the ground of crystallochemical analysis of products of experiments and the conformity with temperature of transformations reactions was ascertain. So, reactions with inheritance of layer pass under minimal temperature of experiments (200-250°C). It is possible that these reactions were typical for upper part of the crystal of sedimentary rocks. The reactions with inheritance of some tetrahedral and octahedral positions at partial destruction of layer - for example by change of dioctahedral structure into trioctahedral one, or silicates into aluminosilicates, require greater energetical expenditure and take place at temperatures 250-300°C.

Still more energy is spend at alteration of layered silicates into the frameworked or some other nonlayered structures, where smaller structural particles are transformed instead of layers and definite tetrahedral and octahedral nets. The noticed conservation of Si - O nets by transformation of heterodesmic structures in neutral conditions can be explained by the stability of ionic-covalent bonds Si - O. But, along with the rise of temperature, the increase of alkalescence of neutral conditions also increases the solubility of silicates, in consequence of which one may expect, that the structural succession will be difficult. In fact, as a set of experiments of transformation of kaolinite into montmorillonite in the presence of  $K_2CO_3$  and  $K_2SO_4$  has shown, along with layered, mixed - layered mica - montmorillonite and micaceous formations in the products of experiments, there are also present framed aluminosilicates - leicite and kalisilite. The formation of the latter we have not studied in details; we can only suppose, that the formation of feldspars in the experiments with KCl by high temperatures, kalisilite and leicite with  $K_2CO_3$  and  $K_2SO_4$  in alkali conditions at low parameters, arises from more disperse phases or from a mineralized vapour phase.

Table II

The transformational reactions with presence of the layered and pseudolayered silicates

Without changing of composition (formation different defects of structure, polytypes, polymorphous)	With a changing of composition (phases reactions)	Degree of inheritance of structure		The conditions of experiments
Ordered kaolinite - - disordered kaolinite	I. In groups of silicates. Hydration $\longrightarrow$ dehydration (halloysite $\longrightarrow$ meta-halloysite, montmorillonite $\longrightarrow$ mixed-layer phase $\longrightarrow$ dehydrational montmorillonite)	layer	Homomorphy	100°C + + P <sub>stress</sub>
	II. Between groups of silicates. Beidellite $\longrightarrow$ random mixed-layer phase $\longrightarrow$ hydromica. Beidellite $\longrightarrow$ regular mixed-layer phase $\longrightarrow$ hydromica, chlorite			100-200°C + PH <sub>2</sub> O + KCl, NaCl + CaCl <sub>2</sub> , + MgCl <sub>2</sub>
Kaolinite - chlorite	Diocahedral montmorillonite $\longrightarrow$ trioctahedral montmorillonite Sepiolite $\longrightarrow$ dehydrational Mg - montmorillonite	Tetrahedral and octahedral nets	Heteromorphy	+ MgCl <sub>2</sub> FeCl <sub>2</sub> P <sub>stress</sub> ★ 200-300°C
	III. Between groups of silicates - aluminosilicates Montmorillonite $\longrightarrow$ random mixed-layer phase $\longrightarrow$ hydromica Kaolinite $\longrightarrow$ beidellite Kaolinite $\longrightarrow$ hexagonal analogue of anortite Sepiolite $\longrightarrow$ Mg - montmorillonite $\longrightarrow$ talc Palygorskite $\longrightarrow$ di- and tri-octahedral montmorillonites Palygorskite $\longrightarrow$ trioctahedral montmorillonite			+ PH <sub>2</sub> O  + CaCl <sub>2</sub> with and without additions + KCl, NaCl CaCl <sub>2</sub> + MgCl <sub>2</sub>
Layered hexagonal analogue of anortite - framework anortite	IV. Between structures of layer-unlayer (frameworks, ribbon and others) Montmorillonite $\longrightarrow$ feldspars Sepiolite $\longrightarrow$ tremolite	Structural elements		300-400°C  + PH <sub>2</sub> O + KCl, NaCl, CaCl <sub>2</sub> + CaCl <sub>2</sub>

★ Temperature of transformation is lowered strongly by P<sub>stress</sub>, because of breaking of structure (Goilo et al., 1966).

The reactions observed above must respond different progressive stages of alteration of the rocks. One may consider, that the observed scheme is relatively similar to that in the nature, when a progressive metagenesis of deposits would take place with the assistance of the interstitial solutions containing K, Na, Ca, Mg.

### Chemical features of the processes

Figure 3 shows compositional changing of consequently transforming phases. Let us note some regularity for all the revealed reactions with the increase of temperatures:

1. Development of layered three-staged structures after original two-staged one, is accompanied by the release of octahedral cations with decrease of bonds Al-OH in the structure (dioctahedral structures) and Mg, Fe-OH (trioctahedral structures). The released cations being in the solution, may be crystallized into compounds, rich with Al, Mg, Fe.

2. Transformation of three-staged layered and pseudo-layered structures at progressive increase of temperature, in contrast with mentioned above, is followed by the desilification. For example, such alterations as montmorillonite  $\rightarrow$  hydromica, beidellite  $\rightarrow$  rectorite  $\rightarrow$  mica, beidellite  $\rightarrow$  tosudite  $\rightarrow$  chlorite, palygorskite  $\rightarrow$   $\rightarrow$  montmorillonite, sepiolite  $\rightarrow$  talc and etc.

3. The further rise of temperature leads to destruction of structures and formation of framed and some other structures; this process is followed by intensive desilification with a sharp decrease of such bonds as Al-OH, (Mg, Fe)-OH.

Thus, the general tendency of layered silicates transformations is clearly controlled by the stability of bond Me-OH. The hydroxyl bond, more stable with Mg than with Al, explains the fact that the trioctahedral forms were more steady, than the dioctahedral ones. As for the peculiarities of formation of frameworked aluminosilicates it is important to mention, that there Al is bound only with oxygen and is in tetrahedral position; in the layered silicates the octahedral Al, bound both with O and OH, prevails over the tetrahedral Al. The composition of structural types of synthesized phases with the value of pH in solutions, leads to the conclusion, that increase of alkalescence of solution favours the formation of such aluminosilicates, where Al like Si is bound with oxygen, while the sour and neutral solutions favours the formation of silicates, where the octahedral Al, bound with the OH-groups, prevails. It appears that those tendencies in the behavior of Al as an amphoter, that are noted in the solutions at low pressures and temperatures, are also observed at the experiments by higher T-P-parameters. Experimentally was established that the stages of phase transformations of the silicates are proved to be closely connected with both the thermodynamical conditions of this transformations (temperature, composition of solution and s.o.) and the crystallochemical features of transformed struc-

tures. In luminous the natural processes of metagenesis and hydrothermal-metasomataical alterations, that are similar to laboratory experimental investigations, for the future experiments, by examining the influence of various environments ( $SO_4$ ,  $CO_3$ -solutions and s.o.), on clay minerals it will be possible to find out more varieties of processes and their structural mechanism, that will help us to evaluate the peculiarity of natural analogies.

#### REFERENCES

- VALYASHKO, M.G. (1958): Some general trends formation of chemical composition of natural waters. In: Mem. F.P. Savarensky labor. hydrogeol. probl. of the Academy of Sciences of the USSR, v. 16, Moscow, p.p. 127-140.
- GOILO, E.A., KOTOV, N.V., FRANK-KAMENETSKIJ, V.A. (1966): The experimental study of the influence of stress and hydrostatic pressure on the crystalline structure of kaolinite under various temperatures. In: Physical research methods of Sedimentary rock minerals. Publ. office "Science", Moscow, p.p. 123-130.
- FRANK-KAMENETSKIJ, V.A., KOTOV, N.V., GOILO, E.A. (1969): Hydrothermal synthesis in the systems halloysite and kaolinite K, Na, Ca, Mg-chlorides under pressure. In: Problems of petrology and genetic mineralogy, vol. I, Publ. office "Science", Moscow, p.p. 143-163.
- FRANK-KAMENETSKIJ, V.A., KOTOV, N.V., KLOCHKOVA, G.N. (1969): Phase transformations of sepiolite and palygorskite at different pressures under hydrothermal conditions. *Geochemistry*, 1, 14-21.
- FRANK-KAMENETSKIJ, V.A., KOTOV, N.V., GOILO, E.A. (1970): Hydrothermal synthesis of mixed-layered phases in the systems kaolinite - K, Na, Ca, Mg-chlorides under pressure. In: The mineralogy, the properties and the practical significance of clays. Publ. office "Science", Moscow, p.p. 39-51.
- FRANK-KAMENETSKIJ, V.A., KOTOV, N.V., KLOCHKOVA, G.N. (1970): Phase transformations of sepiolite and palygorskite in the hydrothermal conditions under pressure in the presence of potassium and sodium chlorides. *Geochemistry*, II: 1312-1321.
- KOTOV, N.V., LEBEDEV, V.I., TARLAKOV, U.P. (1970): Mixed-layered phases as a products alteration of kaolinite and metahalloysite at heating in hydrothermal conditions under pressure. *Dokl. Akad. Nauk S.S.S.R.*, 191/4/: 901-904.
- KOTOV, N.V., SHITOV, V.A. (1971): Phase and structural alterations of dioctahedral montmorillonite under pressure. *Mem. Leningrad State University, geol.-geogr.sci.*, 2/12/: 34-48.
- TOMASHENKO, A.N., FRANK-KAMENETSKIJ, V.A., KOTOV, N.V.,

(1971): On synthesis of rectorite from gels. Dokl. Akad. Nauk, S.S.S.R., 199/I/: 186-188.

FRANK-KAMENETZKIJ, V.A., KOTOV, N.V., GOILO, E.A. (1966): Strukturänderung von Tonmineralen unter verschiedenen thermodynamischen Bedingungen, I. Kristall und Technik, 1/3/: 465-475.

FRANK-KAMENETZKIJ, V.A., KOTOV, N.V., GOILO, E.A. (1968): Strukturveränderungen von Tonmineralen bei verschiedenen thermodynamischen Bedingungen, 2. Kristall und Technik, 3/3/: 643-660.

FRANK-KAMENETZKIJ, V.A., KOTOV, N.V., SCHITOV, V.A., GOILO, E.A. (1970): Strukturveränderungen von Tonmineralen bei verschiedenen thermodynamischen Bedingungen, 3. Kristall und Technik, 5/I/:129-144.

FRANK-KAMENETZKIJ, V.A., KOTOV N.V., GOILO, E.A. , KLOTCHKOVA, G.N. (1971): Structural transformations of some clay minerals under pressure in hydrothermal conditions. In: Y. Takeuchi/Editor/, Mineral. Soc. Japan. Spec. Pap. I, Tokyo, p.p. 88-97.

EGGLESTON, R.A., BAILEY, S.W. (1967): Structural aspects of dioctahedral chlorite. Amer. Miner., 52/5-6/: 673-689.



KINETICS OF ALTERATION OF K-FELDSPAR TO KAOLINITE  
AND ITS APPLICATION TO THE GENESIS  
OF KAOLIN DEPOSITS

Y. Tsuzuki, S. Mizutani and H. Shimizu\*

Department of Earth Sciences, Faculty of Science, Nagoya University,  
Nagoya, Japan

H. Hayashi

Government Industrial Research Institute, Nagoya, Japan

ABSTRACT. - K-feldspar was experimentally treated with acid solutions containing various concentration of  $H^+$  and  $K^+$  at 210-270°C in silica glass tubes. Amounts of Si, Al and K in the solutions were determined after some of the experimental runs. The alteration product was kaolinite in general, but amorphous material in strong acid solution. This result is explained by using  $\log [Al^{+++}]$  vs.  $\log [H_4SiO_4]$  diagram.

The rate of reaction depends on chemical composition of solution and temperature. On a basis of the experimental results, the alteration process can be expressed by the following rate formula,

$$\alpha = 1 - \exp(-kt^n)$$

where  $\alpha$  is kaolinite fraction of the solid,  $t$  is time, and  $k$  and  $n$  are constants.

Assuming that Al is inert and Si and K behave as mobile components, formation of kaolin deposits is illustrated in a model involving a kinetic process. In a case that Al is considered to be a mobile component, alteration process is also discussed on  $\log [Al^{+++}]$  vs.  $\log [H_4SiO_4]$  diagram.

---

\*Present Address: Narumi China Co., Ltd., Narumi, Aichi, Japan.

## INTRODUCTION

The essential process of formation of hydrothermal kaolin deposits are considered to be an alteration of feldspar during permeation of hydrothermal acid solution through it. This process occurs in an open system, and the mineral assemblage resulted does not represent an equilibrium state. To study this process basically, therefore, an experiment of hydrothermal alteration must be done from a kinetic point of view.

Since Correns and von Engelhardt's experimental work (1938), many investigations have been done on the reaction between solution and feldspar. Hemley and Jones (1964) discussed the alteration process based on their experimental results, and Helgeson (1968) and Helgeson et al. (1969) studied it theoretically, assuming that the process progressed under partial equilibrium state. Tsuzuki and Mizutani (1969, 1971), however, pointed out that the rate of attainment of equilibrium depends largely on the relative rate of reaction to the material transfer, and discussed the alteration process based on kinetics of hydrothermal experiment. In the present work, hydrothermal alteration of K-feldspar in acid solution was experimentally studied, and the precipitation process from solution is discussed together with mineral alteration from a kinetic viewpoint in an open system.

## EXPERIMENTAL

Microcline separated by means of heavy liquid from perthite from India is exclusively used; the average grain size about 0.01 mm in diameter. The experimental method of alteration is almost the same as that of the previous work reported by Tsuzuki and Mizutani (1969, 1971). After each alteration experiments, Si, Al and K contents of the solutions were determined by atomic-absorption spectrophotometry and flame photometry, and mineral compositions of the solid estimated quantitatively by X-ray diffraction.

K-feldspar was generally altered to kaolinite. In high  $H^+$  solution, however, no kaolinite was formed and some amorphous material rich in silica was found instead. The change of Al, Si and K in the solution with time was different for different runs as shown later. In low  $H^+$  solution, dissolution of Al is much less in amount.

## REACTION KINETICS

Generally, the reaction proceeds rapidly in a solution with high  $H^+$  and low  $K^+$  concentration and at high temperature. The types of

reaction are diversified when expressed in terms of kaolinite fraction of solid versus time. Some reactions are low in rate at first and become high, and then slow down gradually as shown in Fig. 1(A). Others progress rapidly in the early stage, then become slower, and hardly reach the ultimate stage as shown in Fig. 1(B).

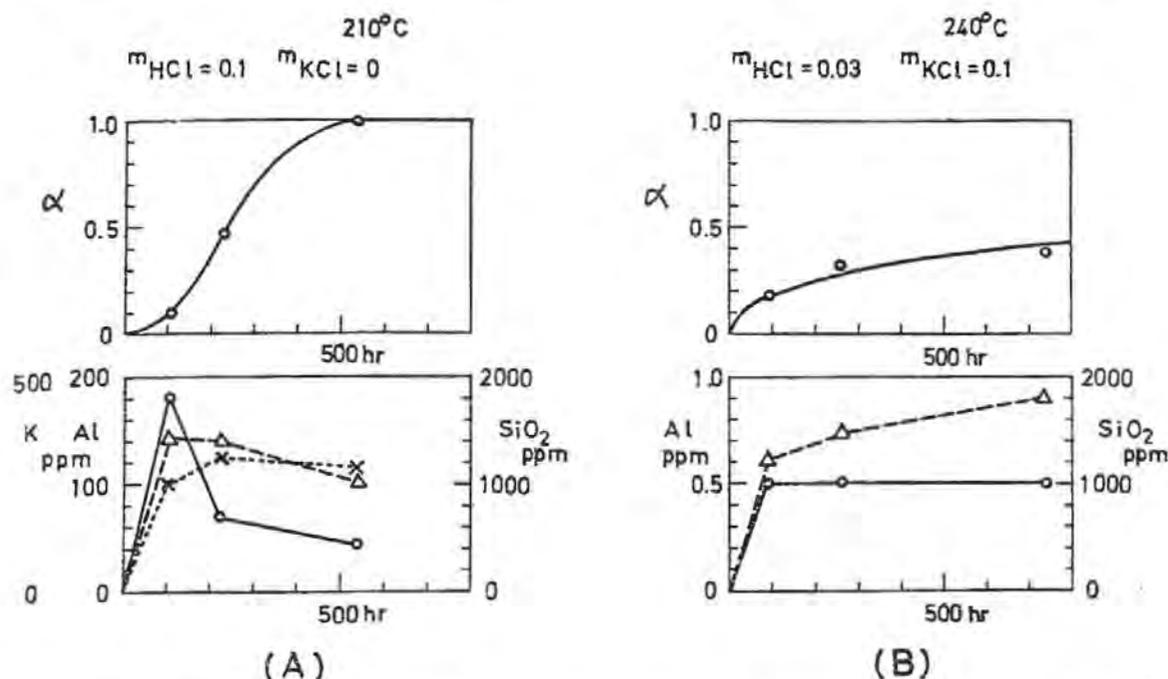


Figure 1. Reaction kinetics of alteration of K-feldspar to kaolinite in hydrothermal solution

$\alpha$  (kaolinite wt. fraction of the solid):  $\circ$ , observed; —, calculated; on the upper diagrams.

Concentration in solution:  $\circ$ , — Al,  $\Delta$ , - - - Si, X, - - - - K; on the lower diagrams.

The kinetic relation can be expressed by the following empirical formula, which was given by Erofeev (1961) for a reaction involving solid,

$$\alpha = 1 - \exp(-kt^n) \quad (1)$$

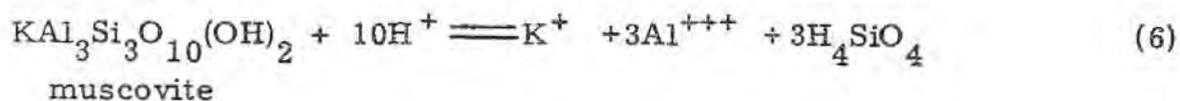
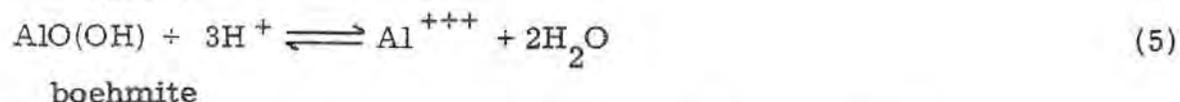
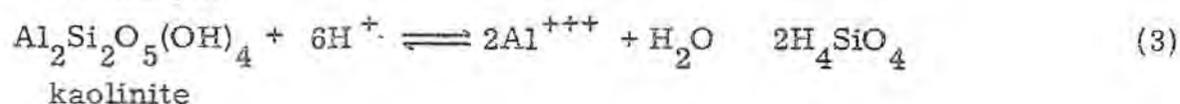
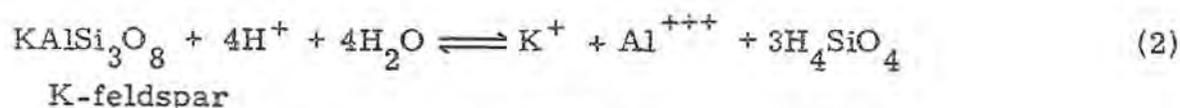
where  $\alpha$  is kaolinite fraction of the solid at time  $t$ , and  $k$  and  $n$  are constant related with temperature and concentration of  $\text{H}^+$  and  $\text{K}^+$ . The curves in Fig. 1 are calculated according to this formula under a given experimental condition using experimentally determined values of the constants. Because this empirical formula does not tell us the mechanism of reaction, the chemical change of solution must be determined experimentally, the result of determination being given and discussed in the next section.

## REACTION PROCESS ON AN EQUILIBRIUM DIAGRAM

According to the present experimental results, the alteration reaction of K-feldspar can be divided into two extreme types, although many intermediate cases are observed. When the reaction occurs rapidly, Si content of solution decreases slightly with reaction time, or maintained almost constant, while Al decreases sharply. This fact, as well as the sigmoidal curve of kaolinite formation (Fig. 1, A), indicates that the K-feldspar is dissolved into solution at first and then kaolinite is precipitated from the solution. Thus Al should be considered as a mobile component.

In a case of slow reaction, on the other hand, Si content of the solution increases slightly with time, or is maintained constant, and Al remains nearly constant throughout whole stage of reaction. This fact shows that the transformation of K-feldspar into kaolinite occurs in solid state, and thus Al is considered as an inert component.

The rapid reaction and even the slow reaction are regarded as a step reaction K-feldspar  $\rightarrow$  solution  $\rightarrow$  kaolinite, if solid transformation is considered as a dissolution immediately followed by precipitation. This step reaction can be treated on  $\log [Al^{+++}]$  vs.  $\log [H_4SiO_4]$  diagram. The relevant reactions are



Equilibrium constants of these equations at elevated temperatures were given by Helgeson (1969), except that of equation (5) which was calculated according to equations proposed by Helgeson (1969). Using these equilibrium constants, the stability relations are shown on  $\log [Al^{+++}]$  vs.  $\log [H_4SiO_4]$  diagram at a given activity of  $H^+$  and  $K^+$  and temperature as shown in Fig. 2.

As Al in solution, however, dissociates to  $Al^{+++}$ ,  $AlOH^{++}$  and  $Al(OH)_4^-$ , activity of  $Al^{+++}$  should be calculated according to the

following equations.



Though  $\text{H}_4\text{SiO}_4$  dissociates to  $\text{H}^+$  and  $\text{H}_3\text{SiO}_4^-$ , the ratio of  $\text{H}_3\text{SiO}_4^-$  to  $\text{H}_4\text{SiO}_4$  is negligibly small in low pH solution,

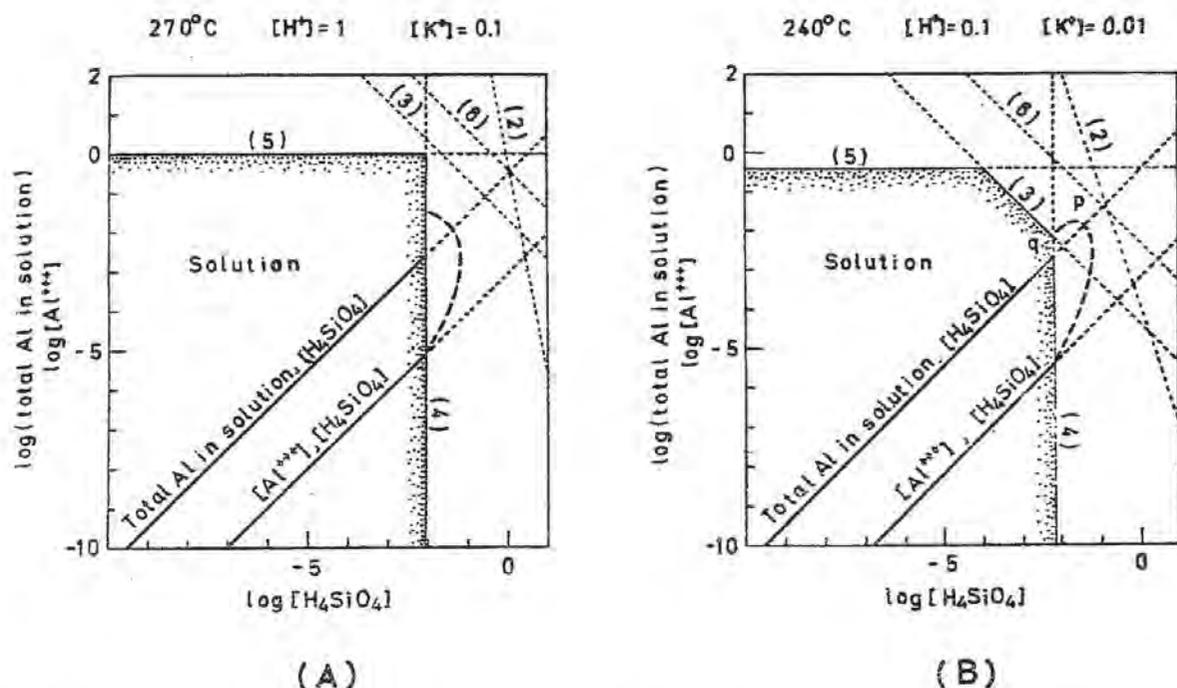


Figure 2. Equilibrium relations on the  $\log [\text{Al}^{+++}]$  vs.  $\log [\text{H}_4\text{SiO}_4]$  diagram and a trace of composition in solution at alteration of K-feldspar on that diagram and on the  $\log [\text{total Al in solution}]$  vs.  $\log [\text{H}_4\text{SiO}_4]$  diagram. No. attached to each line corresponds to No. of equation in the text.

Activity coefficient of ions and molecules in solution is assumed to be unity in the following discussion. When K-feldspar is dissolved perfectly, the molar ratio of total Al in solution to  $\text{H}_4\text{SiO}_4$  in the solution equals to 1/3. If  $\log [\text{total Al in solution}]$  is taken on the ordinate, the change of the chemical composition of solution owing to K-feldspar dissolution is expressed by a straight line which passes the point ( $\log [\text{total Al in solution}] = 0$ ,  $\log [\text{H}_4\text{SiO}_4] = 0.477$ , which corresponds to  $m\text{Al} = 1$ ,  $m\text{H}_4\text{SiO}_4 = 3$ , respectively), and it declines 45° to the both axes. The trace on  $\log [\text{Al}^{+++}]$  vs.  $\log [\text{H}_4\text{SiO}_4]$  diagram is a line which is parallel to that on  $\log [\text{total Al in solution}]$  vs.  $\log [\text{H}_4\text{SiO}_4]$  diagram but differs by  $\log [\text{Al}^{+++}/\text{total Al in so-}$

lution] on the ordinate from the latter.

The change of  $[Al^{+++}]$  and  $[H_4SiO_4]$  proceeds from lower left to upper right on the diagram and reaches the precipitation line for a certain mineral. Then, the mineral begins to be precipitated and the trace of chemical change of concentrations in solution bends into a different trend. The course of chemical change in the solution after that can be estimated by assuming the rate of dissolution and precipitation. If a reaction proceeds under partial equilibrium as discussed by Helgeson (1968), chemical composition of the solution changes along boundary line between a mineral and solution. However, chemical composition of solution actually should enter into the mineral field under a metastable state. The change of composition in solution continues until K-feldspar disappears or until it reaches dissolution line of K-feldspar.

The diagram under a strong acid solution is shown in Fig. 2(A). Since kaolinite precipitation line is far from the solution area, kaolinite is under unstable state. The trace of K-feldspar dissolution crosses the silica precipitation line at first and silica (amorphous) begins to precipitate and the trace bends like the broken line in the figure. The boehmite precipitation line is situated in such a high  $[Al^{+++}]$  region that the trace will not reach it before K-feldspar disappears. This agrees with the result of the experiment.

An example under a general condition of kaolinite formation is shown in Fig. 2(B). Silica (amorphous) precipitates at first and the solution perhaps changes along the broken line; and kaolinite precipitation begins around point "p", too. Probably, amorphous silica and kaolinite coexist around point "q". The line of sericite precipitation is so far from the solution area that it is not precipitated. This also agrees with experimental result.

#### ALTERATION OF FELSIC ROCK AND FORMATION OF KAOLIN DEPOSITS

During the hydrothermal alteration of rock, solution reacts to the rock, and both the solution and the rock change their compositions. The solution then migrates to the adjacent part of the rock.

When slightly acid solution reacts to a felsic rock which consists of K-feldspar and silica or silica glass, it is reasonably considered that Al is inert,  $K^+$  is mobile and is not precipitated as mineral, and Si is mobile and is precipitated as amorphous silica or quartz. Although, for such a case, the  $\log [Al^{+++}]$  vs.  $\log [H_4SiO_4]$  diagram is useful to the interpretation of natural hydrothermal alteration, the scheme proposed by Tsuzuki and Mizutani (1969, 1971) can be better used incorporated with kinetic formula



## REFERENCES

- CORRENS, C.W. and von ENGELHARDT, W. (1938): Neue Untersuchungen ueber die Verwitterung des Kalifeldspates. *Chem. d. Erde.* 12, 1-22.
- EROFEEV, B.V. (1961): Reaction rate of processes involving solids with different specific surfaces. *Reactivity of Solids, Proc. 14th Intl. Symp. Reactivity of Solids, 1960*, 273-282.
- HEMLEY, J.J. and JONES, W.R. (1964): Chemical aspects of hydrothermal alteration with emphasis on hydrogen metasomatism. *Econ. Geol.* 59, 538-569.
- HELGESON, H.C. (1968): Evaluation of irreversible reactions in geochemical processes involving minerals and aqueous solutions - I. Thermodynamics relations. *Geochim. et Cosmochim. Acta.* 32, 853-877.
- HELGESON, H.C. (1969): Thermodynamic of hydrothermal systems at elevated temperatures and pressures. *Am. Jour. Sci.* 267, 729-804.
- HELGESON, H.C., GARRELS, R.M. and MACKENZIE, F.T. (1969): Evaluation of irreversible reactions in geochemical processes involving minerals and aqueous solutions - II. Applications. *Geochim. et Cosmochim. Acta*, 33, 455-481.
- IWAO, S. (1968): Zonal structure in some kaolin and associated deposits of hydrothermal origin in Japan. Genesis of the kaolin deposits. Rept. 23 Session Czechoslovakia 1968, *Intl. Geol. Cong.* 107-113.
- TANEMURA, M. (1954): Kaolin deposits in Nittai-Kawauchi, Tomoe and Kampaku Mines, Tochigi Prefecture (in Japanese). *Bull. Geol. Surv. Japan*, 5, 647-656.
- TSUZUKI, Y. and MIZUTANI, S. (1969): Kinetics of hydrothermal alteration of sericite and its application to the study of alteration zoning. *Proc. Intl. Clay Conf. 1969*, 1, 513-522.
- TSUZUKI, Y. and MIZUTANI, S. (1971): A study of rock alteration process based on kinetics of hydrothermal experiment. *Contr. Mineral. and Petrol* 30, 15-33.

# KINETICS AND MECHANISMS OF DISSOLUTION OF FITHIAN ILLITE IN TWO COMPLEXING ORGANIC ACIDS

W.H. Huang and W.D. Keller

Department of Geology, University of South Florida  
Tampa, Florida 33620, U. S. A.

**ABSTRACT.** - Eight grams of the  $< 2 \mu$  fraction of Fithian illite were intermittently shaken up to 520 days, in 500 ml each of solution of 0.01 M salicylic and tannic acids, at room temperature. Aliquots of centrifuged solutions were analyzed for pH, the major elements, Si, Al, Fe, Mg, K, Ca, and Na. The pH, 3 to 3.5, of the solutions remained relatively unchanged throughout the reaction.

The cations were dissolved at different rates in the two acids. Al, K, Fe, and Mg were dissolved incongruently and preferentially with respect to Si in tannic and salicylic acids, respectively, by factors of 1.3 - 1.3, 2.4 - 1.7, 15.5 - 24, 4.8 - 3.9. The dissolution of Al, K, Mg, up to 60 days followed a first-order reaction, whereas the solution of Si and Fe appeared to be controlled by a diffusion reaction, according to a model for the peripheral attack on a disk-shaped particle in which the reacted layer acts as a diffusion barrier. Diffusion rates of Si (tetrahedral) were similar in both acid solutions, and were lower than those of Fe (octahedral).

## INTRODUCTION

Dissolution kinetics of clay minerals in inorganic acids have been extensively studied to determine the specific ions in tetrahedral and octahedral coordinations (Brindley and Youell, 1951; Osthaus, 1956), the structures of clay minerals (Gastuche and Fripiat, 1962; Gastuche, 1963; Ross, 1967, 1968), and the dissolution rates and activation energies of the reactions (Cloos et al., 1960). Reports on the kinetics of dissolution of clay minerals in organic acids, however, are notably fewer.

Complexing organic acids whose functional groups, such as carboxyl, hydroxyl, and amino are typically present in humus and other organic matter of geologic environments, dissolved clay mi-

nerals in significantly different ways than did inorganic acids (Huang and Keller, 1971). In a study of equilibrium dissolution of clay minerals we found that Al and Fe were dissolved preferentially with respect to Si in strongly complexing acids. In this paper are reported the kinetics of illite dissolution in salicylic and tannic acids and the trend of structural decomposition after dissolution.

## EXPERIMENTAL

Eight grams of the  $< 2 \mu$  fraction of Fithian illite were intermittently shaken in separate 500 ml portions of 0.01 M salicylic and tannic acids at room temperature for different periods of time up to 520 days. Salicylic acid is aromatic and mono-hydroxy in structure, whereas tannic acid is believed to be a mixture of aliphatic and polyhydroxy carboxylic acid (Hem, 1965).

After selected reaction times the clay suspensions were centrifuged at 15,000 rpm for 2 hours, and the supernatant liquids (showed no Tyndall cone) withdrawn. Then, 500 ml of newly prepared acid solutions were added to the samples for continued reactions. The pH was immediately measured. Si in the supernatant solution was determined colorimetrically, except that in tannic acid solution (colored) it was run by atomic absorption. Al, Na, and K in the solution were determined by atomic flame emission, and Fe, Mg, and Ca, by atomic absorption (Huang and Keller, 1970, 1971).

After the last extraction (about 520-day dissolution) the clay samples were x-rayed to determine structural changes in the illite resulting from its reaction with the organic acids.

## KINETICS AND MECHANISMS OF DISSOLUTION

### Incongruency of dissolution

Incongruent dissolution of clay minerals has been observed to occur commonly in laboratory dissolution experiments, as well as in geologic weathering environments. To determine the incongruency of dissolution of illite by complexing salicylic and tannic acids, the fractional amounts of Si, Al, Fe, Mg, and K dissolved were divided by the fractional amounts of them present in the original bulk analyses; this yielded the fraction ( $\alpha$ ) dissolved. These fractions were plotted against time of dissolution, as shown in Figs. 1, and 2. Since  $\alpha$  values for framework cations yielded dissimilar curves, obviously the framework cations from illite were dissolved at significantly different rates. Among the framework cations, Fe was dissolved relatively rapidly followed in order of decreasing rate by Mg, K, Al, and Si, in both salicylic and tannic acids. That the

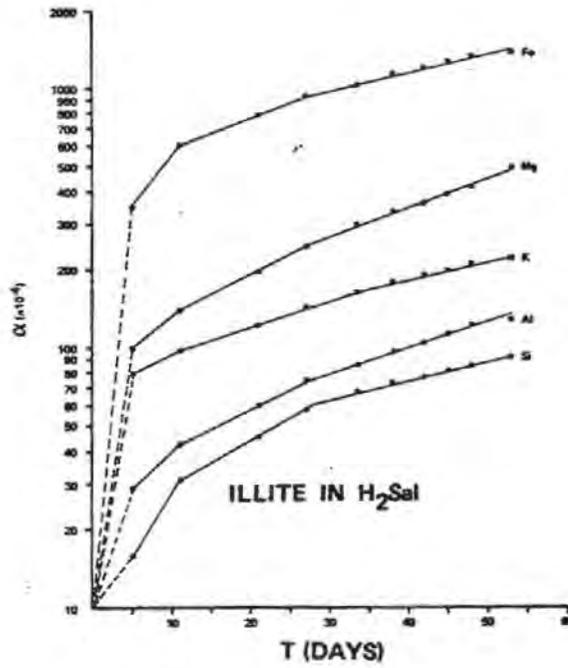


Figure 1. Fraction of cations dissolved from Fithian illite in 0.01M salicylic acid, as a function of time.

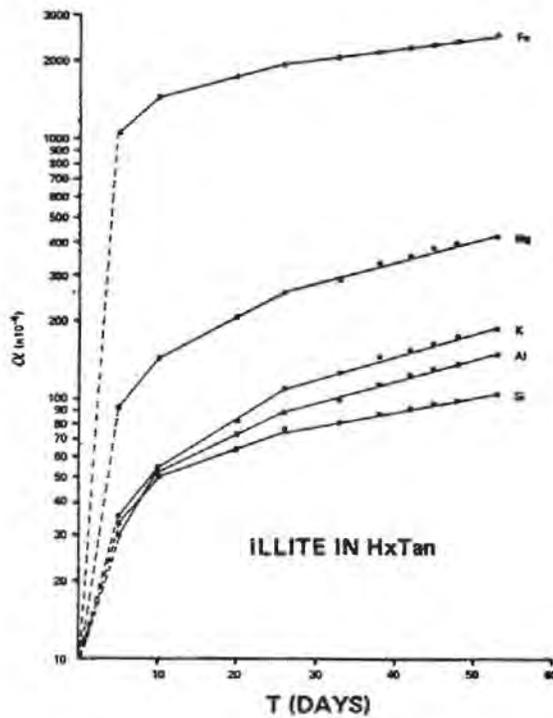


Figure 2. Fraction of cations dissolved from Fithian illite in 0.01M tannic acid, as a function of time.

relative rates of dissolution of Al and Fe were higher than that of Si in the organic acids is in contrast to dissolution in inorganic aqueous solutions where Si was always dissolved faster than Al or Fe.

Inasmuch as the changes in the pH of organic acid solutions of illite, Table I, were rather small, in the range of 3.0 to 3.5, the interaction of organic acids with sesquioxides resulted in the formation of complex organomineral compounds. This mechanism accounts for the relatively high dissolution rates of Al and Fe in organic acids (Huang and Keller, 1972).

Table I

Changes of pH in dissolution of Fithian illite in salicylic acid ( $H_2Sal$ ) and tannic acid ( $H_xTan$ ) as a function of time in days

<u>Time</u>	<u><math>H_2Sal</math></u>	<u><math>H_xTan</math></u>
0	3.01	3.40
1	3.25	3.03
3	3.16	3.17
5	3.12	3.19
11	3.09	3.22
21	3.09	3.27
26.5	3.07	3.34
33.3	3.06	3.37
38	3.05	3.39
42	3.05	3.36
45	3.03	3.40
48	3.03	3.41
53	3.03	3.41

## Diffusion-controlled reactions for Si and Fe

The dissolution of silicate minerals in inorganic aqueous solution is commonly governed by either a diffusion process (Ross, 1968; Luce et al., 1972), or a first-order reaction (Osthanus, 1956). To evaluate the dissolution reactions of framework cations from illite in complexing acids, the  $\alpha$  values for cations were plotted against the square root of time ( $\sqrt{t}$ ), Fig. 3. The linear relationships for Si and Fe in Fig. 3 indicate that dissolution of Si and Fe followed the parabolic rate expression,  $\alpha^2 = kt$ , which is an expression for a diffusion-controlled reaction.

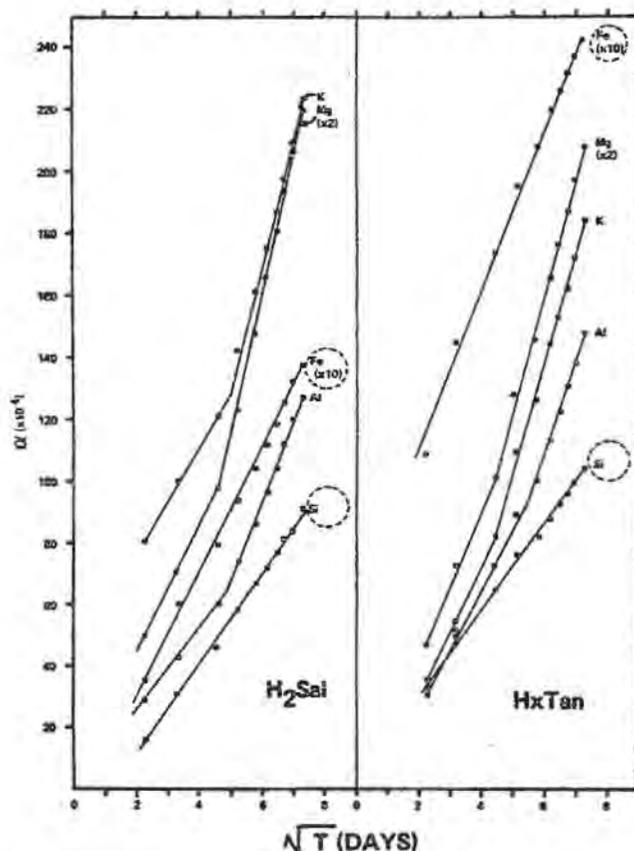


Figure 3. Fraction dissolved ( $\alpha$ ) versus  $\sqrt{t}$  of cations in 0.01M salicylic and tannic acids.

Assume a model for the peripheral attack on a disk-shape particles of illite in which the reacted layer acts as a diffusion barrier, and that Si and Fe ions do not diffuse backward into the mineral particles. Then the exact solution of diffusion constants ( $k$ ) is obtained as follows:

$$\frac{dy}{dt} = \frac{k}{y} ; y^2 = 2kt \quad (1)$$

$$\text{since } y = r [1 - (1 - \alpha)^{1/2}]$$

where  $r$  = mean diameter of particle  
 $\alpha$  = fraction loss of ion

$$\text{therefore } y^2 = r^2 [1 - (1 - \alpha)^{1/2}]^2 = 2kt$$

$$\therefore [1 - (1 - \alpha)^{1/2}] = \left( \sqrt{\frac{2k}{r}} \right) \sqrt{t} \quad (2)$$

As shown by the data for Si and Fe in Fig. 4, the linear relationships for Si and Fe indicate that dissolution of Si (and Fe) follows this model in which the complexing acids attack disk-shaped particles. Attack proceeds from the circumference to the center during which the reacted layer (probably amorphous layer, or Al-organic complex layer?) acts as a diffusion layer. Since the data for Al show non-linearity in the plots, dissolution of Al is not controlled by the diffusion process. The diffusion constants ( $k$ ) for Si and Fe in two complexing acids were calculated and shown in Table II. The rate constants of Si (tetrahedral) were similar in both acid solutions, and were lower than those of Fe, which presumably is coordinated octahedrally, as might be expected.

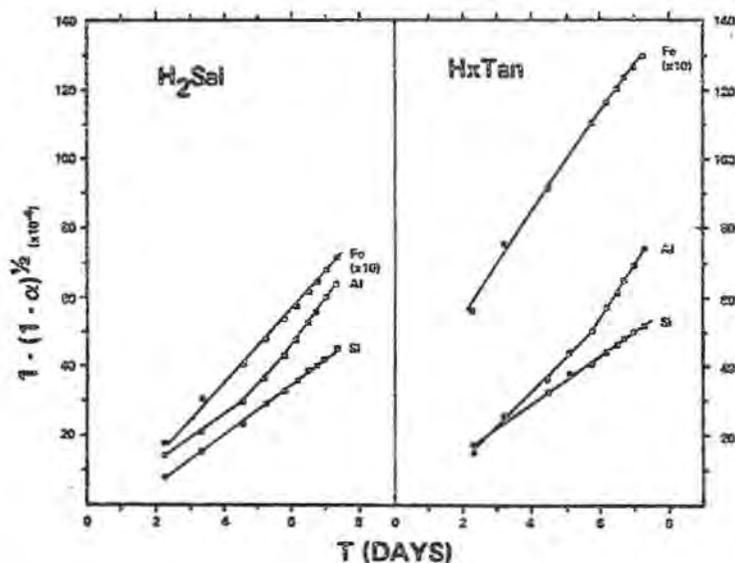


Figure 4. Plots of  $(1 - (1 - \alpha)^{1/2})$  versus  $\sqrt{t}$  for Si, Fe, and Al dissolved from Fithian illite by 0.01M salicylic and tannic acids.

Table II

Diffusion constants\* for Si (and Fe) from illite in salicylic and tannic acids, expressed as  $\text{cm}^2/\text{sec}$

	<u>Salicylic acid</u>	<u>Tannic Acid</u>
Si	$3.38 \times 10^{-26}$	$2.95 \times 10^{-26}$
Fe	$7.25 \times 10^{-24}$	$1.18 \times 10^{-23}$

\*Assume  $r = 0.3 \mu$ , and disk-shape particle

#### First-order reaction for Al, K, and Mg

Since Al is complexed by salicylic and tannic acids (Huang and Keller, 1971, 1972), and K and Mg are highly soluble in the solutions, the dissolution of these cations may be governed by a first-order rate law. Osthau (1956) showed that dissolution of Al from montmorillonite and nontronite followed the first-order reaction.

The rate constants ( $k_1$ ) of the first-order reaction may be expressed as follows:

$$\ln (1 - \alpha) = - k_1 t + \text{constant} \quad (3)$$

or:

$$\log (1 - \alpha) = - \frac{k_1 t}{2.303} + \text{constant} \quad (4)$$

In Figs. 5 and 6 where  $\log (1 - \alpha)$  is plotted against time for Al, K and Mg, the solution curves for these ions follow straight lines, indicating a first-order reaction. The rate constants are listed in Table III. The data show that (1) the constants for each ion in two complexing acids were found to be much the same, and (2) the constant for Mg was the largest, followed by K, and Al. That higher rate constants of Mg and K occurred in dissolution of illite by acids may be attributed to ion-exchange reactions rather than from destruction-dissolution of framework by organic acids, because it is unlikely that K or Mg would be chelated (Sillén and Martell, 1964). Dissolution of Al, however, is primarily (99% of Al) a complexing reaction at  $\text{pH} = 3.0 - 3.5$  (Huang and Keller, 1972).

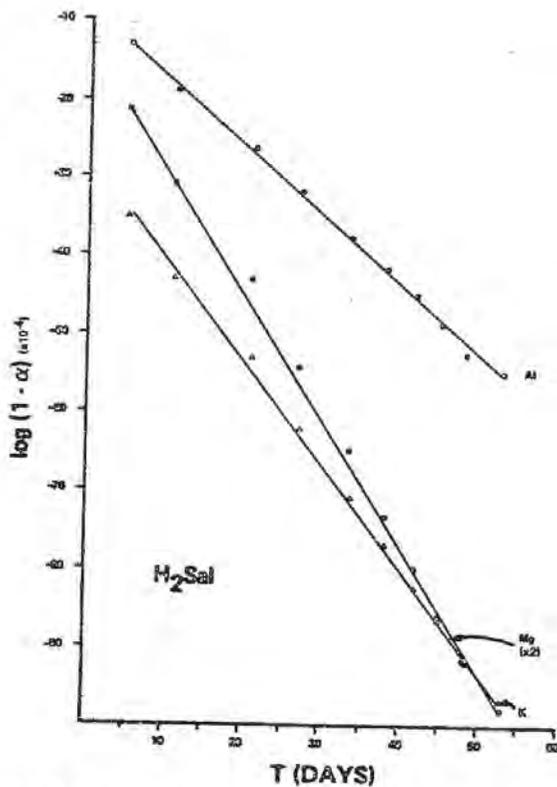


Figure 5. Plot of  $\log(1 - \alpha)$  versus  $t$  for Al, K, and Mg dissolved from Fithian illite in 0.01M salicylic acid.

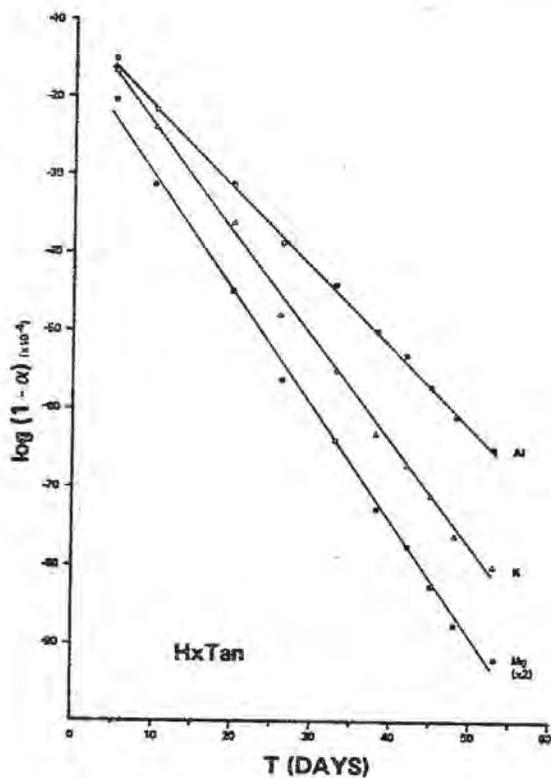


Figure 6. Plot of  $\log(1 - \alpha)$  versus  $t$  for Al, K, and Mg dissolved from Fithian illite in 0.01M tannic acid.

Table III

First-order rate constants for Al, K, and Mg from illite in salicylic and tannic acids, expressed as  $\text{sec}^{-1}$

<u>Ions</u>	<u>H<sub>2</sub>Sal</u>	<u>H<sub>x</sub>Tan</u>
Al	$2.36 \times 10^{-9}$	$2.51 \times 10^{-9}$
K	$3.57 \times 10^{-9}$	$3.70 \times 10^{-9}$
Mg	$8.44 \times 10^{-9}$	$7.85 \times 10^{-9}$

### Summary of kinetic changes

Dissolution of illite, nearly similar in both salicylic and tannic acids, took place by two kinetic mechanisms. Al was complexed following a first-order reaction. K and Mg were dissolved, in part by ion exchange following first-order law. Dissolution of Si and Fe was by a diffusion reaction. Diffusion rates of Si were similar in both acids but lower than those of Fe—presumably because of stronger Si bonding in tetrahedral sites than Fe bonding in octahedral sites. Since it is possible that some iron may be present in Fithian illite as a sulfide this might be a contributory source of Fe.

### STRUCTURAL CHANGES DURING DISSOLUTION OF THE CLAY

Two recognizable changes in the 001 spacing occurred during dissolution of the illite in salicylic acid, but in tannic acid changes were less pronounced. This is presumably due to the fact that fractional dissolution of K over Si in salicylic acid was found to be higher than in tannic acid, Fig. 7, yielding more K pulled out from the structure in salicylic acid.

X-ray diffractograms in Fig. 8 show illite before reaction, and after 520 days dissolution in salicylic acid. The typical broad 001 spacing (from 10.05 to 10.65 Å) of illite was modified in most cases (Fig. 8 C, D) by sharpening of the 9.59 Å component. Simultaneously, the wider-spacing components (10.05 to 10.15 Å) were converted to either 9.59, or to a uniformly expanding sequence of spacings in the low 2-theta direction.

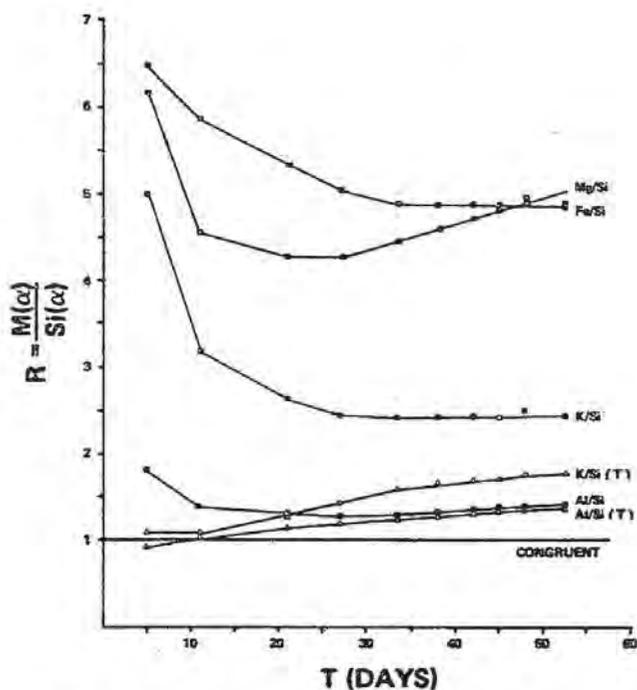


Figure 7. Ratios of fractions of dissolved cations over dissolved Si in salicylic acid, and K/Si (T) and Al/Si (T) for tannic acid.

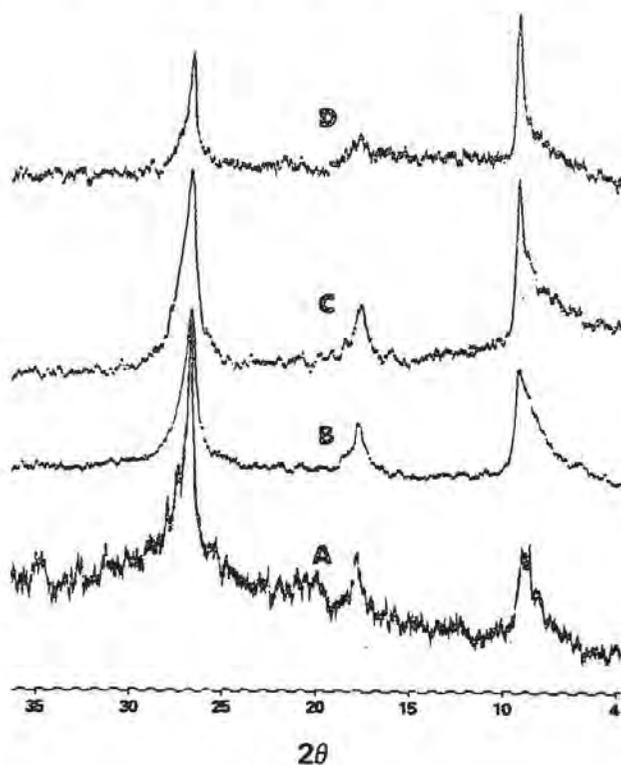


Figure 8. X-ray diffraction traces of oriented specimens of Fithian illite before reaction (A), and after 520 days dissolution (B, C, D, three different samples). Ni-filtered,  $Cu K\alpha$  radiation.

Our interpretation of these changes is only tentative at this time because we must refrain from heating or processing chemically the clay still under dissolution until it has been dissolved further. Tentatively, we interpret the sharpening and intensity increase at 9.59 Å as being due to removal of K and accompanying collapse of otherwise 10Å illite packets. The expanding portion may be that fraction of the illite which had a montmorillonite-heritage and is returning to an increasing ratio of montmorillonite-rich mixed layering. The expansion could possibly be due to an increase in hydration, or to entrance of salicylate molecules. After the experiment is carried further, we plan to heat to collapse, treat with glycol, run IR spectra, and other conventional clay-mineral chemical treatments.

#### REFERENCES

- BRINDLEY, G.W. and YOUELL, R.F. (1951): A chemical determination of "tetrahedral" and "octahedral" aluminum ions in a silicate. *Acta Cryst.* 4, 495-496.
- CLOOS, P., GASTUCHE, M.C. and GROEGAERT, M. (1960): Cinétique de la destruction de la glauconite par l'acide chlorhydrique étude préliminaire. *Intern. Geology Congr.*, 21st Rept. Session, Norden, pt. 24, 35-50.
- GASTUCHE, M.C. (1963): Kinetics of acid dissolution of biotite. II. Interfacial rate process calculated from chemical determinations assuming a given model of attack. *Proc. Int. Clay Conf.*, 1, 77-83.
- GASTUCHE, M.C. and FRIPIAT, J.J. (1962): Acid dissolution techniques applied to the determination of the structure of clay and controlled by physical method. *Science of Ceramics*, 1, 121-138.
- HEM, J.D. (1965): Reduction and complexing of manganese by gallic acids. U.S. Geol. Surv. Water Supply Pap. 1667-D, 28pp.
- HUANG, W.H. and KELLER, W.D. (1970): Dissolution of rock-forming silicate minerals in organic acids: Simulated first-stage weathering of fresh mineral surfaces. *Amer. Miner.*, 55, 2076-2094.
- HUANG, W.H. and KELLER, W.D. (1971): Dissolution of clay minerals in dilute organic acids at room temperature. *Amer. Miner.*, 56, 1082-1095.
- HUANG, W.H. and KELLER, W.D. (1972): Geochemical mechanics for the dissolution, transport, and deposition of aluminum in the zone of weathering. *Clays and Clay minerals*, (in press).
- LUCE, R.W., BARTLETT, R.W. and PARKS, G.A. (1972): Dissolution kinetics of magnesium silicates. *Geochim. Cosmochim. Acta*, 36, 35-50.
- OSTHAUS, B. (1956): Kinetic studies on montmorillonites and nontronite by the acid dissolution technique. *Clays and Clay Minerals*, *Nat. Acad. Sci. - Nat. Res. Council Pub.*, 327, 404-417.

ROSS, G.J. (1967): Kinetics of acid dissolution of an orthochlorite mineral. *Canadian Jour. Chem.*, 45, 3031-3034.

ROSS, G.J. (1968): Structural decomposition of an orthochlorite during its acid dissolution. *Canadian Mineral.*, 9, 522-530.

SILLÉN, L.G. and MARTELL, A.E. (1964): Stability constants of metal-ion complexes. *Chem. Soc. London Spec. Pub.* 17, 754pp.

## NEW DATA ON IRON OXIDES IN THE WEATHERING ZONE

F. V. Chukhrov, B. B. Zvyagin, L. P. Ermilova, A. I. Gorshkov  
Institute of ore Geology and Mineralogy, Academy of Sciences  
of the USSR, Staromonetny, 35, Moscow, Zh-17, USSR

**ABSTRACT.** - Iron oxides are important constituents of clays and soils. Being variable in structure composition and degree of crystallinity they may be highly sensitive to the conditions of formation and environment. The development of techniques of investigation, particularly the application of electron diffraction have permitted to reveal the lowest degrees of crystallinity; structural peculiarities of these phases and their relations to the better crystallized iron oxides-hydroxides.

Of great interest is the so called "brown amorphous iron hydroxide" which is obtained from  $\text{Fe}^{3+}$  salt solutions. Its nature was initially revealed by Towe and Bradley (1967). An analogous substance was found in natural conditions, and a name ferrihydrite - was proposed for it (Chukhrov et al., 1971), which was confirmed by the Commission on new minerals of the IMA. Some general data on ferrihydrite and its occurrence in nature are given below.

### COMPOSITION

According to Towe and Bradley (1967) the theoretical composition of the brown amorphous phase is  $2.5 \text{ Fe}_2\text{O}_3 \cdot 4.5 \text{ H}_2\text{O}$  ( $\text{Fe}_2\text{O}_3$ -83.12 $\text{H}_2\text{O}$ -16.88%), specific weight  $3.96 \text{ g/cm}^3$ , paramagnetic. The compositions of natural ferrihydrites are somewhat different what in particular is attributed to the fact that the quantities of  $\text{H}_2\text{O}^+$  and  $\text{H}_2\text{O}^-$  hardly correspond completely to chemically bounded and chemical free water. The iron oxides from thermal waters of Tshelken are of a special interest since their total water content is lower than the theoretical one in ferrihydrite. This is to be explained by the

presence of some transitional forms towards hematite. Very fine particles of hematite were indeed indentified by selected area electron diffraction in aggregates of ferryhidrite. The high silica content is remarkable. Its presence is connected with its intensive adsorption by iron hydroxides (Harder, Flehming, 1970).

## DIFFRACTION PATTERNS

Many authors failed to obtain satisfactory diffraction patterns of the "amorphous brown iron hydroxide" (Weiser, 1935). X-ray diffraction patterns with distinct reflections were firstly received by Giessen (1966) and independently by Towe and Bradley (1967) for products precipitated from the trivalent iron nitrate solutions. Perhaps the iron hidroxide of an iron rust, studied by Miyake (1939) is also of the same kind.

The main diffractational characteristics received by different authors as well as by the present authors are given in the Table I. The indices are related to a hexagonal cell containing four layers of a hexagonal close packing of O or OH, H<sub>2</sub>O.

As Fe<sup>3+</sup> -ions may occupy only a part of the octahedral positions (between 1/3 and 2/3 of them) the a-axis is chosen as the second by its length translation in the plane of close packing, although reflections, which could not be indexed with a  $\sqrt{3}$ -times shorter a-translation are hardly seen in the patterns. So it is clear that the main distinguishing feature of all these oxides is a sequence of the indicated five reflections, where the reflections 113 at d 1.97 Å is most symptomatic, and those at d 2.5 and 1.5 Å may be groups of not always resolved reflections forming diffuse bands. In the extreme case when only these two bands are seen without the intermediate reflections, the substance may be considered being in the initial stage of crystallization and defined as protoferrihydrite.

The natural ferrihydrites studied by the present authors are partly X-ray amorphous or give only the strongest lines. Therefore electron diffraction (especially selected area diffraction) was applied as the most effective diagnostic tool.

## DTA

Before distinct X-ray diagrams of the "brown amorphous iron hydroxide" were received, many authors had established that it gives DTA-curves, where except of an endothermic peak at 100-150° (removal of weakly bonded water), there was an exothermic peak between 300-400°C (formation of hematite). It is noteworthy

that fresh ferrihydrites give a single peak at 300-350°C; ferrihydrites precipitated more than 30 years ago give two weak (partly overlapping) peaks near 200 and 450°C. The reasons for it may be the increase of the crystalline dimensions and the increase of the strength of the water bond.

Table I

Certain reflections of synthetic and natural ferrihydrites

hkl	Giessen, 1966	Towe, Bradley, 1967	Chukhrov et al., 1971	Jackson, Keller, 1970	Towe, Lowens- tamm, 1967	Miyake, 1939
110	2.52 vs	2.54 s	2.50 m	2.52 m-s	2.54 s-m	2.56 s
112	2.25 s	2.24 m-s	2.21 w	2.23 m-s	2.24 s	2.28 vw
113	1.97 s	1.98 m	1.96 w	1.98 vw	1.98 m	2.09 vw
114	1.72 s	1.72 w	1.72 vw	1.70 vw	1.72 w	
300	1.48 vs	1.47 s	1.48 m	1.47 m	1.47 s	1.48 s

### IR SPECTRA

Towe and Bradley (1967) have observed the presence of molecular water bands at 3450 and 1620  $\text{cm}^{-1}$ . These are also present in the IR spectra of the natural ferrihydrites. The positions of the OH-stretching oscillations are constant, and the positions of some maxima of the bending oscillations of  $\text{H}_2\text{O}$  vary for different samples. All ferrihydrites give an additional band in the range 930-1020  $\text{cm}^{-1}$  which is due to the presence of silica. Stretching and bending bands of hydroxiles, not belonging to water molecules, are not present in the IR spectra of ferrihydrites. Protoferrihydrite has the same IR-spectra as ferrihydrite.

### FORMATION AND TRANSFORMATIONS OF FERRIHYDRITE

In the course of slow reactions at  $\text{pH} \sim < 3$  and  $\sim > 9.5$  stable goethite is formed; rapidly proceeding reactions at  $\text{pH} \sim < 9.5$  lead to formation of unstable ferrihydrite. The formation of ferrihydrite in result of chemical oxidation of  $\text{Fe}^{2+}$  requires such high concentrations of iron and such intense oxidation factors, that it is

practically impossible in nature. At very rapid precipitation of iron hydroxide, protoferrihydrite is formed. Previously such a phase was received by Towe and Bradley from a mixture of solutions of an alkali and a salt of trivalent iron. It follows from our data that such precipitate in the same solution after some hours pass into ferrihydrite.

For the first time ferrihydrite was found by one of the authors in the mines of some Altay localities, where it was precipitated from solutions percolating through sulphide ores and containing divalent iron.

It was established in result of special investigations that ferrihydrite is a typical mineral of geologically recent precipitates. Its formation is caused by rapid oxidation in connection with the vital functions of iron bacteria and first of all Gallionella, Leptothrix and Toxothrix. The relicts of such bacteria composed of ferrihydrite or protoferrihydrite were found in all iron oxides deposited in all cold iron springs with pH of water near 7 in different parts of the USSR.

It was also found as a newly formed sediment in many mines. According the X-ray data the hydroxide described by Jackson and Keller (1970) formed in the basalt lavas under lichen of Hawaii island is represented by ferrihydrite. The hydroxide from the rice field solis of Japan (Iwasa, 1965) gives ferrihydrite DTA curves; its formation is connected with the activity of iron bacteria.

Ferrihydrite is a typical low temperature unstable mineral in form of which the main quantity of iron hydroxide is deposited from the solutions of the weathering zone. At ageing in oxidation conditions it spontaneously transforms in a stable phase - hematite. Undoubtedly the origin of hematite in many sedimental rocks and ores follows the same mechanism.

It is established that in moderate acid or alkaline solutions ferrihydrite transforms into hematite at 60°C. This is consistent with the data on transformation of the "brown amorphous iron hydroxide" into hematite in result of ageing (Torno and Krause, 1933). In the waters of rivers, lakes and ocean ferrihydrite spontaneously transforms into hematite. In our experiments with synthesized ferrihydrite its partial transformation into hematite at pH 10.5 and room temperature already occurred after two weeks. We have found that a fine admixture of colloid silica reduces the transformation speed; a synthetic ferrihydrite at pH 7 and temperature 60°C was completely transformed into hematite during 15 days; natural ferrihydrite from Karaoba deposit containing 6% SiO<sub>2</sub> did not change at the same conditions. Some iron bacteria in solutions may greatly accelerate the oxidation of Fe<sup>2+</sup>; as a result is the ferrihydrite formation.

As a direct hematite formation at the temperatures of the hypergene (supergene) processes is impossible, ferrihydrite is to be considered as the only protohematite phase in the hypergenesis zone. Apparently the transformation ferrihydrite - hematite occurs when

ferrihydrite is not subjected to transformation into goethite. In dependence on formation conditions ferrihydrite appears as proto-goethite or as protohematite.

A number of experiments has been made to reveal the influence of the ions of di- and trivalent iron on ferrihydrite. Samples of synthetic and natural ferrihydrites have been treated with solutions of iron vitriol, Mohr's salt, iron bicarbonate, iron alum at different pH-values. It was established that under influence of  $\text{Fe}^{2+}$  ions at pH 7 ferrihydrite transforms into goethite, this transformation being checked by electron and X-ray diffraction patterns, electron micrographs and DTA. The reason of the different influence of  $\text{Fe}^{2+}$  and  $\text{Fe}^{3+}$  ions is connected with the fact that in water solutions trivalent iron ions form hydrocomplexes like  $\text{Fe}(\text{OH})^{2+}$ ,  $\text{Fe}(\text{OH})_2^+$ , when  $\text{Fe}^{2+}$  may exist in the form of simple ions which can penetrate in the structure and after oxidation stimulate its rearrangement.

#### ON THE STRUCTURE OF FERRIHYDRITE AND ITS RELATION TO OTHER IRON OXIDES

Taking into account the chemical composition and specific weight Towe and Bradley (1967) have interpreted the above described diffraction pattern as corresponding to a pseudohexagonal structure, where  $\text{Fe}^{3+}$  occupy octahedral positions of a hexagonal close packing in such a way, that in 4 successive per repeat layers the portions of occupied positions are  $2/3$ ,  $1/3$ ,  $1/3$ ,  $1/3$ . It was believed that the corners of octahedra are occupied by atoms O and molecules  $\text{H}_2\text{O}$ . Thus the structure is described by a formula  $\text{Fe}_5\text{O}_8 \cdot 4\text{H}_2\text{O}$ . In analogy with hematite some octahedra of successive layers (but no more than two per repeat) were allowed to have common faces. In the structural schemes the orientation of the positive poles of the molecules  $\text{H}_2\text{O}$  were indicated.

These ideas may serve as a good basis for explanation of the properties of ferrihydrite and its relations to other iron oxides from structural points of view. It is worth only to make some refinements and detailizations of the initial structural scheme in order to get a better understanding of the structure and of the principal possibilities of its formation and transformations.

Apparently there is no necessity for octahedra of successive layers to have common faces, since single Fe-octahedra may preferably have a common face with an empty octahedron and common corners with occupied octahedra. As in the case of aluminium oxides (Hsu, Bates, 1964) in the medium of crystallization single octahedra adjoining together by edges firstly form hexagonal rings, which in turn form pieces of layers, populated by iron-atoms according the hematite-law. Let us call them "2/3-layers". At the

next stage when the condensation process continues in the third dimension additional Fe-octahedra may adjoin only the hollow octahedra in the middle of the hexagonal rings from both sides of the two-dimensional layers, thus forming two layers occupied according the antihematite (carbonate) law ("1/3-layers"). In sum three-sheet layers "1/3-2/3/1/3" arise, which are in some respect unequivocally constructed structural units, which are presumably characteristic for protoferrihydrite. In dependence on concentration of Fe-atoms and the speed of crystallization these units may be subjected to further condensation giving different structures.

If the structural units are joined through intermediate single Fe-octahedra, which also form "1/3-layers", a structure with a 4-layer repeat arises "1/3-2/3-1/3-1/3-1/3-2/3-1/3...". There are two possibilities of positioning of the Fe-octahedra of the intermediate "1/3-layer" against each of two adjacent three-storied layers when Fe-octahedra will have only common corners. As a consequence the three-storied layers must be randomly displaced in the direction *b* of an orthogonal cell, on multiples  $b/3$  ( $b$  8.9 Å). In the diffraction pattern separate reflections only with  $k = 3n$  (or  $k - h = 3n$  for a hexagonal cell) may exist. The ratio Fe/O = 5/12 corresponds to the structure of Towe and Bradley's phase or ferrihydrite. All the corners at a boundary between 1/3 - and 2/3 - layers are shared by three, between 1/3 - and 1/3 - layers - by two Fe-octahedra. The formers lack a half and others - a unity of a positive valency. It is impossible to give preference for some O and to form around them groups H<sub>2</sub>O, leaving the others without H. There are not also separate groups OH. In principle each H<sup>+</sup> must belong to two O in an equal way. Between consequent "2/3 - layers" chains O-H-O-H-O may be traced, which are perhaps responsible for the observed IR- and DTA- characteristics of ferrihydrite. Its formula should be more explicitly written as Fe<sub>5</sub>[O<sub>4</sub>H<sub>3</sub>]<sub>3</sub>.

If the structural units are joined directly, without intermediate layers, a sequence of layers "1/3-2/3-1/3-1/3-2/3-1/3-1/3-2/3-1/3..." is obtained. As the consequent "2/3-layers" have opposite orientations the real repeat is of six layers. Such a structure is also subjected to random displacement of the "1/3-2/3-1/3" - layers. Between consequent "2/3 - layers" chains O-H-O-H-O may be traced. The formula is 2{Fe<sub>4</sub>[O<sub>3</sub>H<sub>2</sub>]<sub>3</sub>}.

The next possibility is when three-storied layers do not exist independently each two "2/3 - layers" being joined by a common "1/3 - layer". The structure "1/3-2/3-1/3-2/3-1/3..." has a repeat of two layers and formula Fe<sub>3</sub>[O<sub>2</sub>H]<sub>3</sub>. At the ideal ratio Fe/O = 1/2 the structure with octahedra having only common corners must be ordered, and reflections with  $k \neq 3n$  ( $k - h \neq 3n$ ) are to be expected in the diffraction patterns. In fact that was observed by us for the magnetic δ-FeOOH studied by means of electron diffraction. Some other samples had given similar diffraction patterns but only with reflections having  $k = 3n$  ( $k - h = 3n$ ). This may be a result

of a random distribution of occupied Fe-octahedra, caused by any slight deviation of the composition from the ratio  $Fe/O = 1/2$ . It should be underlined that the ordered structure is to be expected in result of a separate process of crystallization. As it is not uniform in population of consequent layers, the structures of goethite and lepidocrocite with the same ratio  $Fe/O = 1/2$  are more favourable and are formed at lower crystallization rate.

When the ratio  $Fe/O$  is more than  $1/2$  it is impossible to escape octahedra having common faces. In the extreme case of the ratio  $Fe/O = 2/3$  there is a hematite sequence of layers " $2/3-2/3-2/3-2/3...$ " with a repeat of six layers, and a formula per unit cell  $Fe_{12}O_{18}$ . The presence of Fe-octahedra sharing faces in it is compensated by displacements of Fe-atoms from central positions and by the uniform distribution of these atoms.

Considering all these structures one may suppose that at ratios  $Fe/O < 2/3$  two opposite factors are simultaneously operative; the preference of the absence of Fe-octahedra with common faces and the tendency of an uniform distribution of Fe-atoms among octahedra. Under such conditions hematite - like (pseudohematite) structures are possible where one empty and two not completely, but partly occupied octahedra are alternating. As the ratio  $Fe/O$  increases there is a natural sequence of structures; proto-ferrihydrite  $\rightarrow$  ferrihydrite  $\rightarrow$  pseudohematite  $\rightarrow$  hematite. It is in accord with iron oxide transformations observed in reality.

## REFERENCES

- CHUCHROV, F.V., ZVYAGIN, B.B., GORSHKOV, A.I., ERMILOVA, L.P., RUDNITSKAYA, E.S. (1971): Towe-Bradley's phase - a product of hypergenesis alteration of ores. *Izvestia AN SSSR, ser. geol.*, N 1.
- Van der GIESSEN, A.A. (1966): The structure of iron (III) oxide-hydrate gel. *J. Inorg. Nucl. Chem.*, 28, N 10.
- HARDER, H., FLEHMING, W. (1970): Quarzsynthese bei tiefen Temperaturen *Geoch., Cosmoch. Acta.* 34, N 3.
- HSU, P.H., BATES, T.F. (1964): Formation of X-ray amorphous and crystalline aluminium hydroxides. *Min. Mag.*, 333, N 264.
- IWASA, J. (1965): Mineralogical studies of iron from minerals in soils. *Bull. Nat. Inst. Agricult. Sci.*, B, N 15.
- JACKSON, T.A., KELLER, W.D. (1970): A comparative study of the role of lichens and "inorganic" processes in the chemical weathering of recent Hawaiian lava flows. *Am. J. Sci.*, 269, N 5.
- MIKAYE, SH. (1939): A study on the corrosion of iron by electron diffraction. *Sci. Papers Inst. Phys. Chem. Research (Japan)*. 36.
- TORNO, H., KRAUSE, A. (1933): Über Sillerferrite. *Zs. anorg. allgem. Chemie.* 211, H. 1-2.

- TOWE, K.M., BRADLEY, W.F. (1967): Mineralogical constitution of colloidal "hydrous ferric oxides". J. Coll. Interface Sci., 24, N 3.
- TOWE, K.M., LOWENSTAM, H.A., NESSON, M.H. (1963): Invertebrate ferritin occurrence in Mollusca. Science, 142, N 3588.
- WEISER, H.B. (1935): X-ray study of the hydrous oxides. VII. Ferric oxides. J. Phys. Chem., 39, N 1.

# THE TRANSFORMATION OF LEPIDOCROCITE TO GOETHITE

U. Schwertmann

Institut für Bodenkunde der Technischen Universität  
München, 805 Freising-Weihenstephan, German  
Federal Republic

R.M. Taylor

C.S.I.R.O., Division of Soils, Private Bag No. 1,  
Glen Osmond, S.A. 5064, Australia

## (EXTENDED ABSTRACT)

Lepidocrocite ( $\gamma$ -FeOOH) being metastable with respect to its polymorph goethite ( $\gamma$ -FeOOH) ( $\Delta F_r^0 = -3,3$  kcal/mol, v. Schuylenborgh 1972) is found to be of considerable persistence in soils and sediments. In an attempt to explain this the transformation of synthetic and natural soil lepidocrocite has been studied in some detail under widely varying conditions.

### Conversion of synthetic lepidocrocite in alkaline solution

In 1 M KOH solution at 80°C the conversion is usually completed in 5-15 hr but is much slower at 20°C and/or in 0.1 M KOH. Poorly crystalline material converts faster than well crystalline one.

The synthetic lepidocrocites generally consisted of thin laths 0.1-1,  $\mu\text{m}$  in length with highly serrated edges in the (001) direction (Fig. 1a). During conversion the "teeth" firstly disappear giving a terraced appearance (Fig. 1b). Finally, when much goethite has been formed, the residual lepidocrocite is present in small cube-like particles (Fig. 1c). During this process the relative solubility in oxalate changes from 0.24 (lep. with a specific surface of 60  $\text{m}^2/\text{g}$ ) to  $< 0.01$  with the final goethite (15-20  $\text{m}^2/\text{g}$ ).

The conversion was followed by quantitative x-ray diffraction using the area of the (120) line of lepidocrocite and the (130) line of goe-

and minimizing orientation effects by pressing the sample in the sampleholder against filter paper. When only very small samples were available quantitative determination with infrared absorption spectroscopy using the band at  $1020\text{ cm}^{-1}$  for lepidocrocite and at  $820\text{ cm}^{-1}$  for goethite has been used with reasonable success.

Conversion-time curves of three different kinds were found (Fig. 2). Type I depicts a reaction which continually increased in rate whereas Type II had a continually decreasing rate of conversion. The third form of the conversion, Type III showed an initial increase followed by a continual decrease in rate, with the maximum occurring approximately at the half conversion time (HCT).

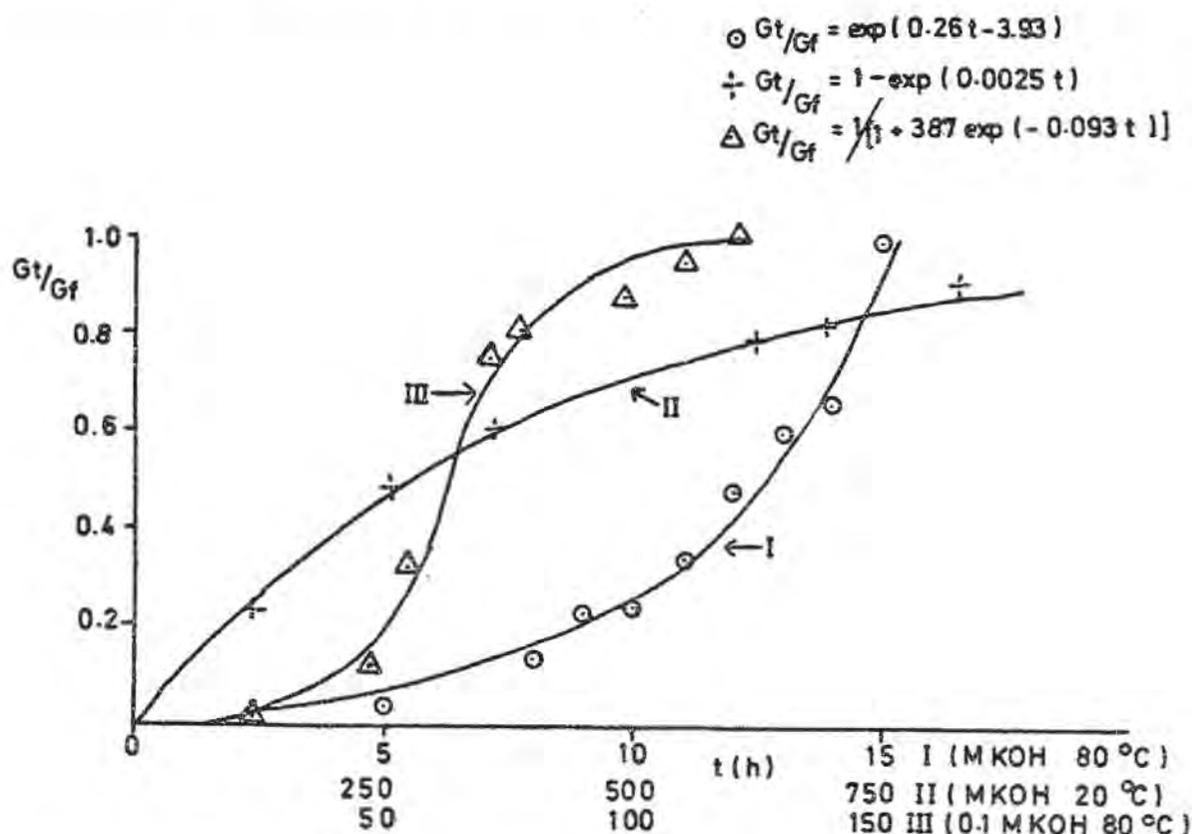


Figure 2. Various time curves for the conversion of synthetic lepidocrocite to goethite under different conditions (see abscissa).

Using an empirical treatment the following linear relationships were derived from these three types of reaction ( $r = 0.965 - 0.998$ ):

$$\text{type I : } \ln G_t/G_f = kt + c$$

$$\text{type II : } \ln L_t = kt + \ln L_0$$

$$\text{type III : } \ln (G_f/G_t - 1) = -k (G_0 + L_0) + \ln L_0/G_0$$

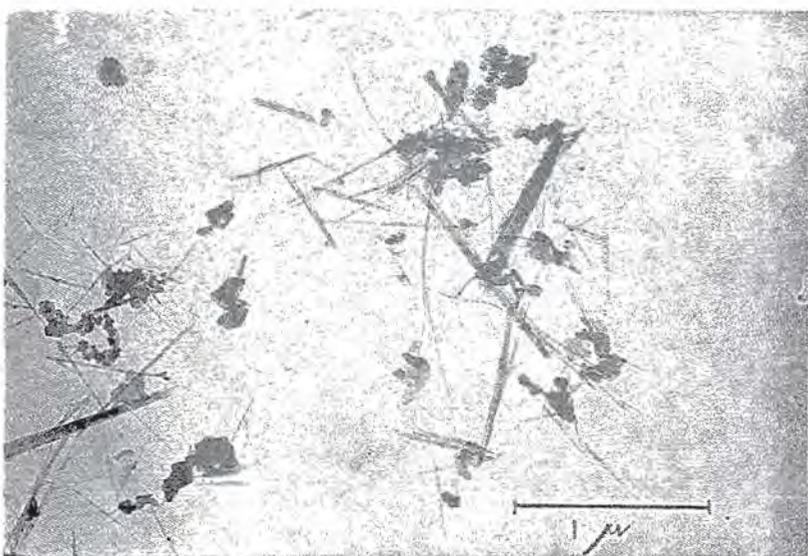
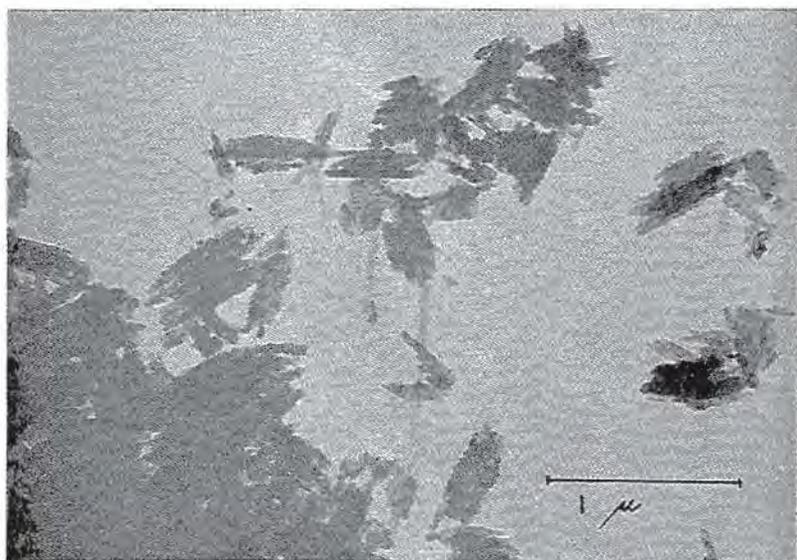


Figure 1 a-c. Electron micrograph of synthetic lepidocrocite (spec. surface  $50 \text{ m}^2/\text{g}$ ) at the beginning (fig. 1 a) and after 5 (fig. 1 b) and 23 hrs. (fig. 1 c) in M KOH at  $80^\circ \text{ C}$ .



in which  $L_0$ ,  $L_t$ ,  $G_0$ ,  $G_t$ ,  $G_f$  are lepidocrocite and goethite concentrations at time  $t = 0$ ,  $t = t$  and after complete conversion ( $f$ ),  $k$  is the reaction constant and  $c$  is a constant which has the meaning of  $G_0$ .

Type I curve seems to indicate that the rate of goethite formation depends mainly on the goethite already formed, i.e. the reaction is seeding itself with goethite the surface area of which (being proportional to its concentration) determines the rate of further crystal growth. In seeding the system artificially the conversion rate is drastically accelerated and the value  $c$  approximates to  $\ln G_0$ , where  $G_0$  is the amount of goethite added.

In seeded systems and at lower temperature (20°C) the dissolution rate and solubility of the lepidocrocite replaces the goethite concentration in determining the rate of reaction. A type II form of curve results in which the lepidocrocite concentration is rate determining. Finally, type III represents a second order catalytic reaction (Frost and Pearson 1962) in which during an initial phase the rate increases with increasing goethite concentration and decreases at a later stage due to depletion of lepidocrocite as a source of iron. We believe this type to be realized under conditions where the dissolution rate of lepidocrocite and the rate of formation of goethite are within the same order of magnitude (e.g. at 80°C in 0.1 M KOH).

These results suggest that the transformation is not topochemical, but proceeds through the solution phase. The main steps governing the rate of transformation are (1) the dissolution of lepidocrocite and (2) the formation of goethite nuclei and subsequent growth each step probably consisting of further substeps. Either of these processes can be rate-determining under appropriate conditions.

#### Conversion of synthetic lepidocrocite in the presence of silicate

Silicate as a common constituent in natural waters is able to considerably retard the conversion of well crystalline lepidocrocite (Fig. 3). The half conversion time increases approximately linearly with increasing Si concentration between 0 and  $0.532 \cdot 10^{-3} \text{M/l}$ . This covers the normal concentration range of soil solutions. As outlined before the shape of the conversion curves fits a linear relationship for  $\ln G_t/G_f$  versus time indicating the formation of goethite crystals as the rate determining process. Again after seeding with 6.8% goethite the influence of silicate can be almost completely eliminated.

The Si concentration in solution showed a decrease during the conversion process approaching a final value in equilibrium with the goethite formed. The major part of the Si removed is highly correlated with the amounts of goethite that have been formed, yielding a relationship of the form  $\ln Si_t/Si_0 = -c G_t/G_f$  where  $Si_t$  and  $Si_0$  are Si concentrations at time  $t$  and zero. This indicates the goe-

thite to be responsible for the Si uptake. The amount of Si taken up per unit weight of goethite (approximately one Si atom per 300-1000 Fe atoms) is linearly correlated with  $Si_t$ . This and some further results indicate that Si is not being adsorbed on the surface of the goethite but rather incorporated into the crystals during their growth. Almost no Si is taken up after the goethite has formed. Also, neither fresh M KOH nor HCl at pH 1.0 - 2.9 extract more than a trace of Si from Si containing goethite.

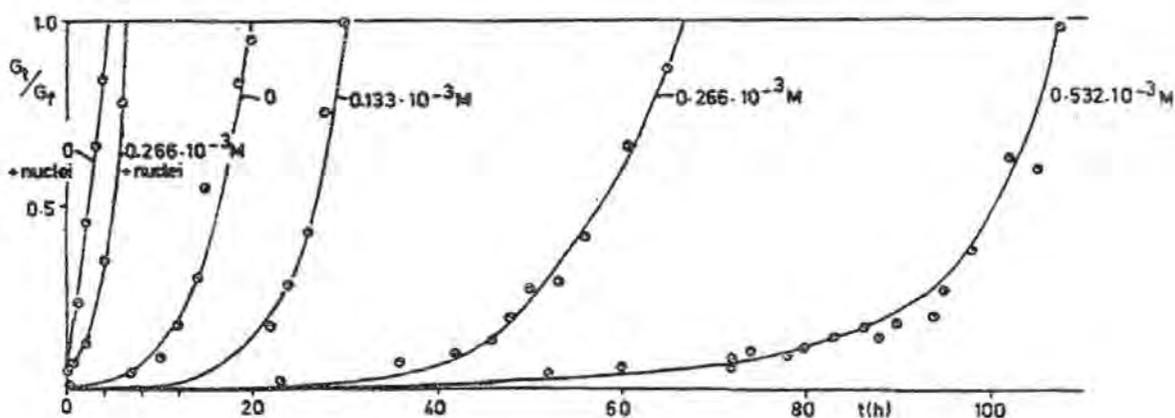


Figure 3. Time curves for the conversion of synthetic lepidocrocite to goethite at 80°C in M KOH and various initial Si solution concentration and in the presence of added goethite. The solid lines were drawn from the best linear fits of  $\log G_t/G_f = kt$ .

To further studying the Si influence Si was added 0, 2, 4, 6 and 8 hrs after the start of the experiment in which the conversion was completed after 21 hrs, without Si addition. As seen from Fig. 4 the addition of Si 4 hrs. or later after the start has no retarding influence on the conversion, although at this stage the conversion is just commencing. This and the seeding experiment mentioned above is evidence that the retarding influence of Si occurs solely during the nucleation stage of the transformation, long before the major part of the Si is taken up by the goethite. At this stage the Si concentration per unit area of goethite is very high and the surface has to cope with the tendency of Si to be taken into the goethite lattice leading to slowed formation and growth of nuclei. The more goethite surface formed during nucleation the less serious will be this tendency so that the later Si is introduced into the system after the start of the conversion the smaller will be its retarding effect.

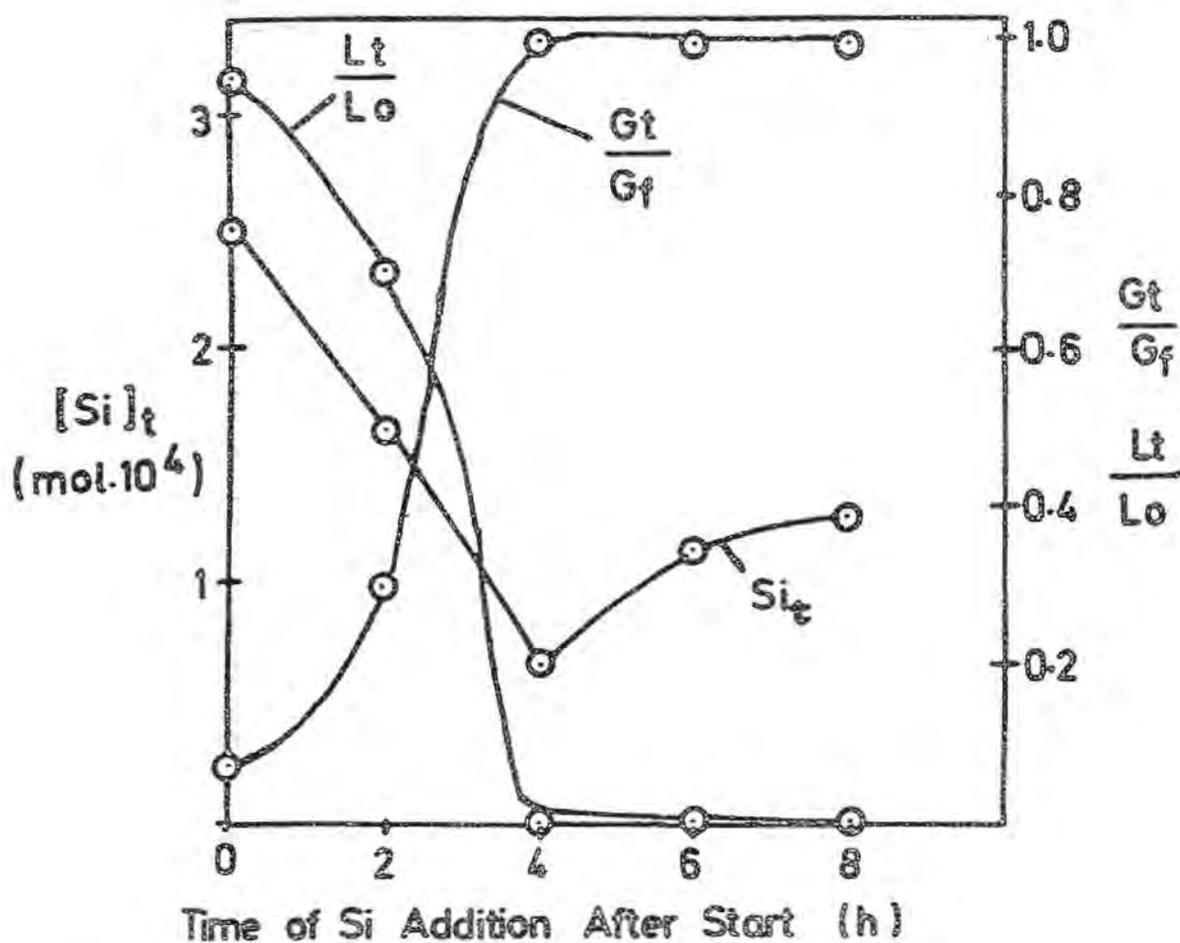


Figure 4. Influence of time of Si addition on the conversion of synthetic lepidocrocite to goethite and the Si uptake in M KOH at 80°C after 30 hours. ( $L_t$ ,  $L_o$ ,  $G_t$ ,  $G_f$  see test).

#### Conversion of natural lepidocrocite

In a further series of experiments the transformation of a natural lepidocrocite has been studied. The lepidocrocite came from a hydromorphic soil (Hangpseudogley) developed in-periglacial solifluction material of Mt. Wellington, Tasmania, Australia. The clay fraction of this soil contains mainly kaolinite with smaller amounts of illite and iron oxides (13-16% Fe, dithionite soluble) predominately in the form of lepidocrocite with traces of goethite. Electron micrographs show large layer silicate flakes, the surface of which is covered with small lath shaped lepidocrocite crystals (Fig. 5a) which resemble somewhat in morphology a synthetic lepidocrocite (Fig. 1a) and can be removed by dithionite (Fig. 5b). Conversion was followed quantitatively by using the (020) line of lepidocrocite or where possible the ratio of this line to the (001) line of kaolinite as an internal standard.

As compared to pure systems the conversion rate of the natural lepidocrocite in M KOH at 80°C is much lower (conversion almost completed after approximately 50 days against less than 1 day in synthetic systems). From the conclusions drawn above this can clearly be contributed to the high Si concentration arising from dissolution of silicates under strong alkaline conditions up to 1000 ppm SiO<sub>2</sub>. This is further substantiated by the observation that seeding the system with synthetic goethite as well as replacing the Si containing KOH by fresh KOH after 3 or 6 days remarkably accelerates the transformation.

Approaching natural conditions and following earlier results of several authors it was then tried to study the conversion of natural lepidocrocite in the presence of ferrous iron in a normal pH range of soils. A preliminary experiment with synthetic lepidocrocite showed a complete conversion with a constant rate in 0.1M FeSO<sub>4</sub> at 80°C after approximately 4 days at pH between 1.5 and 2.0 (due to some hydrolysis of FeSO<sub>4</sub>). At the same pH but without Fe<sup>2+</sup> (using H<sub>2</sub>SO<sub>4</sub>) no conversion took place.

A typical goethite formed under these conditions from natural lepidocrocite is shown in Fig. 6.

Replacing FeSO<sub>4</sub> by FeCl<sub>2</sub> completely inhibited the conversion. At room temperature no measurable conversion took place in 0.005 - 0.5M FeSO<sub>4</sub>.

The influence of Fe<sup>2+</sup> concentration was studied at 70°C in closed bottles. As seen from Fig. 7 the lepidocrocite seems to convert under these conditions with a constant rate over most of the conversion. Furthermore, whereas in 0.1 and 0.03 M FeSO<sub>4</sub> solution the conversion was completed after 400 hrs it has just begun in 0.01 whereas it has not yet started in 0.003 M solution. A plot of the rate constant obtained from these linear curves against log of initial [Fe<sup>2+</sup>] yields a linear relationship (r = 0.94) showing that below a certain Fe<sup>2+</sup> concentration the conversion rate may be almost zero.

In a further experiment in 0.5 M FeSO<sub>4</sub> at room temperature the pH was adjusted in the beginning to 3 and 6 respectively. Although being run under N<sub>2</sub> a pH drop could not be avoided but whereas at an initial pH 3 no conversion was noted after 53 days the conversion was completed after this period at an initial pH 6.

In a similar experiment under N<sub>2</sub> at pH 4.5 and 6 the pH was adjusted from time to time. The results show that at pH 6 where the conversion was followed to completion the conversion-time curve fits to the equation  $\ln (L/K)_t = (L/K)_0 - kt$  for the decrease in lepidocrocite (not shown) and  $\ln (G/K)_t - (G/K)_0 = \ln (G/K)_f - kt$  for the increase in goethite (Fig. 8) indicating first order kinetics. The reaction proceeds faster at pH 6.0 than at pH 4.5. At pH 7 and 8 the lepidocrocite is converted to a ferromagnetic black compound (probably hydroxy magnetite).

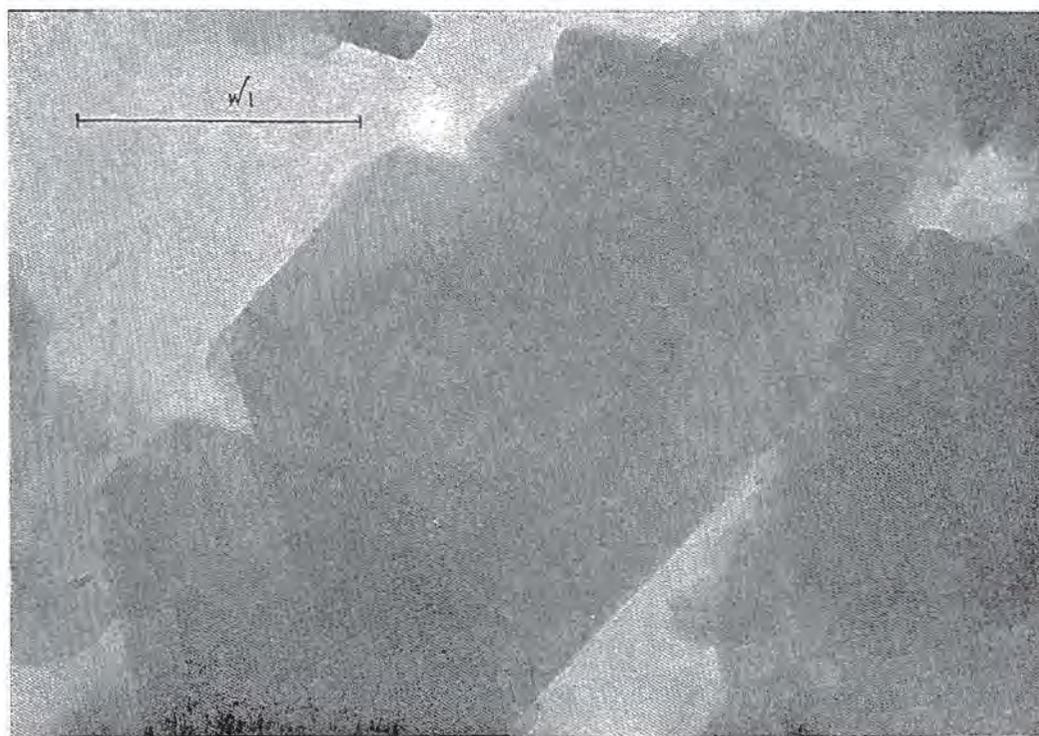
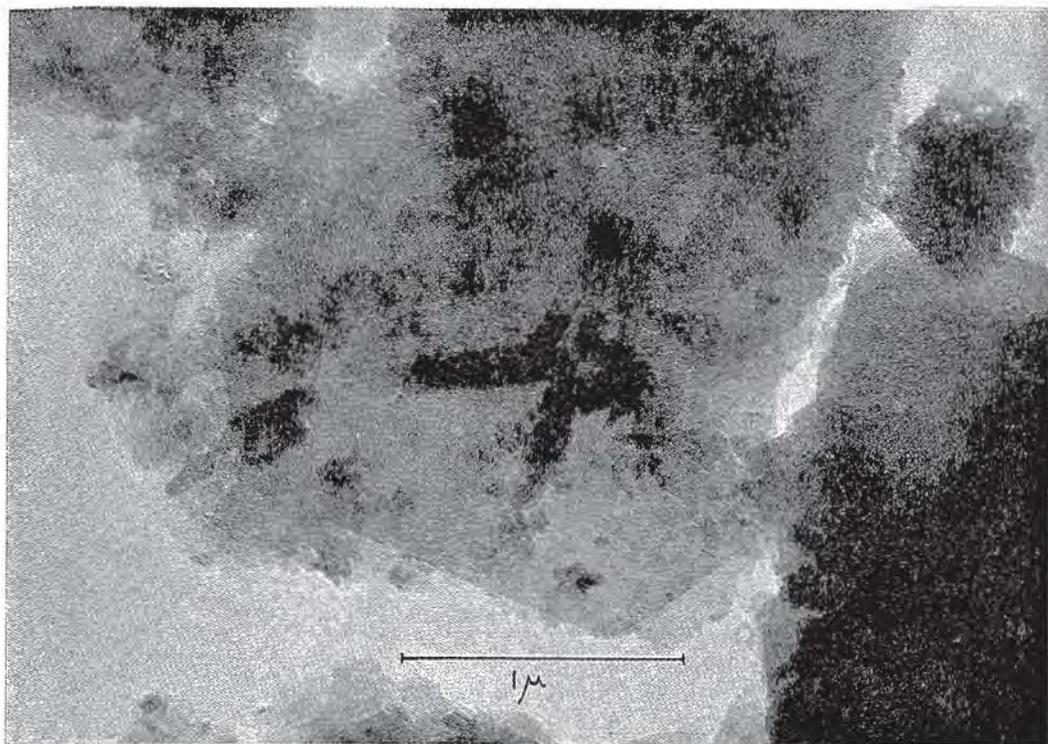


Figure 5 a, b. Electron micrograph of the clay fraction showing large layer silicate flakes and lath shaped lepidocrocite crystals on their surface (5 a). Same after deferration with dithionite (5 b).





Figure 6. Electron micrograph of goethite formed from soil lepidocrocite in 0.1 M  $\text{Fe SO}_4$  solution at  $80^\circ \text{C}$  after 160 hours.



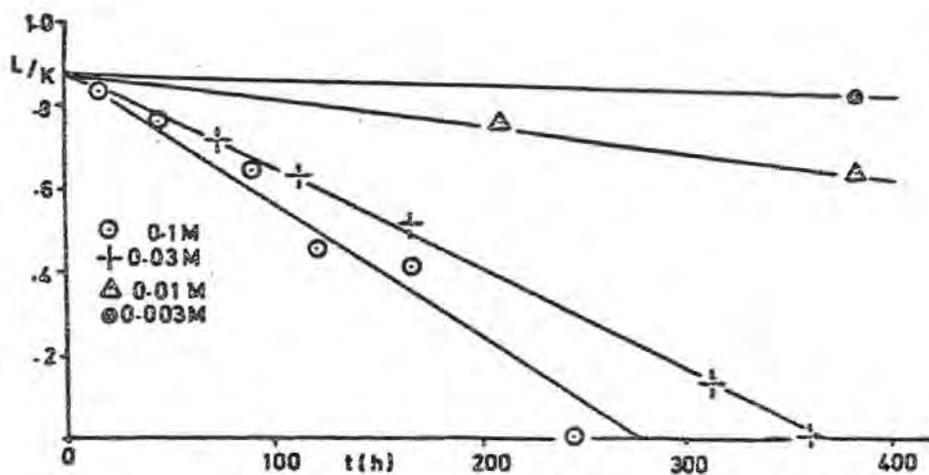


Figure 7. Decrease of soil lepidocrocite with time in 0.1, 0.003, 0.01 and 0.003 M  $\text{FeSO}_4$  solution at  $70^\circ\text{C}$ .

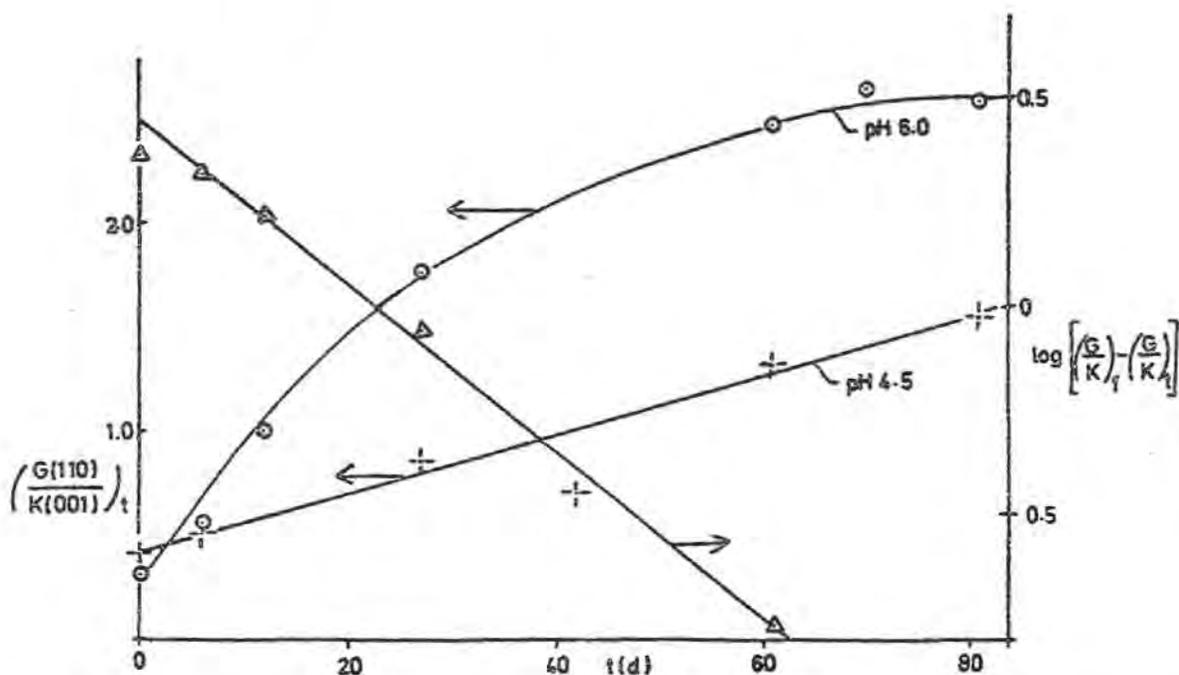


Figure 8. Normal and log plot (pH 6) of goethite concentration formed with time from soil lepidocrocite in 0.5 M  $\text{FeSO}_4$  solution at room temperature and at pH 6 and pH 4.5 respectively.

### Conclusions

The transformation of metastable lepidocrocite to its stable polymorph goethite proceeds via solution. Under strong alkaline conditions  $\text{Fe}(\text{OH})_4^-$  monomers are most likely the form in solution. From this goethite nuclei are formed at a rate which, among other fac-

tors, depends on the degree of supersaturation with respect to goethite ( $pK_s \sim 44$  against  $\sim 43$  for lepidocrocite, Langmuir 1971). The nuclei themselves are seeded by Fe from the lepidocrocite.

Among the factors influencing the rate of this process are the solubility and dissolution rate of the lepidocrocite (or any source of ferric iron) which increases with increasing temperature and alkalinity of the solution (according to  $FeOOH + OH + H_2O \rightleftharpoons Fe(OH)_4^-$ ) and with decreasing crystallinity of the lepidocrocite. As well known a very rapid transformation to goethite can be obtained with freshly precipitated ferric hydroxide under strong alkaline conditions.

Various constituents of natural solutions may be able to influence the overall process. For soluble silicate it is concluded from these experiments that a few ppm  $SiO_2$  may retard the conversion by reducing the nucleation rate. Small amounts of Si, like other elements can be incorporated into the goethite lattice explaining why extremely pure samples of natural goethite often contain some Si.

A constituent which accelerates the conversion is  $Fe^{2+}$ . It has been shown with ferric sulphate (Lieser et al. 1959) that  $Fe^{2+}$  increases the dissolution rate of ferric compounds by surface adsorption of  $Fe^{2+}$  and electron transfer. This also explains the influence of pH in such a system because at low pH the adsorption of  $Fe^{2+}$  by the positively charged lepidocrocite will be low whereas at higher pH ( $>7$ )  $Fe^{2+}$  will be inactivated by oxidation. Fischer (1972) recently demonstrated the same effect with the transformation of amorphous ferric hydroxide to goethite.

With regard to the initial question why lepidocrocite appears to be stable in soils and sediments over long periods of time the following conclusion may be permitted. The rate of nucleation of goethite appears not to be the rate limiting step. This is based on the observation that the majority of the lepidocrocite occurrences (which are mainly restricted to systems in which ferrous iron occurs due to anaerobic conditions) also contain at least some goethite. Therefore these systems are naturally seeded and Si concentration in solution although high enough will not inhibit the conversion to goethite.

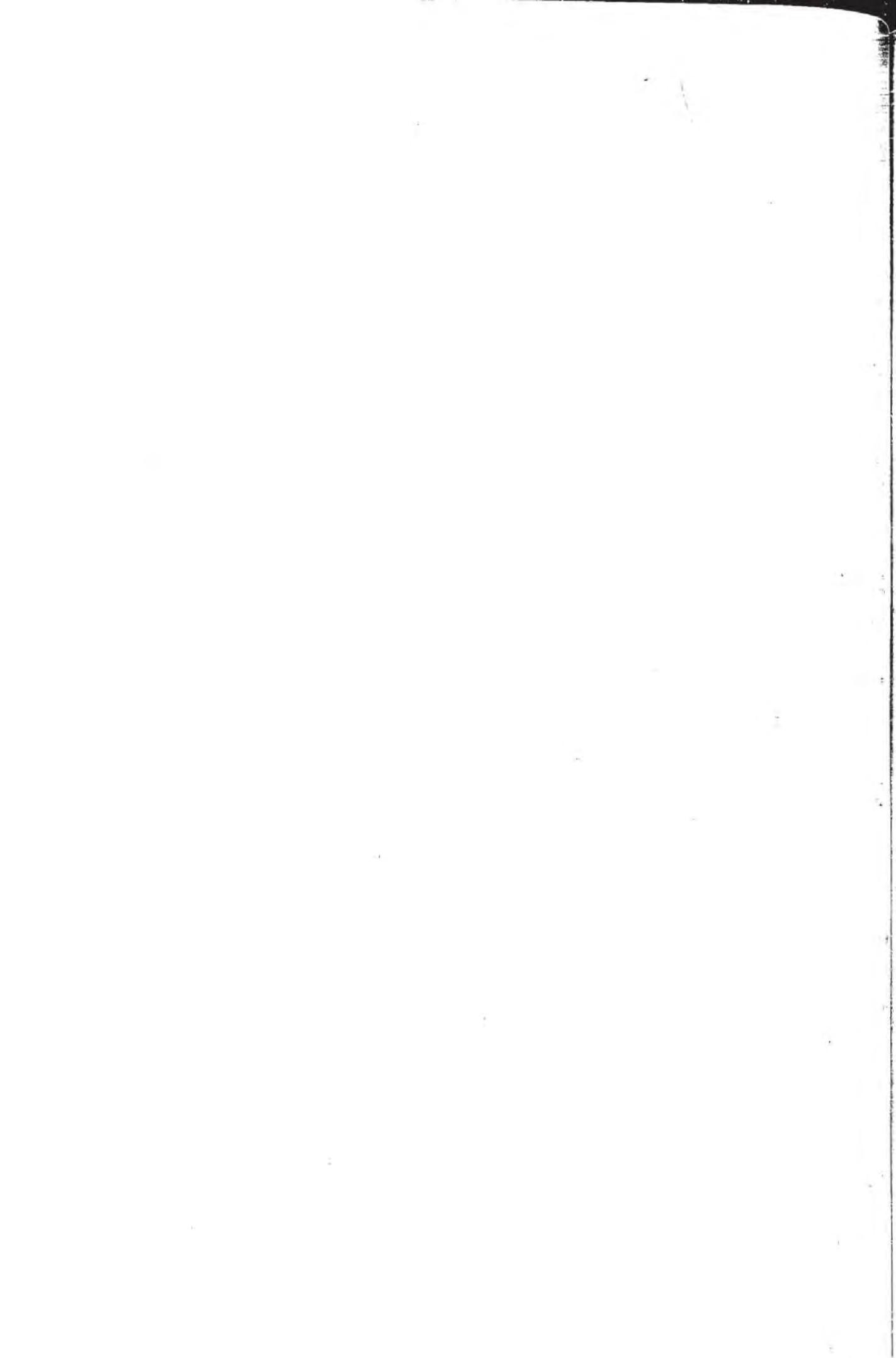
It is more likely therefore to assume that the solubility of lepidocrocite and its low dissolution rate is responsible for its high persistence in soils. This is due to an unsuitable pH (low solubility) and a low  $Fe^{2+}$  concentration (low dissolution rate) even under anaerobic conditions.

## REFERENCES

- For further details and references see  
SCHWERTMANN, U. and TAYLOR, R.M. (1972): The transformation of lepidocrocite to goethite. The influence of silicate on the transformation of lepidocrocite to goethite. *Clays. Clay Min.* **20**.  
SCHWERTMANN, U. and TAYLOR, R.M. (1972): The in vitro transformation of soil lepidocrocite to goethite. *Trans. Int. Soc. Soil Sci. Comm.* V and VI Stuttgart-Hohenheim.

## ADDITIONAL REFERENCES

- FISCHER, W. (1972): Die Wirkung von zweiwertigem Eisen auf Auflösung und Umwandlung von Eisen (III)-hydroxiden. *Trans. Int. Soil Sci. Soc. Comm.* V and VI Stuttgart-Hohenheim.  
FROST, A.A. and PEARSON, R.G. (1962): *Kinetics and mechanism*. 2nd edition J. Wiley, New York.  
LANGMUIR, D. (1971): Particle size effect on the reaction goethite = hematite + water. *Amer. J. Sci.* **271**, 147-156.  
LIESER, K.H. and SCHROEDER, H. (1959): Die Kinetik der Auflösung des wasserfreien Eisen (III) sulfats in Eisen (II)-ionenhaltigen Lösungen. *Z. Electrochem.* **64**, 252-257.  
SCHUYLENGORGH, J.v. (1972): Summary report. *Trans. Int. Soil Sci. Soc. Comm.* V and VI Stuttgart-Hohenheim.



GEOCHEMISTRY OF TRACE ELEMENTS DURING THE GENESIS  
OF COLOURED BENTONITES

J. Linares, F. Huertas, M. Lachica and E. Reyes

Estación Experimental del Zaidín. C.S.I.C. Granada, Spain

**ABSTRACT.** - Manifestations of volcanic activity, associated to the Alpidic orogenic cycle, are common in the zone of Cabo de Gata (SE Spain). Some dacitic tuffaceous formations underwent an hydrothermal alteration to bentonites. In Sierra de Gata the bentonites are pale or white coloured and in Serrata de Nijar the bentonites are red, green, brown, blue and white in colour.

The genesis of the coloured bentonites is investigated from a physico-chemical point of view, taking into account chemical, spectrographic, X-ray and field data.

The whole genetic process, from the parent rock to the bentonite, is studied through the geochemical balance of the major elements; so, there is removal of silica and alkalines and enrichment in magnesium. On the other hand, a spectrographic determination of trace elements was carried out. This study reveals that  $\text{Cr}^{3+}$ ,  $\text{Ni}^{2+}$  and  $\text{Co}^{3+}$ , among others, are concentrated in the coloured bentonites. This fact is in accordance with the crystal field theory in the sense that these cations have a high crystal field stabilization energy (CFSE) in octahedral coordination.

Likewise, it is suggested that the process of hydrothermal alteration begins with the change from an octahedral symmetry, for the transition element, to a seven coordination complex in the form a pentagonal bipyramid, due to the pairing of electrons of a water molecule with a vacant  $t_{2g}$  orbital of the transition element. This seven coordination activated state being the rate determining step in the process. The difference between the CFSE in octahedral and pentagonal bipyramidal coordination gives the magnitude of the contribution to the activation energy for the hydrolisis process. For Cr, Ni and Co this difference is high, so that, its hydrolisis will be very slow. Thus they will have a tendency to be concentrated in the bentonites contributing to its colour.

## INTRODUCTION

In the Cabo de Gata region, Almería (SE Spain) several cenozoic volcanic manifestations associated to the Betic orogeny (Alpidic cycle) are found.

Alteration zones showing processes of hydrolisis, sulfatation, carbonatation, silification and oxidation are common in this region (Linares et al. 1972). One of them has been the massive transformation of dacite tuffs into bentonite, giving broad deposits of great economic importance.

Both, the region and the bentonites have been studied since long (For a review see Linares, 1963). A striking fact is the presence, in some localized placers, of coloured bentonites (green, blue, red and brown) while the common bentonites are white.

This paper deals with the relation between the content of transition trace elements in bentonites and altered volcanic rocks and the origin of colour. Electronic transitions within orbitals caused by light absorption must be the origin of colour in bentonites, as it is general in a great number of other silicates and minerals.

## MATERIALS AND METHODS

### Description of samples

a) "Frente de Archidona" zone: This deposit is located at the southeastern side of the Serrata de Nijar, between Cerro Blanco and Cerro Colorado (Fig. 1).

In this restricted zone there is evidence of a strong alteration by an ascending hydrothermal fluid. The bentonite bed is at least 20 m thick.

Figure 2 sketches the relative disposition of samples, whose descriptions are the following:

<u>Sample</u>	<u>Description</u>
FA-1	Dacitic conglomerate
FA-2	Altered volcanic tuffs
FA-3	Altered volcanic tuffs
FA-4	Red bentonite
FA-5	White bentonite
FA-6	White bentonite
FA-7	Green bentonite
FA-8	Green bentonite

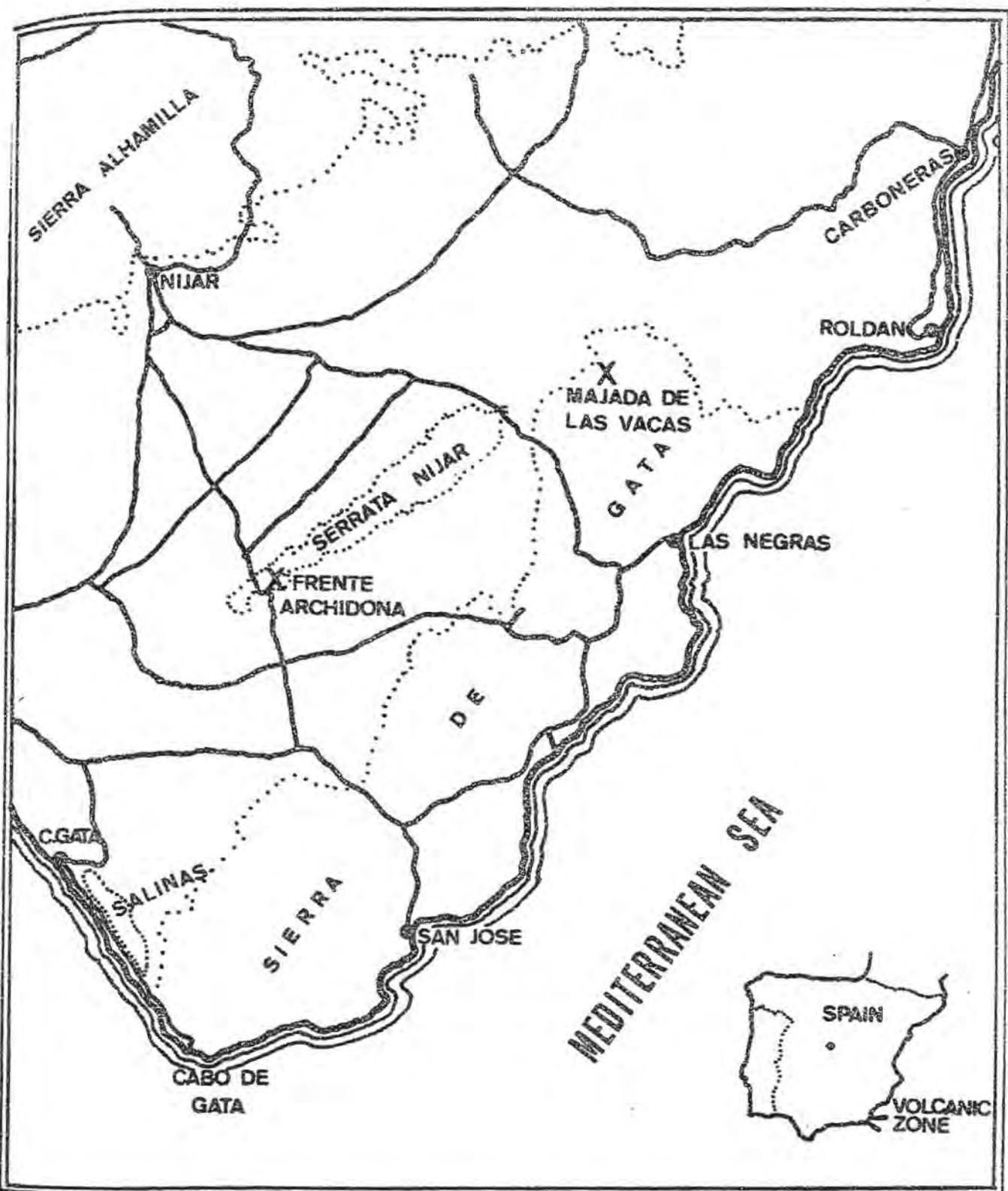


Figure 1. Sample localities.

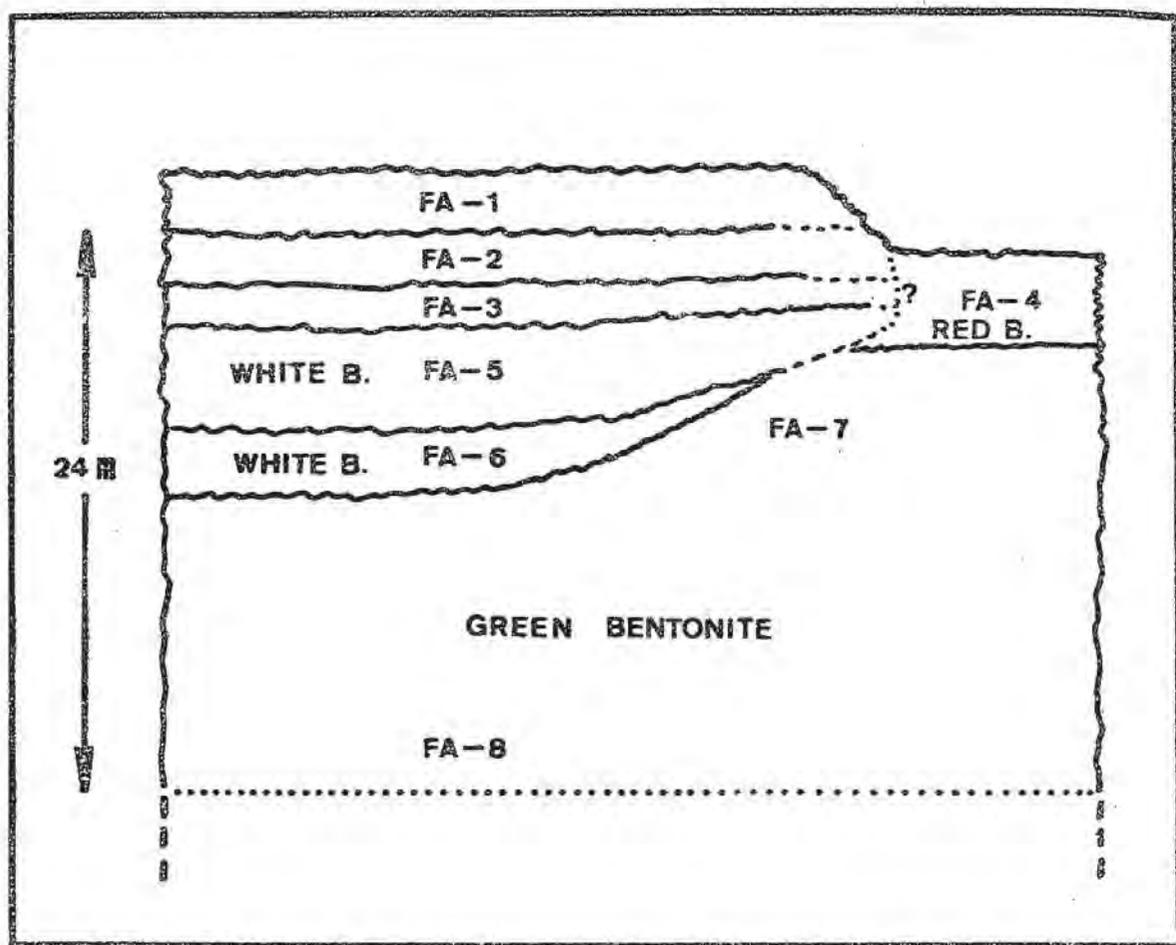


Figure 2. Sketch of the "Frente de Archidona" deposit.

As may be observed in the field sample FA-1, at the top, does not show any alteration evidence and seems to lie unconformably over sample FA-2. So, there is not a genetic alteration relation between them.

b) "Majada de las Vacas" zone: This outcrop has been described by Linares (1963) and by Martin Vivaldi, Linares and Alias (1964). It belongs to the northern region of Sierra de Gata (Fig. 1). In this zone a dacitic tuff is altered merging gradually to a pale-green bentonite, through the following sequence:

<u>Sample</u>	<u>Description</u>
MV-1	Yellow-gray altered dacitic tuff
MV-2	Altered tuff
MV-3	Altered tuff
MV-4	Very altered tuff
MV-5	Pale-green bentonite

The alteration seems to be due to an hydrothermal fluid ascending through a vertical fracture. The samples are arranged from center to the margin of the fracture. The distance between MV-1 and MV-5 is about 3 m.

### Experimental methods

a) X-ray diffraction: The mineralogical analysis was carried out with a Philips diffractometer PW 1010, equiped with scintillation counter and pulse-high discriminator. The operating conditions were: 34 kV and 28 mA, with Cu K radiation Ni-filtred. The diagrams obtained were: powder for the bulk sample and sand fraction, and oriented aggregates and powder for the clay fraction, following the usual methods.

b) Chemical analysis: Major elements were determined following the wet method of Huertas and Linares (1970), which is a modification of the methods proposed by Shapiro and Brannock (1962) and by Voinovitch et al. (1966).

The sample is submmitted to an alkaline disgregation, so that silica is solubilized and later determined by colorimetry by means of the silico-molybdc reduced complex. On other aliquot of the sample, and acid treatment was carried out to bring it into solution (except silica), and Al, Fe, Ti, Ca and Mg were determined by complexometry and Na and K by flame photometry.

The ferrous ion was determined by the Jakob's method (1940).

c) Spectrochemical analysis: For the semiquantitative analysis the method proposed by Mitchell (1964) was used with minor modifications. It was carried out with a Hilger automatic quartz spectrograph E. 492, equiped with a Hilger D.C. Source unit FS. 141. The operating conditions were: D.C. Arc at 9 A; slit 8 mm long and 20 u wide; image into the plane of the slit; two exposures par sample of 55 sec each; electrodes made from Morganite SG, 305H pure carbon; cathode reduced in diameter to 2.8 mm with boring of 1 mm in diameter and 8 mm deep. The sample was mixed with an equivalent amount of pure carbon powder. The plater employed were: Ilford Long Range Spectrum (8000-3300 Å) and Ilford Chromatic G. 30 (3500-2485 Å). The spectra were worked out by means of a Judd Lewis Comparator L. 46.

## EXPERIMENTAL AND DISCUSSION

### Mineralogy

In both zones, "Frente de Archidona" and "Majada de las Vacas", even the least altered rocks contain montmorillonite in variable amount, and quartz, plagioclase and biotite as main components.

This fact is in accordance with the lack of fresh rocks in the zone as evidenced by field observation.

Quartz, plagioclase and biotite are minor constituents in the bentonites. The montmorillonite is dioctahedral in all cases with a (060) spacing ca. 1.49 Å. The iron content of the octahedral layer must be low since parameter is not higher than 9.00 Å (Mac Ewan, 1961).

The plagioclase composition was not determined because of its advanced state of alteration.

### Geochemistry of major elements

The chemical analysis of the samples is summarized in Tables I and II. The oxide alumina molal ratios for the samples are shown in Tables III and IV.

In the "Majada de las Vacas" outcrop the genetic process is very simple consisting of a leaching of silica, iron, calcium and alkalis with subsequent enrichment of magnesium, through the gradual sequence rock-to-bentonite.

Table I

#### Chemical Analysis of samples from "Frente de Archidona"

	<u>FA-2</u>	<u>FA-3</u>	<u>FA-4</u>	<u>FA-5</u>	<u>FA-6</u>	<u>FA-7</u>	<u>FA-8</u>
SiO <sub>2</sub>	60.33	58.11	51.31	55.37	63.11	59.65	60.44
Al <sub>2</sub> O <sub>3</sub>	12.50	19.21	18.82	17.95	6.76	16.08	13.53
Fe <sub>2</sub> O <sub>3</sub>	4.16	6.34	7.18	5.01	3.88	1.11	1.10
FeO	0.81	0.03	0.04	0.04	0.04	0.82	1.75
TiO <sub>2</sub>	0.63	1.37	0.22	0.56	1.17	0.12	0.40
MgO	4.72	3.55	9.33	7.47	5.11	3.88	4.69
CaO	3.90	1.44	2.75	3.16	1.37	3.16	2.00
Na <sub>2</sub> O	3.07	2.27	1.99	2.17	4.90	3.60	4.67
K <sub>2</sub> O	1.89	0.68	0.45	0.37	2.83	2.38	3.30
CO <sub>2</sub>	0.08	-	-	0.57	-	0.42	0.16
H <sub>2</sub> O(+)	8.11	7.59	8.13	7.46	10.83	8.08	8.45
	<u>100.20</u>	<u>100.59</u>	<u>100.21</u>	<u>100.13</u>	<u>100.00</u>	<u>99.30</u>	<u>100.49</u>

Table II

Chemical analysis of samples from "Majada de las Vacas"

Sample	MV-1	MV-2	MV-3	MV-4	MV-5
SiO <sub>2</sub>	68.80	69.00	66.33	63.98	60.12
Al <sub>2</sub> O <sub>3</sub>	15.28	17.70	18.42	20.34	24.35
Fe <sub>2</sub> O <sub>3</sub>	3.17	2.09	2.01	2.10	2.45
FeO	0.04	0.11	0.03	0.03	0.03
TiO <sub>2</sub>	0.41	0.20	-	-	-
MgO	0.21	0.25	1.46	2.57	3.67
CaO	1.12	0.67	0.72	0.78	0.84
Na <sub>2</sub> O	2.71	2.98	2.32	2.16	2.06
K <sub>2</sub> O	2.54	1.80	1.25	0.83	0.73
H <sub>2</sub> O(+)	6.48	6.24	6.71	6.85	6.44
	100.78	100.96	99.25	99.64	100.69

Table III

Molar ratios of samples from "Frente de Archidona"

	$\frac{\text{SiO}_2}{\text{Al}_2\text{O}_3}$	$\frac{\text{Fe}_2\text{O}_3}{\text{Al}_2\text{O}_3}$	$\frac{\text{MgO}}{\text{Al}_2\text{O}_3}$	$\frac{\text{CaO}}{\text{Al}_2\text{O}_3}$	$\frac{\text{TiO}_2}{\text{Al}_2\text{O}_3}$	$\frac{\text{Na}_2\text{O}}{\text{Al}_2\text{O}_3}$	$\frac{\text{K}_2\text{O}}{\text{Al}_2\text{O}_3}$
FA-2	8.23	0.25	0.95	0.56	0.06	0.40	0.16
FA-3	5.14	0.21	0.46	0.4	0.09	0.19	0.03
FA-4	4.64	0.24	1.25	0.26	0.01	0.17	0.02
FA-5	5.26	0.18	1.05	0.32	0.04	0.20	0.02
FA-6	15.94	0.36	1.91	0.36	0.21	1.18	0.44
FA-7	6.30	0.07	0.61	0.35	0.01	0.36	0.15
FA-8	7.58	0.13	0.87	0.27	0.01	0.56	0.26

Table IV

Molar ratios of samples from "Majada de las Vacas"

	<u>MV-1</u>	<u>MV-2</u>	<u>MV-3</u>	<u>MV-4</u>	<u>MV-5</u>
$\text{SiO}_2/\text{Al}_2\text{O}_3$	7.65	6.63	6.12	5.34	4.19
$\text{Fe}_2\text{O}_3/\text{Al}_2\text{O}_3$	0.13	0.08	0.07	0.07	0.06
$\text{MgO}/\text{Al}_2\text{O}_3$	0.03	0.03	0.20	0.32	0.38
$\text{CaO}/\text{Al}_2\text{O}_3$	0.13	0.07	0.07	0.07	0.06
$\text{Na}_2\text{O}/\text{Al}_2\text{O}_3$	0.29	0.28	0.21	0.17	0.14
$\text{K}_2\text{O}/\text{Al}_2\text{O}_3$	0.18	0.11	0.07	0.04	0.03

On the contrary, in the "Frente de Archidona" deposit three-different processes seem to occur; a) leaching of all elements, except Mg, (FA-2 to FA-3 and FA-5 step); b) gain of elements (FA-5 to FA-6 step), and, c) other involving the coloured bentonites (FA-4, FA-7 and FA-8) which have an intermediate behaviour.

The alteration rock-to-bentonite must be effected by an hydrothermal fluid of magmatic origin (Linares et al. 1972).

The process seems to be constituted by a first step of hydrolysis characterized by the change of constituents of the parent rock into gels which later are transformed into montmorillonite under the effect of the environmental conditions (Linares et al. 1972). The montmorillonite thus formed may be of the beidellite type, essentially constituted by the cations possessing less mobility from a geochemical point of view. In a second stage the ions of the hydrothermal solution (silica, Na, K, Mg,  $\text{CO}_3\text{H}^-$ , etc) can react with the ions removed from the hydrolized parent rock originating the neoformation of a montmorillonite chemically different from the previous one. This new montmorillonite could be constituted by the cations with a higher mobility, being a true montmorillonite.

The process in the "Majada de las Vacas" outcrop must be due only to hydrolysis, while in "Frente de Archidona" the hydrolysis, the transformation and neoformation of montmorillonite and a siliification (sample FA-6) are superposed as a result of the later magmatic step of the hydrothermal fluid.

#### Geochemistry of trace elements

In Tables V and VI are summarized the result of the spectrochemical analysis. The elements have been arranged according to Taylor and White (1966).

Table V

Spectrochemical analysis of samples from "Frente Archidona"

	<u>FA-1</u>	<u>FA-2</u>	<u>FA-3</u>	<u>FA-4</u>	<u>FA-5</u>	<u>FA-6</u>	<u>FA-7</u>	<u>FA-8</u>
Rb	100	30	10	-	-	30	30	50
Ba	250	125	50	3	100	30	200	250
Pb	10	15	10	80	30	10	3	10
Sr	60	45	30	10	30	100	60	60
La	30	30	30	50	150	T	100	50
Th	150	150	150	150	150	300	150	150
Zr	100	100	100	30	30	200	30	30
Sn	3	5	10	10	10	5	1	10
Mo	2	4	3	7	3	1	3	3
Mn	10	10	T	7000	10	200	30	10
Cu	T	++	T	+++	++	++	+	+
Co	-	-	-	3	3	-	10	3
Ni	5	15	7	50	10	20	30	50
Li	30	30	20	30	20	20	20	30
V	-	-	-	-	-	+	+	++
Cr	1	2	2	1	1	1	30	20
Ca	30	30	30	20	20	30	20	20
Ag	-	-	-	1	-	1	1	1

Note: Values are in ppm. The crosses are relative amount.  
T means traces.

The first group contains the elements occurring in 8-12 fold coordination and forming dominantly ionic bonds. All the elements are similar to the potassium, and so, Pb and Sr are included because of their ability to substitute potassium. A decrease in concentrations is observed in the intermediate stage of alteration for all the elements.

Among the elements of the rare-earths group only La was determined, showing an irregular distribution.

The group of high charge cations (Zr type) have also an irregular distribution. These elements can not enter into silicate lattices and occur as complex ions.

In the ferromagnesian group are placed the elements with a six-fold coordination, so are included Li, Ti, Cu and Zn. This group

Table VI

Spectrochemical analysis of samples from  
"Majada de las Vacas"

	<u>MV-1</u>	<u>MV-2</u>	<u>MV-3</u>	<u>MV-4</u>	<u>MV-5</u>
Rb	100	100	30	10	10
Ba	1000	300	1000	1000	300
Pb	15	5	30	70	30
Sr	100	100	100	100	100
La	30	50	T	200	T
Th	150	200	150	150	150
Zr	200	300	200	200	200
Sn	2	5	3	3	3
Mo	1	1	1	1	1
Mn	200	200	200	300	100
Cu	+	+++	++	++	+
Co	-	-	-	-	-
Ni	2	4	2	2	2
V	10	10	10	10	10
Cr	-	1	1	1	1
Ca	15	20	30	30	30

is the most important from the point of view of this paper. These elements are easily hydrolized and a great number of them are also transition elements. As can be seen from Table V the transition elements are concentrated in the coloured bentonites. This conclusion is in accordance with the genesis of the bentonites and explain their colour as it will be discussed later.

The distribution and content of the trace elements in the "Majada de las Vacas" outcrop is very different from those of the "Frente de Archidona" deposits. The most striking feature is the low content of the transition elements through the "Majada de las Vacas" suite. This must be in relation with the genesis of the parent volcanic rocks. In fact, the studies carried out by some of us show clearly that the vulcanism of "Majada de las Vacas" is younger than that of the "Frente de Archidona". Taking into account the trace elements distribution during the magmatic differentiation (see for instance the classical work of Wager and Mitchell, 1951 or Curtis, 1964) the transition elements are concentrated in the first stages

of this magmatic evolution. Thus, a gradual distribution of this elements occurs as a time function.

In the case presented in this paper the older volcanic rocks (F. Archidona), richer in metallic elements, produce strong coloured bentonites, while the younger ones (M. Vacas), low in metabolic cations, originate pale coloured bentonites, but in other cases white bentonites are originated (not described in this paper).

The white bentonite formed in the "Frente de Archidona" deposits may be neofomed, while the coloured ones must be originated through an hydrolitic process.

These conclusions seem relevant for the study of volcanic zones, because the transition elements content can serve as a "stratigraphic" indicator in order to make a relative correlation among different volcanic manifestations. In the zone of Cabo de Gata this method is being utilized by the authors due to the complex volcanic history (unpublished results).

### Geochemistry of the alteration and crystal field theory

The process of hydrolisis of silicates may be considered as a transfer from the lattice ions to the environmental solution. The transition elements, as stated above, are localized in silicates in octahedral sites (six-fold coordination), but in solution are also found as hexahydrated ions. Burns (1970) has pointed out, that the crystal field stabilization energies (CFSE) for these elements are equivalent in silicates and in solutions, except if there are distorsion phenomena of the Jahn-Teller type in lattices.

The removal of an ion from the crystalline lattice depends on the accessibility of the water molecules to the ion. This process can be seen as a substitution reaction, from a kinetic point of view, beginning with the formation of an activated complex. Thus, the crystal field theory can provide an insight into the substitution reactions involving metal ions (Basolo and Pearson, 1958, and Burns, 1970).

The process is believed to proceed through a seven-coordinate transition state possessing the configuration of a pentagonal bipyramid. One water molecule can share electrons from oxygen with an empty  $t_{2g}$  orbital from the octahedral cation, so as to form a complex of seven ligands. The formation of this activated complex is the rate-determining step in the reaction. Later, the complex is destroyed spontaneously providing residues of an hydroxysilicate and a metallic hydroxysilicate. Finally, other water molecules enter into reaction leading to a metallic hydroxide and an hydroxysilicate residue.

This process can take place if in the metallic ion, vacant  $t_{2g}$  orbitals are present. Thus for the ions with  $d^1$  and  $d^2$  configurations, having  $t_{2g}$  vacancies, the reaction of substitution proced faster than in the case of the  $d^3$  ions with no vacancies. Ions of the  $d^4$ ,  $d^5$  and

$d^6$  (high-spin) type need an additional energy in order to pair electrons and leave some  $t_{2g}$  orbital empty. The substitution reaction will be faster in  $d^7$ ,  $d^8$  and  $d^9$  configuration since there are not any vacancies. Finally, ions with  $d^6$  configurations (low-spin) will show very low reaction because the  $t_{2g}$  orbital are completely filled.

However, this reasoning can be made more quantitative considering the necessary activation energy to pass from six to seven-fold coordination (from octahedral to pentagonal bipyramidal configurations). A high and positive value for this energy should indicate that the rate of hydrolysis should be slow; on the contrary, for high and negative values the hydrolysis will go faster.

Data for this activation energy, taken from Burns (1970), are shown in Table VII. As can be seen,  $Cr^{3+}$ ,  $Ni^{2+}$  in high-spin and  $Co^{3+}$  and  $Fe^{2+}$  in low-spin have high and positive values, so that these cations will be very slow in the substitution reactions and very resistant to the mobilization.

Table VII

Crystal field activation energies for the substitution mechanism: octahedral - pentagonal bipyramid symmetry

No of electrons	Ion	High-spin state E	Low-spin state E
1	$Ti^{3+}$	- 0.128	- 0.128
2	$Cr^{3+}$ , $Mn^{4+}$	- 0.256	- 0.256
3	$Cr^{3+}$ , $Mn^{4+}$	0.426	0.426
4	$Cr^{2+}$ , $Mn^{3+}$	0.107	0.298
5	$Mn^{2+}$ , $Fe^{3+}$	0	0.170
6	$Fe^{2+}$ , $Co^{3+}$	- 0.127	0.852
7	$Co^{2+}$ , $Ni^{3+}$	- 0.256	0.534
8	$Ni^{2+}$	0.426	0.462
9	$Cu^{2+}$	0.107	0.107

Source of data: Basolo and Pearson (1958) p. 109.

These are the reasons for the concentration of the transition elements in coloured bentonites.

Hawkins and Roy (1963) arrive to the same conclusion for nickel. They alter synthetic basalts hydrothermally and find that all the Ni in the basalt is accumulated in the octahedral layer of the montmorillonite originated as a product of alteration.

In conclusion, the relative concentration of Cr, Ni and Co during the alteration process is clearly demonstrated in this paper by spectrochemical and field evidences.

The presence of these ions among others, is the origin of the colour in the bentonites.

Finally, it can be concluded that crystal field theory explain quantitatively the reluctance to the hydrolisis of the transition trace elements.

#### ACKNOWLEDGEMENTS

The authors wish to express their thanks to Mr. J. Rodriguez Robledo for marking the X-ray diffraction pattern, and to Mr. E. Barahona Fernandez for their valuable comments. Finally we express our appreciation to "Minas de Gador S.A." for the kindness and facilities offered us during our repeated visits to their bentonite workings.

#### REFERENCES

- BASOLO, F. and PEARSON, R.G. (1958): Mechanism of Inorganic Reactions. John Wiley & Sons. New York.
- BURNS, R.G. (1970): Mineralogical applications of Crystal field theory. Cambridge Univ. Press. London.
- CURTIS, C.D. (1964): Applications of the crystal-field theory to the inclusion of trace transition elements in minerals during magmatic differentiation. *Geochim. Cosmochim. Acta.* 28, 389-403.
- HAWKINS, D.B. and ROY, R. (1963): Distribution of trace elements between clays and zeolites formed by hydrothermal alteration of synthetic basalts. *Geochim. Cosmochim. Acta.* 27, 785-795.
- HUERTAS, F. and LINARES, J. (1970): Análisis químico de silicatos. Report Extac. Exp. Zaidín. 20 pags.
- JAKOB, J. (1940): Gufa para el análisis químico de rocas. C.S.I.C. Madrid.
- LINARES, J. (1963): Las bentonitas de Cabo de Gata. Doctoral Thesis. Univ. Granada.
- LINARES, J., HUERTAS, F., REYES, E., TERRER, A., PUY, J.L., AGUSTIN, V. and MARTINEZ, J.J. (1972): The bentonites

from the volcanic region of Cabo de Gata, Almería (SE Spain). Field trip nº 3. 1972 Int. Clay Conf. Madrid.

MACEWAN, D.M.C. (1961): In: X-ray Identification and Crystal Structure of Clay Minerals, G. Brown editor. Mineralogical Society. London.

MARTIN VIVALDI, J.L., LINARES, J. and ALIAS, L. (1964): The genesis of the montmorillonite in the Cabo de Gata bentonites. 1963 Int. Clay Conf. Stockholm. 2, 229-236.

MITCHELL, R.L. (1964): The spectrochemical analysis of soils, plants and related materials. Commonwealth Agric. Bur., Farnham Royal, Bucks.

SHAPIRO, L. and BRANNOCK, W.W. (1962): Rapid analysis of silicate, carbonate and phosphate rocks. Geol. Surv. Bull. 1144-A. 56 pag.

TAYLOR, S.R. and WHITE, A.J.R. (1966): Trace elements in andesites. Bull. vulcanol. 29, 177-194.

VOINOVITCH, I.A., DEBRAS - GUEDON, J. and LOUVRIER, J. (1966): The analysis of silicates. Israel Prog. Sci. Trans. Jerusalem.

WAGER, L.R. and MITCHELL, R.L. (1951): The distribution of trace elements during strong fractionation of a basic magma. Geochim. Cosmochim. Acta. 1, 129-208.

## ADDITIONAL CONTRIBUTION

### REMARQUES SUR LA TRANSFORMATION DE QUELQUES MINÉRAUX EN MILIEU ALCALIN

S. Caillere

Muséum National d'Histoire Naturelle, Laboratoire de Minéralogie,  
61, rue Buffon, Paris 5<sup>me</sup>, France

H. Besson, S. Henin

Institut National de la Recherche Agronomique  
Station d'Agronomie, C.N.R.A., Route de Saint-Cyr,  
78-Versailles, France

ABSTRACT. - In saturated boiling solutions of  $\text{CO}_3\text{K}_2$  various substances containing oxides of Si Al Mg mixed or combined give typical minerals: kaliophilite, talc, Mg or K aluminates or phlogopite.

In saturated boiling solutions of  $\text{CO}_3\text{Na}_2$  the same materials give sodalite, stevensite, Mg aluminate and dawsonite. However,  $\text{CO}_3\text{Na}_2$  seems to be less active.

### INTRODUCTION

Depuis quelques années nous avons été amenés à développer des recherches concernant l'évolution ou la genèse des minéraux phylliteux en milieux alcalins (Besson, Caillère, Hémin, 1969-1971).

La technique opératoire est la suivante: 1 g du minéral ou du mélange initial est placé dans un béccher en gaffon de 250 cc. contenant une solution de 100 cc. renfermant 100 g de  $\text{CO}_3\text{K}_2$  ou de  $\text{CO}_3\text{Na}_2$ . On maintient à l'ébullition ménagée jusqu'à dessiccation et obtention de cristaux humides. On ajoute ensuite 100 cc. d'eau et après dissolution du carbonate, on évapore à nouveau. L'ensemble humectation-dessiccation constitue un "cycle". Cette technique

a été étendue à des minéraux autres que les phyllites, par exemple diverses formes de silice ou d'alumine cristallisée ou amorphe, des feldspaths, etc.

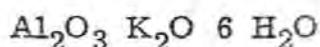
### Résultats obtenus avec $\text{CO}_3\text{K}_2$

a) Minéraux silicoalumineux. Les résultats publiés récemment montrent qu'en présence de  $\text{CO}_3\text{K}_2$  des minéraux silicoalumineux comme la kaolinite ou des mélanges d'opale et de gibbsite donnent assez généralement la kaliophilite  $\text{K}_6(\text{AlSiO}_4)_6$  (Besson, Caillère, Hénin, 1972).

Toutefois, ces évolutions sont plus ou moins rapides puisqu'il suffit de 4 cycles pour transformer la kaolinite, alors qu'au bout de 30 l'orthose n'est pas sensiblement modifiée.

Parmi les facteurs qui semblent inhiber ces transformations, figure l'excès d'un constituant dans la solution. Par exemple les réactions sont plus rapides quand on renouvelle le liquide d'attaque de la montmorillonite, on accélère aussi le processus en ajoutant un excès d'alumine qui sert de fixateur à la silice libérée (Besson, Caillère, Hénin, 1972).

Par contre s'il n'y a pas une quantité suffisante de silice dissoute, par exemple dans le cas où l'on fait agir le quartz au lieu de l'opale, il se forme un aluminat de K bien cristallisé de formule:



Un excès d'alumine en solution joue également un rôle retardateur dans le mélange kaolinite gibbsite dont l'hydroxyde évolue en aluminat. Deux autres facteurs liés à la constitution des matériaux mis en expérience, semblent également freiner la synthèse de la kaliophilite: l'absence d'hydroxydes et l'existence de certains groupements, par exemple Si - Al - K. Ainsi la muscovite et l'orthose sont très résistantes au traitement. Par contre, dans le cas où il s'agit d'une liaison Si - Al - Na comme dans l'albite, le minéral se transforme en kaliophilite.

b) Les mélanges d'hydroxydes d'Al et de Mg donnent en quelques cycles des aluminates de magnésium de type  $[\text{xAl}_2\text{O}_3 \text{ yMgO} \text{ zH}_2\text{O}]$  "x" étant voisin de 1, "y" de 7 et "z" pouvant osciller entre 13 et 15.

c) Quant au mélange  $\text{SiO}_2$  et  $\text{Mg}(\text{OH})_2$  il fournit assez aisément du talc, toujours associé à un gel silicomagnésien.

d) Enfin le mélange d'hydroxydes d'Al et de Mg en présence de  $\text{SiO}_2$  permet d'obtenir plus ou moins rapidement un produit renfermant environ 50% de phlogopite (Besson, Caillère, Hénin, 1971) associée à un gel.

Si l'on part de minéraux, il apparaît un certain nombre de particularités: si l'orthose évolue en phlogopite en présence de Mg

(OH)<sub>2</sub>, par contre le talc et l'antigorite, en présence de gibbsite, résistent et se retrouvent intacts en fin d'opération. La liaison Si - O - Mg semble donc elle aussi particulièrement stable dans ces conditions. Remarquons qu'il se forme alors de l'aluminate de K, ce qui révèle l'attaque de l'hydroxyde d'alumine.

L'ensemble de ces résultats peut être situé sur un diagramme triangulaire.

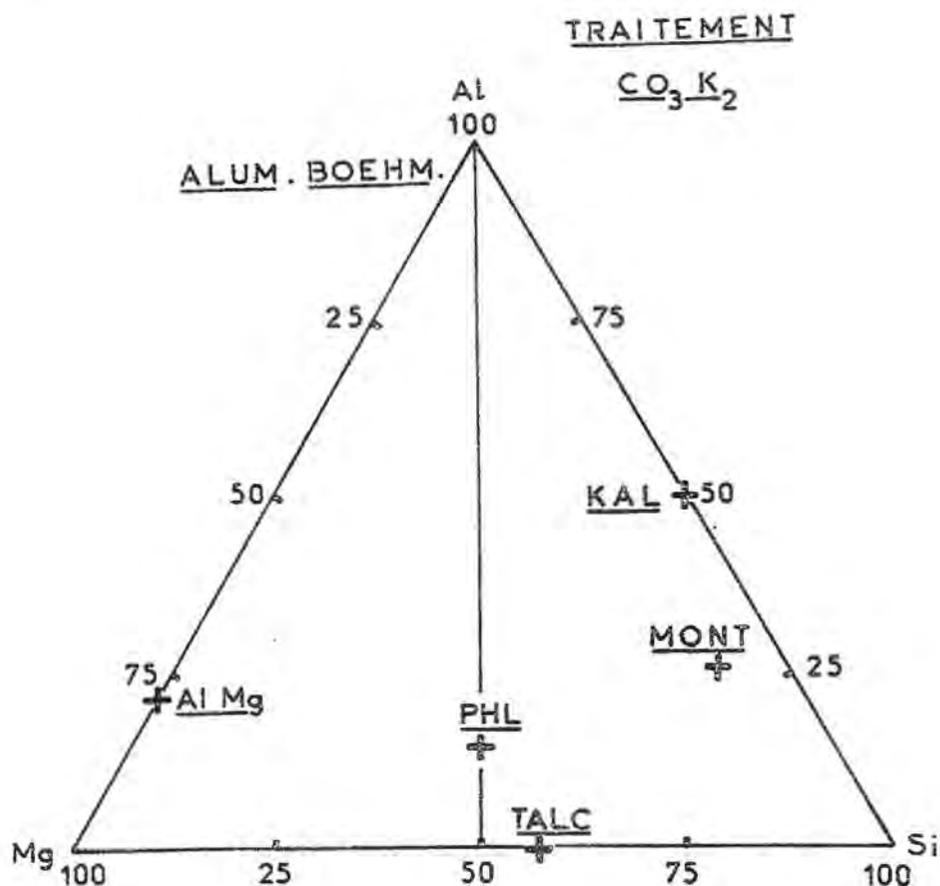


Figure 1. Principaux minéraux caractéristiques tendant à se former dans les systèmes Si - Al - Mg traités par  $\text{CO}_3\text{K}_2$  concentré

On remarquera qu'un certain nombre de composés caractéristiques se forment préférentiellement. La genèse de ces corps stables paraît facilitée quand certaines liaisons sont déjà présentes initialement. Ainsi la kaolinite évolue plus vite en kaliophillite qu'un mélange opale-gibbsite; Al tend à prendre la coordinance 4. L'aluminate de Mg donne plus aisément la phlogopite en présence de silice qu'un mélange brucite-gibbsite-silice. Par contre, d'autres liaisons comme Si - Al - K ou Si - Mg inhibent le processus d'évolution.

## Résultats obtenus avec $\text{CO}_3\text{Na}_2$

Si l'on remplace  $\text{CO}_3\text{K}_2$  par  $\text{CO}_3\text{Na}_2$  on est conduit à faire des observations analogues. La Fig. 2 représente l'essentiel des résultats.

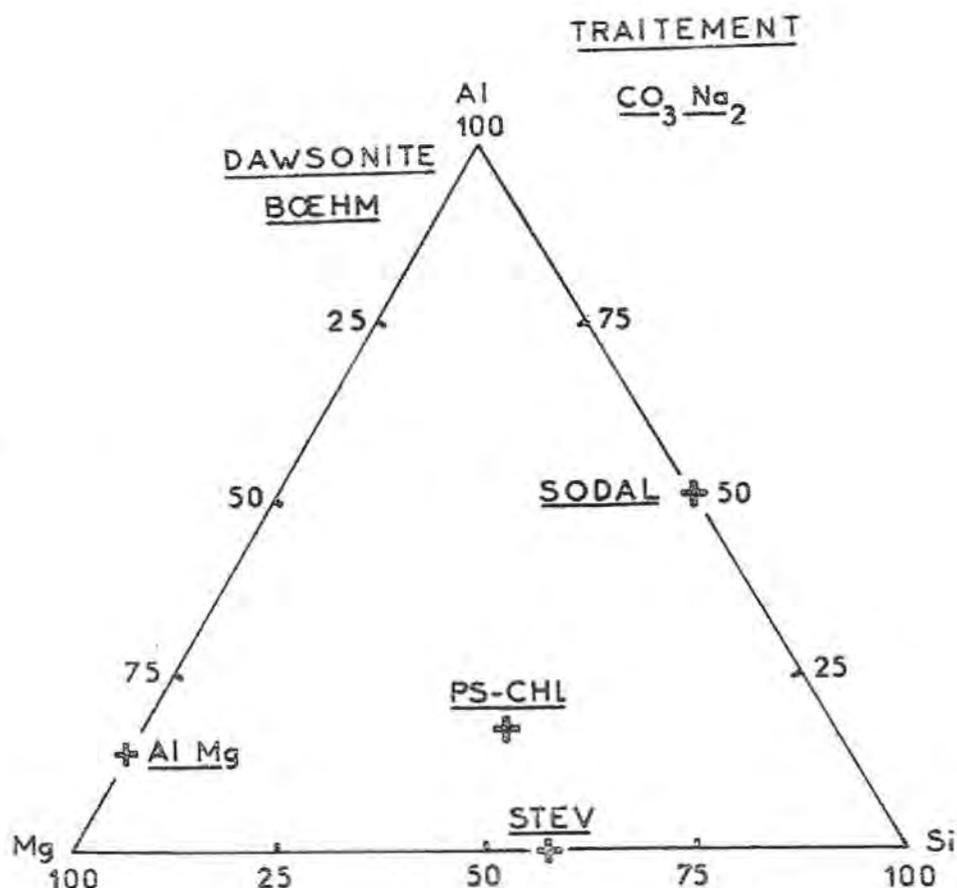


Figure 2. Principaux minéraux caractéristiques tendant à se former dans les systèmes Si - Al - Mg traités par  $\text{CO}_3\text{Na}_2$  concentré

On constate que la kaliophilite est remplacée par l'hydrosodalite dont la formule est  $2 \text{NaOH Na}_6 (\text{Al SiO}_4)_6$ , dans laquelle les deux molécules de NaOH peuvent être remplacées par des molécules d'eau (Besson, Caillère, Hénin, 1969).

Dans quelques cas le système Si - Al tend à donner des zéolites voisines de la phillipsite. Le mélange des hydroxydes d'alumine et de magnésium évolue en aluminat de Mg.

Mais il existe des différences importantes: le système  $\text{SiO}_2 - \text{Mg}(\text{OH})_2$  se transforme lentement en donnant non pas le talc, mais un produit mal cristallisé de type stévensite. Quant aux systèmes Si - Al - Mg ils conduisent à des zéolites voisines de la gmélinite et non à la vermiculite ou à la saponite qui seraient l'équivalent de la phlogopite en milieu sodique. Enfin la montmorillonite qui,

en présence de  $\text{CO}_3\text{K}_2$ , donnait la kaliophilite et le talc, fournit ici une chlorite gonflante.

Ainsi les traitements à l'aide du  $\text{CO}_3\text{Na}_2$  confirment dans leurs grandes lignes les conclusions déjà dégagées avec  $\text{CO}_3\text{K}_2$ . Toutefois  $\text{CO}_3\text{Na}_2$  apparaît comme moins actif que son homologue potassique en particulier vis-à-vis de la formation de minéraux magnésiens. Par ailleurs, le feuillet de la montmorillonite n'évolue pas en présence de  $\text{Mg}(\text{OH})_2$ .

Remarquons qu'à la place de l'aluminate de K obtenu par traitement de la gibbsite par  $\text{CO}_3\text{K}_2$ ,  $\text{CO}_3\text{Na}_2$  donne naissance à la dawsonite:  $\text{CO}_3 \text{Na Al}(\text{OH})_2$  associée à de la boehmite.

Les mélanges à parties égales des deux carbonates ont tendance à donner les mêmes produits que  $\text{CO}_3\text{K}_2$  seul, l'ion K semblerait donc avoir une action dominante.

En conclusion, en présence de carbonates alcalins il tend à se former certains composés spécifiques.

L'accélération des processus de néogenèse peut être favorisée par la composition des systèmes initiaux: présence d'hydroxyles ou de certaines liaisons.

Par ailleurs, on peut préciser des données complémentaires à la notion de "système d'agression". L'un de nous, en effet (Henin, Pedro, Robert, 1968) avait déjà souligné le fait que l'altération d'un minéral peut être sensiblement modifiée par la présence dans le milieu réactionnel de certains éléments peu solubles entrant dans la composition des produits de néogenèse. Tel est le cas du comportement des feldspaths alcalins en présence de  $\text{Mg}(\text{OH})_2$ .

Ces résultats laissent prévoir que dans le milieu naturel superficiel la présence de  $\text{CO}_3\text{Na}_2$  doit entraîner la formation de produits phylliteux relativement assez mal cristallisés (stévensites, pseudochlorites), l'apparition de tectosilicates, (hydrosodalites), de zéolites et d'autres minéraux comme la dawsonite.

## BIBLIOGRAPHIE

- BESSION, H., CAILLERE, S., HENIN, S. (1969): Conditions de préparation de l'hydrosodalite à basse température. C.R. Acad. Sci., Paris, 269, 1367-1368.
- BESSION, H., CAILLERE, S., HENIN, S., PROST, R. (1969): Préparation de la sodalite et de la noséane à basse température, à partir de minéraux phylliteux. Bull. Gr. Fr. Argiles, XXII, 5-16.
- BESSION, H., CAILLERE, S., HENIN, S. (1971): Sur la formation par voie expérimentale d'un minéral micacé voisin de la phlogopite. C.R. Acad. Sci., Paris, 272, 1-3.
- BESSION, H., CAILLERE, S., HENIN, S. (1971): Nouvelle méthode de synthèse d'un silicate du groupe de la néphéline: la kaliophilite. C.R. Acad. Sci., Paris, 272, 2749-2752.

BESSION, H., CAILLERE, S., HENIN, S. (1971): Préparation d'un silicate voisin de la phlogopite. Bull. Gr. Fr. Argiles, XXIII, 173, 180.

BESSION, H., CAILLERE, S., HENIN, S. (1972): Sur l'évolution de la montmorillonite en milieu alcalin potassique. Bull. Gr. Fr. Argiles (sous presse).

HENIN, S., PEDRO, G., ROBERT, M. (1968): 9 th International Congr. of Soil Sc. Transactions 3, paper 9, 79-90.

à consulter:

WEY, R., PEREYRON, A., GUTH, J.L. (1971): Etude du diagramme  $\text{Na}_2\text{O} - \text{Li}_2\text{O} - \text{Al}_2\text{O}_3 - \text{SiO}_2 - \text{H}_2\text{O}$  dans le domaine de formation des zéolites. C.R. Acad. Sci., Paris, 272, 181-184.

BESSION, H., CAILLERE, S., HENIN, S. (1972): Evolution du système Si - Al - Mg en présence de solutions concentrées de carbonate de potassium. Bull. Gr. Fr. Argiles (sous presse).

WALL ROCK ALTERATION IN THE NEOGENE  
HYDROTHERMAL AREAS IN GUTIN MOUNTAINS (RUMANIA)

O. Anton

Geological Institute, Bucarest, Rumania

ABSTRACT. - The regional relationship between hydrothermal solutions, host rocks, ore distribution and clay mineralization in the Gutin Tertiary volcanic Mountains (North Rumania) was investigated.

Four main clay minerals zones have been identified, inside to the outside of the veins as follows: a) the illitic zone; b) the illite, montmorillonite  $\pm$  kaolinite zone; c) the kaolinite, montmorillonite  $\pm$  chlorite zone, and d) the kaolinite, chlorite zone.

The zonal distribution of the mixed-layer clay minerals as the development of the polymorph forms of illite give us informations concerning the evolution of the equilibria relations between hydrothermal solutions and the wall rock minerals.

INTRODUCTION

The neogene volcanic activity in the northern part of Rumania has started in high Tortonian with acid piroclastic products and rhyolites. But the andesitic rocks and their accompanying piroclastic products characterize the hole neogene volcanism in this part of Rumania. The successive ejections of lavas were attributed (Giuseca, D., 1958; Ianovici, V. et al., 1961) to three main volcanic cycles: the first with rhyolites and an amphybolic andesite; the second with successive ejections of dacites and andesites closed by a large flow of andesite with pyroxene and hornblende, and, the third cycle dominated by a pyroxenic andesite. After the first two cycles a large hydrothermal activity have changed the initial aspect of the volcanic products.

In the complexity of hydrothermal manifestations one can distinguish two different phases separated by their manner of penetration in the host rocks and by their physico-chemical parameters, successive in time: one in which the solutions have penetrated in the hole andesitic mass by a diffusional process affecting chiefly the iron-magnesian minerals with old structure preserved, and another, characterized by a fissural circulation of the hydrothermal solutions and the formation of an alteration halo around the channel, with the complete disappearance of the primary structure.

In the zone of Gutin Mountains, the first phase is considered a hypostage of the hydrometasomatic phenomena, described in a propylitic andesite. This phase is developed in the mass of each end andesite of a cycle and considered a typical metasomatic process with the regional chloritization of iron-magnesian minerals (epidotization, carbonatization subordinated) and feldspars unaffected.

The amphyboles, hydrated minerals, transform directly in chlorite (pennine-clinocllore) whereas pyroxen has an intermediate uraltitic stage (hydration without major lattice change) towards the chlorite formation.

This propylitic andesite is the main country rock of the next hydrometasomatic phase, rich in  $H_2O$ ,  $K_2O$ ,  $SiO_2$ ,  $CO_2$ , S, responsible for a range of transformation expanded in an alteration halo around the veins. The content in these elements vary from one cycle to another, for each cycle with an areal variation, affecting the pattern of the hydrometasomatic minerals in the alteration envelope. The wall rock alteration starts with a K-metasomatism in other parts of volcanic range but the content in  $K_2O$  widely change so that in the eastern part of Gutin Mountains this type of metasomatism is absent. Illite is the only K-mineral present so that we can talk about a low-grade K-metasomatism.

#### MINERAL ASSEMBLAGES AND THE PATTERN OF HYDROTHERMAL ALTERATION PRODUCTS

The penetration of the hydrothermal solutions in the rock adjoining a channel leads to a great range of mineral transformations in function of the intensity of hydrolitic attack, leaching processes, change in P-T conditions and the variations of the cation/hydrogen ion ratio. There were distinguished several clay minerals assemblages with a clear zonal distribution dependent on the distance from the channel of hydrothermal circulation and the depth of the consideration point.

From the inside to the outside of the vein we can consider four main zones with the following mineral assemblages:

1-the illitic zone - with illite the only clay mineral present in the space of the channel, associated with quartz,

2-the illite, montmorillonite + kaolinite zone - in which montmorillonite add to assemblage of the zone 1 in amounts increasing with the distance from the channel; kaolinite is subordinated and can or cannot appear.

3-the kaolinite, montmorillonite + chlorite zone - kaolinite becoming the main clay mineral in the assemblage, montmorillonite, even illite are present, sometimes chlorite,

4-the kaolinite, chlorite zone - in which little amounts of montmorillonite can appear.

All these zones are quartz present in crystals similar by size and shape with the clay minerals.

There are not a geometrical limit between different zones, their edges being overlapped.

X-ray diffraction and infrared absorption studies give us detailed informations (Anton, O., 1979) permitting precise considerations upon the distribution of mixed-layer structures and polymorph forms around the veins.

Illite is present in hydrothermal products in its  $2M_1$ , 1M and Md forms.  $2M_1$  polymorph characterize only the space of the channel, outside the vein 1M form is the only stacking mode for the illite lattice. Towards the edge of the zone 2, 1Md polymorph become more and more frequent.

Mixed-layer structures show a geometrical arrangement too. In the proximity of the vein, where montmorillonite begin to be present, regular mixed-layering illite-montmorillonite add to the mineral assemblage. Outward, randomness characterize the type of interstratified illite-montmorillonite with variations in illite and montmorillonite amounts related to the distance from the channel. Chlorite as vermiculite take part to mixed-layering in the external zones, the amount of these components changing too with the distance from the channel.

A different position, referring to the four diagrammatic zones before presented, have several veins with a pyrophyllite-dickite-quartz association. There are grouped in a limited area (Steam-pului Valley) in the eastern part of Gutin Mountains. The relationship with the host rock are similar for pyrophyllite as for illite, doing, together with the microscopical aspects, their identification very difficult.

The detailed microscopical studies pointed out the formation of pyrophyllite by a hydrothermal reaction between dickite and quartz with the appearance of the fibro-radiar arrangement, at the border with a reaction front evident. It seems to be a hydrothermal reaction similar to the experimental formation of hydralsite by Roy and Osborn (1954).

Considered like the products of a local variation in physico-chemical conditions, these veins cross the high mentioned alteration zones.

A vertical zonality can be described too, the supergen acti-

vity being responsible for the leaching of the interlayer cations in the 2:1 and 2:2 structures. Md polymorphs and random mixed-layering characterize this part of profile.

Montmorillonitic structures show variation in the interlayer occupancy. Like illite structure, montmorillonite structures lose their interlayer cations becoming unstable.

The mixed-layer structures identified here confirm the evolution of the clay mineral structures towards an 1:1 Md kaolinite type lattice.

In this zone halloysite is present too.

Referring to before mentioned zones of alteration envelope around the veins, at deeper level (100 m. below) has been noted an important development of montmorillonite and chlorite with extensional restrictions for illite and kaolinite towards a propylitic level (still 150 m. below).

Together with these vertical variations in mineralogical assemblages, it is observed a general restriction of the alteration envelope more and more to the close vicinity of the main vein to propylitic level.

Accompanying clay minerals, carbonate minerals are present in veinlets, sometimes inside the fissure siderite developing in needle formations, outside with large calcite crystals. Dolomite are like calcite widely disseminated in clay mineral mass.

Pyrite in an usual associated mineral.

Gypsum and alunite characterize the supergene zone.

Secondary quartz crystals develop in veins and veinlets, sometimes permitting to describe quartzitic masses.

#### SEQUENCES OF ALTERATION TYPES. CORRELATION WITH SULFIDES ASSEMBLAGE

Time succession and distribution for these high mentioned clay minerals together with their accompanying nonclay minerals were discussed generally in the conception of Hemley and Jones (1964) and Meyer and Hemley (1967).

We consider here a specific hypostage of propylitic alteration, the term of propylite being applied to an andesite with the iron-magnesian minerals entirely chloritized and fresh feldspars.

The change in the intensity of hydrogen metasomatism and the decreasing in temperature lead to the before presented zones considered contemporaneously developed.

With a low  $K_2O$  content, hydrolitic attack in the rocks adjoining the channels start with the formation of illite. The initial P-T conditions were favorable for the  $2M_1$  polymorph. Advancing in the host rock, the P-T and chemical conditions change and 1M form become stable.

Under the variation of the cation/hydrogen ion ratio, the entire range of described clay minerals appear. Toward the fresh rock or propylitic andesite we describe an andesite or propylitic andesite with weak clay mineralization in respect to propylitic alteration like an external zone in wall rock hydrometasomatic phenomena.

It must be mentioned the restricted changes in the chemical characteristics of the solutions responsible for the development of pyrophyllite-dickite-quartz association, like the variations in time for the general chemistry of the solutions expressed in the appearance of an iron-rich chlorite and siderite central in carbonate veins. The iron-rich chlorite accompany  $2M_1$  illite or crosses all the high mentioned alteration zones.

Illite is considered here with a wide range of stability, only the manner of stacking being more sensitive in the P-T variations.

The interstratified structures can be regarded as valuable steps in the evolution of equilibria between different clay minerals.

Like in the hole neogene volcanic range, from Hungary to Rumania (see also Széky-Fux, V., 1970), the propylitization of the andesite is considered the main premetallo-genetic process, genetically connected with the second phase of hydrothermal alteration.

Illitization (described in many geological works as sericitization) are the main synmetallo-genetic process, together with carbonatization, silicification and the hole range of main mentioned clay minerals. The hydrothermal solutions cross all the products of a volcanic cycle so that the high mentioned synmetallo-genetic processes affect all these rocks.

There are also postmetallo-genetic clay minerals - those connected with supergene alteration or owing to late iron-rich phase.

The ore body are represented by galena and sphalerite veins, pyrite and chalcopyrite subordinated, in the region in which intense K-metasomatism are widespread, gold and silver mineralization being present.

At deeper level, where propylitic alteration develops, pyrite and chalcopyrite represent the main sulfide minerals.

The high presented alteration assemblages so related to metallo-genetic process, provide valuable informations for prospection activities.

## REFERENCES

- ANTON, O. (1970): Presence of illite minerals in the hydrothermal alteration products in the Cavnic zone. Rev. Roum. Géol. Géoph. Géogr. 14, 1, 35-43.
- GIUSCA, D. (1958): Die Entwicklung des Vulkanismus in der Gegen von Baia Mare. Geol. Congr. Carp.-Balk. Assoc., Kiew.

- HEMLEY, J.J. and JONES, W.R. (1964): Chemical aspects of hydrothermal alteration with emphasis on hydrogen metasomatism. *Econ. Geol.* 59, 538-569.
- IANOVICI, V. et al. (1961): Aperçu général sur la géologie de la région de Baia Mare. *Assoc. Géol. Carp.-Balk.*, V-ème Congr.
- MEYER, Ch. and HEMLEY, J.J. (1967): In "Geochemistry of hydrothermal ore deposits", edited by H.L. Barnes, Holt, Rinehart and Winston, Inc.
- ROY, R. and OSBORN, E.F. (1954): The system  $Al_2O_3-SiO_2-H_2O$ . *Am. Mineralogist*, 39, 853.
- SZEKY-FUX, V. (1970): Petro- and metallogenetic problems of Carpathian post-magmatic ore mineralization. *Acta Geol. Acad. Sci. Hung.* 14, 223-241.

## AUTHOR INDEX

Adami, A. ....	301	Hayashi, H. ....	377
Angel, B.R. ....	71	Henin, S. ....	429
Antón, O. ....	435	Herbillón, A. ....	241
Aomine, S. ....	263	Huang, W.H. ....	385
Bailey, S.W. ....	3	Huertas, F. ....	415
Bausch, W.M. ....	325	la Iglesia Fernández, A.	227
Besson, H. ....	429	Ikawa, H. ....	185
Brindley, G.W. ....	41	Jacobs, H. ....	59
Caballero, M.A. ....	313	Katz, M. Ya. ....	327
Caillère, S. ....	429	Keller, W.D. ....	385
Chaussidon, J. ....	129	Klotchkova, G. ....	365
Chukrov, F.V. ....	397	Kossovskaya, A.G. ....	341
Cruz-Cumplido, M. ....	59	Kotelnikov, D.D. ....	343
Drits, V.A. ....	15	Kotov, N. ....	365
	327	Lachica, M. ....	415
Ermilova, L.P. ....	397	Linares, J. ....	415
Eswaran, H. ....	271	Maksimovic, Z. ....	87
Frank-Kamenetskij, V..	365	Martín-Vivaldi, J.L. ....	227,
Freund, F. ....	29		313
Fripiat, J.J. ....	59	Mendelovici, E. ....	193
García-Verduch, A. ...	173	Méring, J. ....	153
Giese Jr., R.F. ....	51	Millot, G. ....	205,
Goilo, E. ....	365		255
Gómez Laverde, C. ....	117	Mizota, Ch. ....	263
Gorshkov, A.I. ....	397	Mizutani, S. ....	377
Hall, P.L. ....	71	Moya, J.S. ....	173
		Nathan, Y. ....	117

dal Negro, A.....	301	Shutov, V.D. ....	327
Nikitina, A.P. ....	283	Siffert, B.....	213
Oinuma, K.....	161	Soggeti, F.....	301
Paquet, H. ....	255	Sokolova, A.L. ....	327
Pham Thi Hang.....	41	Sudo, T.....	161
Pigorini, B. ....	301	Sys, C. ....	271
Poncelet, G.....	241	Taylor, R.M.....	405
Rautureau, M. ....	153	Tchoubar, C. ....	153
Reyes, E. ....	415	Tsuzuki, Y. ....	377
Rimsaite, J.....	353	Tulloch, R.J.....	143
Rodrique, L. ....	241	Udagawa, S. ....	185
Roth, C.B. ....	143	Velde, B. ....	285
Rousseaux, J.M.....	117	Veniale, F.....	301
Rouxhet, P.G. ....	117	Wey, R.....	213
Sarkisyan, S.G.....	343	White, J.L. ....	87
Schwertmann, U.....	405	Wiewióra, A. ....	101
Shimizu, H. ....	377	Wolfe, R.W.....	51
Shimoda, S. ....	161	Zvyagin, B.B. ....	283
			397